Resource Estimation and the Kunwarara Magnesite Deposit

by

Stella M. Searston

Submitted in fulfilment of the
requirements for the degree of
Master of Economic Geology
University of Tasmania, December, 1998

CONTENTS

ACKNOWLEDGEMENTS

The following companies are thanked for their support and input:

- Queensland Metals Corporation for the project
- BFP Consultants for the use of Gemcom Software
- Ravensgate Resources for the use of Medsystems Software

The many individuals involved in "hotline" support, including:

- Darcy Milburn
- Steve Wilcock
- Roger Cooper
- Steve Hyland

Thanks also to Charles Melton and Rocky O'Callaghan for the inspiration, and most importantly, Roger for getting me through it.

ABSTRACT

The Kunwarara magnesite deposit, in Central Queensland was selected as a study site to evaluate the use of different resource calculation methodologies on tonnages and grades within the deposit.

Initial appraisal consisted of classical statistics completed on 6 frequently analysed elements, magnesium, silica, manganese, iron, calcium and aluminium. Sample distribution was skewed, and indicative of mixed sample populations. This was attributed to a combination of factors, the most important being groundwater geochemistry in particular changes in pH. Samples were then split by lithology into sand, silt and clay fractions, and the statistics re-run. Again, the main factor controlling sample distribution was suggested to be groundwater geochemistry.

Variography was completed for three dimensional and downhole orientations. Results showed that there were coherent ranges for magnesium, iron, aluminium, and manganese in the sand fraction. The silt lithology displayed better variograms from all elements, with only calcium returning unclear variogram ranges. In the silt fraction, iron and magnesium were not clear, while the remaining elements displayed clear ranges. A feature of all variograms was the "noise" displayed. This was attributed to the mixed sample populations of each element and the sampling technique employed on the minesite.

Five resource calculation techniques were tested: inverse distance squared and cubed, ordinary kriging and indicator kriging on both composite and raw data. Tonnage and grade curves produced for each method indicated that there was relatively little difference between the methods in terms of tonnage or grade estimation. Generally, the inverse distance cubed method produced the highest tonnages and grades, while the indicator kriging (raw data) method returned the most conservative grades and tonnages. By evaluating the variance, mean and median returned from each block model, it was determined that indicator kriging was the most appropriate resource calculation method.

Using the indicator kriging method on raw assay data, a number of block sizes were evaluated. The 100 x 100 x 3 metre block size showed the minimum sample variance and is of sufficient size to allow for easy mine planning in a 3 million tonne per annum operation.

CHAPTER 1

1.0 Introduction

Queensland Metals Corporation hold title to one of the largest known cryptocrystalline magnesite deposits in the world, at Kunwarara in central Queensland. Resources at the commencement of mining were some 500 million tonnes of nodular magnesite.

Kunwarara forms a case study for the evaluation of different computerised resource estimation techniques. This study attempts to document the effects of such calculations upon the tonnages and grades to be expected in the deposit, and also to determine the effects of changes in ore block size on the tonnage and grade curves produced by each evaluation technique.

Resource calculations are the foundation stone of any successful mining operation. From the geological resource, the mining method, plant design, and eventual output are all designed. A poor selection of resource evaluation methodology can make the difference between a robust mining operation, and a break-even or sub-economic scenario. By evaluating computerised techniques, the study attempts to define the most accurate methodology for the current mining operation.

1.1 Definition of Resource Estimation

Resource estimation is a process used to determine the best possible geological assessment of the quality and quantity of a particular commodity, based on a given set of data points, so that the commodity can be profitably extracted. A mineable resource is where a commodity has been evaluated in terms of all known factors including geology, but where the mining method, extraction method, financial aspects and environmental aspects have all been considered.

1.2 Background

A number of processes lead to the mineable resource. The initial exploration program focuses on the "hypothetical", or the search for an economic commodity concentration. Steps in this process include targeting of a particular commodity, ground selection, regional reconnaissance, prospecting, and anomaly definition. Once located, an anomaly is subjected to verification by detailed mapping, geochemical and geophysical surveying, possibly costeaning or trenching, and initial drilling using rotary air blast, aircore or percussion drilling.

The next step involves deposit development. The mineralisation is more clearly defined using geological techniques such as reverse circulation percussion and diamond drilling, and the prospect advances to pre-feasibility study stage. Engineering studies, preliminary metallurgical testwork, and environmental aspects of extraction are completed. If the resource and extraction techniques appear feasible, scoping studies and a full feasibility study are commissioned. At this point, factors such as cut-off grades, mineability and dilution are assessed.

A feasibility study is the point at which project economics are fully evaluated. This consists of the best available resource estimate based on data available, full scale engineering and metallurgical studies, evaluation of environmental and heritage considerations, and a determination of the operating and capital costs, projected revenue, financial backing and social constraints of mine start-up.

Assuming a positive, robust conclusion to the feasibility study, mine construction and exploitation of the defined resource then follow. The mine start-up comes with three inherent risks – financial, business and technical. Financial risk is related to interest rates, exchange rates and commodity prices. Business risks are those associated with the financing of an exploration effort, deposit development and mine exploitation. Technical risk is directly associated with exploration, deposit development and mine production costs.

By far the largest contribution to any project's risk is the technical aspect, and this is also generally the simplest to reduce by increasing the knowledge about the deposit at the pre-mine stage. From a geological perspective, the most important factors are those which allow the resource to be quantified and the verification of methods used. The resource is the basis of the mine and the cornerstone for the evaluation of the correct mining method, plant and extraction techniques.

The geologist's input involves determining mineralisation boundaries such as the extent of the deposit, mineralogy, grade, tonnage, density and controls on mineralisation such as folds, faults or lithology. In addition, the geologist is expected to provide information on the framework of the deposit – the regional and local geological environment.

Once such factors have been documented, or at least considered, the resource estimate can be undertaken. The first step of a resource estimation process is to evaluate the known geology of a deposit. Are there lithological or structural controls? Is the genesis of the deposit likely to provide information as to higher grade mineralisation? What is the primary mineralogy? Is the mineralisation liable to require detailed metallurgical testwork due to its fine grained or refractory nature?

The next step is to assess the shape, limits and dimensions of a deposit. The more regular a deposit shape, the less likelihood there is in a major

error in estimation of size or grade. A second corollary is that mineralisation hosted in a more regular deposit shape can more readily be approximated by use of samples of limited size, such as one metre lengths of drill core or one metre intervals of drill chips.

In addition, an evaluation of the assay distribution of the commodity and any "poisons" or deleterious elements must be made. Such an evaluation can determine if there is a natural, or statistical, cut-off for economic extraction, whether there are definite patterns to the mineralisation such as a normal distribution, or whether certain elements are preferentially related to a particular lithology.

The final point, prior to the actual resource calculation, is to determine the specific gravity of the commodity, or its host rock. The resource calculation then uses the known deposit boundaries, geology, structure and mineralisation to estimate the tonnage and grade of the commodity, via ore blocks of defined thickness, width and grade.

1.3 Review of Estimation Techniques

1.3.1 Traditional Techniques

Resource estimates can be completed using either traditional or non-traditional methods. Traditional methods rely on estimating the volume of mineralisation in relation to known sample points, generally drillholes. Assay values are then assigned to the volumes via geometrical weighting techniques. Traditional methodologies include sections, contours, and polygons.

Sections are produced from lines of drillholes preferably sited on standard grid patterns at right angles, or close to right angles to the mineralisation being evaluated. A section normally shows the trace of the drillhole, geology downhole and the assay values and intervals. For reasons of sampling accuracy, usually only reverse circulation percussion or diamond drillholes are utilised.

Surfaces are drawn to approximate the boundaries of mineralisation, ensuring that each "block" outlined follows the assumed dip of the mineralisation. Each block's area is calculated, and a grade assigned by averaging the drillhole grades over the width of the block. A typical section example is shown in Figure 1-1.

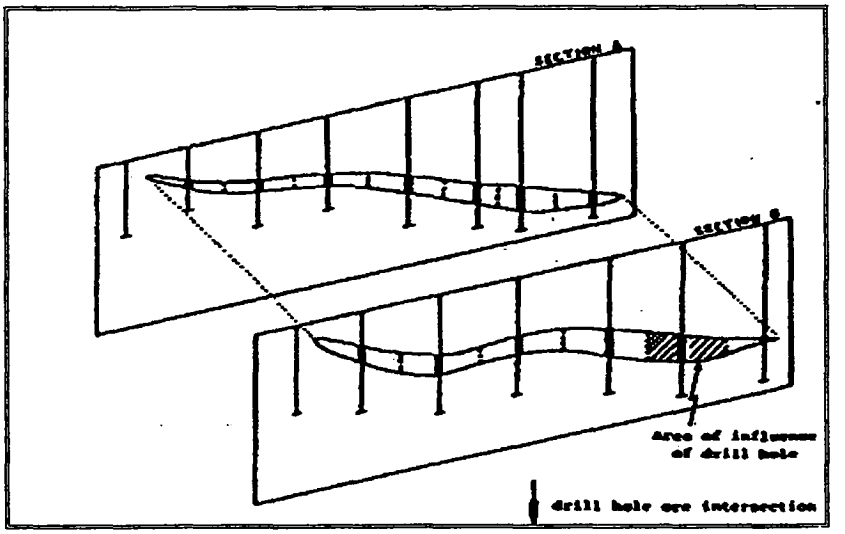

Figure 1-1 Sectional Calculation Method

(reproduced from King, H., McMahon, D, and Bujtor, G. (1982), A guide to the understanding of Ore Reserve Estimation, Supplement to AusIMM Proceedings No. 281, March, 1982).

Contour calculations involve assigning various grade weights between two samples on a regular, proportional basis, so that each grade weight is an equal proportion of the difference in grade between the two samples. Grade weights of the same value are joined up, and the area underlain by each grade weight calculated by using either a planimeter or a digitiser. The result is a contour plan, as shown in Figure 1-2

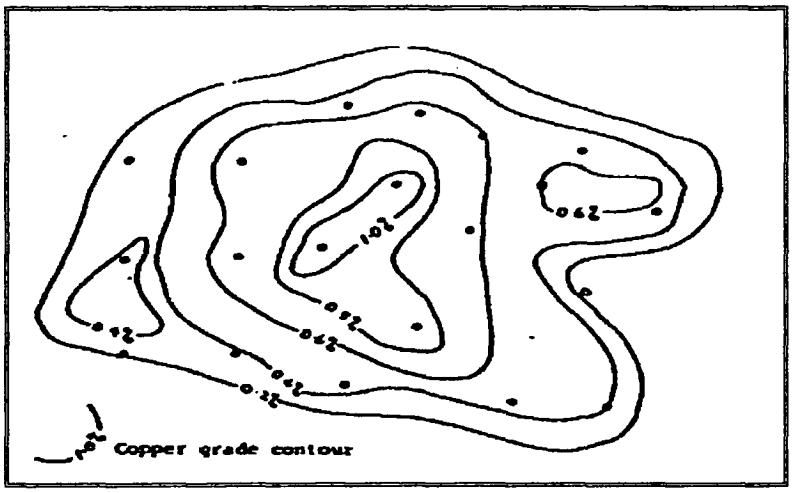

Figure 1-2 Contour Calculation Method

(reproduced from King, H., McMahon, D, and Bujtor, (1982), A guide to the understanding of Ore Reserve Estimation, Supplement to AusIMM Proceedings No. 281, March, 1982).

Polygons use individual drillholes to calculate a grade and thickness value for the mineralisation intercepted by that hole. Polygon ore blocks may be truly polygonal, triangular, rectangular, or square in shape. Boundaries for each block are generally assumed to be half way between adjacent drillholes. Figures 1-3 and 1-4 give examples of polygonal and triangular resource calculation methodologies.

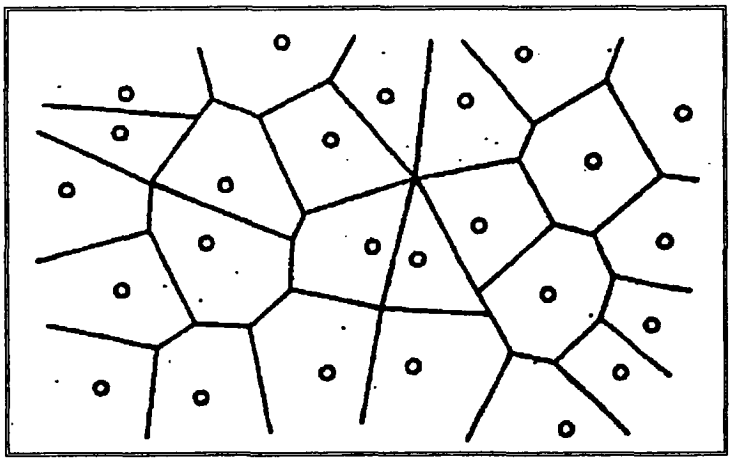

Figure 1-3 Polygonal Resource Calculation Diagram

(reproduced from Royle, A.G. (1980), Estimating Global Ore Reserves in a Single Deposit, Minerals Science and Engineering, Volume 12, No 1, pp 37-50)

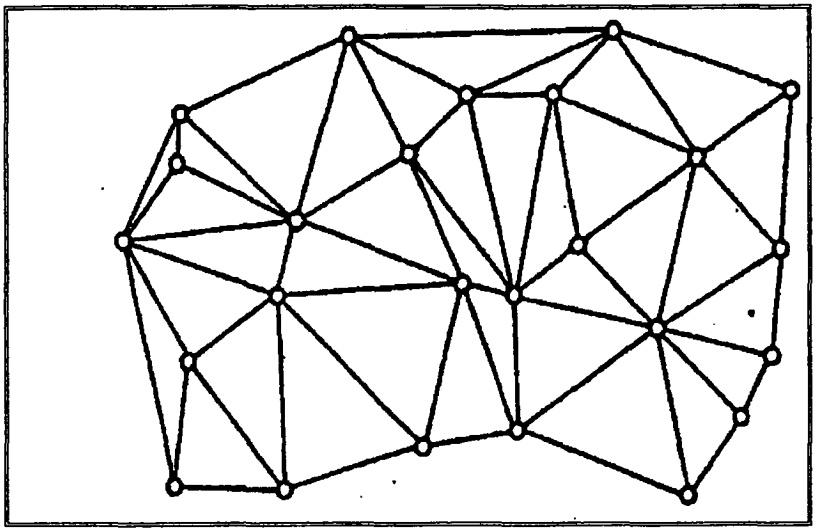

Figure 1-4 Triangular Resource Methodology Diagram

(reproduced from Royle, A.G. (1980), Estimating Global Ore Reserves in a Single Deposit, Minerals Science and Engineering, Volume 12, No 1, pp 37-50)

In general, the traditional methods tend to overestimate volumes, particularly at the corners of surfaces or polygons, and more particularly, when the polygon volumes or surface volumes vary widely between adjacent sections (Snowden, 1995). Assumptions as to continuity, and trends are implicit in the calculations, and may lead to errors in estimation, particularly if the mineralisation plunges in an orientation which is not the same as the strike (Kim, 1993).

A similar overestimation can occur with grade. Most traditional methods simply extend the area of influence of a sample to half the distance of the sampling grid, so that a series of samples taken 25 metres apart will have a radius of influence of 12.5 metres. This gives a disproportionately high weighting to isolated high grade drillholes. In the case of a polygonal estimate, the average grade of a polygon is based on the grade in a single drillhole, leading to biased grade estimates.

The overestimation is frequently countered by assigning various correction factors, such as cutting of high grade values, or superimposing a dilution factor on the ore block. Traditional methods also have two other drawbacks. The first being that they are time consuming, and being laboriously manually completed are subject to human vagaries in attention to detail and repeatability. The second problem relates to difficulties in determining the margin of error in the volume and grade calculations.

1.3.2 Transitional Technique – Inverse Distance Weighting

Inverse distance weighting was the initial response to the problems of overestimation. The technique allows assays which are closest to the defined ore block to have the most impact on the grades within the block. Generally, an orebody is divided up into blocks of equal area or volume.

Each block is then subject to a pre-defined set of search parameters to determine which assay values are the closest in space to the block. Only assays from within the search radius are used to assign values to the individual block. Assay values are assigned a weighting dependent on the distance from the drillhole to the block, as shown in Figure 1-5.

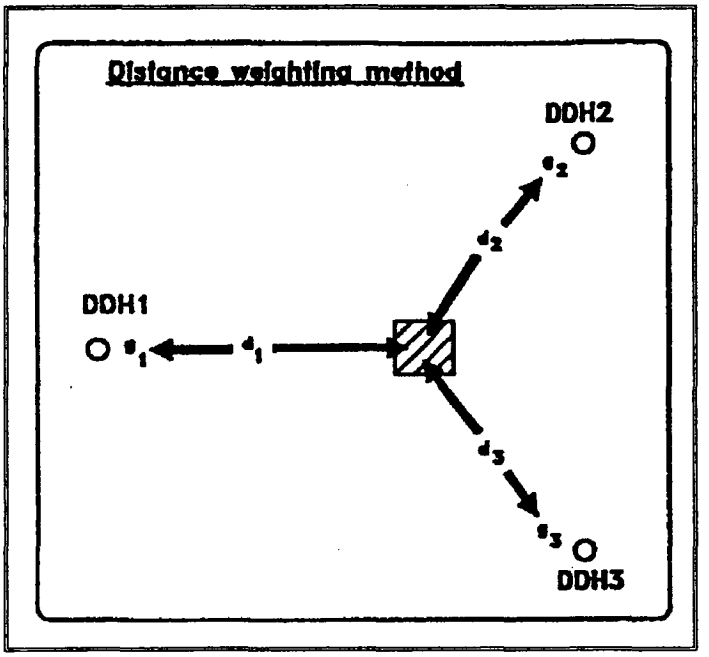

Figure 1-5 Weighting Factors, Inverse Distance Technique

(reproduced from Snowden, V. (1995), Applied Mining Geostatistics. Shortcourse presented at University of Tasmania, November, 1995)

$$\text{Grade of block} = \frac{[g1/(d1)^m + g2/(d2)^m + g3/(d3)^m]}{[1/(d1)^m + 1/(d2)^m + 1/(d3)^m]}$$

DDH 1 to 3 are the drillholes, g1 to g3 are the grades to be used in the calculation, and d1 to d3 are the distances from the block to the drillholes, and m is the selected power.

The weight is inversely proportional to the distance to an arbitrary power "m", between the sample and the centre of the block. The most common "m" powers used are squared and cubed, and selection of the required power more an arbitrary decision than a function of the change in variation of mineralisation over the calculated distance.

Although frequently presented as a "geostatistical" resource calculation method, inverse distance weighting is not a geostatistical method, and it cannot produce an estimation of the errors in the grade and volume calculations.

1.3.3 Geostatistical Techniques

Non-traditional techniques include ordinary kriging and conditional simulation, and various modifications of the kriging process such as multiple and indicator kriging. These techniques allow some precision into the mineralisation estimation procedure by assessing grade continuities along with mineralisation orientation trends.

The major tool of a geostatistical estimate is the variogram. Variography allows an assessment of the continuity and direction of mineralisation, the variability of the assay results, and the range of influence of drillholes to be made. Each variogram can be assessed in terms of the nugget effect, range of influence, and sill.

Two samples which are taken at exactly the same point may not have exactly the same assay value, and the difference between the two samples is the nugget effect. The nugget effect is most commonly a high value where small scale structures such as veining, or coarse gold distributions exist. In large, massive deposits, such as a nickel laterite, there may be a very small nugget effect, meaning that there is not much variation in assay values between sample values taken from the same location.

By increasing the distance between the locations of individual sample pairs, variability may increase to the point where the samples simply have no relationship to each other. The point of no relationship is measured from the y-axis of the variogram, and represents the sill. The same point, on the x-axis gives the range of influence, or the last point at which samples can be correlated. An example of a variogram is shown in Figure 1-6, with the sill, range and nugget values calculated.

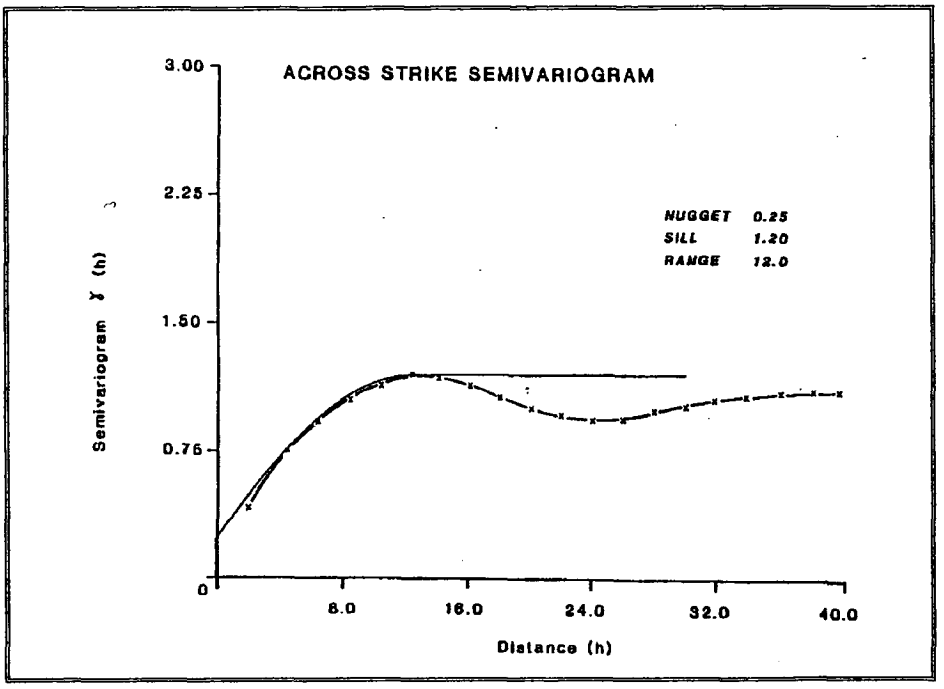

Figure 1-6 Example of a Semi-Variogram

Semi-variograms can be calculated for specific geological or structural directions, such as along strike, down dip, down plunge or across strike.

Kriging uses the information gained from the variography to estimate the grade of an ore block by weighting surrounding assays on the basis of the magnitude of the assay, and the distance to the assay from the ore block. At the same time, the technique minimises the sample variance within the ore block. Figure 1-7 shows the relationship of the surrounding drillholes to the ore block being estimated.

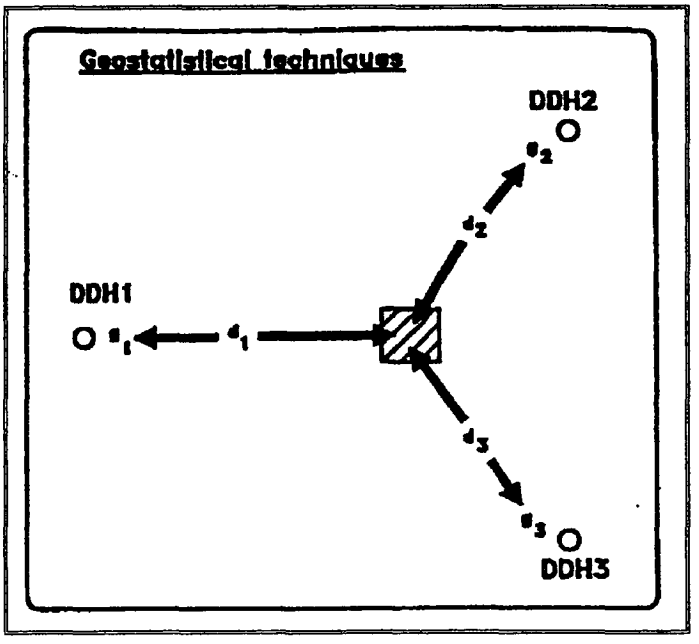

Figure 1-7 Weighting Factors, Kriging Techniques

(reproduced from Snowden, V. (1995), Applied Mining Geostatistics. Shortcourse presented at University of Tasmania, November, 1995)

In this instance,

Grade of the Block = $\lambda 1g1 + \lambda 2g2 + \lambda 3g3$

assuming that $\lambda 1+\lambda 2+\lambda 3$ are all equal to 1. $\lambda 1$ to $\lambda 3$ is the weighting factor assigned to minimise estimation variance.

Which method of kriging to employ is dependent on the type of distribution revealed by the classical statistical evaluation of data undertaken. If data are normally distributed, and the variograms are robust, ordinary kriging is a useful tool.

Indicator kriging is employed when the mineralisation under study has a complex distribution (highly skewed, for example), as the method allows the assignment of probabilities to an ore block independent of sample distribution types. Figure1-8 shows the application of an indicator kriged model to an ore block.

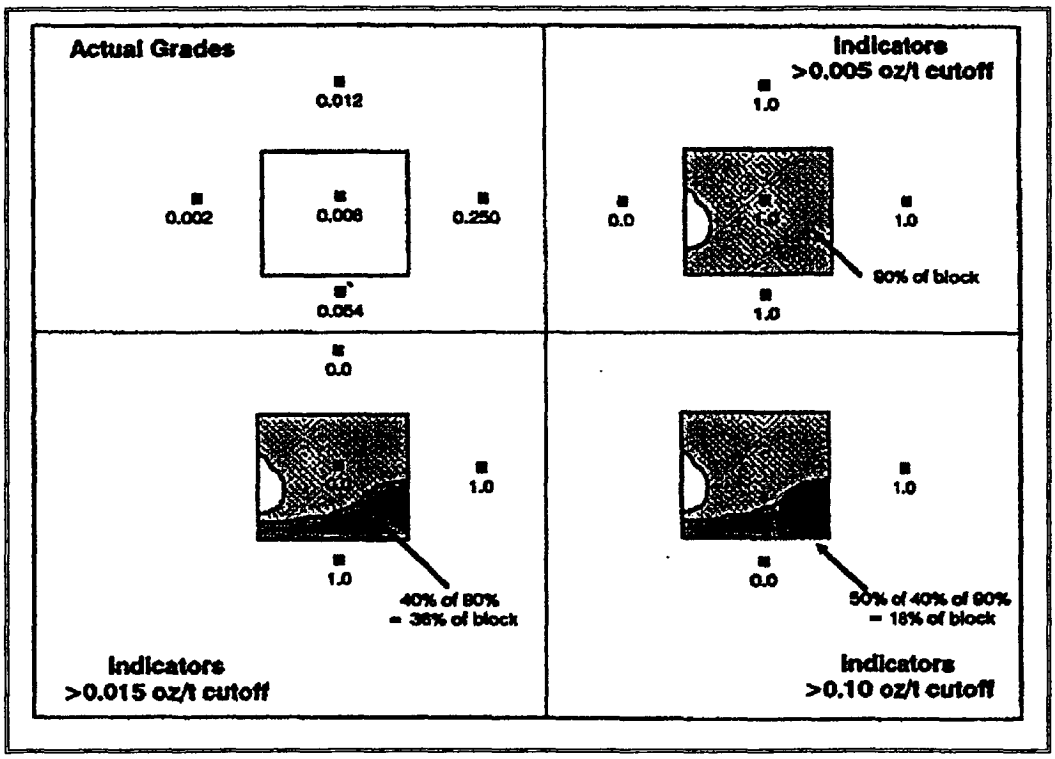

Figure 1-8 Indicator Kriging Approach to Resource Estimation

(reproduced from Dagbert, M. (1990), Approaches to Ore Reserve Estimation – Indicator Approach, in Snowden Associates Newsletter, May, 1990)

Probability kriging involves assay values being sorted by increasing value, and then being assigned a cumulative frequency based on the assay value. More unusual kriging routines, such as disjunctive, multi-gaussian and rank order kriging have also been reported, e.g. Francois-Bongarcon (1986), Verly (1983) and Verly and Sullivan (1985).

In general, the following criteria should be used when selecting a kriging method for a deposit (Snowden, 1995)

- Normal distribution — Ordinary Kriging
- Highly skewed distribution — Indicator or Probability Kriging

Conditional simulation as a resource estimation technique is a relatively new technique in the geostatistical inventory, but also relies on variography. A model of a deposit is built to reproduce all known values from drillholes, and to possess the same mean, variance and variography as the actual deposit itself. Generally, this is achieved by running a number of different conditions for the deposit model, and assessing the variability between models. The completed simulated model is able to provide a more complete picture of the uncertainty involved in the resource calculation. The methodology is normally employed for deposits which require careful modelling of short-scale variability, such as the assessment of blending requirements for mill feed, or evaluation of dilution effects.

1.4 Mining Units

Selective mining is dependent on the standard mining unit, or the smallest block of ore capable of being mined. Selective mining units (SMUs) are frequently chosen to reflect the operational cut-off grade utilised in the mine plan. Thus, the SMU is the smallest volume which can be classified as ore or waste (Journel, 1985). If the grade estimated within the SMU is greater than the cut-off grade used, then the block is classified as ore. If less than the cut-off grade, the block is classified as either low grade or waste.

Generally, the SMU is dependent on the type of deposit, with a high tonnage, low grade deposit having a larger SMU than a low tonnage, high grade or highly complex body. In practice, the upper limit of an SMU may be constrained by the size of the mining equipment used. In the case of an underground mine, the SMU may be directly related to the size of the bucket of the loader feeding the ore haulage system. In an opencut operation, this may equate to a dragline bucket, haul truck load capacity or the size of the excavator used.

1.5 Estimation Bias

One of the larger problems in calculating mineable reserves is that the majority of mining decisions and forward mine planning are based on small sample populations generated by exploration drilling. The resource figure generated from the exploration data is reported to the stock exchange, and forms the basis for annual reconciliation figures.

In practice however, day to day mining decisions are not based on the exploration data, but on larger volumes of information generated by blasthole sampling or close spaced mine drilling. This allows a degree of selectivity of resource grade not available in the exploration data, to ensure

the mill receives the best possible grades, while low grade material or waste is sent to the appropriate stockpile. The use of the blasthole information to determine mill feed results in a difficulty with reconciliation of mill figures back to the original exploration data.

For example, an ore reserve reported for a particular year will have a defined tonnage and grade, based on the exploration sampling. Figures kept by the mining operation in terms of tonnage mined and treated and grade recovered are then reconciled to the ore reserve, and the remaining ore in the ground is the basis for the following year's reserves. However, as the ore extracted has been based on better spaced information than the exploration drilling, the reconciliation is possible for either the tonnage extracted, or the grades treated.

A partial explanation for this can be gained by evaluating the "regression effect" or the conditional bias involved in the resource calculation.

The regression effect is caused by exploration or blasthole data overestimating the grade in higher grade areas, and underestimating the grade in designated low grade areas. This may result in higher than expected grades on the low grade stockpiles, or lower than expected grades being delivered to mill. The regression effect is illustrated graphically in Figure 1-9. The ellipse contains the variation of data points which result when block grades are plotted against the initial sample grades.

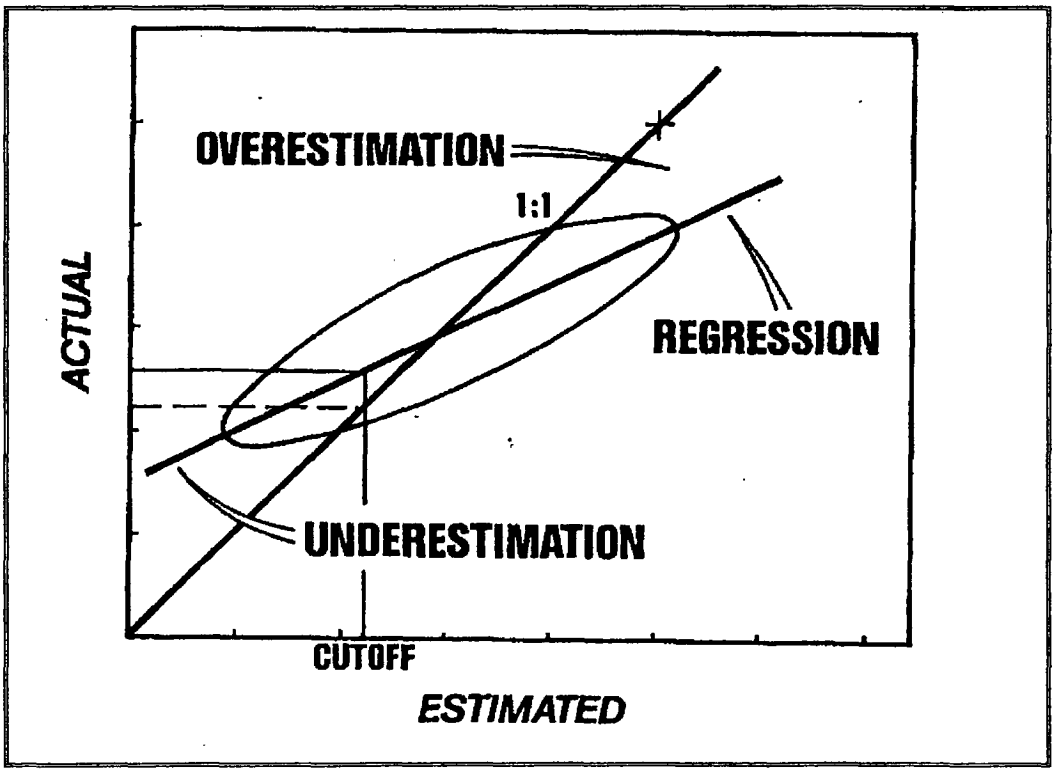

Figure 1-9 Regression Effect

(reproduced from Snowden, V. (1995), Applied Mining Geostatistics. Shortcourse presented at University of Tasmania, November, 1995)

The effect is caused by changes in the variability of a data set in relation to the amount of data used to calculate an ore block. If a deposit is mined as a single block of ore, it will have negligible block variance. As this is not practical in terms of mining and milling constraints, the assessment of variation within the SMU blocks is required. Figure 1-10 shows the relationship of ore blocks at the same cut-off grade to samples, where the blocks have more tonnes at a lower grade, than the samples do. In this instance, samples have a lower grade, but a higher tonnage, than do the corresponding ore blocks.

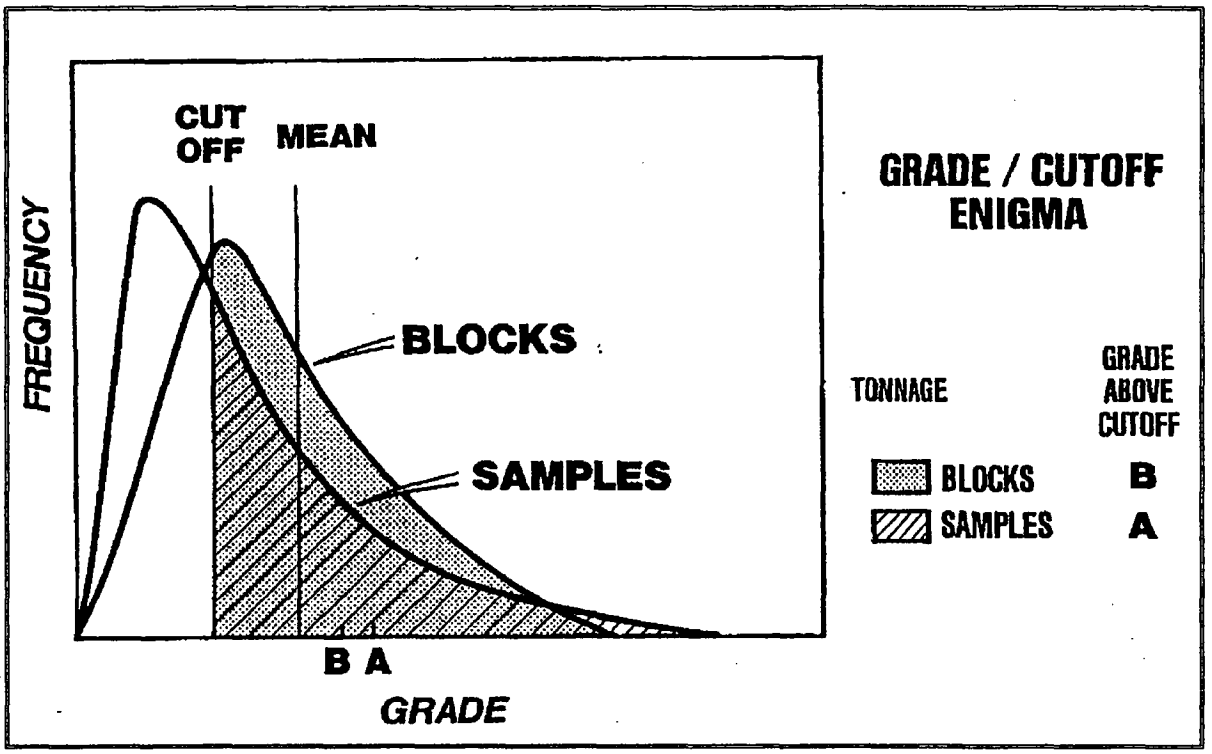

Figure 1-10 Grade/Tonnage Regression Effect

(reproduced from Snowden, V. (1995), Applied Mining Geostatistics. Shortcourse presented at University of Tasmania, November, 1995)

Block variance for any size block can be calculated using Krige's Relationship (Kim, 1993), whereby

$$\sigma^2_{(v/D)} = \sigma^2_{(o/D)} - \sigma^2_{(o/v)} = \gamma(D,D) - \gamma(v,v)$$

o	is the assay value being assessed
v	is the ore block
D	is the entire deposit
γ	is the average dispersion variance
$\sigma^2_{(v/D)}$	is the block variance
$\sigma^2_{(o/D)} - \sigma^2_{(o/v)}$	is the difference of two dispersion variance, and is generally equal to the sill, derived from the variography.

Estimation variance is the estimation of the variability of the error between the actual grade of an ore block, and that estimated during the resource calculation. It allows an estimate of how well (or poorly) the resource calculation is reflecting the mineralisation. The larger the variance, the worse the resource calculation is doing.

From a combination of the estimation variance and the block variance, the conditional bias of the estimation process is reviewed, and adequate sample spacing for the mining operation can be determined.

1.6 Kunwarara

Kunwarara was selected as a case study to evaluate the impact of various geostatistical resource modelling techniques on tonnage and grade, and to determine whether changes in block sizes for the mining process affect resource tonnages and grades.

As a result of well-documented biases, more traditional non-computer related resource methods were ignored in favour of the inverse distance weighting and geostatistical methods. At the same time, the experimental conditional simulation geostatistical technique has not been utilised due to the method complexity, and lack of readily available run-of-mine software.

The following chapters outline the evaluation of Kunwarara in terms of regional and local geological reviews, assessment of the statistical variation of the six major elements in the deposit, calculation of three-dimensional and downhole variograms, and completion of inverse distance weighted, ordinary and indicator kriged modelling to determine the most appropriate resource calculation technique for the deposit.

CHAPTER 2 - PROJECT BACKGROUND

Any successful resource evaluation requires an assessment of the setting of the deposit to be modelled. In the case of an existing mining operation, the metallurgical process and mining process need to be outlined. Mining processes involve an idea of the capacity of the equipment to be utilised, the type of operation, location and trucking distance of stockpiles, for example. The metallurgical process route needs to be defined in terms of ore handling, blending requirements, possible contaminants, and the final end-product.

Outlined below is a summary of the location details of the deposit, in addition to a précis of the mining and metallurgical processes.

2.1 Location

The Kunwarara Magnesite Deposit is located some 70 kilometres northwest of the Central Queensland town of Rockhampton, close to the small township of Marlborough, see Figure 2-1.

2.2 Access

The mine is accessed via the all weather Bruce Highway, the main north-south highway in Queensland to the small township of Kunwarara north of Rockhampton, and thence by 6 kilometres of gravel roads.

2.3 Tenure

The area of the deposit is held under Mining Lease 5868, and EPM's 4121 and 4117.

2.4 Corporate Background

Queensland Metals Corporation (QMC) is an Australian listed company with approximately 3000 shareholders. In 1985, the company discovered the Kunwarara magnesite deposit, the world's largest magnesium carbonate deposit (QMC Annual Report, 1997) and since that time has established a number of projects to utilise the resource. In 1998, the QMAG and Enviromag projects were in commercial operation.

QMAG is a large magnesite processing and refractory magnesia operations, producing 120 000 tonnes per annum of deadburned magnesia and 30 000 tonnes per annum of electrofused magnesia. QMAG was formed as a joint venture in 1987 between Pancontinental Mining Limited and Radex Australia Pty Ltd, with initial construction of the mine and plant processing facilities in 1991. Enviromag was established in 1993 as a joint

venture between ICI Australia, QMC and CSIRO to produce calcined magnesia and magnesium hydroxide.

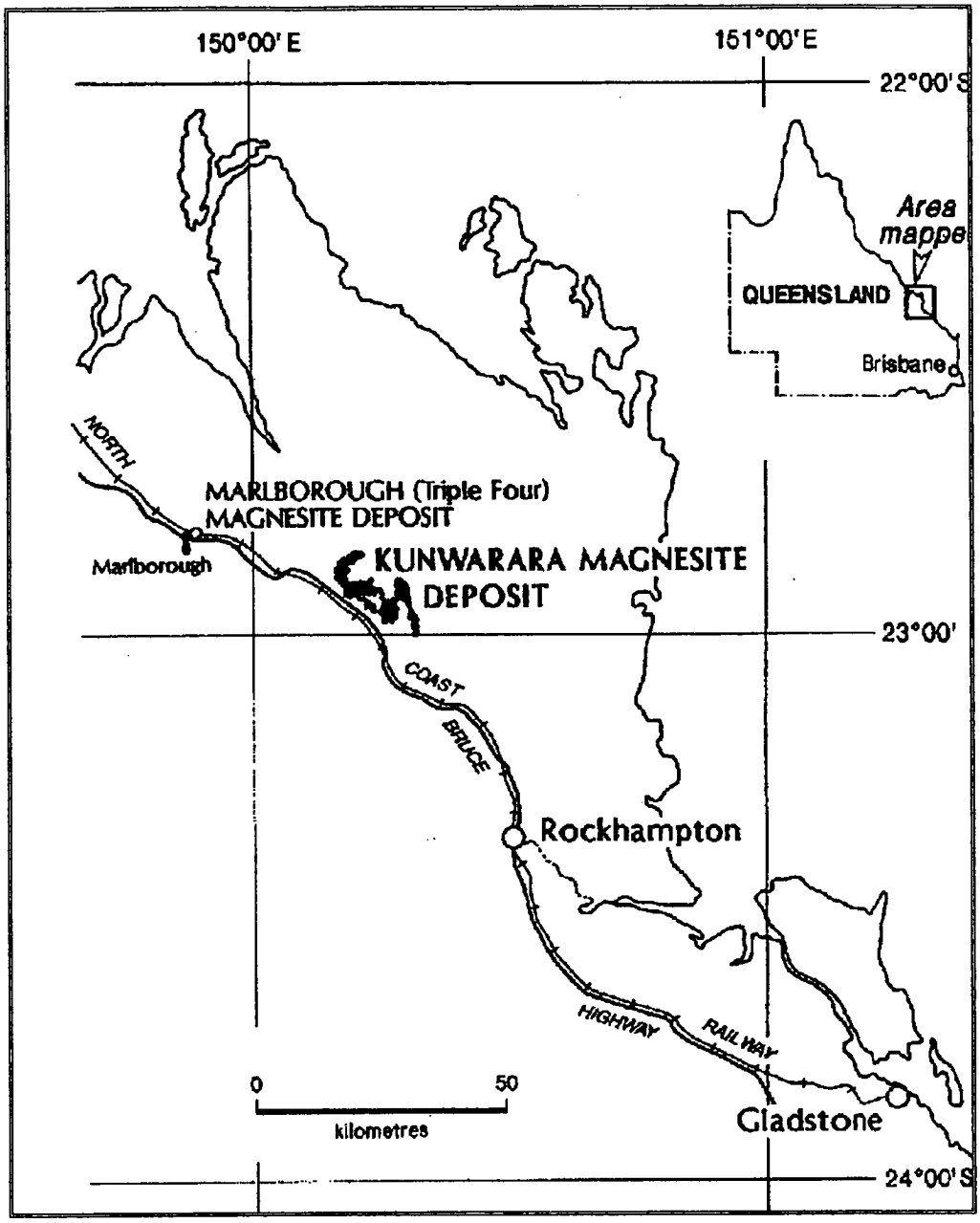

Figure 2-1 ***Location Plan, Kunwarara Magnesite Deposit***

(plan reproduced from Milburn, D. and Wilcock, S. (1994), The Kunwarara Magnesite Deposit, Central Queensland, in Holcombe, R.J., Stephens, C.J. and Fielding C.R., editors, Capricorn Region Central Coastal Queensland, 1994 Field Conference Manual, Geological Society of Australia, Queensland Division)

The Kunwarara project was rationalised during 1997 firstly by QMC acquiring 100% ownership of QMAG and Enviromag, and secondly through the creating of the Australian Magnesium Corporation (AMC). As part of the formation of AMC, QMC sold all of its magnesium metal interests to AMC. This included the technology, a portion of the Kunwarara deposit, and all the relevant licences. AMC is designed to exploit research undertaken by CSIRO and QMC to convert magnesia to magnesium metal. A full feasibility study into the Australian Magnesium process is expected to be completed by the end of 1998.

2.5 Mining Operation

Ore is currently mined at the rate of approximately 3 million tonnes per annum, from 3 metre high benches in three separate open pits, using 100 tonne excavators in the opencut mine and 50 tonne dump trucks for transport. The operation is free-dig and ore is stockpiled approximately 1 kilometre from the pit and blended for processing.

Following screening, and crushing if required, ore is placed into either a crushed or uncrushed stockpile, and then processed according to grade requirements.

The first phase beneficiation plant is located on site, and this plant is fed from magnesite material which has been upgraded using a series of washers and screens. Beneficiation consists of both high grade and low grade gravity cyclones and drums respectively, which are used to separate components according to bulk density. Further washing and screening of the resultant separated product occurs to ensure no impurities remain.

Prior to being transported to the Pankhurst Refractory plant in Rockhampton, the beneficiation product is stockpiled and subjected to stringent quality control approvals.

2.6 Product

At the Pankhurst plant, the raw magnesia undergoes heat treatment to produce calcined magnesia. This involves heating the raw product to approximately 1050 degrees Celsius to drive off carbon dioxide. Screening, crushing, magnetic separation and finally blending are then used to upgrade the calcined magnesia to a homogeneous mixture of known magnesium grade. A flowsheet for the magnesite calcination process is shown in Figure 2-2.

The final product from the Pankhurst plant is deadburned and electrofused magnesia. The relatively stable non-reactive deadburned material results from the heating of calcined magnesia to temperatures over 1500 degrees Celsius, the process being documented in Figure 2-3. It is primarily used in furnaces, kilns and cement works, in the form of high density briquettes.

Electrofused magnesia results from taking the calcined magnesia to temperatures over 2800 degrees Celsius, and the product is more stable than deadburned magnesia. Its primary use is in nuclear reactors, rocket nozzles and high temperature furnaces. The process flowsheet for the electrofusing operation is shown in Figure 2-4.

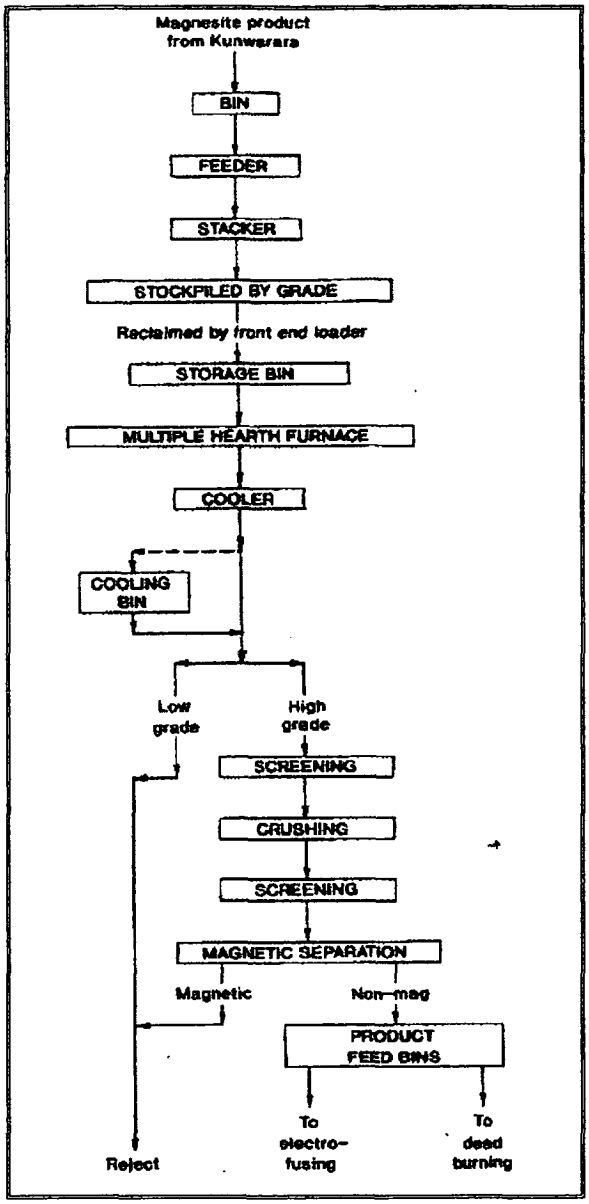

Figure 2-2 Parkhurst Operation Magnesite Calcination Circuit Flowsheet

(reproduced from Hill, B.F. (1992), Magnesite and magnesia production by Queensland Magnesia (Operations) Pty Ltd at Kunwarara and Rockhampton, Qld. In AusIMM Bulletin, July, 1992.

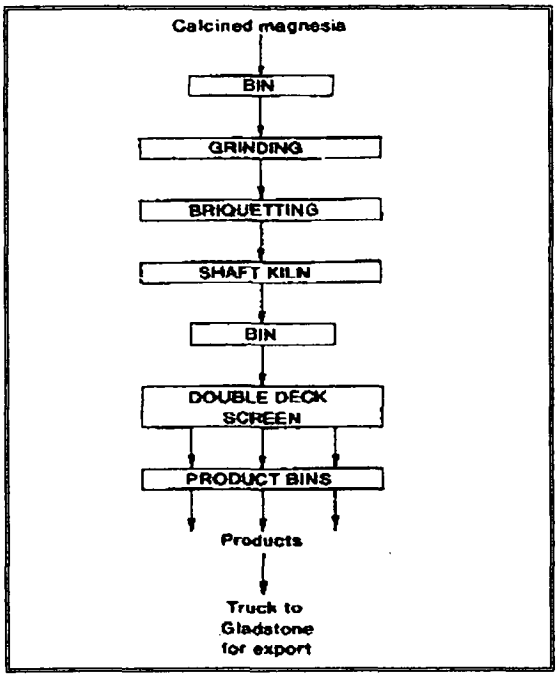

Figure 2-3 Parkhurst Operation Magnesite Briquetting and Deadburning Circuit Flowsheet

(reproduced from Hill, B.F. (1992), Magnesite and magnesia production by Queensland Magnesia (Operations) Pty Ltd at Kunwarara and Rockhampton, Qld. In AusIMM Bulletin, July, 1992.

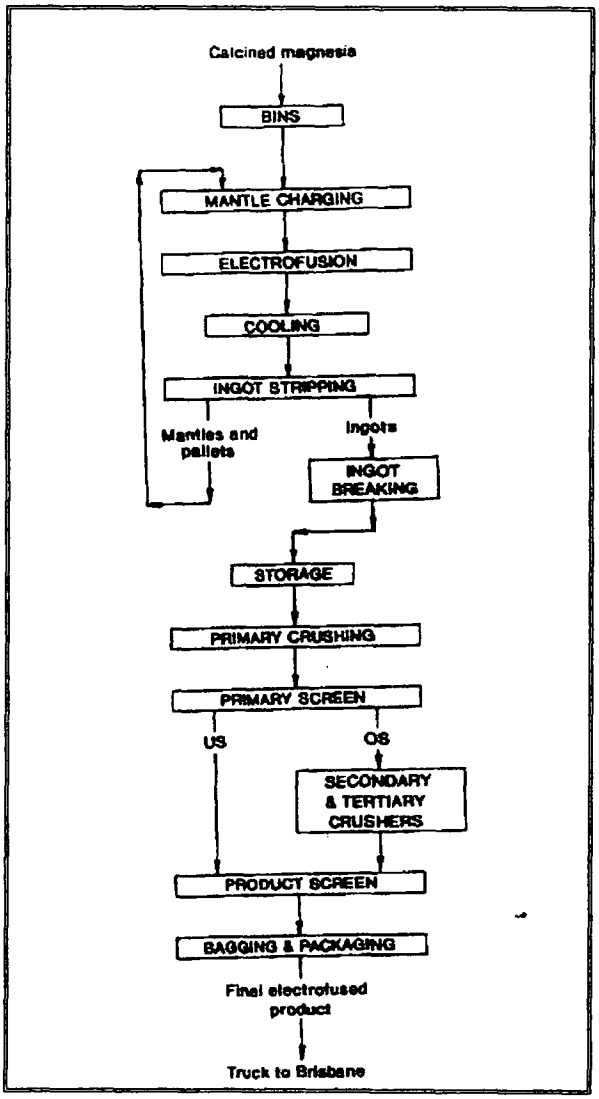

Figure 2-4 Parkhurst Operation Magnesite Electrofusing Circuit Flowsheet

(reproduced from Hill, B.F. (1992), Magnesite and magnesia production by Queensland Magnesia (Operations) Pty Ltd at Kunwarara and Rockhampton, Qld. In AusIMM Bulletin, July, 1992.

CHAPTER 3 - GEOLOGY

A clear and concise understanding of the geological setting and genesis of a deposit is mandatory prior to any resource calculation being undertaken. The regional geological outline explains where the deposit is situated in relation to the development of a province as a whole, while the local geology provides an framework for the mineralisation setting.

Unless these parameters have been evaluated, a resource model will simply be based on assay values, and local controls such as favourable stratigraphic units, faults or fractures ignored. This leads to a poorly informed resource model, and will probably result in a sub-economic mining operation.

3.1 Exploration History

Magnesite occurrences in the general vicinity of the Kunwarara deposit have been known since the early 1900s. References in the early literature of the region (e.g. Dunstan, 1913, Brooks 1964) are to magnesite veins and lenses, later noted as occurring in the vicinity of minor intrusions in weathered ultramafic rocks (Ridgway, 1948).

Nodular magnesite was also known to occur in the Rockhampton district, although its origins remained unknown, due to the lack of exposure of the source material under soil cover.

QMC personnel were approached by a prospecting syndicate in early 1985, and recognised the sedimentary origin of a magnesite rich horizon exposed in a creek bank near the township of Marlborough (Burban, 1990).

Subsequent research of open file data held by the Queensland Geological Survey and Queensland Department of Mines by QMC located references to intersections of sediment hosted magnesite in drillholes sunk by oil shale exploration companies. Twinning of these holes in early 1985 led to the recognition of the Kunwarara magnesite deposit (Burban, 1990).

3.2 Regional Setting

The Kunwarara deposit is situated within the Yarrol Province of the New England Fold Belt or Orogen (Murray, et al 1987). This orogen constitutes the youngest, eastern-most portion of the Tasman Orogenic Zone (Day et al 1978), and probably developed between the Silurian at the earliest, and Triassic at the latest. Figure 3-1 depicts the structural units of the New England Orogen. The recognition of the Yarrol province as part of the New England Fold Belt is comparatively recent, and much of the current literature is devoted to the establishment of definitions of the belt based on terrane analysis.

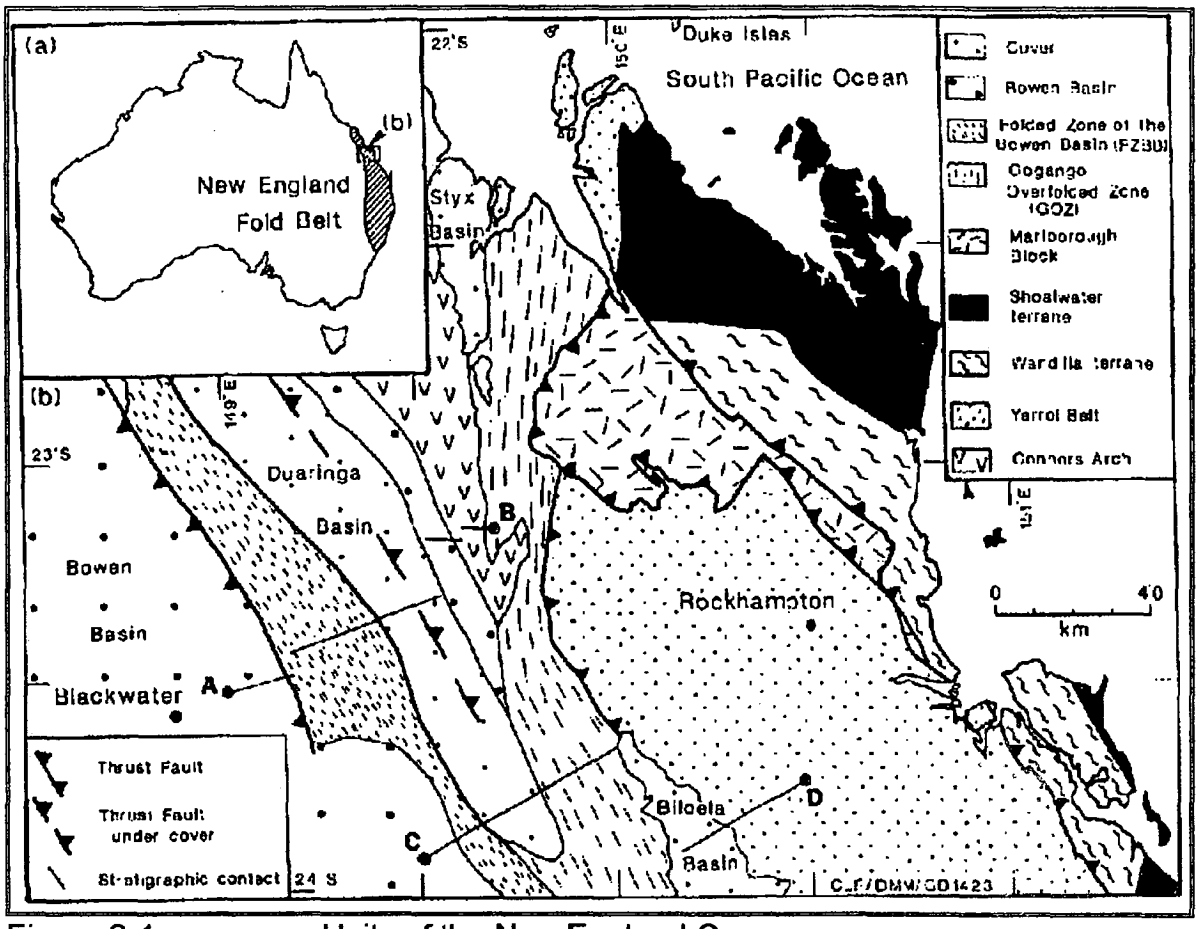

Figure 3-1 Units of the New England Orogen

(Plan reproduced from Ferguson, C.L., Henderson, R.A. and Leitch, E. (1994) in Holcombe, R.J., Stephens, C.J. and Fielding, C.R, editors, Capricorn Region Central Coastal Queensland 1994 Field Conference Guidebook. Note in original plan, the lines A, B, C, D, represented regional cross-sections not applicable to this thesis)

Descriptions of rocktypes and definitions of sedimentary units from earlier work such as Day et al (1978), have not yet been fully incorporated into the latest understandings of the geological evolution of the area, and are beyond the scope of this review.

Descriptions of the Yarrol province from the 1970's and early 1980's consisted of a terrane of structurally bounded sedimentary rocks in three distinct sub-provinces. The area was termed the Craigilee-Yarrol Province by Henderson, 1980, and the descriptions of the sub-terranes are summarised from this work.

The Craigilee-Yarrol Province is a narrow strip of primarily marine sediments of Late Silurian, Devonian and Carboniferous age (Henderson, 1980) lying parallel to the Central Queensland coastline. It is bounded to the west by the deformed margin of the Bowen Basin, of Permo-Triassic age, and to the east by the Proserpine Province, of Mesozoic age. Major fault systems, such as the Broad Sound, Tungamull, Boyne River and Yarrol Faults separate the Craigilee-Yarrol Province into three separate sub-provinces. The Craigilee Subprovince forms a dismembered

basement to the central Yarrol and eastern Coastal Sub-Provinces, see Figure 3-2.

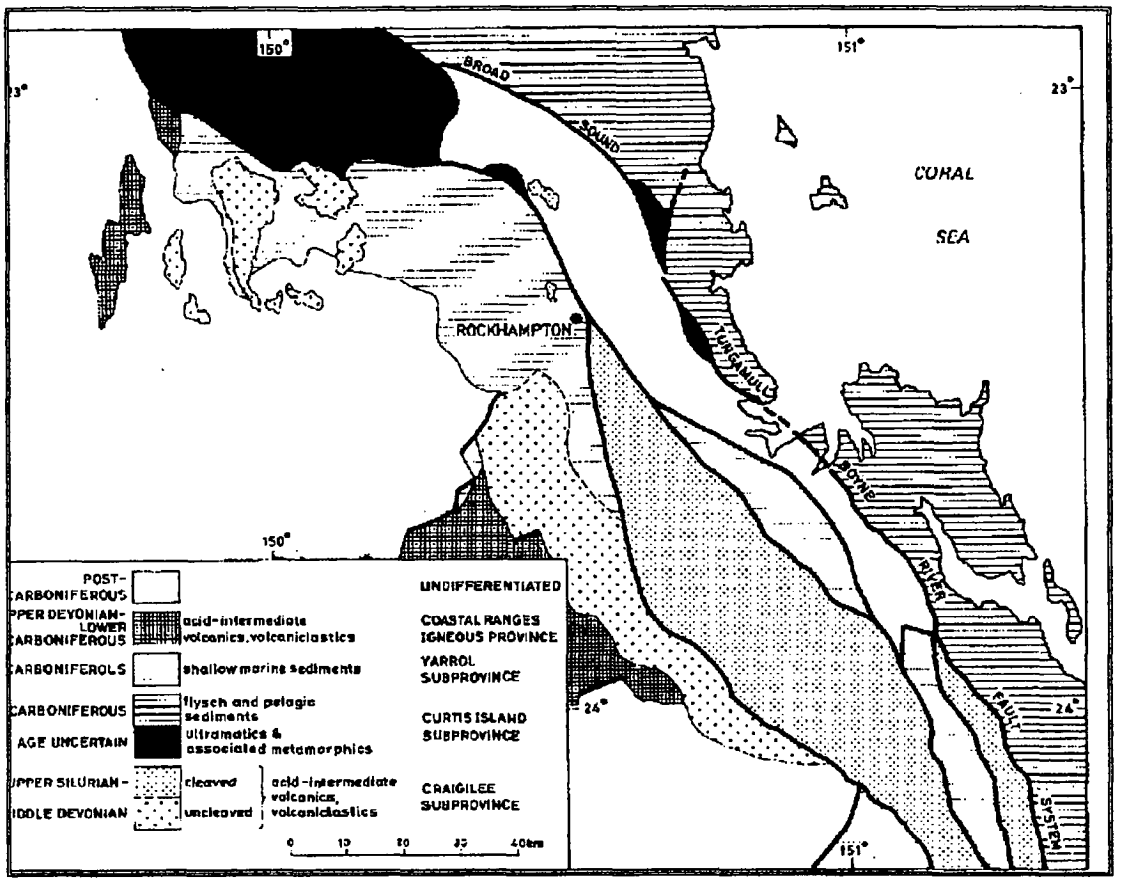

Figure 3-2 Craigilee-Yarrol Province

(Plan reproduced from Henderson, R.A. (1980), Structural Outline and Summary Geological History for Northeastern Australia, in Henderson, R.A. and Stephenson, P.J. editors, The Geology and Geophysics of Northeastern Australia, Geological Society of Australia, Queensland Division, July, 1980)

The Craigilee Subprovince consists of a thick, structurally complex sequence of marine sediments interbedded with acid to intermediate volcanics and volcaniclastics (Henderson, 1980) and are interpreted as tightly folded from the presence of a strongly developed slaty cleavage. Both age and stratigraphic relationships for the sub-province are not well understood, however fossils ranging in age from ?Late Silurian to Middle Devonian have been recorded (Henderson, 1980)

The Yarrol Subprovince comprises Upper Devonian and Carboniferous marine sediments which unconformably overlie elements of the Craigilee Sub-Province, and acid to intermediate volcanic and volcaniclastic rocks of Late Devonian age (Henderson, 1980) of the Coastal Ranges Igneous Province. The sequence has a maximum thickness of 6 kilometres, thinning toward the structural contact with the Bowen Basin to the west. Predominant rocktypes are pelites, arenites, volcaniclastics, limestone and conglomerates. The sediments have been folded into open folds which are partially dismembered by faulting and disrupted by younger, post-Carboniferous granitoid intrusions.

The Coastal Sub-Province which is postulated from fossil evidence (Fleming et al 1975) to be of probable Carboniferous age, comprises cleaved, structurally complex terrestrial to marine sediments. In the west of the province, are cherts, pelites, volcaniclastic arenites and limestones, which grade into immature greywackes with a minor volcaniclastic and detrital carbonate component in the centre of the terrain. The eastern portion of the sub-province consists of quartz greywackes and pelites, metamorphosed to schists and gneiss.

The bounding fault system between the Yarrol and Coastal Sub-Provinces contains ultramafic bodies, associated with phyllites, schists and amphibolites (Henderson, 1980). Murray, (1974) regarded these bodies as being emplaced by thrusting during the Permian.

Later regional interpretations of the geology of the area, such as Murray et al (1987) and Fergusson et al (1990) recognised the Yarrol Province as the northernmost portion of the New England Fold Belt. As in the southernmost New England Province, parallel belts were equated with volcanic arc, forearc basin and subduction complex assemblages, and were recognised as being originally continuous over the entire length of the fold belt.

In the Rockhampton/Gladstone area, the New England Fold Belt consists of the Yarrol, Marlborough, Wandilla and Shoalwater terranes, refer Figure 3-1.

The Yarrol terrane comprises Devonian through to Permian sedimentary and volcanic rocks, which were deposited into a forearc basin. The island arc assemblage from which the volcanic component is derived is situated to the west of the terrane, and formed the Connors-Auburn Arch. During the Late Palaeozoic to early Mesozoic (Fergusson et al 1990), mafic to silicic plutons intruded the basin and volcanic arch.

The contact between the Wandilla and Yarrol terranes is structural, and the two areas are separated by the Marlborough terrane. Discontinuous serpentinite bodies and a zone of undated ultramafics and metamorphic thrust sheets adjacent a major fault mark the Marlborough terrane. The metamorphics are of uncertain derivation, and comprise schists and gneisses.

The Wandilla terrane is predominantly a tectonic melange, consisting of greenstones, cherts, mudstones, greywackes and tuffs, while the adjacent Shoalwater terrane consists of a variably metamorphosed Palaeozoic succession of quartzose turbidites and mudstones.

Paleogeographic studies and the reconstruction of the evolutionary history of the northern Yarrol Province, such as that proposed by Murray et al (1987) are necessarily complex. The tectonic model for the area (Murray et al 1987) attributes the changes in deposition and stratigraphy to change

from a convergent continental margin to a dextral transform margin during the Middle Carboniferous as a results of a collision of a mid ocean ridge with the offshore trench. A brief evolutionary summary for the Rockhampton/Gladstone area is given below, and presented schematically in Figure 3-3.

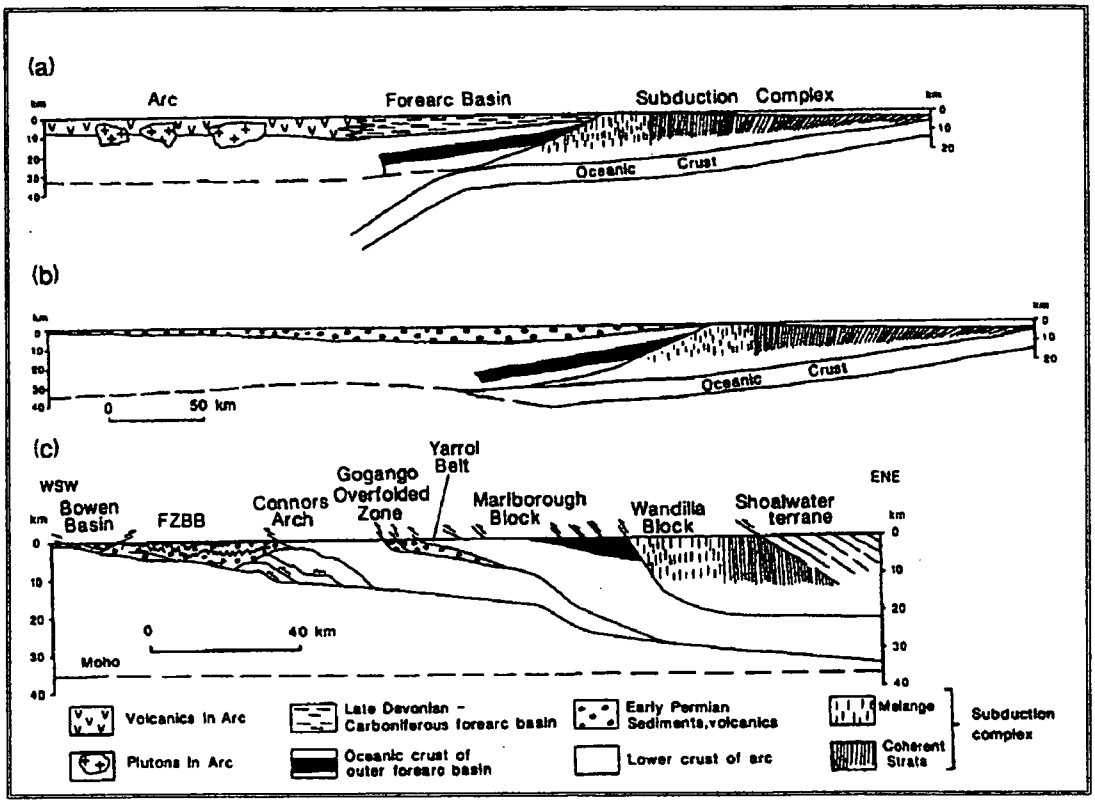

Figure 3-3 Cross-Section Through New England Fold Belt, Showing Evolution from (a) Late Carboniferous to (b) Early Permian and (c) Late Permian to Early Triassic.

(Plan reproduced from Ferguson, C.L., Henderson, R.A. and Leitch, E. (1994) in Holcombe, R.J., Stephens, C.J. and Fielding, C.R, editors, Capricorn Region Central Coastal Queensland 1994 Field Conference Guidebook)

Initial wide-spread deposition in the Yarrol Province occurred during the Silurian to Middle Devonian, when calc-alkaline volcanics, volcaniclastics and limestones of the Calliope Island Arc were deposited (Murray et al, 1987). The origin of the volcanics is somewhat equivocal. Published literature identifies the andesite and subordinate basalt flows as typical of volcanic island arcs (Marsden (1972)), while dissenting opinions e.g. Baker (1982) attribute the presence of localised silicic pyroclastics to a continental margin setting. The latest interpretations appear to favour the island arc setting for the volcanics, based on unusual Na_20/K_20 ratios of the rocks (Murray et al, 1987).

Offshore from the active volcanic arc, debris and sediments collected downslope in a forearc basin. The western portion of the Wandilla Slope and Basin is possibly Silurian to Middle Devonian age (Murray et al, op cit.) Rocktypes in the Rockhampton region of the basin include altered basaltic flows, radiolarian cherts and jaspers, and local dacitic to andesitic tuffs.

At the end of the Middle Devonian, rocks of the Calliope Island Arc were folded with accompanying granite plutonism (Day et al 1978). Then, in the Late Devonian and Early Carboniferous, subaerial volcanics comprising thick andesite flows, and subordinate rhyolitic, dacitic and basaltic lavas were deposited. These volcanics form the Connors-Auburn Volcanic Arch.

To the east of the volcanic arch, the Yarrol Forearc Basin formed. The southern portion of the Yarrol Forearc Basin was probably deposited unconformably over the folded elements of the Calliope Island Arc. Basin fill was predominately of volcaniclastic origin, sourced from the volcanic arcs to the west, with some primary volcanic flows (Marsden, 1972). In the Rockhampton area, the volcanics are intermediate to silicic in composition and are probably of Late Devonian to Carboniferous age. During periods of volcanic quiescence, ooliths and oolitic limestones developed.

Further to the east, in the Wandilla Slope and Basin area, volcaniclastic flysch type sequences were deposited. In addition, oolitic limestones, probably sourced from the Yarrol Forearc Basin and transported via turbidity currents, were deposited as oolitic greywackes in the Wandilla Basin.

During the Middle and Late Carboniferous, volcanism apparently waned, while marine sedimentation continued in the Yarrol Forearc Basin, as did deep water sedimentation in the Wandilla Slope and Basin. Granitoids, possibly relating to the waning of the volcanic arc, were emplaced in the Connors-Auburn Arch.

Imbricate thrust slices, and regional melanges typical of subduction complexes then developed, causing a fundamental difference in deformational styles across the Yarrol fault system. In general, the strata of the Yarrol Forearc Basin are folded into gentle, open folds, with no regionally developed axial plane cleavage (Murray et al, 1987), whereas the Wandilla Slope and Basin sequences have been multiply deformed, and have at least one penetrative cleavage.

3.3 Deposit Geology

Kunwarara is situated within a shallow, predominantly freshwater sedimentary basin surrounded by low relief hills of granite, metamorphosed sediments, and ultramafic serpentinites.

3.3.1 Basement Geology

In a regional context, the Kunwarara deposit is situated on the boundary between the Marlborough and Wandilla Terranes, and is located in a Tertiary basin developed adjacent a regional fault. The hills enclosing the basin consist of cherts, argillites, gabbros, dolerites and serpentinites. The basin floor is granite, and the deposit is developed primarily over the

granite portion of the basement, although the southeastern area has developed over serpentinite.

3.3.2 Metasediments

The metasediments belong to the Doonside Formation, part of the metasedimentary package which makes up the Wandilla Terrane. In the vicinity of Kunwarara, the Doonside Formation consists of red, green, white, grey and black cherts and argillites (Charlton, 1992). Outcrop is poor, and limited to exposures in dry creek beds.

3.3.3 Serpentinites

Serpentinite units at Kunwarara are predominantly massive, and contain chrysotile, antigorite, lizardite, magnetite and brucite. Table 3-1 details the main serpentinite types (after Charlton, 1992):

SERPENTINITE TYPE	DESCRIPTION
Massive Serpentinite	Massive; no apparent structure; slickensided; slickenside infill of magnesite or chalcedony; magnesite veins common
Blocky Serpentinite	Massive, highly jointed; joint directions random
Globular Serpentinite	Confined to contact aureole of intrusions; relict calcic orthopyroxene pseudomorphed to bastite.
Schistose Serpentinite	Schist-like texture
Sheared Serpentinite	Lateritic to gossanous sheared and silicified serpentinite; chrysoprase to chalcedonic vein infill.
Foliated Serpentinite	Located parallel to, or adjacent fault zones; play appearance
Brecciated Serpentinite	Angular fragments of massive serpentinite in matrix of serpentinous minerals.

Table 3-1 Serpentinite Varieties in Deposit Area

Intruding the serpentinites are a sequence of gabbroic sills and dolerite dykes. Dykes may very from 30 cm to over 20 metres in width.

3.3.4 Granites

Granite and granodiorite bodies have intruded along a north-westerly trending belt which runs sub-parallel to the main structural trends in the deposit area. In addition, two small micro-syenite plugs occur in the west of the mining lease.

3.4 Basin Geology

The magnesite deposit occupies a 22 kilometre long arc-shaped depression, possibly a half-graben, bounded by the Tungamull Fault to the east. Sediments within the graben have been classified into six main lithofacies, based on colour, grainsize, and mineralogical composition (Charlton, 1992). A cross-section through the deposit showing the local geology is illustrated in Figure 3-4.

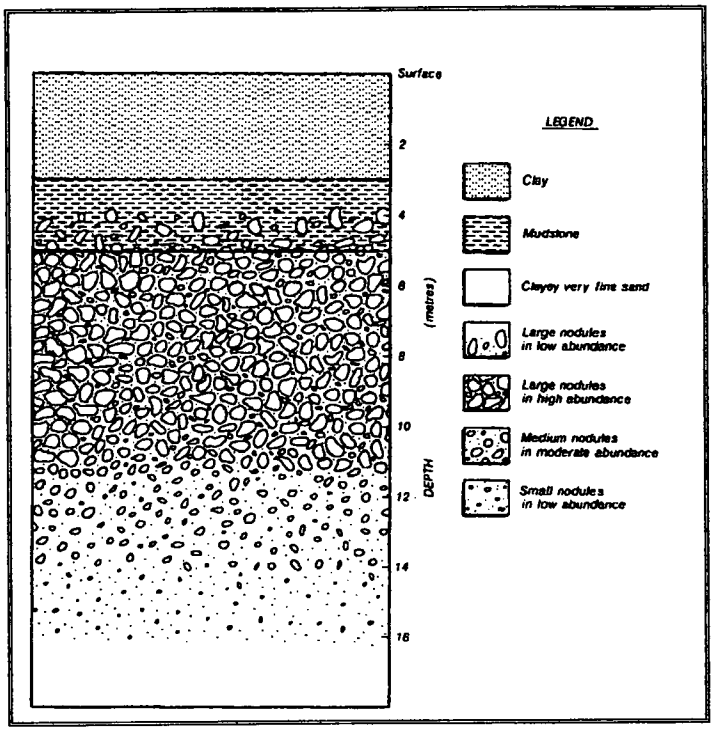

Figure 3-4 Typical Cross-section Through Kunwarara, Showing Typical Geological Units and Zones of Magnesite Concentration

(plan reproduced from Milburn, D. and Wilcock, S. (1994), The Kunwarara Magnesite Deposit, Central Queensland, in Holcombe, R.J., Stephens, C.J. and Fielding C.R., editors, Capricorn Region Central Coastal Queensland, 1994 Field Conference Manual, Geological Society of Australia, Queensland Division)

3.4.1 Unconsolidated gravels and sand

Basal beach or river sands and gravels overlie basement granites and serpentinites. Thicknesses of the unit average 10 metres, with the average depth from surface varying between 20 and 40 metres.

Gravels consist of unconsolidated, well rounded quartz pebbles and cobbles in a fine grained sandy matrix. The sandy units are fine grained, and uncemented and are comprised of a reddish sandy mud, with wispy white layers of magnesite rich mud.

The gravels are interpreted as being deposited in a high energy fluvial environment, while the sand interbeds are indicative of a decrease in depositional energy.

3.4.2 Fine grained sandstone

The transition from the unconsolidated ?river sands to the overlying sandstone is generally sharp. The sandstone unit is weakly indurated, reddish in colour at the base and grey toward the top. It has a thickness of between 5 and 20 metres. Sands are generally fine to medium grained, and composed of feldspars, quartz, minor magnetite and clay.

Wispy manganese veinlets occur as dendritic veinlets and as small globules within the sandstone mass. Magnesite nodules are common, particularly in the upper portion of the sandstone. The majority of the magnesite is porcelainous in nature, and occurs in nodules up to 300 mm in size.

Fluvial channels have been intersected, suggesting a fluvial flood plain environment of deposition.

3.4.3 Green sandy siltstones

Sandy, olive green to green, poorly cemented sandy siltstones overlie the fine grained sandstone horizon. Thickness of the unit varies between 3 and 15 metres.

The coarser, clastic component of the unit comprises quartz and feldspar grains, with matrix silts and smectites. Schmid (1987) noted that the silt is composed mainly of finely crystalline illite, with "basket weave" textures. Manganese veinlets and globules are common.

Magnesite occurs in the unit in the form of small, porous nodules to 40 mm in size.

This unit is interpreted as being deposited in a low energy fluvial environment.

3.4.4 Black clays and silts

A zone of black clays overlie the darker sandy siltstones with a sharp contact, and form the ubiquitous black soil cover of the Kunwarara area.

The clay unit is generally massive, but may contain localised layers of darker, manganiferous, silty material. Fine grained sands may be locally present. The unit is generally devoid of magnesite.

The clays were probably deposited by low energy fluvial floodplain processes, or via sheet flooding.

3.4.5 Fluvial channel fill deposits

Early channel fill deposits occur within the fine grained sandstone unit. They are between 1 and 2 metres thick, and up to 30 metres in width. Tabular in shape, the elongate bodies often taper at the ends. Channel sediments consist of fine grained sands, magnesite nodules and gravels.

Fluvial wash-out channels cut across the fine grained sandstone, green siltstone and dark siltstone units. The channels are generally massive, steep sided, and U-shaped. Ranging between 1 and 20 metres thick, and up to 100 metres wide, the channels consist of fine sands, magnesite nodules and rare basal coarse sands.

Fine-grained massive channel fill deposits of dark grey to black siltstones occur within the dark siltstone unit, and can be differentiated from it by a higher coarse clastic component, and rounded magnesite nodules.

3.5 Deposit Genesis

The initial model for formation of the deposit was suggested by Schmid (1987), by analogy with Salda Lake in Turkey.

The geological setting was interpreted as a small, closed basin rimmed by basement hills. In the vicinity of the magnesite deposit, the basement was overlain by wind blown sands, forming coastal dunes. River systems drained into this lacustrine environment from headwaters sourced within the enclosing basement hills. Silt and sand material was then deposited as broad sheets. Seasonal evaporation or draw down of the water level in the closed lake allowed evaporation to take place at or near the surface of the mud, resulting in chemical precipitation of magnesite in the form of nodules (Milburn and Wilcock, 1994)

Charlton, 1992 suggested modifications to the initial method of formation, relating to changes in the course of the Fitzroy River. Following the formation of a half-graben associated with the Tungamulla Fault and associated erosion of the surrounding granites and granodiorites, the Fitzroy River flowed through the graben into Broadsound Bay.

Deposition of the coarse gravels at the base of the Kunwarara sequence is a direct result of this. As the sediment load in the river channel built up, the river was diverted south, and finer grained sediments were deposited in the basin as a result of sheet flooding and crevasse splays. Formation of dolomite nodules (the precursor to the magnesite nodules of today) could be related to occasional interactions of the sediments with sea waters due to tidal incursions.

3.6 Magnesite Nodules

Mineralisation consists of a flat-lying, magnesite rich zone approximately 11 metres thick, and defined by a 5% magnesite by mass cut-off (Milburn and Wilcock, 1994), stretching for approximately 15 square kilometres.

The Kunwarara deposit includes four zones of higher grade magnesite in KG1, KG2, Oldman North and Oldman South, two of which, KG1 and KG2, are currently being mined and a prospect, Oldman West. The locations are shown in Figure 3-5.

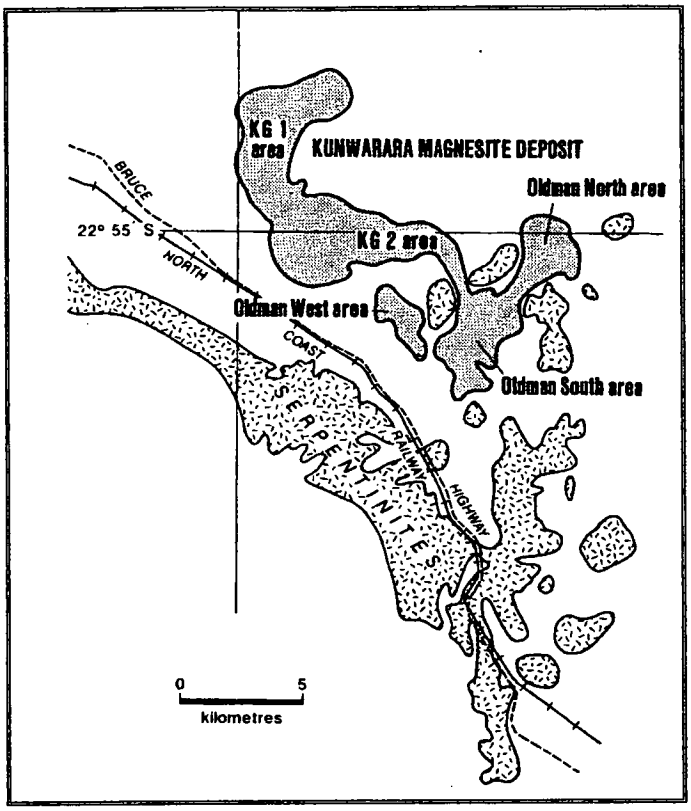

Figure 3-5 Location Plan, Higher Grade Magnesite Zones, Kunwarara

(after Burban, B. (1990) Kunwarara Magnesite Deposit, in Hughes, F.E. , editor, Geology of the Mineral Deposits of Australia and Papua New Guinea, AusIMM Monograph 14)

Magnesite is concentrated within the sandstone and siltstone intervals, in the form of 0.01 to 50 centimetre magnesite nodules. Thin interbeds of magnesite muds have also been logged in the sand lithology. The mined magnesia consists of two types, described below.

3.6.1 Bone Magnesite

Bone magnesite is a white, dense and compact porcelainous magnesite, with a rough surface and conchoidal fracture. It has a relatively high density, and is non-porous. Bone magnesite forms large nodules up to 50 cm across, and aggregates of nodules to 1 metre across. Internal dehydration cracks are common, as are small "seed" nodules of magnesite encased in the larger nodules (Burban, 1990)

3.6.2 Porous Magnetite

A more common nodule variety than the bone magnesite, the porous nodules are, as the name suggests, porous, softer, lighter and prone to inclusions of non-magnesite material. Burban (1990) notes that porosity may vary from low (10%) to high (20%) to extreme (>50%), where the magnesite nodule may have the appearance of volcanic scoria.

3.7 Conclusions

In terms of deposit modelling, the salient features of the geological review of Kunwarara are:

- Flat-lying and laterally continuous deposit
- Thin geological units
- Nodular, and therefore irregular nature of mineralisation
- Restriction of magnesite nodules to two lithologies, namely sandstone and siltstone
- Development of two distinct nodule types, bone and porous magnesite
- Strong influence of a shallow evaporative basin on the development and location of the deposit.

The resource model to be constructed will require thus require careful modelling to take into account the thin lithologies, and the mixed nature of the magnesite nodule distributions.

CHAPTER 4 – CLASSICAL STATISTICS - ASSAYS

Assay values were provided by Queensland Metals Corporation staff for the following elements: magnesium (MgO), calcium (CaO), silicon (SiO_2), iron (Fe_2O_3), aluminium (Al_2O_3) and manganese (Mn_3O_4).

Using Gemcom software, a basic statistical evaluation was undertaken for each element on uncomposited, raw assay data. A total of 10014 data points were available for each element.

4.1 Magnesium

Summary statistics for magnesium are given in Table 4-1.

Maximum MgO Value	98.50	
Minimum MgO Value	0	
Number of Samples ≤ 0	36	
Total Population	10014	
	Ungrouped Data	Grouped Data
Mean	92.63	92.69
Median	N/A	93.86
Geometric Mean	N/A	N/A
Natural LOG Mean	N/A	N/A
Standard Deviation	7.09	7.14
Variance	50.36	51.05
Log Variance	N/A	N/A
Coefficient of Variation	0.076	0.077
Moment 1 about Arithmetic Mean	0	0
Moment 2 about Arithmetic Mean	50.36	51.05
Moment 3 about Arithmetic Mean	3071.77	-2944.81
Moment 4 about Arithmetic Mean	265921	250583
Moment Coefficient of Skewness	-8.59	-8.07
Moment Coefficient of Kurtosis	104.84	96.13

Table 4-1 Magnesium Summary Statistics

Magnesium displays a strongly negatively skewed distribution. Figure 4-1 illustrates this by displaying the data as a normal histogram distribution. Values show a tapering tail away from the 86 percentile mark, and a cluster of values at between approximately 90 and 98%.

Figure 4-2 illustrates a zoomed display of the normal histogram, with data cut to the 75% magnesium assay level. The plot clearly shows the negatively skewed magnesium distribution, but also the irregularity of the assay values. Such irregularities may have a number of causes, such as sampling error, effect of weathering, or separate magnesium populations.

When converted to a log normal histogram plot as shown in Figure 4-3, the only information conveyed is the skewed distribution range, and an obviously mixed sample population.

Figures 4-4 and 4-5 show magnesium data represented as a normal probability plot and log probability plot respectively. Both plots strongly suggest that there are mixed sample populations.

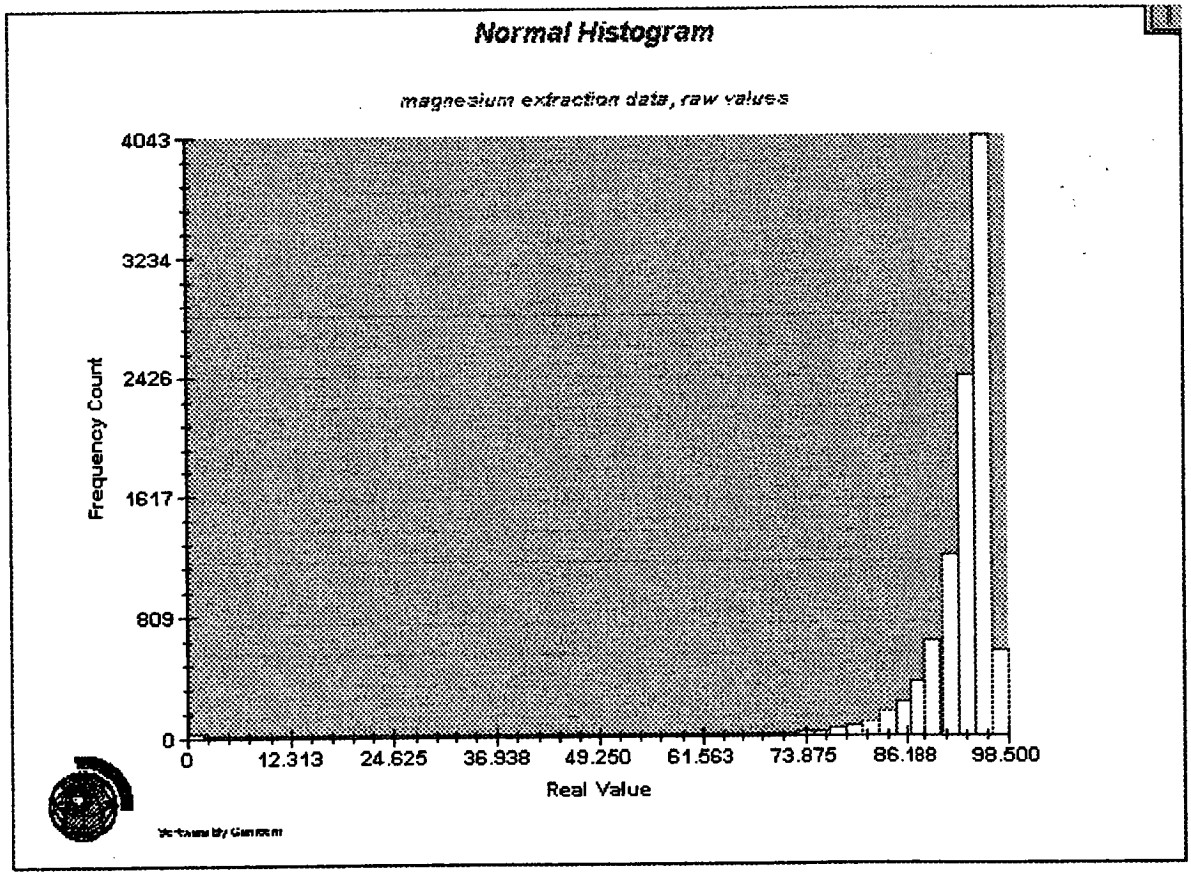

Figure 4-1. Normal Histogram, Uncut Magnesium Values

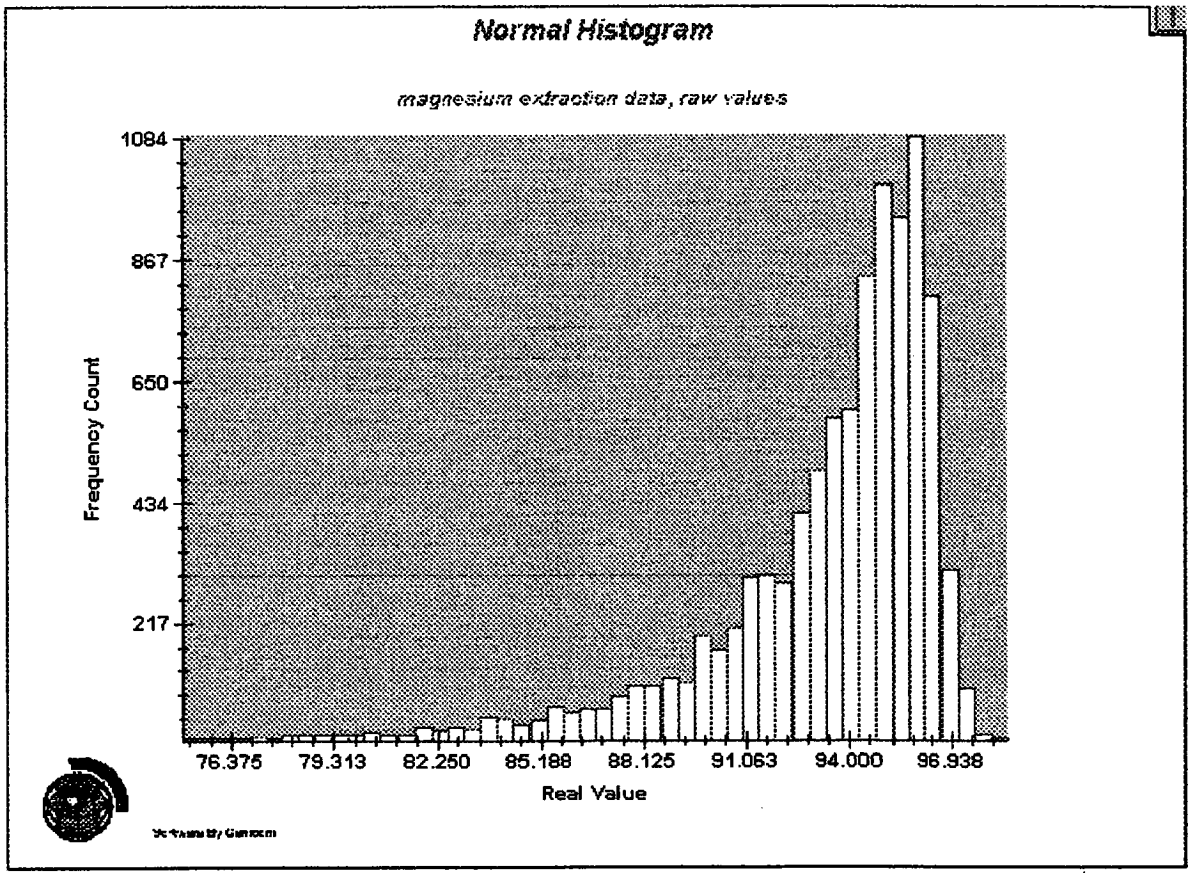

Figure 4-2 Normal Histogram, Magnesium Values Top-cut to 75%

Figure 4-3 Log Normal Histogram, Magnesium

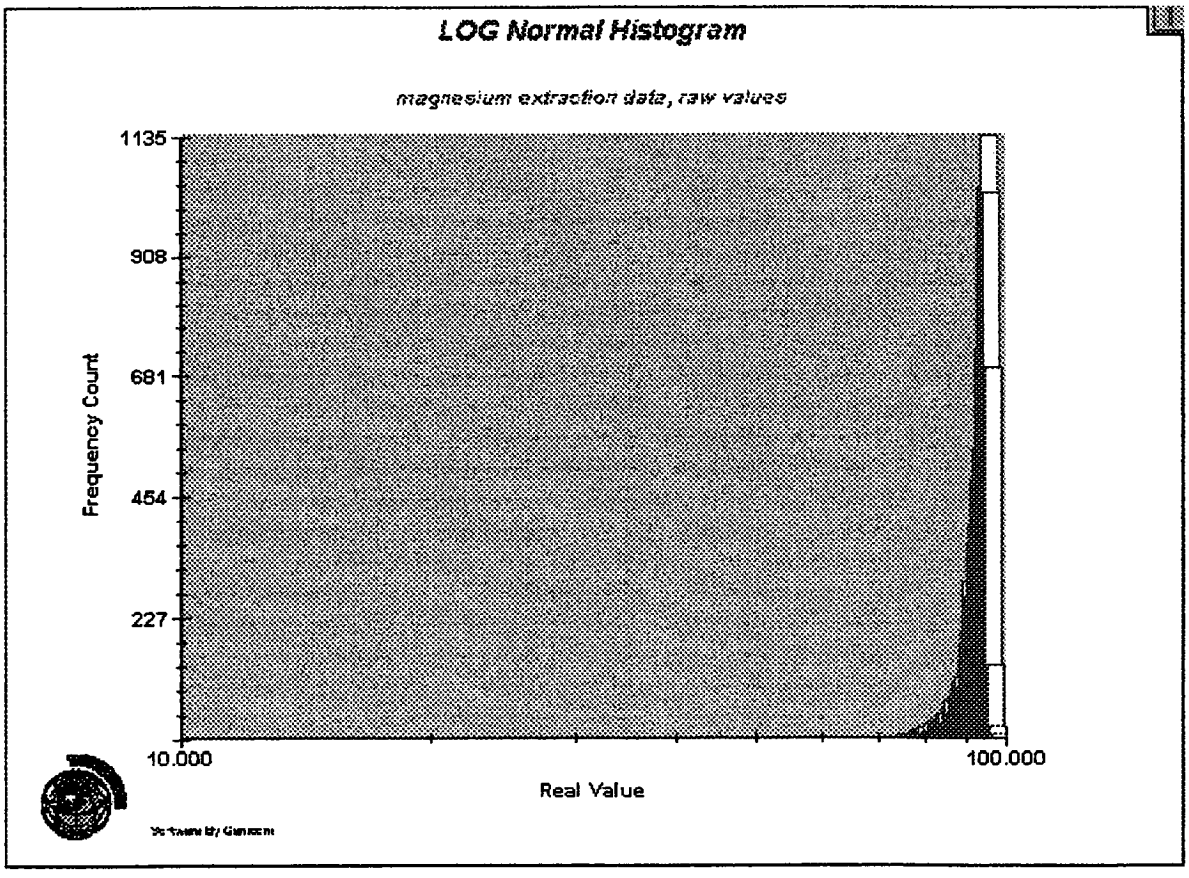

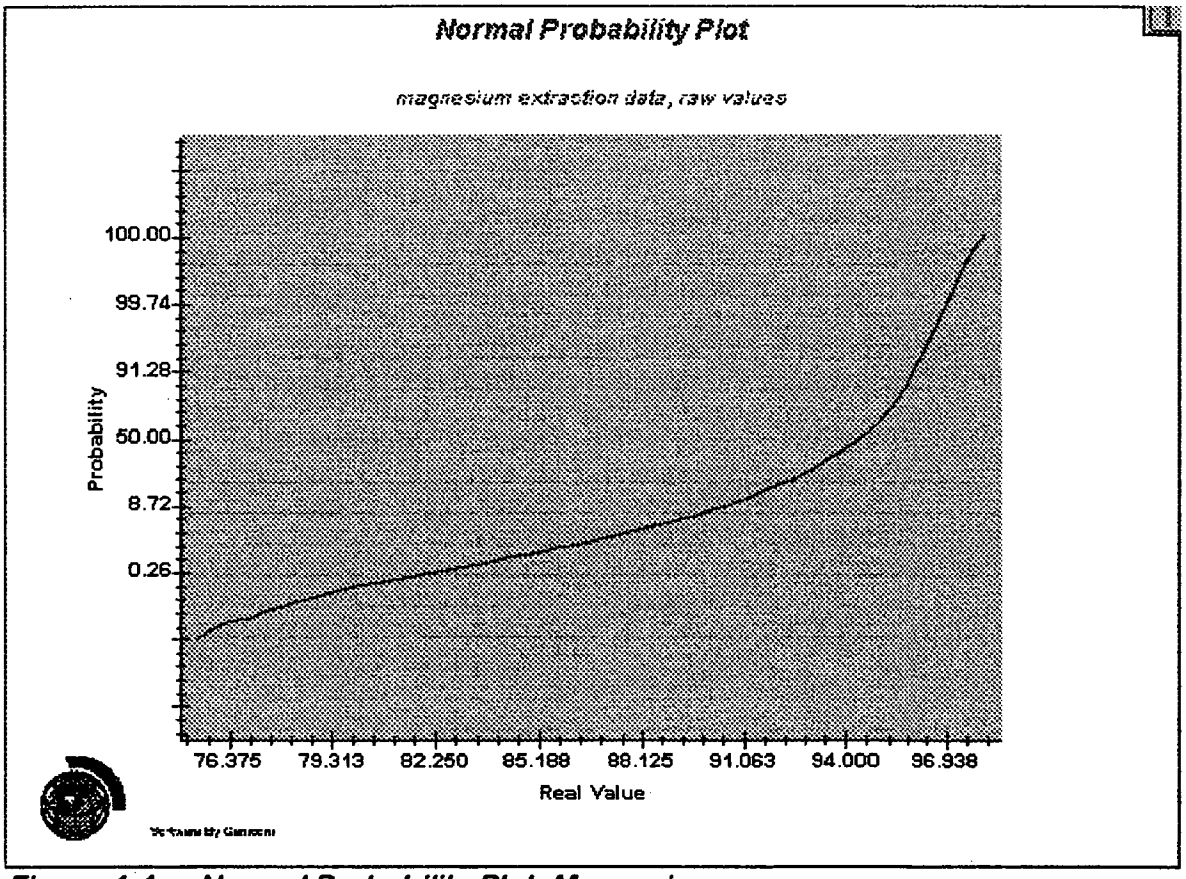

Figure 4-4 Normal Probability Plot, Magnesium

Figure 4-5 Log Normal Probability Plot, Magnesium

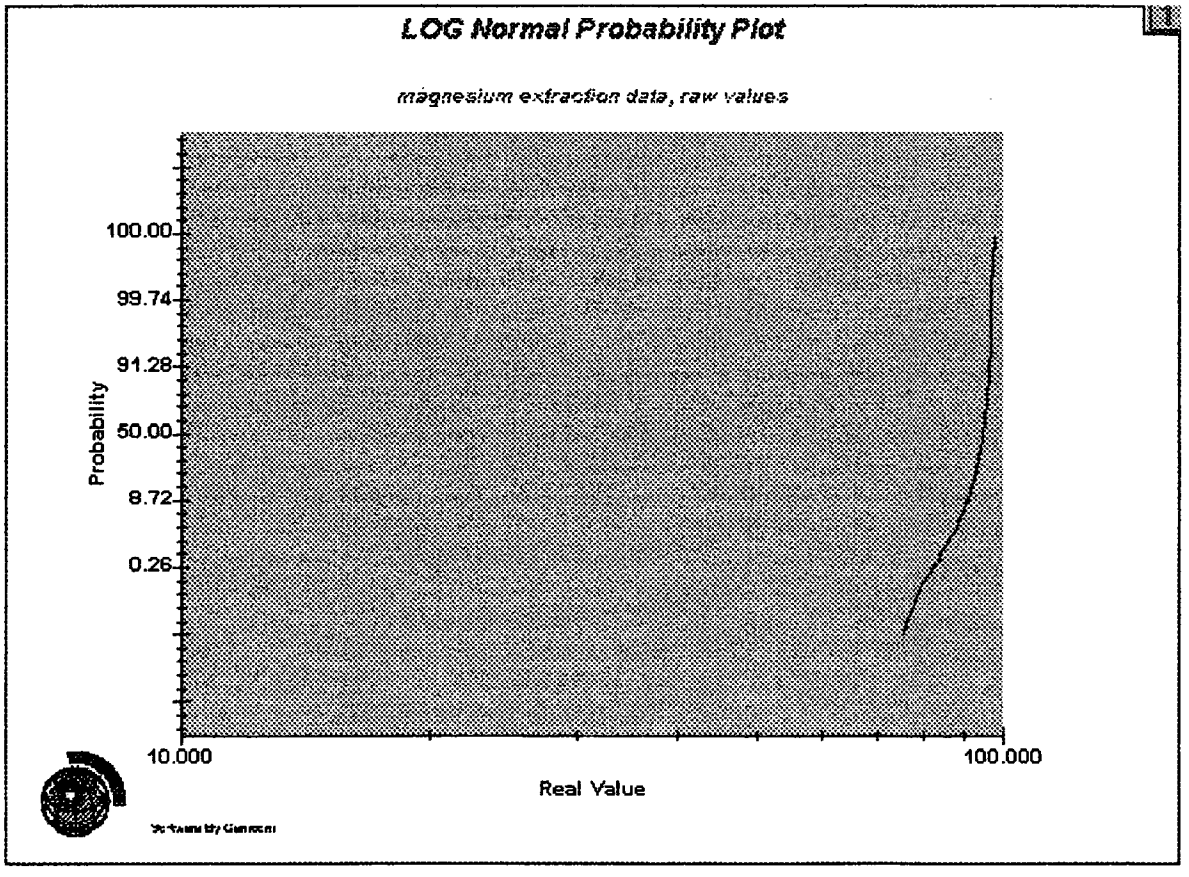

4.2 Silica

The summary statistics for silica are presented in Table 4-2. The silica distribution is mildly positively skewed. Across the deposit, silica averages 1.8%, but assays may reach as high as 24.8% silica.

Maximum SiO_2 Value	24.8	
Minimum SiO_2 Value	0	
Number of Samples ≤ 0	3887	
Total Population	10014	
	Ungrouped	Grouped
Mean	1.80	1.96
Median	N/A	1.36
Geometric Mean	N/A	N/A
Natural LOG Mean	N/A	N/A
Standard Deviation	2.10	1.97
Variance	4.43	3.19
Log Variance	N/A	N/A
Coefficient of Variation	1.16	1.009
Moment 1 about Arithmetic Mean	0	0
Moment 2 about Arithmetic Mean	4.43	3.91
Moment 3 about Arithmetic Mean	16.81	16.16
Moment 4 about Arithmetic Mean	175.18	160.36
Moment Coefficient of Skewness	1.80	2.08
Moment Coefficient of Kurtosis	8.90	10.44

Table 4-2 Silica Summary Statistics

The normal data distribution, see Figure 4-6, is dominated by the number of null assay values. Null values represent areas which have silica below the assay detection limit

The silica data was lower cut to edit the null values, and to focus in on the distribution of positive silica values, by top-cutting to 6% silica. The resulting histogram is shown in Figure 4-7. The silica population is highly mixed in the upper levels of the assay values.

Figure 4-8 is a graphic representation of a log transform of the silica data. The distribution is obviously mixed, with a poorly sorted upper range, and a marked tail toward the lower silica grades.

Figures 4-9 and 4-10 are normal and log normal probability plots respectively. Both indicate very mixed sample populations, and mildly skewed data

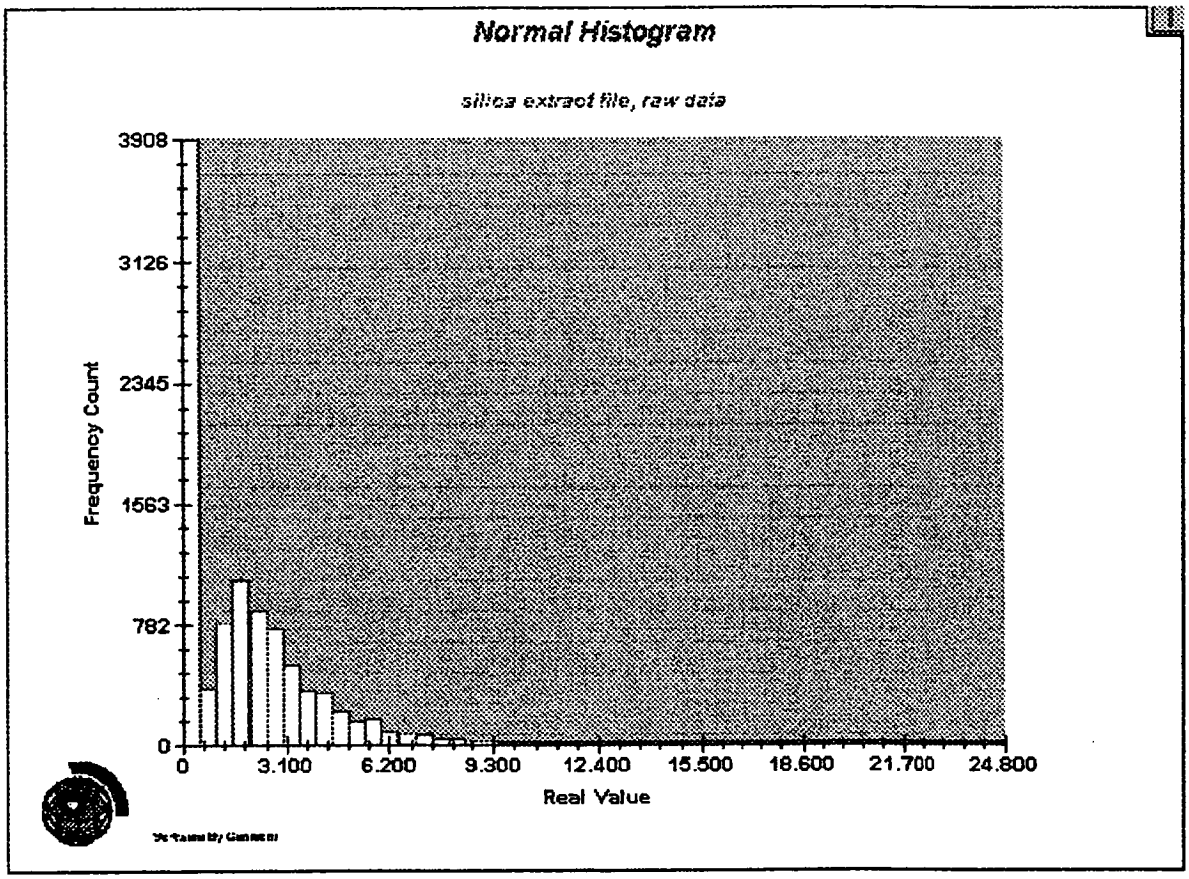

Figure 4-6 Normal Histogram, Uncut Silica Values

Figure 4-7 Normal Histogram, Silica Lower Cut of 0% and Top-Cut of 6%

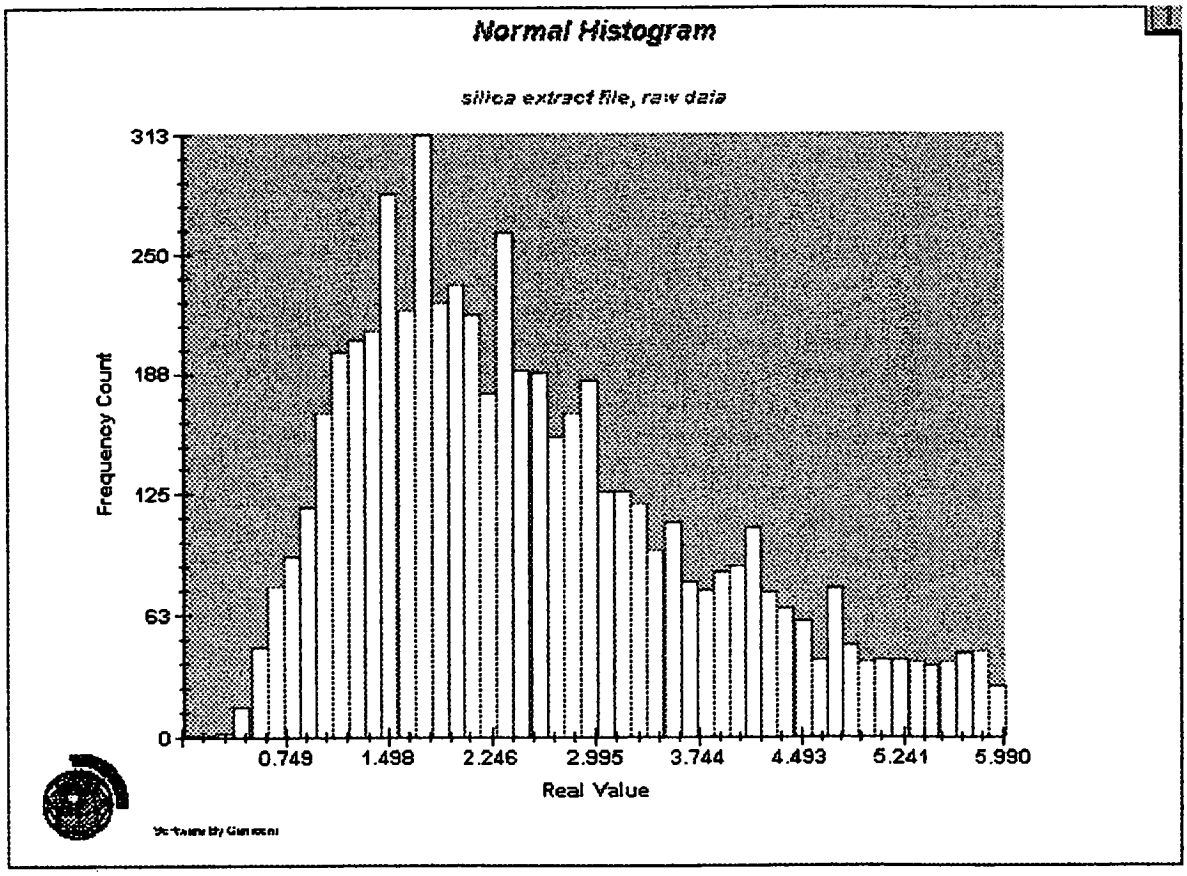

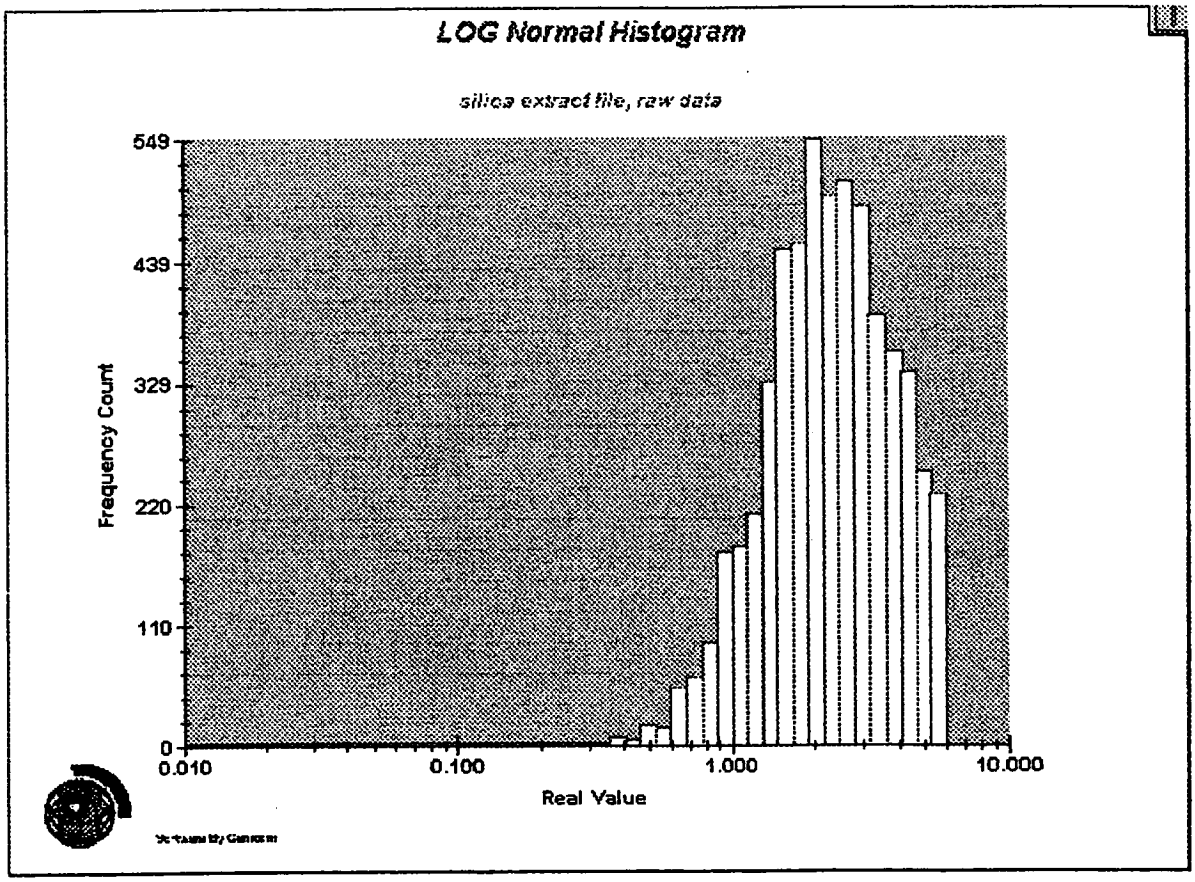

Figure 4-8 Log Normal Histogram, Silica

Figure 4-9 Normal Probability Plot, Silica

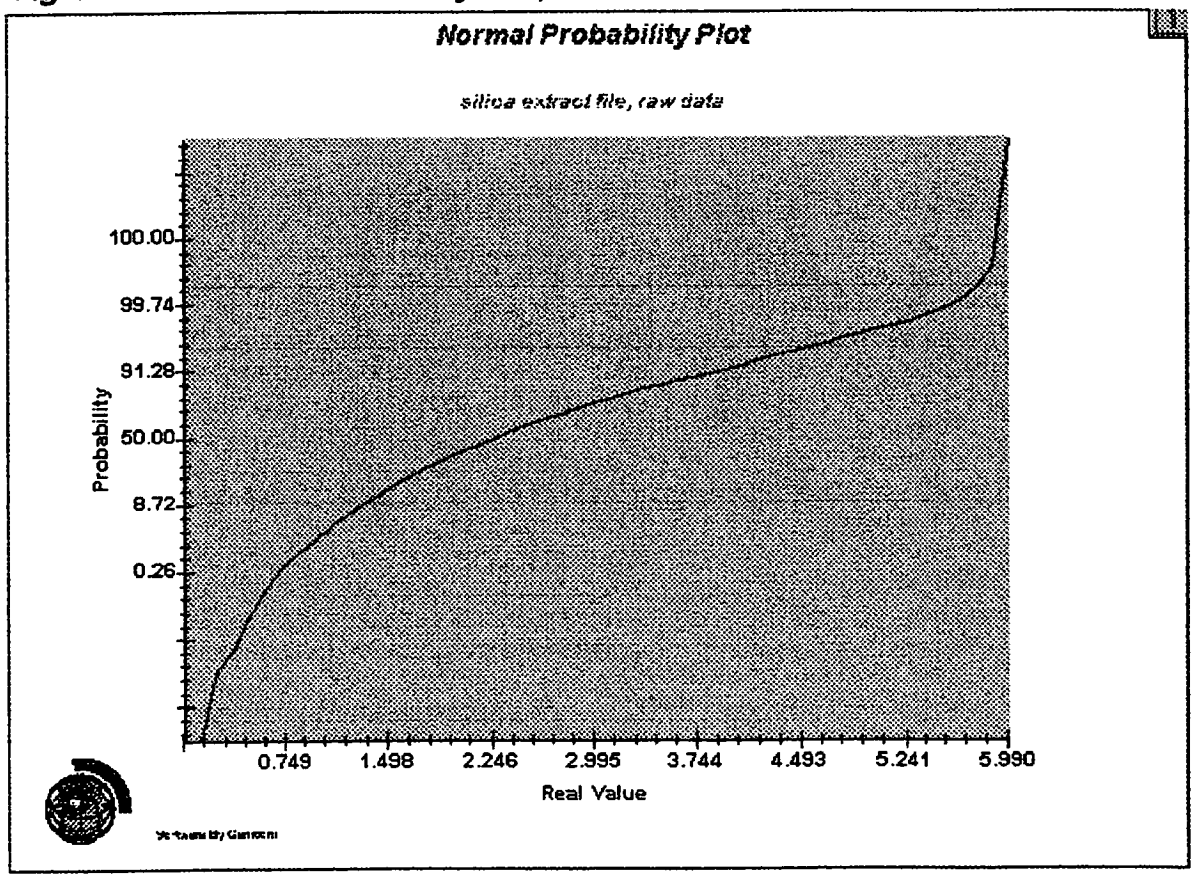

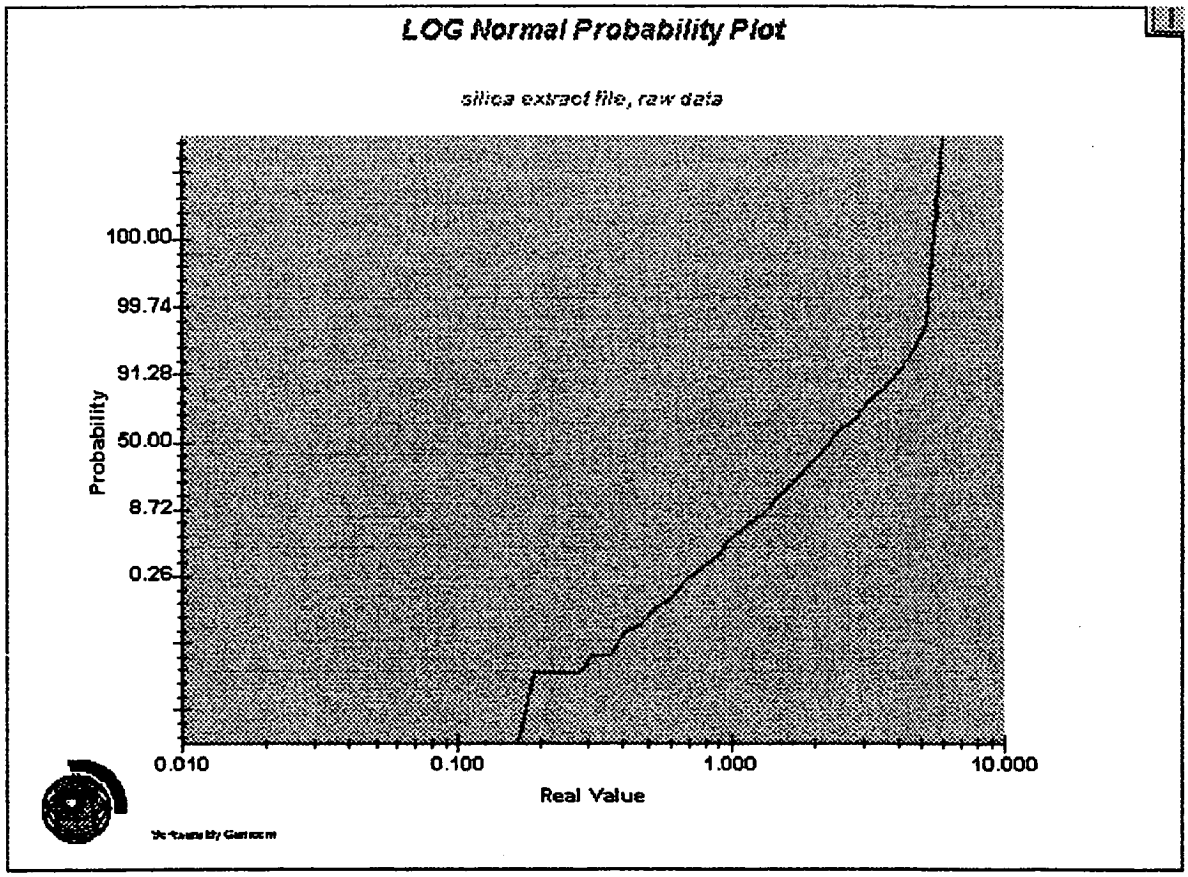

Figure 4-10 **Log Normal Probability Plot, Silica**

4.3 Manganese

Manganese data statistics are summarised in Table 4-3. The values are highly positively skewed, with an average value returned of between 0.12 and 0.26% MnO.

Maximum Mn_3O_4 Value	16	
Minimum Mn_3O_4 Value	0	
Number of Samples ≤ 0	1192	
Total Population	10014	
	Ungrouped	Grouped
Mean	0.12	0.26
Median	N/A	0.26
Geometric Mean	N/A	N/A
Natural LOG Mean	N/A	N/A
Standard Deviation	0.17	0.15
Variance	0.03	0.02
Log Variance	N/A	N/A
Coefficient of Variation	1.34	0.57
Moment 1 about Arithmetic Mean	0	0
Moment 2 about Arithmetic Mean	0.03	0.02
Moment 3 about Arithmetic Mean	0.39	0.39
Moment 4 about Arithmetic Mean	6.33	5.71
Moment Coefficient of Skewness	77.26	98.50
Moment Coefficient of	89.04	9801

Table 4-3 Manganese Summary Statistics

Figure 4-11 shows the normal histogram data distribution for manganese, which is dominated by the number of zero assay values returned. No skew is apparent from the plot.

Figure 4-12 is a zoomed example of the same histogram, with a lower cut of 0.01% and top cut of 6% applied to the assays. The distribution is clearly highly positively skewed, with a tail of higher grade values.

When log transformed, Figure 4-13, manganese data begins to approach a log normal distribution, but still indicates that there are mixed sample populations.

The normal and log normal probability plots are shown in Figures 4-14 and 4-15 respectively. Again, both plots show mixed sample populations, and a skewed distribution of manganese assay values.

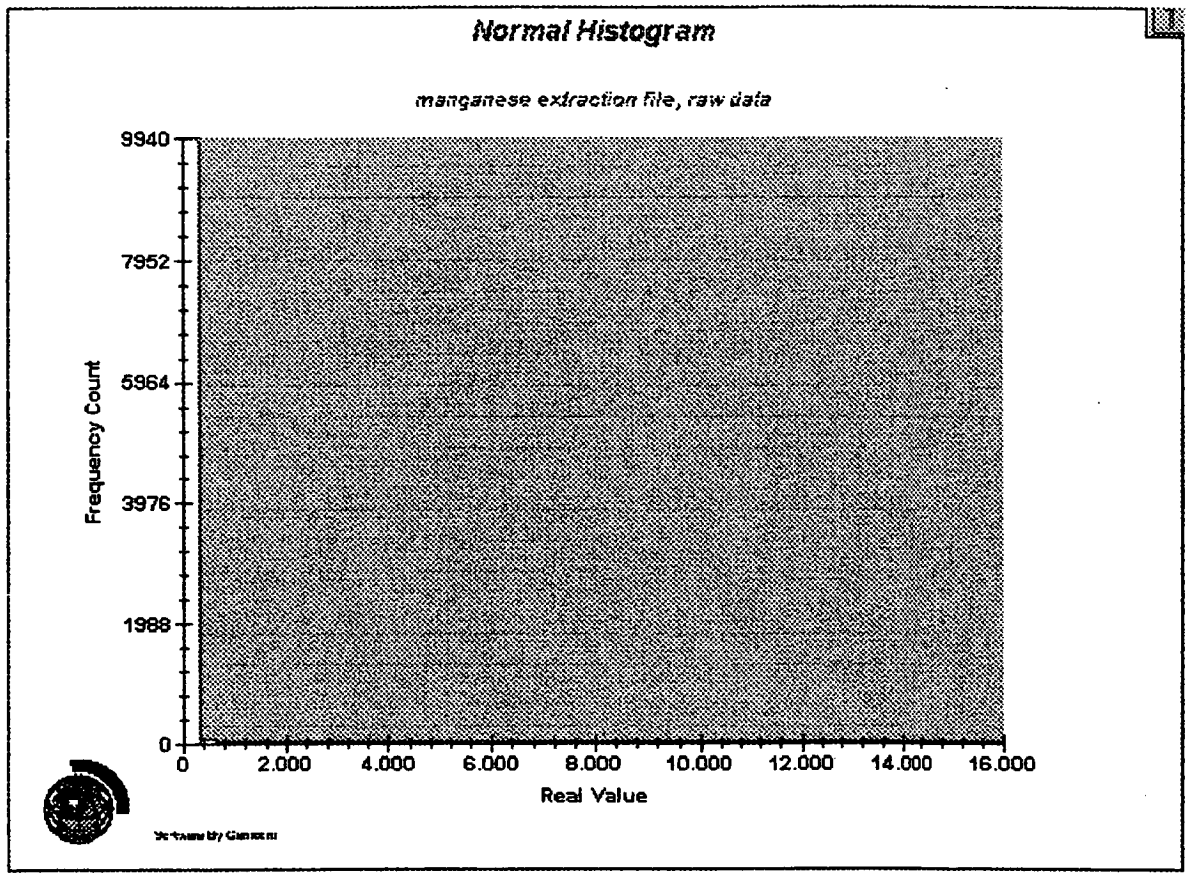

Figure 4-11 Normal Histogram, Uncut Manganese Values

Figure 4-12 Normal Histogram, Lower Cut of 0.01%, Top-Cut of 1.5%

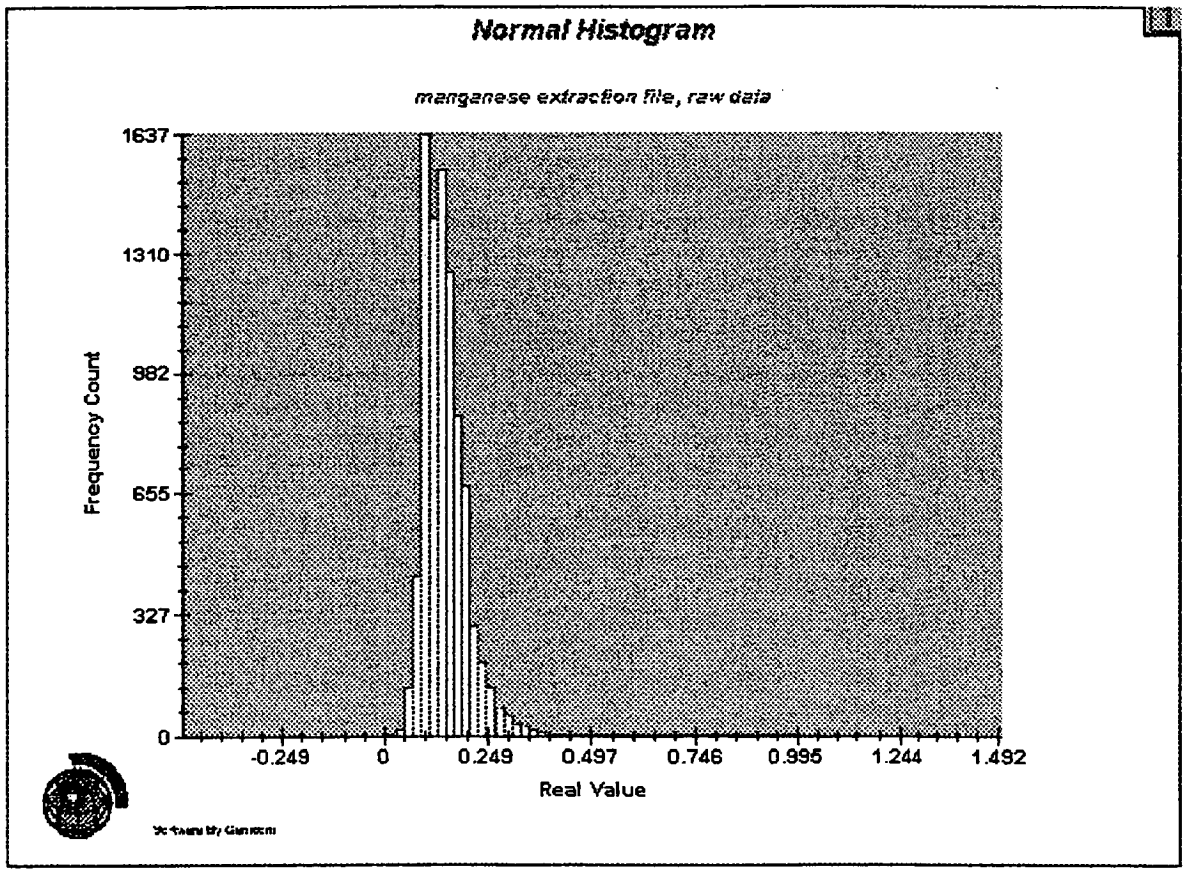

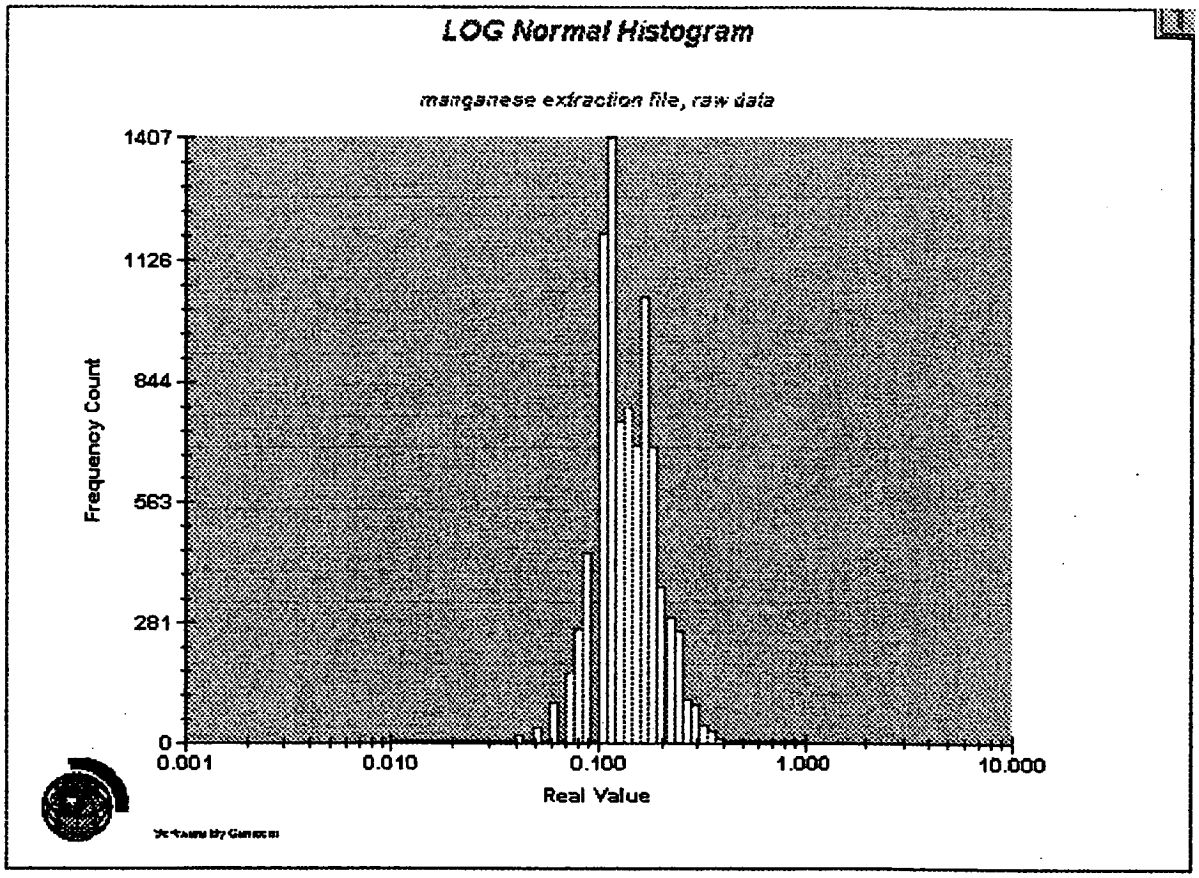

Figure 4-13 Log Normal Histogram, Manganese

Figure 4-14 Normal Probability Plot, Manganese

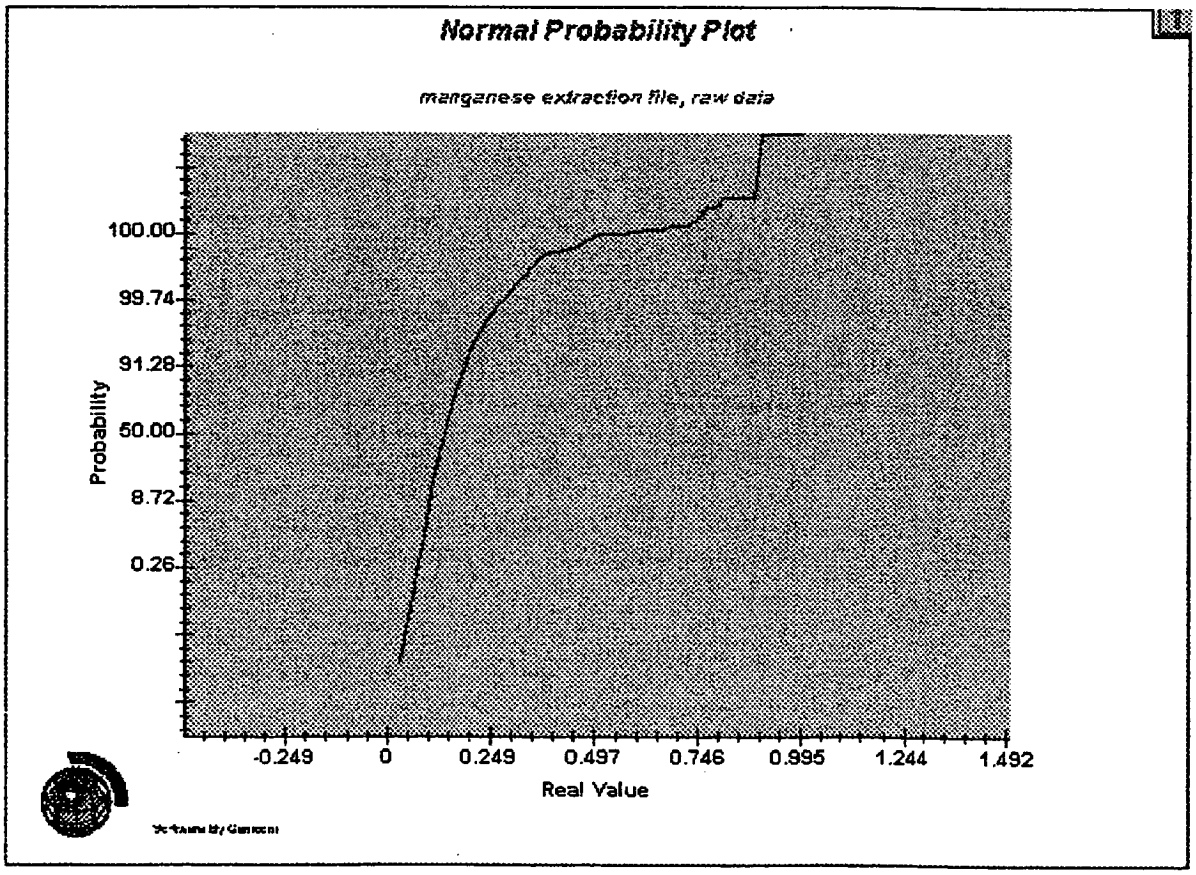

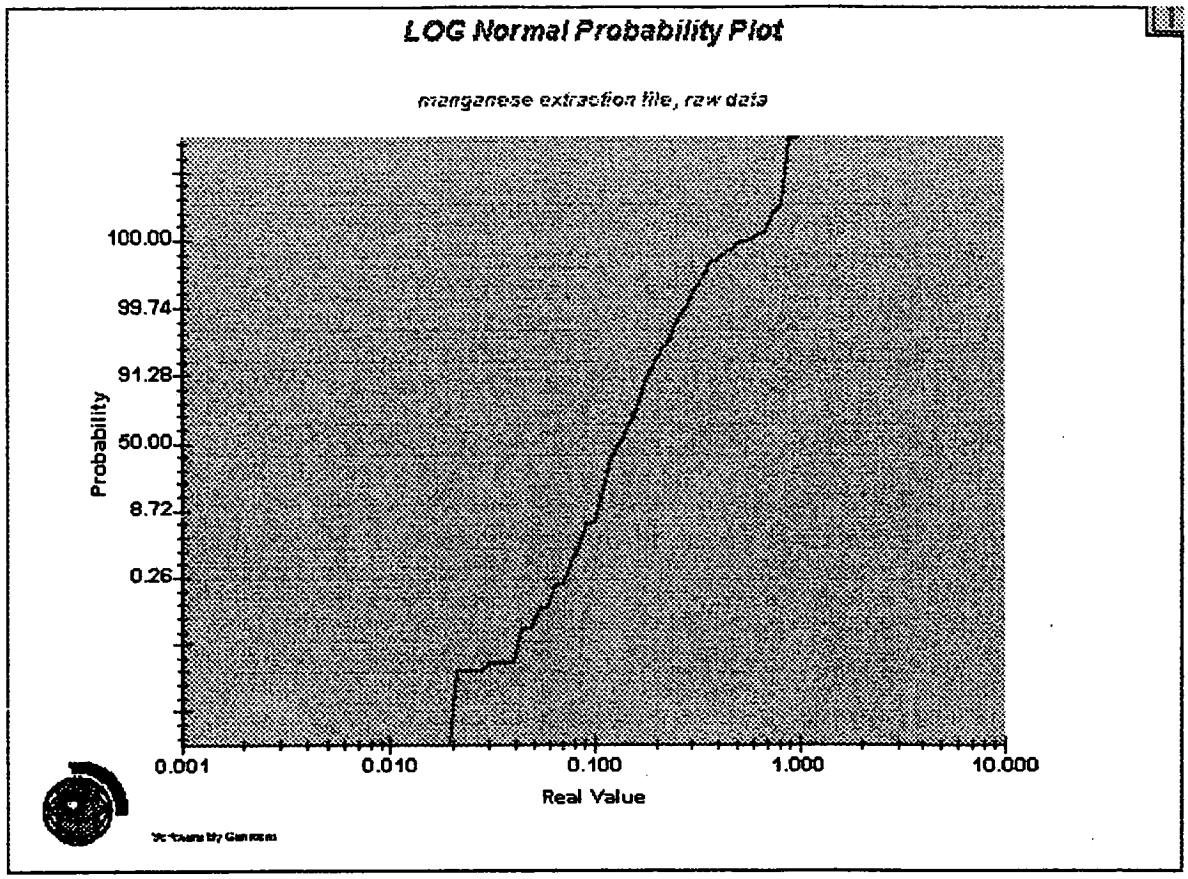

Figure 4-15 Log Normal Probability Plot, Manganese

4.4 Iron Oxide

Iron data summary statistics are given in Table 4-4. Values are grouped around 0.2% Fe_2O_3, and the data display a slight positive skew.

Maximum Fe_2O_3 Value	3.70	
Minimum Fe_2O_3 Value	0	
Number of Samples ≤ 0	238	
Total Population	10014	
	Ungrouped	Grouped
Mean	0.20	0.19
Median	N/A	0.17
Geometric Mean	N/A	N/A
Natural LOG Mean	N/A	N/A
Standard Deviation	0.15	0.16
Variance	0.024	0.027
Log Variance	N/A	N/A
Coefficient of Variation	0.78	0.82
Moment 1 about Arithmetic Mean	0	0
Moment 2 about Arithmetic Mean	0.024	0.027
Moment 3 about Arithmetic Mean	0.025	0.058
Moment 4 about Arithmetic Mean	0.061	0.058
Moment Coefficient of Skewness	6.35	5.57
Moment Coefficient of Kurtosis	97.67	80.02

Table 4-4 Iron Oxide Summary Statistics.

Figure 4-16 shows the iron data, and illustrates the slight positive skew in the distribution. When top-cut to 1% iron, and null values removed, see Figure 4-17, there is clearly a mixed population of iron values.

The log normal transformation, Figure 4-18, indicates that iron has an almost log normal distribution, but a strongly mixed sample population.

Figures 4-19 and 4-20 display the normal and log normal probability plots for the iron samples.

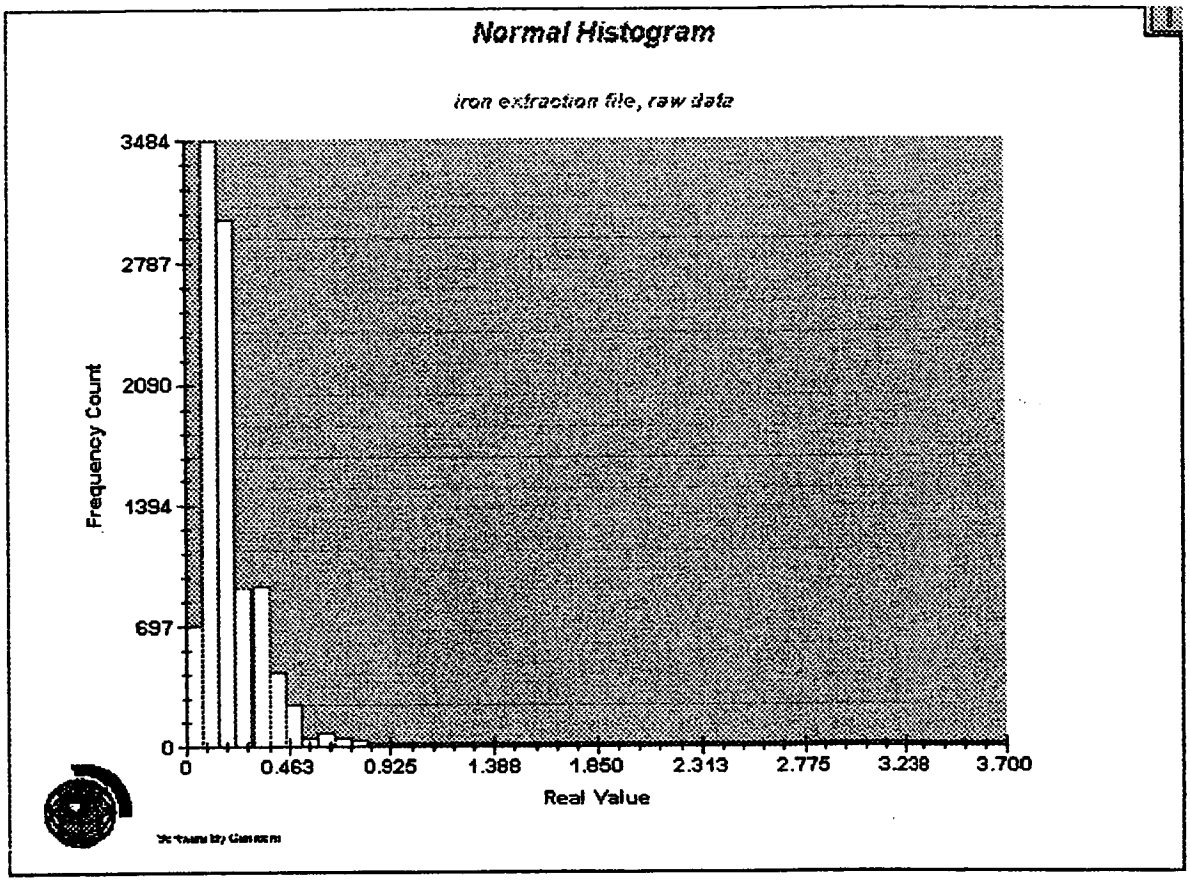

Figure 4-16 Normal Histogram, Uncut Iron Values

Figure 4-17 Normal Histogram, Lower Cut of 0.01%, and Top Cut to 1%

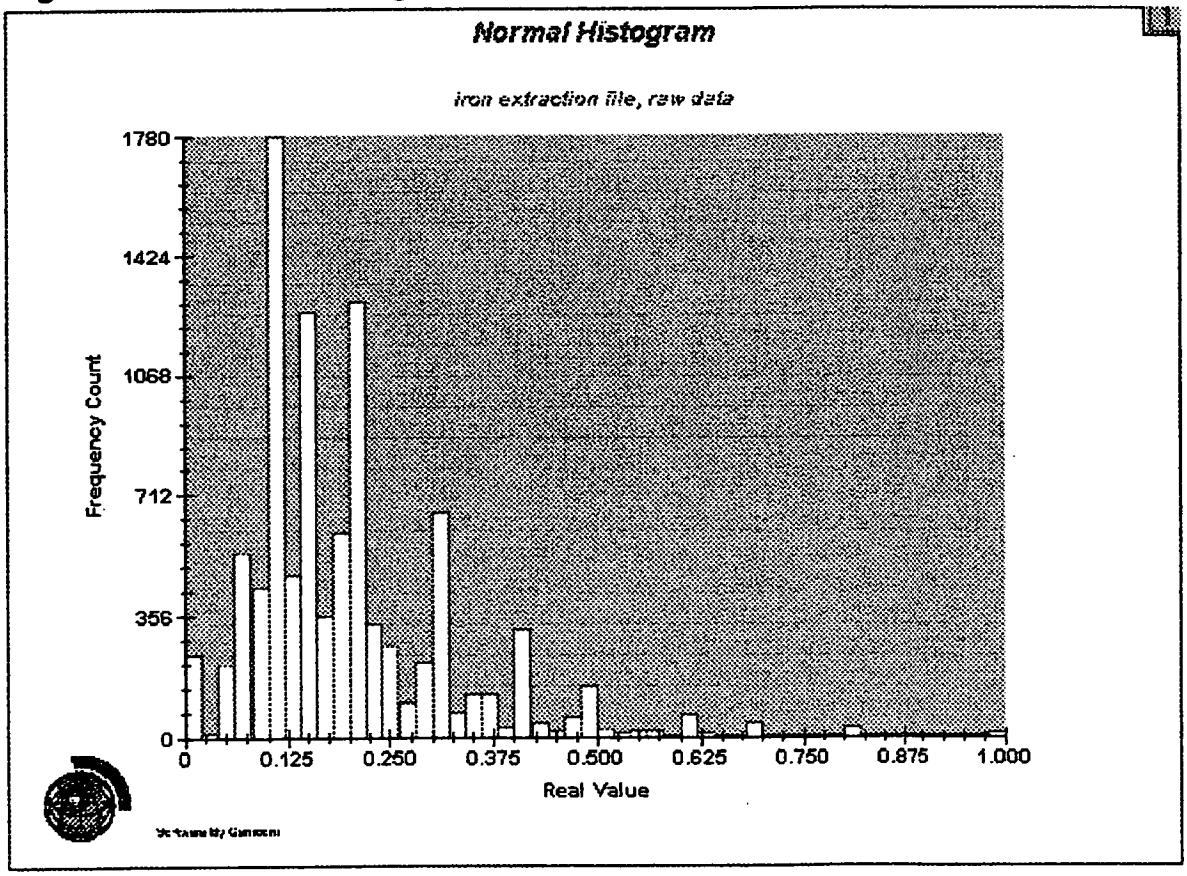

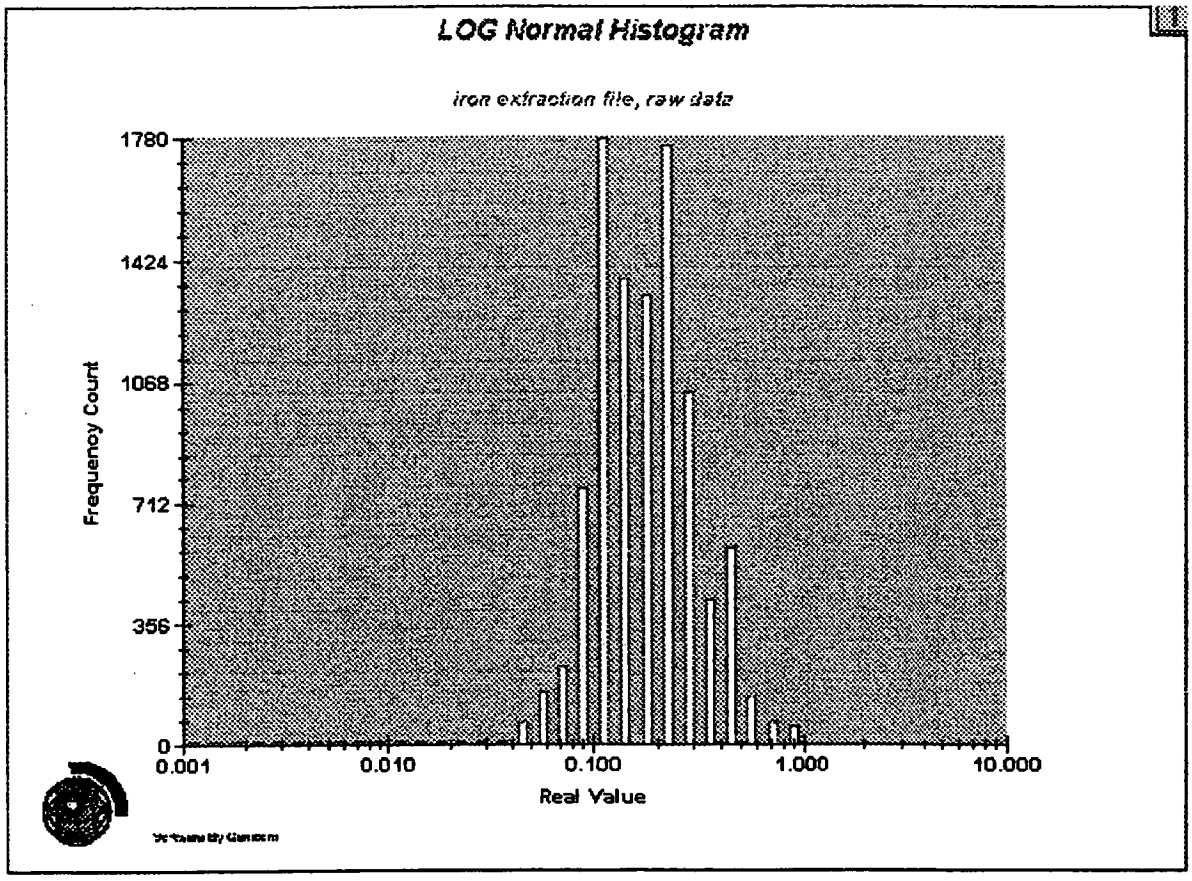

Figure 4-18 Log Normal Histogram, Iron

Figure 4-19 Normal Probability Plot, Iron

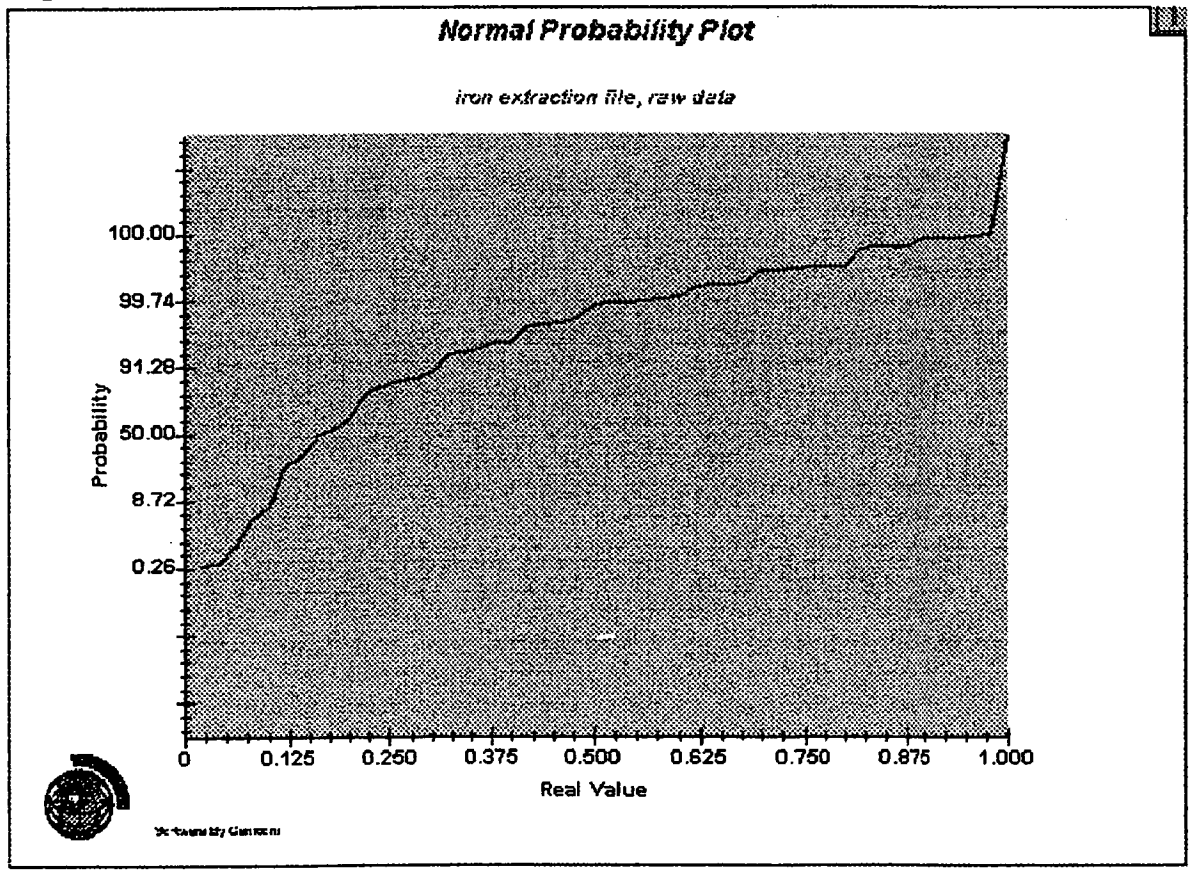

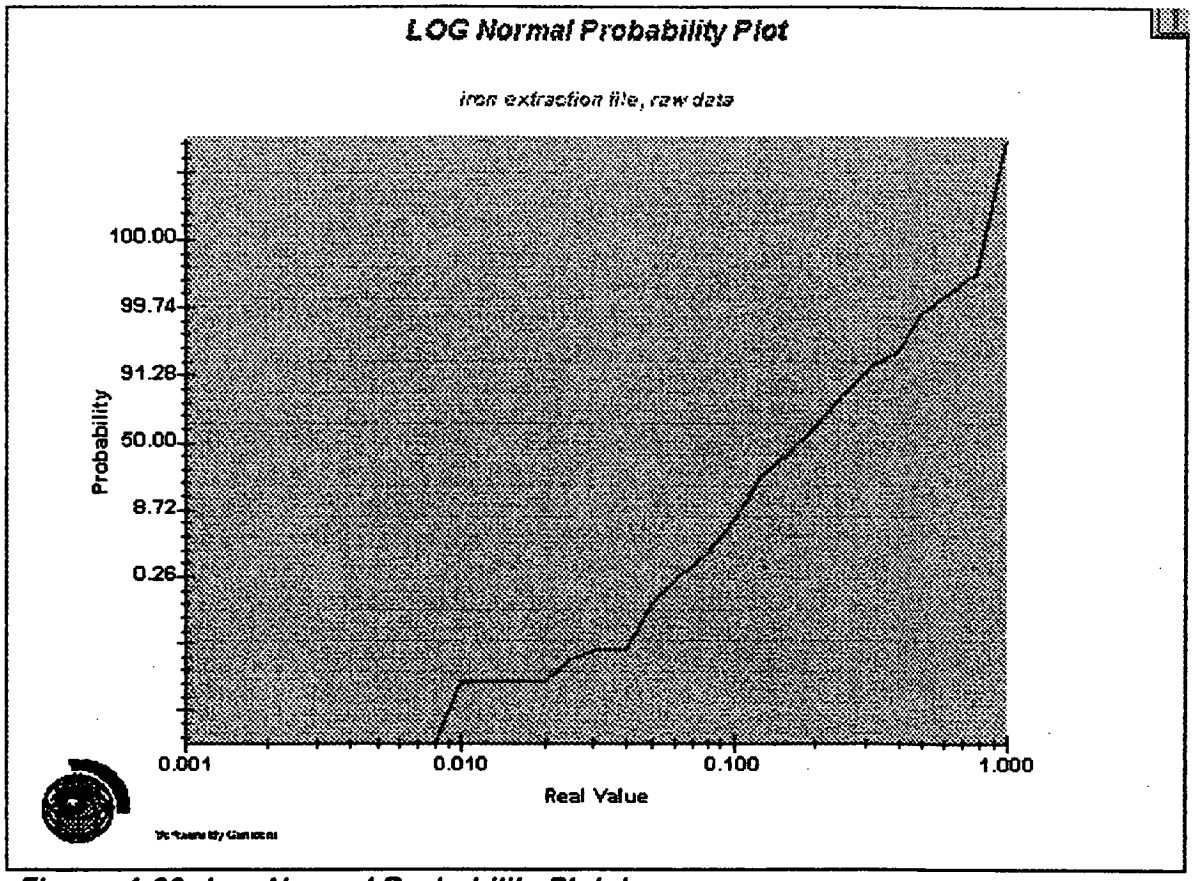

Figure 4-20 Log Normal Probability Plot, Iron

4.5 Calcium

Calcium assay values are statistically summarised in Table 4-5. Calcium averages between 3 and 3.3%, and shows a slight positive skew to the data distribution.

Maximum CaO Value	35.90	
Minimum CaO Value	0	
Number of Samples ≤ 0	3886	
Total Population	10014	
	Ungrouped Data	Grouped
Mean	3.05	3.29
Median	N/A	2.41
Geometric Mean	N/A	N/A
Natural LOG Mean	N/A	N/A
Standard Deviation	4.04	3.88
Variance	16.33	15.10
Log Variance	N/A	N/A
Coefficient of Variation	1.32	1.18
Moment 1 about Arithmetic	0	0
Moment 2 about Arithmetic	16.33	15.10
Moment 3 about Arithmetic	170.54	165.49
Moment 4 about Arithmetic	418.17	3240.74
Moment Coefficient of	2.58	2.81
Moment Coefficient of	12.81	14.20

Table 4-5 Calcium Summary Statistics

Figure 4-21 is a normal histogram plot of all the calcium data, and reflects the strong influence of the number of assays returned with no calcium values.

When the data are top-cut to 13% , and the null values removed, the skewed nature of the calcium distribution is apparent, Figure 4-22.

The log normal distribution, Figure 4-23 shows a positively skewed sample distribution, with a long assay tail toward the higher grade values. Given the alkaline environment of deposit formation, it is suggested that the higher values represent more calcareous nodules or actual samples of calcrete.

Figures 4-24 and 4-25 display the normal and log normal probability plots respectively.

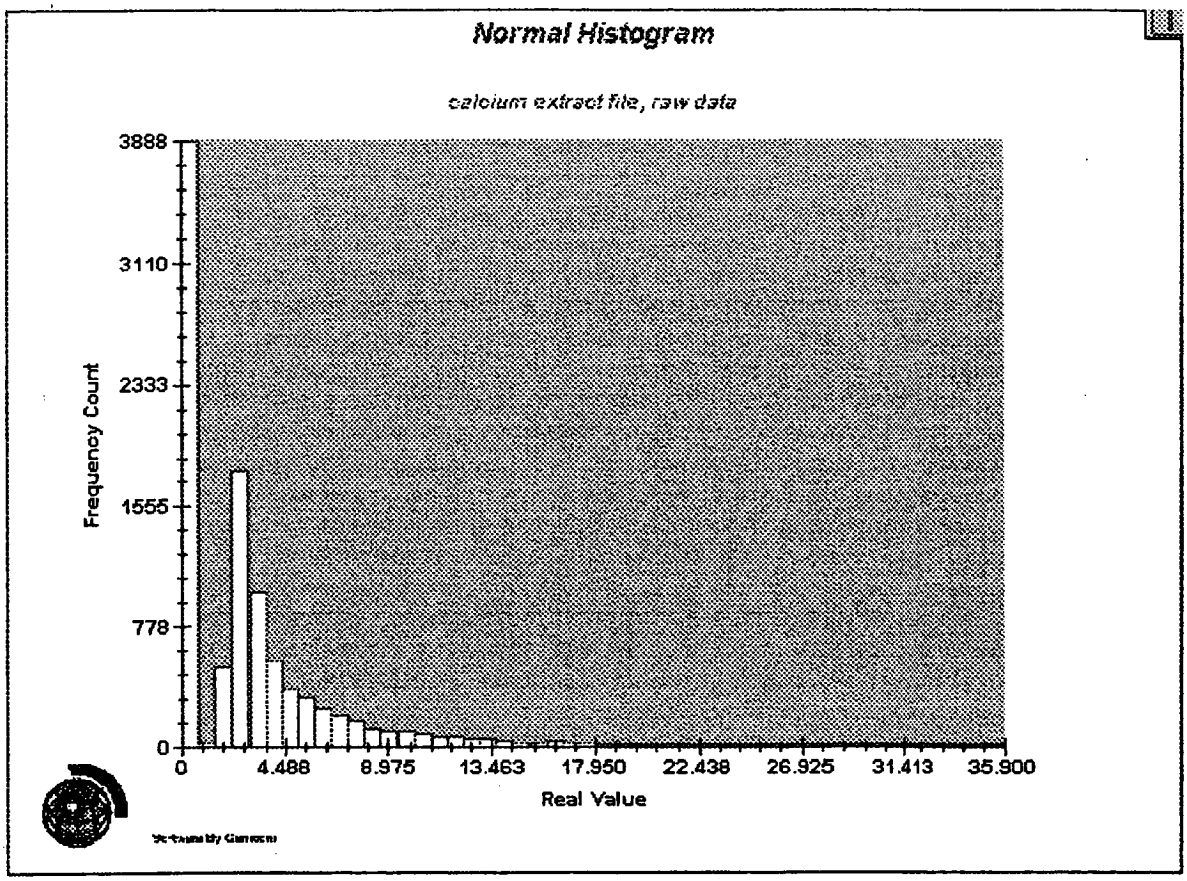

Figure 4-21 Normal Histogram, Uncut Calcium Values

Figure 4-22 Normal Histogram, Lower Cut of 0.01% and Top Cut of 13%

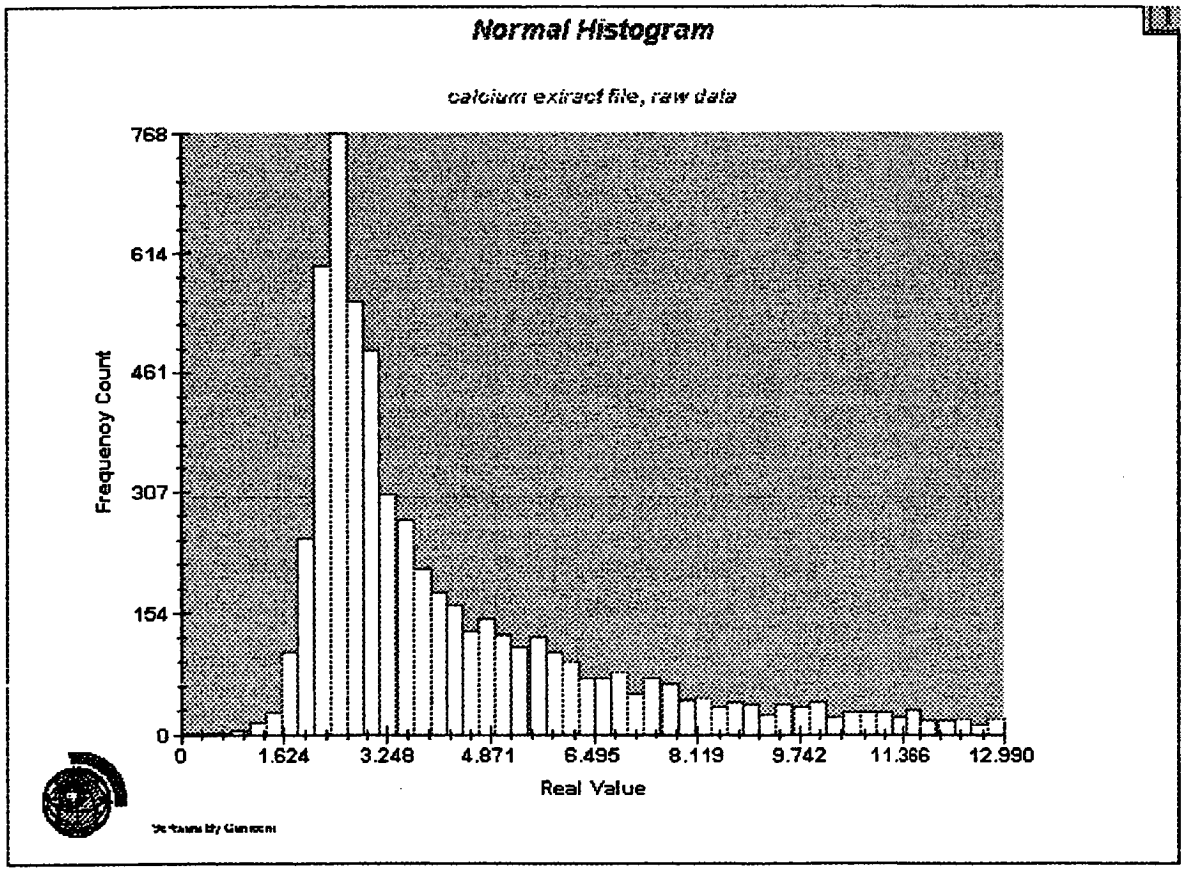

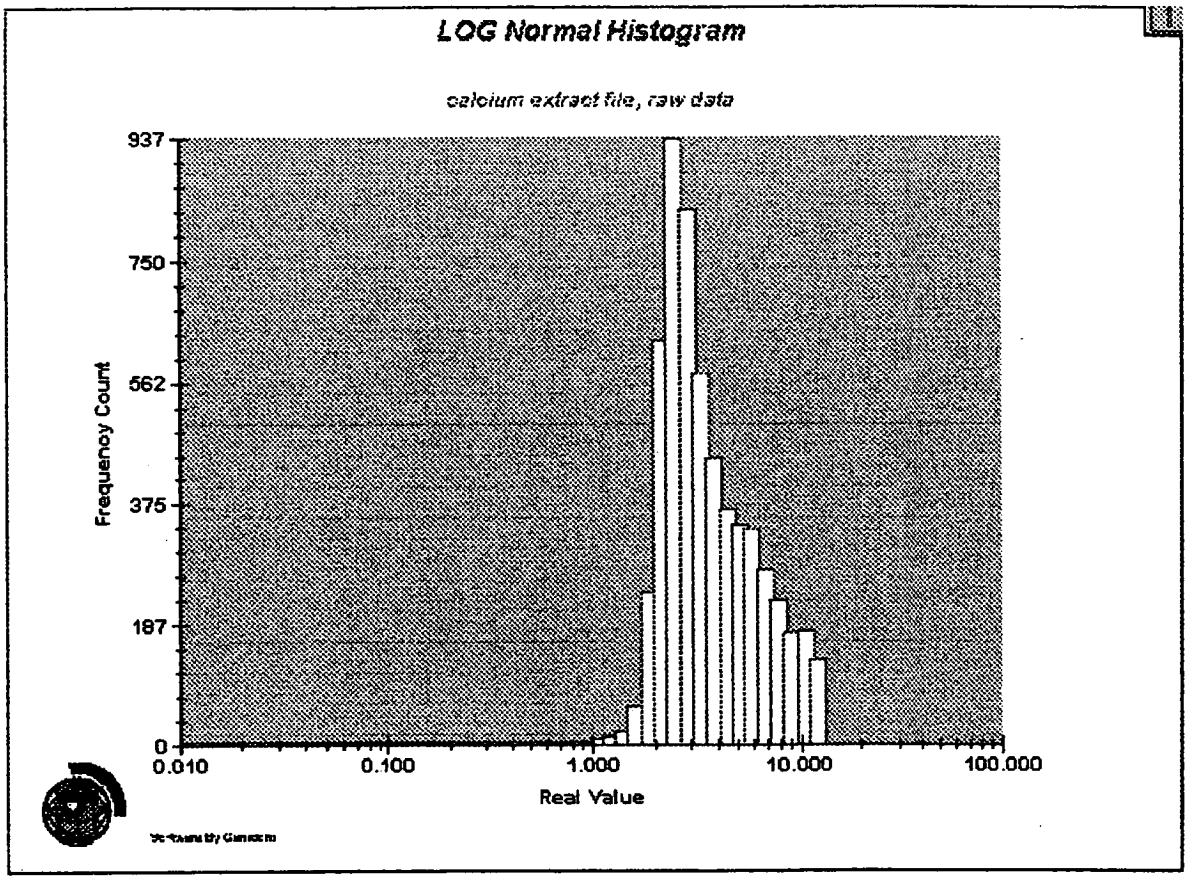

Figure 4-23 **Log Normal Histogram, Calcium**

Figure 4-24 **Normal Probability Plot, Calcium**

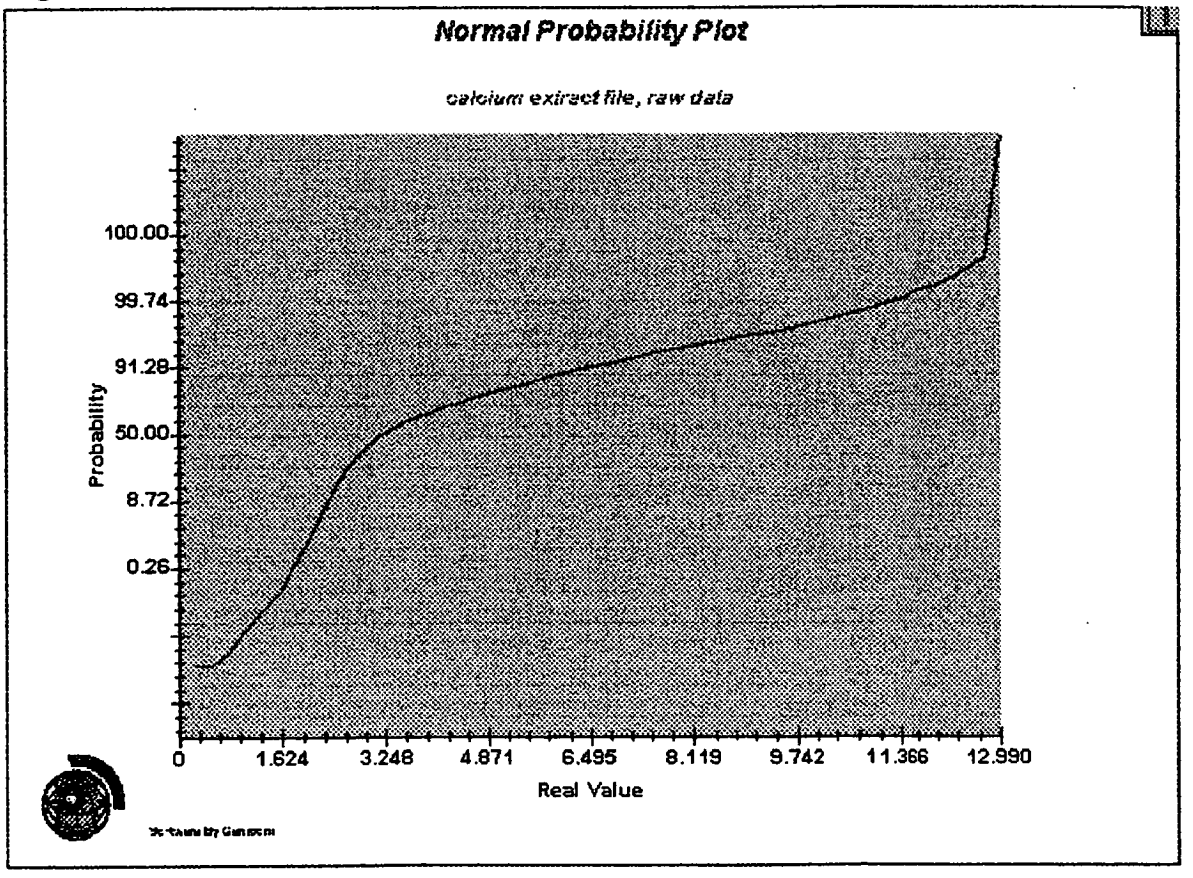

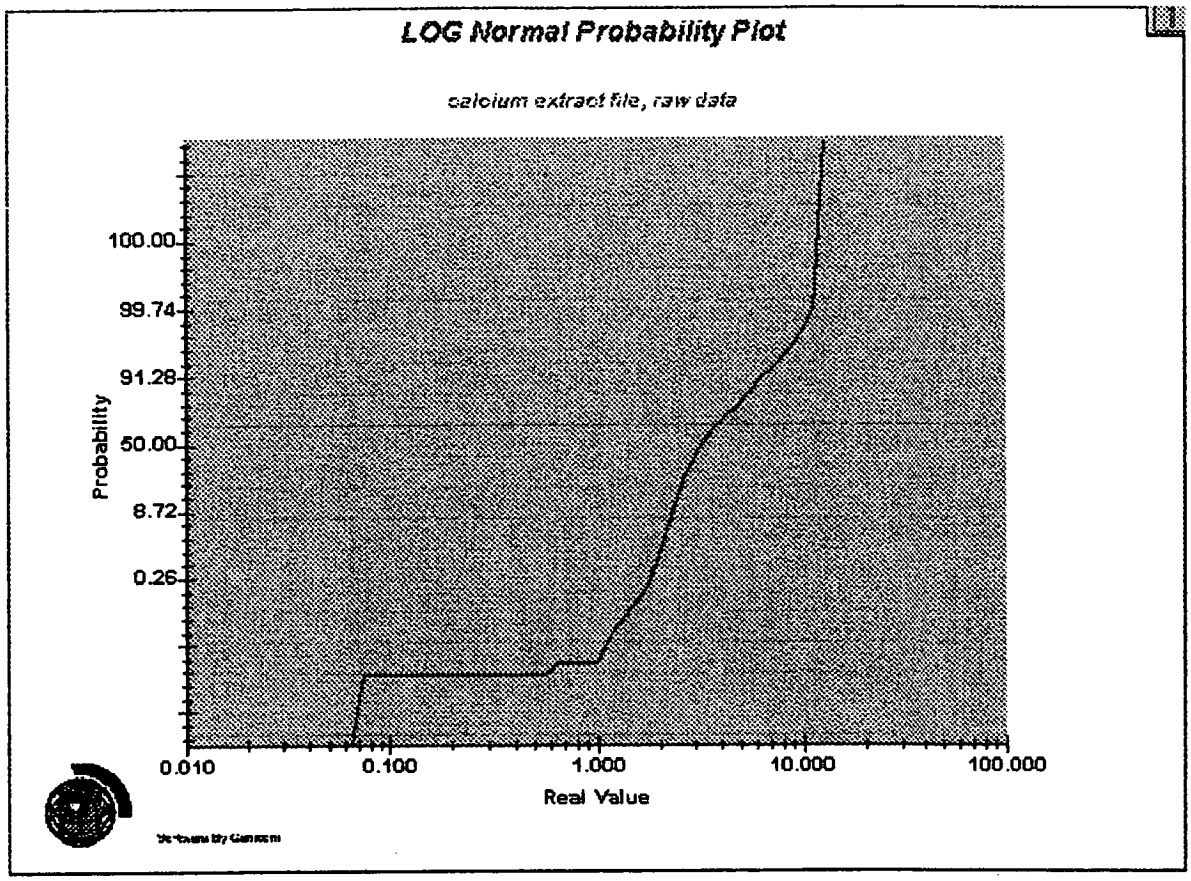

Figure 4-25 **Log Normal Probability Plot, Calcium**

4.6 Aluminium

The aluminium data was evaluated using 10014 sample points. Summary statistics are illustrated in Table 4-6. Aluminium averages 0.22%, with an assay high of 13%.

Maximum Al_2O_3 Value	13.00	
Minimum Al_2O_3 Value	0	
Number of Samples ≤ 0	67	
Total Population	10014	
	Ungrouped	Grouped
Mean	0.22	0.20
Median	N/A	0.16
Geometric Mean	N/A	N/A
Natural LOG Mean	N/A	N/A
Standard Deviation	0.22	0.24
Variance	0.051	0.059
Log Variance	N/A	N/A
Coefficient of Variation	0.99	1.16
Moment 1 about Arithmetic Mean	0	0
Moment 2 about Arithmetic Mean	0.051	0.059
Moment 3 about Arithmetic Mean	0.23	0.22
Moment 4 about Arithmetic Mean	2.68	2.54
Moment Coefficient of Skewness	19.90	15.70
Moment Coefficient of Kurtosis	1032.51	719.41

Table 4-6 Aluminium Summary Statistics

Figure 4-26 shows a normal histogram of the aluminium distribution. The histogram is dominated by the null values. Figure 2-27 is a zoomed section of the histogram, with assays lower cut to 0.1% aluminium, and top-cut to 1.6%. The distribution is positively skewed, shows the effect of mixed sample populations and also indicates that the distribution has a long tail of higher grade aluminium assays.

The aluminium log normal histogram, Figure 4-28, shows a mixed sample population, and a distribution which is approaching log normal.

Figures 4-29 and 4-30 show the normal and log normal probability plots for aluminium assay distribution, respectively. Both plots again show the mixed nature of the sample populations.

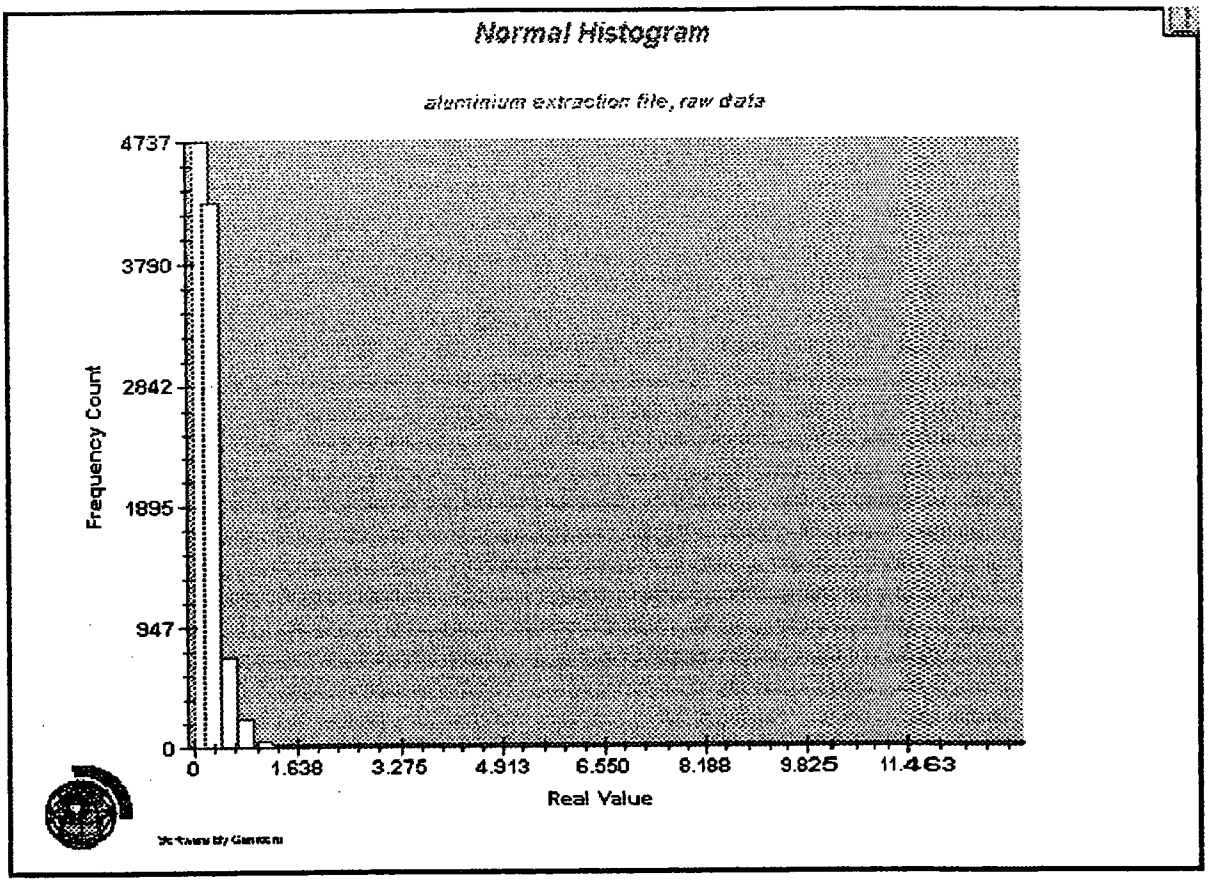

Figure 4-26 Normal Histogram, Uncut Aluminium Values

Figure 4-27 Normal Histogram, Lower Cut to 0.01% and Top Cut to 1.6%

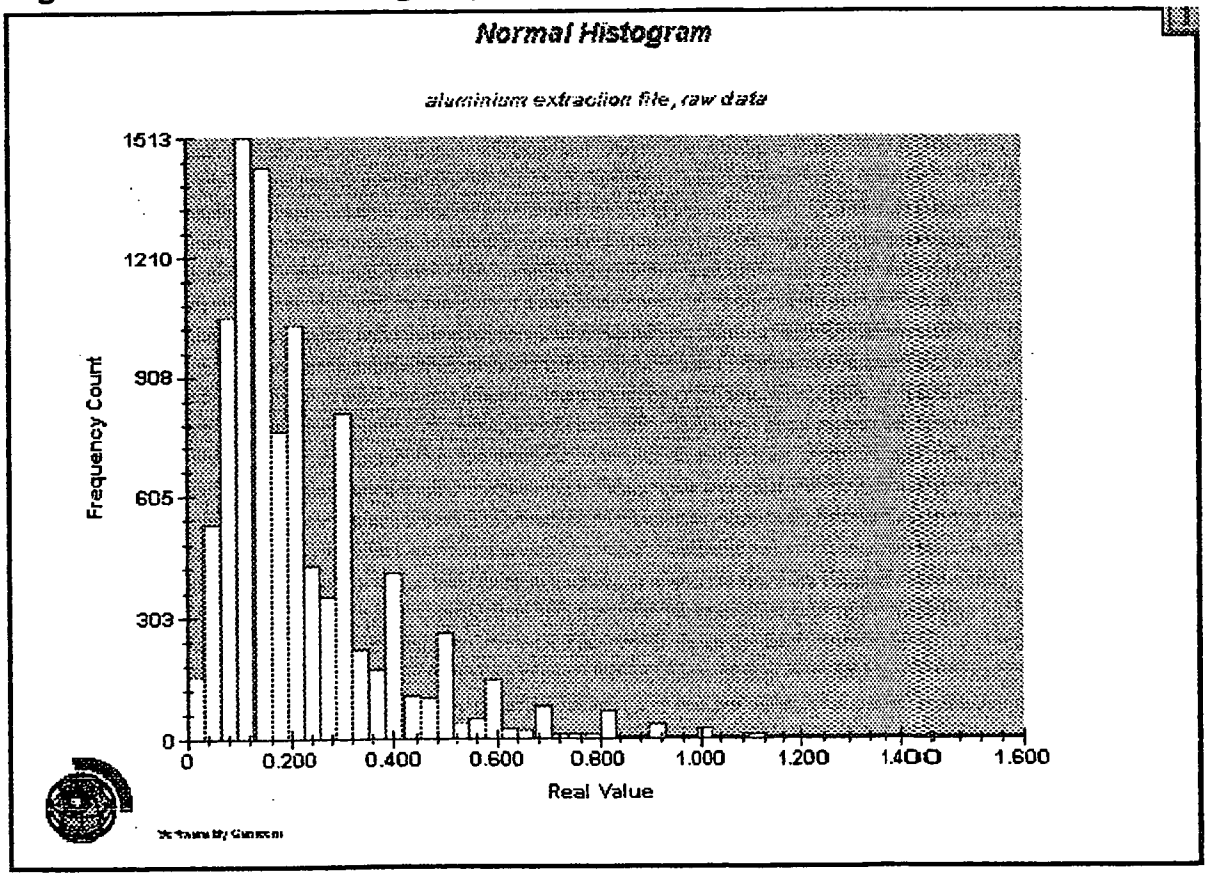

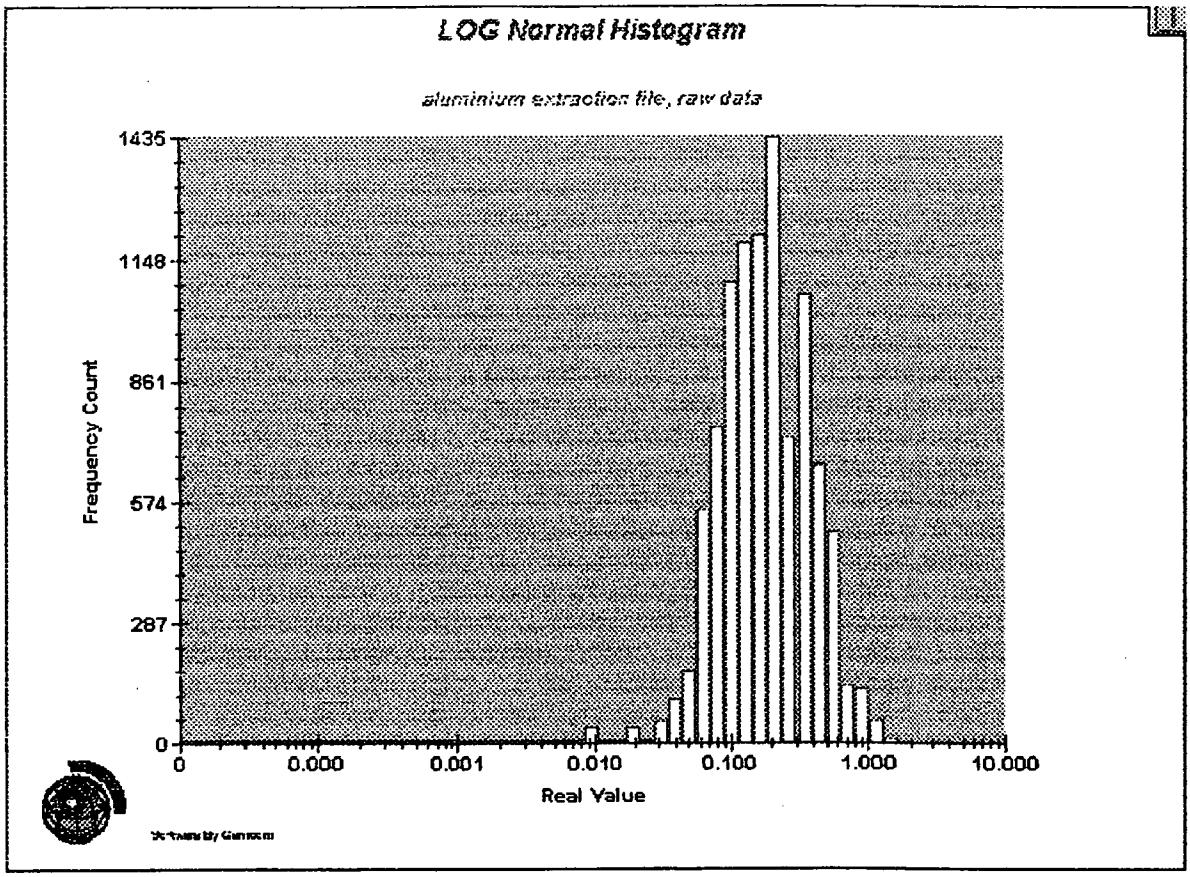

Figure 4-28 **Log Normal Histogram, Aluminium**

Figure 4-29 **Normal Probability Plot, Aluminium**

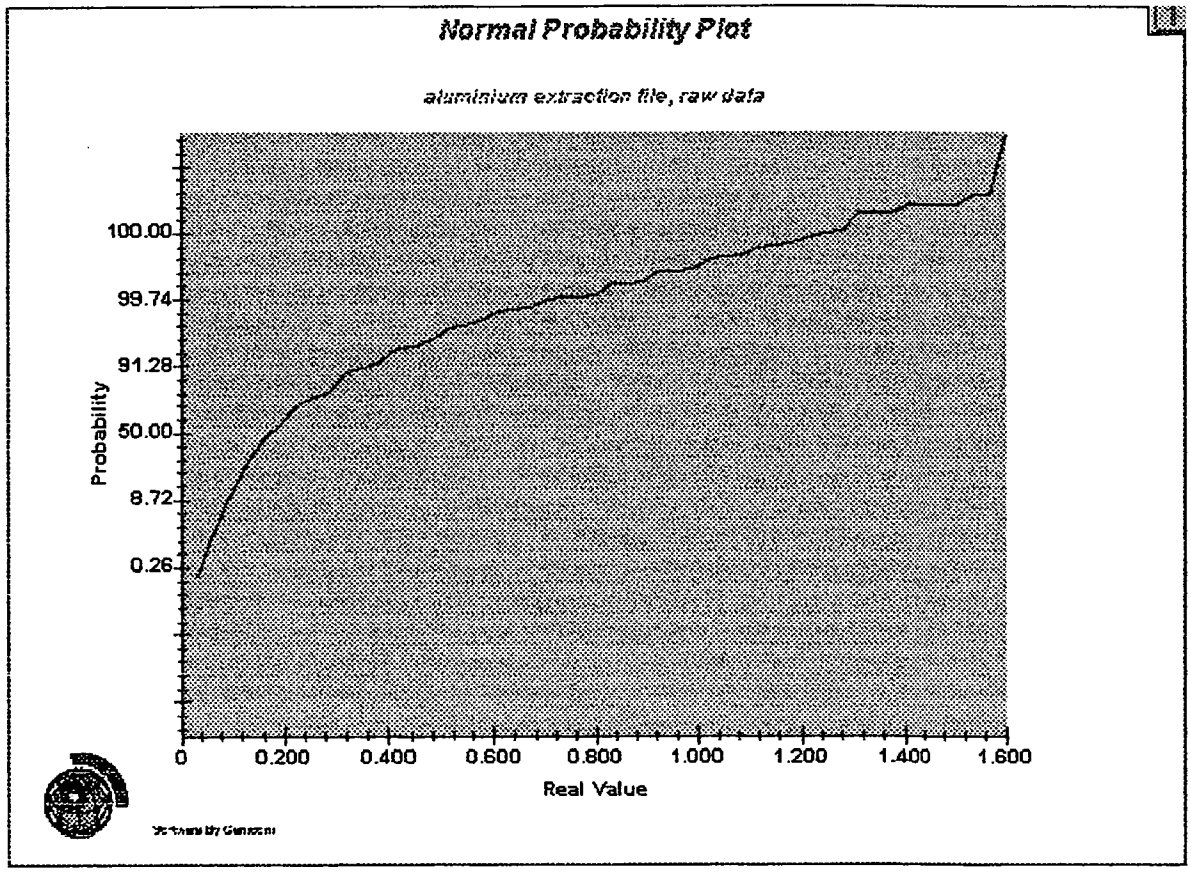

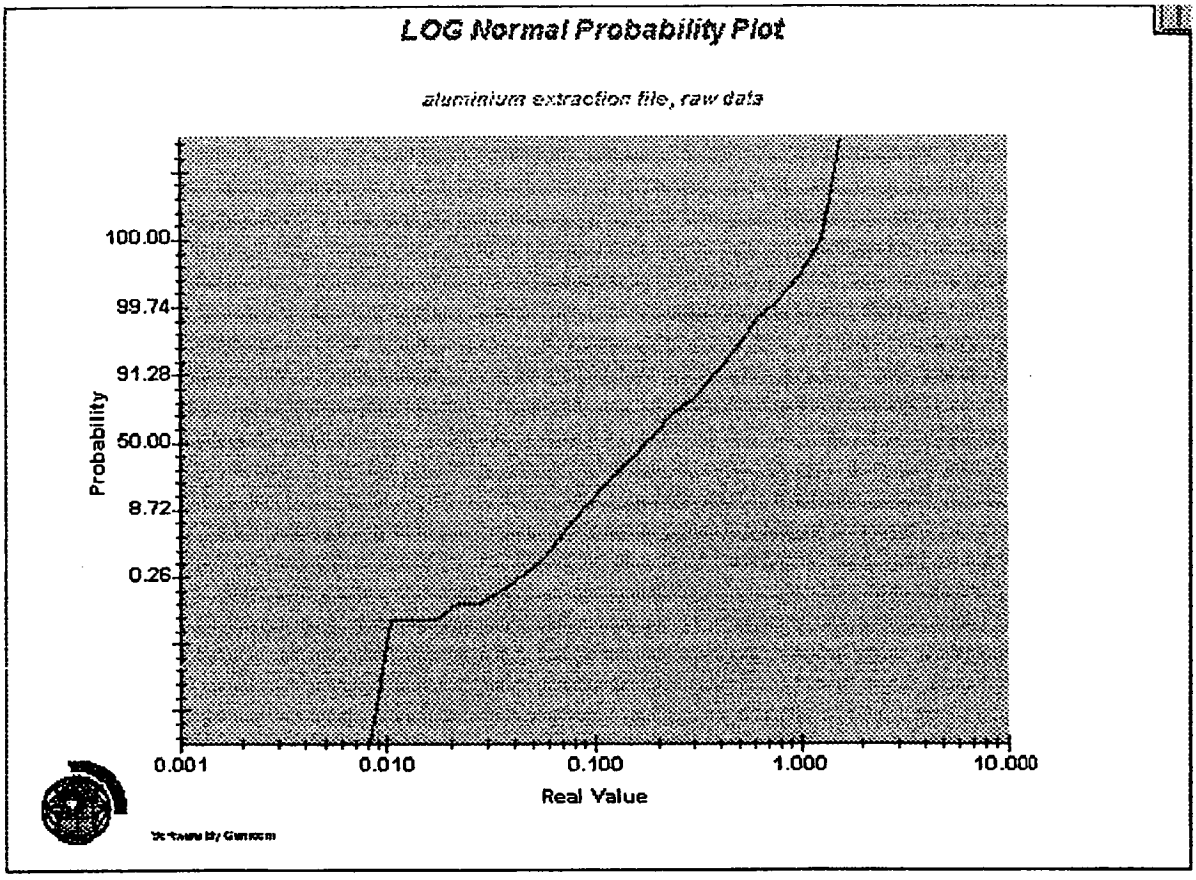

Figure 4-30 ***Log Normal Probability Plot, Aluminium***

4.7 Discussion

Evaluation of the raw assay values indicates that magnesium, calcium, iron, aluminium, manganese and silica all have mixed sample populations, and display variously skewed sample distributions. The mixed populations reveal that the raw assays have a distribution which may be controlled by distinct geological or mineralogical factors. The populations and distributions are suggested to be related to underlying basement geology, changes in position of redox fronts, changes in water table levels, and changing pH conditions, and this is discussed more fully below.

Studies by Canterford et al (1987) indicated that the distributions of magnesium and calcium were related, as were iron and manganese, and lastly, silica and aluminium. The paired elements were reported to respond in a similar manner to changes in the chemical and weathering environment, and as a result, tend to show similar sample distribution and population patterns.

The proposed genesis of Kunwarara has a normal drainage system of near neutral pH changing to strongly alkaline conditions in a closed basin, under arid weathering conditions.

Weathering results from the contact of fresh rock to atmospheric conditions, and is controlled by the amount of water and oxygen interacting

with the rock. A complex system of oxidising and reducing conditions develops, where Eh and pH increase progressively toward the surface. Lower in a weathering profile, the environment is mildly reducing, due to the consumption of oxygen in weathering, while in the upper portion of the profile, more oxidising conditions prevail (Lawrance, 1995).

Superimposed on this weathering profile is the effect of the alkaline water table. Magnesium in the weathering profile is probably derived from serpentine in the underlying basement lithologies, and surrounding basement hills. Serpentine is stable only in contact with solutions which are undersaturated in silica, and at temperatures at less than 500 degrees Celsius (Krauskopf and Davis, 1995). and given that the interpreted origin for Kunwarara is a drainage system, the major contributor of free magnesium cations is probably hydrolysis reactions.

Primary magnesium cations are produced by the hydrolysis of minor remnant olivine in the underlying ultramafic basement according to the reaction:

$$((Mg, Fe)_2SiO_4) + 10H_2O = 2Mg^{2+}+2Fe(OH)_3+H_4SiO_4\ (aq)+4OH^-+6H^++6e^-$$

and by the hydrolysis of serpentine.

A tendency of the hydrolytic reactions is to increase the pH toward more alkaline conditions, but this is to some extent countered by the formation of ferric iron, and the accompanying liberation of hydrogen ions, and thus the production of acid conditions. As slightly more hydrogen ions are produced than hydroxyl anions, the resulting pH would tend toward acid or neutral conditions.

In the case of the hydrolysis of olivine, some of the silica may not remain in solution under acid to neutral conditions, but precipitate out as cryptocrystalline or opaline silica. At the same time, ferric oxide may either precipitate as amorphous masses or form goethite or haematite.

A second source of magnesium cations can be from the transformation of serpentine into nickeliferous serpentine via the an ionic exchange reaction:

$$Mg_3Si_2O_5(OH)_4 + Ni^{2+} = (Mg_2Ni)Si_2O_5(OH)_4 + Mg^{2+}$$

as well as via the hydrolysis of serpentine. However, serpentine will only react when all of the olivine has been consumed (Trescases, 1992). The mixed magnesian population may thus be partially due to the difference in rate of production of magnesium cations from the two reactions above.

More magnesium would be liberated from areas which have not undergone serpentinisation of the olivine groundmass, as olivine is generally less stable in a tropical environment (Trescases, 1992), than from serpentinised bedrock.

During evolution of the closed Tungamulla basin, more alkaline conditions prevailed, either as a result of seawater incursions, or as a direct result of development of a playa lake system. Under alkali pH conditions, magnesium may precipitate out as concretions or as calcrete equivalents (Trescases, 1992) in a solid solution series with calcium.

Bulk chemical analyses of the magnesite nodules (Canterford et al, 1987) indicate that there are marked differences in grain size, nodule shape and porosity in nodules from different locations within the deposit. Nodules displayed different core and skin compositions, with samples ranging in composition from dolomite ($CaMg(CO_3)_2$) to magnesite (MgO).

This chemical change will be reflected in the assay values, as the magnesium percentage returned will be dependent on which portion of a nodule is sent for assay, the mineralogy of the nodule and where the nodule is sourced in the deposit.

It is suggested that the long tail on the magnesium distributions may relate to fluctuations in the alkaline water table in response to pH changes from dry to wet season conditions, and this resulting change is evidenced by the number of differing nodule types recognised by Canterford et al, 1987.

Calcium in the weathering environment shows a similar behaviour to magnesium. Calcium ions were probably released as part of the breakdown of anorthite, which is a hydrolitic reaction producing hydroxyl anions, and a tendency toward more alkaline conditions.

Calcium, in the saline lake conditions proposed for deposit formation, would have precipitated as nodules or calcrete in conjunction with magnesium. Mixed sample populations are probably a reflection of localised pH fluctuations at the time of precipitation.

Manganese is generally present in rock forming minerals in several oxidation states (Trescases, 1992) including Mn^{2+}, Mn^{3+} and Mn^{4+}, but most commonly as Mn^{2+}. Oxidation in the weathering environment has the effect of converting Mn^{2+} to Mn^{4+} species, with the resultant formation of manganite, pyrolusite and "wad" as oxidation minerals coating fractures and joints. Higher grade manganese samples may represent manganiferous fracture coatings.

The position of the water table generally controls the location of oxidising/reducing fronts, and thus, the location of the transformation of Mn^{2+} species to Mn^{4+} ions. The redox front is the usually the point where water logged lithologies are in contact with drier lithologies. This location generally corresponds with the position of the watertable, but in a drainage channel, the redox front may be lower than the standing water table due to incorporation of oxygen in higher volume water discharges.

Manganese deposition therefore, is controlled by water table movement, and the related movement of the redox front (Lawrance, 1997). The mixed sample population and the skewed nature of the manganese assays probably reflects water table movement, and the effect of meandering drainage channels on manganese precipitation.

As the production of Mn4+ ions releases acid, the manganese assays may also represent two distinct generations of formation. The first would be related to initial dissolution of manganese from the basement lithologies, and the second to groundwater movement after the main alkaline pH conditions which resulted in magnesium nodule formation.

Manganese precipitation requires more acid to neutral pH conditions, and the mixed sample population may represent fluctuations in the water table, and in

Iron gives one of the more problematic distributions. Like manganese, iron may be present in bedrock in different valency states, as Fe^{2+} or Fe^{3+}. During weathering, the ferrous iron is oxidised to ferric iron at the redox front, via the following reaction:

$$Fe^{2+} + 3H_2O = Fe(OH)_3 + 3H^+ + 3e^-$$

with ferric iron becoming the only stable oxidation state. Minerals formed include goethite, haematite and amorphous iron oxides. Ferric iron is also produced from the hydrolysis of minerals such as olivine in the underlying basement ultramafic lithologies. The reaction is acid forming, and two generations of iron formation are probable, prior to, and after, the alkaline magnesian nodule forming event.

The iron sample populations probably reflect changes in the local water table levels, changing redox front positions, and the generation of formation of the iron mineral.

Silica and aluminium distributions are complex in that both elements are major rock-forming constituents. Significant variations in the silica histograms could in part be due to the changing rocktypes down the profile from low silica content clays at surface through to higher silica content sands and gravels at the base of the sequence.

A second explanation is that the upper level silica values represent silica mobility in solution. In this instance, silica would be derived from the weathering of silicates in the underlying bedrock. Silica dissolution is pH dependent, and generally is the result of hydrolitic reactions, as shown above for olivine. As noted above, partial precipitation of silica as amorphous or opaline silica may have occurred during this phase of weathering. Morris and Fletcher (1987) noted that silica solubilities increased as a direct result of the oxidation of ferrous to ferric iron. As ferric iron is produced as part of the olivine weathering process, the silica

dissolution may have been increased, and amorphous silica precipitates may have been partially dissolved.

During the formation of the magnesium nodules, silica would have remained in solution, as the mineral is highly soluble in alkaline conditions (Trescases, 1992). With cessation of the saline nodule forming episode, silica re-precipitation would have resulted with a change back to more acid/neutral pH. As the silica would precipitate only when pH conditions were suitable, there would be scattered silica concentrations in the sequence reflecting the changing pH values.

Canterford et al (1987) noted that in scanning electron microprobe analyses, the silica content of the skins of nodules tended to be higher than that measured at the nodule centre, suggesting that again, pH conditions were variable during nodule formation, and that the more acid requirements for precipitation of silica were met only toward the end of the nodule forming process.

Aluminium rich minerals are generally relatively inert in the upper weathering environment, and not subject to hydrolysis in the same manner that the calcium and magnesian minerals are. In the pH range of hydrolitic reactions, three types of aluminosilicate hydrolysis reaction are possible, and may produce either gibbsite, kaolinite or smectite.

As the pH conditions changed to reflect the formation of the magnesite nodules in a strongly alkaline environment, aluminium would have become highly soluble as an anionic species.

Thus, the mixed sample populations recorded in the histogram distributions may be the result of fluctuating pH and water table conditions, varying hydrolitic reactions, and may also be due to underlying basement lithological variations.

Overall, the sample distributions for the six main elements are skewed and represent mixed populations, which may not be directly related to lithologies. Based on this information, the most reliable evaluation technique would be an indicator kriging method.

CHAPTER 5 - CLASSICAL STATISTICS - LITHOLOGY

Each assay type was separated into lithological profile units, using the four logged lithologies supplied by QMC – sand, clay, silt and gravel. Upon extraction, it was found that gravel was never analysed for magnesium, and so the statistics are only evaluated for the first three rock types.

5.1 Magnesium

Table 5-1 shows the magnesium summary statistics for sand, clay and silt.

	SAND		SILT		CLAY	
Maximum MgO value	98.5		98.3		98	
Minimum MgO value	0		0		0	
Number of Samples ≤ 0	5235		3288		931	
Total Population	5235		3288		931	
	Un-grouped	Grouped	Un-grouped	Grouped	Un-grouped	Grouped
Mean	92.84	92.81	92.95	92.93	91.27	91.24
Median	N/A	94.69	N/A	94.23	N/A	92.47
Geometric Mean	N/A	N/A	N/A	N/A	N/A	N/A
Natural LOG Mean	N/A	N/A	N/A	N/A	N/A	N/A
Standard Deviation	8.13	8.08	4.84	4.88	6.26	6.30
Variance	66.24	65.41	23.51	23.82	39.22	39.75
LOG Variance	N/A	N/A	N/A	N/A	N/A	N/A
Coefficient of Variation	0.87	0.87	0.05	0.05	0.06	0.06
Coefficient of Skewness	-8.51	-8.42	-6.61	-6.37	-7.60	-7.33
Coefficient of Kurtosis	92.92	91.48	96.10	90.57	97.43	92.23

Table 5-1 Magnesium Summary Statistics by Lithology

Magnesium typically shows a skewed assay distribution in each lithology code. Sand, in general, has larger standard deviation and shows more assay variance than the other two lithologies, and a slightly higher magnesian assay value.

Figures 5-1 to 5-6 are normal histogram and log normal histogram plots respectively for magnesium in each lithology.

Magnesium values in sand are highly skewed, and still represent mixed sample populations. The samples still display the long assay tail on the lower grade samples. A similar distribution is evident from magnesium in silt, although the silt distribution has a more marked tail. Clay magnesian values are also negatively skewed, although samples begin to approach a normal distribution toward 100% magnesium assays.

Thus, the magnesium sample populations are apparently independent of host lithology, and are probably then related to a combination of basement lithology and weathering reactions.

To model the magnesian sample population, an indicator kriging methodology should be used.

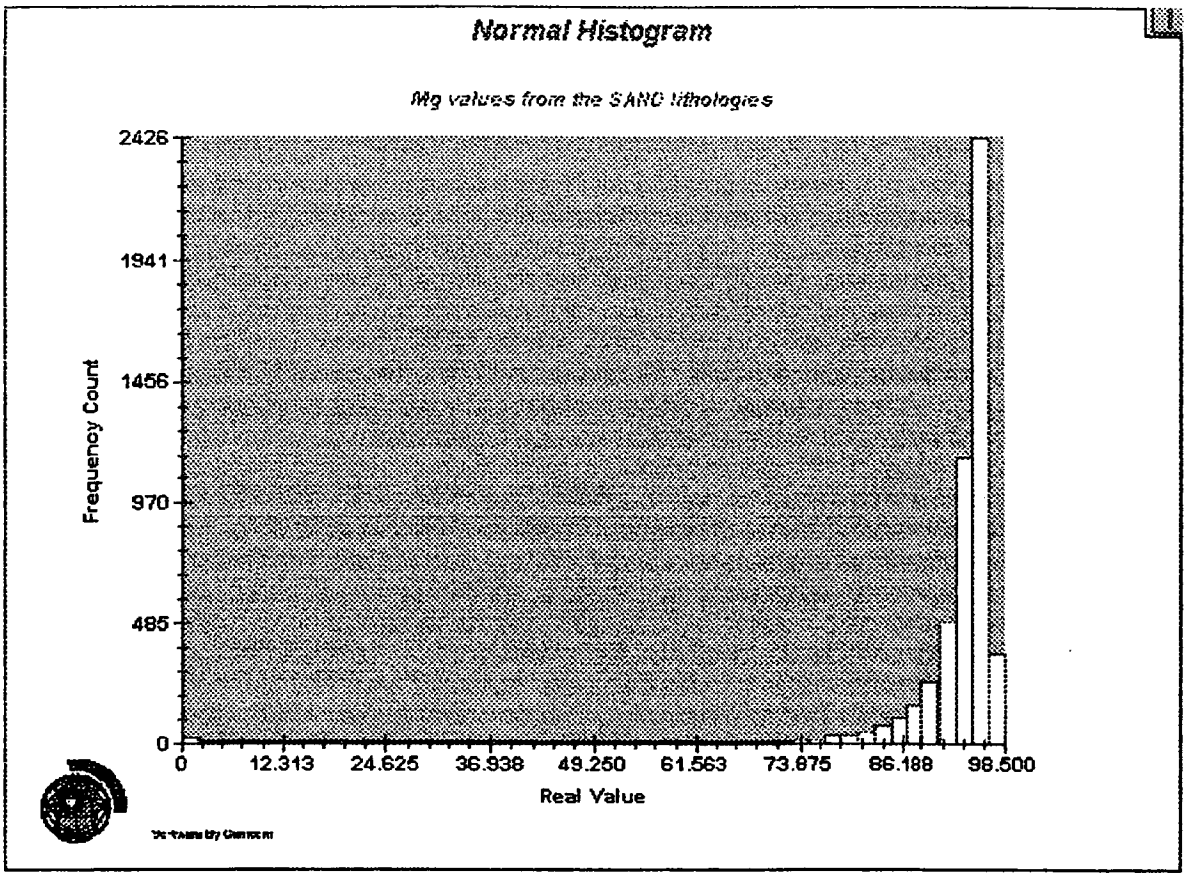

Figure 5-1 Normal Histogram, Magnesium Distribution - Sand

Figure 5.2 Log Normal Histogram, Magnesium Distribution - Sand

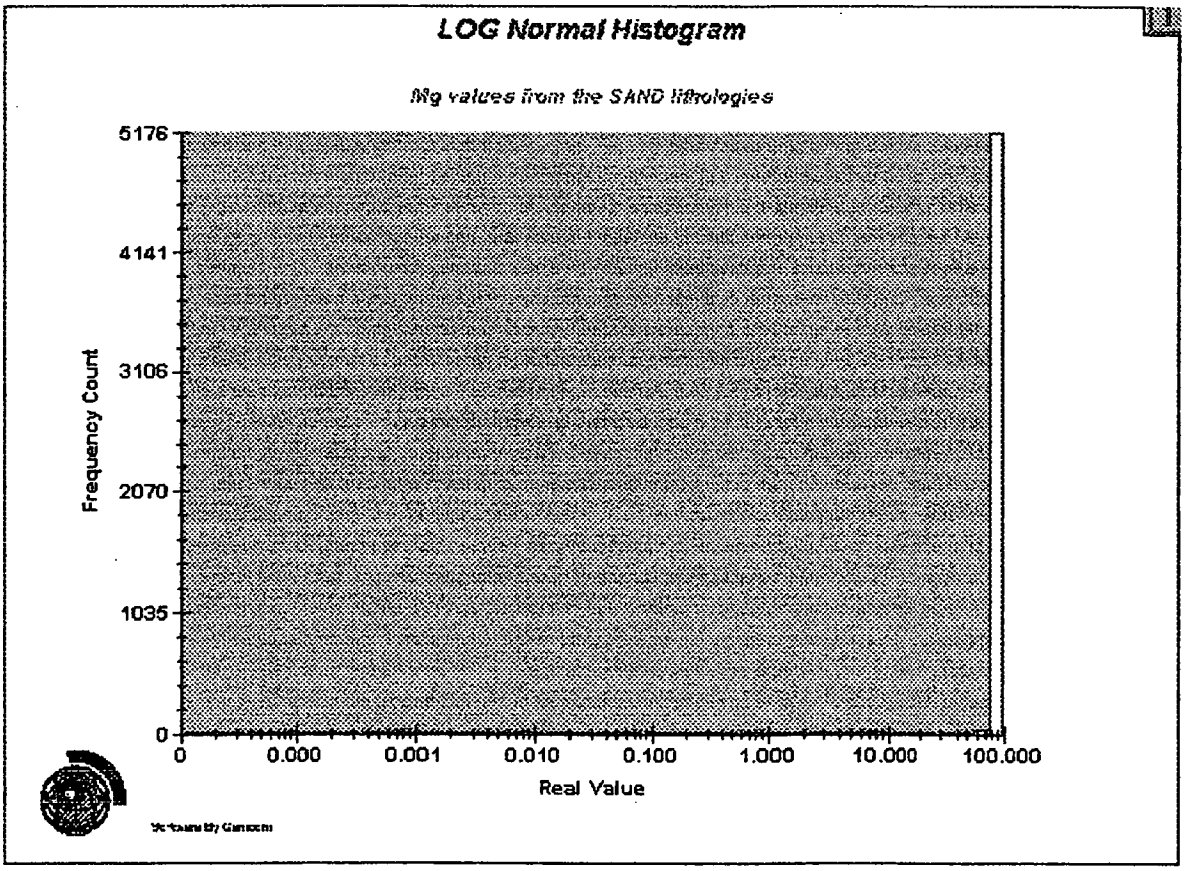

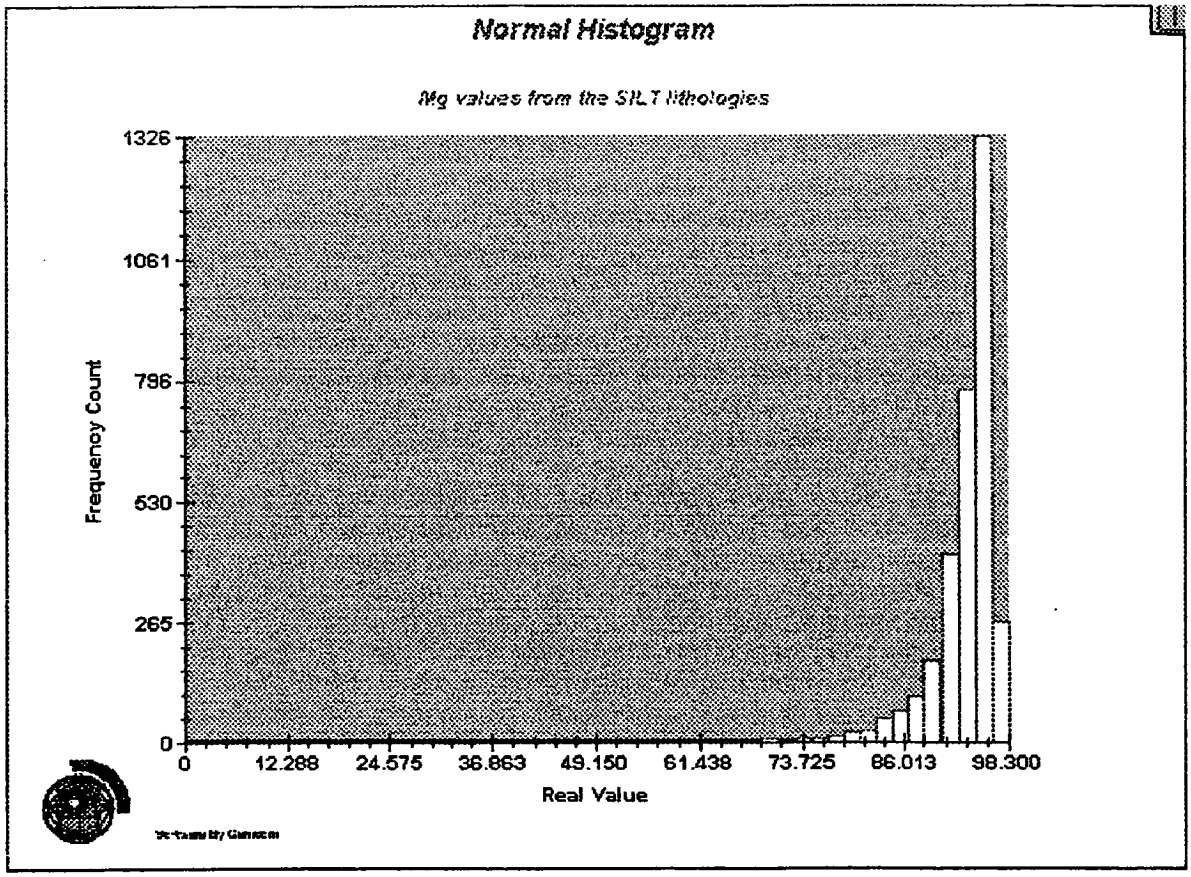

Figure 5.3 Normal Histogram, Magnesium Distribution - Silt

Figure 5.4 Log Normal Histogram, Magnesium Distribution - Silt

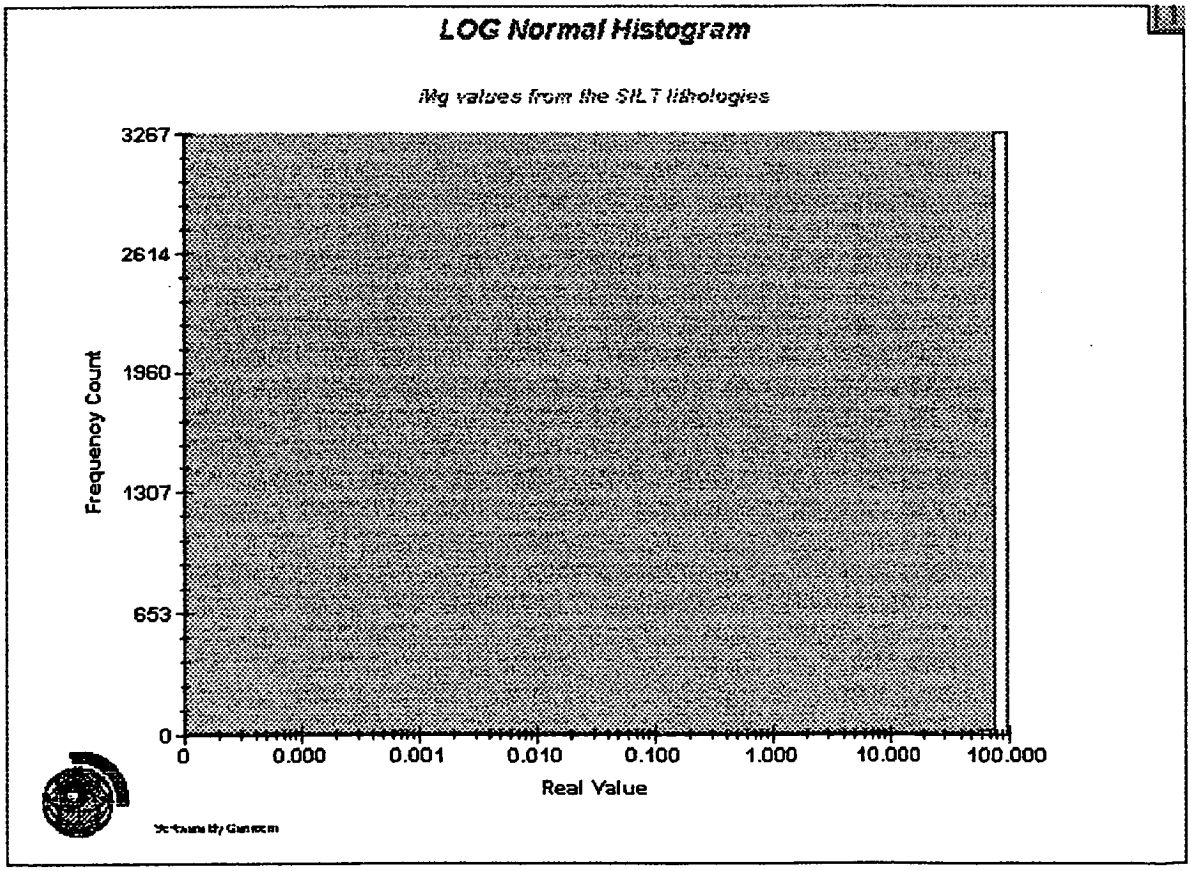

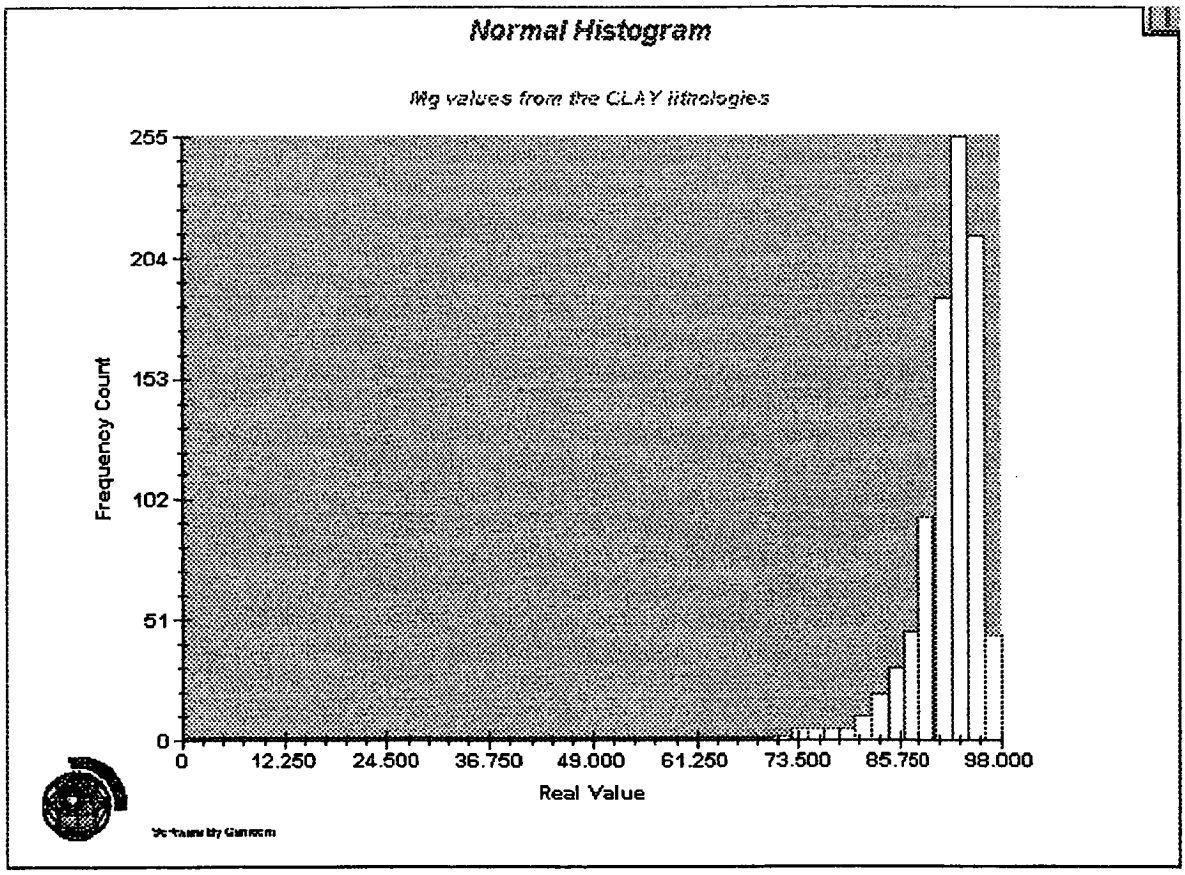

Figure 5..5 Normal Histogram, Magnesium Distribution - Clay

Figure 5.6 Log Normal Histogram, Magnesium Distribution - Clay

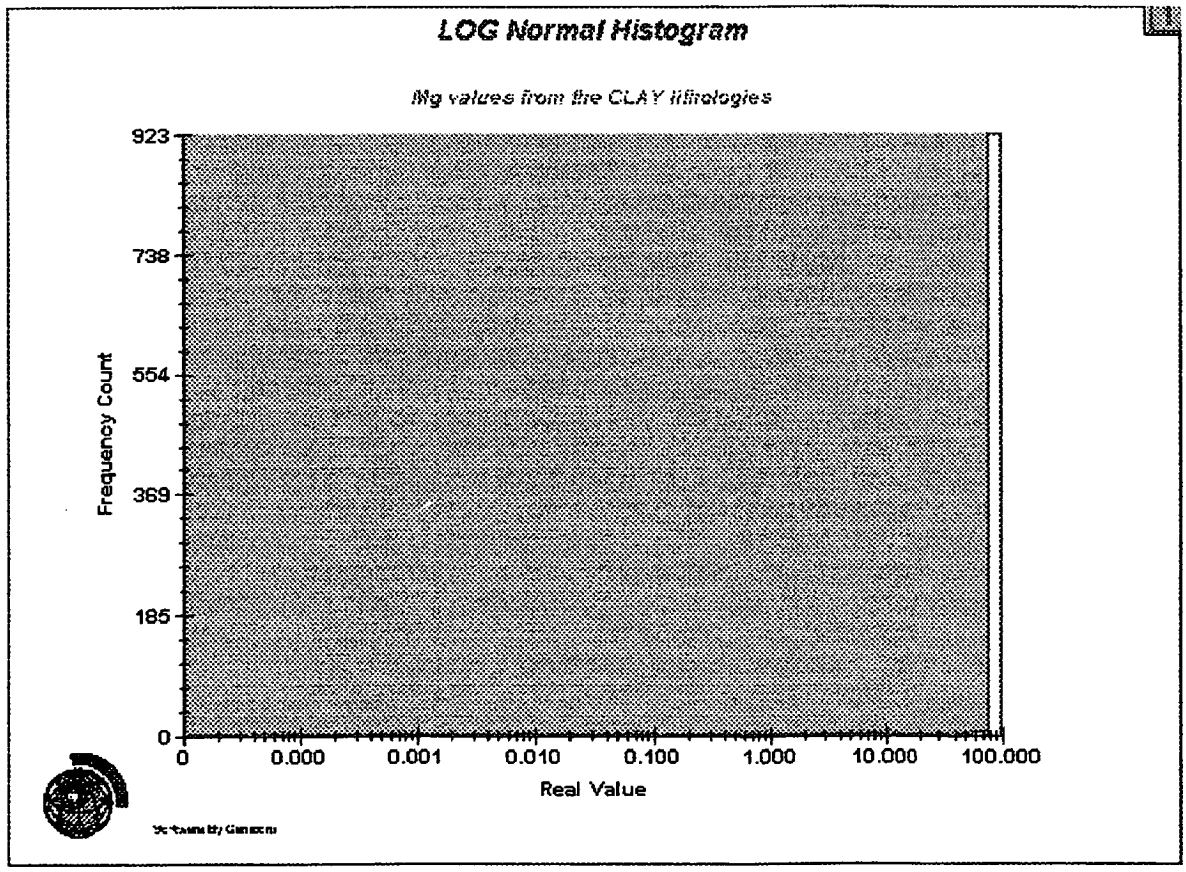

5.2 Silica

Summary statistics for the silica assay results by lithology are shown in Table 5-2.

	SAND		SILT		CLAY	
Maximum SiO_2 value	12.7		18.6		17.89	
Minimum SiO_2 value	0		0		0	
Number of Samples ≤ 0	1847		1924		108	
Total Population	5235		3288		931	
	Un-grouped	Grouped	Un-grouped	Grouped	Un-grouped	Grouped
Mean	1.52	1.56	1.48	1.58	3.54	3.57
Median	N/A	1.35	N/A	0.31	N/A	3.17
Geometric Mean	N/A	N/A	N/A	N/A	N/A	N/A
Natural LOG Mean	N/A	N/A	N/A	N/A	N/A	N/A
Standard Deviation	1.61	1.57	2.26	2.20	2.59	2.56
Variance	2.61	2.48	5.15	4.84	6.71	6.58
LOG Variance	N/A	N/A	N/A	N/A	N/A	N/A
Coefficient of Variation	1.06	1.00	1.53	1.38	0.73	0.71
Coefficient of Skewness	1.54	1.65	1.94	2.04	1.26	1.32
Coefficient of Kurtosis	7.13	7.61	8.02	8.59	6.01	6.11

Table 5.2 Silica Summary Statistics by Lithology

The silica data distributions still display a slight positive skew, and a mixed sample population, as evidenced by Figures 5-7 to 5-12, which are normal and log normal histogram plots for sand, silt and clay lithologies respectively.

Silica distribution is apparently independent of the lithology type. Given the interpreted deposit formation conditions, the silica would have been primarily in solution, precipitating only as isolated pockets of amorphous material when pH conditions were favourable, and the major control on the location of the silica would be the location of the water table.

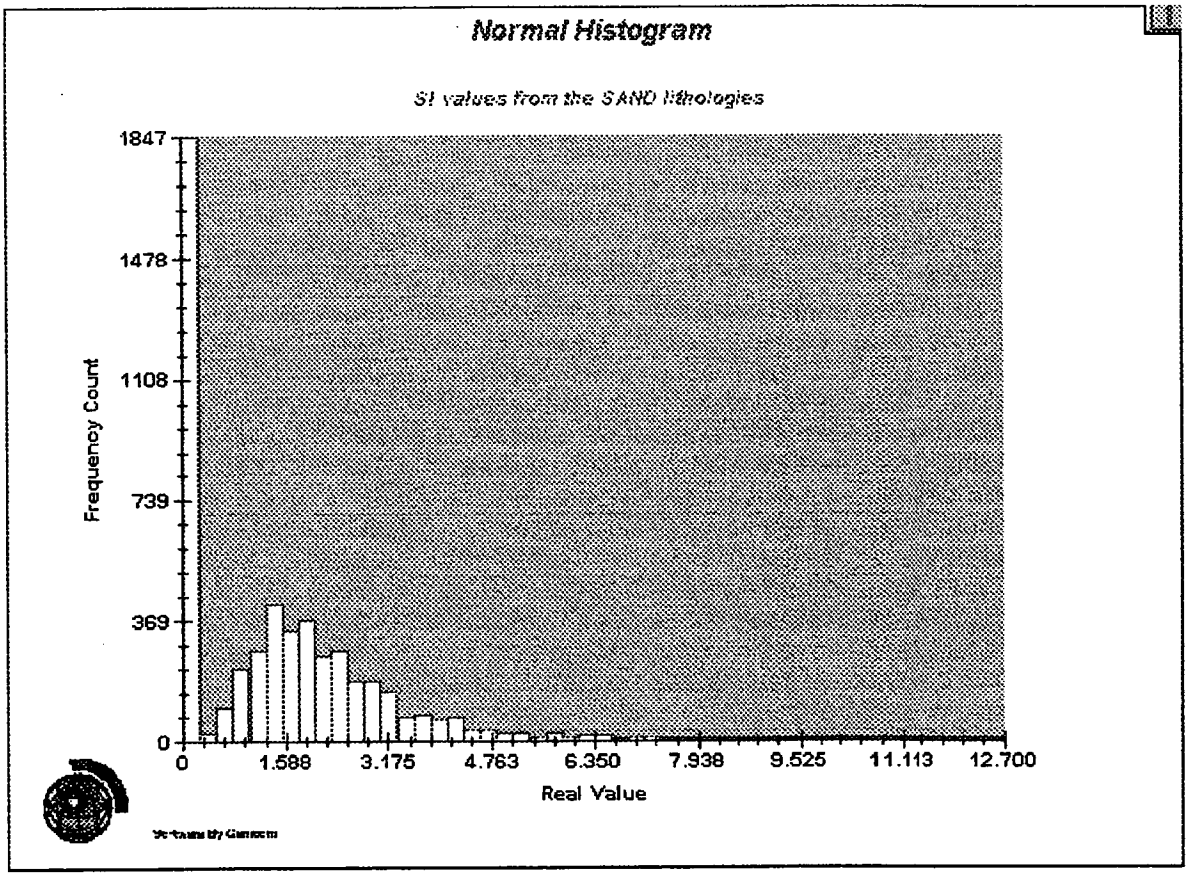

Figure 5-7 Normal Histogram, Silica Distribution – Sand

Figure 5-8 Log Normal Histogram, Silica Distribution – Sand

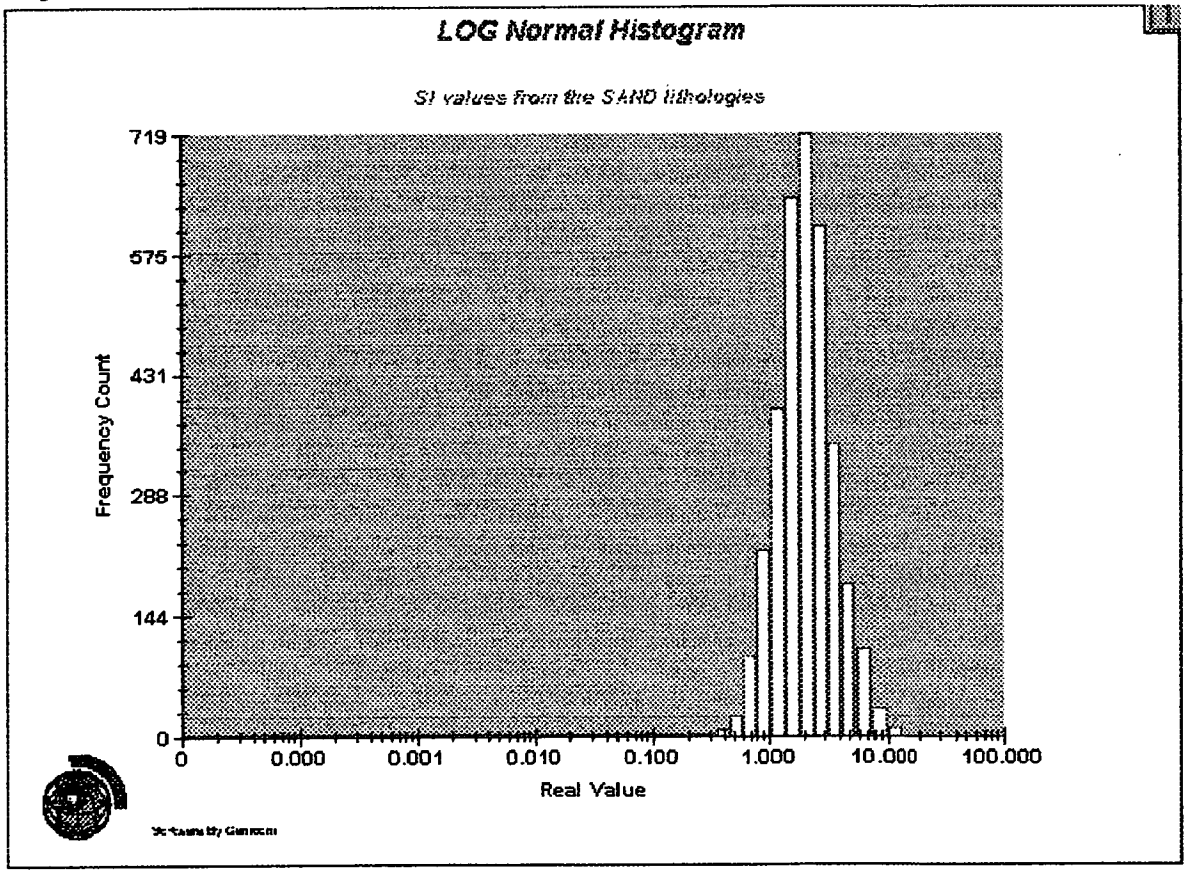

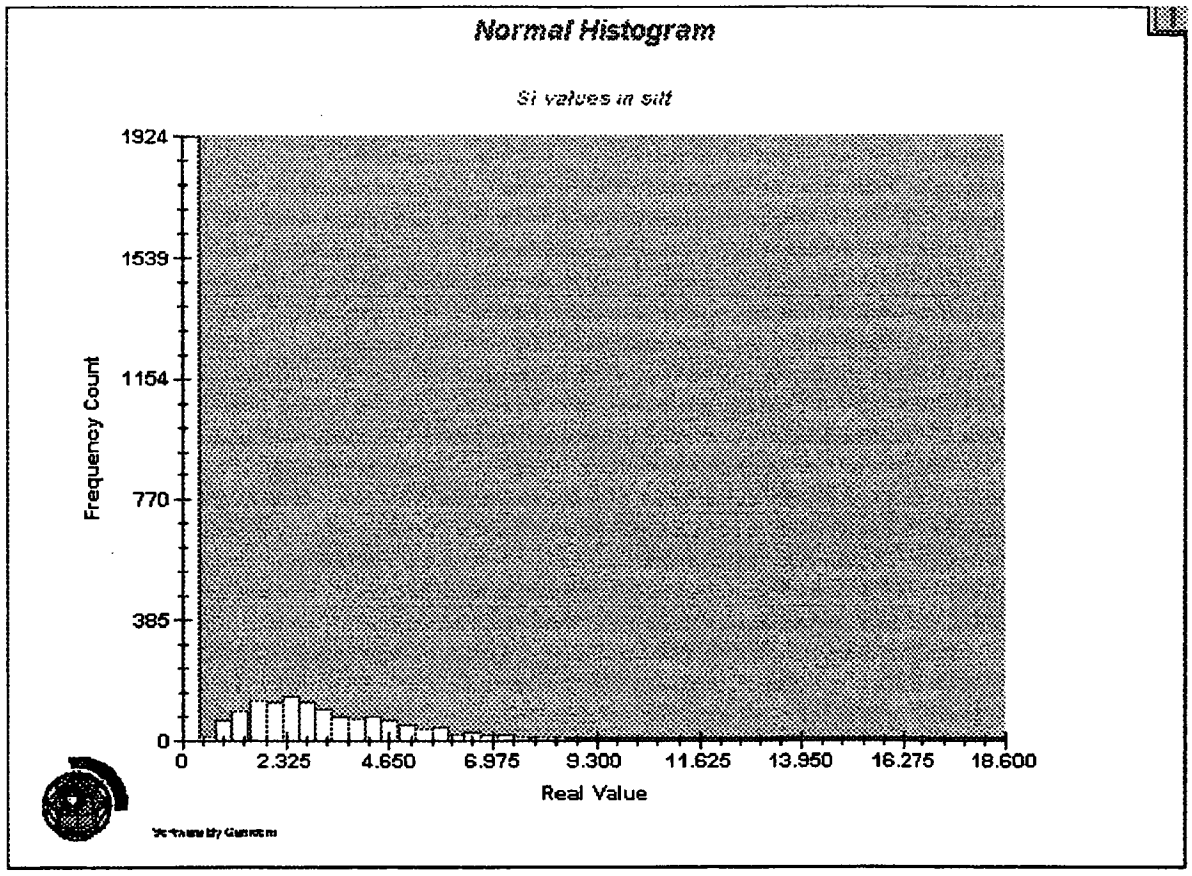

Figure 5-9 Normal Histogram, Silica Distribution – Silt

Figure 5-10 Log Normal Histogram, Silica Distribution – Silt

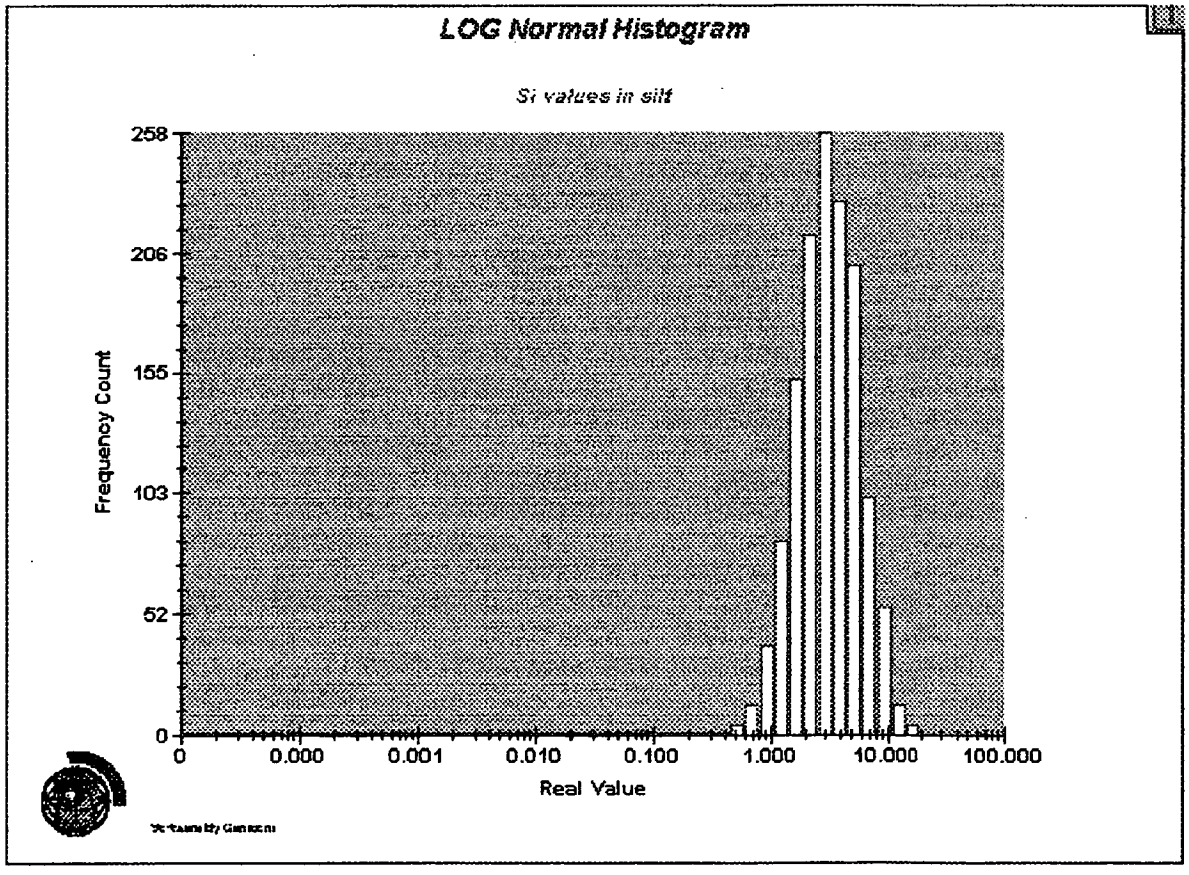

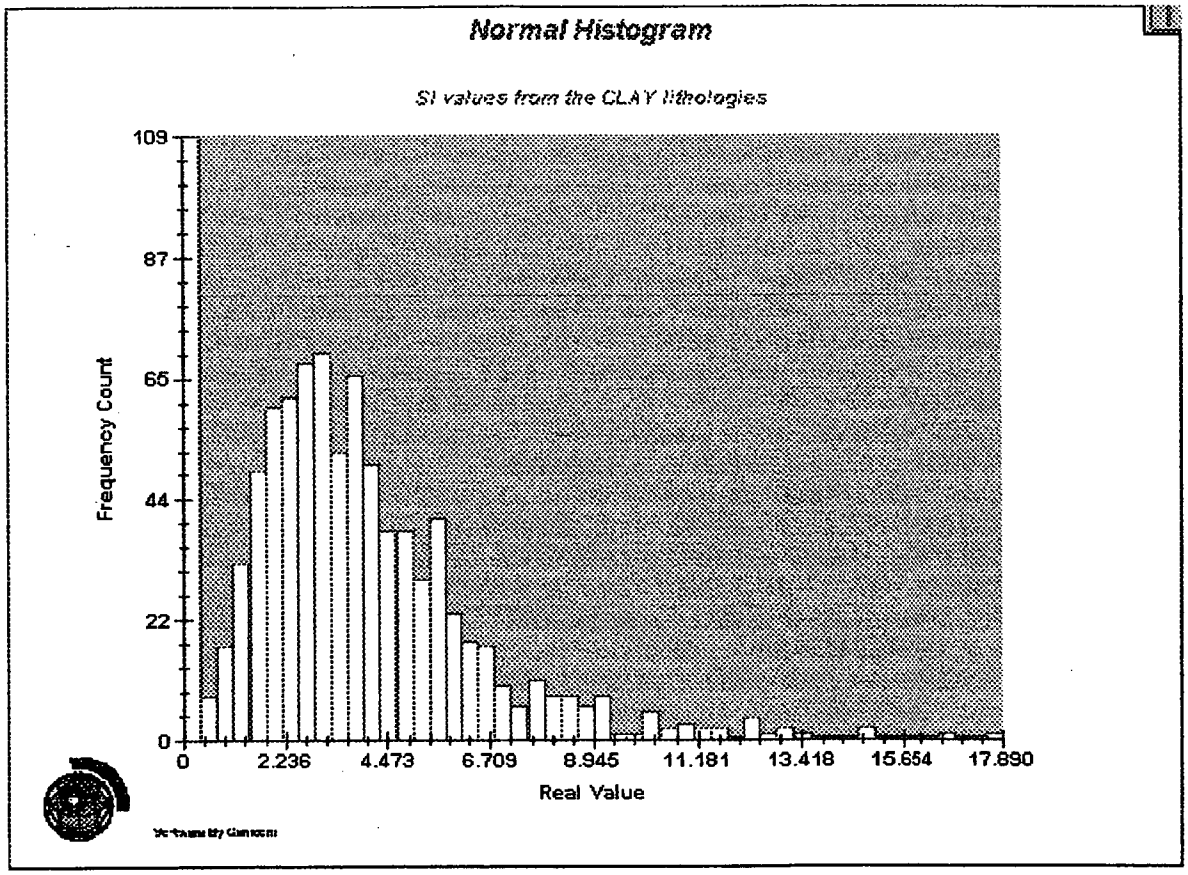

Figure 5-11 Normal Histogram, Silica Distribution – Clay

Figure 5-12 Log Normal Histogram, Silica Distribution, - Clay

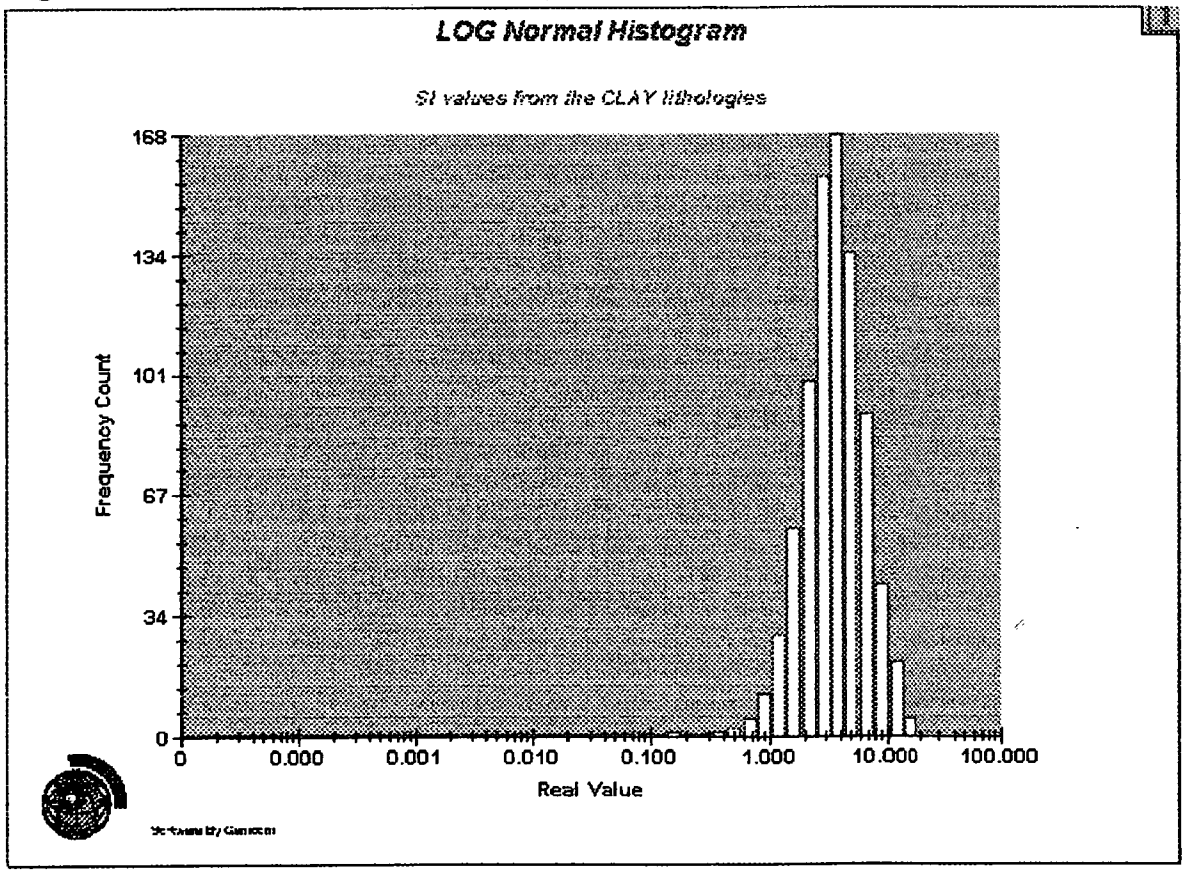

5.3 Manganese

Summary statistics for the manganese assays are shown in Table 5-3.

	SAND		SILT		CLAY	
Maximum MgO value	17.00		15		8	
Minimum MgO value	1.69		0		0	
Number of Samples ≤ 0	0		2		22	
Total Population	4498		3289		926	
	Un-grouped	Grouped	Un-grouped	Grouped	Un-grouped	Grouped
Mean	8.44	8.46	4.34	4.29	2.16	2.15
Median	N/A	8.74	N/A	4.06	N/A	1.97
Geometric Mean	7.98	8.00	N/A	N/A	N/A	N/A
Natural LOG Mean	2.07	2.07	N/A	N/A	N/A	N/A
Standard Deviation	2.68	2.67	2.09	2.09	1.34	1.32
Variance	7.19	7.14	4.39	4.39	1.80	1.76
LOG Variance	0.12	0.12	N/A	N/A	N/A	N/A
Coefficient of Variation	0.31	0.31	0.48	0.48	0.62	0.61
Coefficient of Skewness	0.04	0.02	0.84	0.84	1.08	1.12
Coefficient of Kurtosis	2.14	2.15	3.90	3.90	4.23	4.35

Table 5.3 Manganese Summary Statistics by Lithology

Histogram and log normal histogram plots for manganese are shown in Figures 5-13 to 5-18.

Manganese in silt and clay lithologies is again a mixed sample population, with a very small positive skew. The samples are approaching a log normal distribution in the sand component.

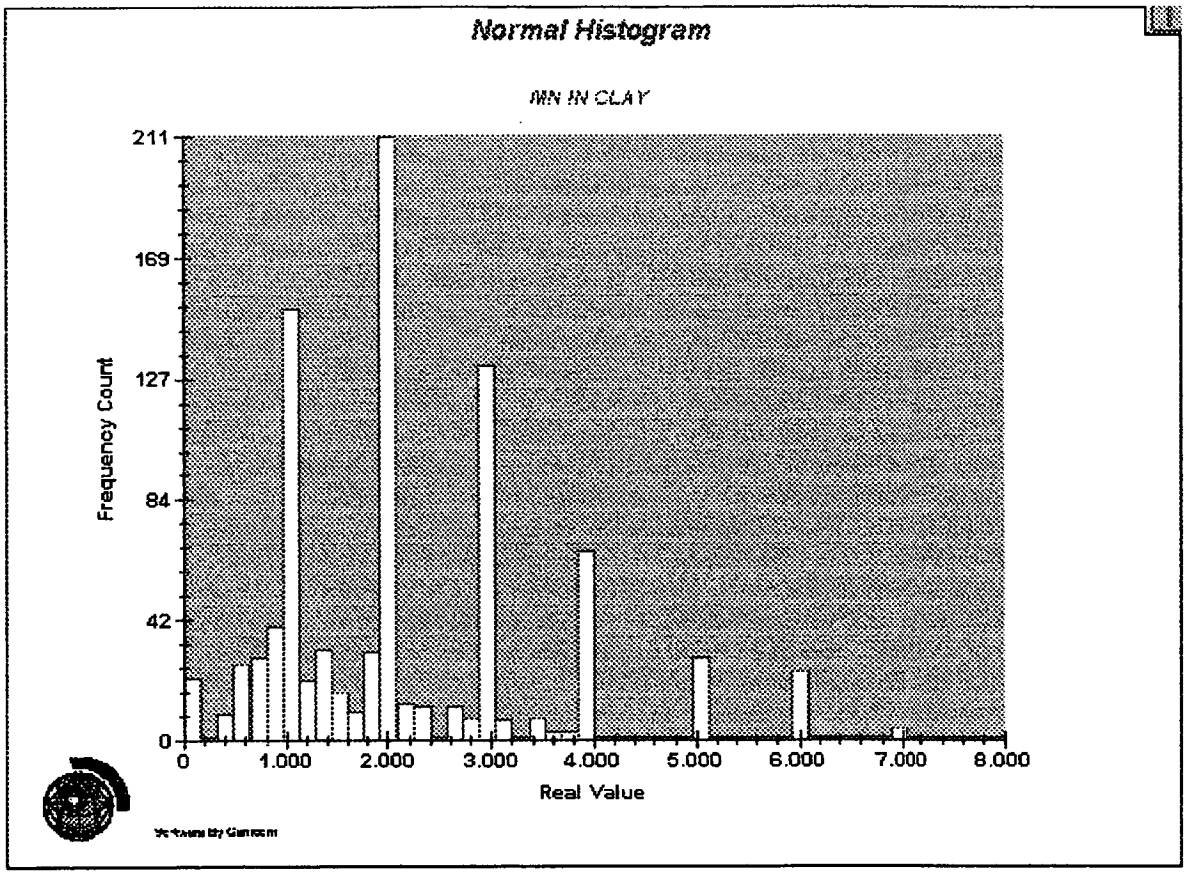

Figure 5-13 Normal Histogram, Manganese Distribution – Sand

Figure 5-14 Log Normal Histogram, Manganese Distribution – Sand

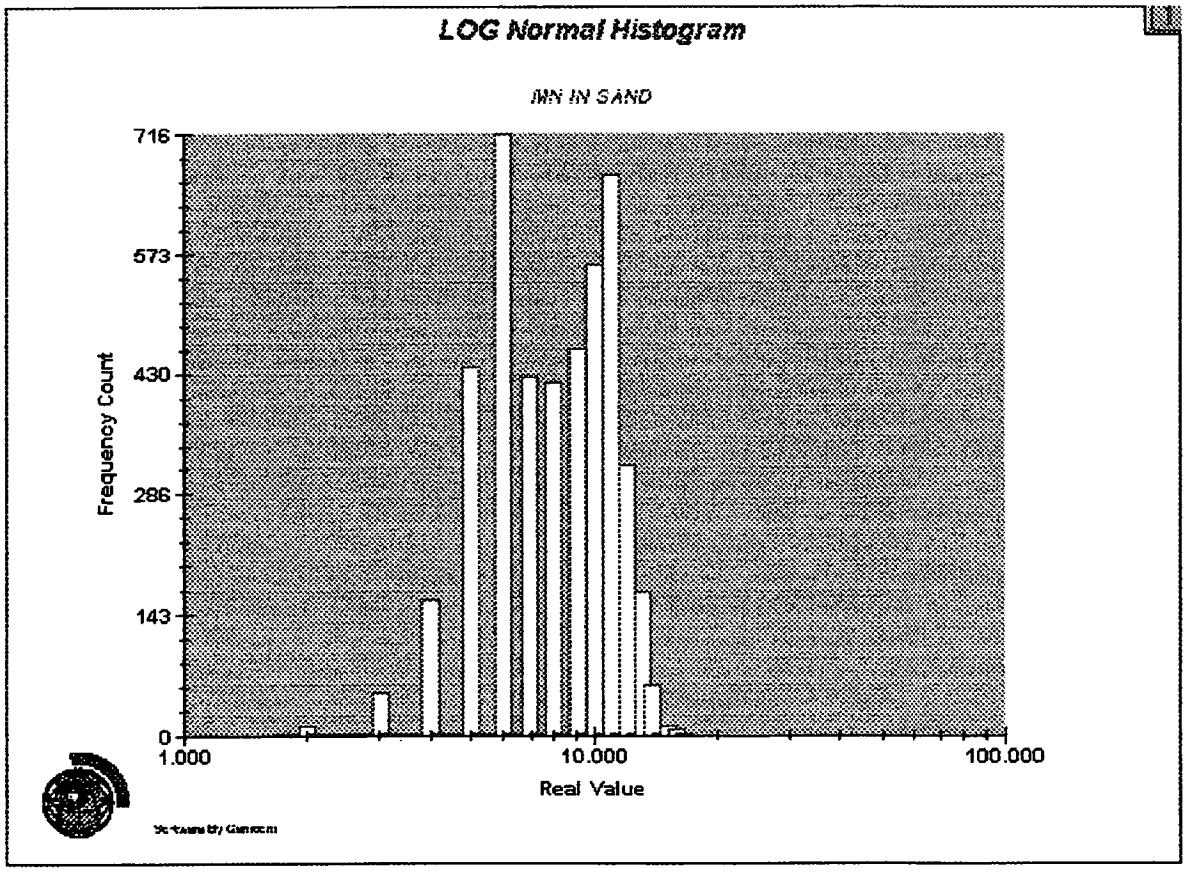

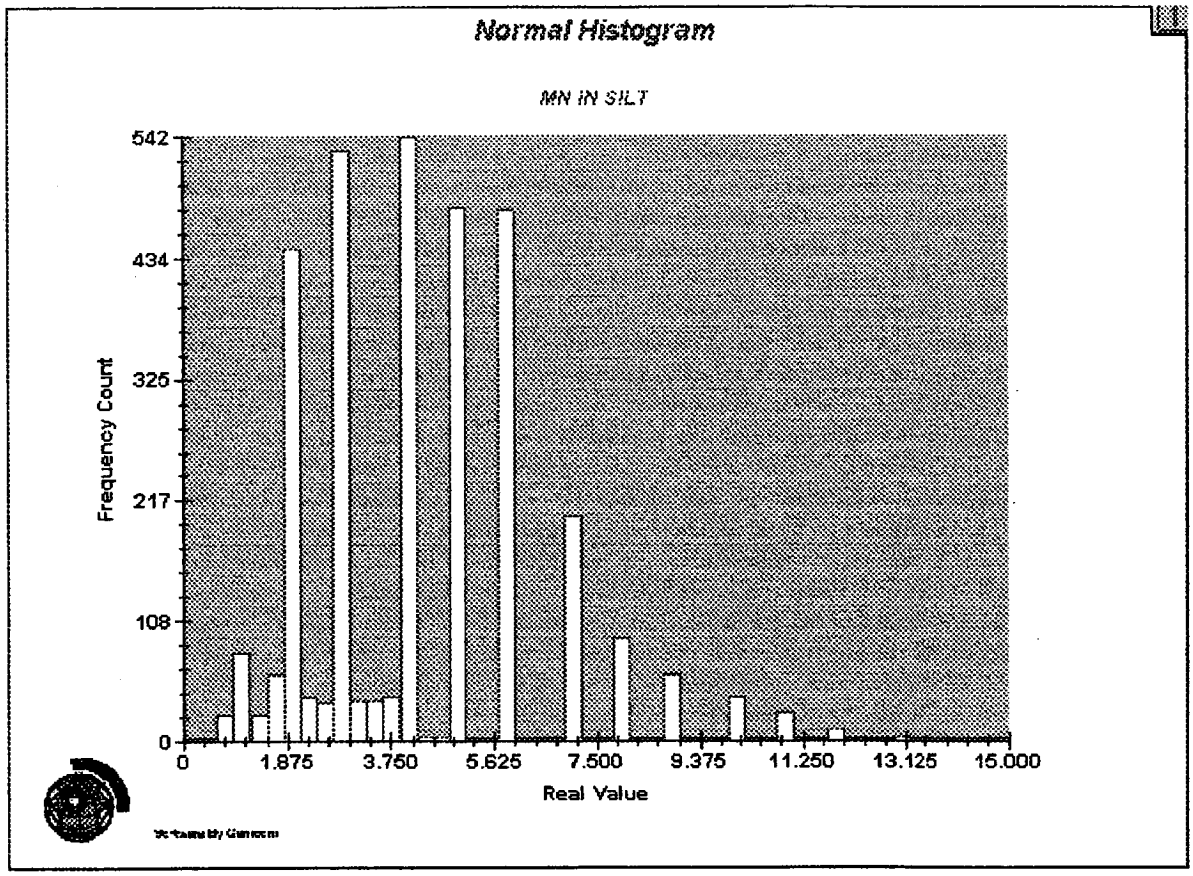

Figure 5-15 Normal Histogram, Manganese Distribution – Silt

Figure 5-16 Log Normal Histogram, Manganese Distribution - Silt

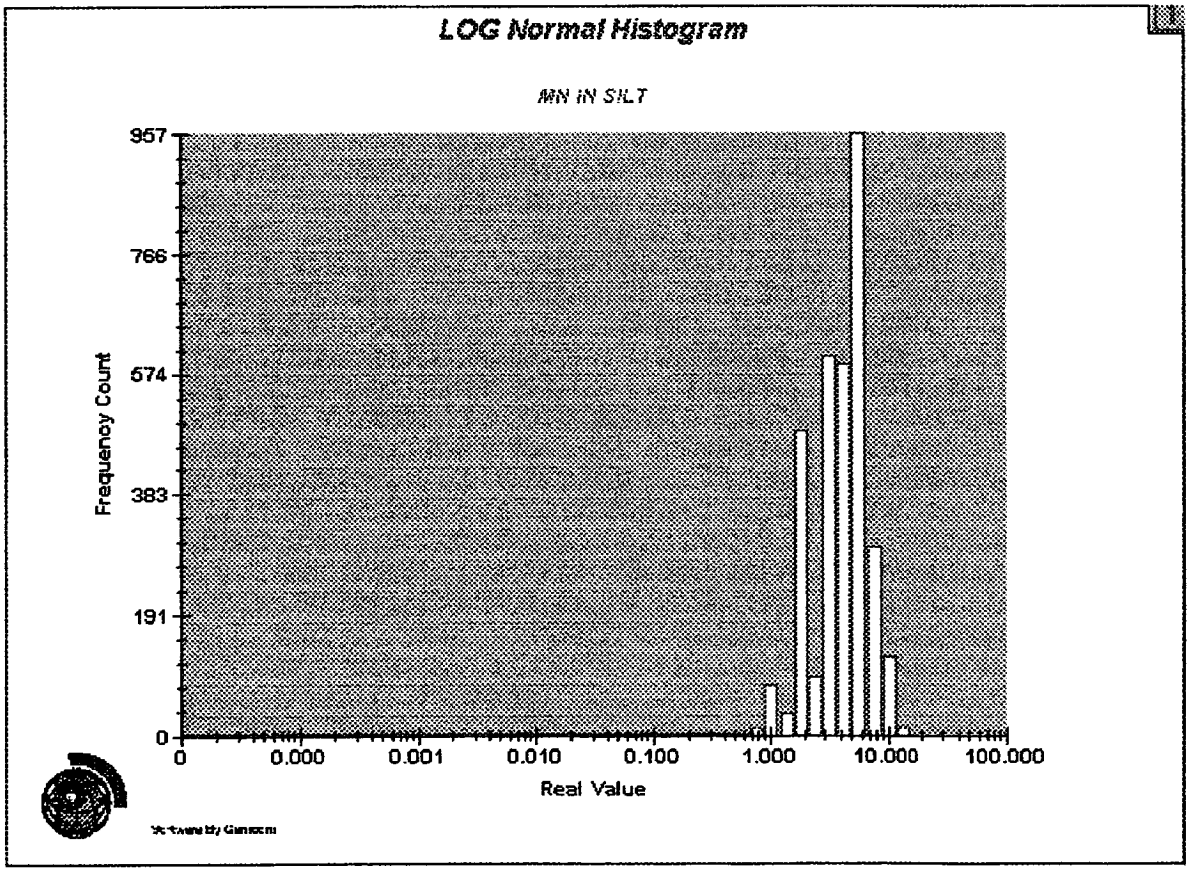

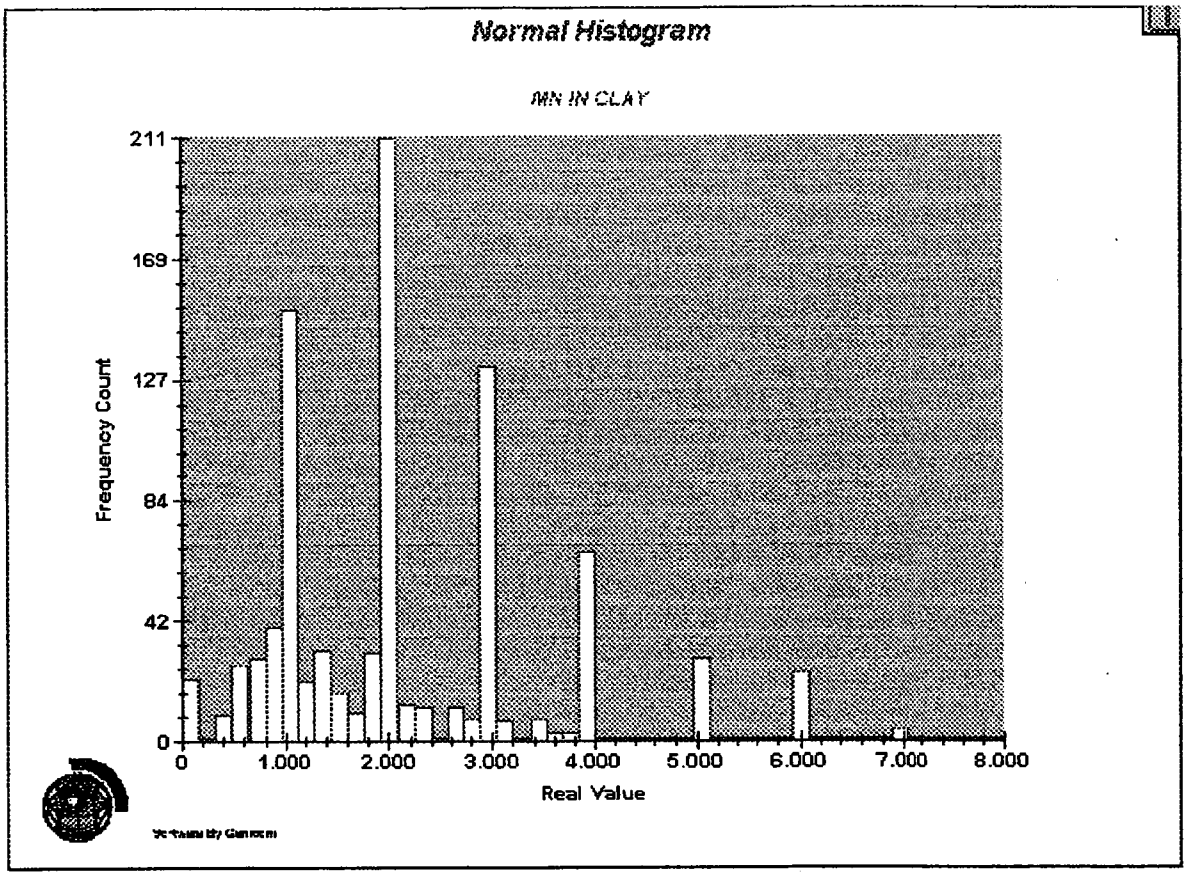

Figure 5-17 Normal Histogram, Manganese Distribution – Clay

Figure 5-18 Log Normal Histogram, Manganese Distribution - Clay

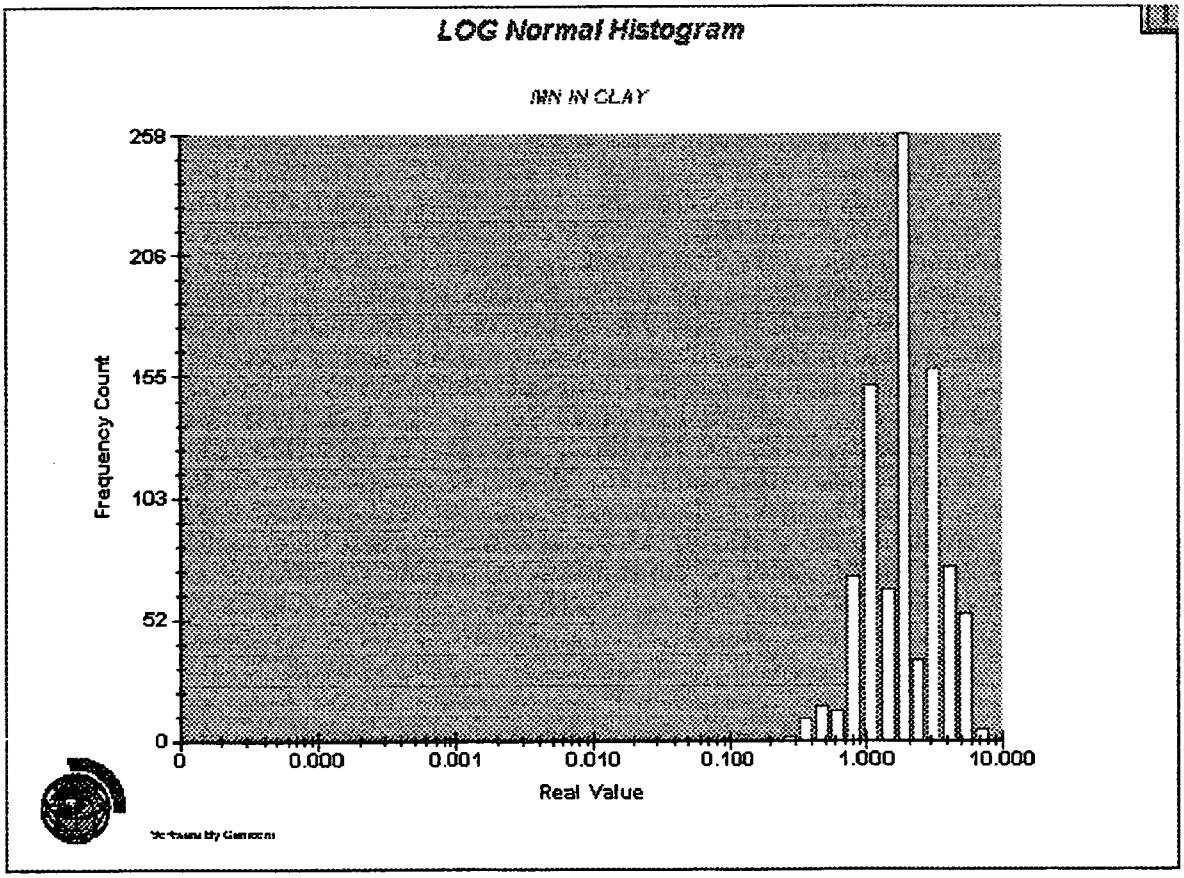

5.4 Iron

Summary statistics for iron by lithology are shown in Table 5-4.

	SAND		SILT		CLAY	
Maximum MgO value	17		15		8	
Minimum MgO value	0.99		0		0	
Number of Samples ≤ 0	0		2		22	
Total Population	5089		3291		929	
	Un-grouped	Grouped	Un-grouped	Grouped	Un-grouped	Grouped
Mean	8.36	8.35	4.34	4.29	2.16	2.15
Median	N/A	8.00	N/A	4.06	N/A	1.97
Geometric Mean	7.86	7.85	N/A	N/A	N/A	N/A
Natural LOG Mean	2.06	2.06	N/A	N/A	N/A	N/A
Standard Deviation	2.75	2.77	2.09	2.09	1.34	1.32
Variance	7.60	7.72	4.38	4.39	1.79	1.76
LOG Variance	0.13	0.13	N/A	N/A	N/A	N/A
Coefficient of Variation	0.32	0.33	0.48	0.48	0.61	0.61
Coefficient of Skewness	0.05	0.08	0.84	0.84	1.08	1.12
Coefficient of Kurtosis	2.20	2.11	3.90	3.90	4.22	4.34

Table 5-4 Iron Summary Statistics by Lithology

The iron distribution has a very small positive skew in each lithology. Samples approach a log normal distribution in the sand fraction, but also strongly indicate two different sample populations. These may reflect two different mineral types, such as goethite or haematite.

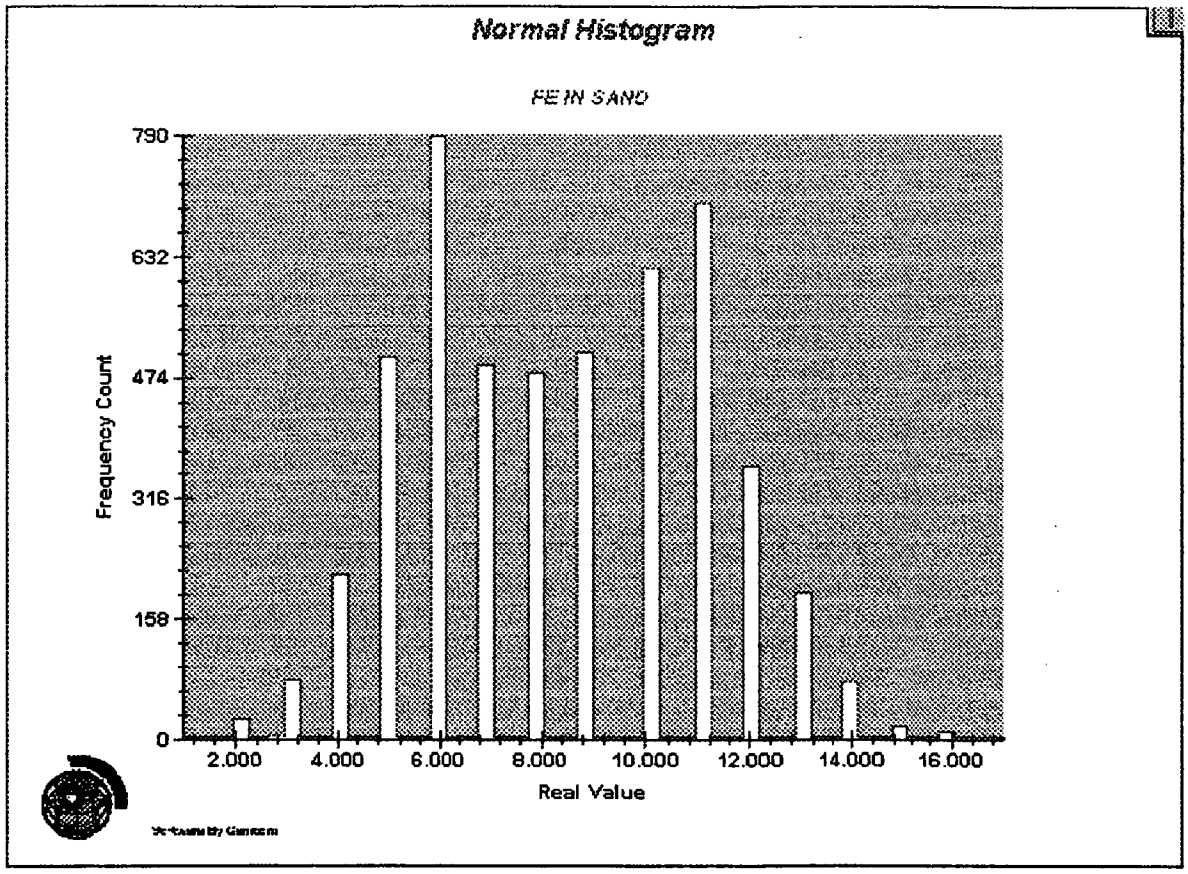

Figure 5-19 Normal Histogram, Iron Distribution – Sand

Figure 5-20, Log Normal Histogram, Iron Distribution, - Sand

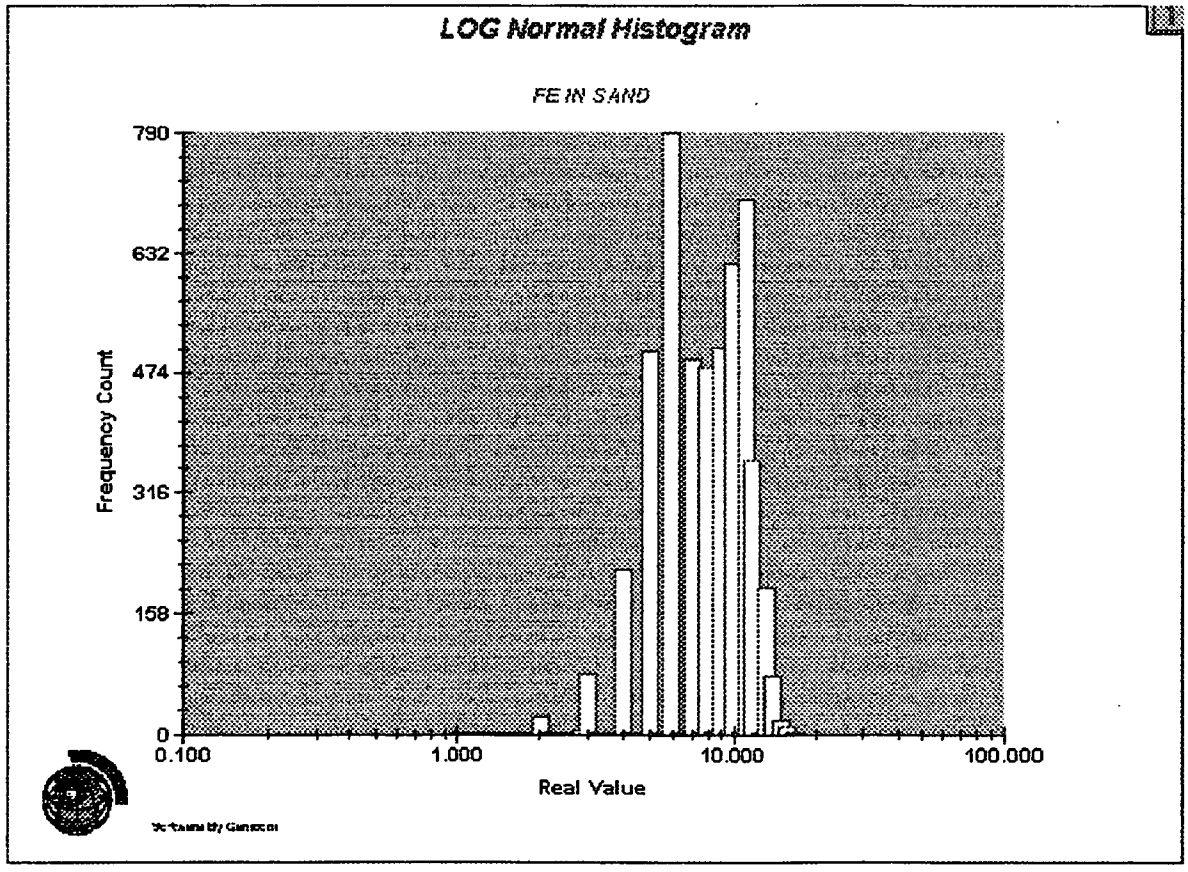

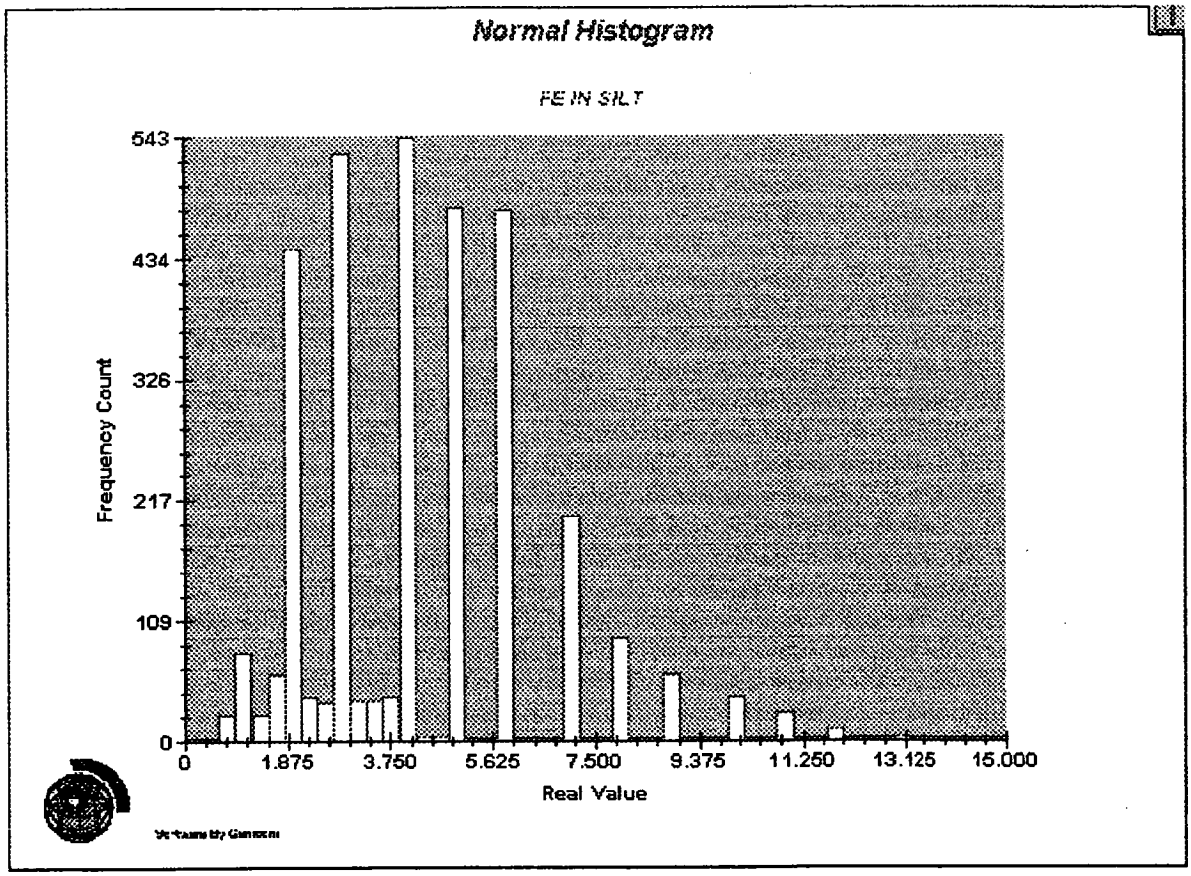

Figure 5-21 Normal Histogram, Iron Distribution – Silt

Figure 5-22 Log Normal Histogram, Iron Distribution – Silt

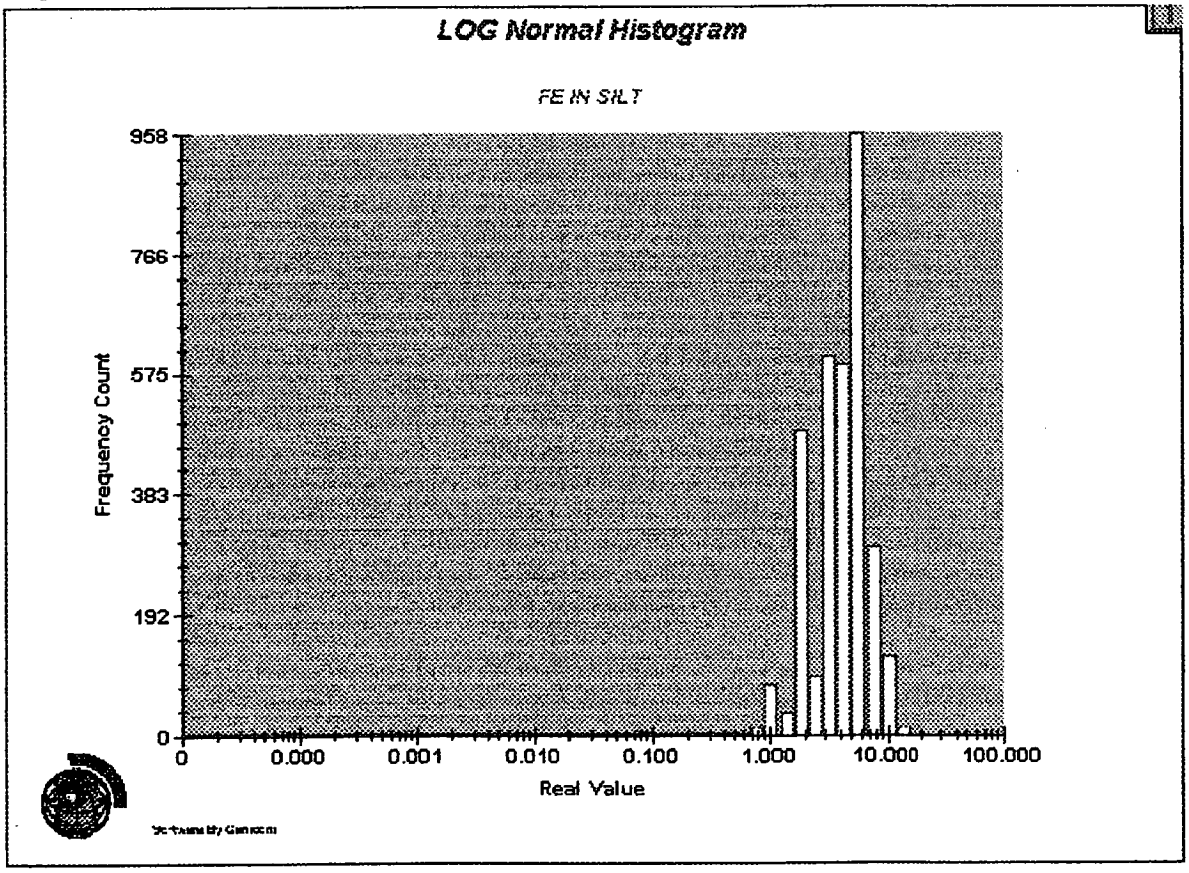

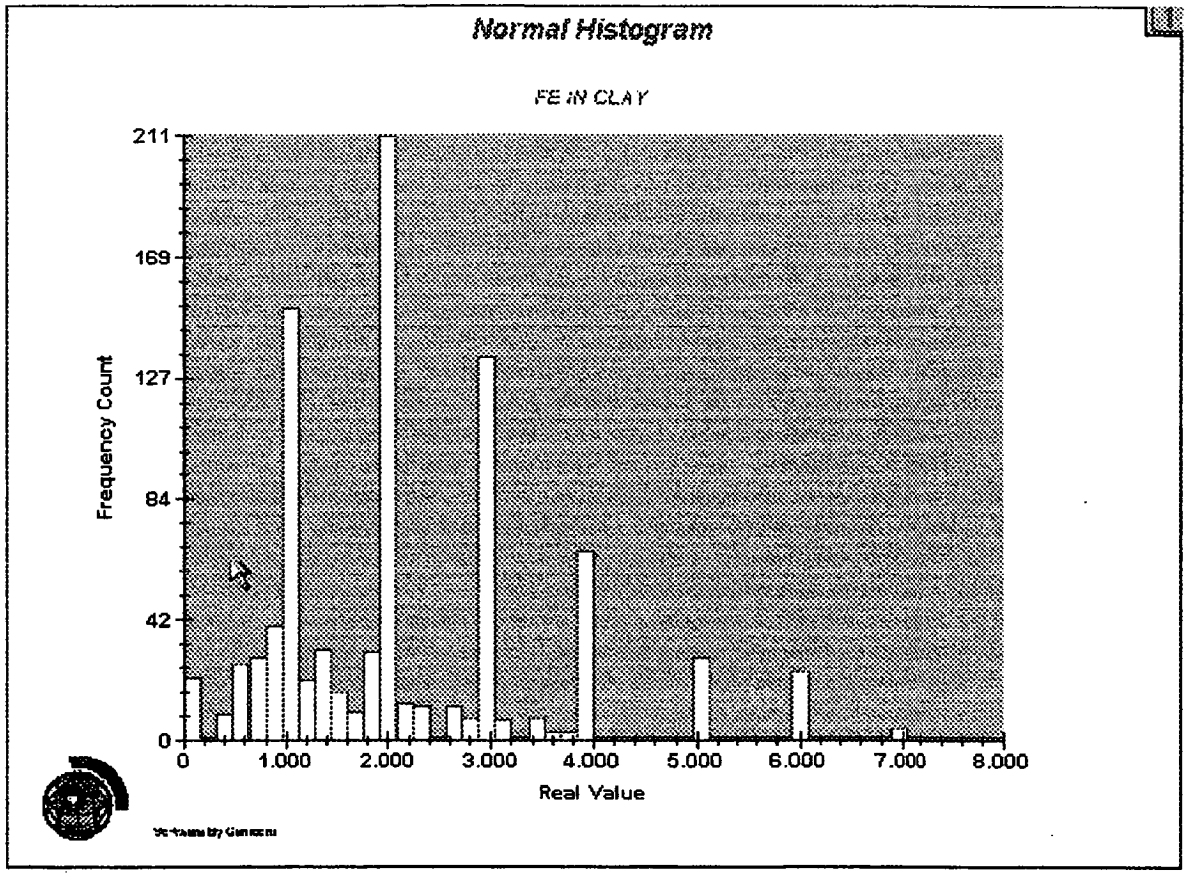

Figure 5-23 Normal Histogram, Iron Distribution – Clay

Figure 5-24 Log Normal Histogram, Iron Distribution – Clay

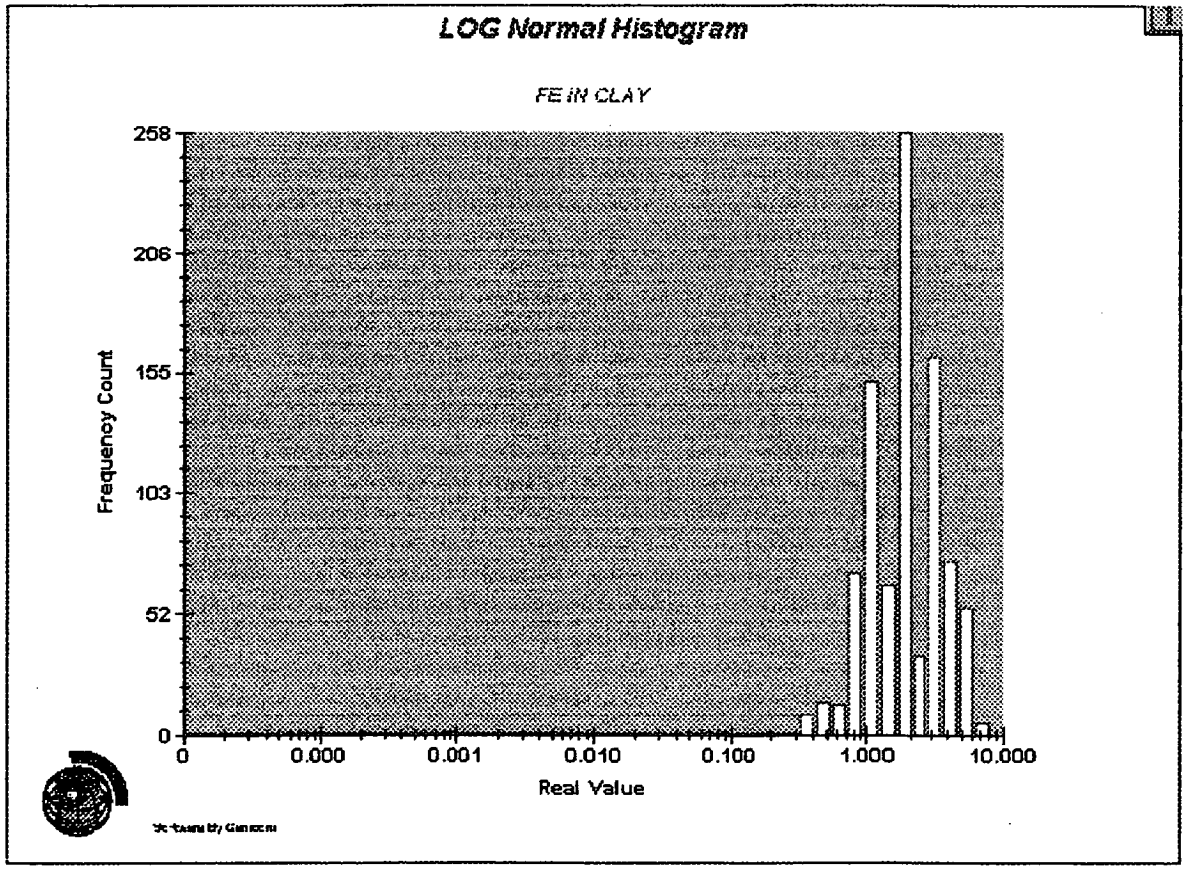

5.5 Calcium

Summary statistics for the calcium assays are presented in Table 5-5 by lithology.

	SAND		SILT		CLAY	
Maximum MgO value	35.2		33.79		35.9	
Minimum MgO value	0		0		0	
Number of Samples ≤ 0	1846		1924		108	
Total Population	5235		3288		931	
	Un-grouped	Grouped	Un-grouped	Grouped	Un-grouped	Grouped
Mean	3.41	3.53	2.17	2.37	3.32	3.37
Median	N/A	2.59	N/A	0.57	N/A	2.65
Geometric Mean	N/A	N/A	N/A	N/A	N/A	N/A
Natural LOG Mean	N/A	N/A	N/A	N/A	N/A	N/A
Standard Deviation	4.21	4.11	3.82	3.71	3.14	3.09
Variance	17.73	16.95	14.59	13.76	9.89	9.60
LOG Variance	N/A	N/A	N/A	N/A	N/A	N/A
Coefficient of Variation	1.23	1.16	1.75	1.56	0.94	0.91
Coefficient of Skewness	2.35	2.49	2.87	3.02	4.03	4.13
Coefficient of Kurtosis	11.29	12.06	13.77	14.77	29.26	29.77

Table 5-5 Calcium Summary Statistics by Lithology

The calcium distributions are positively skewed in each lithology, and have a long high grade assay tail. Sample distribution does not appear to be primarily related to lithology, and thus may reflect basement rocktype trends or fluctuations in pH during nodule and calcrete formation.

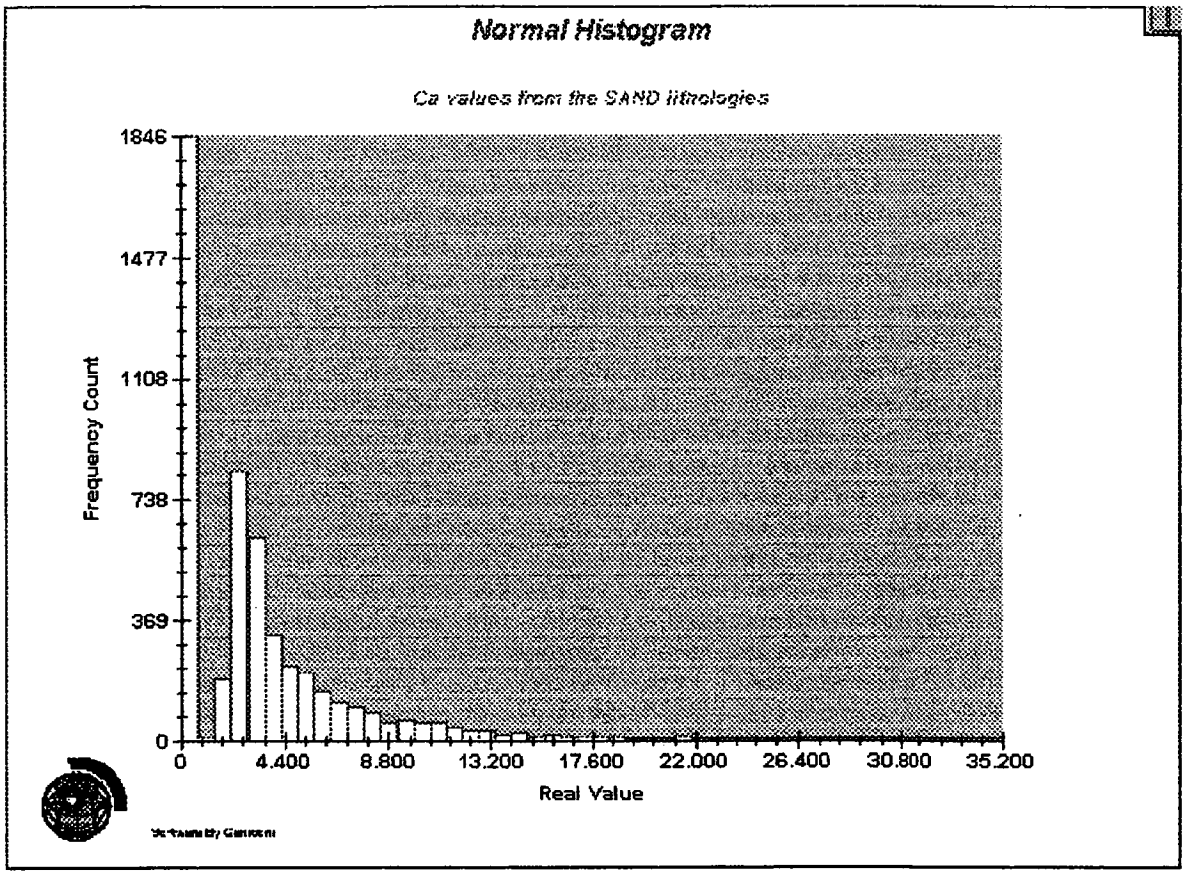

Figure 5-25 Normal Histogram, Calcium Distribution – Sand

Figure 5-26 Log Normal Histogram, Calcium Distribution – Sand

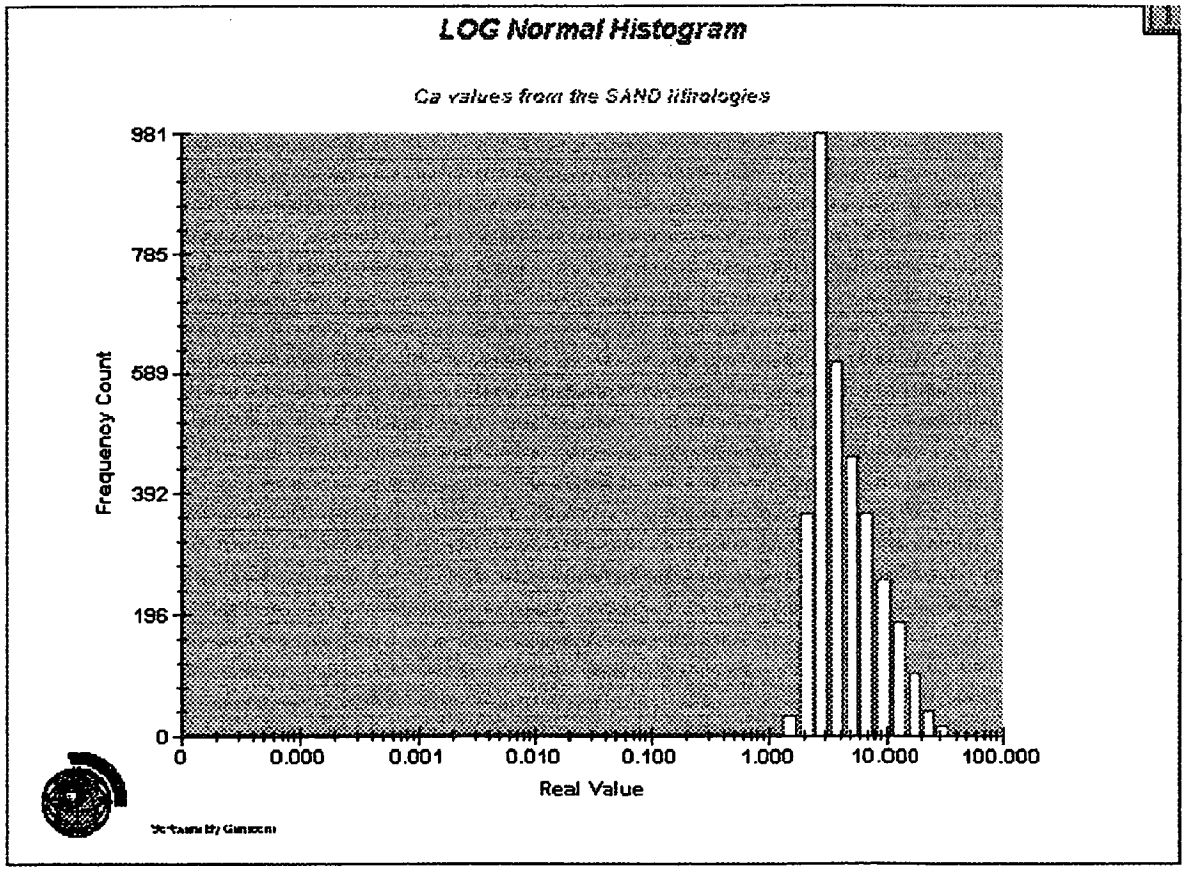

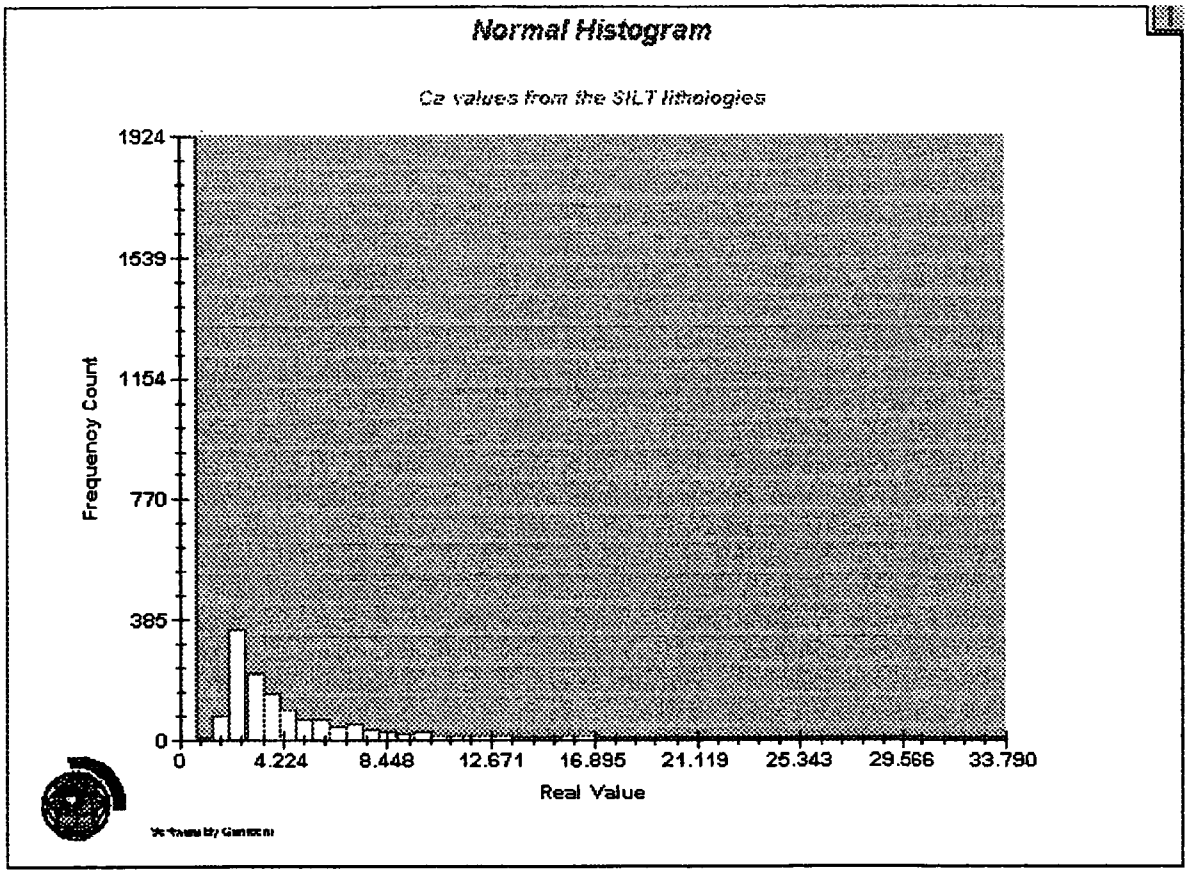

Figure 5-27 Normal Histogram, Calcium Distribution – Silt

Figure 5-28 Log Normal Histogram, Calcium Distribution – Silt

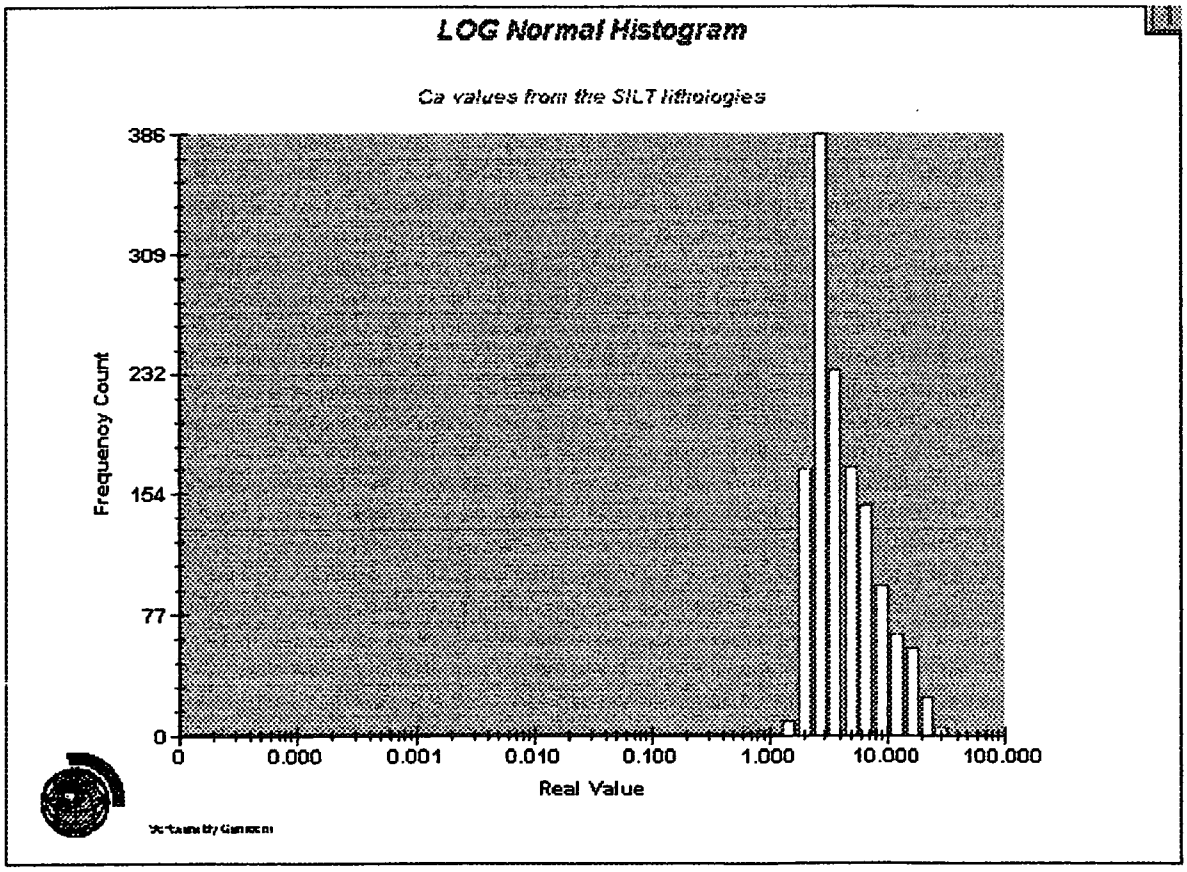

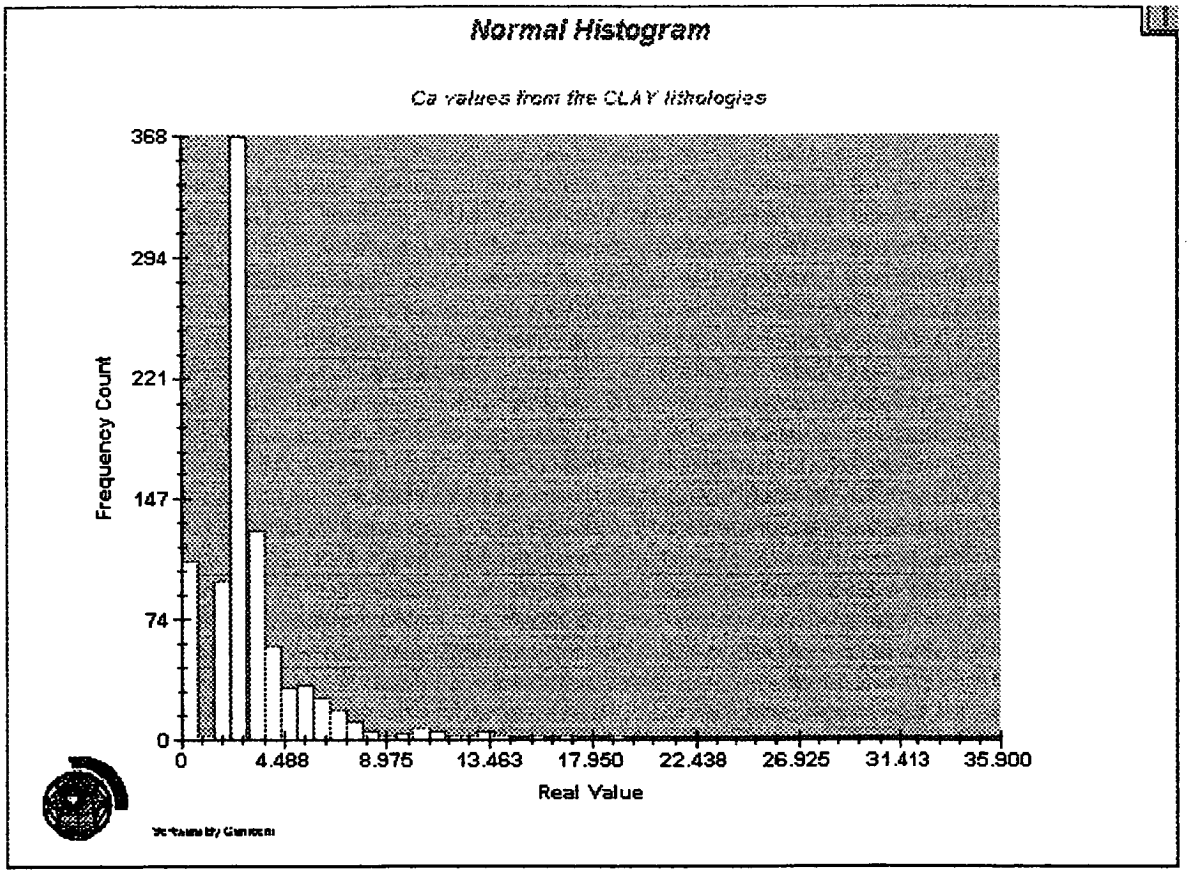

Figur3 5-29 Normal Histogram, Calcium Distribution – Clay

Figure 5-30 Log Normal Histogram, Calcium Distribution – Clay

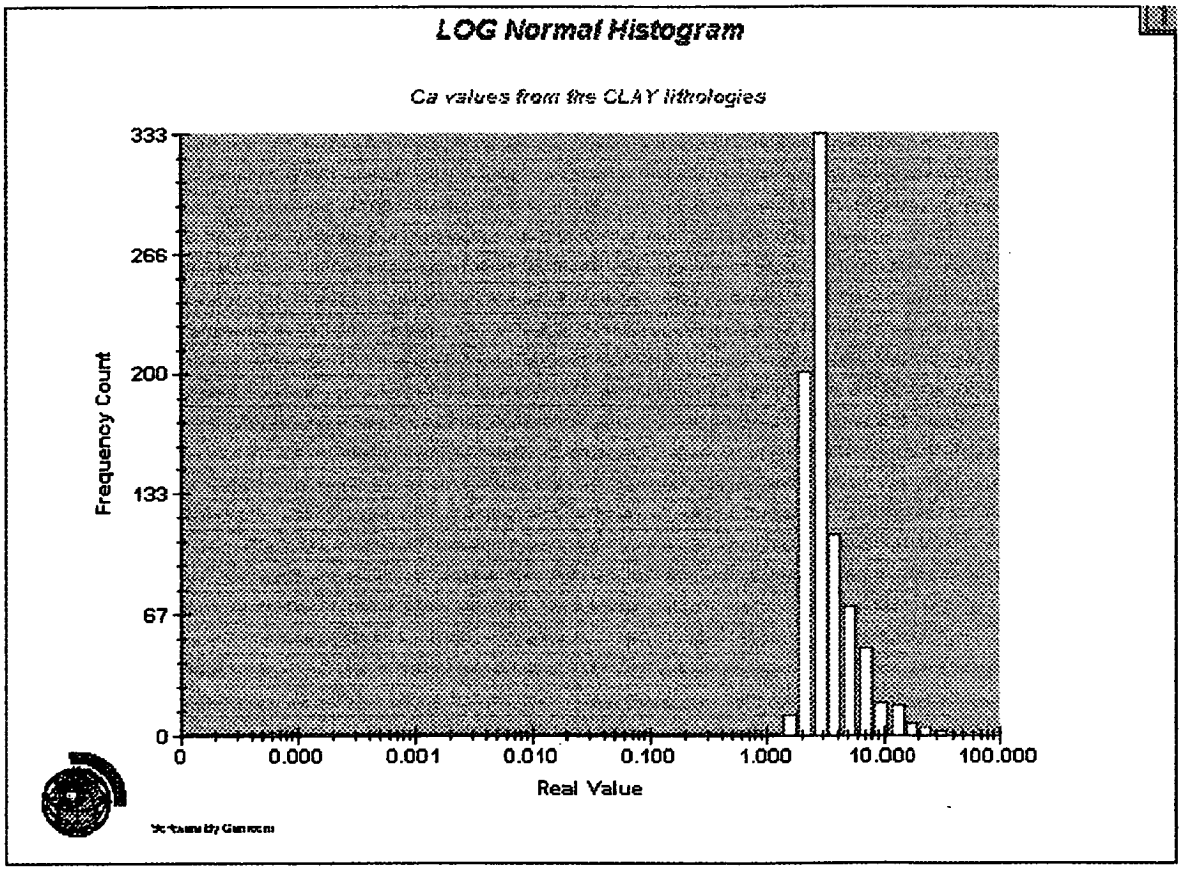

5-6 Aluminium

	SAND		SILT		CLAY	
Maximum MgO value	17.00		15.00		8.00	
Minimum MgO value	0.99		0		0	
Number of Samples ≤ 0	0		2		22	
Total Population	5152		3287		922	
	Un-grouped	Grouped	Un-grouped	Grouped	Un-grouped	Grouped
Mean	8.40	8.39	4.34	4.29	2.16	2.15
Median	N/A	8.01	N/A	4.06	N/A	1.97
Geometric Mean	7.90	7.88	N/A	N/A	N/A	N/A
Natural LOG Mean	2.06	2.06	N/A	N/A	N/A	N/A
Standard Deviation	2.76	2.78	2.09	2.09	1.33	1.31
Variance	7.63	7.75	4.39	4.39	1.77	1.73
LOG Variance	0.13	0.13	N/A	N/A	N/A	N/A
Coefficient of Variation	0.05	0.08	0.48	0.48	0.61	0.61
Coefficient of Skewness	2.21	2.12	0.84	0.84	1.06	1.10
Coefficient of Kurtosis	2.02	2.11	3.90	3.90	4.18	4.31

Table 5-6 Aluminium Summary Statistics by Lithology

The aluminium distribution shows a positive skew in all lithologies, and a mixed sample population. The samples are probably related to different clay types within the various lithologies.

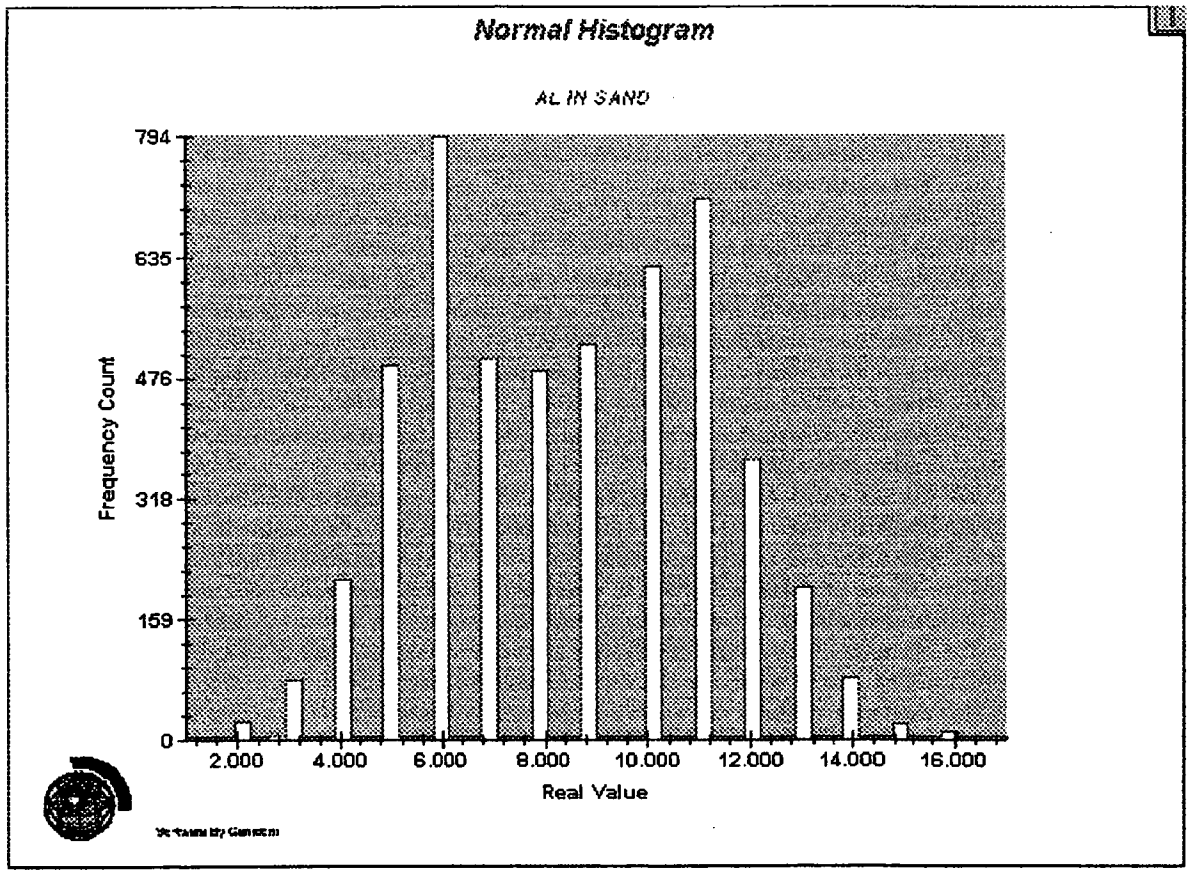

Figure 5-31 Normal Histogram, Aluminium Distribution – Sand

Figure 5-32 Log Normal Histogram, Aluminium Distribution – Sand

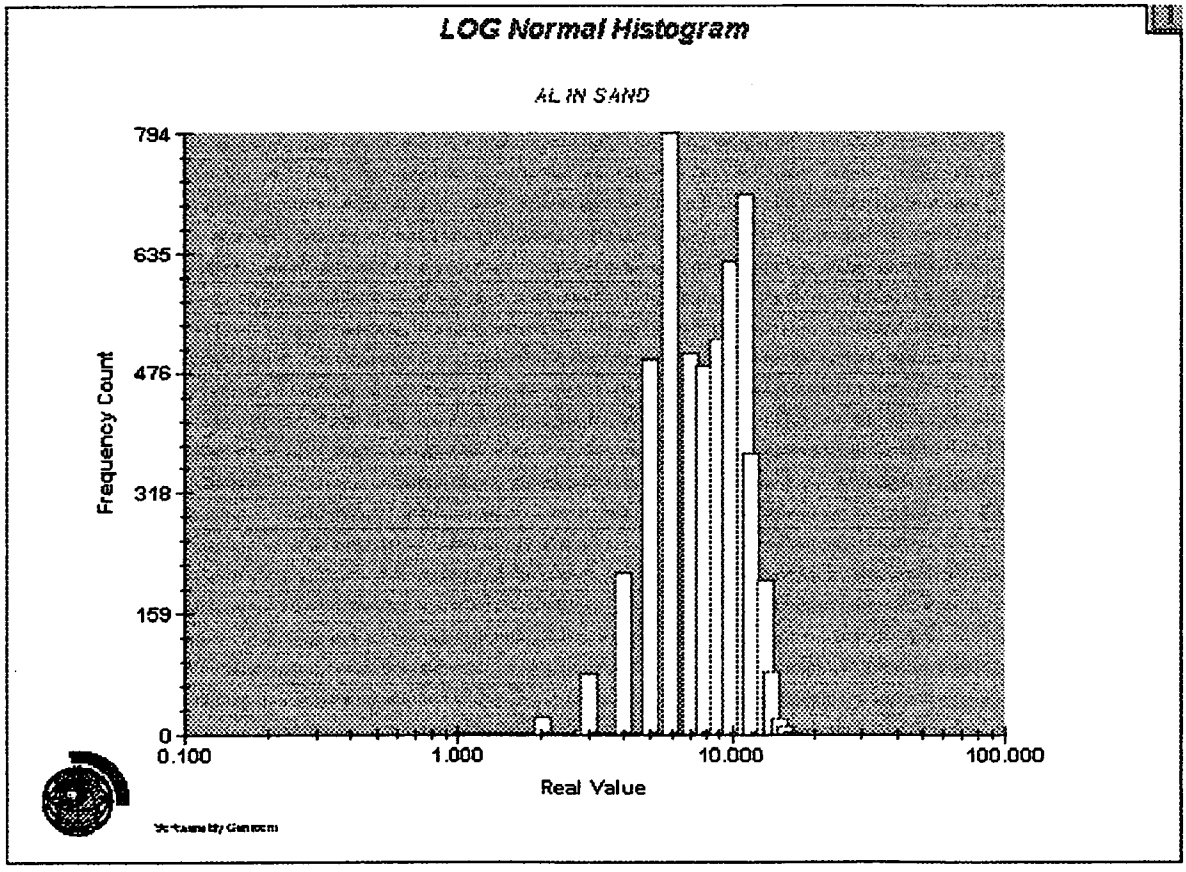

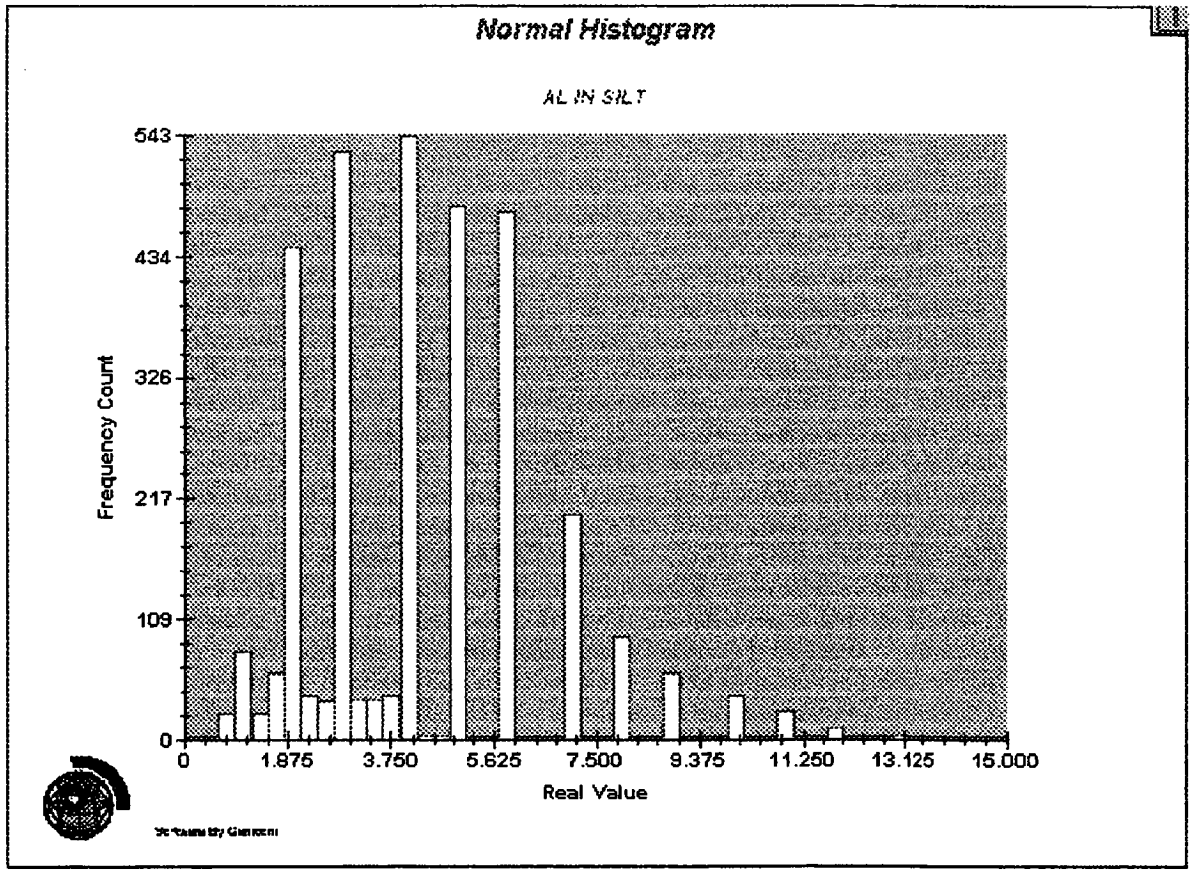

Figure 5-33 Normal Histogram, Aluminium Distribution – Silt

Figure 5-34 Log Normal Histogram, Aluminium Distribution – Silt

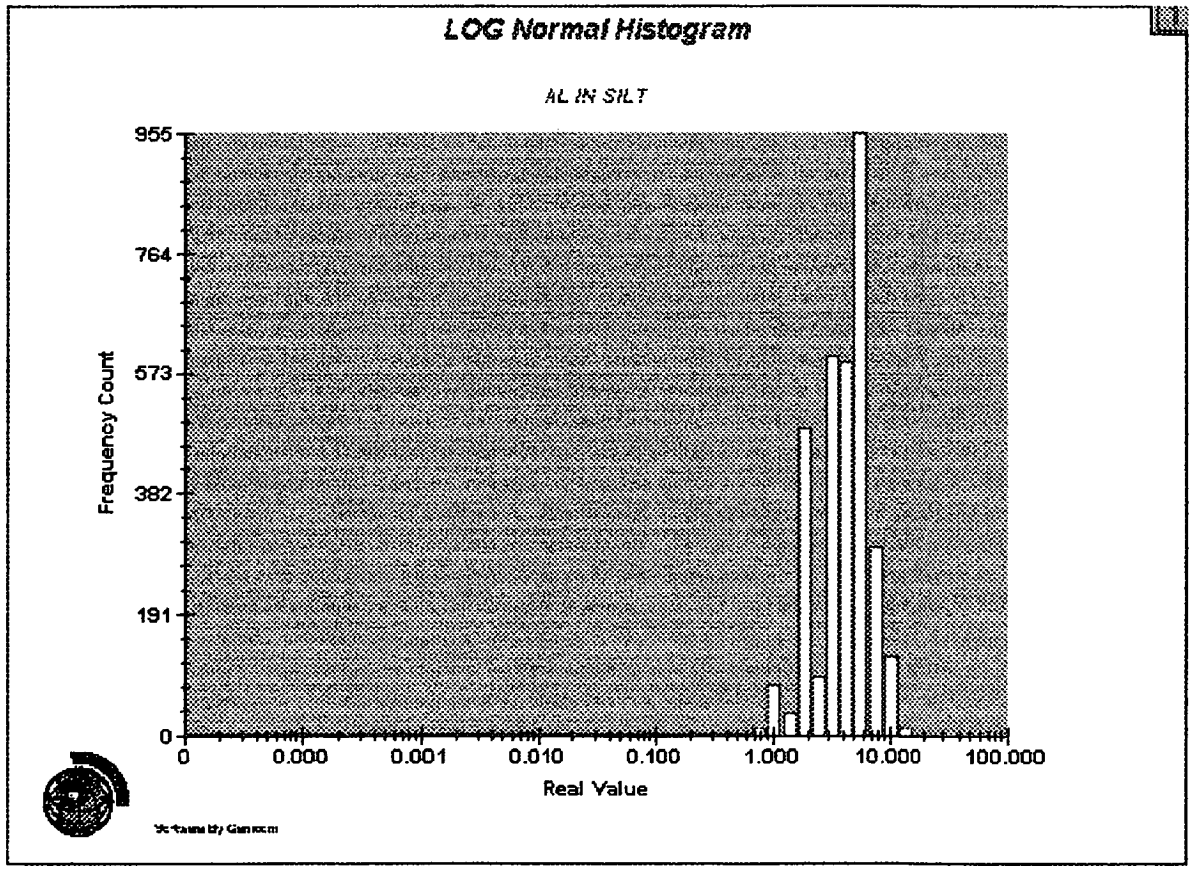

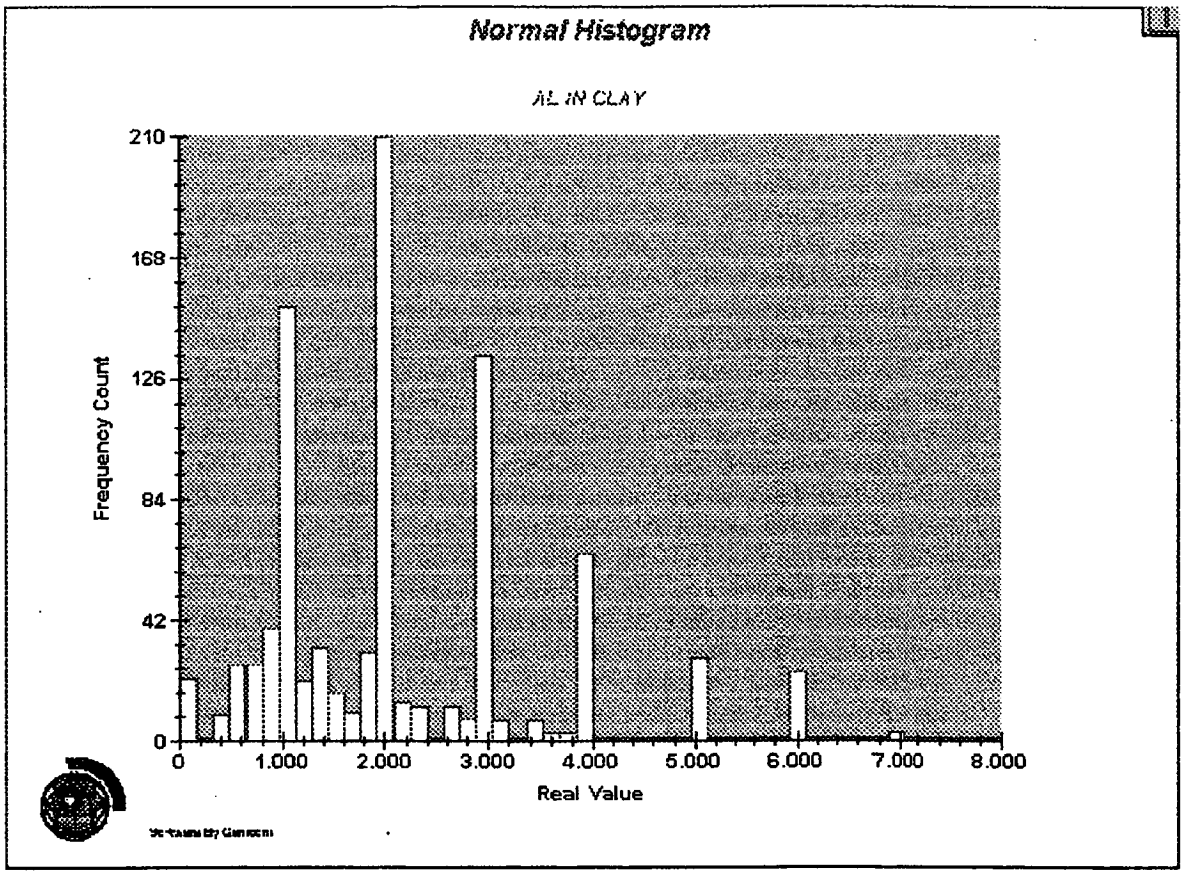

Figure 5-35 Normal Histogram, Aluminium Distribution – Clay

Figure 5-36 Log Normal Histogram, Aluminium Distribution – Clay

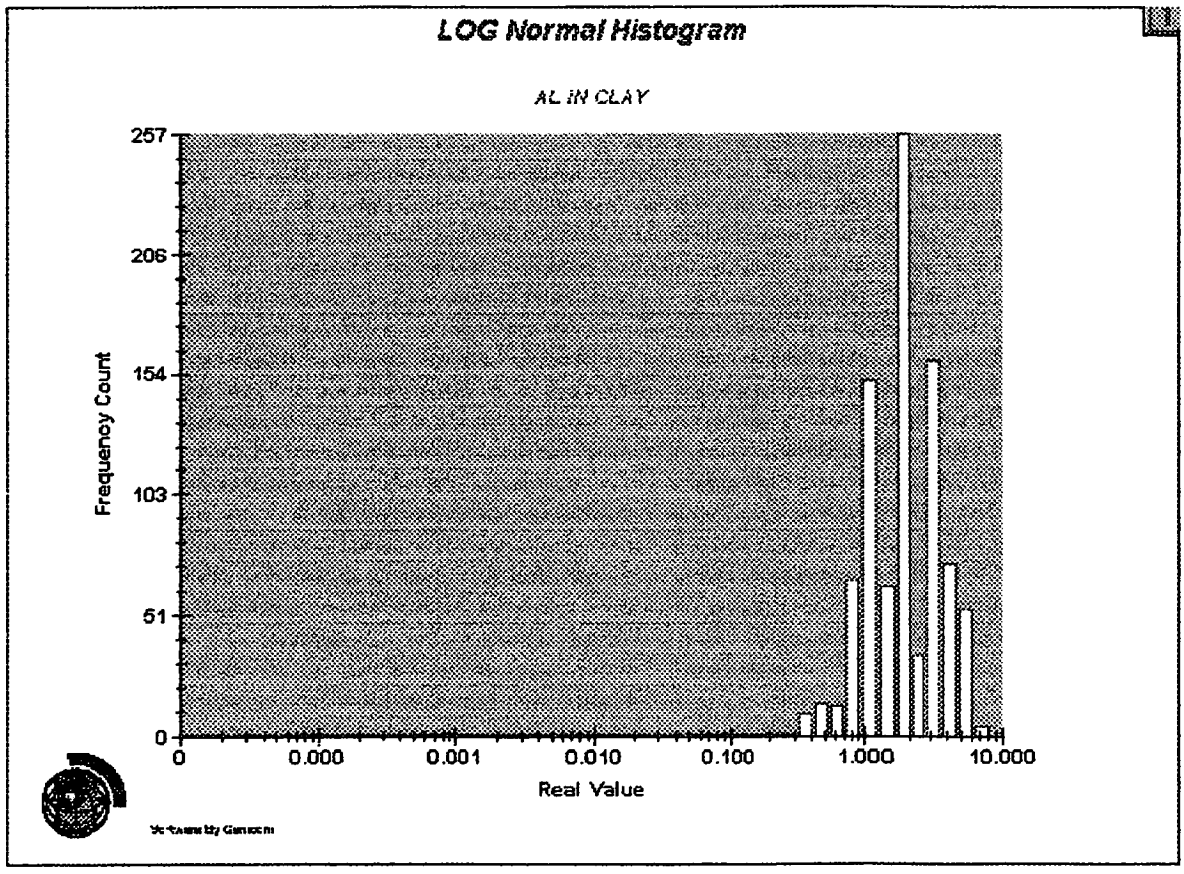

CHAPTER 6 – VARIOGRAPHY

6.1 Standard Orientations, 3-D Variograms

Three-dimensional variograms were calculated for all assay values, based on the various lithological categories. Each assay value and lithology were evaluated using Gemcom software, and a standard set of 12 orientations. The variogram orientations are indicated in Table 6-1, and presented in Appendix 1.

Variogram	Azimuth	Spread (degrees ±)
1	000	90
2	000	15
3	030	15
4	060	15
5	090	15
6	120	15
7	150	15
8	180	15
9	080	45
10	135	45
11	045	45
12	000	90

Table 6-1 Three-Dimensional Variogram Orientations

6.2 Magnesium

6.2.1 Sand

All of the directions for magnesium in the sand lithology show a range of between 100 and 200 metres, and have two structures with an unusual dip between the structures. The first structure has a range of between 50 to 75 metres, averaging 60 metres, and a sill ranging between 0.8 and 0.9. The second structure is longer, at 150 to 200 metres, with a sill of 0.1. The nugget effect is low, ranging from 0 to 0.1. Overall, the distribution is not quite anisotropic, as the east-west ranges tend to be slightly shorter than the north-south.

6.2.2 Silt

The magnesium in silt has a very high nugget effect, and two ranges, one at 300 metres north-south, and the second at 250 metres, east-west.

Unfortunately, the variograms are noisy, and the level of distortion may indicate a high degree of element mobility in the silt layer.

6.2.3 Clay

Little real interpretation was returned from the variography. The 060 direction shows a long range (600 metres) with considerable noise. The long range follows on from a shorter structure at 75 metres, which apparently equates to the sill. The nugget effect is low.

6.3 Silica

6.3.1 Sand

Silica in sand has no apparent structures, and the majority of the variography indicates sand is omnidirectional. There is a relatively high nugget effect. One structure is visible within a 50 metre range, at 120 degrees azimuth.

6.3.2 Silt

The distribution of silica in silt is possibly isotropic. In the 0 to 90 degree arc, the range is of the order of 75 to 125 metres. Several of the variograms do not reach the sill. All have only one structure visible, and that structure is apparently spherical. The nugget effect is not able to be discriminated, but may be high. In the 90 to 180 degree quadrant, no recognisable or interpretable variograms were returned, and the anisotropy of the system remains unknown.

6.3.3 Clay

Silica in clay behaves in an isotropic manner, and the variography may be reflecting two different silica types, the first being mobile silica, the second the actual clay component. Mobile silica may be the source of the noise in the variograms. The 600 metre long range visible may simply be reflecting an individual clay type. The nugget effect is high, approximately 0.5.

6.4 Manganese

6.4.1 Sand

Manganese values in sand are almost isotropic. There is a range of 50 to 100 metres, averaging 75 metres, with a single structure, and a nugget effect which approaches zero.

6.4.2 Silt

Manganese shows two separate ranges in the silt fraction. The first, and longer, in the 120 to 300 degree area is approximately 500 metres, while the second is a shorter range of 75 degrees, at a sill of 0.23, visible in the remaining variogram directions. The nugget effect was not clear from the variography, but is apparently low.

6.4.3 Clay

Two structures are visible in the manganese in clay. One structure is at approximately 50 metres, with a sill of 0.7, and the second structure has a sill of 0.3, and a range of 225 metres, approximately. The nugget effect is low.

6.5 Iron

6.5.1 Sand

The sand component for iron has an isotropic nature between 300 and 060 directions. The range is approximately 75 metres, and the variography suggests almost no nugget effect.

6.5.2 Silt

The iron in silt variograms show two structures, one short range at 25 metres, with a 0.72 sill, and the second a very long range, 600 metre structure. The longer range structure has a more gaussian distribution than the shorter, spherical range.

6.5.3 Clay

The iron in clay variography indicates a consistent range of 300 metres for all of the directions except north-south. The omnidirectional variogram is not interpretable, while some of the variograms have two clear structures, and others only one, but all display considerable noise.

6.6 Calcium

6.6.1 Sand

None of the variograms run for calcium in the sand lithology produced definite ranges. If the approach of the curve to the sill is accepted, there is an omnidirection to the variogram, with a nugget of approximately 0.3, and a range of 120 metres for a single spherical structure.

6.6.2 Silt

Ranges from the calcium in silt variography are from 75 to 100 metres, with no clear directional focus. Only one of the variograms reaches the sill, which renders interpretation difficult. The nugget effect is very low, and there is an apparent hole effect directly beyond the interpreted range, which may be due to cross-cutting structures in the silt.

6.6.3 Clay

Calcium in clay shows a highly directional nature. The range in the 045 degree direction is 675 metres, and the orthogonal 150 degree direction is 125 metres. The nugget effect at 0.4 is relatively high.

6.7 Aluminium

6.7.1 Sand

The aluminium in sand variograms are truly omnidirectional. There is a very low nugget effect, with two structures, and a sill approaching 1 at between 50 and 60 metres. The second structure is smooth to a range of 400 metres, which suggests that interparticle relationships continue beyond the 200 metre intercept with the sill.

6.7.2 Silt

Aluminium in silt shows two structures, and an isotropic behaviour. The total range is 600 metres in all directions. There is a very low nugget effect. The first structure comprises the majority of the sill at 0.8, and has a range of 50 metres. The second structure is at 600 metres.

6.7.3 Clay

Aluminium in the clay lithology is isotropic in behaviour. The nugget is low, and the range is approximately 300 metres, with the first structure having a sill of around 0.7 and a range of 50 metres, and the second structure a sill of 0.1 and a range of 300 metres.

Overall, aluminium displays a similar omnidirectional behaviour irrespective of lithology.

6.8 Downhole Variography.

Using Medsystems, a number of downhole variograms were completed for the different elements. Each variogram was calculated with a lag distance of one, and then two metres. Results are included in Appendix 2.

6.8.1 Magnesium

The magnesium variogram returned from 1 metre lags shows a downhole range of up to 11 metres. There is a hole effect visible, which may be due to lithological changes downhole. The 2 metre lag variogram has a similar 11 metre range, and a slight hole effect.

6.8.2 Silica

Silica values for both the 1 and 2 metre lags give clear variograms. The nugget effect is approximately 0.2, and the range is 6 metres, assuming a sill of 1.

6.8.3 Manganese

Manganese values show clear and unambiguous downhole relationships for both the 1 and 2 metre lags. The nugget effect is 0, and the downhole range from 8 to 11 metres using 1 metre lags, and the range is 11 metres in the 2 metre lag.

6.8.4 Iron

The iron variograms downhole indicate the data is too sparse for reasonable interpretation. Using the 2 metre lag , there is a high nugget effect of 0.8, and a range of 5 metres. The large difference resulting from the use of 1 or 2 metre lag samples indicates the variograms should be treated with caution. The 1 metre lag has a strong hole effect, and no clear range or nugget effect. This may be due to different lithologies strongly influencing the iron distribution.

6.8.5 Calcium

Calcium displays a low nugget effect, and a range of 4 metres. There is a strong hole effect at a 1 metre lag, with a final range increase at 11 metres. The 2 metre lag indicates the 11 metre range is more typical.

6.8.6 Aluminium

Both the 1 and 2 metre lags in the aluminium variograms show a moderate nugget effect. The 1 metre lag has a range of 6 metres, and displays a strong hole effect. The 2 metre lag has a range of 11 metres and shows no

hole effect. Thus, for aluminium, the 2 metre lag variogram parameters should be utilised.

6.8.7 Magnesium by Lithology

The magnesium assays were then separated by lithology, and downhole variograms using a 2 metre lag run for sand, clay and silt. The resulting variograms are included in Appendix Two.

The magnesium in sand variogram shows a moderate nugget effect of 0.6, and a range of 10 metres. Extreme values shown at the end of the variogram are probably the result of low pair numbers in the variogram.

The silt unit variogram shows a very low nugget effect, approximately 0, but does not reach the sill. This may be due to the range being longer than the actual thickness of the silt unit.

In the clay fraction, the variogram is not capable of being interpreted. The unit thickness is possibly too small to allow enough data to be viewed across the deposit using a 2 metre lag, to produce a meaningful relationship.

6.9 Discussion

All of the variograms generated display considerable noise. This may be partly due to the basic sampling technique employed on site, which results in non-extractable variation in the samples. It is also probably due to the populations under examination being heterogeneous, giving multiple populations in each variogram which obscure subtle relationships within each individual population.

Most of the variography was found to produce at the minimum, a range and direction. Few of the variograms are strongly anisotropic, but there is a considerable difference in the nugget effect between different elements and different lithologies.

For modelling purposes, the following ranges are indicated, see Table 6-2. As the only commodity being mined is magnesia, the modelling described in the next chapter is only for the magnesium distribution. The ranges established for magnesium in sand will be used to inform the block model search ellipse and will also be used for sample weighting.

Element and Lithology	Strike Axis (degrees)	Across Strike (m)	Along Strike (m)	Downhole (m)
MAGNESIUM				***11***
Sand	000	100	175	10
Silt	000	250	300	?
Clay	000	?	600	?
SILICA				***6***
Sand	NA	?	?	
Silt	000	100	100	
Clay	000	600	600	
MANGANESE				***11***
Sand	000	75	75	
Silt	000	500	75	
Clay	000	225	225	
IRON				***5***
Sand	000	75	75	
Silt	000	600	600	
Clay	000	300	300?	
CALCIUM				***11***
Sand	000	120?	120?	
Silt	000	100?	100?	
Clay	045	150	675	
ALUMINIUM				***11***
Sand	000	200	200	
Silt	000	600	600	
Clay	000	300	300	

Table 6-2 Variogram Ranges, All Elements

CHAPTER 7 - RESOURCE CALCULATIONS

7.1 Database

The resource database was supplied by Queensland Metals Corporation, and consists of 4769 drillholes. Holes were drilled by QMC as exploration drilling, and Queensland Magnesia as run-of-mine assay holes.

Drilling is completed using rotary air blast rigs, with samples collected in a tray which surrounds the rod string. Samples are deposited on the ground in one metre intervals. Sampling is frequently wet, which results in fines being washed into the vegetation cover on which the samples are dumped. Colour plates 7-1 to 7-3 show, in order, a completed drillhole undergoing geological logging, sample layout, and a close-up of a metre which has considerable magnesite nodules

Assay samples are taken by "scooping" a sample from each one metre pile into predetermined composite lengths. Sample composites are determined on the basis of whether a hole is for exploration or run-of-mine requirements.

Assay results are input with the lithological logging into an Access database. On receipt of the database from QMC, holes were checked on screen for azimuth and direction errors, and a validation process run using Gemcom software to locate technical errors such as inconsistent sample intervals.

All data used for the modelling process was sourced directly from the QMC Access database.

7.2 Compositing

Orebody sampling at Kunwarara has been undertaken at many different sample intervals, producing a heterogeneous sample database. Normally, such data would be composited to standard one or two metre sample intervals. Compositing is generally used to combine individual samples of smaller lengths to standard longer lengths using weighted averages to give the grade of the longer sample.

Two problems were identified with the Kunwarara data in compositing magnesium data. The first problem is related to the longer sample intervals, of up to 8 metres in the database. When such an interval is composited to one metre values, for example, the average for the entire 8 metres is then assigned to each one metre interval. This leads to an artificial smoothing of the data.

Colour Plate 7-1 Geological Logging of a Completed Drillhole, with Drillrig in Background.

Colour Plate 7-2 Layout of One Metre Drill Samples Awaiting Composite Sampling

Colour Plate 7-3 Close-up of One Metre Sample Showing Typical Magnesite Nodule Intersection

If the opposite approach was taken, and longer composite lengths used, then many of the relatively narrow rocktype intersections would either not be represented at all, or be represented by a small fraction of the composite length.

Unlike many gold deposits, the variation in sample lengths does not appear to be related to close-spaced sampling of high grade material. Sample intervals are irregular in both high and low grade magnesium zones. In addition, the sample lengths are relatively constant between adjacent holes, so that calculations based on adjacent holes are unlikely to be significantly biased.

As a consequence, the resource evaluation was run using raw assay values, and the raw database sampling intervals, although a three metre composite model was included in the evaluation process as both a check and an aid to data interpretation.

7.3 Three Dimensional Solid Modelling

Gemcom software was used to wireframe model the geology of the Kunwarara deposit, using the lithological definitions from drillhole logging by site geologists. Four lithologies, gravel, sand, clay and silt, were used.

The more usual process of linking sections of digitised interpretations was not utilised in the wireframe, due to the very thin nature of the lithologies, and the scale of the horizontal distances in the deposit. The perceived risk in the use of sections is in the difficulty of reproducing three-dimensional behaviour between sections using straight lines to connect points on one section with points on the next section.

Instead, the upper surface of each lithology was modelled as an individual surface, using a Laplace algorithm. The smoothing factor in the algorithm was set to zero to avoid over-interpretation, and a grid of 100 x 100 metres used. The surfaces produced were validated for irregularities, and then used to cut a solid blank which covered the limits of drilling.

By successive Boolian operations, in which the surfaces were used as cutting tools on a blank solid constructed around the outline of the limits of drilling, a model of each lithology was produced. The resultant solids were validated, and assigned rock code identifiers.

The coded solids were then used to overstamp rockcodes into the block model, depending on the percentage of any given block which lay within the solid. A value of 50 percent was chosen as the criterion for assigning blocks with a particular rock code. Thus, a value of 51% silt would result in a block being assigned to the silt lithology. The overstamping was undertaken down the geological profile from surface, with clay written first, then silt and finally sand.

7.4 Block Modelling

Block modelling for the deposit was undertaken using Gemcom's PCMine program. The initial evaluation was completed using 25 x 25 x 1 metre block sizes, which allowed an effective penetration rate of one drillhole to each block. Note that the longer length samples did result in an apparent high ratio of blocks to samples, however.

The following resource methods were used on that block spacing:

- Inverse distance squared
- Inverse distance cubed
- Ordinary kriging
- Indicator kriging (raw data)
- Indicator kriging (composite data)

To ensure a meaningful comparison between techniques, the sample search parameters used were the same for each method, as were the number of samples used to inform a block. Ore block samples for the purposes of the evaluation were a standard 25 x 25 x 1 metre size.

Where applicable, the limits of the indicators for the indicator kriging runs were drawn directly from the element by lithology distributions involved. Each of the three main lithologies, clay, silt and sand, was calculated in an independent run, and then combined into a single final model for each method. Results of the modelling process were used to produce grade/tonnage curves.

The density of 1.9 tonnes per cubic metre used to calculate tonnages was supplied by QMC, and is the run-of-mine density figure. (S. Wilcock, pers comm.)

7.5 Grade Tonnage Curves

The grade tonnage curves for the individual lithologies and each calculation type are shown in Figures 7-1 to 7-15, in order of increasing complexity of resource calculation.

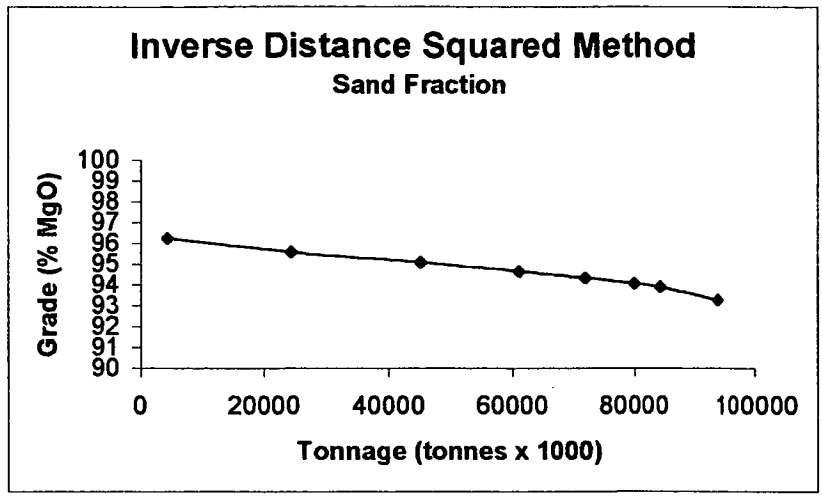

Figure 7-1 Inverse Distance Squared, Sand

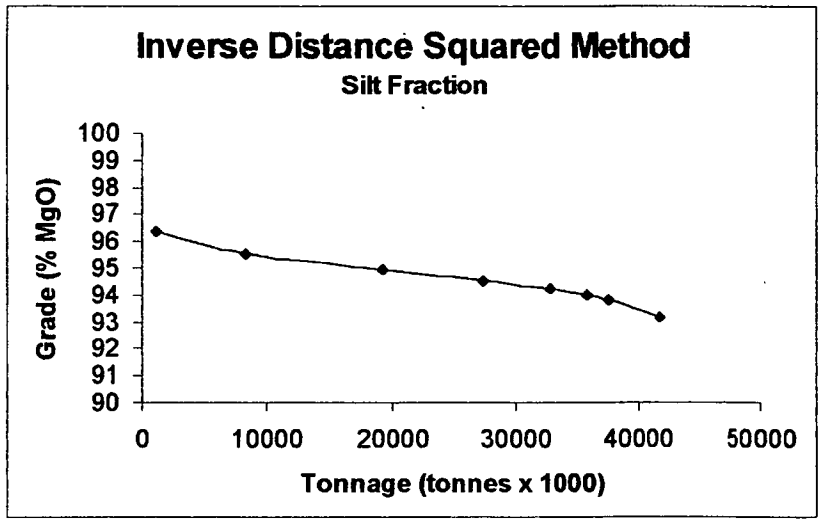

Figure 7-2 Inverse Distance Squared, Silt

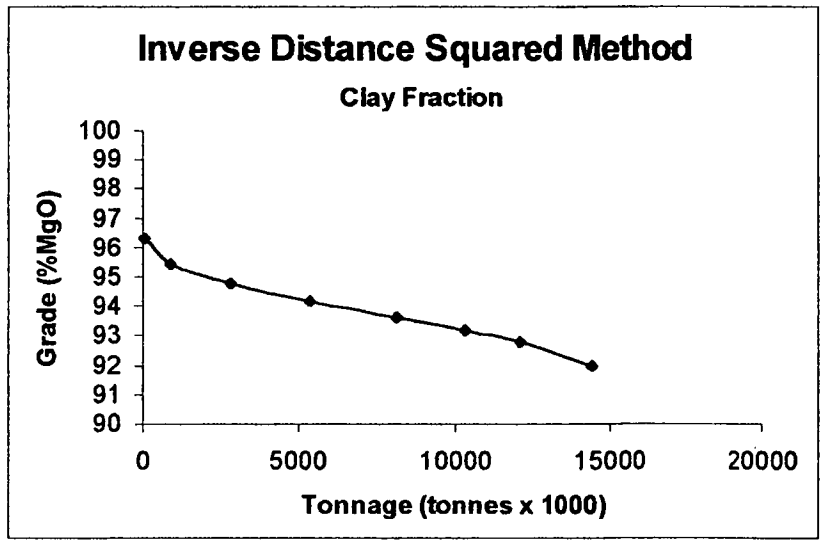

Figure 7-3 Inverse Distance Squared - Clay

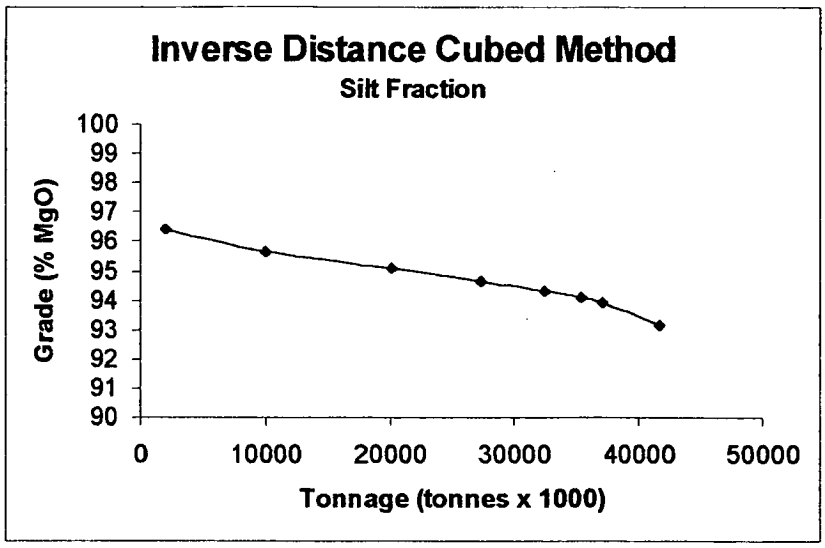

Figure 7-4 Inverse Distance Cubed - Sand

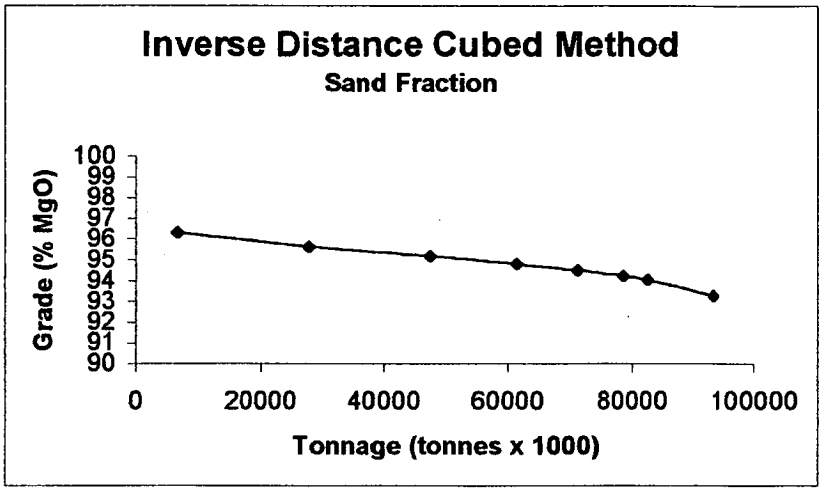

Figure 7-5 Inverse Distance Cubed - Silt

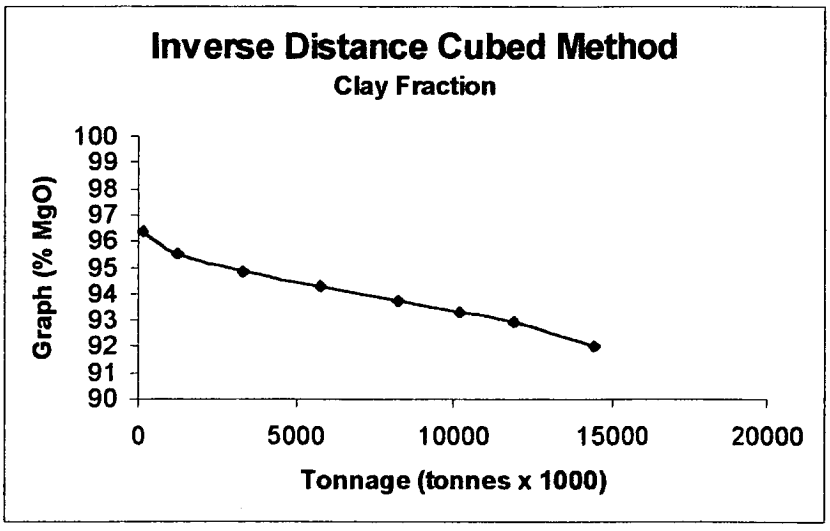

Figure 7-6 inverse Distance Cubed - Clay

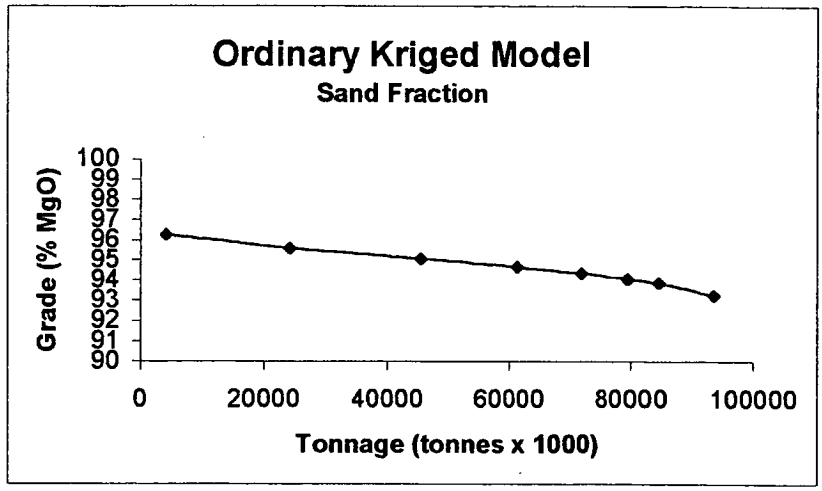

Figure 7-7 Ordinary Kriging - Sand

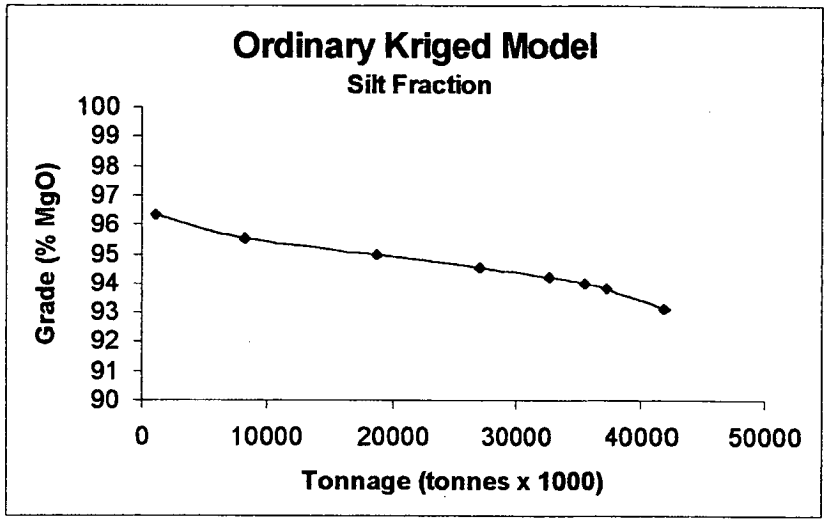

Figure 7-8 Ordinary Kriging - Silt

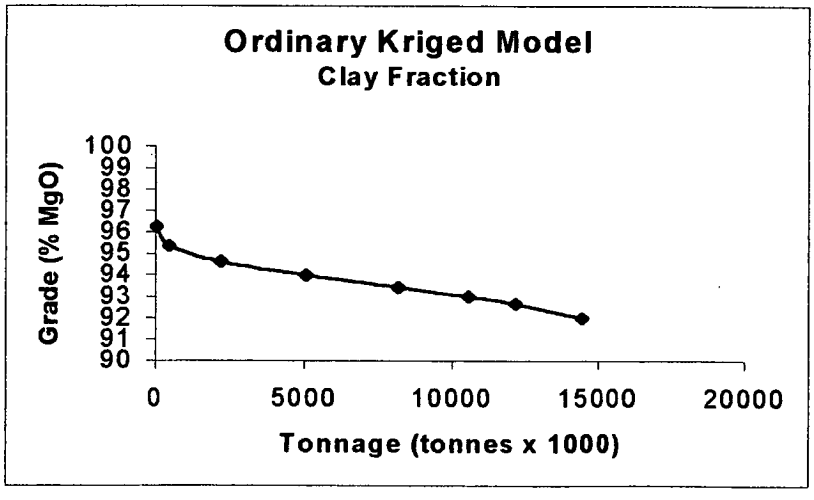

Figure 7-9 Ordinary Kriging - Clay

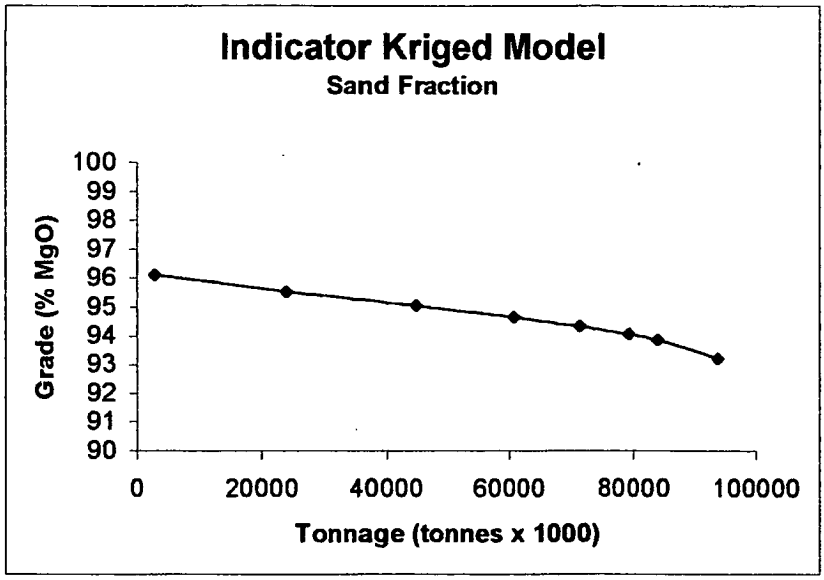

Figure 7-10 Indicator Kriging, Raw Data - Sand

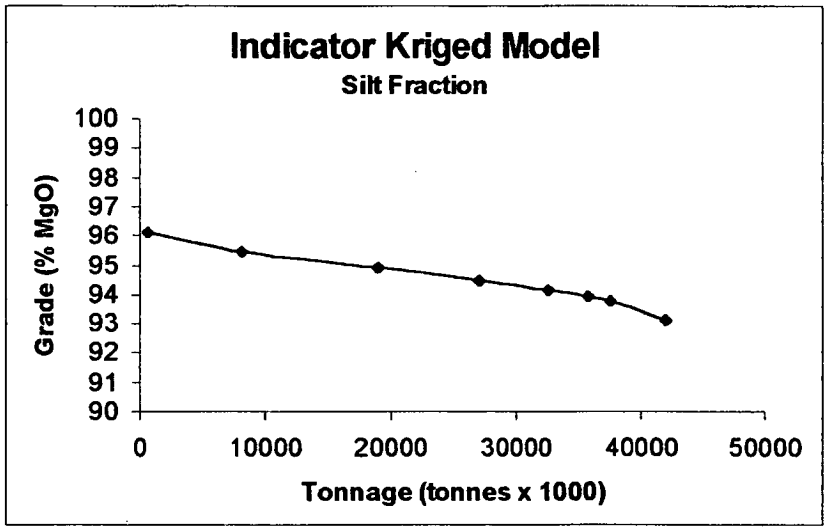

Figure 7-11 indicator Kriging, Raw Data - Silt

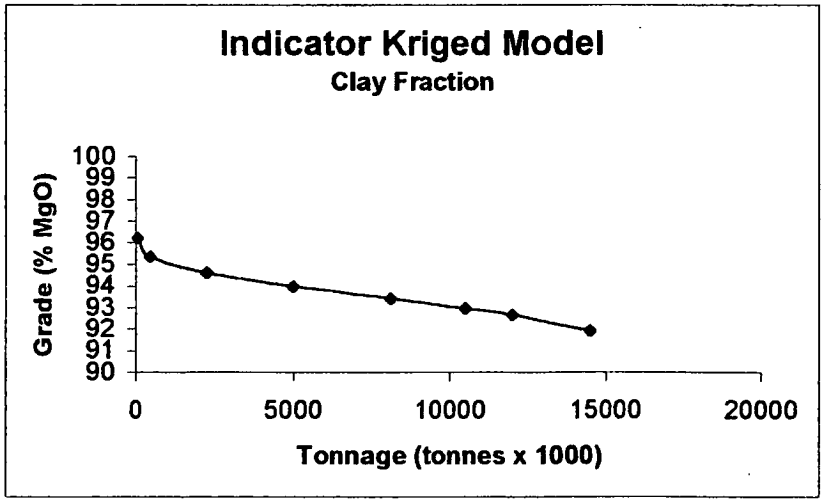

Figure 7-12 Indicator Kriging, Raw Data - Clay

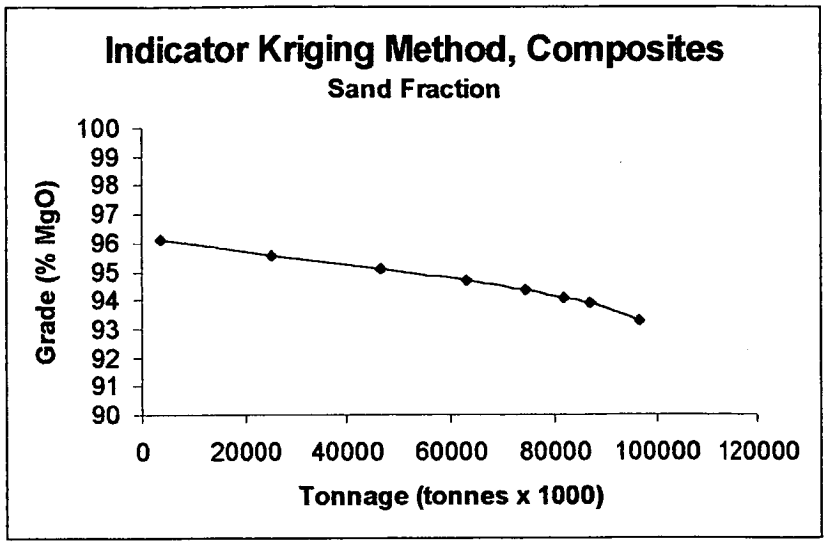

Figure 7-13 Indicator Kriging, Composites - Sand

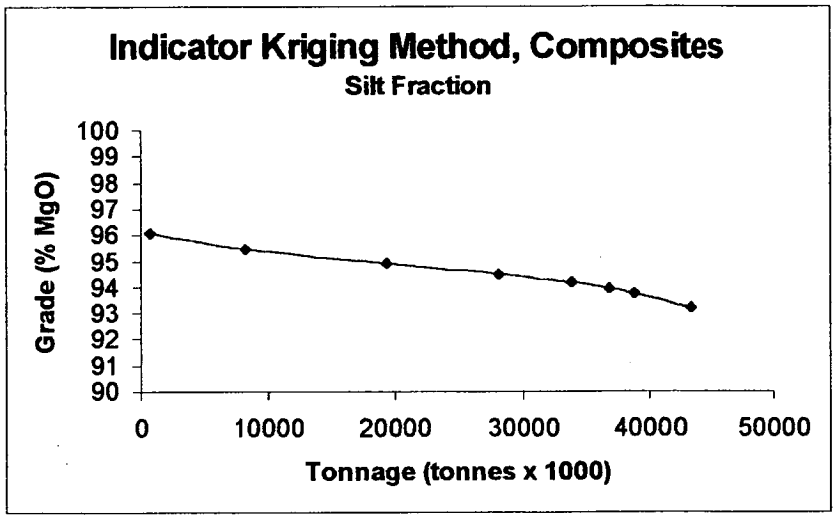

Figure 7-14 Indicator Kriging, Composites - Silt

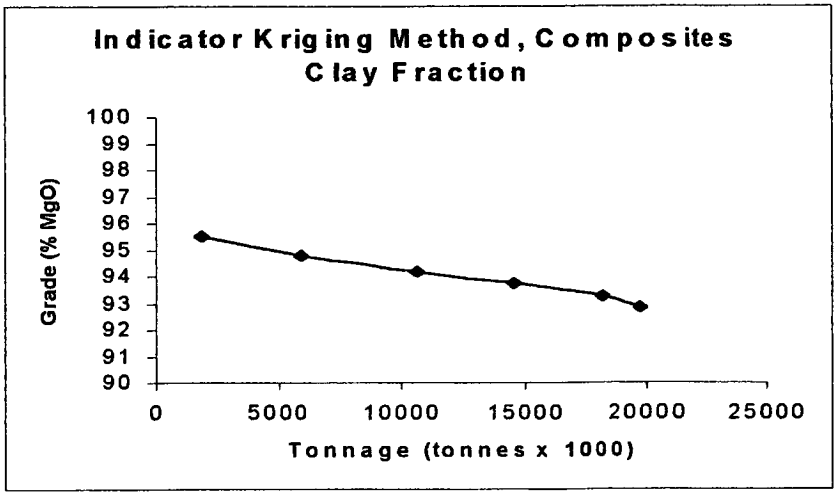

Figure 7-15 Indicator Kriging, Composites - Clay

7.6 Discussion

The grade tonnage curves show that the Kunwarara deposit is extremely unusual in its tonnage versus grade behaviours. The majority of the techniques give a relatively close approximation for tonnage and grade, as shown in Figures 7-16-18.

In the sand fraction, inverse distance squared and ordinary kriging return similar grades and tonnages, whilst the indicator kriged composites and indicator kriged raw data return the most conservative tonnage and grade figures. Indicator cubed methodology gives the highest tonnages and grades.

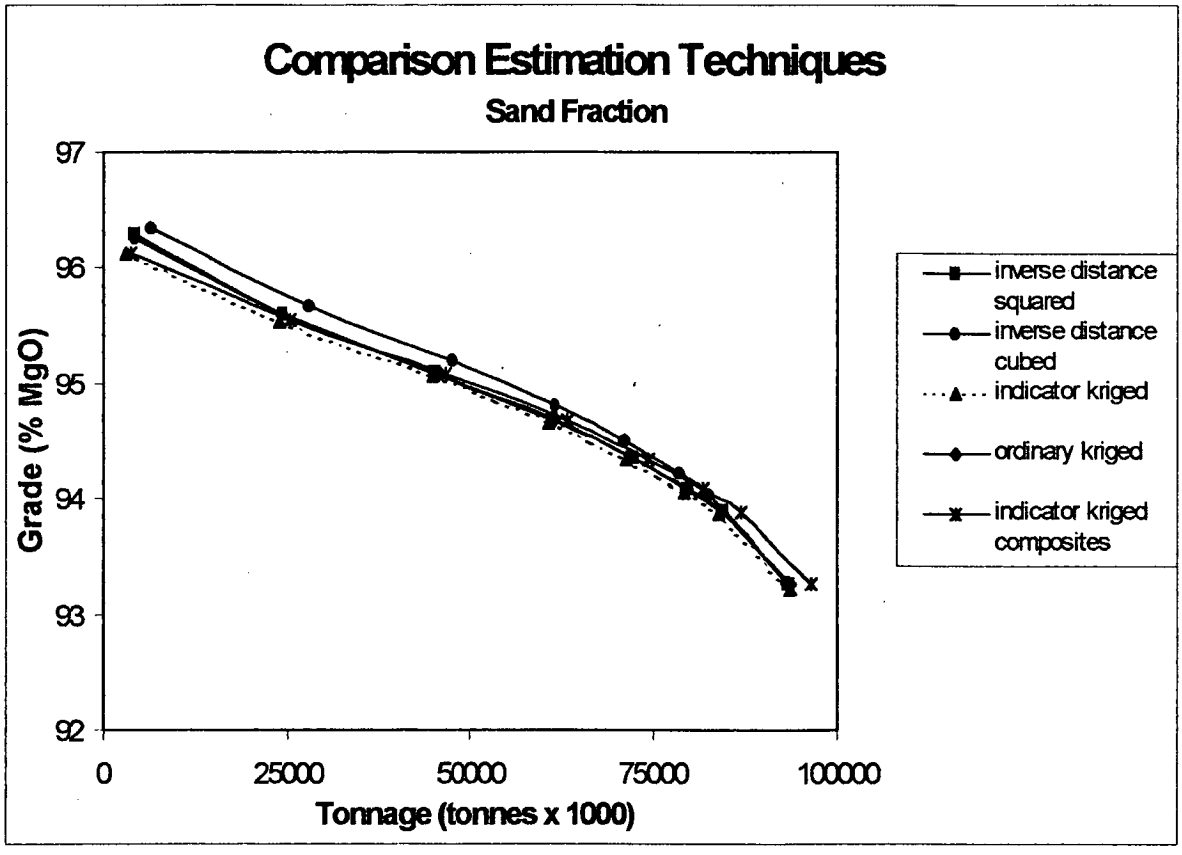

Figure 7-16 Composite Tonnage Grade Curves, Sand Fraction

Values in the silt fraction indicate that the ordinary kriging and inverse distance squared results are similar, with the indicator kriging raw data and indicator kriging composite data returning comparable grades and tonnages, and the inverse distance cubed fraction again giving higher tonnages and grades.

In the clay fraction, the indicator kriged composite samples are notably higher in both tonnage and grade. Inverse distance cubed and squared methods show the next highest grade and tonnage figures, while the ordinary and indicator kriging raw data values are the most conservative.

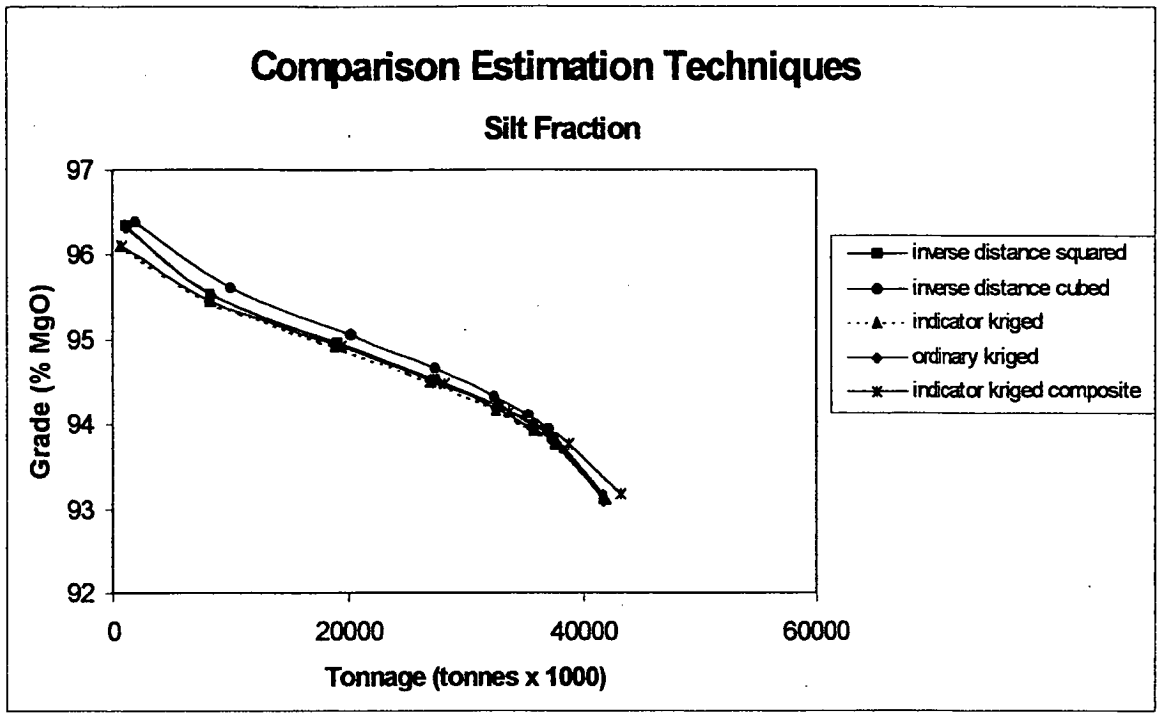

Figure 7-17 Composite Tonnage Grade Curves, Silt Fraction

Figure 7-18 Composite Tonnage Grade Curves, Clay Fraction

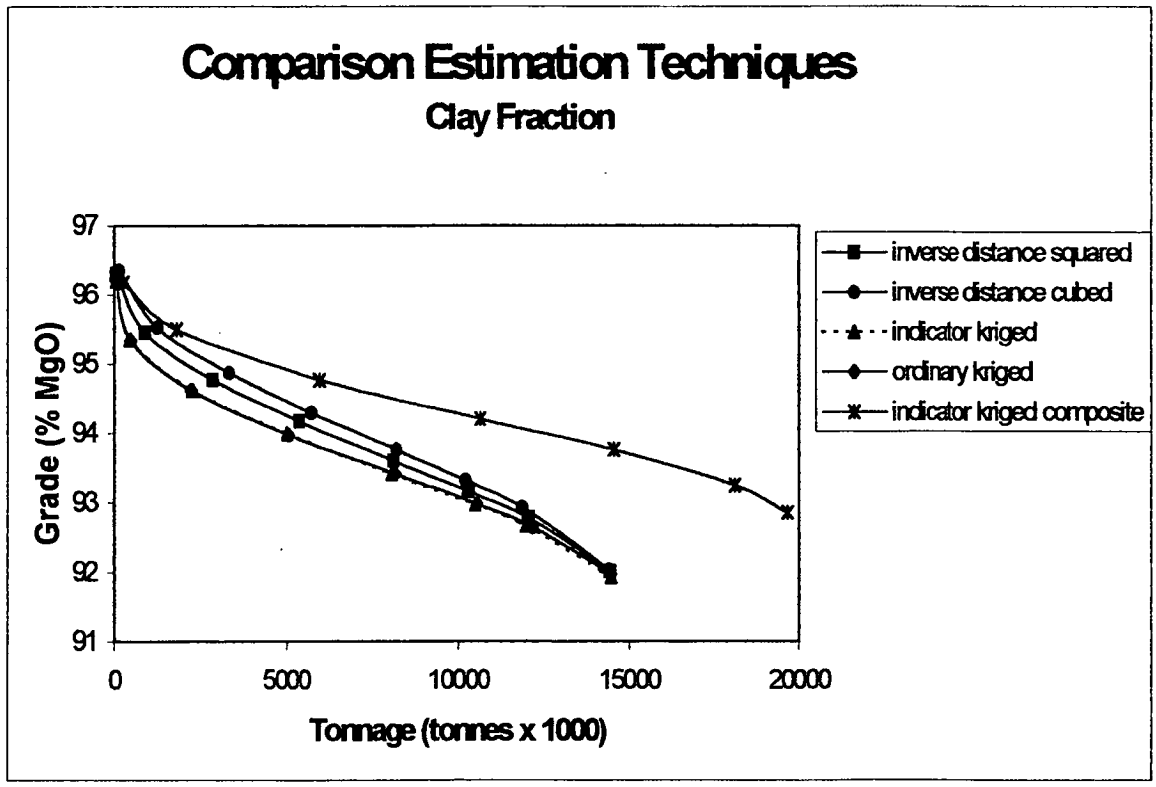

The clay fraction shows an unusual distribution in comparison to the silt and sand lithologies, for the indicator kriging composite method. This is attributed to a combination of a very narrow lithological horizon, and the compositing of samples to a 2 metre interval. In the raw dataset, a sample taken over an 8 metre interval might well straddle the clay/silt boundary, for example, but would be assigned to the thickest lithology, which would be silt. When the samples are composited, this 8 metre interval would become 4 separate 2 metre intervals, and the clay fraction would be given the same assay value as the silt layer. As a result, there are more blocks informing the clay layer in the composite indicator krige run, and thus, both a higher grade and higher tonnage results.

A comparison of the original input data and the output grades different models is shown in Table 7-1, for the grouped data.

	Raw	ID2	ID3	OK	IKR	IKC
Maximum MgO value	98.50	97.95	98.33	97.45	96.21	96.19
Mean	92.81	72.24	68.2	72.25	72.04	74.11
Median	94.69	92.58	92.26	92.54	92.97	93.10
Standard Deviation	8.08	38.65	40.77	38.66	38.53	37.16
Variance	65.41	1494.59	1662.30	1494.80	92.97	1380.88
Coefficient of Variation	0.87	0.53	0.59	0.53	0.53	0.50
Coefficient of Skewness	-8.42	-1.26	-1.01	-1.27	-1.27	-1.43
Coefficient of Kurtosis	91.48	2.63	2.04	2.63	2.63	3.06

Table 7-1 Input and Output Grades

Key:

- Raw = input raw assay values
- ID2 = inverse distance squared method
- ID3 = inverse distance cubed method
- OK = ordinary kriging method
- IKR = indicator kriging method, raw assay values
- IKC = indicator kriging method, composited assay values

The datasets above show that the different resource calculation methods have not cut the upper sample values, with all of the highest grade samples from the different methods within 2% of the highest grade raw data value. The large change in mean values between the raw data set and the different methodologies is largely due to smoothing of the data because of the block to sample ratio, and the estimation processes involved.

The comparison of the input and output grades clearly shows the indicator kriging method on the raw data to have a variance which most closely

approximates that of the input data (input data variance is 65.41, indicator kriging raw data variance is 92.97. The remaining techniques give a much wider block variance range, with the highest variance reached in the indicator kriging composite method and the inverse distance cubed method.

In terms of grades, the following variations were noted, see Table 7-2.

Method	Mean	Variation Mean %	Median	Variation Median %
Raw	92.81	0	94.69	0
ID2	72.24	22	92.58	2.2
ID3	68.20	26	92.26	2.5
OK	72.25	22	92.54	2.2
IKR	72.04	22	92.97	1.8
IKC	74.11	20	93.10	1.6

Table 7-2 Grade Variations Between Methods.

Key:

- Raw = input raw assay values
- ID2 = inverse distance squared method
- ID3 = inverse distance cubed method
- OK = ordinary kriging method
- IKR = indicator kriging method, raw assay values
- IKC = indicator kriging method, composited assay values

The marked difference between the variations in mean and median, approximately a factor of 10, is a product of the mean being susceptible to extreme or outlier sample values, and the smoothing of the grade distribution in the block model which generates the outlier values.

Overall, the examination of the tonnage and grade curves for the various lithologies, the variations in mean, median, and in particular, the variance values suggest that the most appropriate method of resource estimation is the indicator kriging technique, utilising raw data values.

The assignment of a category to the resource is problematic. The mixed sample population, and skewed nature of the distribution suggest that the individual drillholes will not produce a representative grade sample of magnesium material. This is partially offset by the consistent high grade samples, which average between 80 and 96% magnesium. In addition, the number of random size samples submitted for assay is a concern, although again, the impact of the sampling is mitigated by the consistent grade. While the tonnage is generally very consistent between methodologies, the grade is inconsistent, and the indicated category is recommended for the tonnage and grade curves generated from this study.

CHAPTER 8 – ORE BLOCK SIZES

8.1 Ore Block Sizes

An evaluation of the impact of the change in block sizes on the Kunwarara deposit was investigated by varying block sizes in individual indicator kriging raw data resource estimations. The following block sizes were modelled, see Table 8-1.

Block Model	Length (m)	Width (m)	Thickness (m)
1	200	200	3
2	100	100	3
3	50	50	3
4	25	25	3
5	25	25	1
6	16	12.5	3

Table 8-1 Block Sizes

The 3 metre bench height was chosen as a standard, as this is already in use in day-to-day mining operations. In the case of the second 25 metre block size, the one metre interval was the base for the previous chapter's evaluation of the different methodologies.

The smallest block size was unfortunately not a standard 12.5 x 12.5 x 3 metres, as the Gemcom software used in the modelling process was unable to interpret beyond a set number of blocks. As a result, the block size had to be modified to meet the limit of blocks in the software, and thus the 16 metre block length.

8-2 Tonnage and Grade Curves

Tonnage and grade curves were prepared for each lithology, for each block size, and these are shown in Figures 8-1 to 8-15. The curves for the indicator krige run for the 25 x 25 x 1 blocks have already been presented as Figures 7-10 to 7-12.

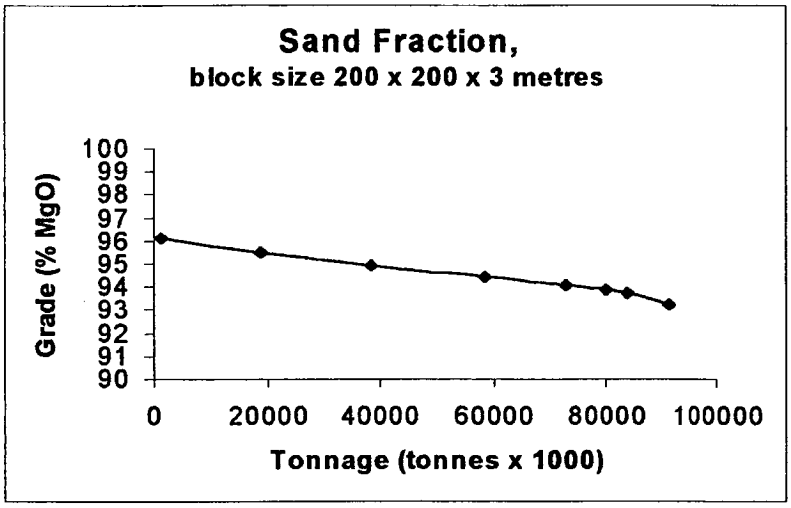

Figure 8-1 Block Size 200 metres, Sand

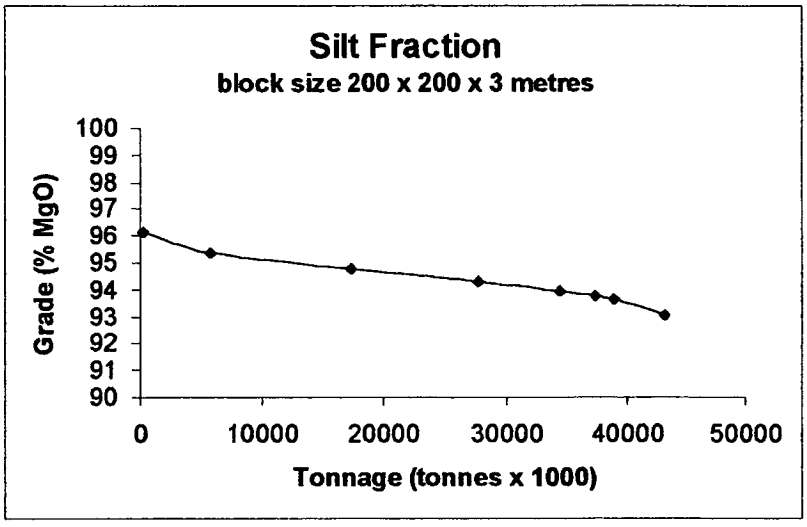

Figure 8-2 Block Size 200 metres, Silt

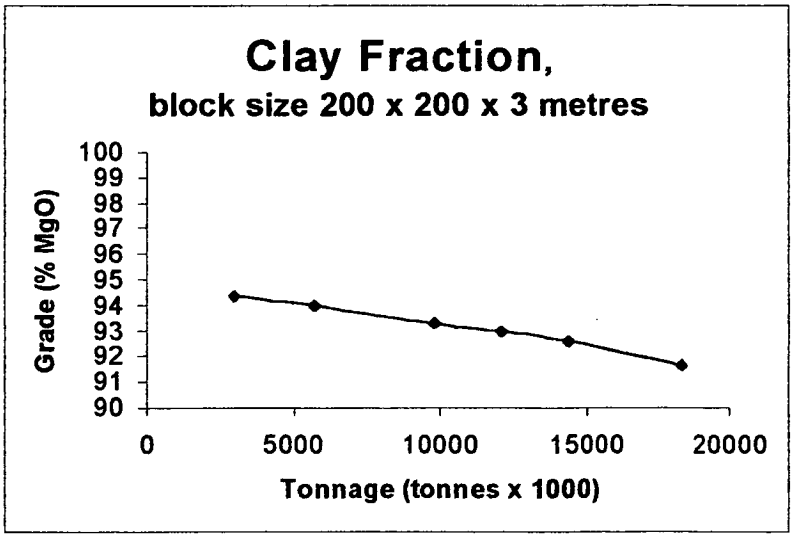

Figure 8-3 Block Size 200 metres, Clay

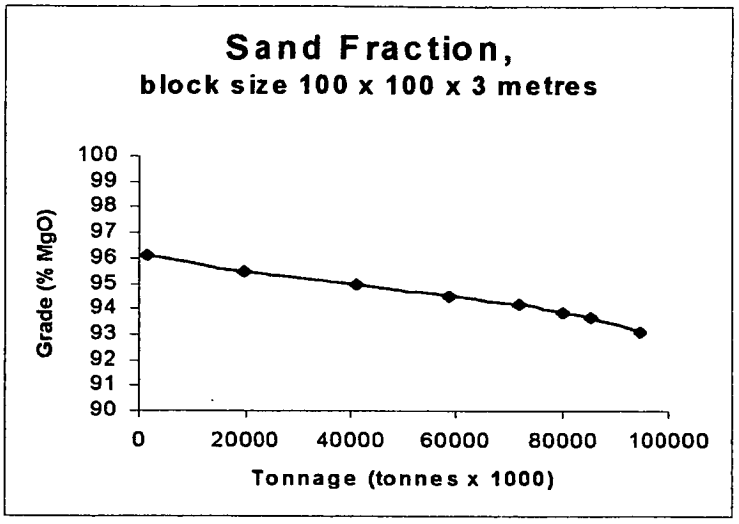

Figure 8-4 ***Block Size 100 metres, Sand***

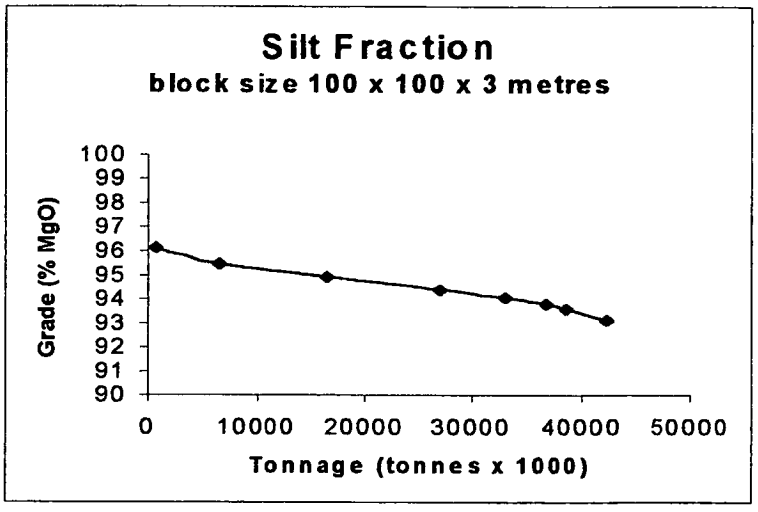

Figure 8-5 ***Block Size 100 metres, Silt***

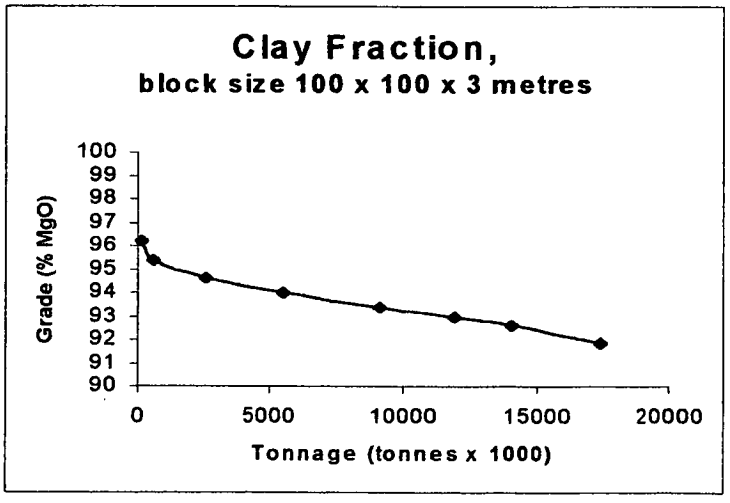

Figure 8-6 ***Block Size 100 metres, Clay***

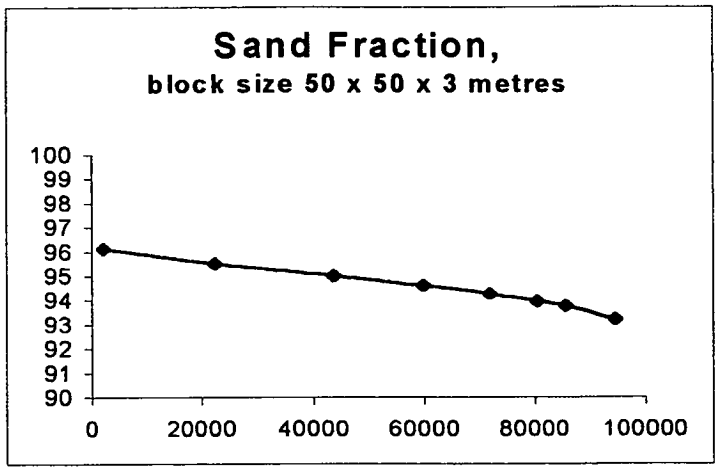

Figure 8-7 Block Size 50 metres, Sand

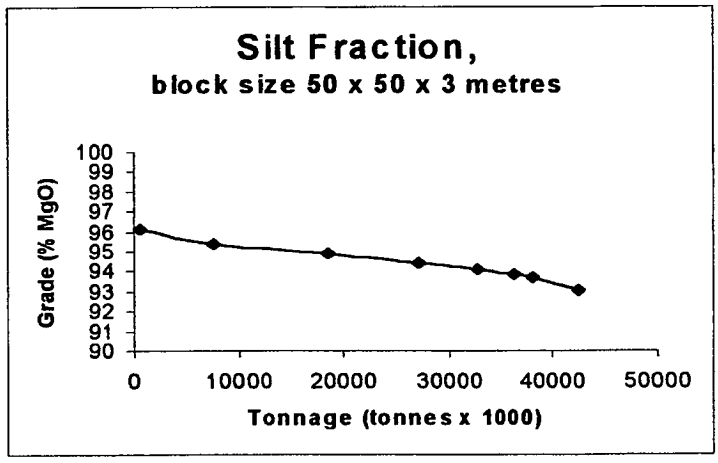

Figure 8-8 Block Size, 50 metres, Silt

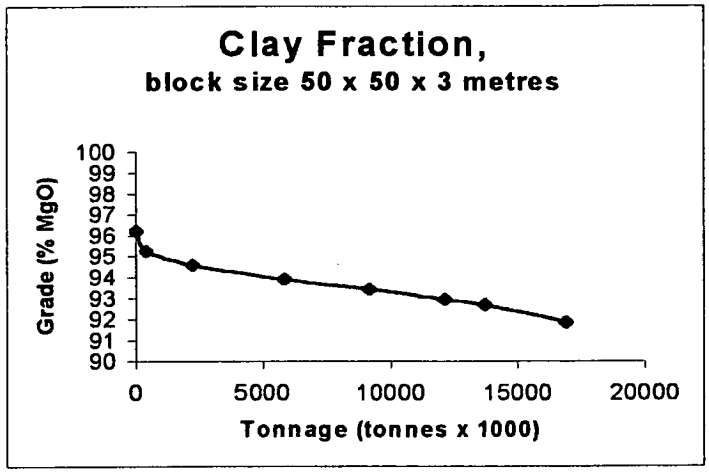

Figure 8-9 Block Size, 50 metres, Clay

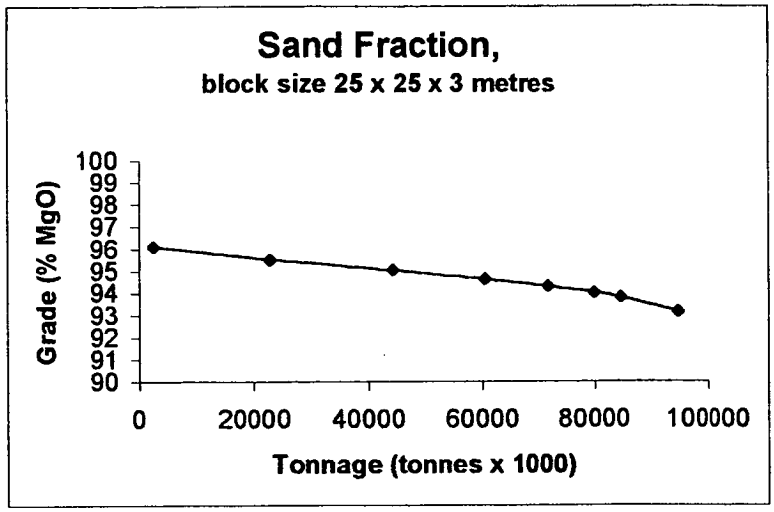

Figure 8-10 Block Size 25 metres, Sand

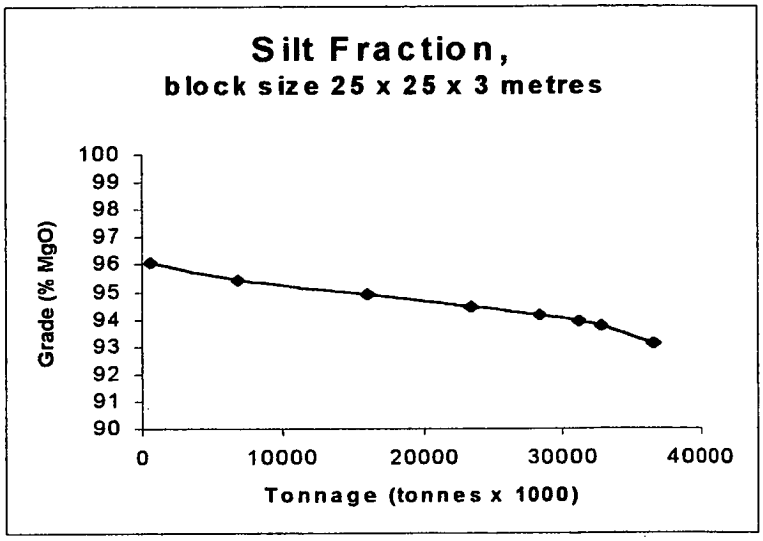

Figure 8-11 Block Size 25 metres, Silt

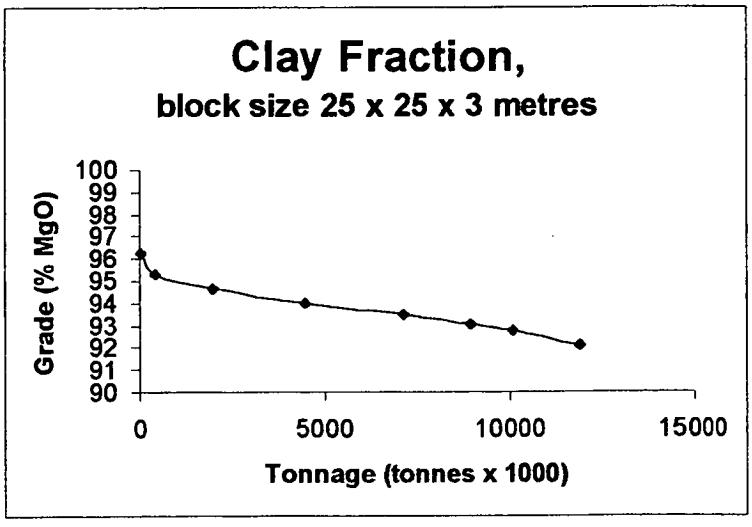

Figure 8-12 Block Size 25 metres, Clay

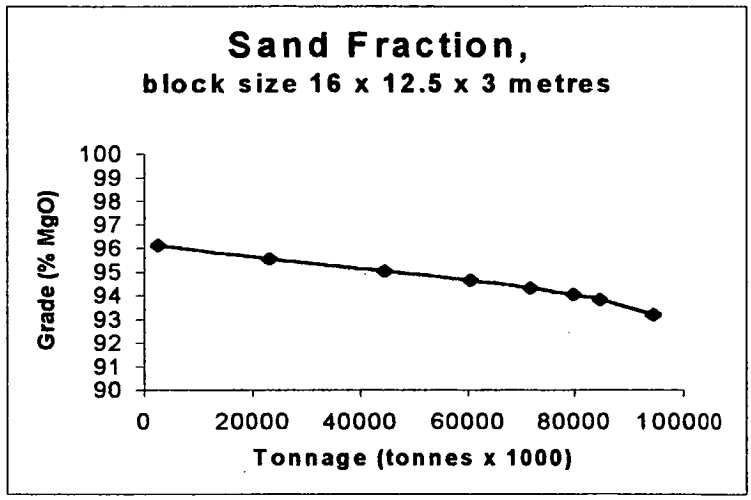

Figure 8-13 Block size 16 metres, Sand

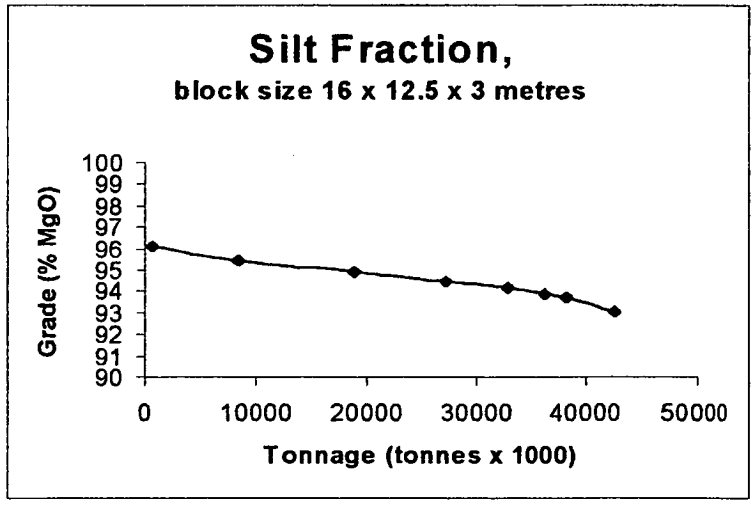

Figure 8-14 Block size, 16 metres, Silt

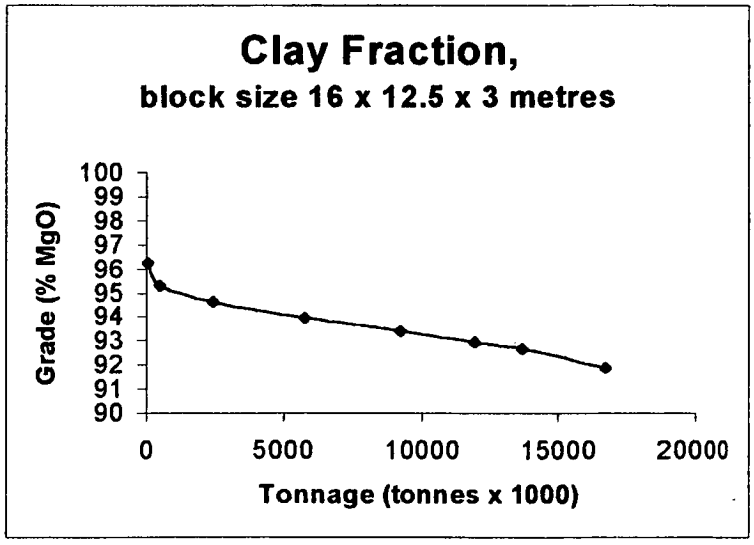

Figure 8-15 Block size, 16 metres, Clay

8.3 Discussion

The choice of block size has a significant impact on the resource at Kunwarara, as illustrated by the change in variances as very large or very small blocks are used. Overall, the smaller the block used, the higher the tonnage and grade in the resulting curve, see Figures 8-16 to 8-18, where the block tonnage and grade curves are plotted by lithology.

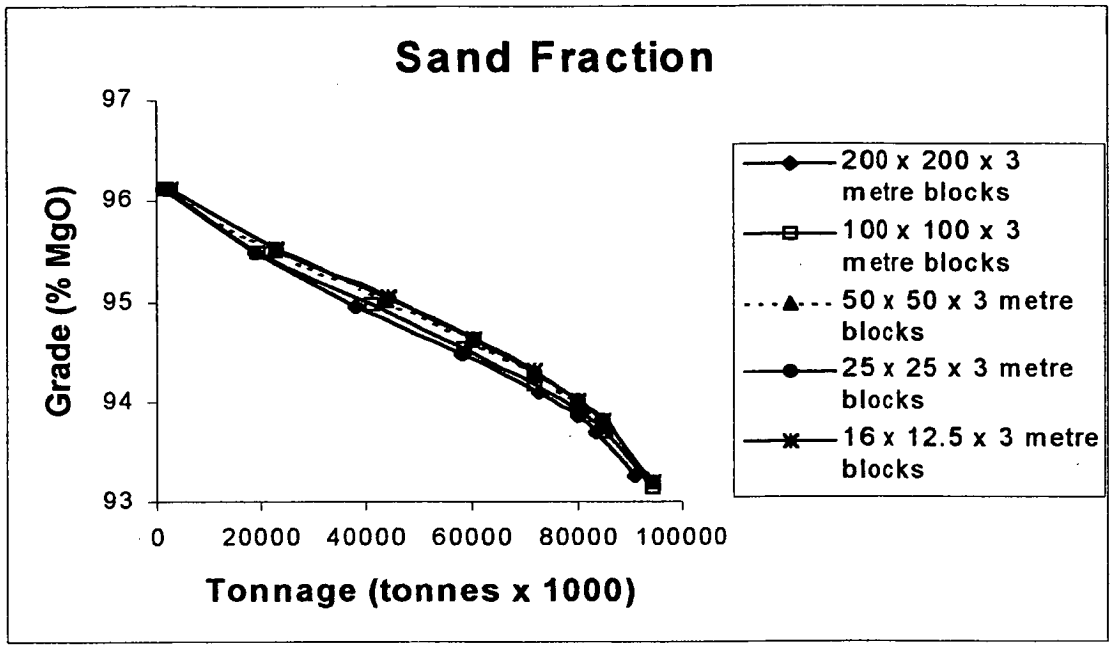

Figure 8-16 Composite Tonnage and Grade, Sand Fraction

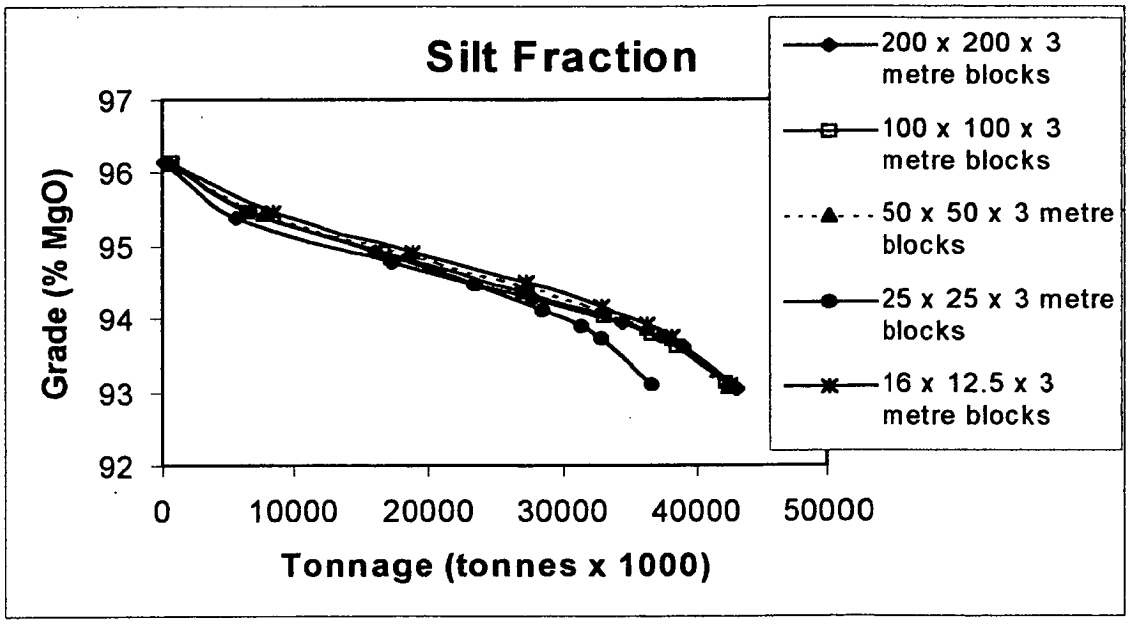

Figure 8-17 Composite Tonnage and Grade, Silt Fraction

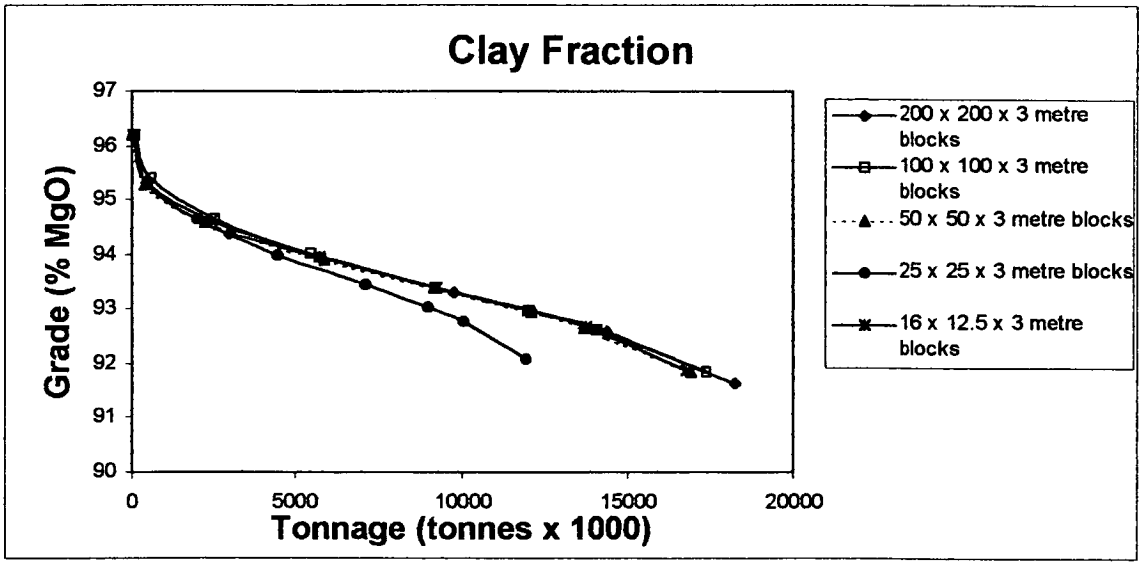

Figure 8-18 Composite Tonnage and Grade, Clay Fraction

A comparison of the original input data and the output grades for the different models is shown in Table 8-2, for the grouped data. A data cut below 85% has been applied to prevent the behaviour of the lowest and most erratic vales in the populations obscuring the choice of block size.

	Raw	200	100	50	25	25 x 1	16
Mean	94.1	93.29	93.20	93.3	92.54	93.13	93.11
Median	94.8	93.68	93.70	93.8	92.80	93.90	93.64
Standard Deviation	2.47	2.05	2.16	2.19	1.82	2.29	2.28
Variance	6.13	4.22	4.68	4.81	3.33	5.24	5.19
Coefficient of Variation	0.87	0.02	0.02	0.02	0.01	0.02	0.02
Coefficient of Skewness	-1.45	-1.32	-1.15	-1.20	-0.82	-1.22	-1.13
Coefficient of Kurtosis	4.82	5.25	4.20	4.36	3.66	4.24	4.03

Table 8-2 Output Data, Various Block Sizes

This table indicates that the majority of the block sizes are reflecting some minor variation away from the raw data distribution. Variation in terms of the mean and median sample values is of the order of less than one percent.

The ratio of block sizes to sample data is shown in Table 8-3.

Block Size	Number of Input Samples	Number of Output Blocks	Ratio
200	5000	500	0.1
100	5000	2100	0.4
50	5000	8500	1.7
25	5000	34300	6.8
25 x 1	5000	102000	20
16	5000	186000	37

Table 8-3 Block Size Ratio

Note all block samples and blocks have been rounded.

The ideal sample versus output ratio for a block model is 1, as then the ratio of blocks to samples is not the cause of smoothing. The closest approximation from the data to 1 is the 100 x 100 x 3 metre block size, at 0.4. The next closest is the 50 x 50 x 3 metre block size at 1.7.

Given the requirement at Kunwarara for three million tonnes of material to be moved per annum, it is suggested that the 100 x 100 x 3 metre blocks be utilised in mine planning. The use of the larger block size also minimises any potential overestimation of tonnage in the resource process.

A cautionary note would be in the use of such large blocks in the clay layer. The thin nature of that lithological unit makes the classification of blocks either in or out on the 50% rule more problematic. Comparatively small changes in thickness in the clay unit can lead to the exclusion of blocks with resultant significant tonnage variations.

CHAPTER 9 DISCUSSION AND CONCLUSIONS

The Kunwarara dataset supplied by Queensland Metals consisted of 4769 drillholes in an Access database. Samples had been assayed for magnesium, silica, manganese, iron, calcium and aluminium. Four major rockcodes had been identified, namely sand, silt, gravel and clay. The gravel layer had not been assayed for magnesium.

Orebody sampling at Kunwarara has been undertaken at many different sample intervals, producing a heterogeneous sample database. Normally, such data would be composited to standard one or two metre sample intervals. Two problems were identified with the Kunwarara data in relation to the magnesium data, one being the relatively long sample intervals which tend to smooth assay values, the second being the tendency for different rocktypes to be included in the one sample interval

Unlike many gold deposits, the variation in sample lengths does not appear to be related to close-spaced sampling of high grade material. Sample intervals are irregular in both high and low grade magnesium zones. In addition, the sample lengths are relatively constant between adjacent holes, so that calculations based on adjacent holes are unlikely to be significantly biased. As a consequence, the resource evaluation was run using raw assay values, and the raw database sampling intervals.

Initial evaluation consisted of a classical statistical review of the raw datasets for each element. The magnesium and calcium distributions were similar, as were iron and manganese, and lastly silica and aluminium. All elements showed mixed sample populations and skewed distributions. This was attributed to a combination of changing pH regimes, fluctuating redox fronts, weathering processes, and the formation of different minerals, for example in the case of iron, the formation of both goethite and haematite.

When the samples were evaluated on the basis of lithology, the distributions remained strongly skewed for magnesium and calcium, but iron and manganese began to approach log normal distributions, suggesting that these elements were in part lithologically controlled. Silica and aluminium sample distributions displayed no correlation with lithology. As a result, it was apparent that indicator kriging was the most appropriate method for modelling the magnesium distribution.

Variography was completed for the different elements, with twelve three-dimensional variograms run and two downhole variograms completed for each element. In addition, magnesium was evaluated downhole by lithology. Results showed that there were coherent ranges for magnesium, iron, aluminium, and manganese in the sand fraction. The silt lithology displayed better variograms from all elements, with only calcium returning unclear variogram ranges. In the silt fraction, iron and magnesium were

not clear, while the remaining elements displayed clear ranges. A feature of all variograms was the "noise" displayed. This was attributed to the mixed sample populations of each element.

Resource modelling was undertaken using inverse distance square, inverse distance cubed, ordinary kriging and indicator kriging techniques. A fifth model used a composite of the magnesium assays for comparison. Standard block sizes of 25 x 25 x 1 metres were employed for each technique, and a standard density of 1.9 tonnes per cubic metre. To ensure a meaningful comparison between techniques, the sample search parameters used were the same for each method, as were the number of samples used to inform a block.

Tonnage and grade curves produced for each method indicated that there was relatively little difference between the methods in terms of tonnage or grade estimation. Generally, the inverse distance cubed method produced the highest tonnages and grades, while the indicator kriging (raw data) method returned the most conservative grades and tonnages. By evaluating the variance, mean and median returned from each block model, it was determined that indicator kriging was the most appropriate resource calculation method. However, the method is still smoothing the data from the skewed input distribution.

Evaluation of the dataset and the tonnage and grade curves suggested that the assigment of a resource category to the deposit would be problematic, and that an indicated category best suited the dataset .

Using the indicator kriging method on raw assay data, a number of block sizes were evaluated. The 100 x 100 x 3 metre block size showed the minimum sample variance and is of sufficient size to allow for easy mine planning in a 3 million tonne per annum operation.

Overall, Kunwarara displays some unusual geostatistical features, which are probably related to the deposit's origin as a chemical precipitate. Further work should include:

- Reconciliation of mining and milling figures to further evaluate the block size question. The blocks will also need to take into account the haulage truck size, and the excavator bucket sizes. Similar deposits, in iron ore for example (Guibal et al 1996), have been modelled using a conditional simulation technique, which more closely mimics the small scale variability of the deposit. This may be the next required step to fully evaluate block sizes

- A careful study of the distribution of magnesium nodules in the sand and silt lithologies to determine what is controlling the distribution, and to make a more careful evaluation of the sample population of the nodules. Are there different nodule types and compositions within the silt layer as opposed to the sand layer?

CHAPTER 10 - REFERENCES

Brooks, J.H. (1964)
Magnesite Deposit, Kunwarara Central Queensland. in *Queensland Government Mining Journal*, Volume 65, p 380

Burban, B. (1990)
Kunwarara Magnesite Deposit. In Hughes, F.E. editor, *Geology of the Mineral Deposits of Australia and Papua New Guinea*, AusIMM Monograph 14, pp 1675 - 1677

Canterford, J.H., Frost, M.T., Lwin, T., McCallum, D.A., McInnes, C.A., Moorrees, C.O., Wilson, B.W. (1987)
The Mineralogy and Geochemistry of the Kunwarara Magnesite Deposit, *unpubl report to QMC*, CSIRO Division of Mineral Chemistry.

Charlton, T.J. (1992)
Geology of the Pointers Range Area and Kunwarara Magnesite Deposit, Rockhampton District, Central Queensland. *unpubl. Honours thesis, University of Queensland.*

Day, R. W., Whitaker, W.G., Murray, C.G., Wilson, I.H. and Grimes, K.G. (1983)
Queensland Geology. *Geological Survey of Queensland Publication*, 383.

Dagbert, M. (1990)
Approaches to Ore Reserve Estimation – Indicator Approach. *Unpubl. newsletter* from Snowden Associates, May, 1990

Day, R.W., Murray, C.G. and Whitaker, W.G., (1978)
The Eastern Part of the Tasman Orogenic Zone. in *Tectonophysics*, Volume 478, pp 327-364.

Dunstan, B. (1913)
Queensland Minerals Index and Guide. *Geological Survey of Queensland*, Publication No 241

Fergusson, C.L., Henderson, R.A., and Leitch, E.C. (1990)
Subduction Complex Melange of the Wandilla Terrane, Palaeozoic New England Fold Orogen, Central Queensland, Australia. in *Journal of Structural Geology*, Volume 12, pp 591-599.

Fergusson, C.L., Henderson, R.A. and Leitch, E.C. (1994)
Tectonics of the New England Fold Belt in the Rockhampton-Gladstone Region, Central Queensland. in Holcombe, R.J., Stephens, C.J. and Fielding, C.R. editors, *Capricorn Region, Central Queensland 1994 Field*

Conference Manual, Geological Society of Australia, Queensland Division, pp 1-16

Fleming, P.J., Murray, C.G. and Whitaker, W.G. (1975)
Palaeozoic invertebrate fossils in the Wandilla Formation, and the Deposition of the Curtis Island Group. *In Queensland Government Mining Journal*, Volume 76, pp 72 - 76.

Henderson, R. (1980)
Structural Outline and Summary Geological History for Northeastern Australia in Henderson, R.A. and Stephenson, P.J. editors, *The Geology and Geophysics of Northeastern Australia.* Geological Division of Australia, Queensland Division, July, 1980. pp 1-26

Hill, B.F. (1992)
Magnesite and magnesia production by Queensland Magnesia (Operations) Pty Ltd at Kunwarara and Rockhampton, Qld. In *AusIMM Bulletin*, July, 1992.

Journel, A. (1985)
Recoverable reserves estimation – the geostatistical approach. In *Mining Engineering*, Volume 37, no 6, June 1985, pp 563-568

Kim, Y. C. (1993)
Introductory Geostatistics and Mine Planning. *unpubl. short course notes*, Department of Mining and Geological Engineering, University of Arizona.

King, H., McMahon D. and Bujtor, G.(1982)
A guide to the understanding of ore reserve estimation. *In Supplement to AusIMM Proceedings No. 281*, March, 1982.

Lawrance, L. (1997)
Regolith Geochemistry. *Unpubl. seminar notes*, 3 day workshop presented at University of Western Australia, Perth, WA, June 25 to 27, 1997.

Marsden, M.A. (1972)
The Devonian History of Northeastern Australia, in *Journal of the Geological Society of Australia*, Volume 19, pp 125 – 162

Milburn, D. and Wilcock, S. (1994)
The Kunwarara Magnesite Deposit, Central Queensland. In Holcombe, R.J., Stephens, C.J. and Fielding C.R., editors, *Capricorn Region Central Coastal Queensland, 1994 Field Conference Manual*, pp 99 – 107.

Morris R.C. and Fletcher, A.B. (1987)
Increased Solubility of Quartz Following Ferrous-Ferric Iron Reactions. In *Nature*, Volume 330, pp 558 – 561

Murray, C.G. (1974)
Alpine-type ultramafics in the Northern Part of the Tasman Geosyncline, Possible Remnant of Palaeozoic Ocean Floor. In *The Tasman Geosyncline, a Symposium*, pp 161 - 181

Murray, C.G., Fergusson, C.L., Flood, P.G., Whitaker, W.G. and Korsch, R.J. (1987).
Plate Tectonic Model for the Carboniferous Evolution of the New England Fold Belt, in *Australian Journal of Earth Sciences*, Volume 34, pp 213 – 236.

Ridgeway, J.E. (1948)
Magnesite deposits at Princhester, Marlborough district. In *Queensland Government Mining Journal*, Volume 42, p 139

Royle, A.G. (1980)
Estimating Global Ore Reserves in a Single Deposit in *Minerals, Science and Engineering*, Volume 12, No. 1, pp 37-50

Schmid, I.H. (1987)
Turkey's Salda Lake – A Genetic Model for Australia's Newly Discovered Magnesite Deposits. in *Industrial Minerals*. August, 1997.

Snowden, D.V. (1995)
Applied Mining Geostatistics. *Unpubl. notes* from Shortcourse presented at Key Centre, University of Tasmania, November, 1995.

Trescases, J.J. (1992)
Chemical Weathering, in Butt, C.R.M. and Zeegers, H. editors, *Handbook of Exploration Geochemistry, Volume 4, Regolith Exploration Geochemistry in Tropical and Subtropical Terrains*. Elsevier Press. pp 25-40

Verly, G. (1983)
The Multigaussian Approach and its Applications to the Estimation of Local Reserves. In *Journal of Mathematical Geology*, Volume 15, No. 2 pp 263-290

Verly, G. and Sullivan, J. (1985)
Multigaussian and Probability Kriging – Application to the Jerrit Canyon Deposit. In *Mining Engineering*, Volume 37, no 6, June 1985 pp 568-574

APPENDIX ONE

Three Dimensional Variograms

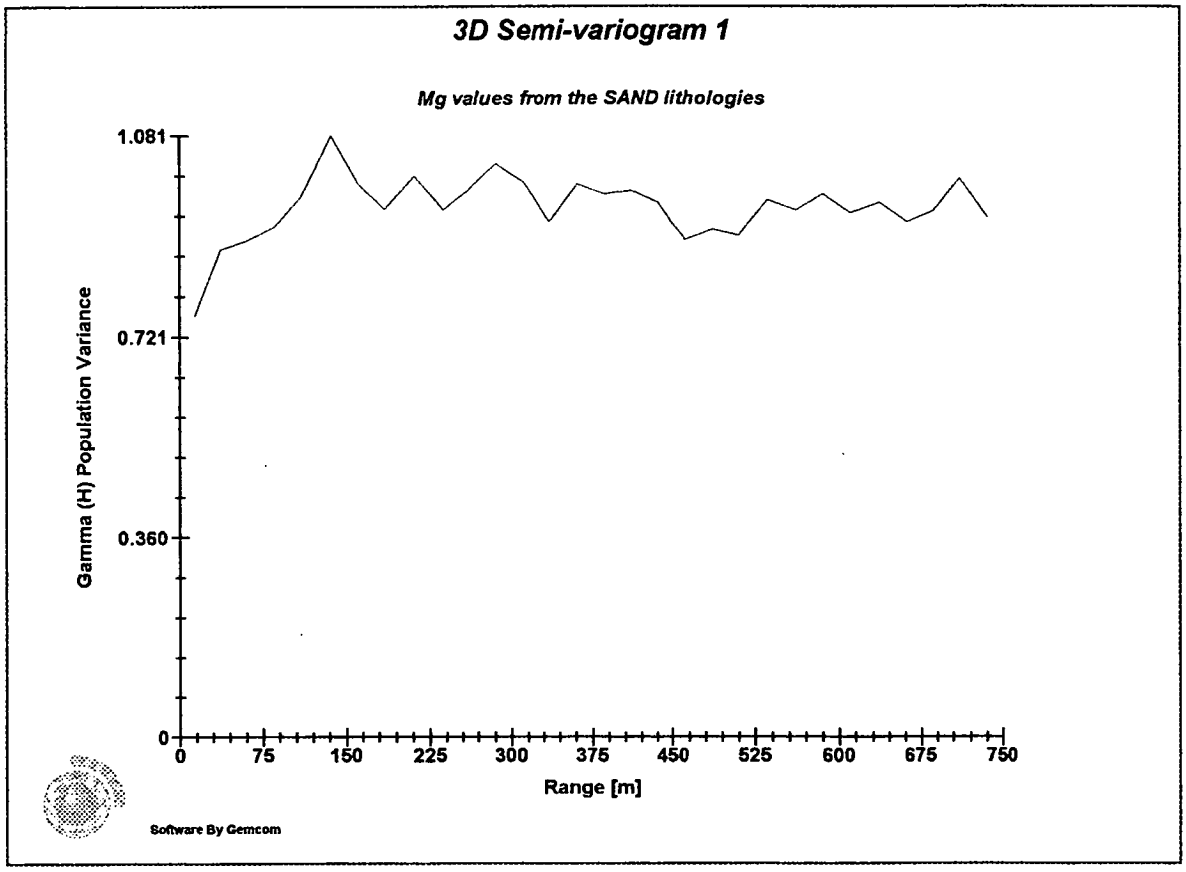
3D Semi-variogram 1
Mg values from the SAND lithologies
1.081
0.721
0.360
0
Gamma (H) Population Variance
0
75
150
225
300
375
450
525
600
675
750
Range [m]
Software By Gemcom

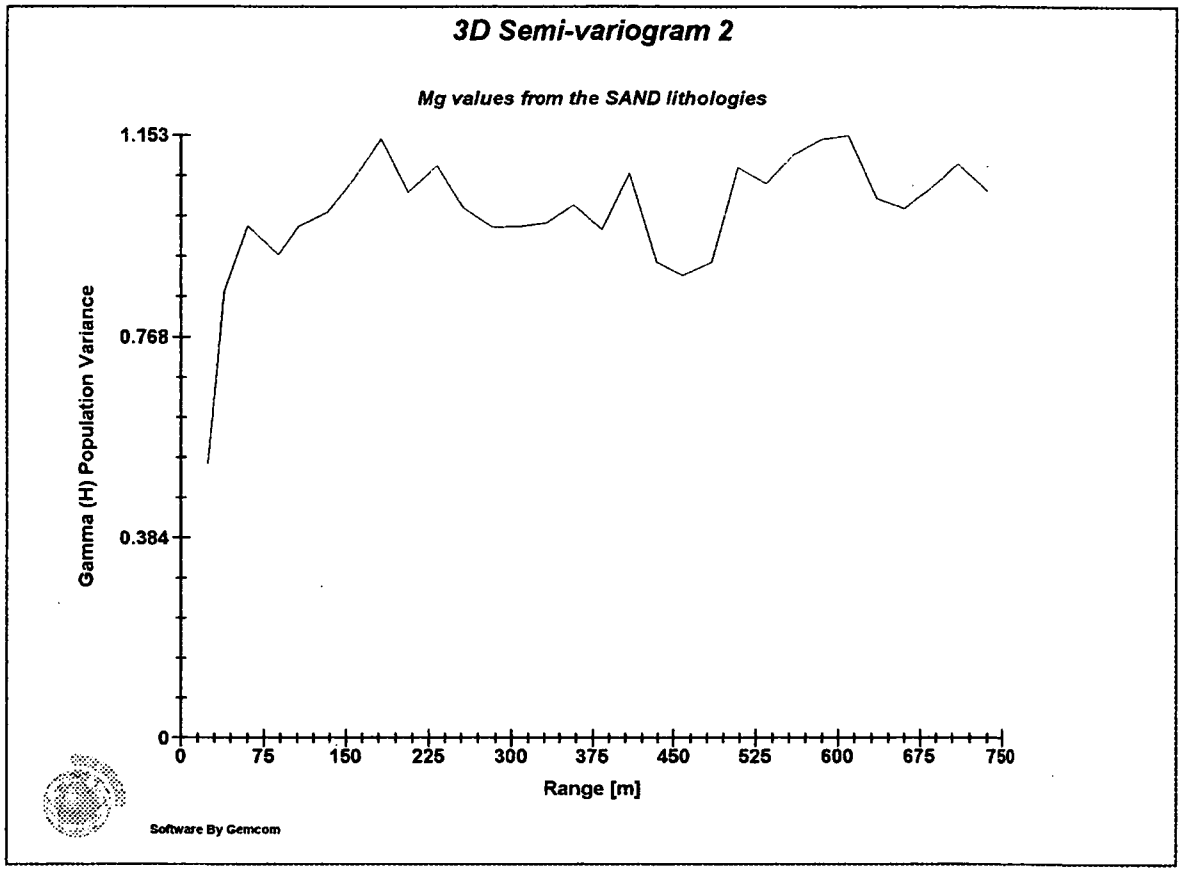
3D Semi-variogram 2
Mg values from the SAND lithologies
Gamma (H) Population Variance
1.153
0.768
0.384
0
0
75
150
225
300
375
450
525
600
675
750
Range [m]
Software By Gemcom

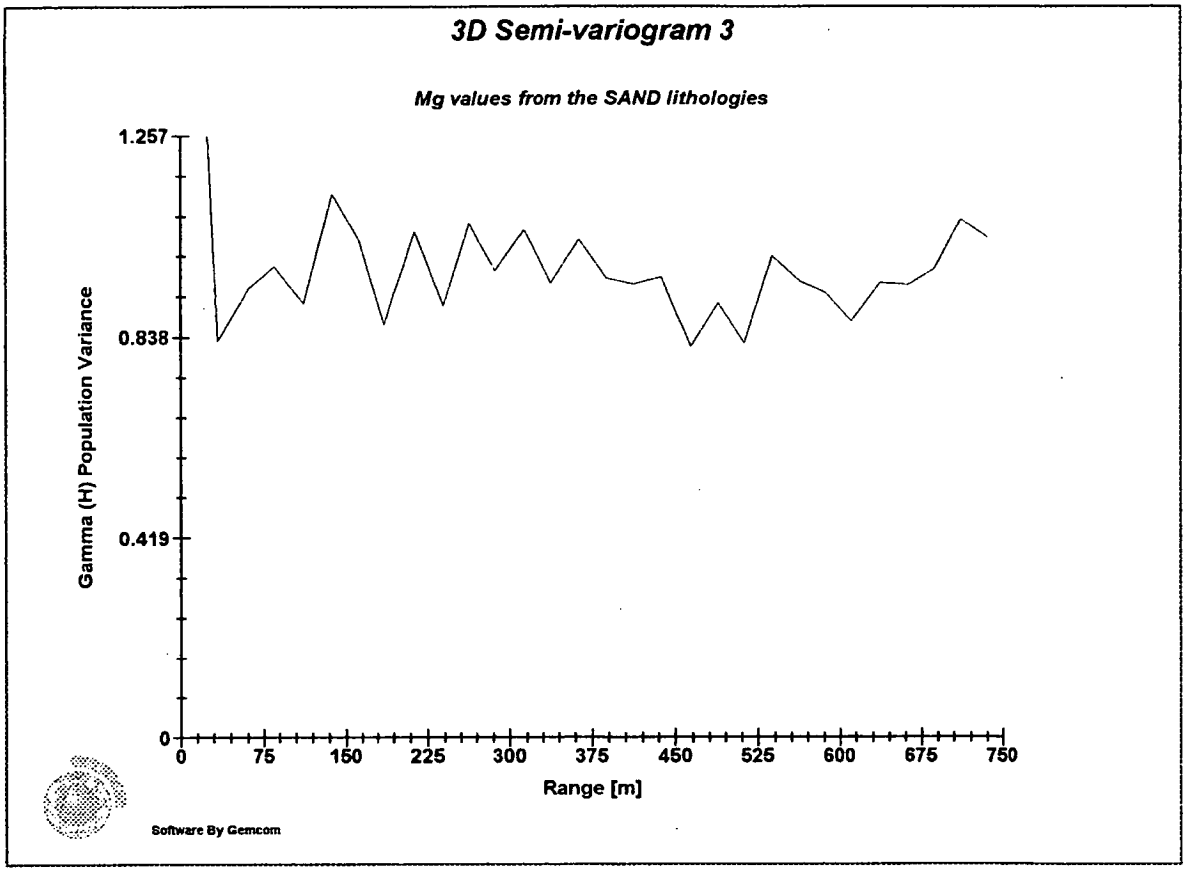
3D Semi-variogram 3
Mg values from the SAND lithologies
Gamma (H) Population Variance
1.257
0.838
0.419
0
0
75
150
225
300
375
450
525
600
675
750
Range [m]
Software By Gemcom

3D Semi-variogram 4

Mg values from the SAND lithologies

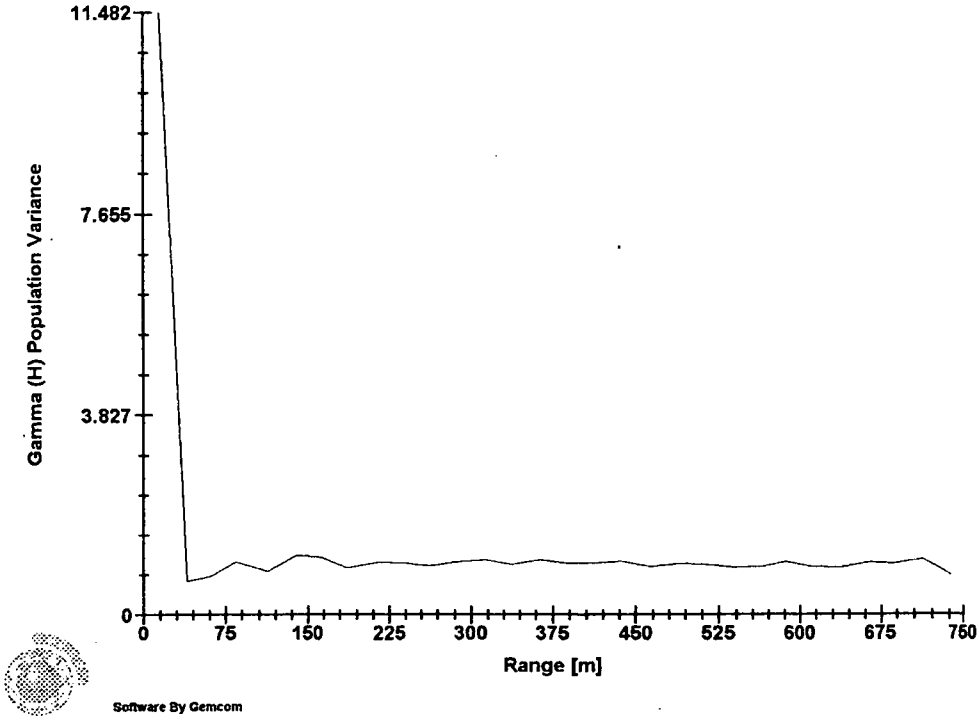

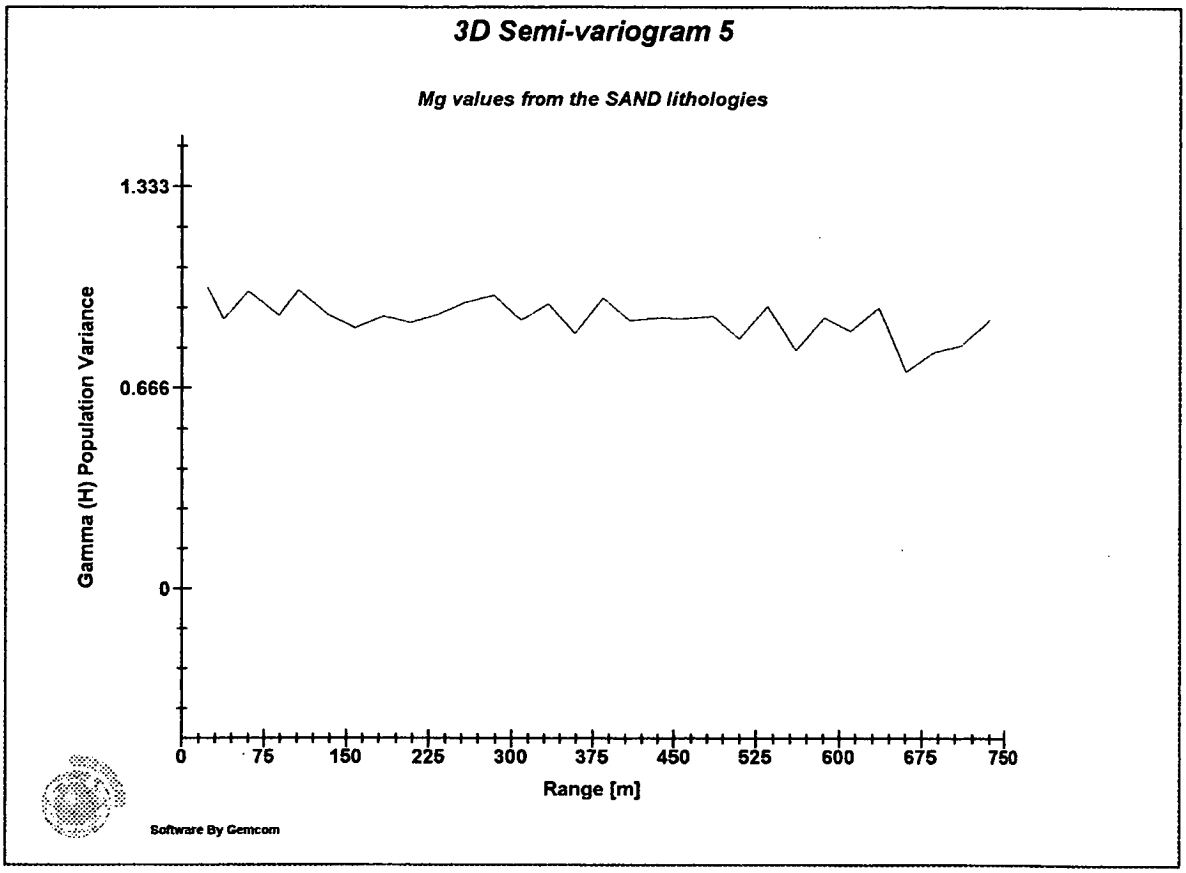
3D Semi-variogram 5
Mg values from the SAND lithologies
1.333
0.666
0
Gamma (H) Population Variance
0
75
150
225
300
375
450
525
600
675
750
Range [m]
Software By Gemcom

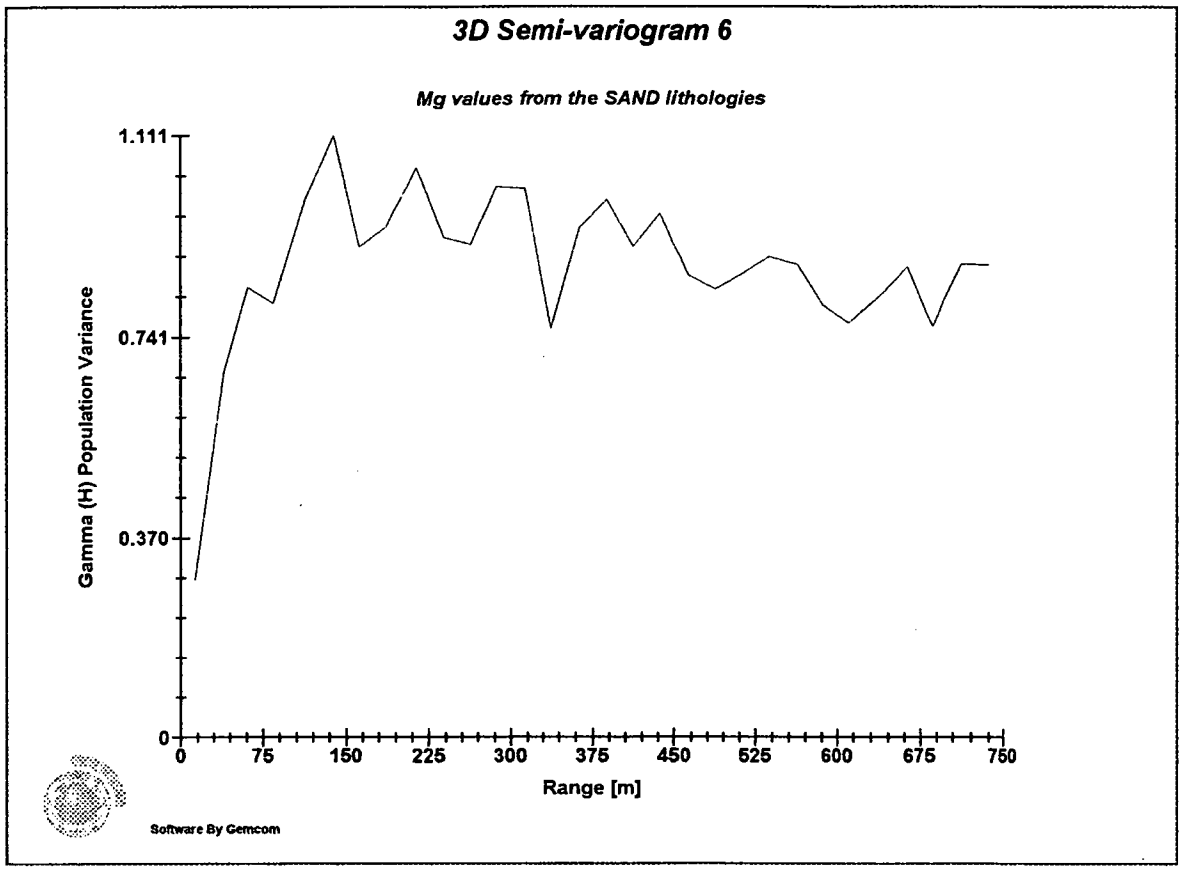
3D Semi-variogram 6
Mg values from the SAND lithologies
Gamma (H) Population Variance
1.111
0.741
0.370
0
0
75
150
225
300
375
450
525
600
675
750
Range [m]
Software By Gemcom

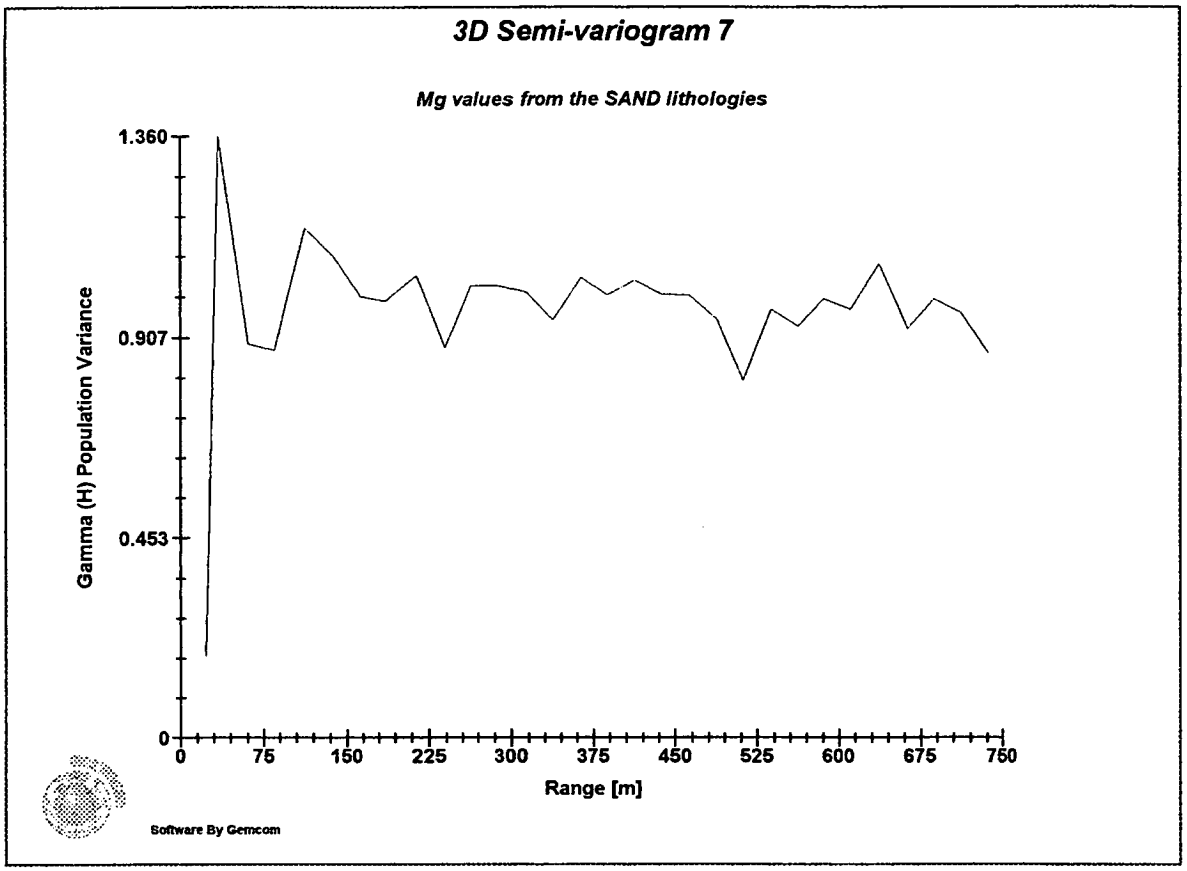
3D Semi-variogram 7
Mg values from the SAND lithologies
Gamma (H) Population Variance
1.360
0.907
0.453
0
0
75
150
225
300
375
450
525
600
675
750
Range [m]
Software By Gemcom

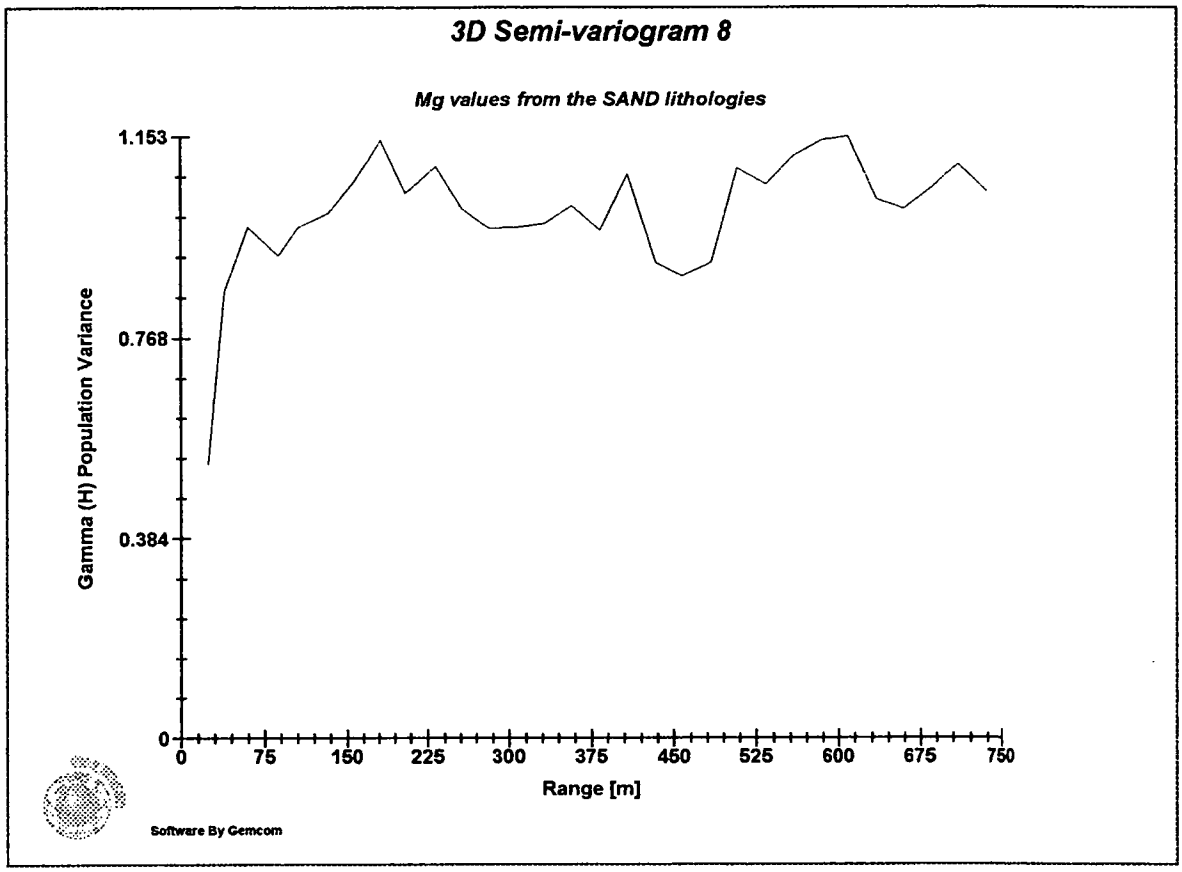
3D Semi-variogram 8
Mg values from the SAND lithologies
Gamma (H) Population Variance
1.153
0.768
0.384
0
0
75
150
225
300
375
450
525
600
675
750
Range [m]
Software By Gemcom

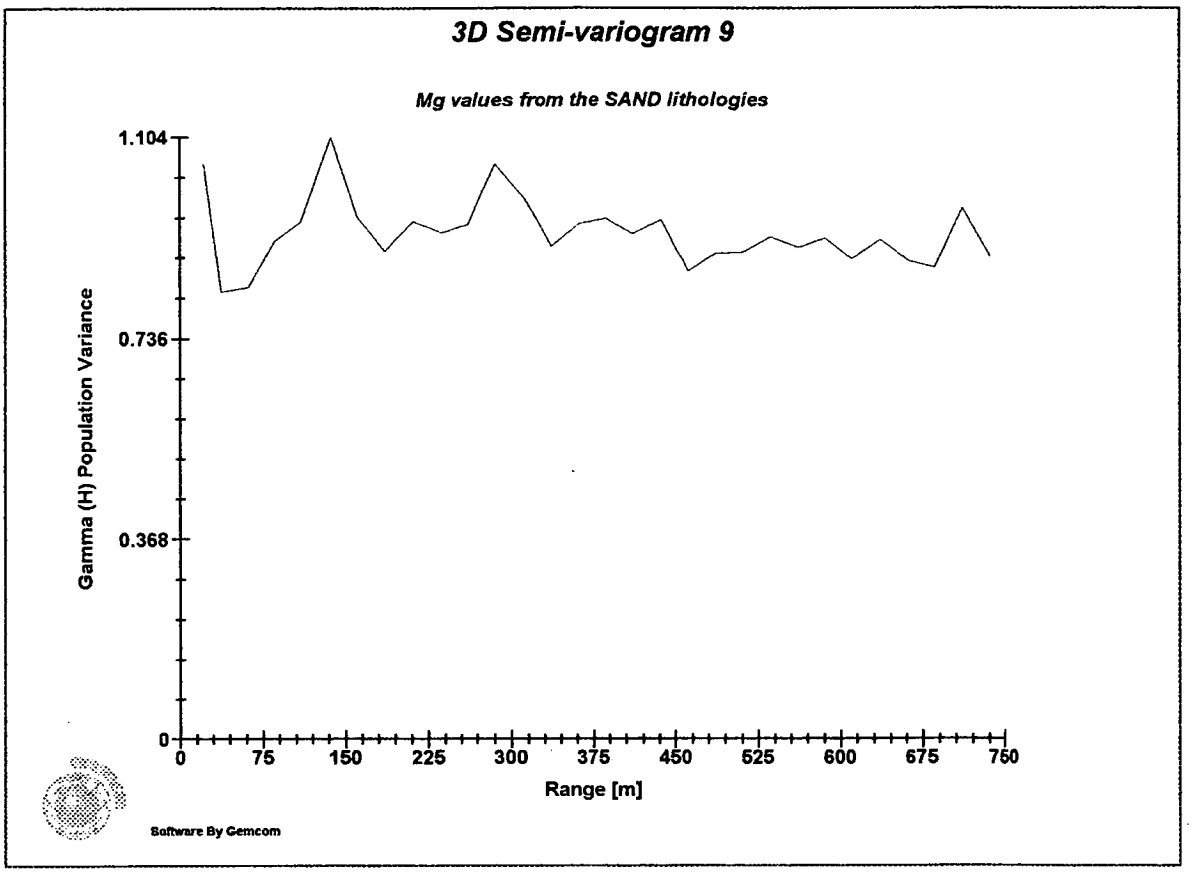
3D Semi-variogram 9
Mg values from the SAND lithologies
1.104
0.736
0.368
0
Gamma (H) Population Variance
0
75
150
225
300
375
450
525
600
675
750
Range [m]
Software By Gemcom

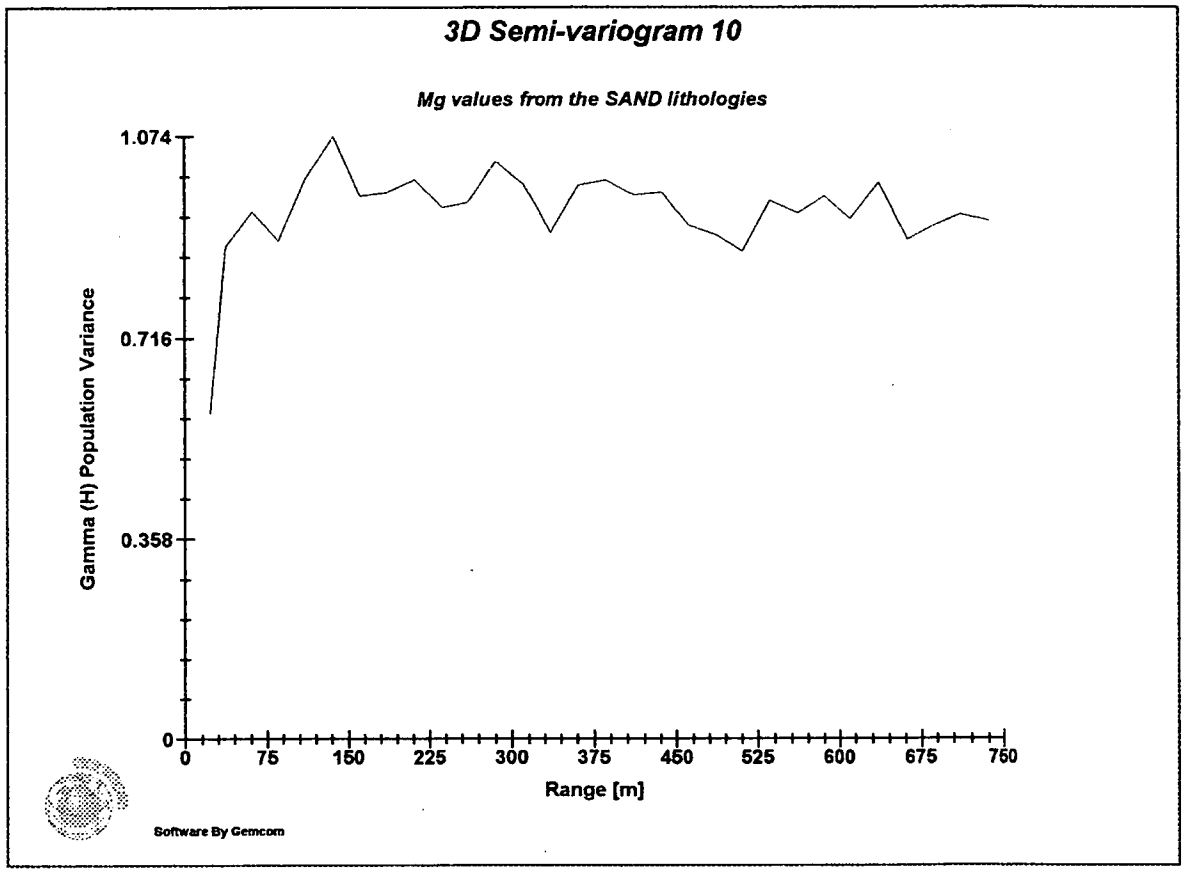
3D Semi-variogram 10
Mg values from the SAND lithologies
Gamma (H) Population Variance
1.074
0.716
0.358
0
0
75
150
225
300
375
450
525
600
675
750
Range [m]
Software By Gemcom

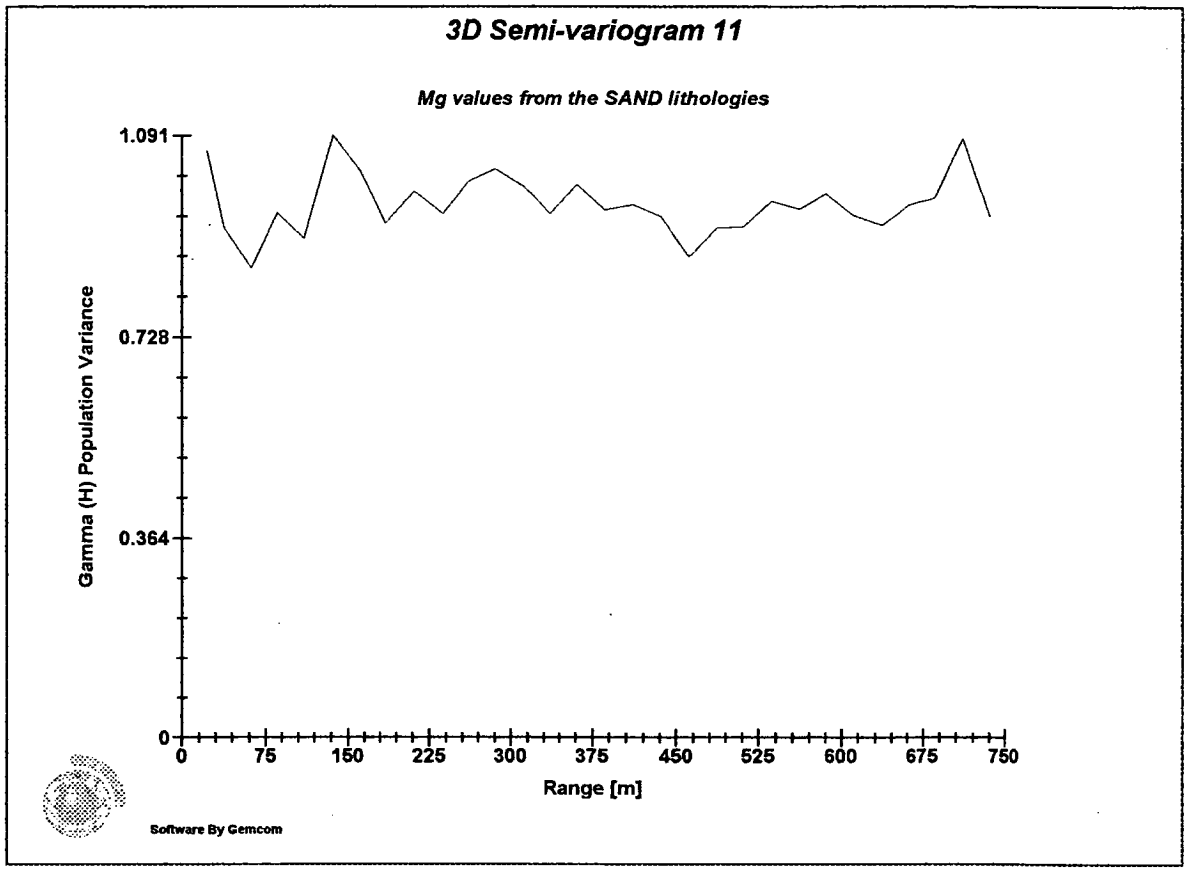
3D Semi-variogram 11
Mg values from the SAND lithologies
1.091
0.728
0.364
0
Gamma (H) Population Variance
0
75
150
225
300
375
450
525
600
675
750
Range [m]
Software By Gemcom

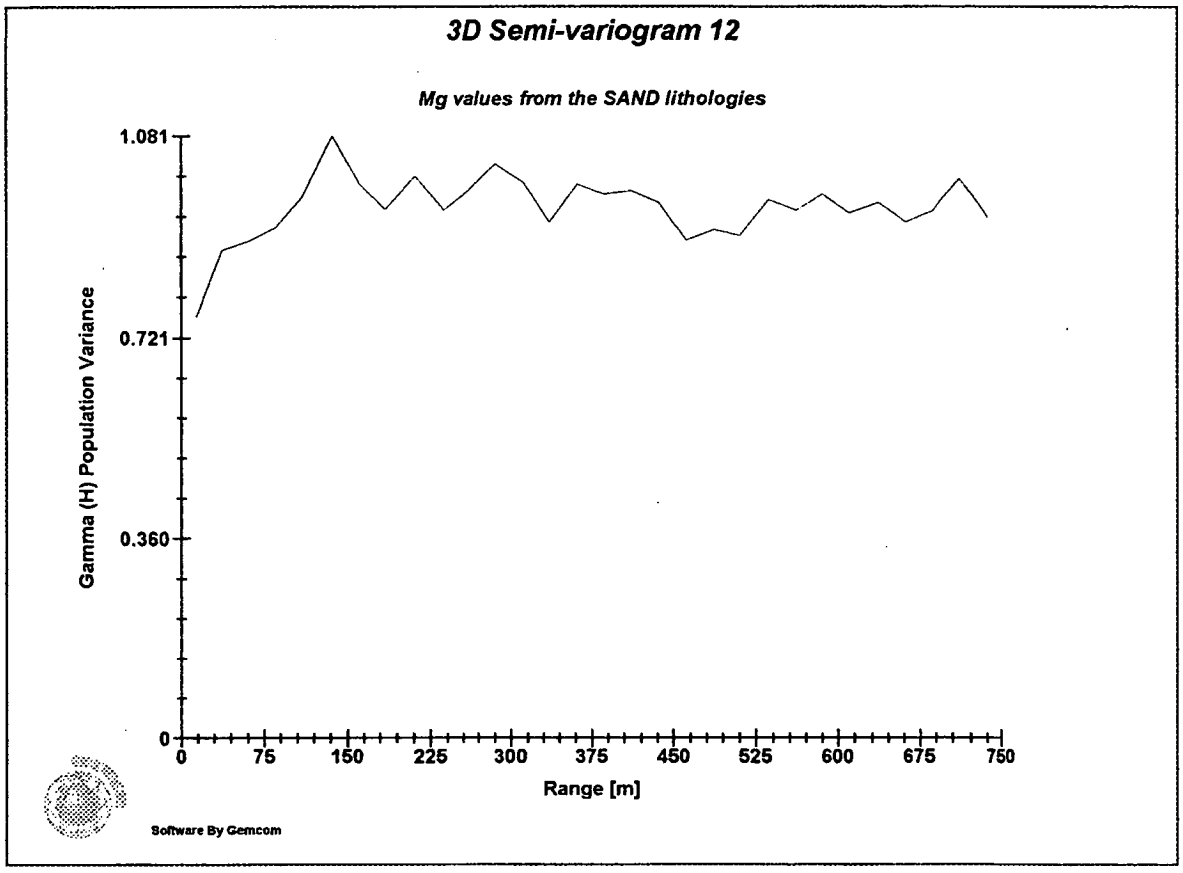
3D Semi-variogram 12
Mg values from the SAND lithologies
Gamma (H) Population Variance
1.081
0.721
0.360
0
0
75
150
225
300
375
450
525
600
675
750
Range [m]
Software By Gemcom

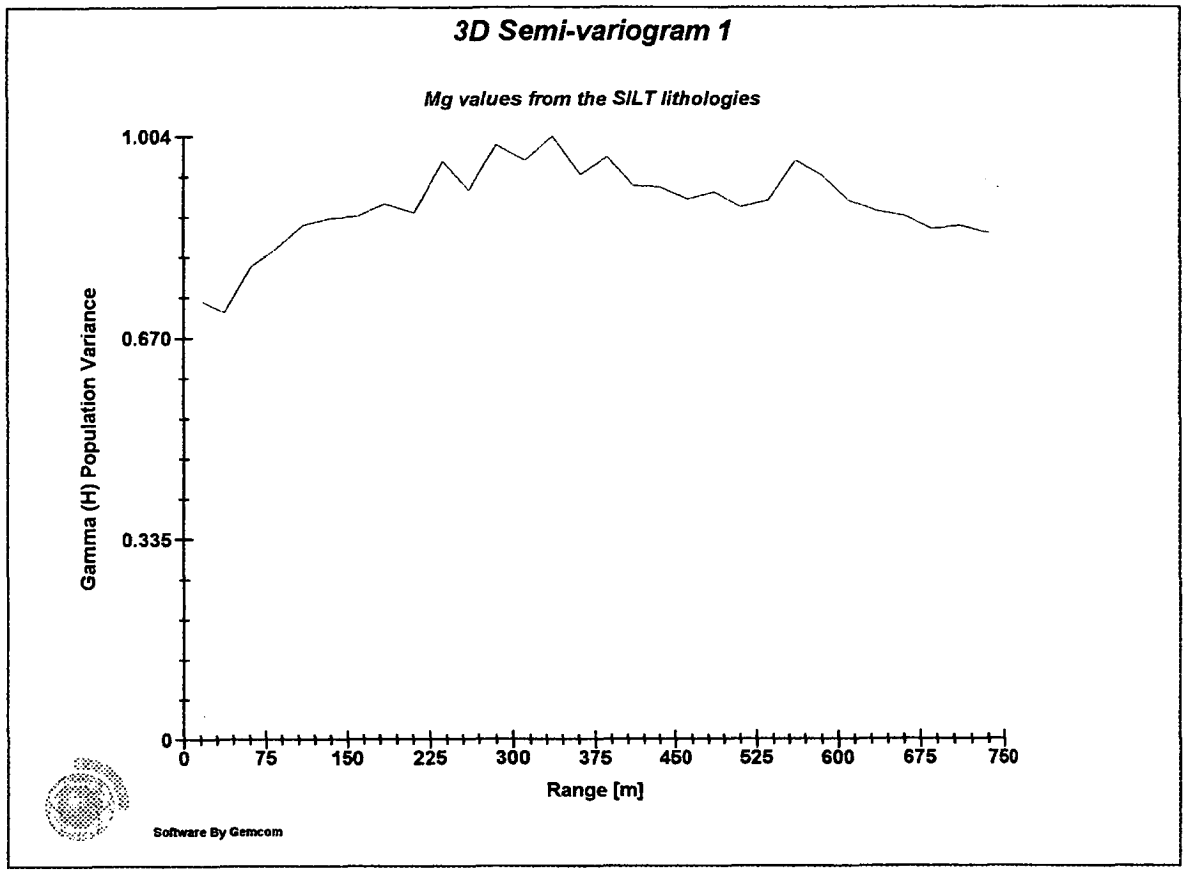
3D Semi-variogram 1
Mg values from the SILT lithologies
Gamma (H) Population Variance
1.004
0.670
0.335
0
0
75
150
225
300
375
450
525
600
675
750
Range [m]
Software By Gemcom

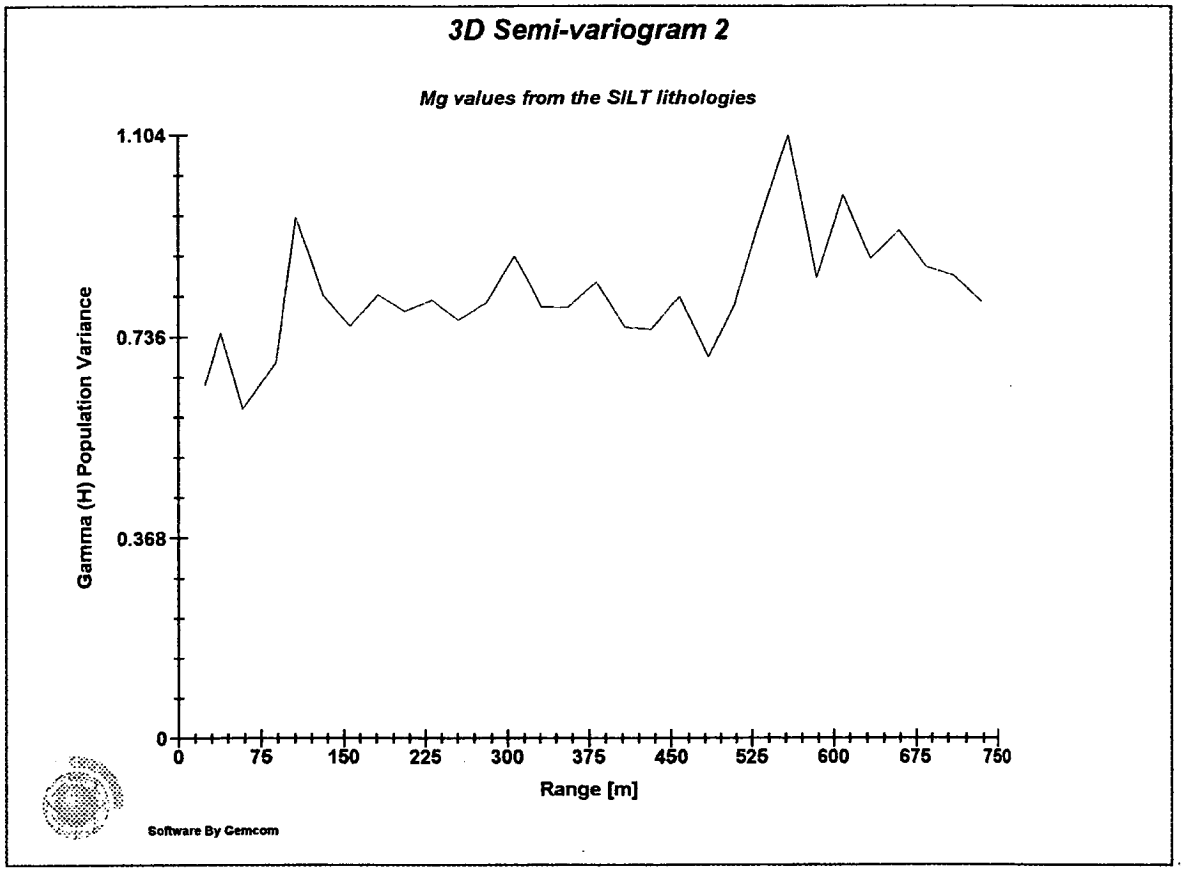
3D Semi-variogram 2
Mg values from the SILT lithologies
Gamma (H) Population Variance
1.104
0.736
0.368
0
0
75
150
225
300
375
450
525
600
675
750
Range [m]
Software By Gemcom

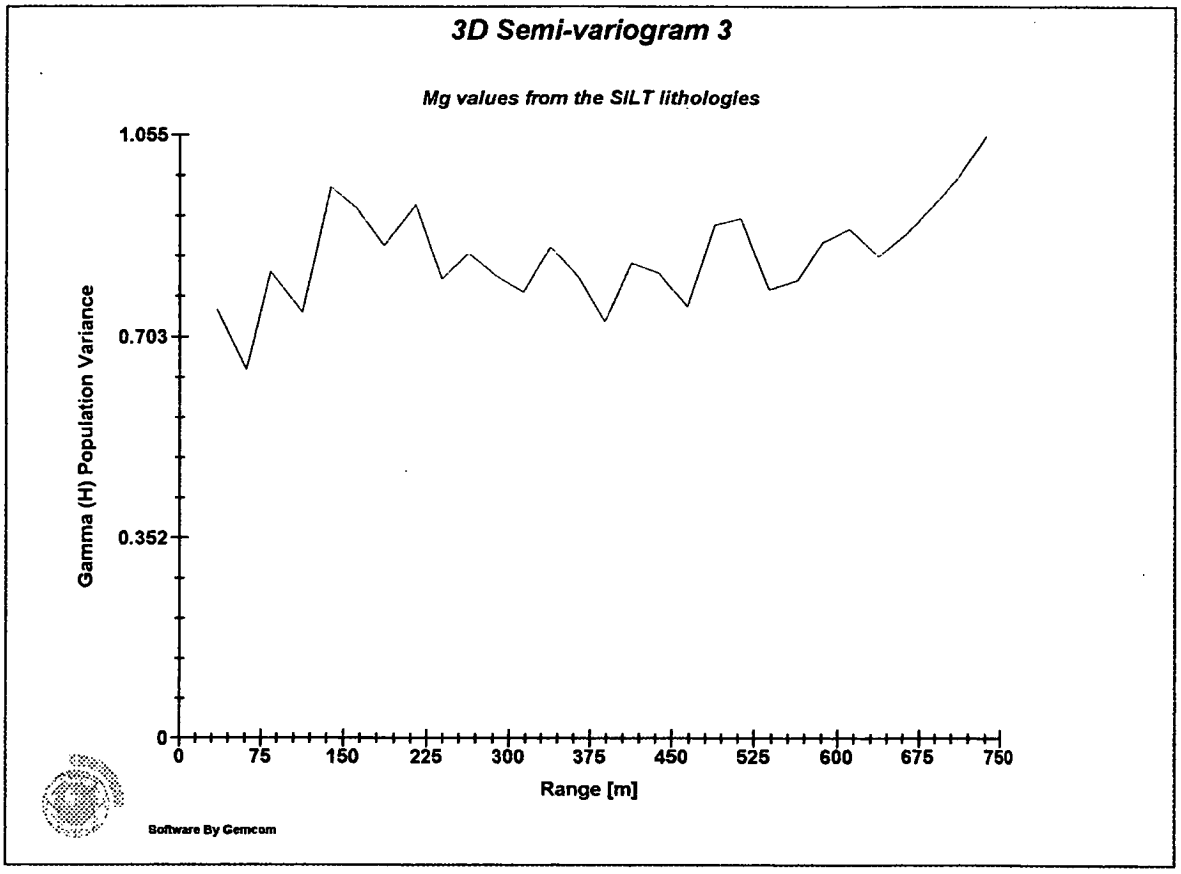
3D Semi-variogram 3
Mg values from the SILT lithologies
1.055
0.703
0.352
0
Gamma (H) Population Variance
0
75
150
225
300
375
450
525
600
675
750
Range [m]
Software By Gemcom

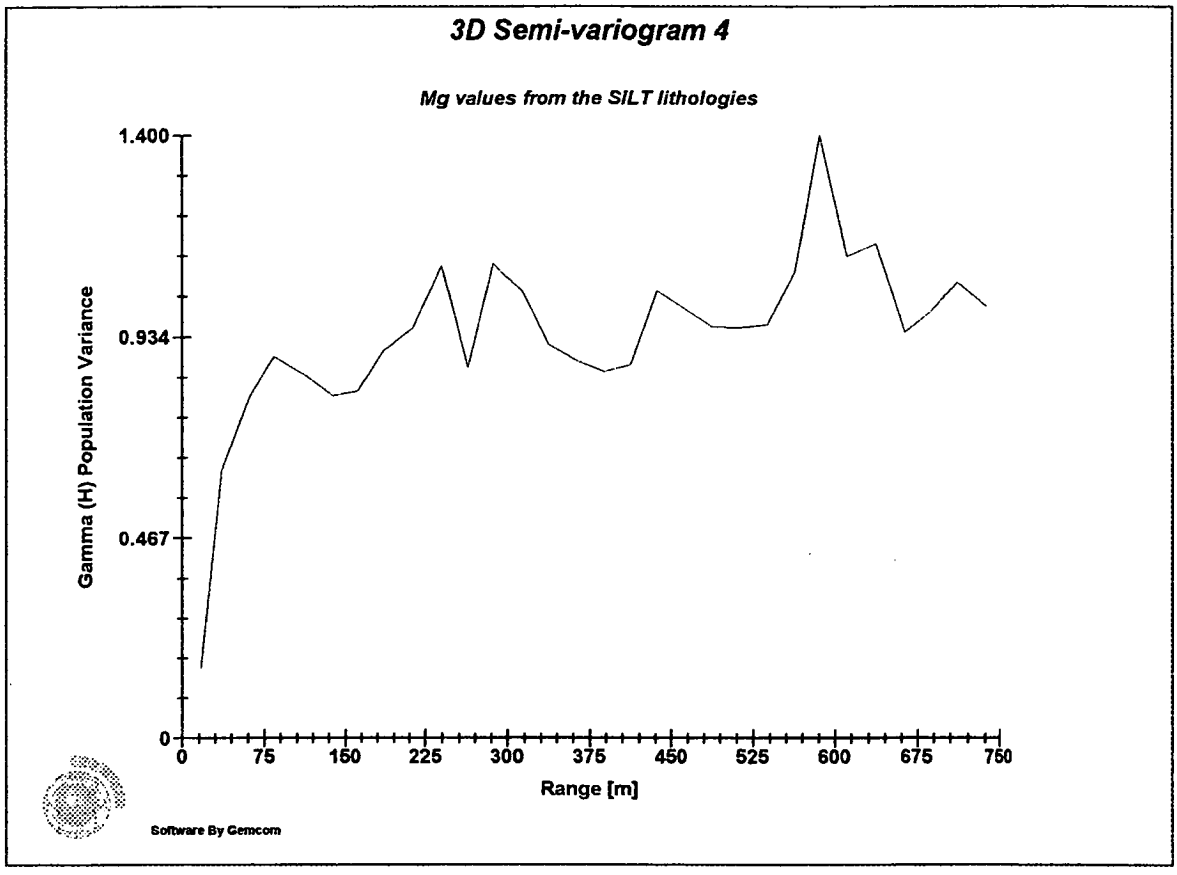
3D Semi-variogram 4
Mg values from the SILT lithologies
Gamma (H) Population Variance
1.400
0.934
0.467
0
0
75
150
225
300
375
450
525
600
675
750
Range [m]
Software By Gemcom

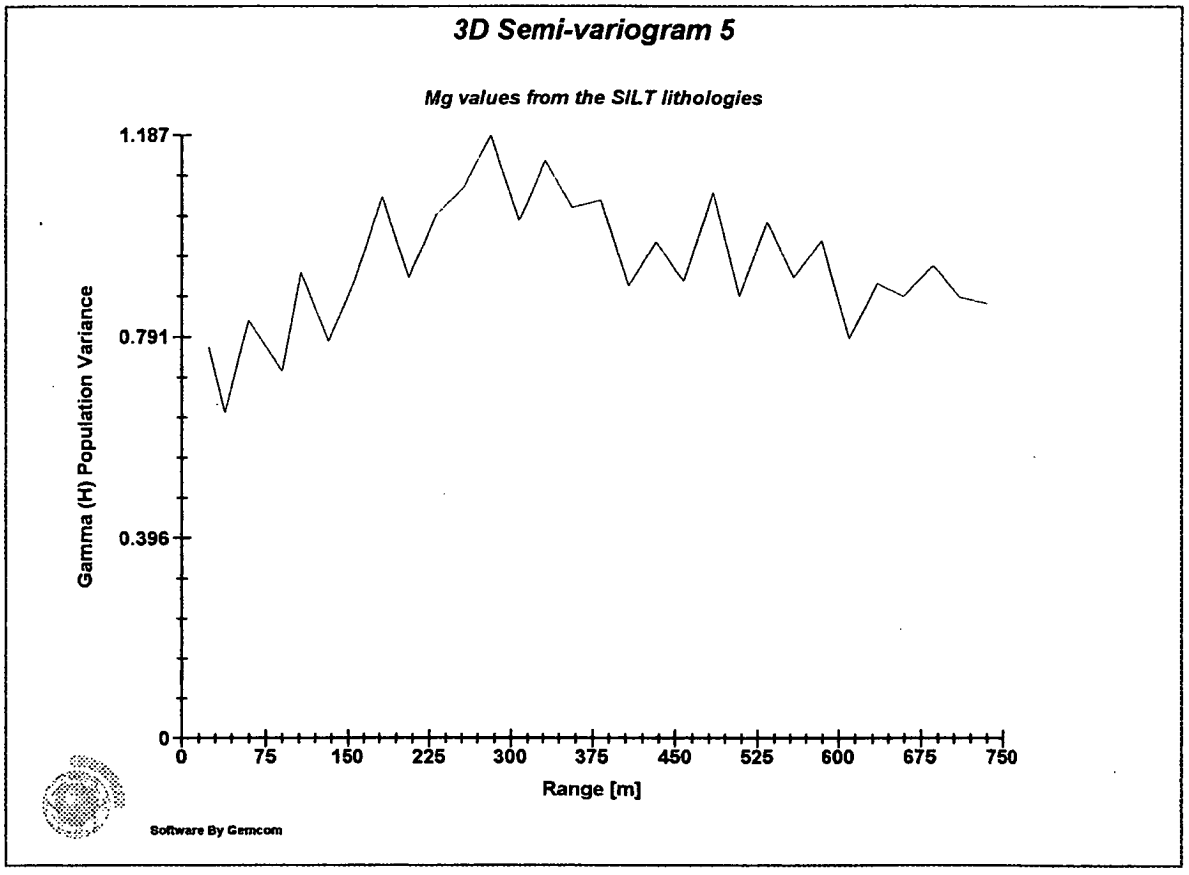
3D Semi-variogram 5
Mg values from the SILT lithologies
1.187
0.791
0.396
0
Gamma (H) Population Variance
0
75
150
225
300
375
450
525
600
675
750
Range [m]
Software By Gemcom

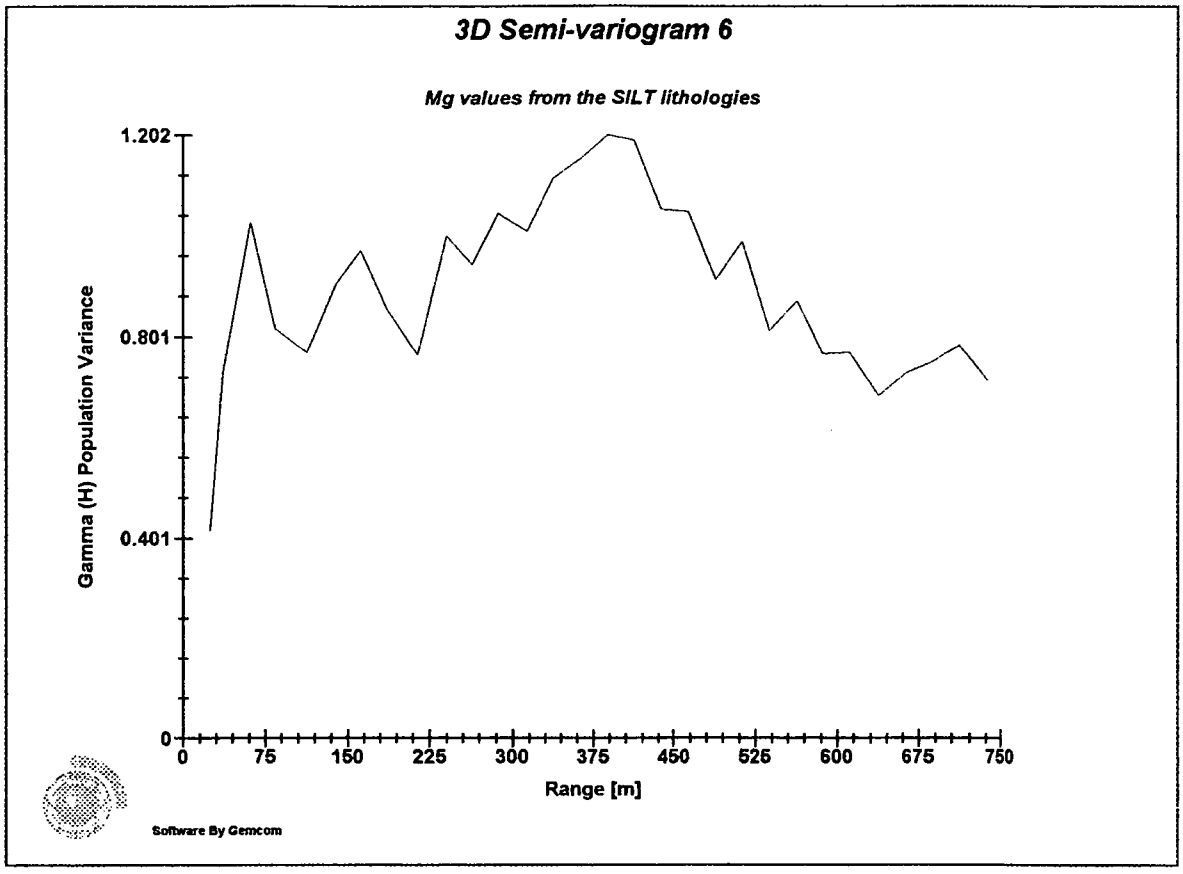
3D Semi-variogram 6
Mg values from the SILT lithologies
Gamma (H) Population Variance
1.202
0.801
0.401
0
0
75
150
225
300
375
450
525
600
675
750
Range [m]
Software By Gemcom

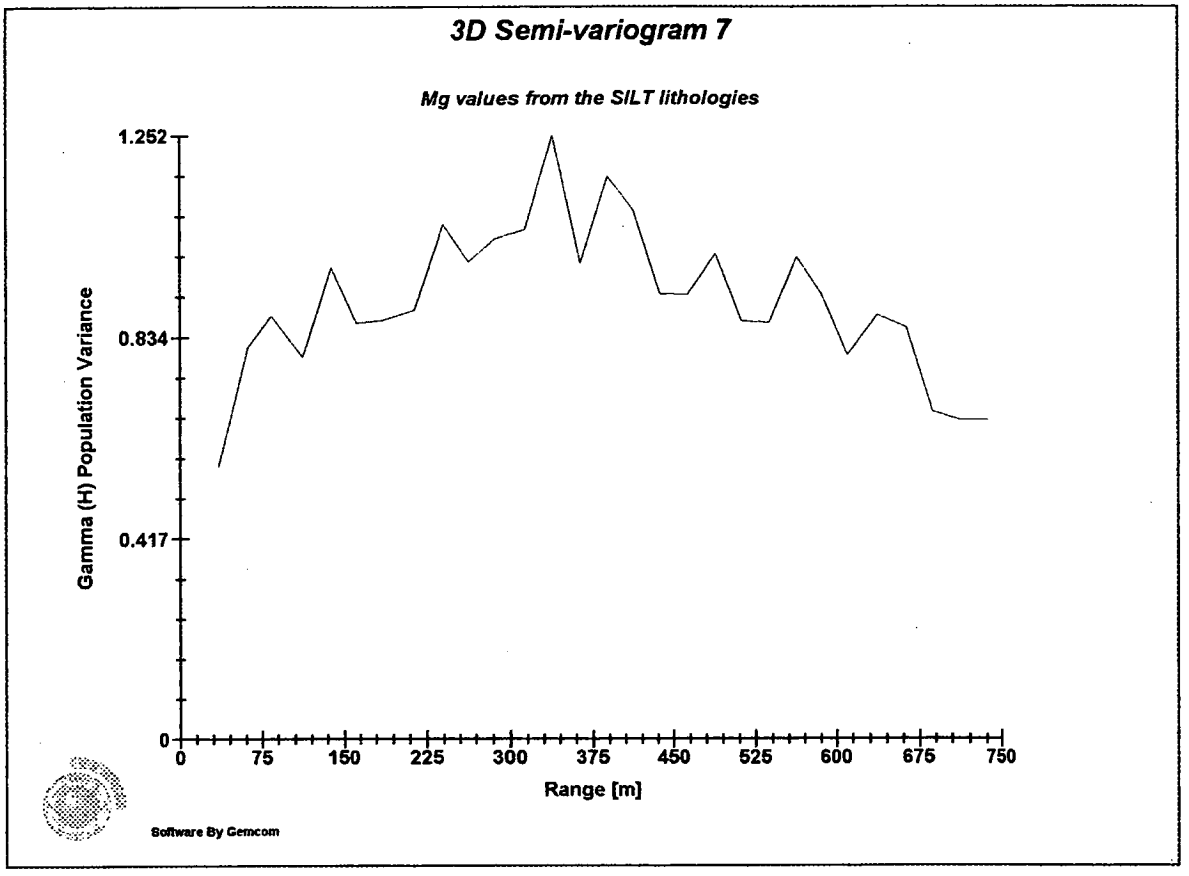
3D Semi-variogram 7
Mg values from the SILT lithologies
Gamma (H) Population Variance
1.252
0.834
0.417
0
0
75
150
225
300
375
450
525
600
675
750
Range [m]
Software By Gemcom

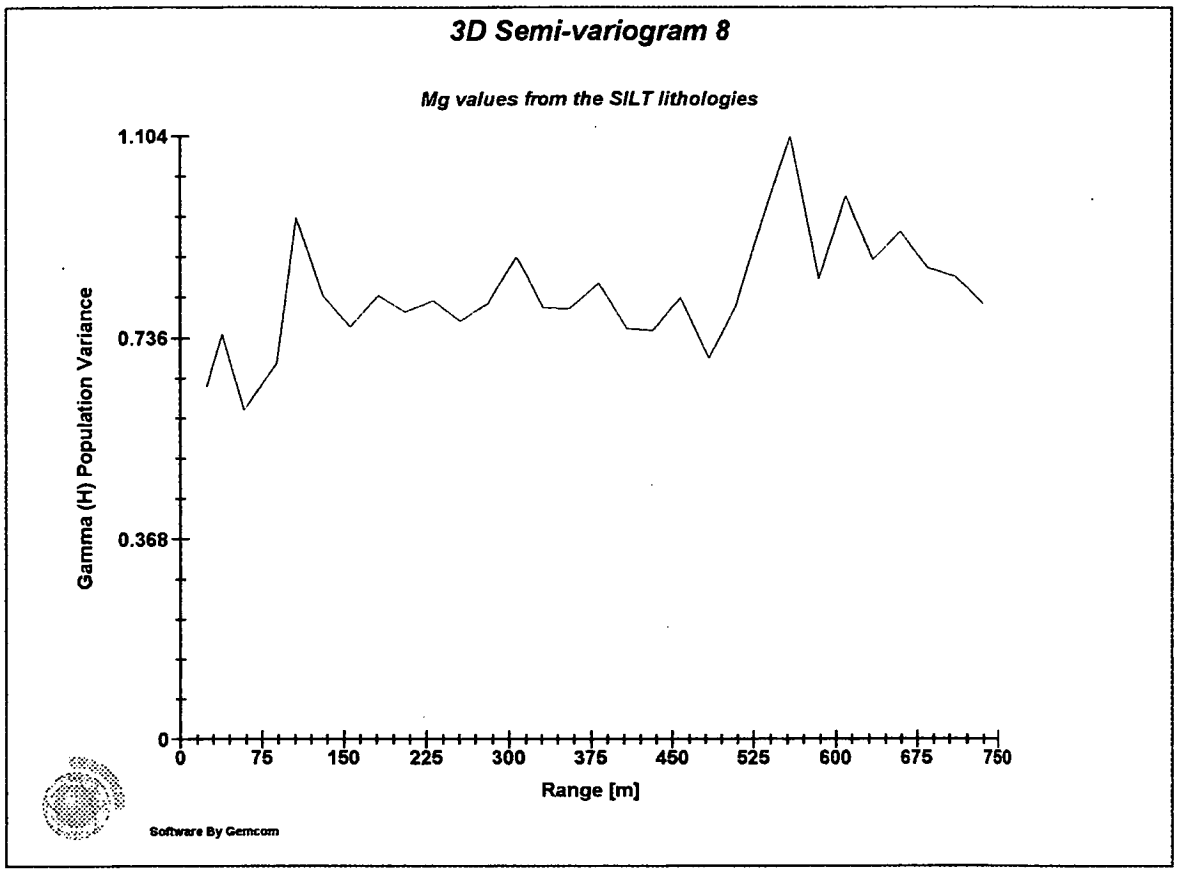
3D Semi-variogram 8
Mg values from the SILT lithologies
Gamma (H) Population Variance
1.104
0.736
0.368
0
0
75
150
225
300
375
450
525
600
675
750
Range [m]
Software By Gemcom

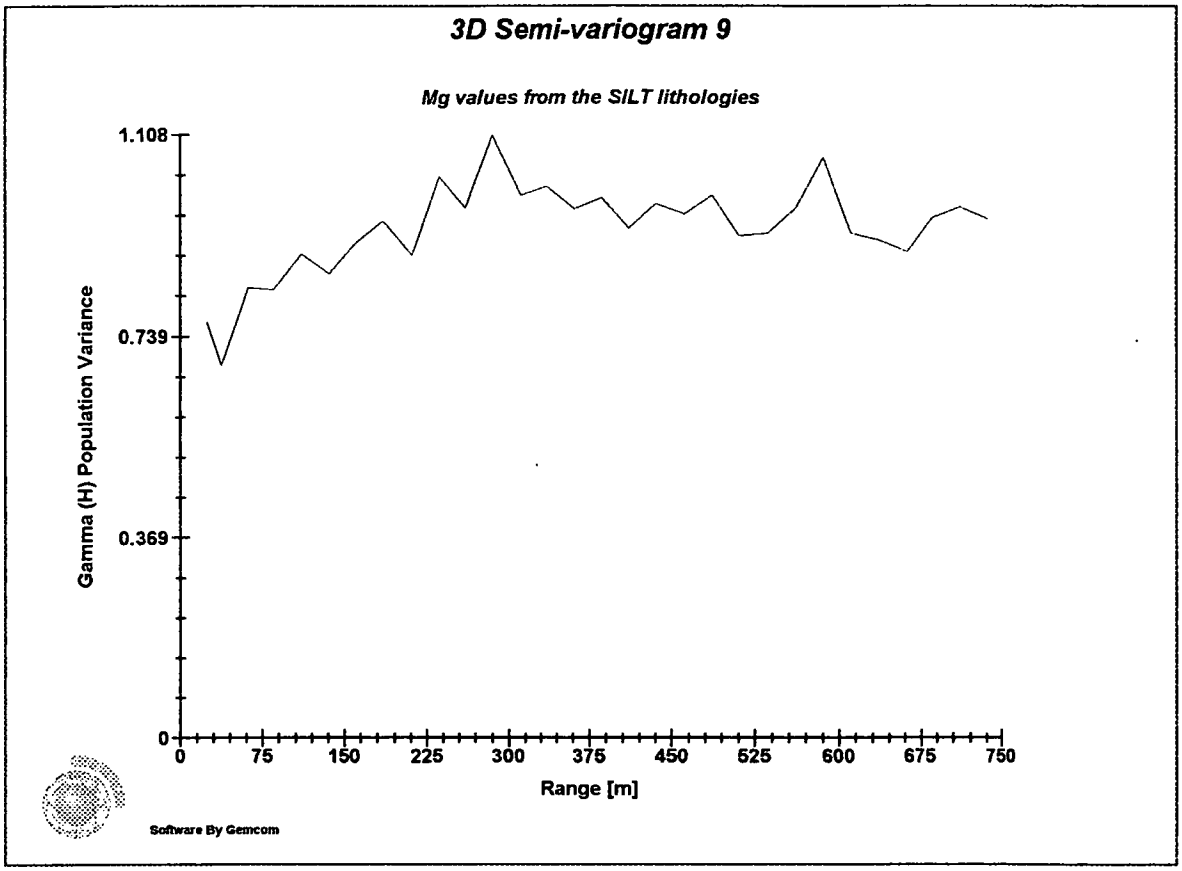
3D Semi-variogram 9
Mg values from the SILT lithologies
Gamma (H) Population Variance
1.108
0.739
0.369
0
0
75
150
225
300
375
450
525
600
675
750
Range [m]
Software By Gemcom

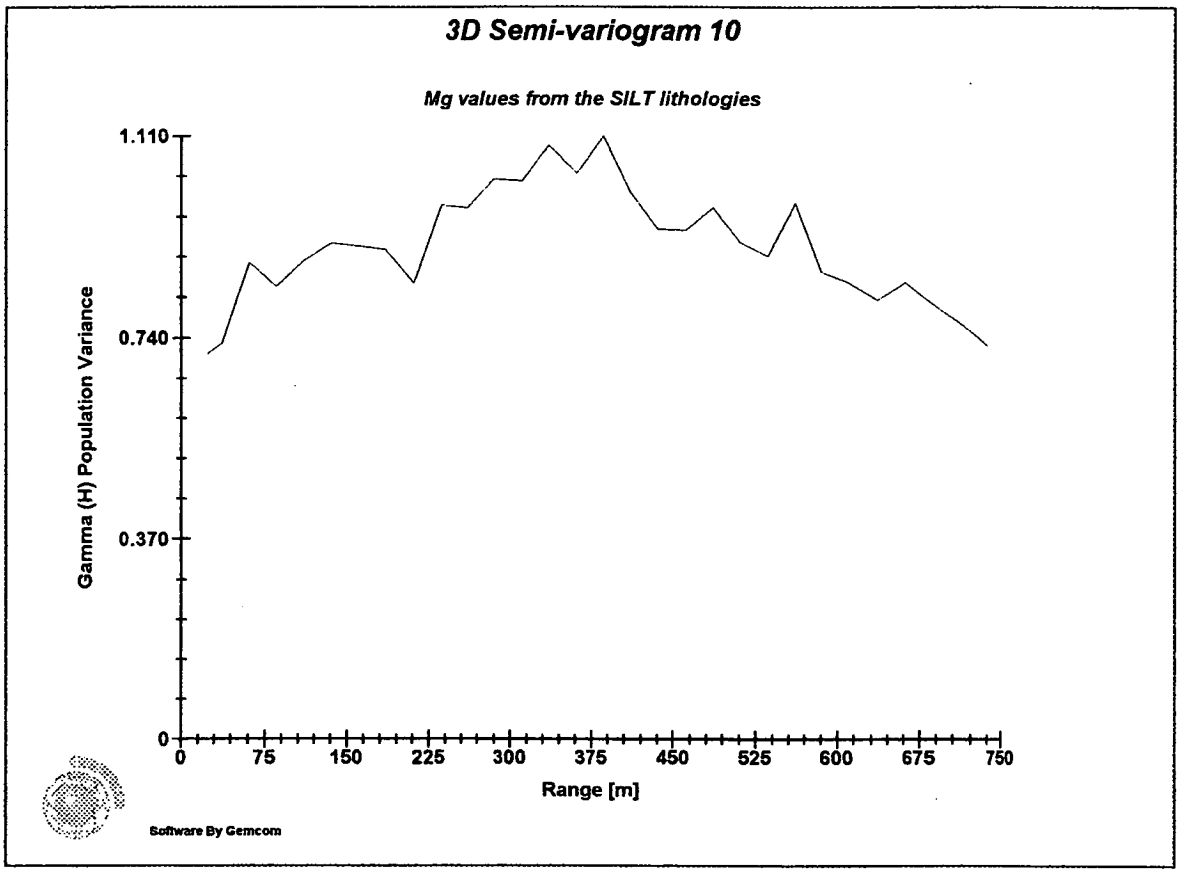
3D Semi-variogram 10
Mg values from the SILT lithologies
Gamma (H) Population Variance
1.110
0.740
0.370
0
0
75
150
225
300
375
450
525
600
675
750
Range [m]
Software By Gemcom

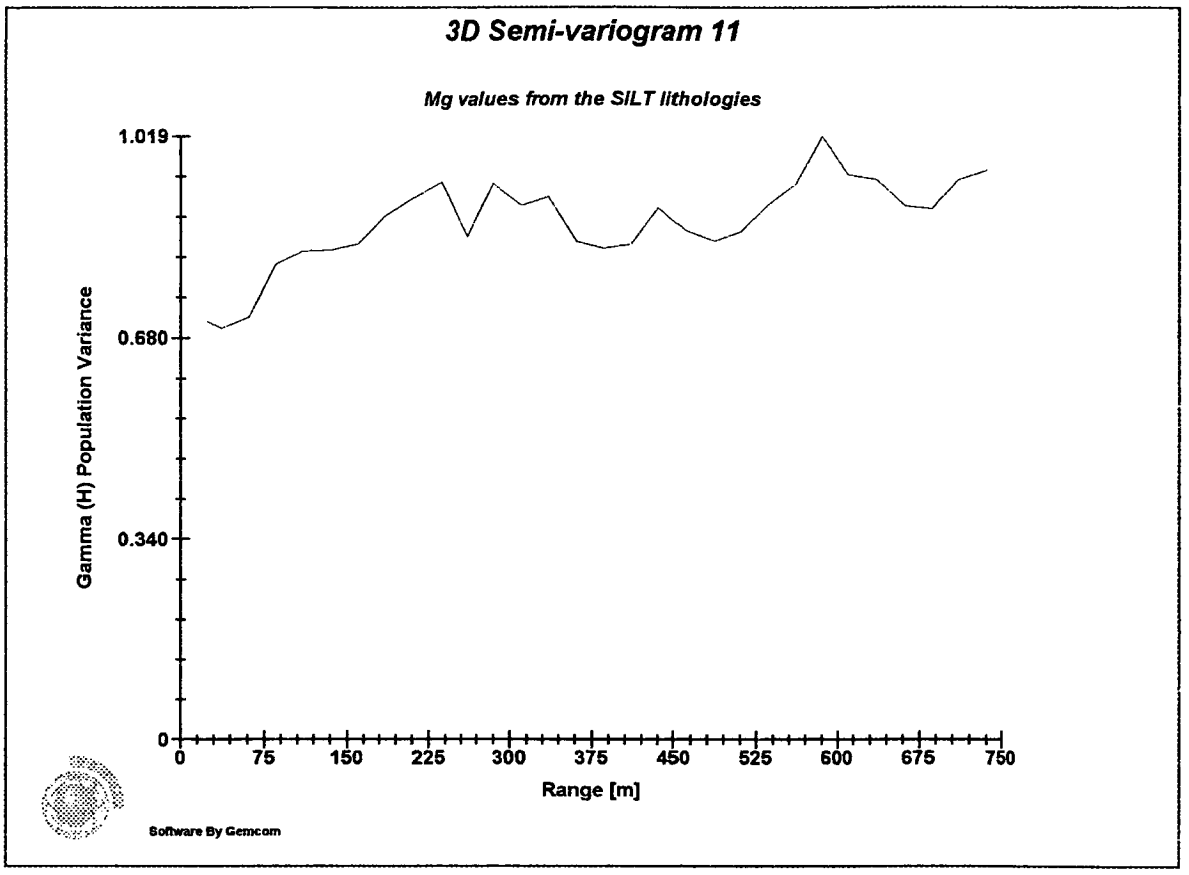
3D Semi-variogram 11
Mg values from the SILT lithologies
Gamma (H) Population Variance
1.019
0.680
0.340
0
0
75
150
225
300
375
450
525
600
675
750
Range [m]
Software By Gemcom

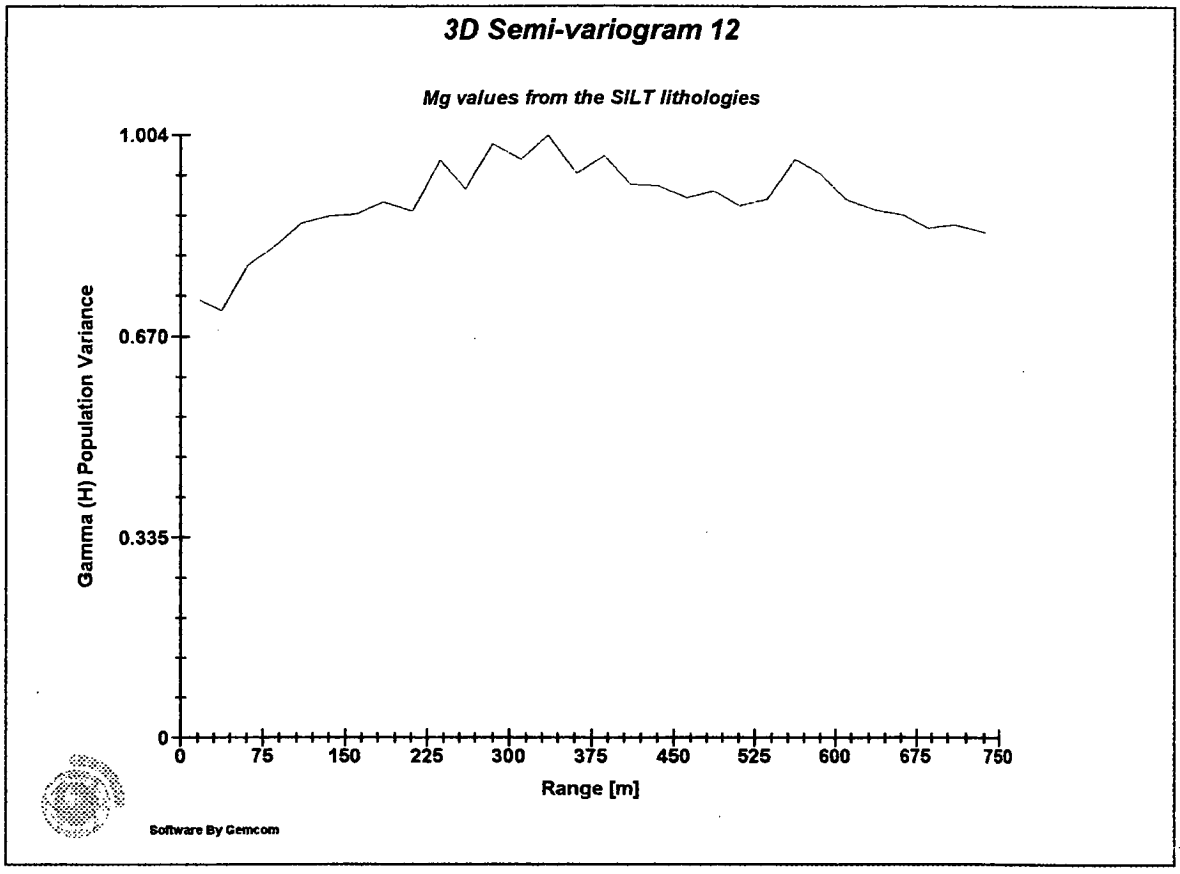
3D Semi-variogram 12
Mg values from the SILT lithologies
1.004
0.670
0.335
0
Gamma (H) Population Variance
0
75
150
225
300
375
450
525
600
675
750
Range [m]
Software By Gemcom

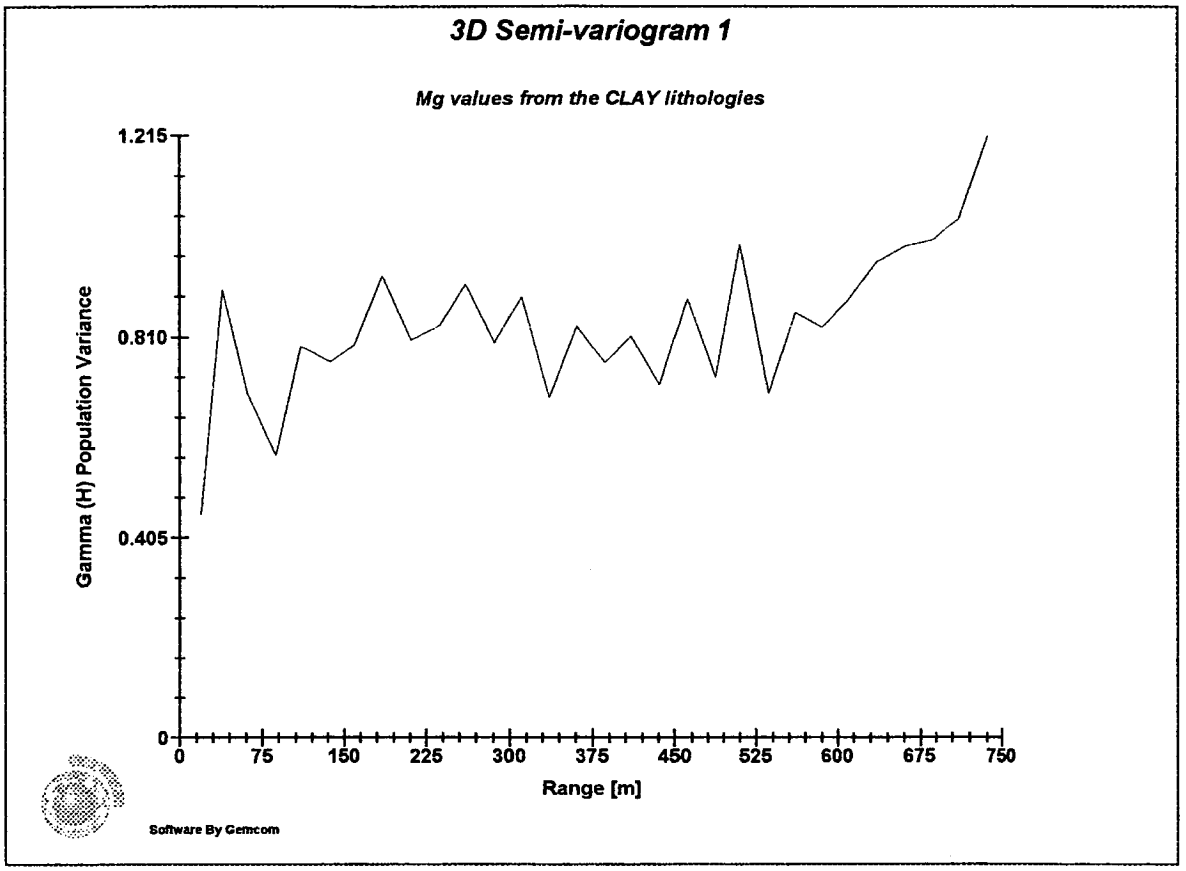
3D Semi-variogram 1
Mg values from the CLAY lithologies
1.215
0.810
0.405
0
Gamma (H) Population Variance
0
75
150
225
300
375
450
525
600
675
750
Range [m]
Software By Gemcom

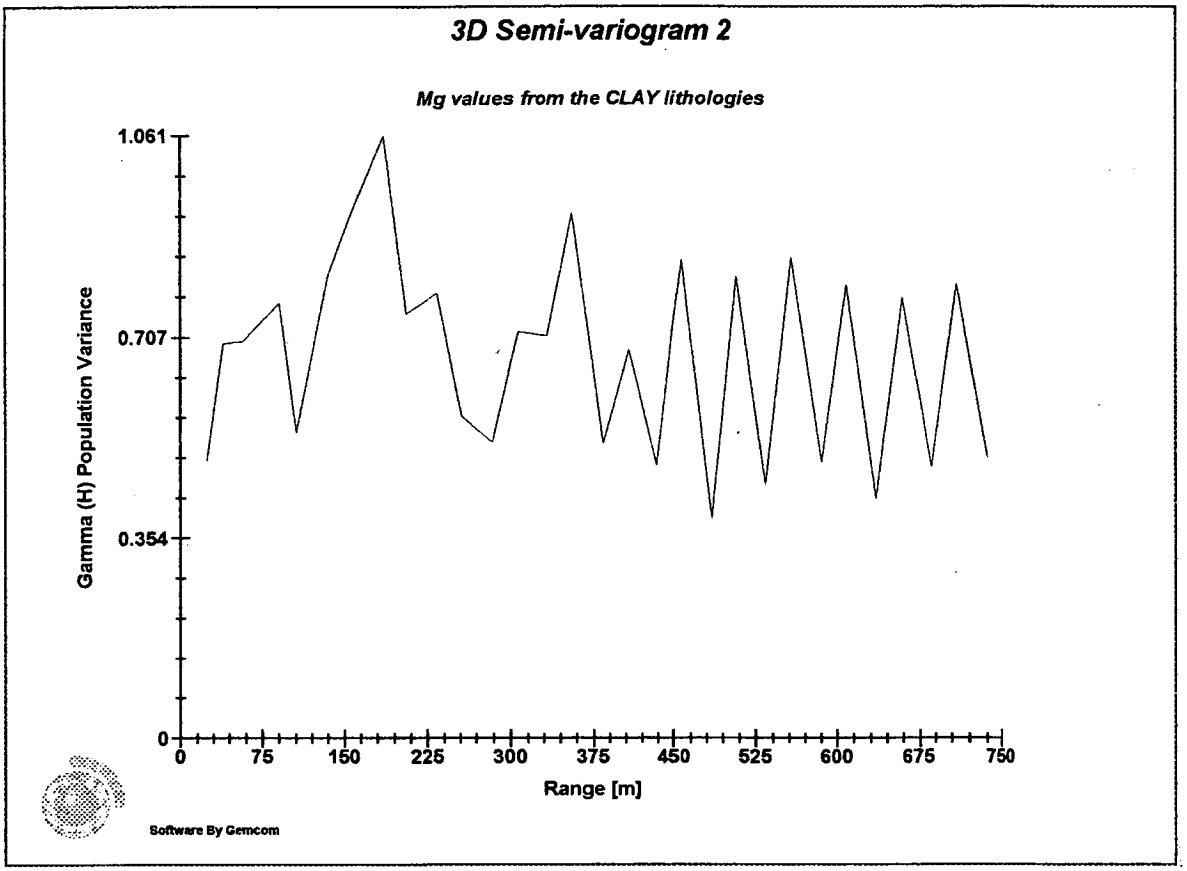
3D Semi-variogram 2
Mg values from the CLAY lithologies
1.061
0.707
0.354
0
Gamma (H) Population Variance
0
75
150
225
300
375
450
525
600
675
750
Range [m]
Software By Gemcom

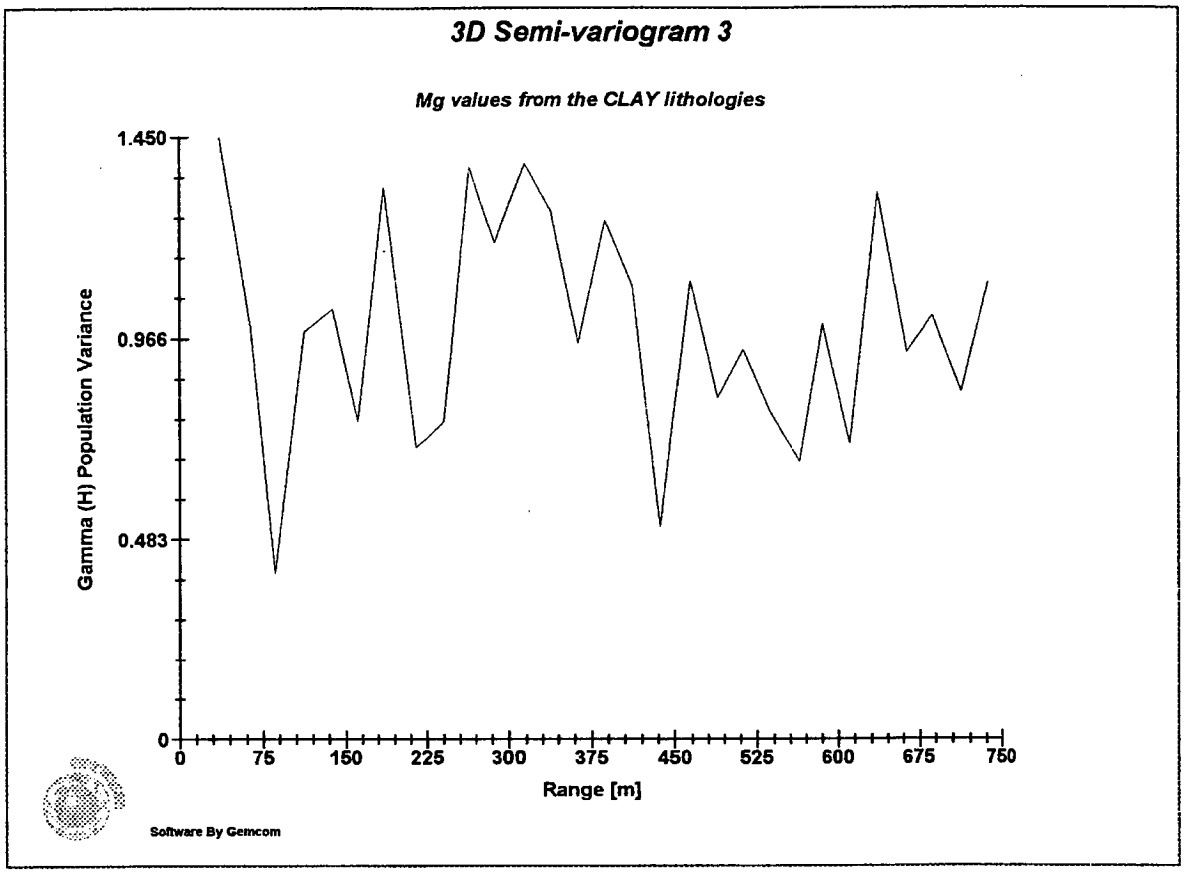
3D Semi-variogram 3
Mg values from the CLAY lithologies
1.450
0.966
0.483
0
Gamma (H) Population Variance
0
75
150
225
300
375
450
525
600
675
750
Range [m]
Software By Gemcom

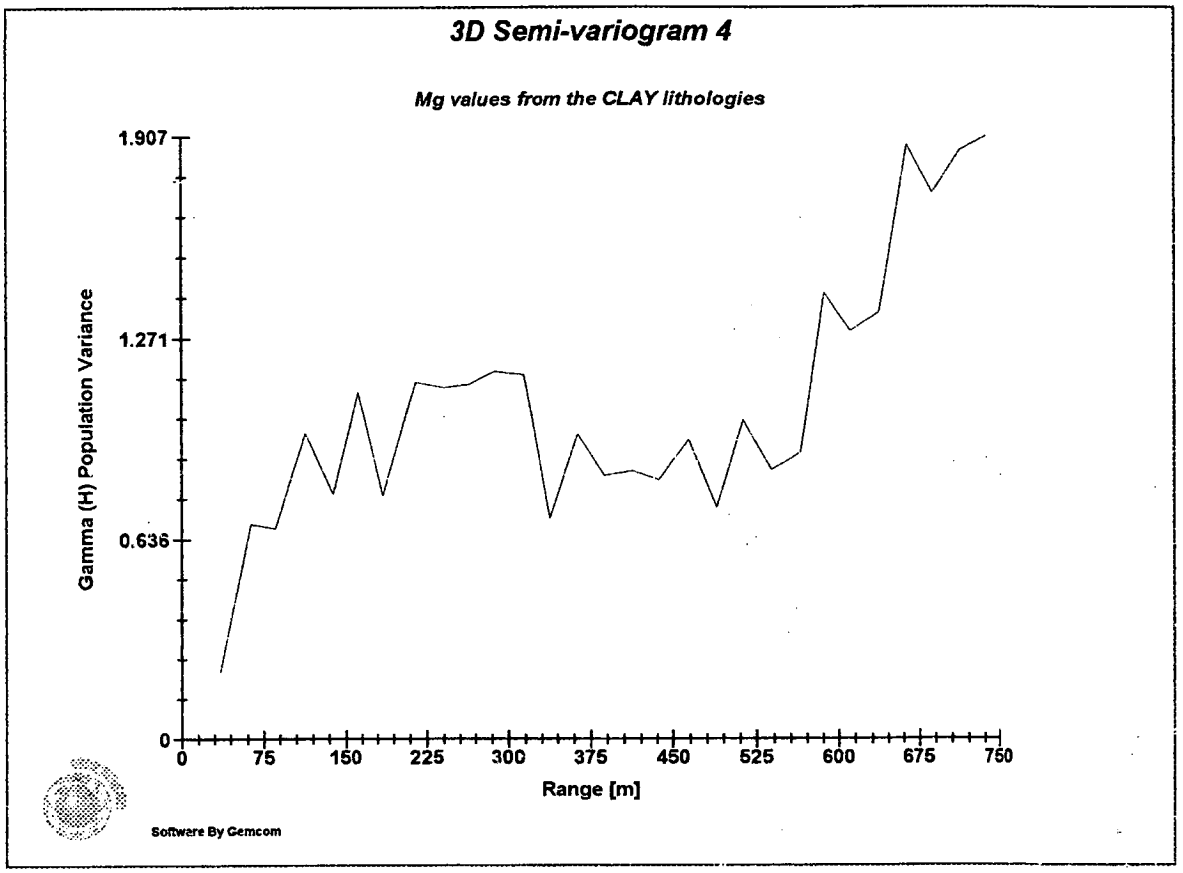
3D Semi-variogram 4
Mg values from the CLAY lithologies
Gamma (H) Population Variance
1.907
1.271
0.636
0
0
75
150
225
300
375
450
525
600
675
750
Range [m]
Software By Gemcom

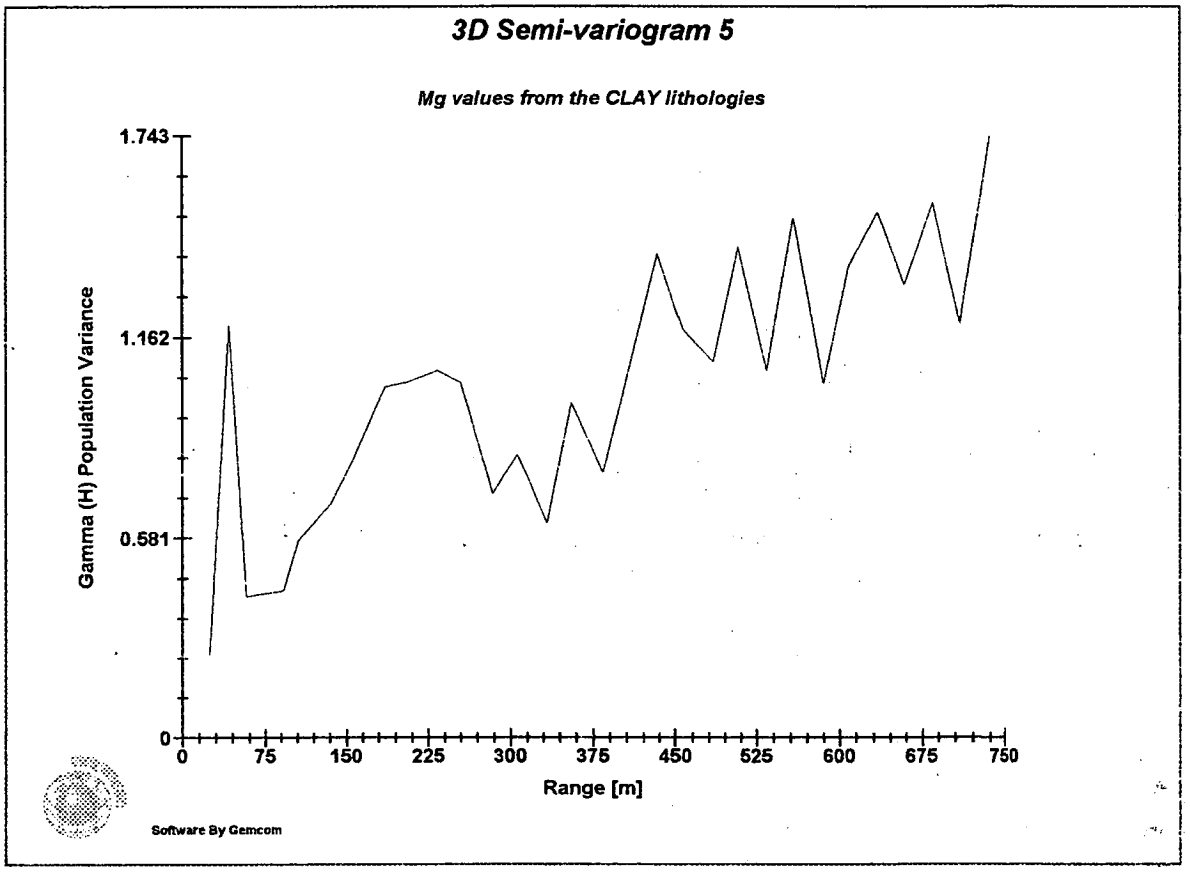
3D Semi-variogram 5
Mg values from the CLAY lithologies
Gamma (H) Population Variance
1.743
1.162
0.581
0
0
75
150
225
300
375
450
525
600
675
750
Range [m]
Software By Gemcom

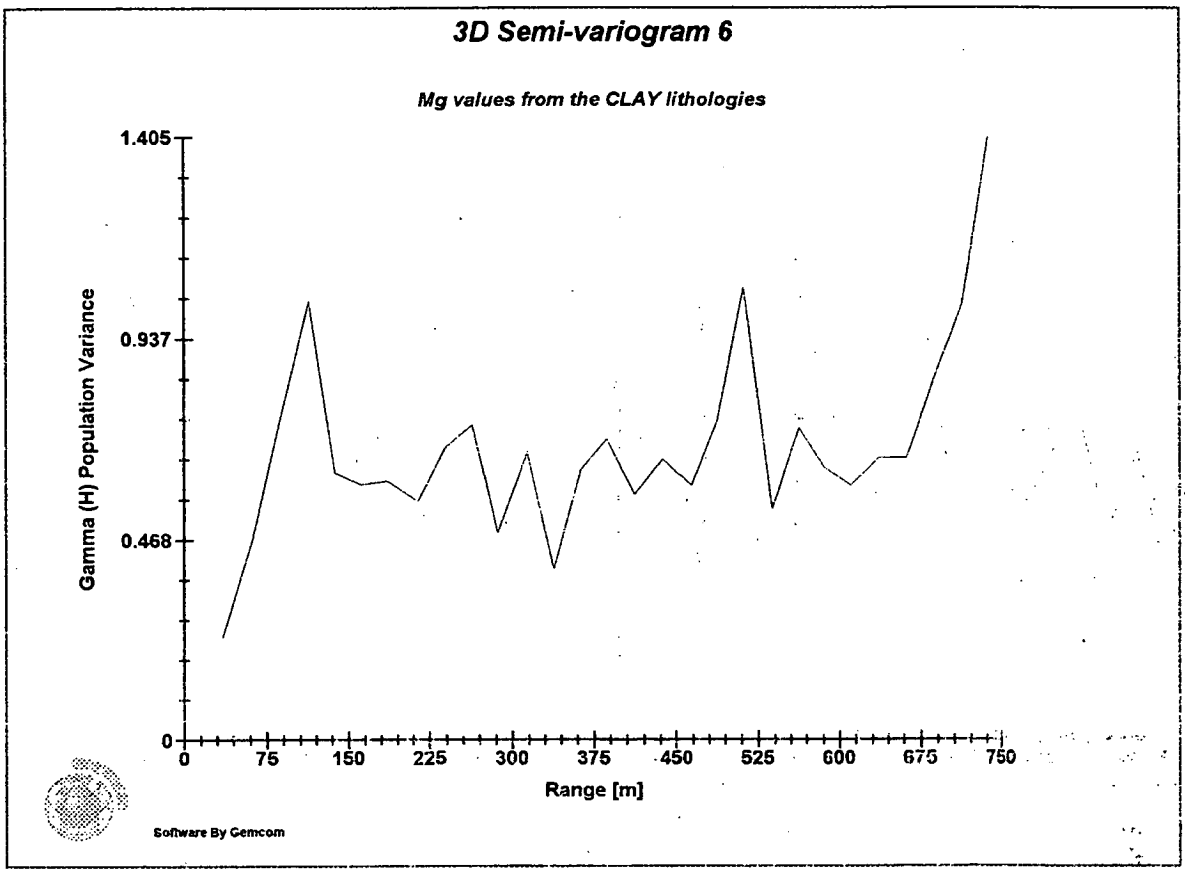
3D Semi-variogram 6
Mg values from the CLAY lithologies
1.405
0.937
0.468
0
Gamma (H) Population Variance
0
75
150
225
300
375
450
525
600
675
750
Range [m]
Software By Gemcom

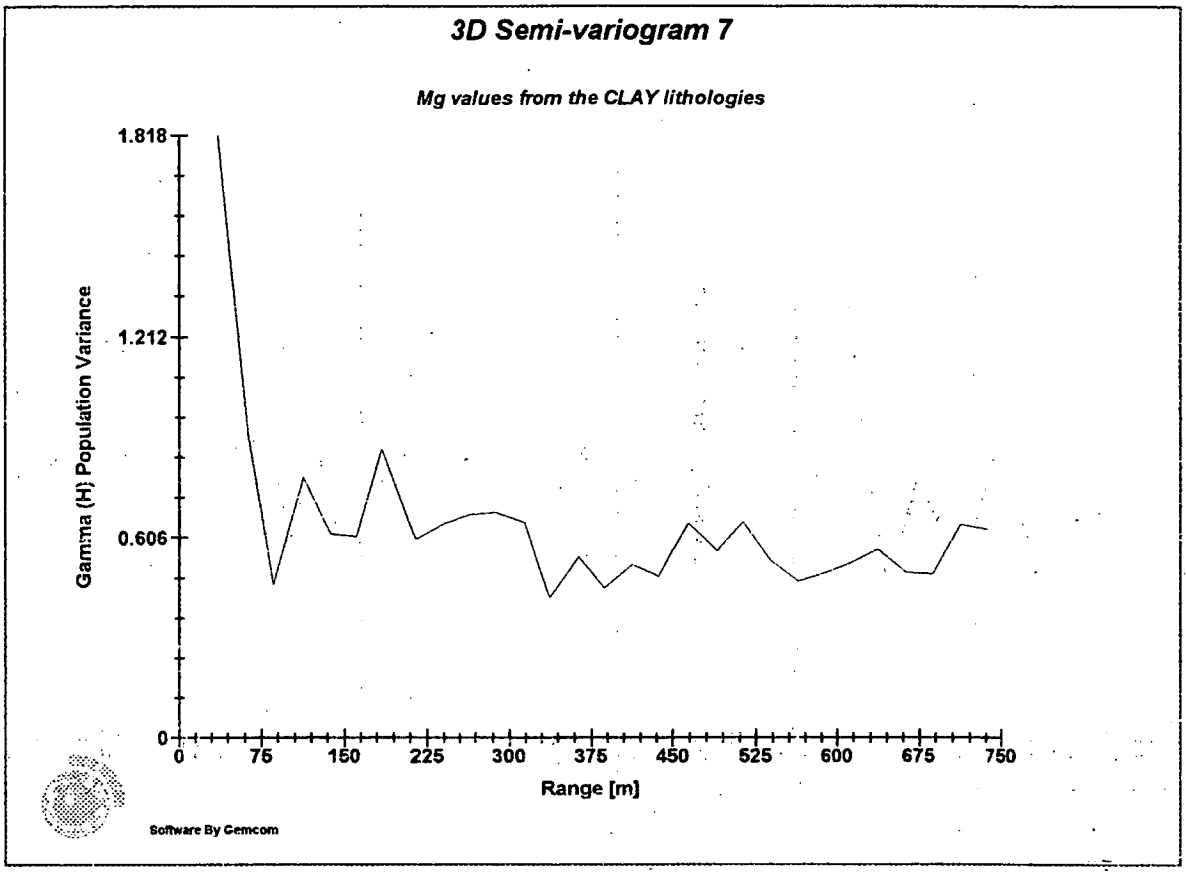
3D Semi-variogram 7
Mg values from the CLAY lithologies
Gamma (H) Population Variance
1.818
1.212
0.606
0
0
75
150
225
300
375
450
525
600
675
750
Range [m]
Software By Gemcom

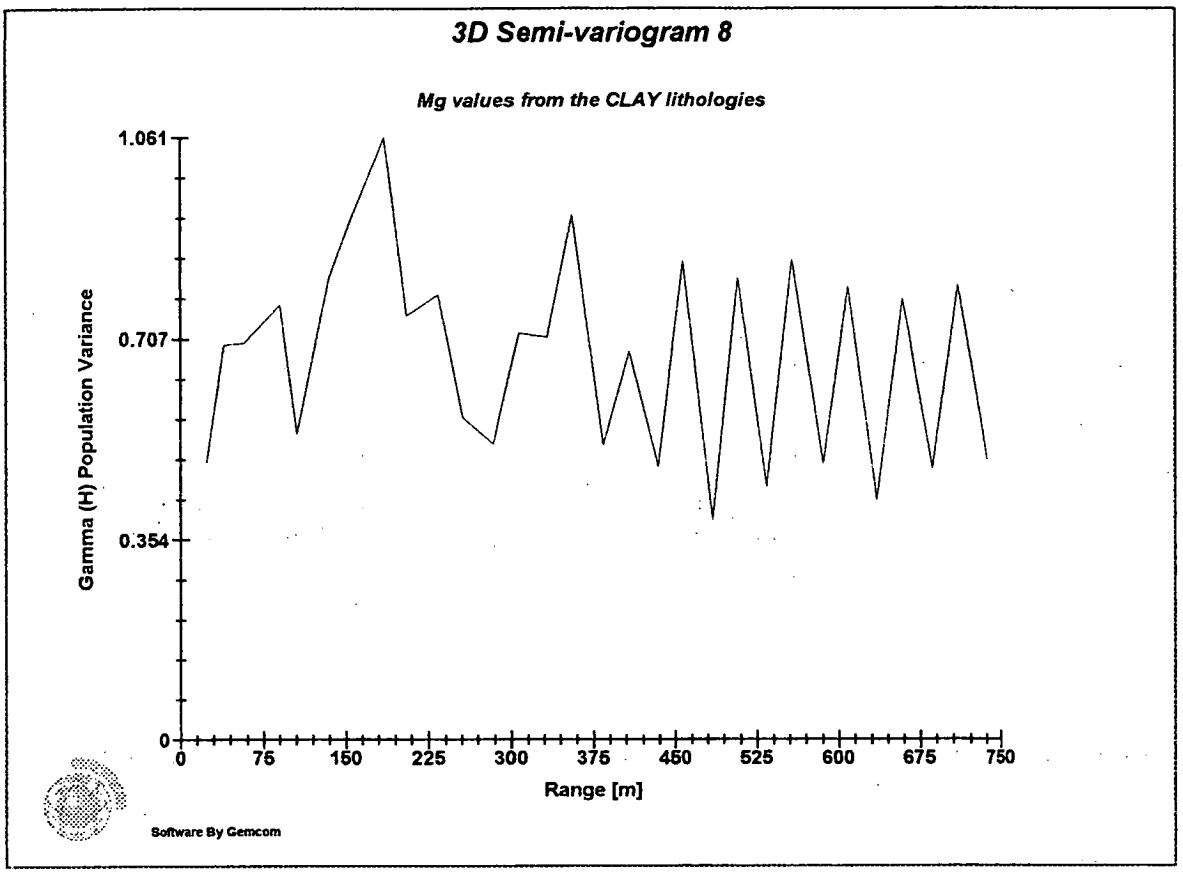
3D Semi-variogram 8
Mg values from the CLAY lithologies
Gamma (H) Population Variance
1.061
0.707
0.354
0
0
75
150
225
300
375
450
525
600
675
750
Range [m]
Software By Gemcom

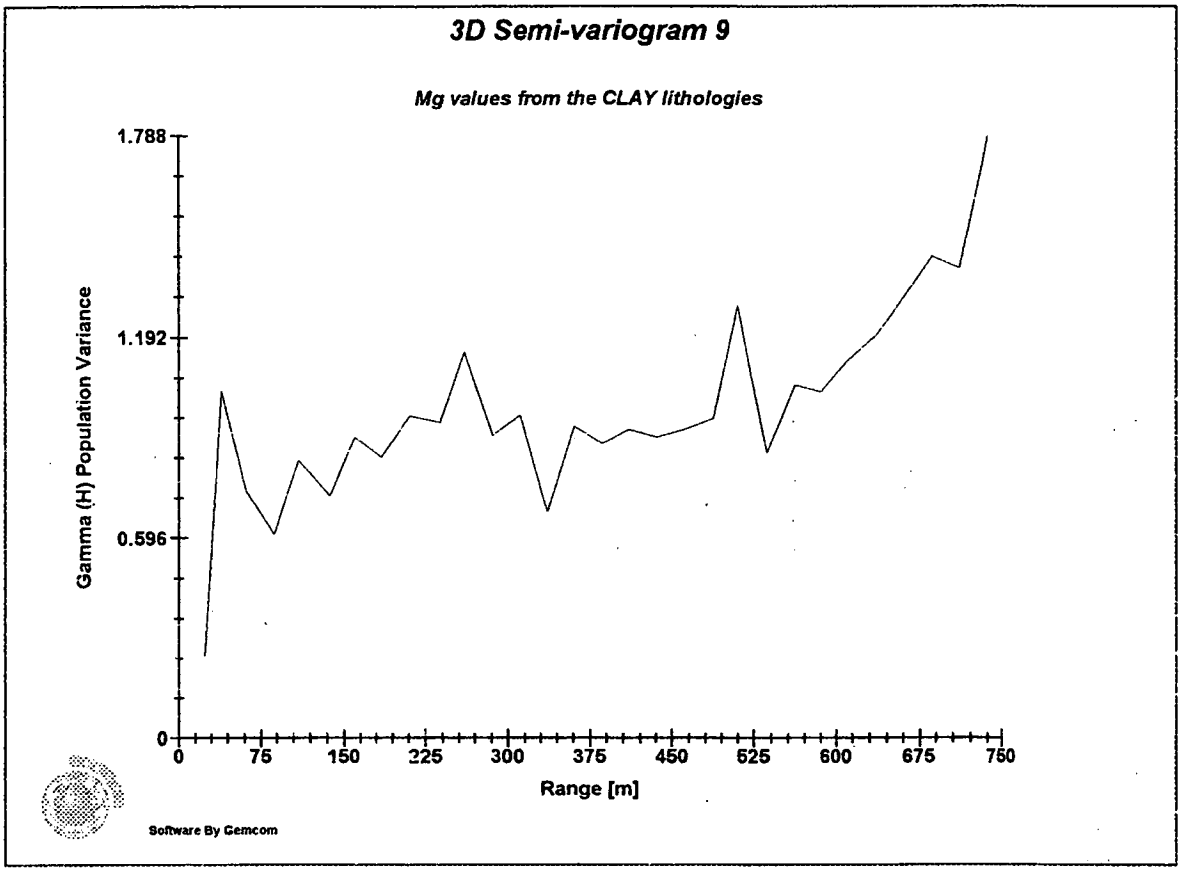
3D Semi-variogram 9
Mg values from the CLAY lithologies
Gamma (H) Population Variance
1.788
1.192
0.596
0
0
75
150
225
300
375
450
525
600
675
750
Range [m]
Software By Gemcom

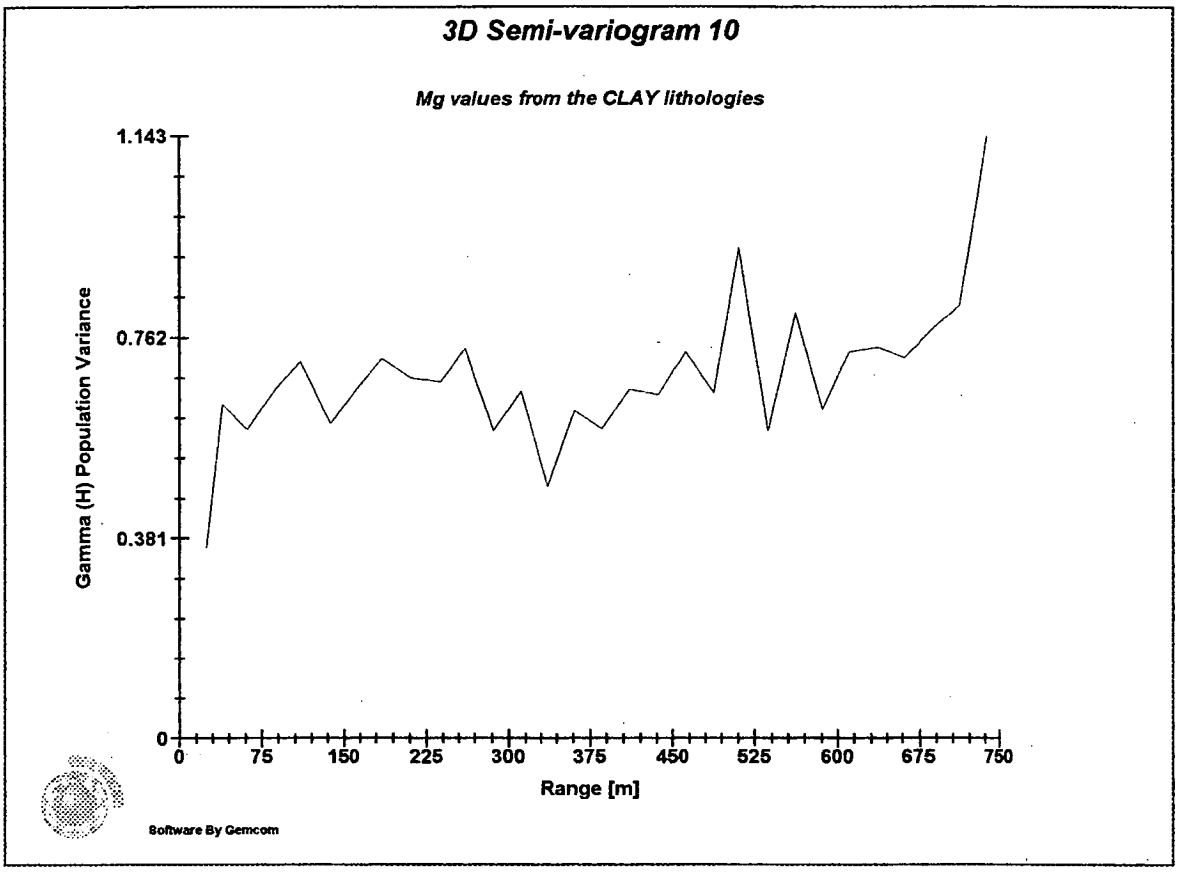
3D Semi-variogram 10
Mg values from the CLAY lithologies
1.143
0.762
0.381
0
Gamma (H) Population Variance
0
75
150
225
300
375
450
525
600
675
750
Range [m]
Software By Gemcom

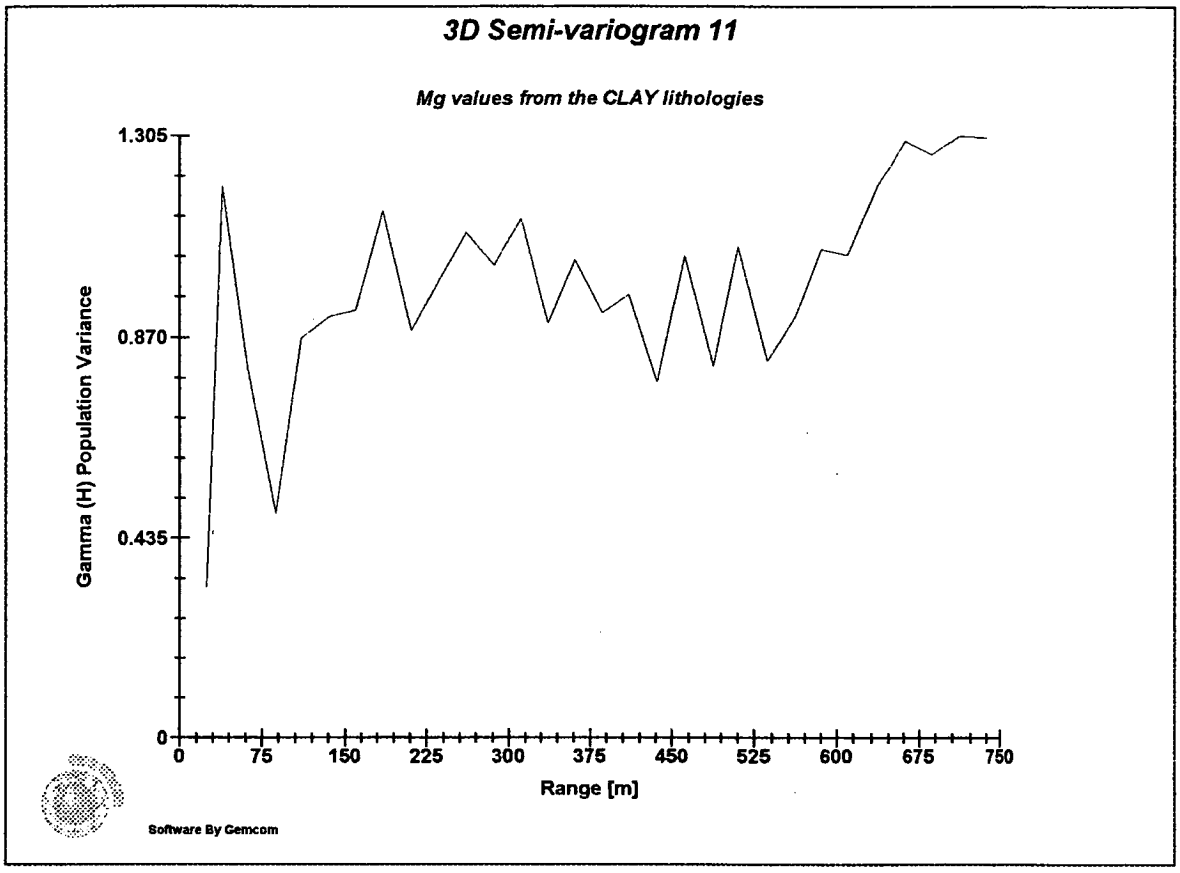
3D Semi-variogram 11
Mg values from the CLAY lithologies
Gamma (H) Population Variance
1.305
0.870
0.435
0
0
75
150
225
300
375
450
525
600
675
750
Range [m]
Software By Gemcom

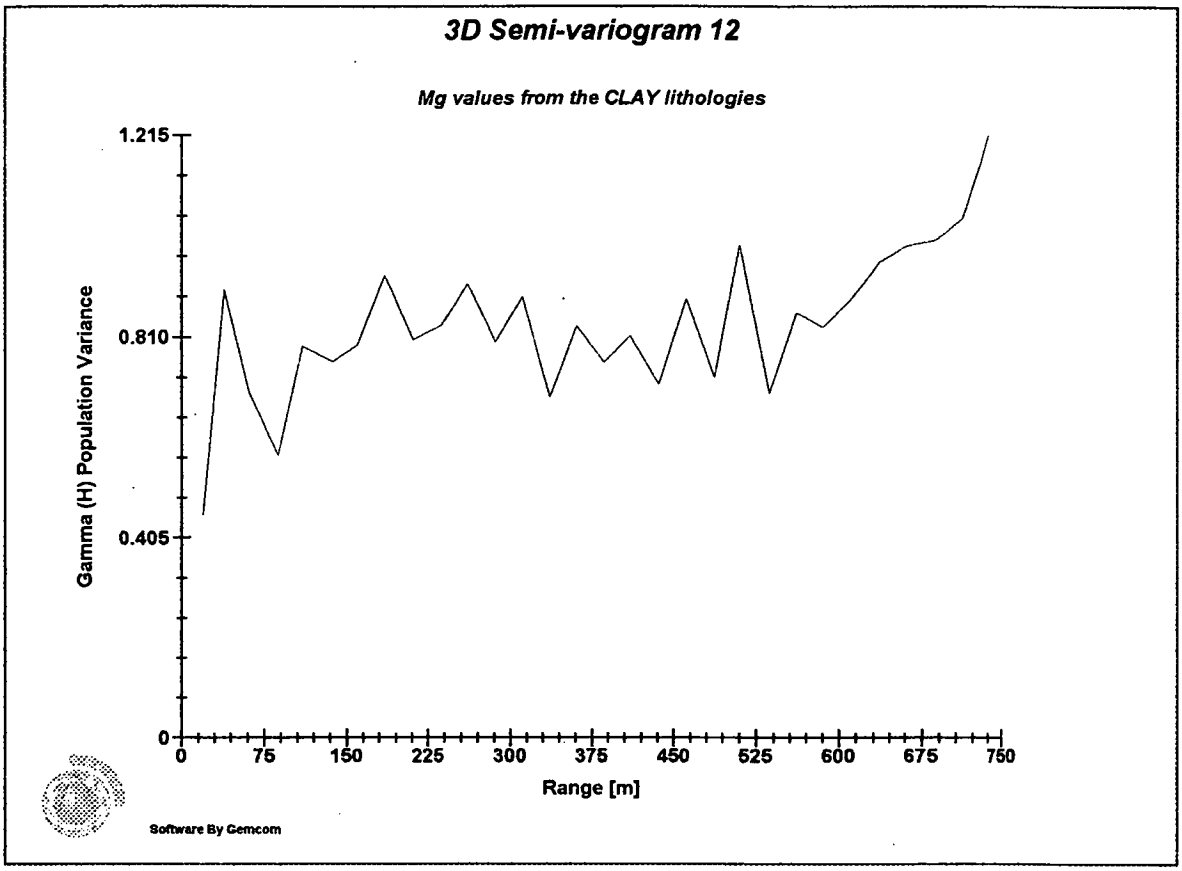
3D Semi-variogram 12
Mg values from the CLAY lithologies
Gamma (H) Population Variance
1.215
0.810
0.405
0
0
75
150
225
300
375
450
525
600
675
750
Range [m]
Software By Gemcom

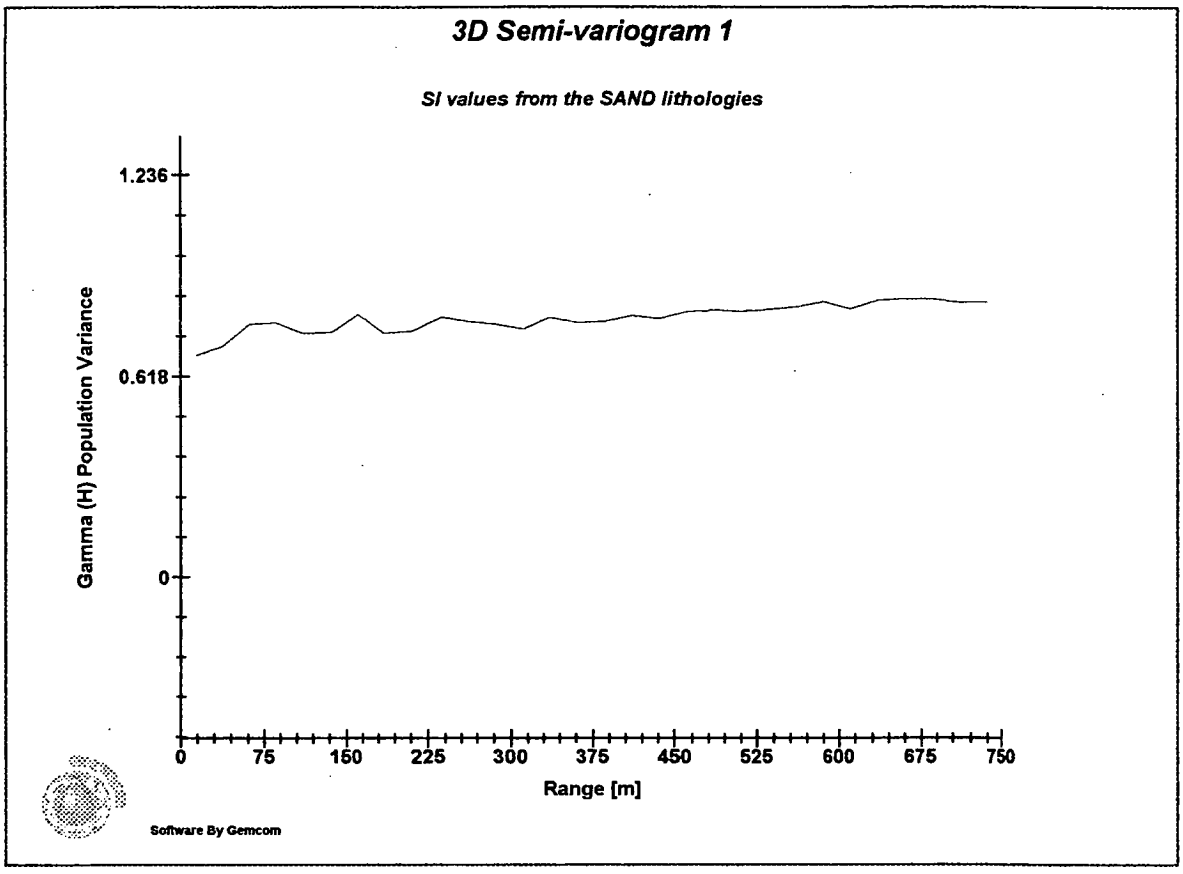
3D Semi-variogram 1
SI values from the SAND lithologies
1.236
0.618
0
Gamma (H) Population Variance
0
75
150
225
300
375
450
525
600
675
750
Range [m]
Software By Gemcom

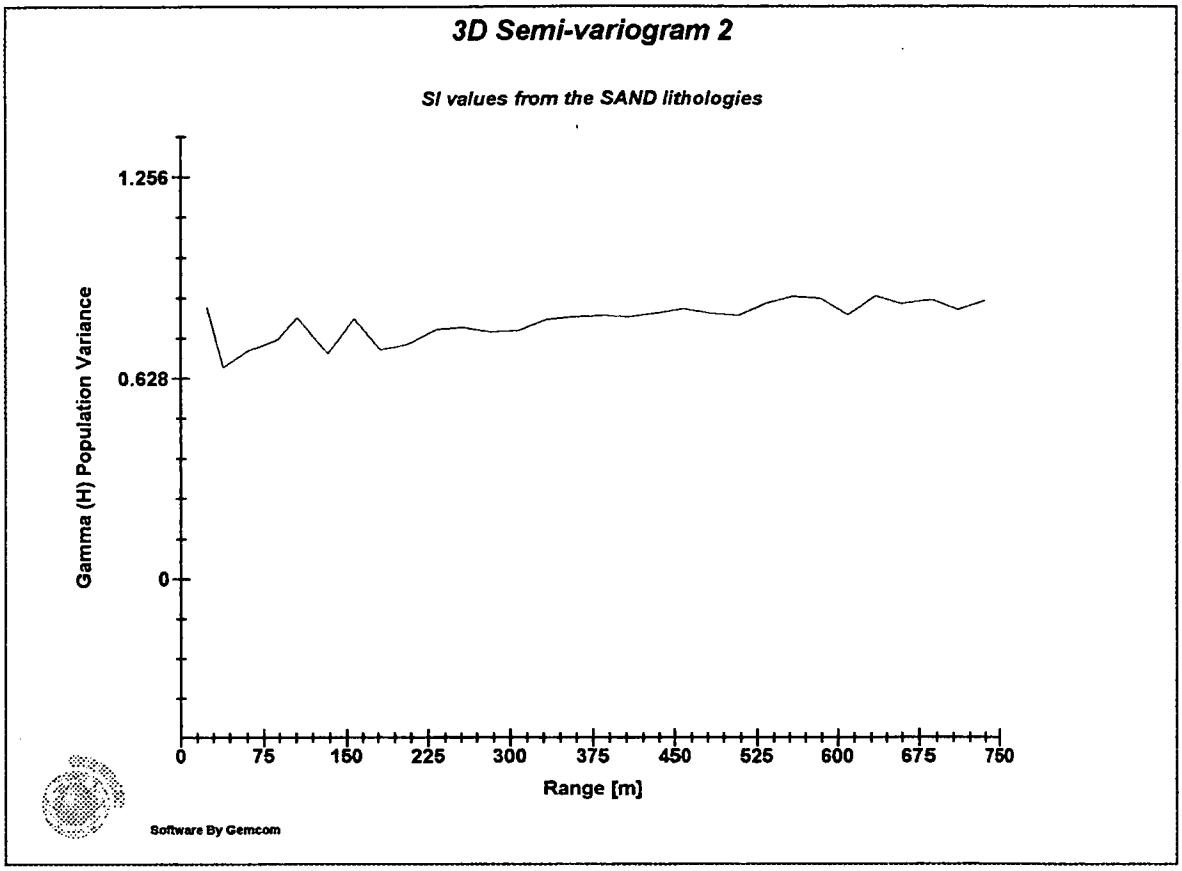
3D Semi-variogram 2
SI values from the SAND lithologies
Gamma (H) Population Variance
1.256
0.628
0
0
75
150
225
300
375
450
525
600
675
750
Range [m]
Software By Gemcom

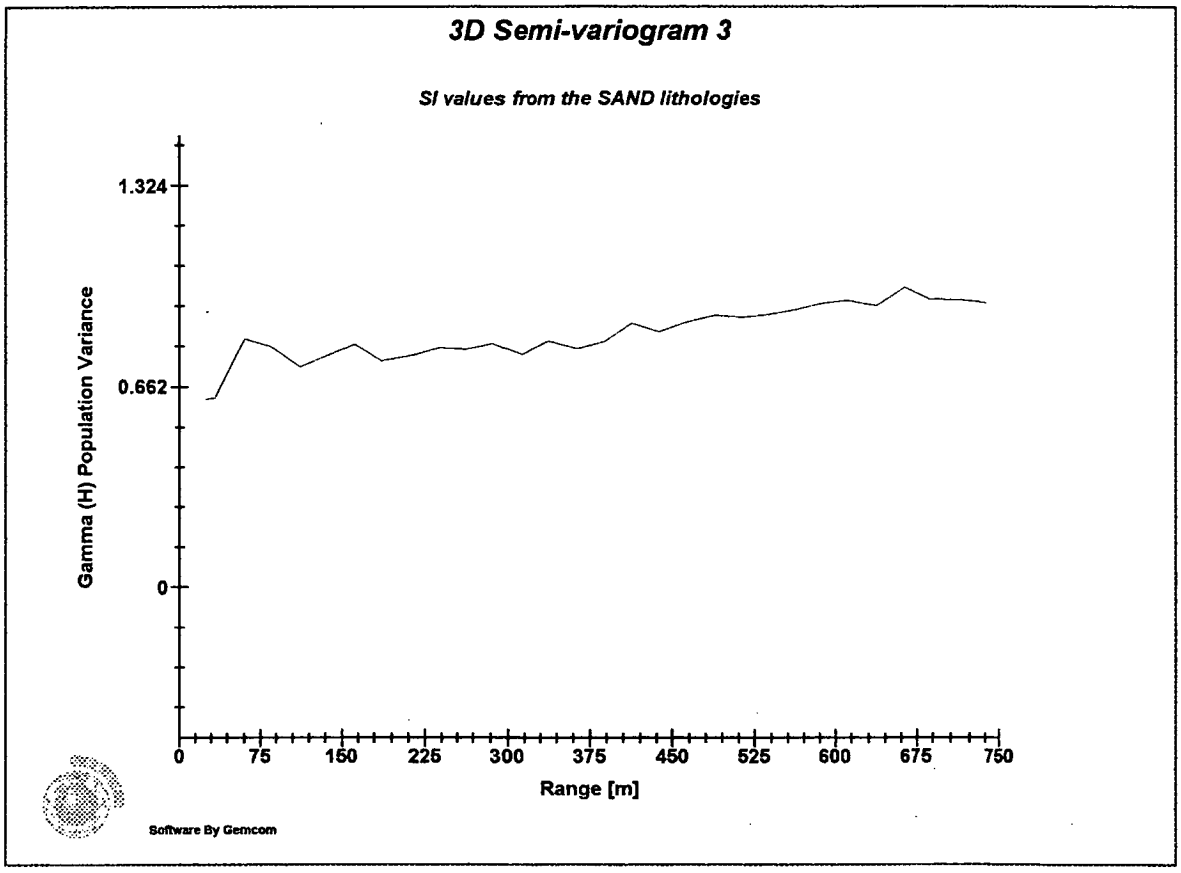
3D Semi-variogram 3
SI values from the SAND lithologies
1.324
0.662
0
Gamma (H) Population Variance
0
75
150
225
300
375
450
525
600
675
750
Range [m]
Software By Gemcom

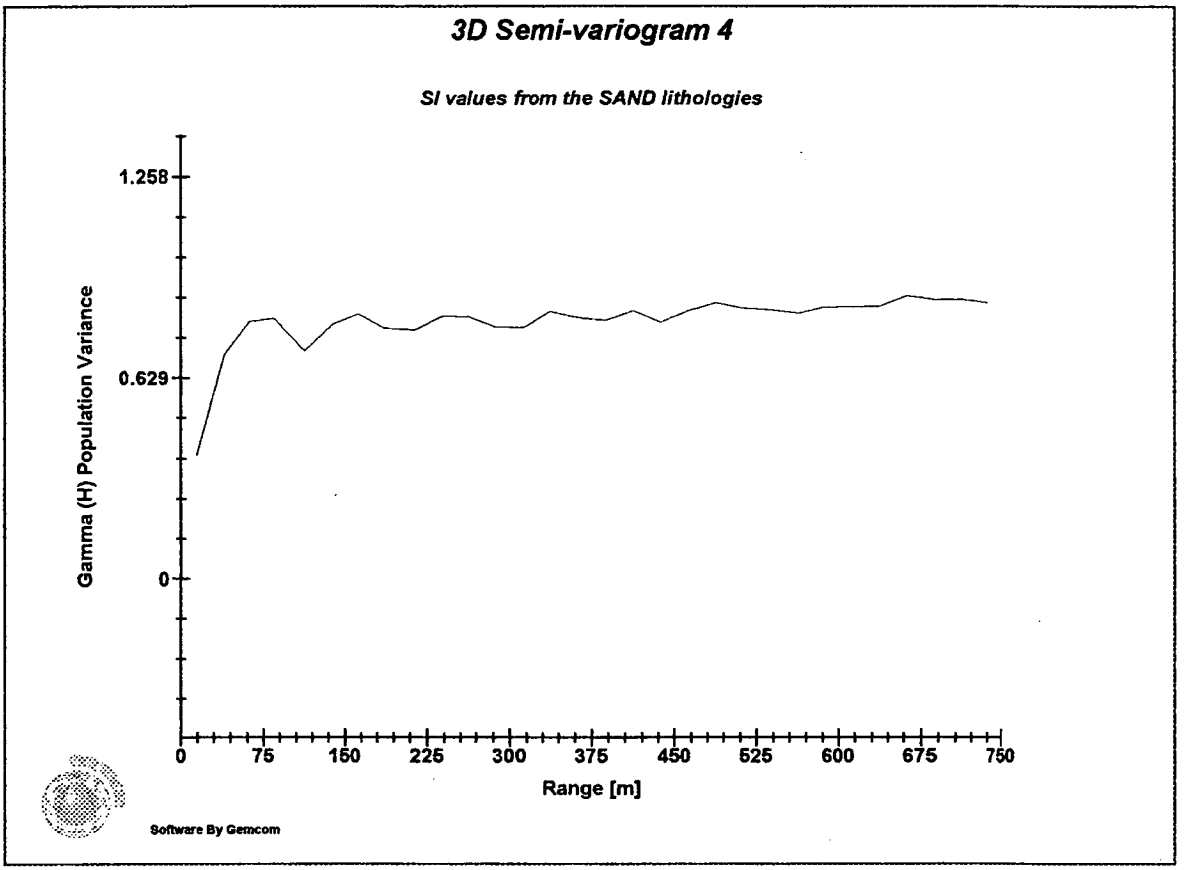
3D Semi-variogram 4
SI values from the SAND lithologies
Gamma (H) Population Variance
1.258
0.629
0
0
75
150
225
300
375
450
525
600
675
750
Range [m]
Software By Gemcom

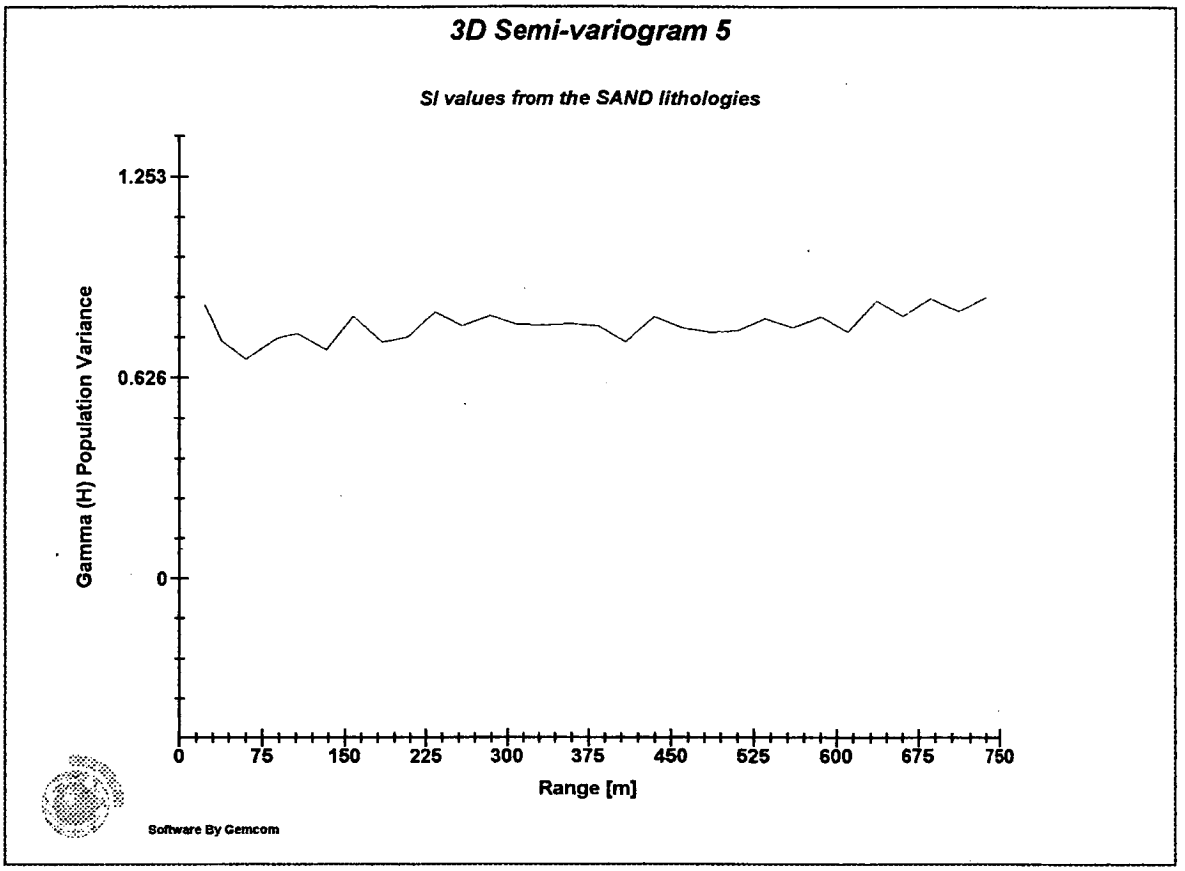
3D Semi-variogram 5
SI values from the SAND lithologies
Gamma (H) Population Variance
1.253
0.626
0
0
75
150
225
300
375
450
525
600
675
750
Range [m]
Software By Gemcom

3D Semi-variogram 6

SI values from the SAND lithologies

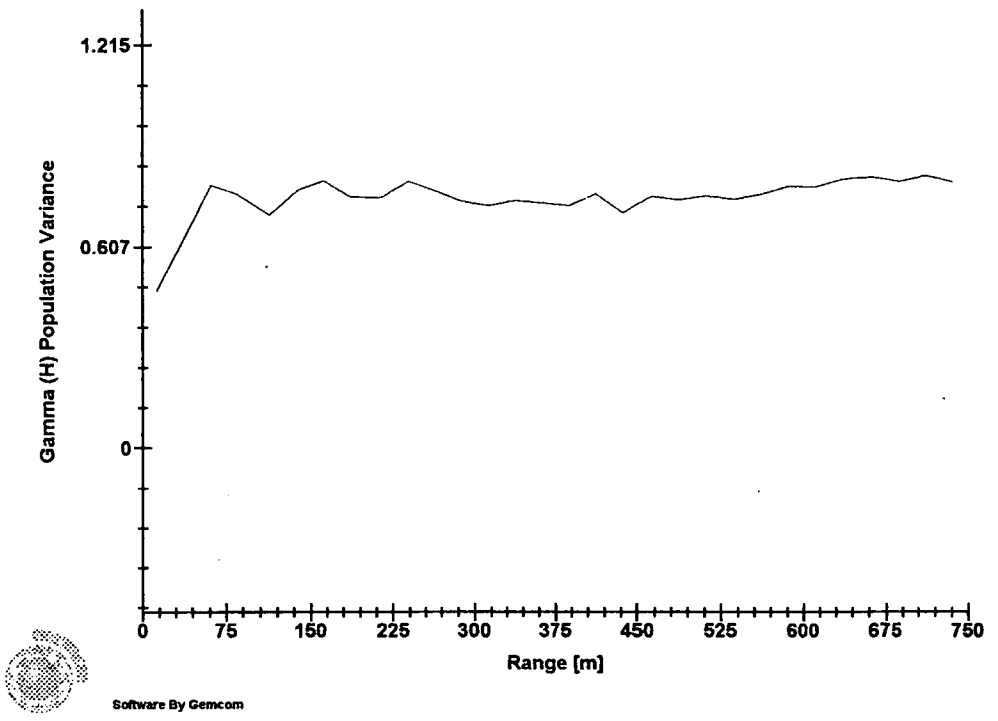

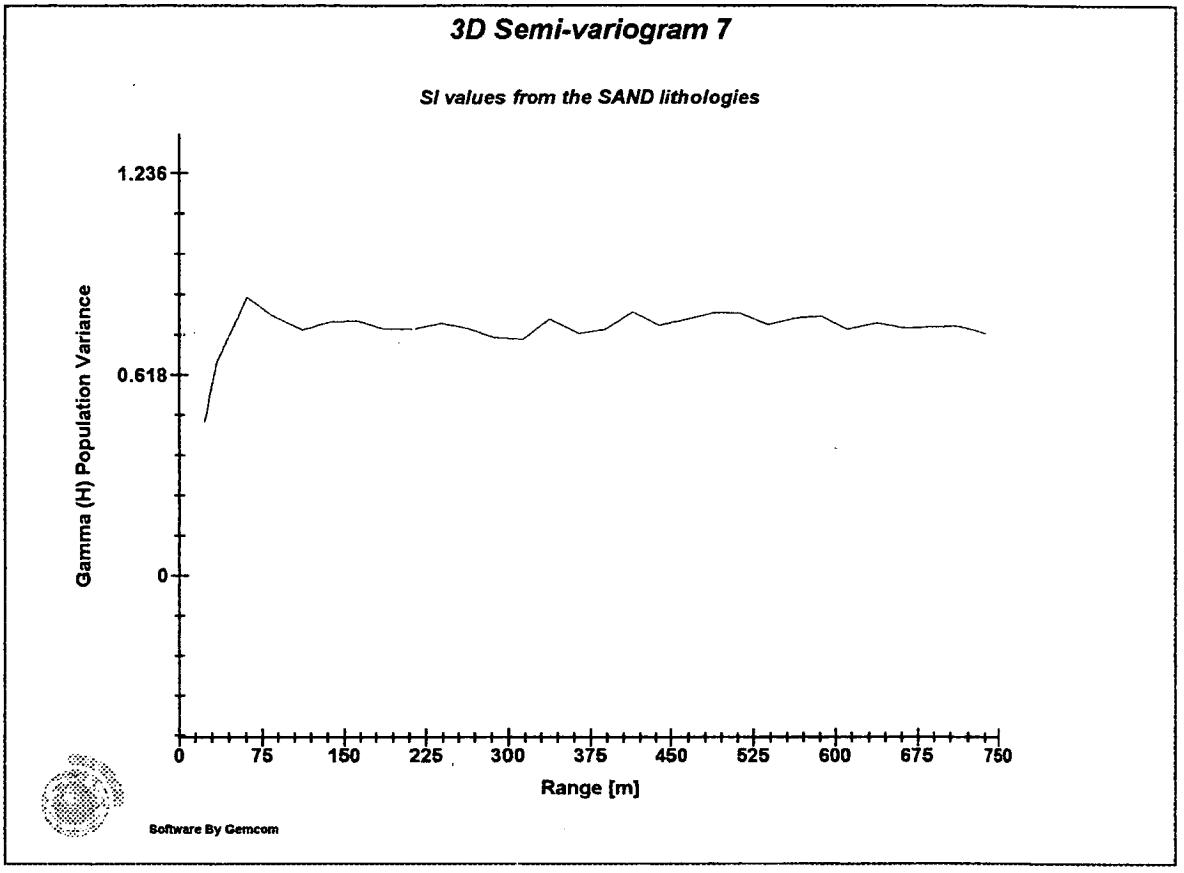
3D Semi-variogram 7
SI values from the SAND lithologies
1.236
0.618
0
Gamma (H) Population Variance
0
75
150
225
300
375
450
525
600
675
750
Range [m]
Software By Gemcom

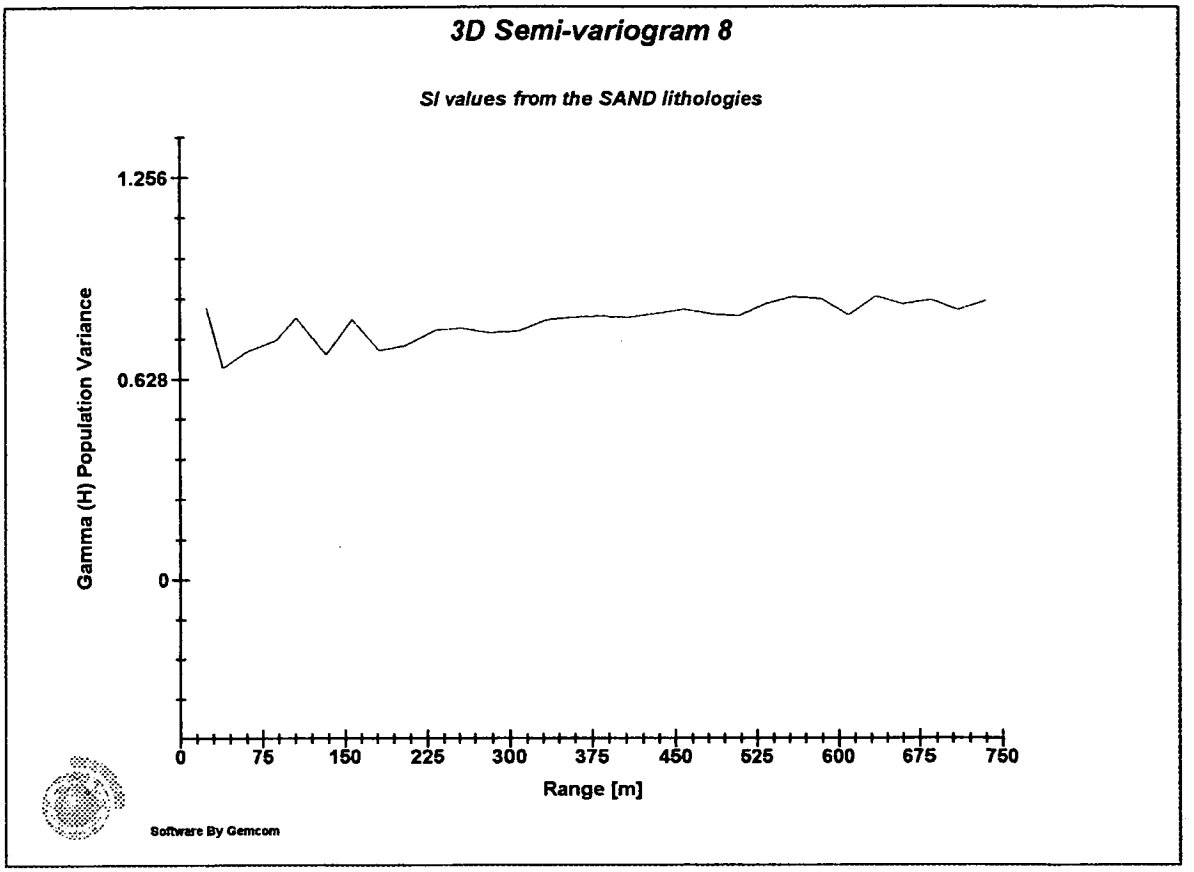
3D Semi-variogram 8
SI values from the SAND lithologies
1.256
0.628
0
Gamma (H) Population Variance
0
75
150
225
300
375
450
525
600
675
750
Range [m]
Software By Gemcom

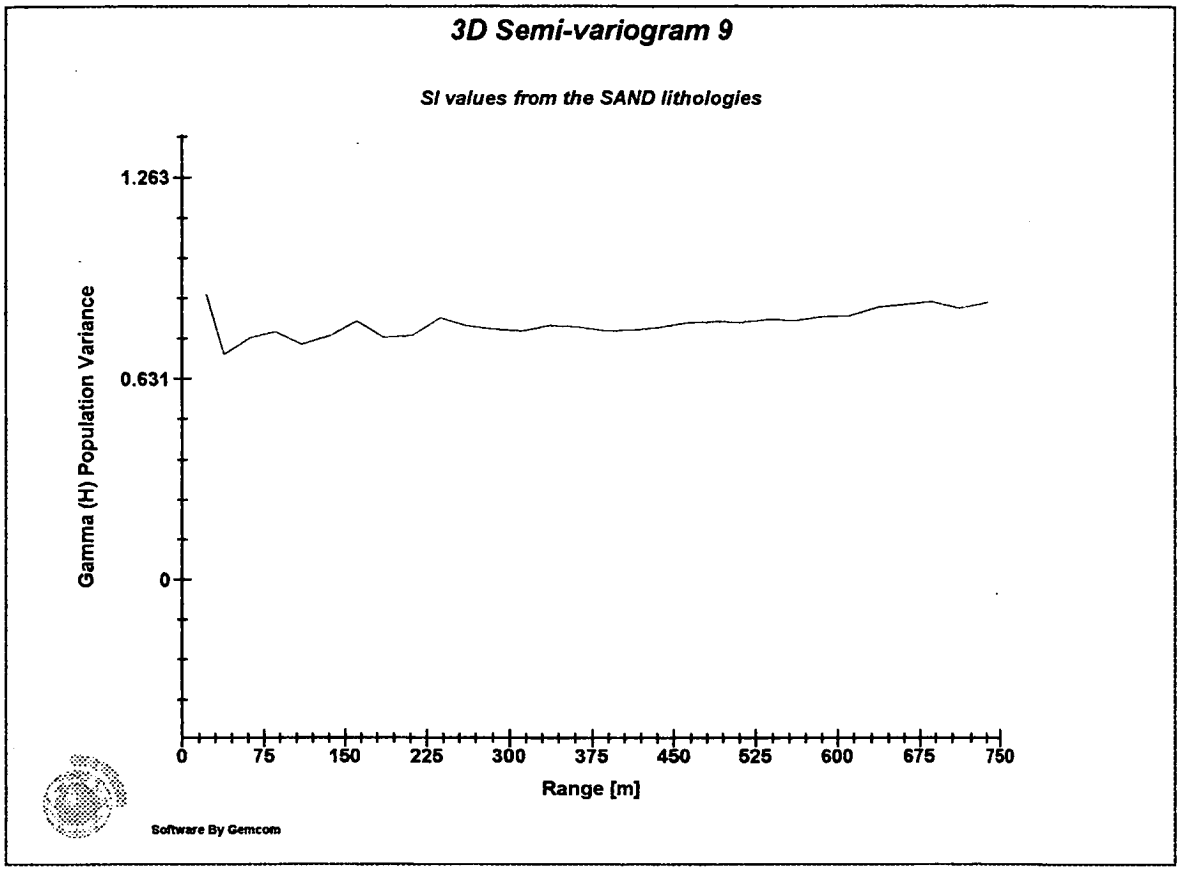
3D Semi-variogram 9
SI values from the SAND lithologies
1.263
0.631
0
Gamma (H) Population Variance
0
75
150
225
300
375
450
525
600
675
750
Range [m]
Software By Gemcom

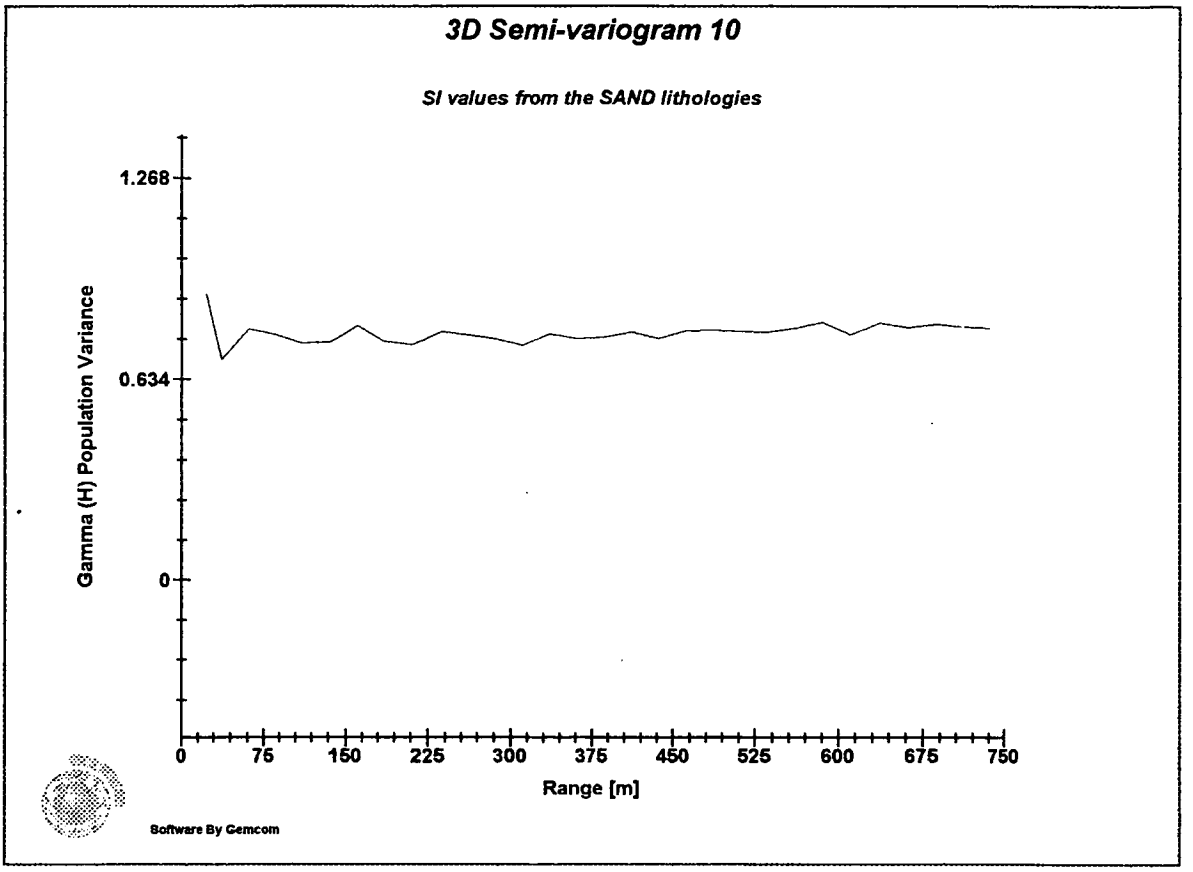
3D Semi-variogram 10
SI values from the SAND lithologies
Gamma (H) Population Variance
1.268
0.634
0
0
75
150
225
300
375
450
525
600
675
750
Range [m]
Software By Gemcom

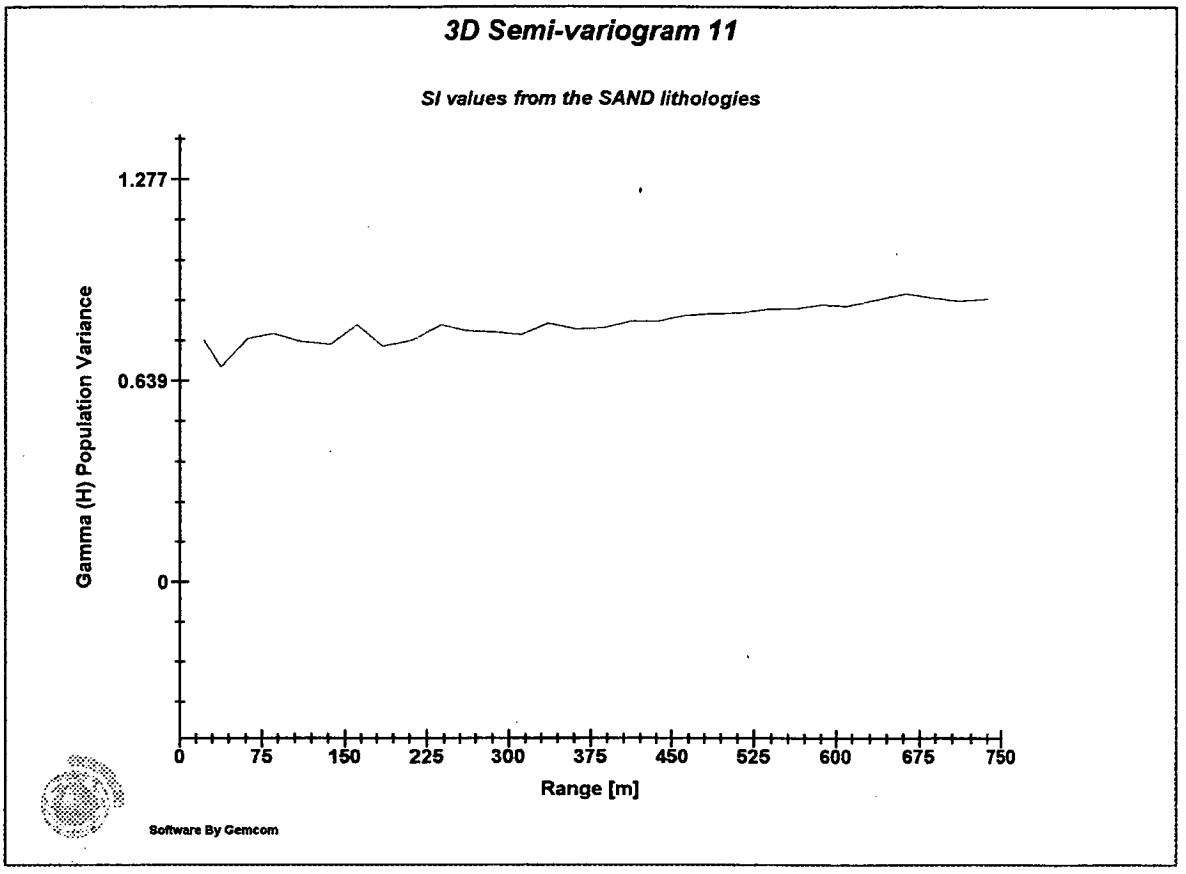
3D Semi-variogram 11
SI values from the SAND lithologies
1.277
0.639
0
Gamma (H) Population Variance
0
75
150
225
300
375
450
525
600
675
750
Range [m]
Software By Gemcom

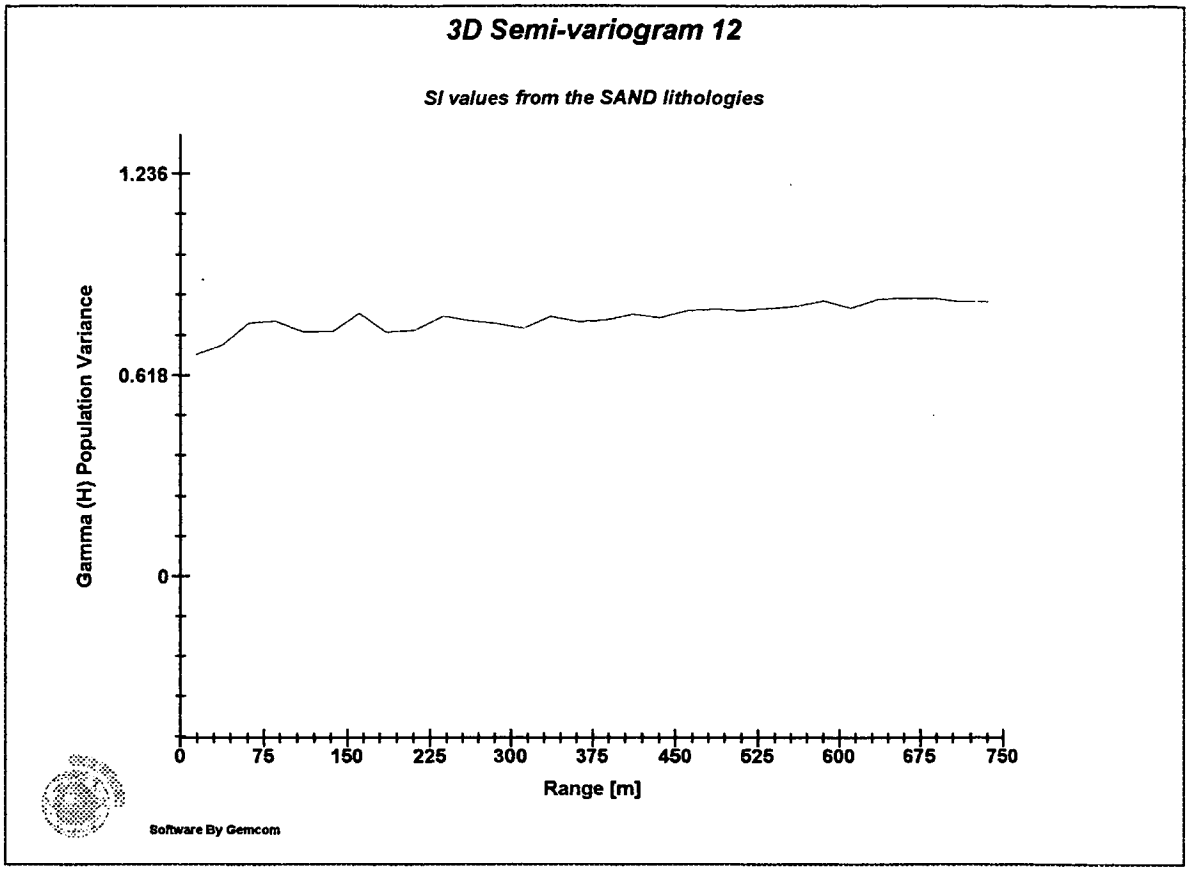
3D Semi-variogram 12
SI values from the SAND lithologies
1.236
0.618
0
Gamma (H) Population Variance
0
75
150
225
300
375
450
525
600
675
750
Range [m]
Software By Gemcom

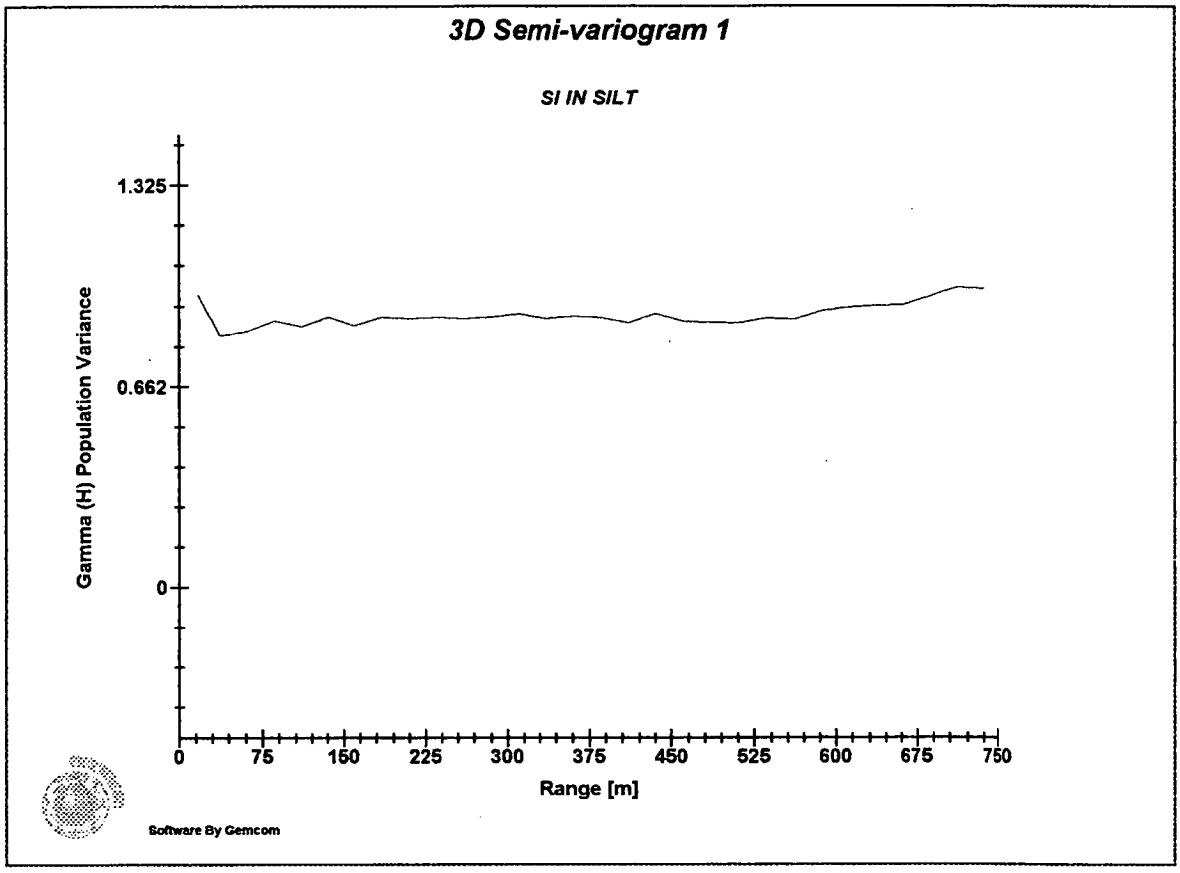
3D Semi-variogram 1
SI IN SILT
1.325
0.662
0
Gamma (H) Population Variance
0
75
150
225
300
375
450
525
600
675
750
Range [m]
Software By Gemcom

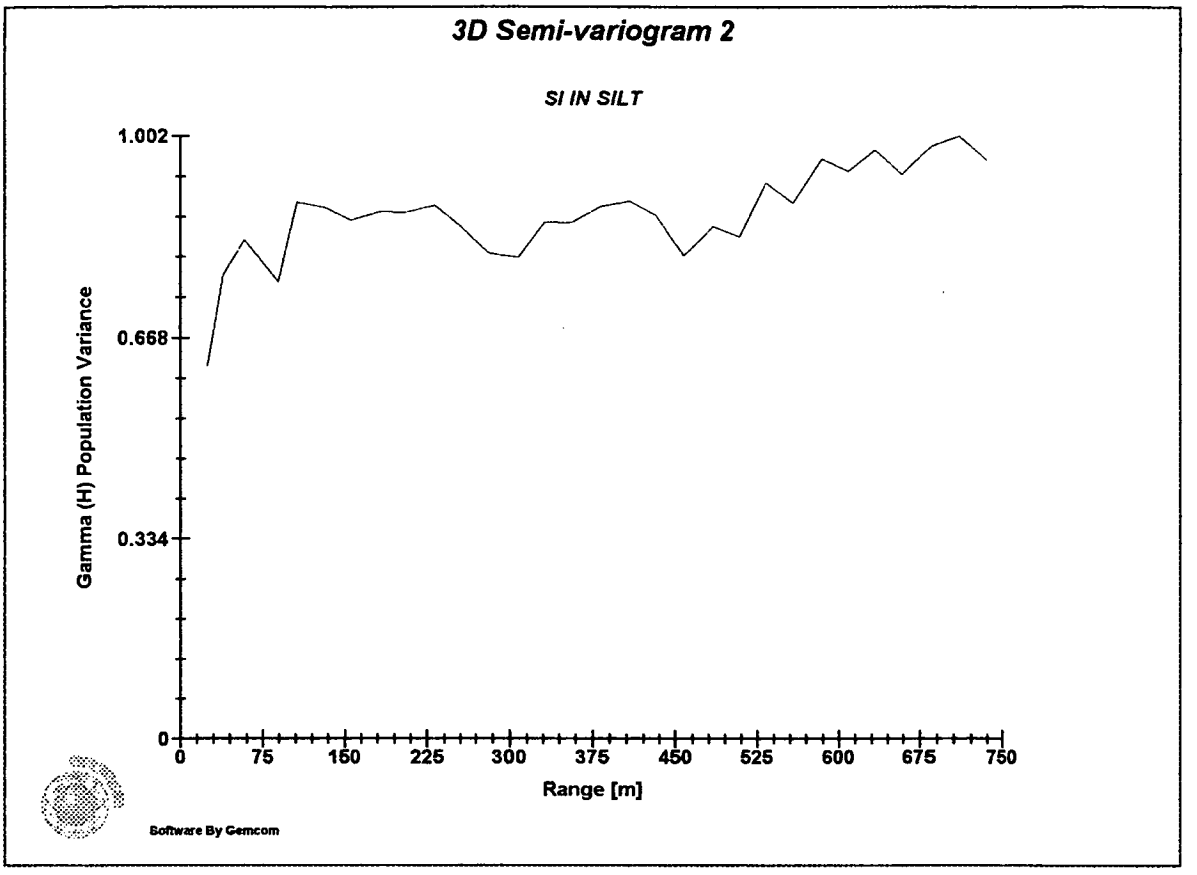
3D Semi-variogram 2
SI IN SILT
1.002
0.668
0.334
0
Gamma (H) Population Variance
0
75
150
225
300
375
450
525
600
675
750
Range [m]
Software By Gemcom

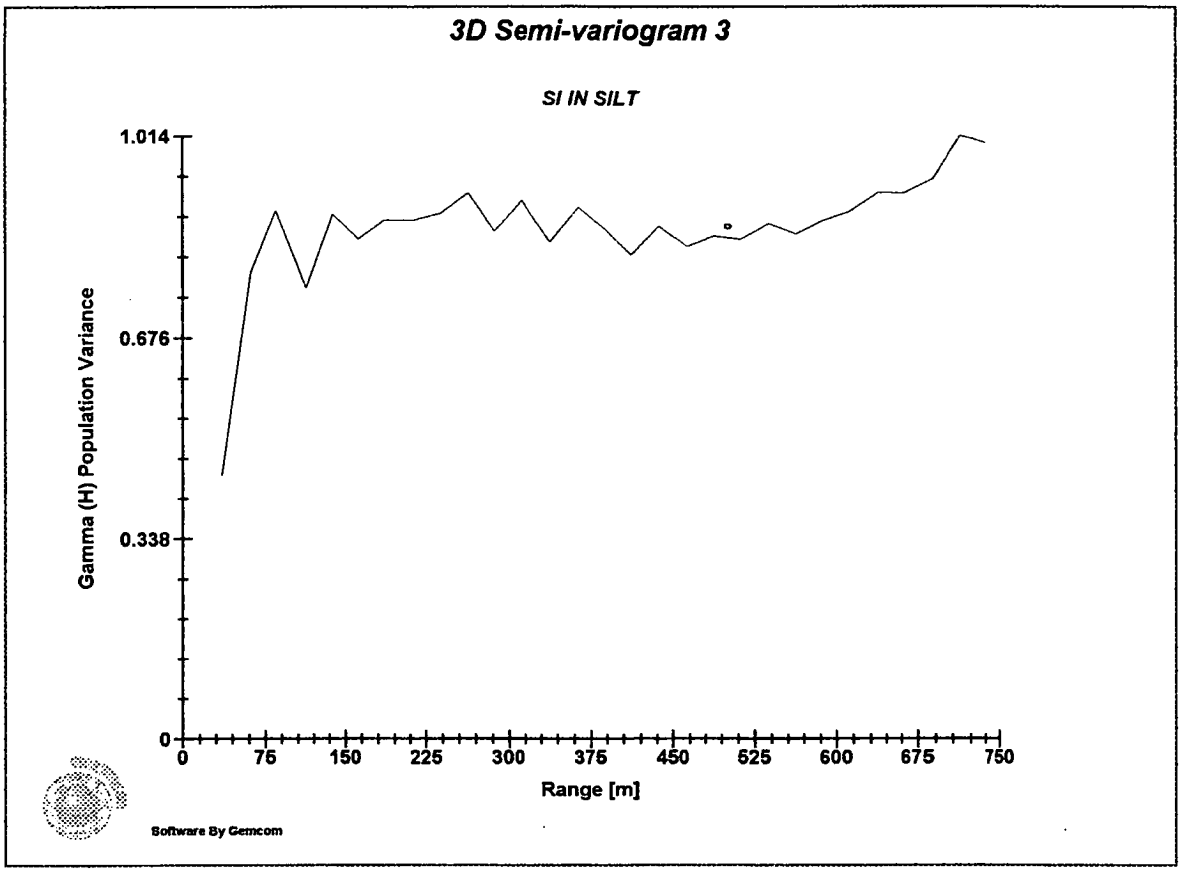
3D Semi-variogram 3
SI IN SILT
1.014
0.676
0.338
0
Gamma (H) Population Variance
0
75
150
225
300
375
450
525
600
675
750
Range [m]
Software By Gemcom

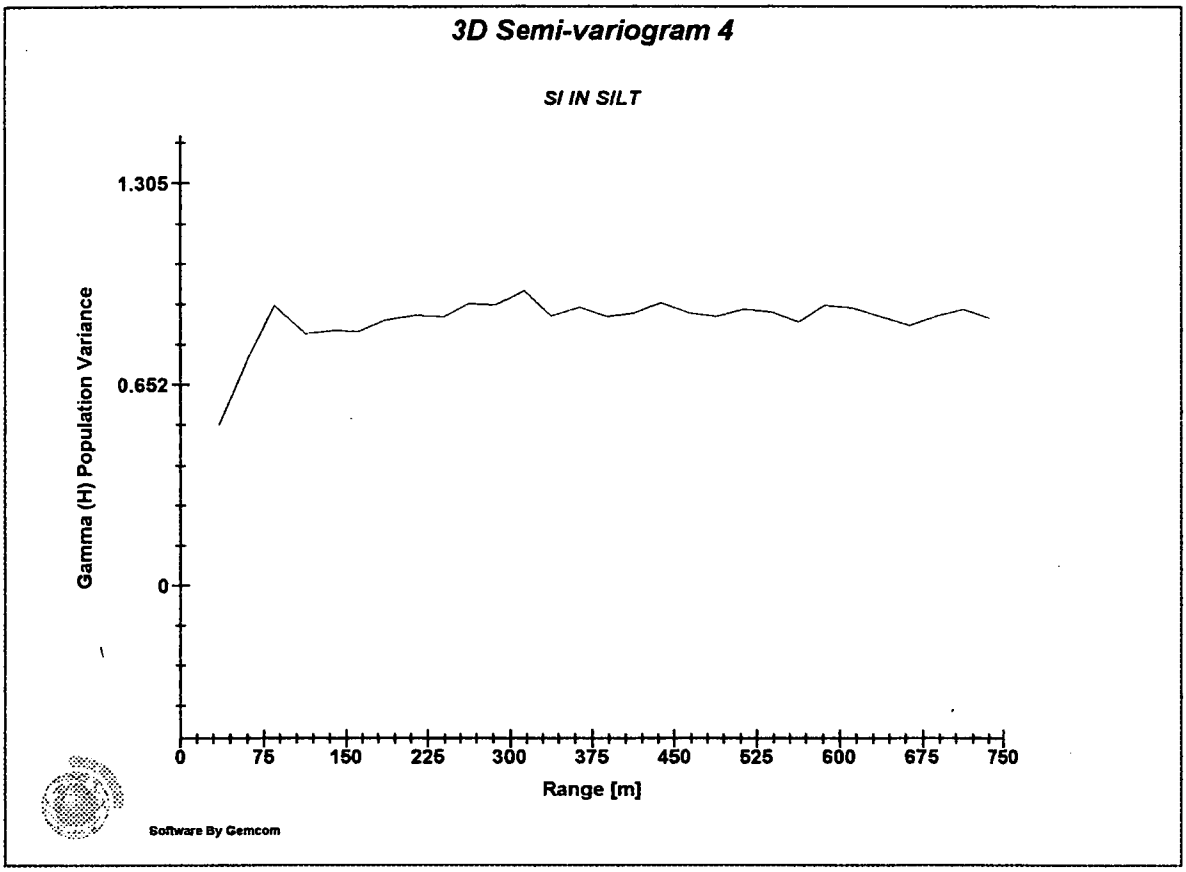
3D Semi-variogram 4
SI IN SILT
1.305
0.652
0
Gamma (H) Population Variance
0
75
150
225
300
375
450
525
600
675
750
Range [m]
Software By Gemcom

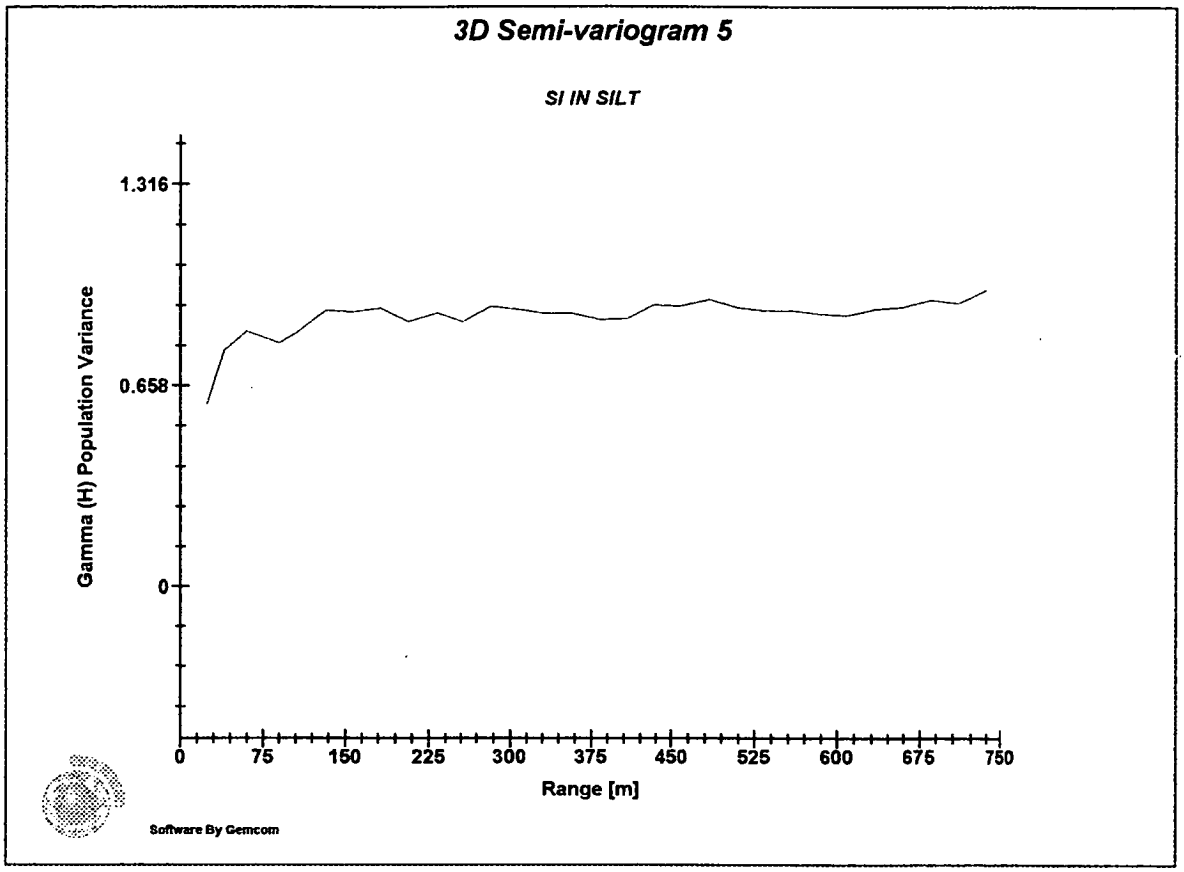
3D Semi-variogram 5
SI IN SILT
1.316
0.658
0
Gamma (H) Population Variance
0
75
150
225
300
375
450
525
600
675
750
Range [m]
Software By Gemcom

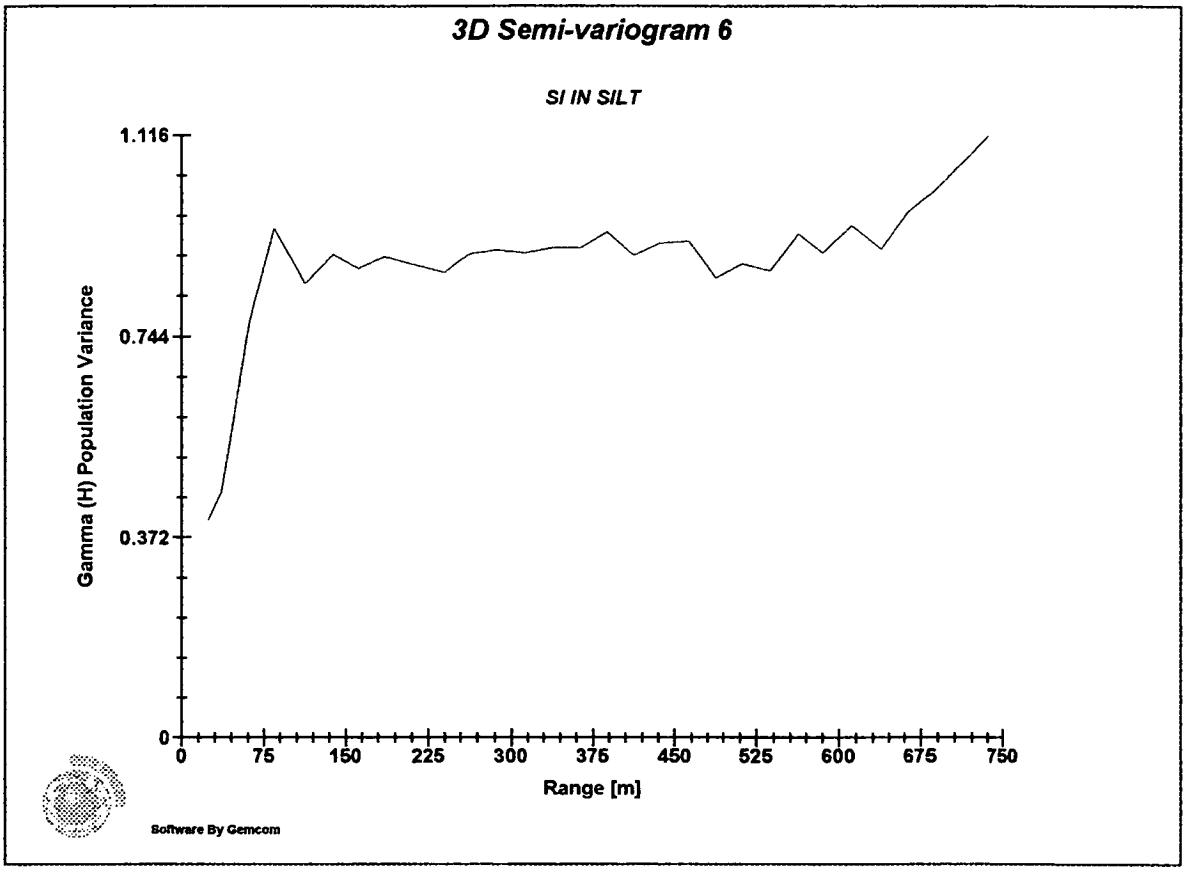
3D Semi-variogram 6
SI IN SILT
1.116
0.744
0.372
0
Gamma (H) Population Variance
0
75
150
225
300
375
450
525
600
675
750
Range [m]
Software By Gemcom

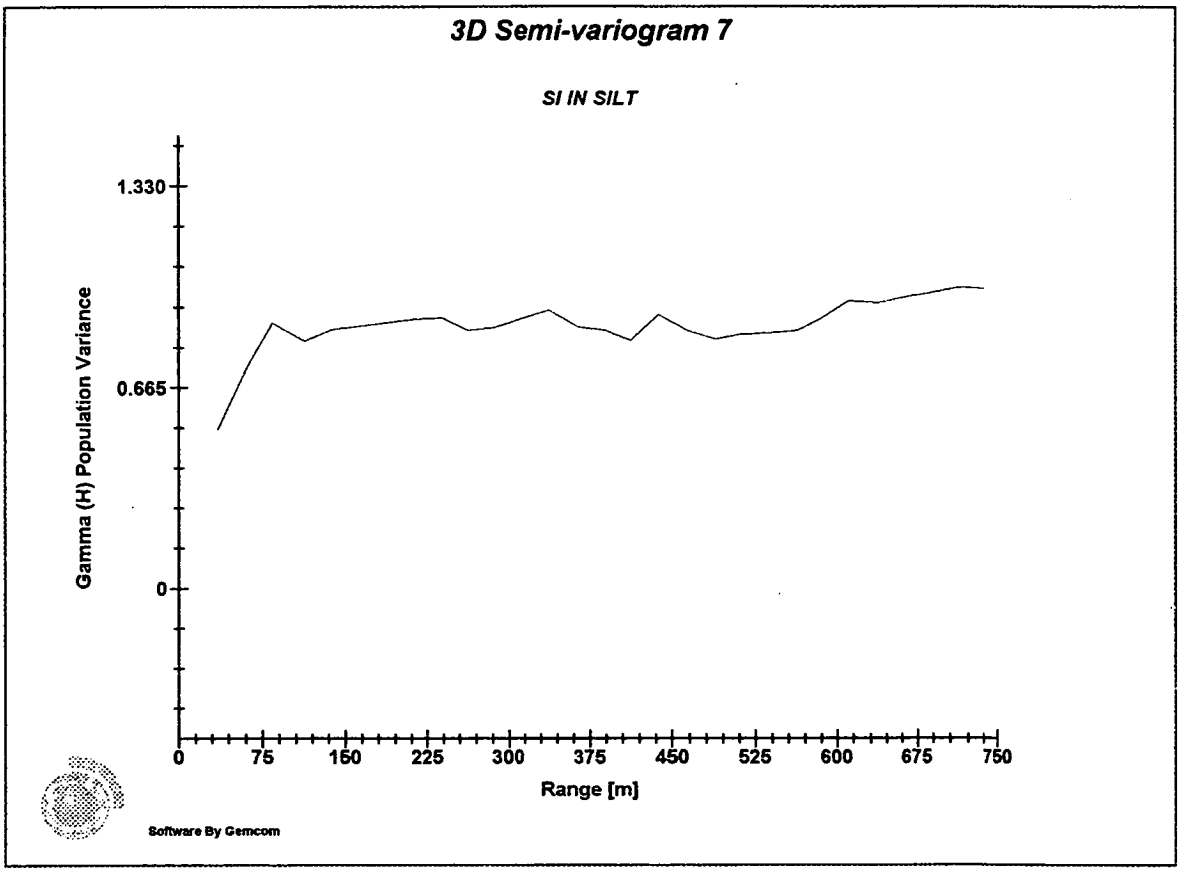
3D Semi-variogram 7
SI IN SILT
1.330
0.665
0
Gamma (H) Population Variance
0
75
150
225
300
375
450
525
600
675
750
Range [m]
Software By Gemcom

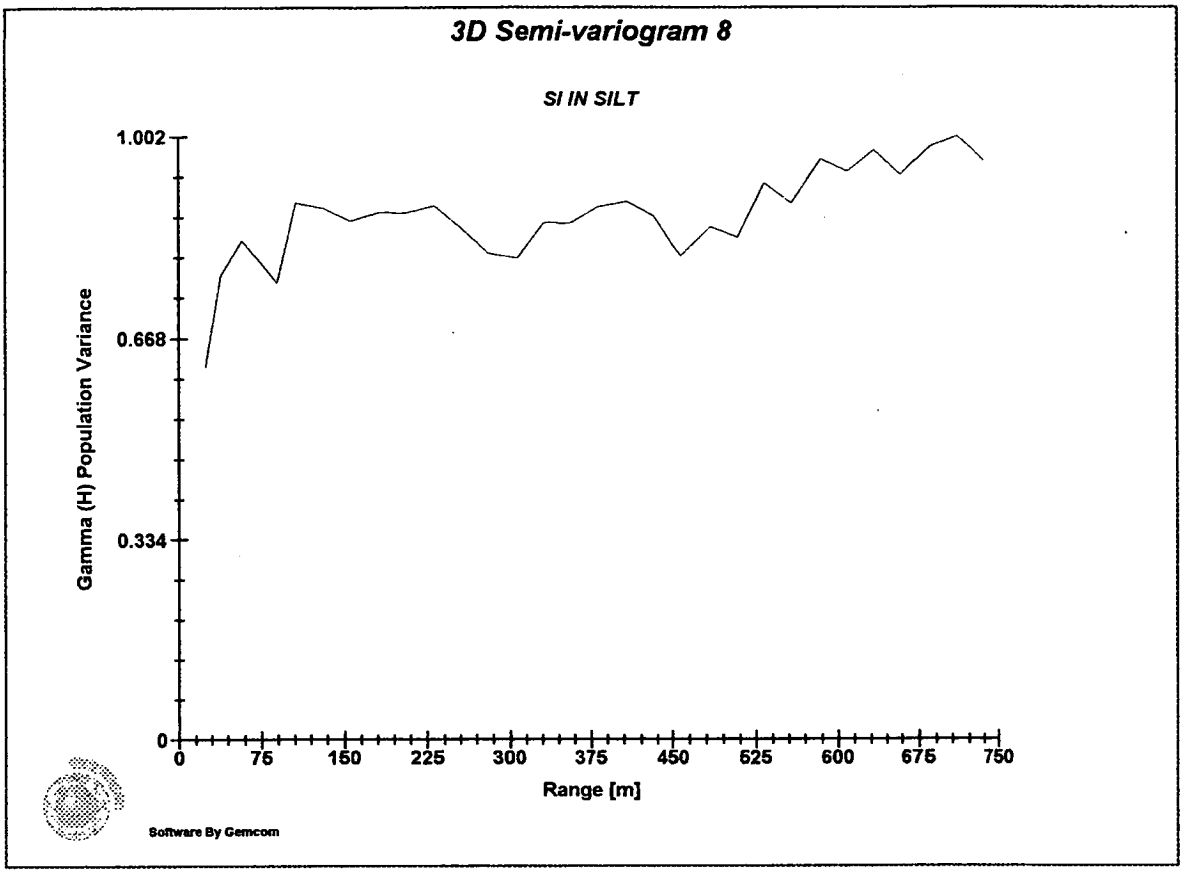
3D Semi-variogram 8
SI IN SILT
1.002
0.668
0.334
0
Gamma (H) Population Variance
0
75
150
225
300
375
450
525
600
675
750
Range [m]
Software By Gemcom

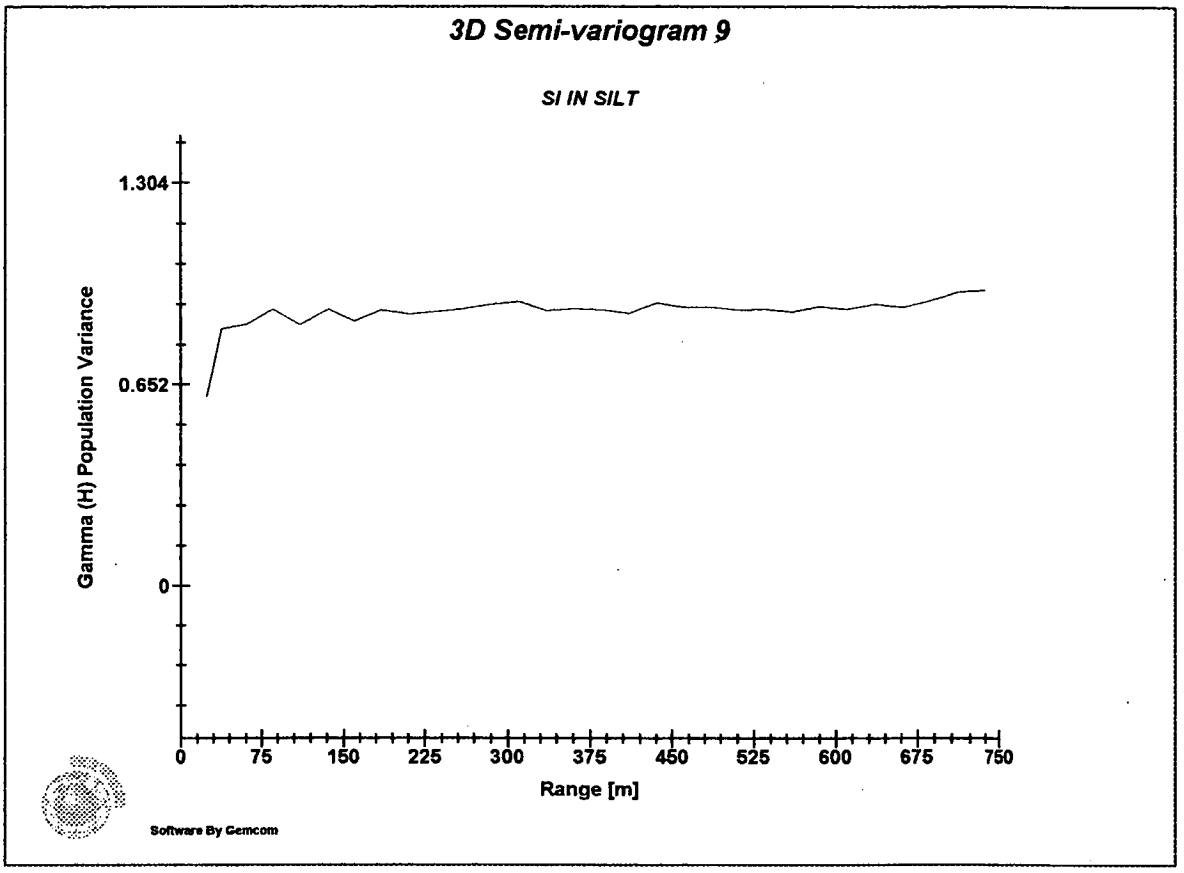
3D Semi-variogram 9
SI IN SILT
1.304
0.652
0
Gamma (H) Population Variance
0
75
150
225
300
375
450
525
600
675
750
Range [m]
Software By Gemcom

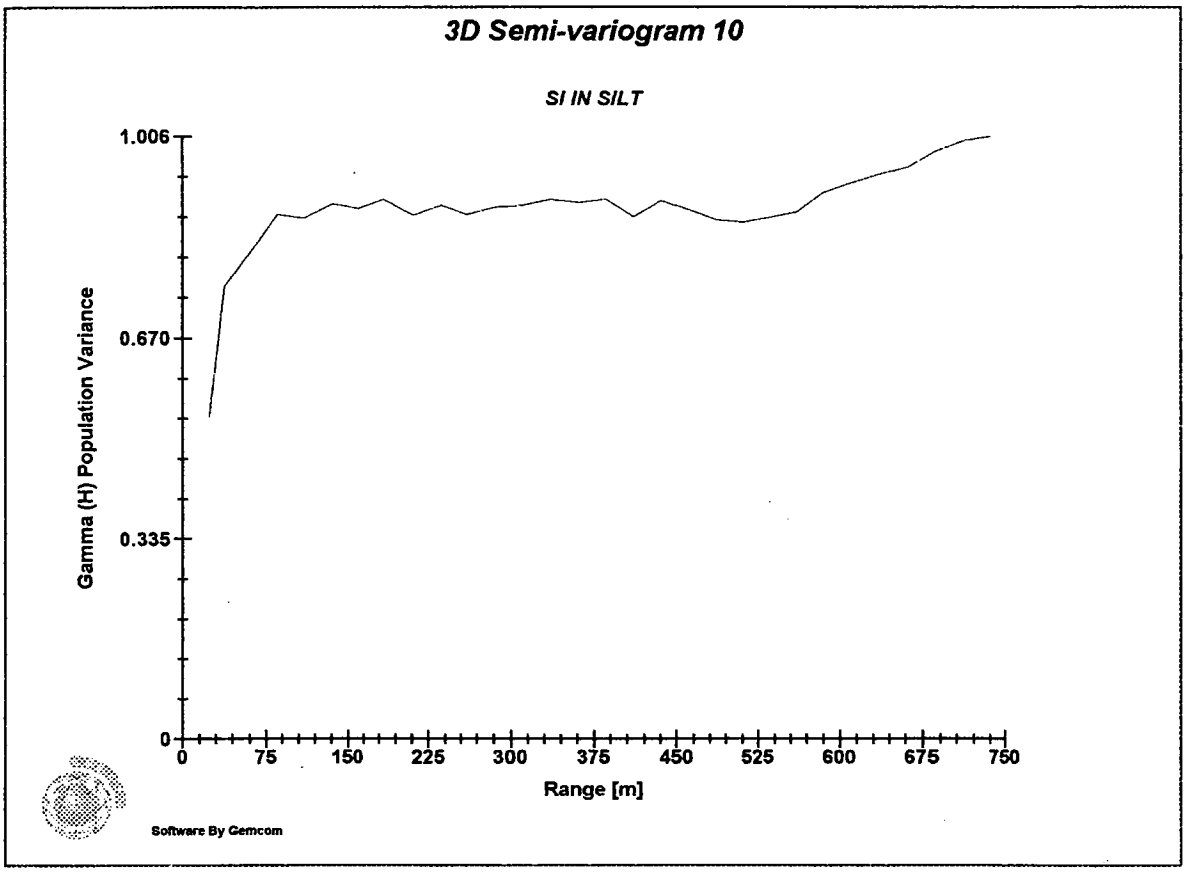
3D Semi-variogram 10
SI IN SILT
1.006
0.670
0.335
0
Gamma (H) Population Variance
0
75
150
225
300
375
450
525
600
675
750
Range [m]
Software By Gemcom

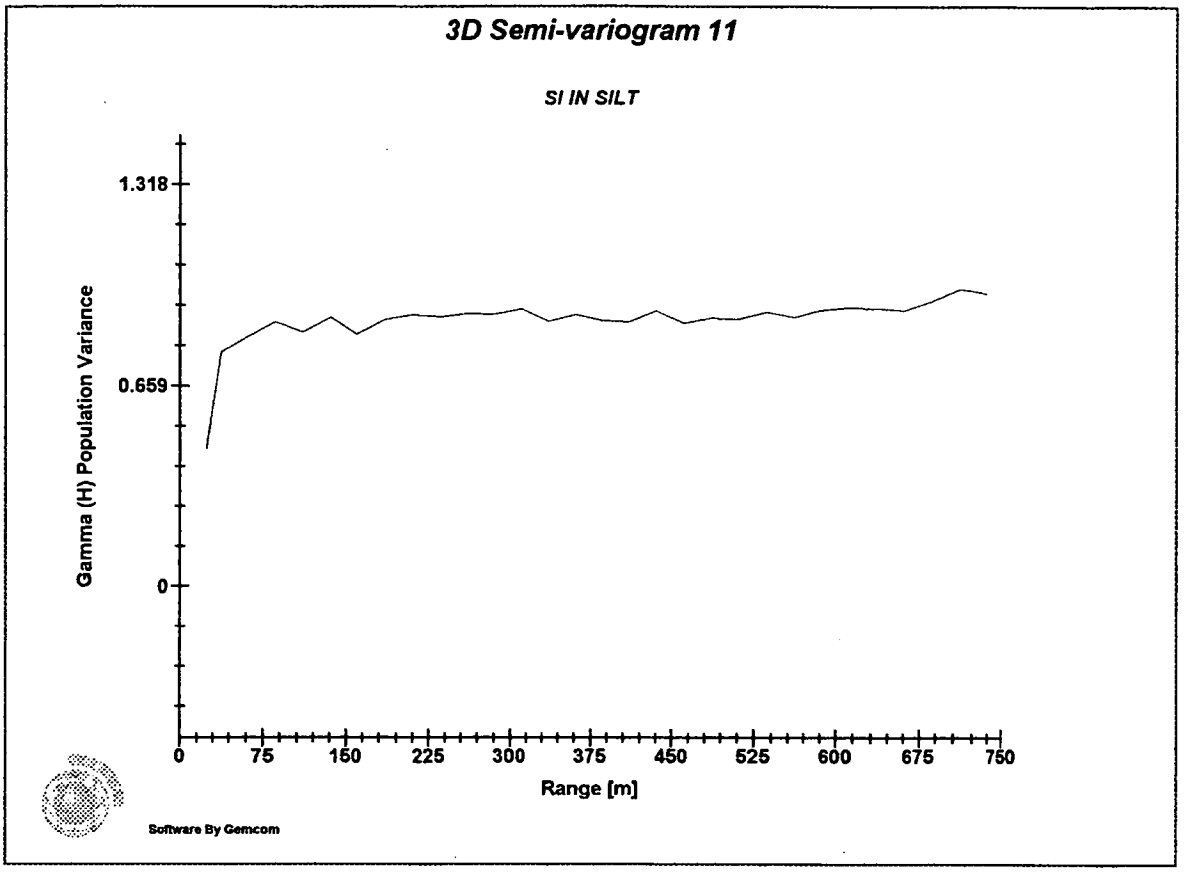
3D Semi-variogram 11
SI IN SILT
1.318
0.659
0
Gamma (H) Population Variance
0
75
150
225
300
375
450
525
600
675
750
Range [m]
Software By Gemcom

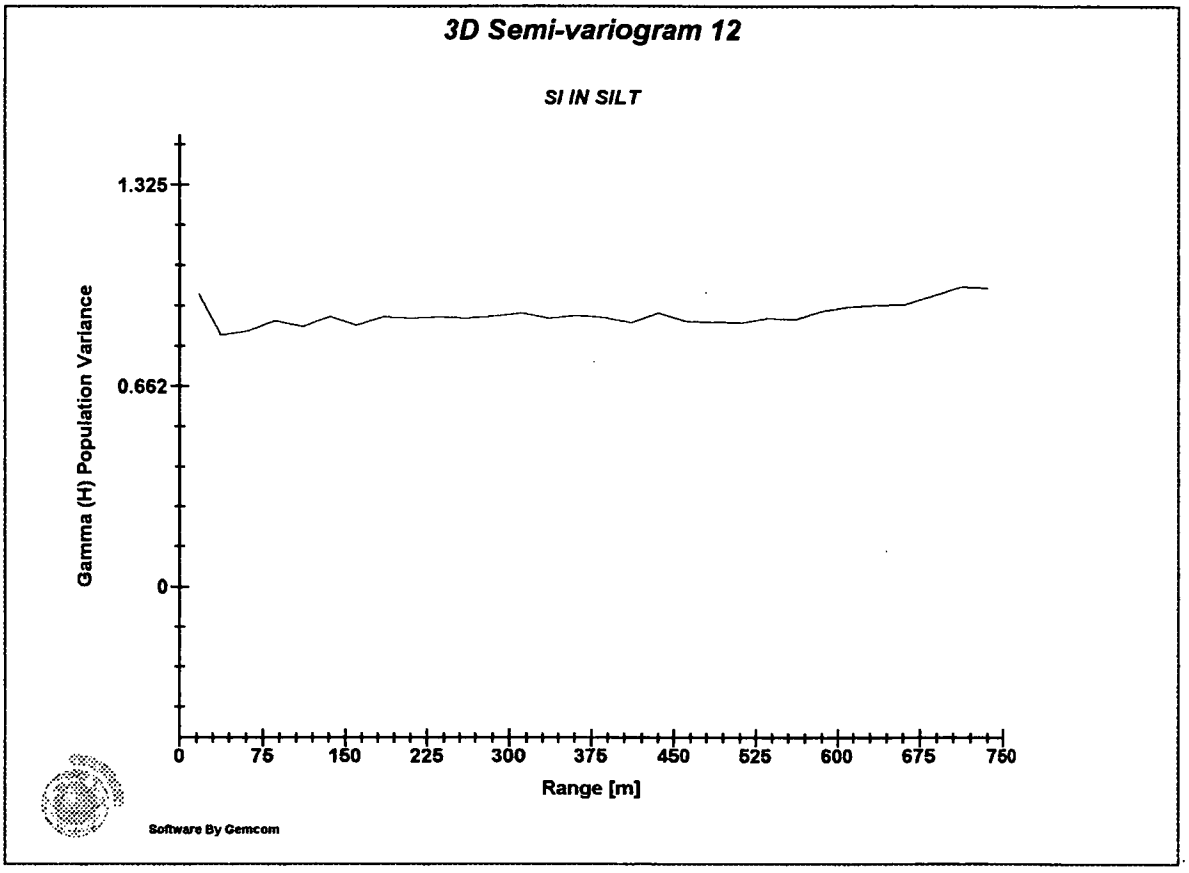
3D Semi-variogram 12
SI IN SILT
Gamma (H) Population Variance
1.325
0.662
0
0
75
150
225
300
375
450
525
600
675
750
Range [m]
Software By Gemcom

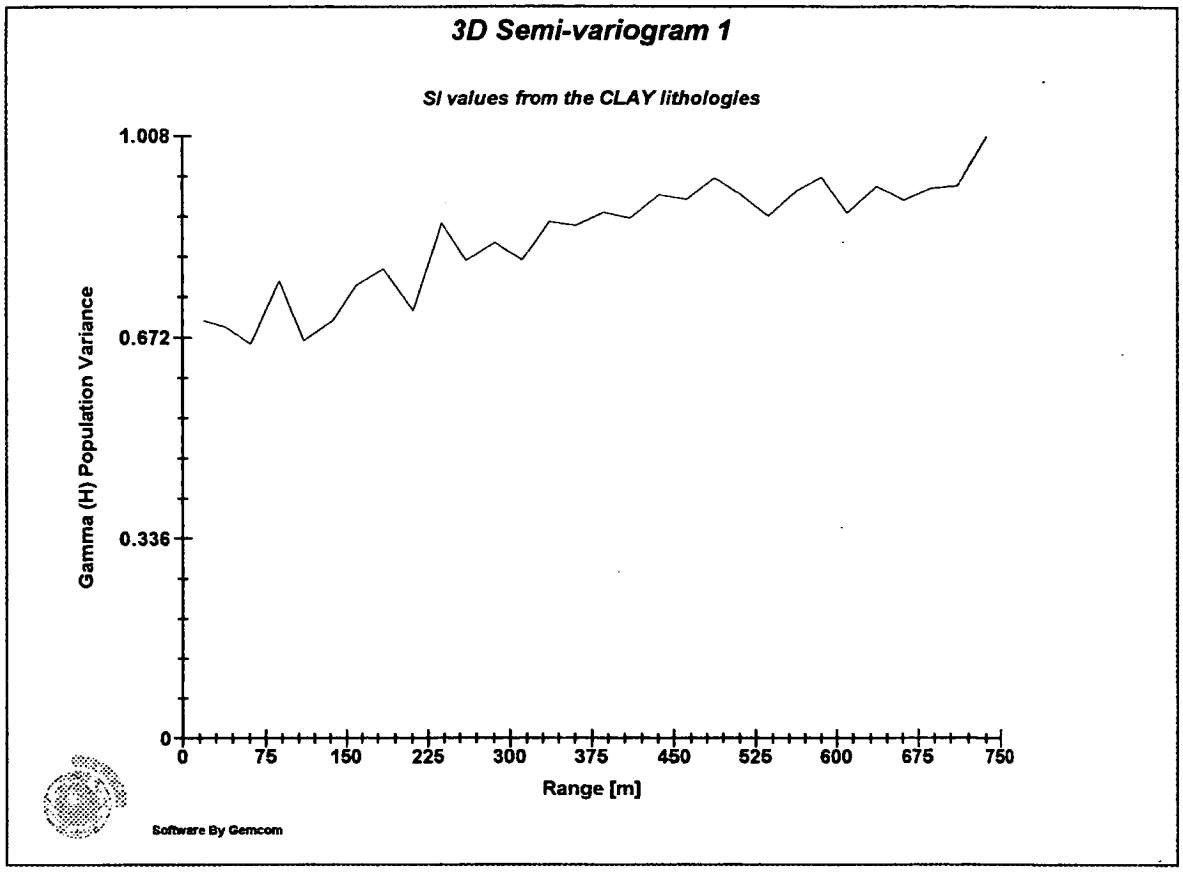
3D Semi-variogram 1
SI values from the CLAY lithologies
1.008
0.672
0.336
0
Gamma (H) Population Variance
0
75
150
225
300
375
450
525
600
675
750
Range [m]
Software By Gemcom

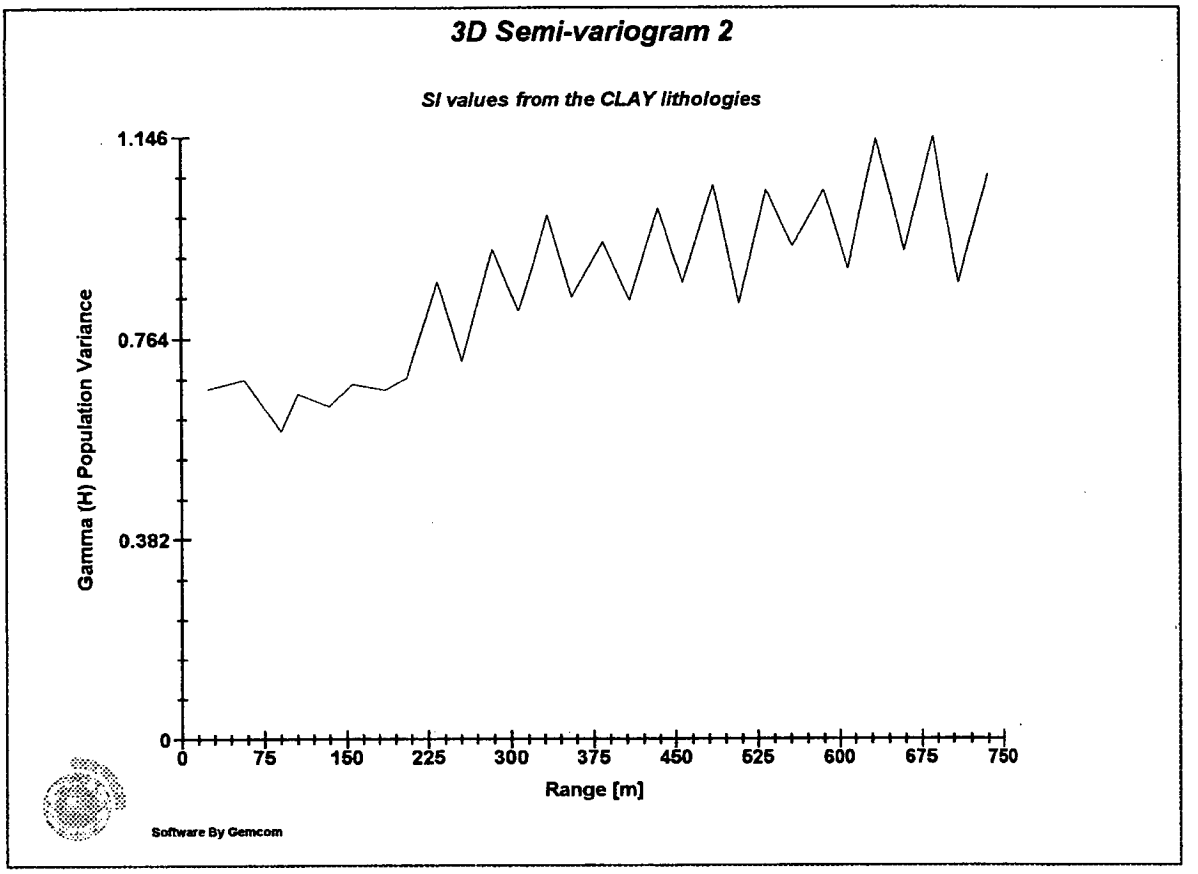
3D Semi-variogram 2
SI values from the CLAY lithologies
1.146
0.764
0.382
0
Gamma (H) Population Variance
0
75
150
225
300
375
450
525
600
675
750
Range [m]
Software By Gemcom

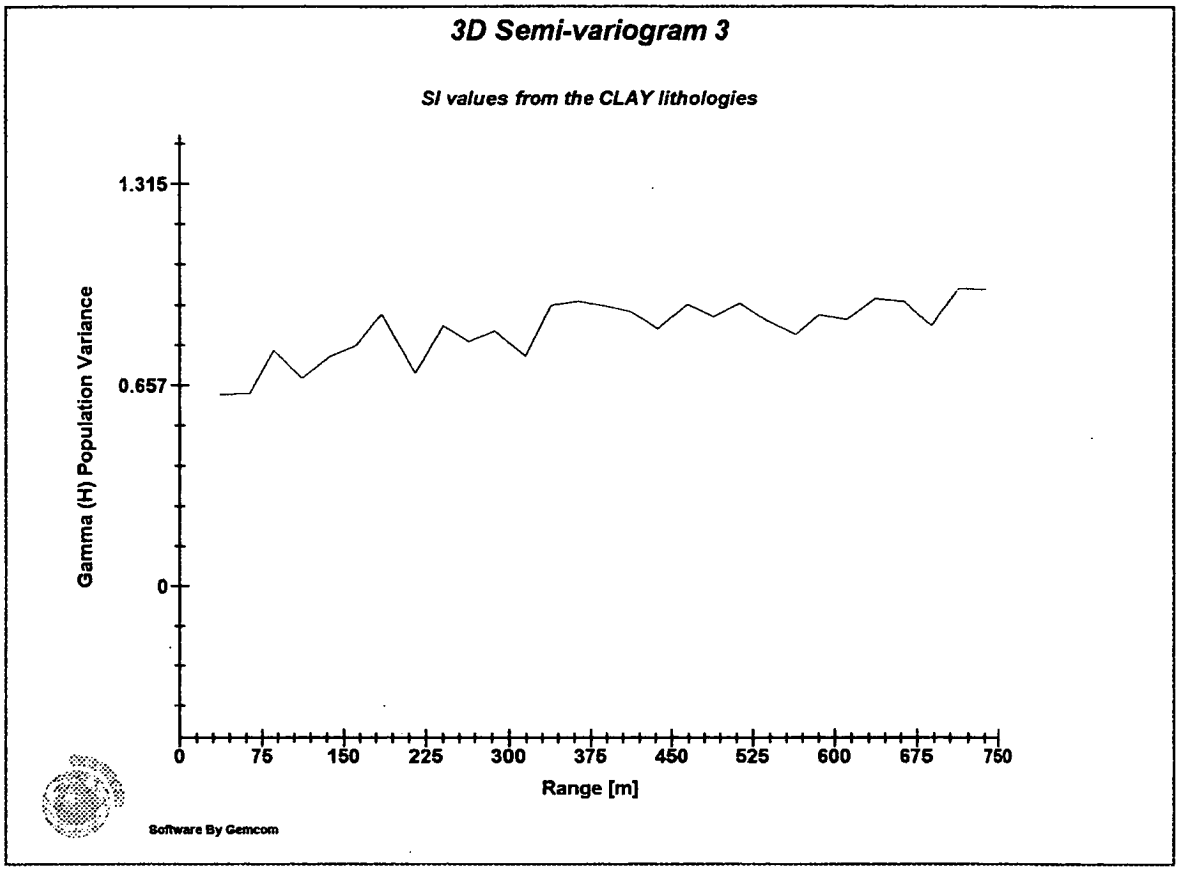
3D Semi-variogram 3
SI values from the CLAY lithologies
Gamma (H) Population Variance
1.315
0.657
0
0
75
150
225
300
375
450
525
600
675
750
Range [m]
Software By Gemcom

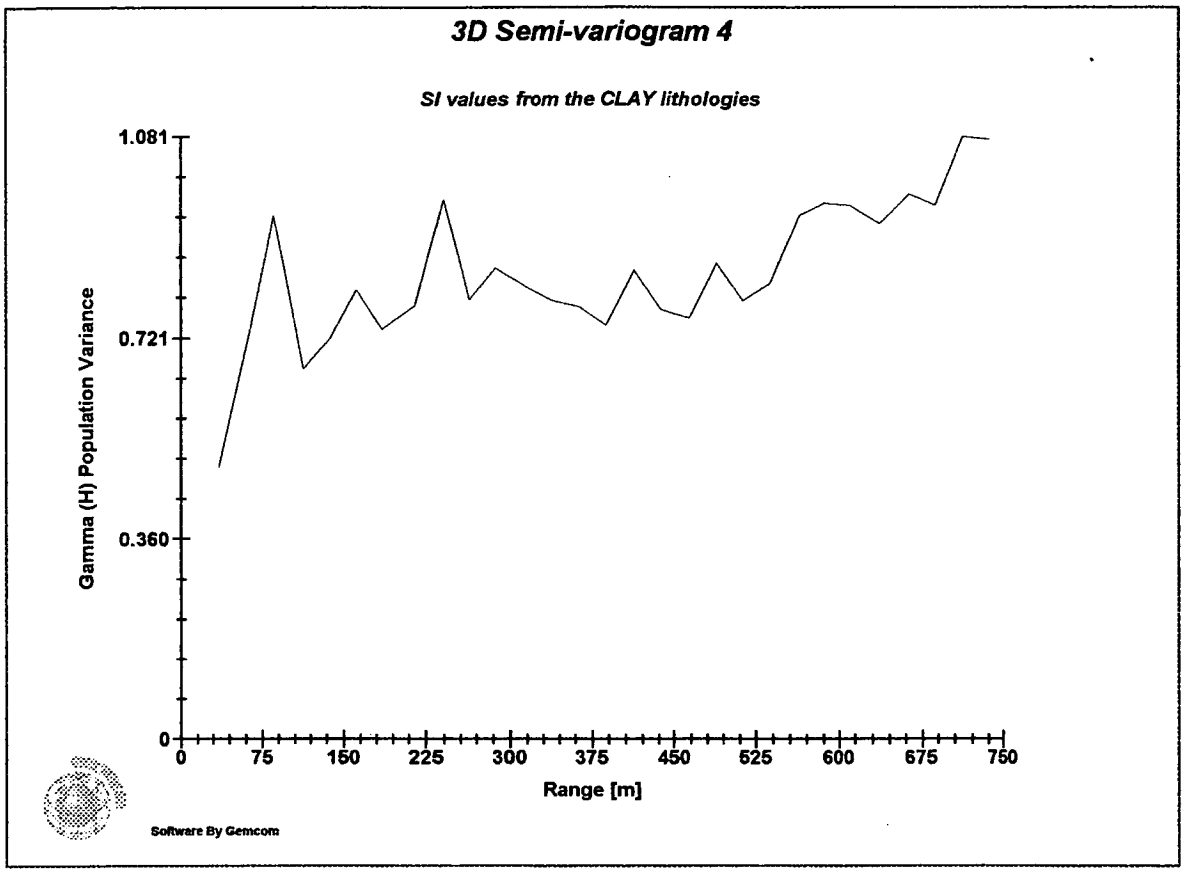
3D Semi-variogram 4
SI values from the CLAY lithologies
1.081
0.721
0.360
0
Gamma (H) Population Variance
0
75
150
225
300
375
450
525
600
675
750
Range [m]
Software By Gemcom

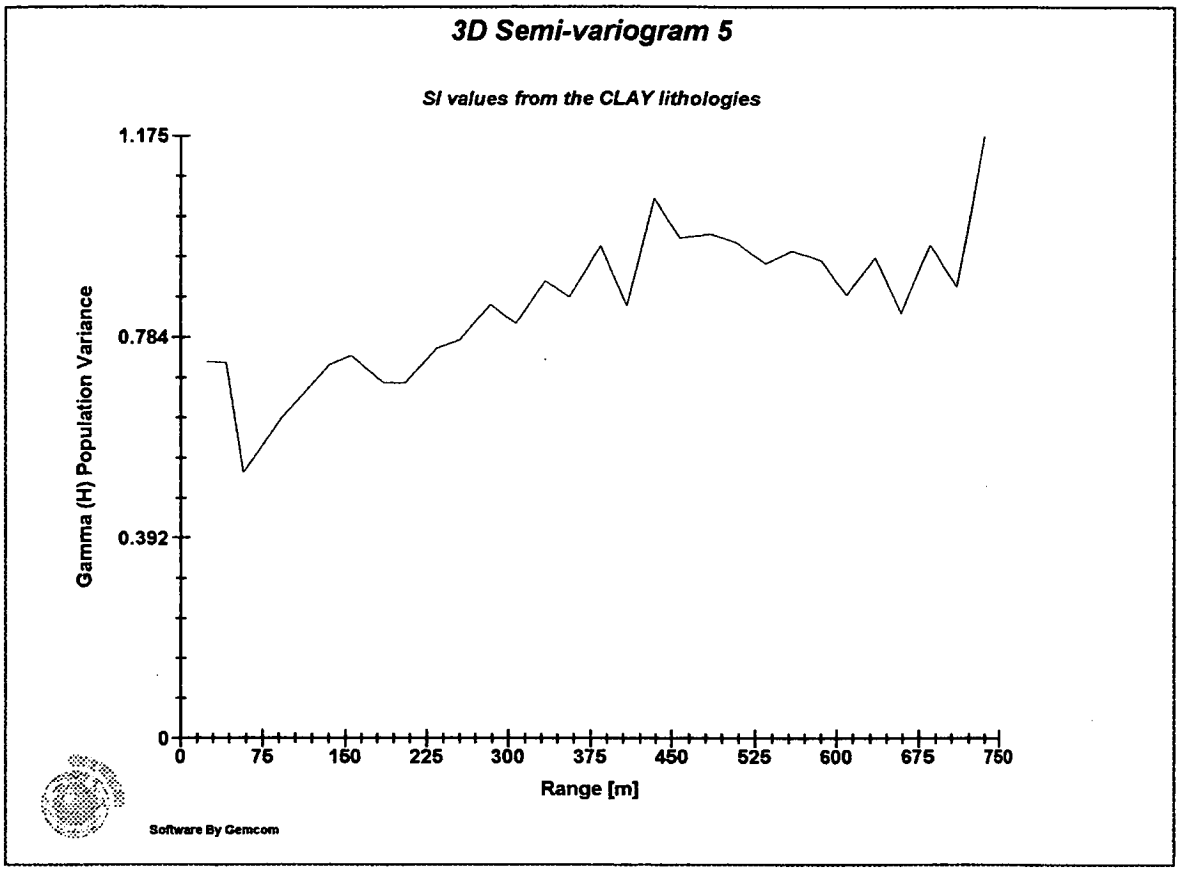
3D Semi-variogram 5
SI values from the CLAY lithologies
Gamma (H) Population Variance
1.175
0.784
0.392
0
0
75
150
225
300
375
450
525
600
675
750
Range [m]
Software By Gemcom

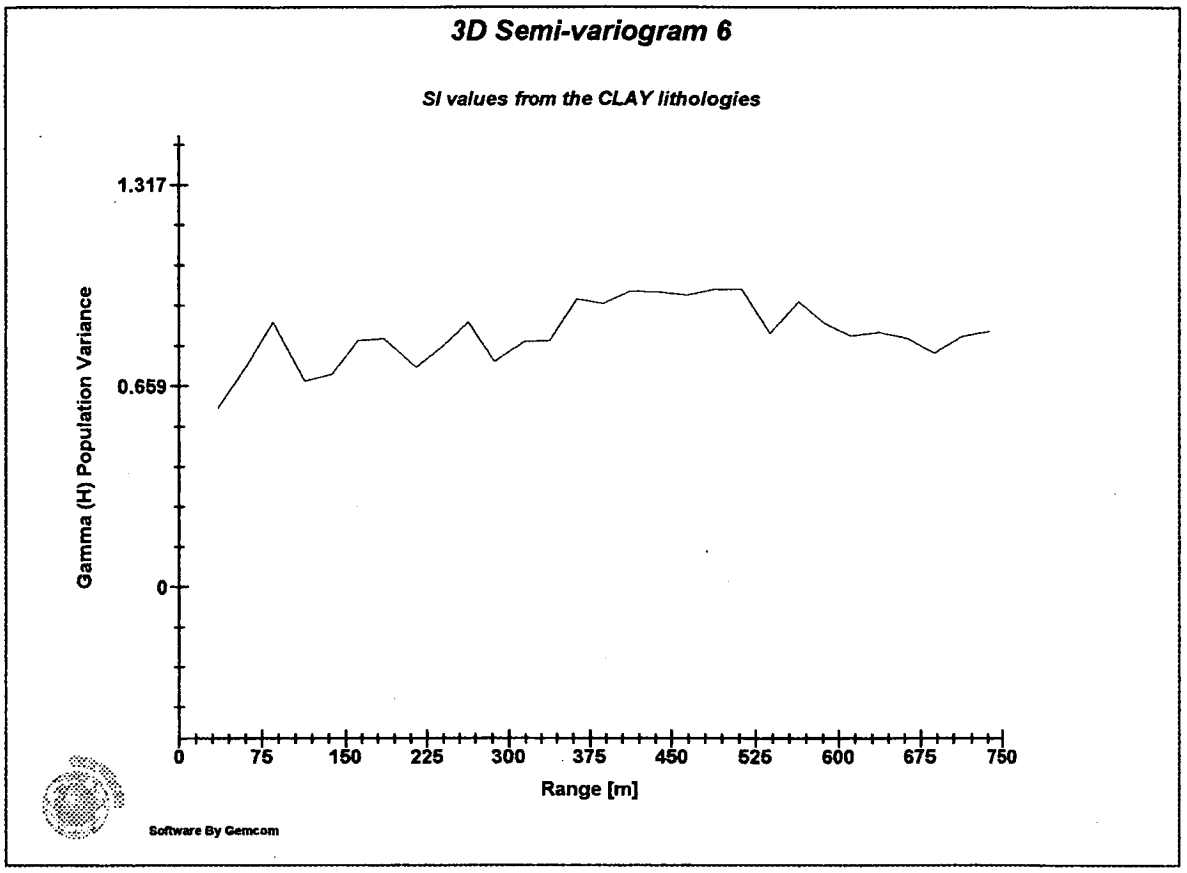
3D Semi-variogram 6
SI values from the CLAY lithologies
Gamma (H) Population Variance
1.317
0.659
0
0
75
150
225
300
375
450
525
600
675
750
Range [m]
Software By Gemcom

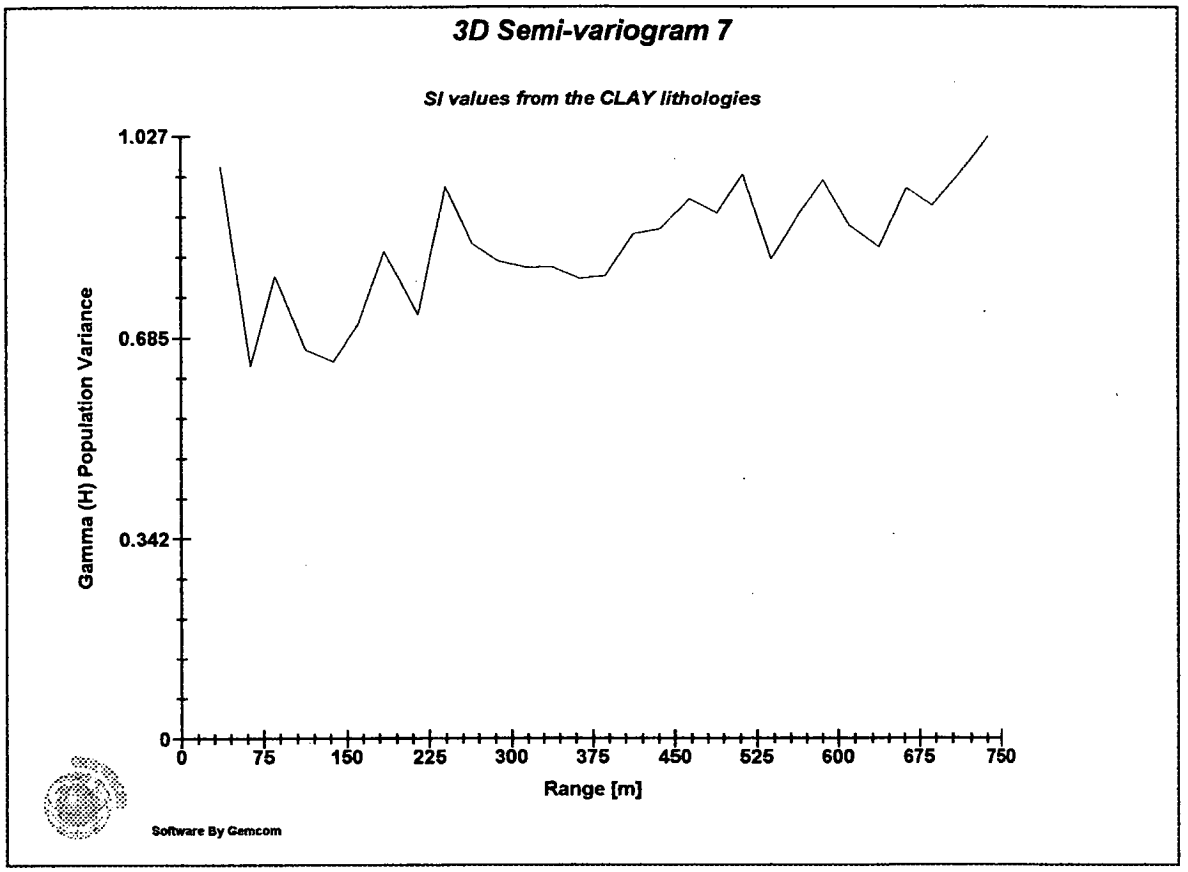
3D Semi-variogram 7
SI values from the CLAY lithologies
1.027
0.685
0.342
0
Gamma (H) Population Variance
0
75
150
225
300
375
450
525
600
675
750
Range [m]
Software By Gemcom

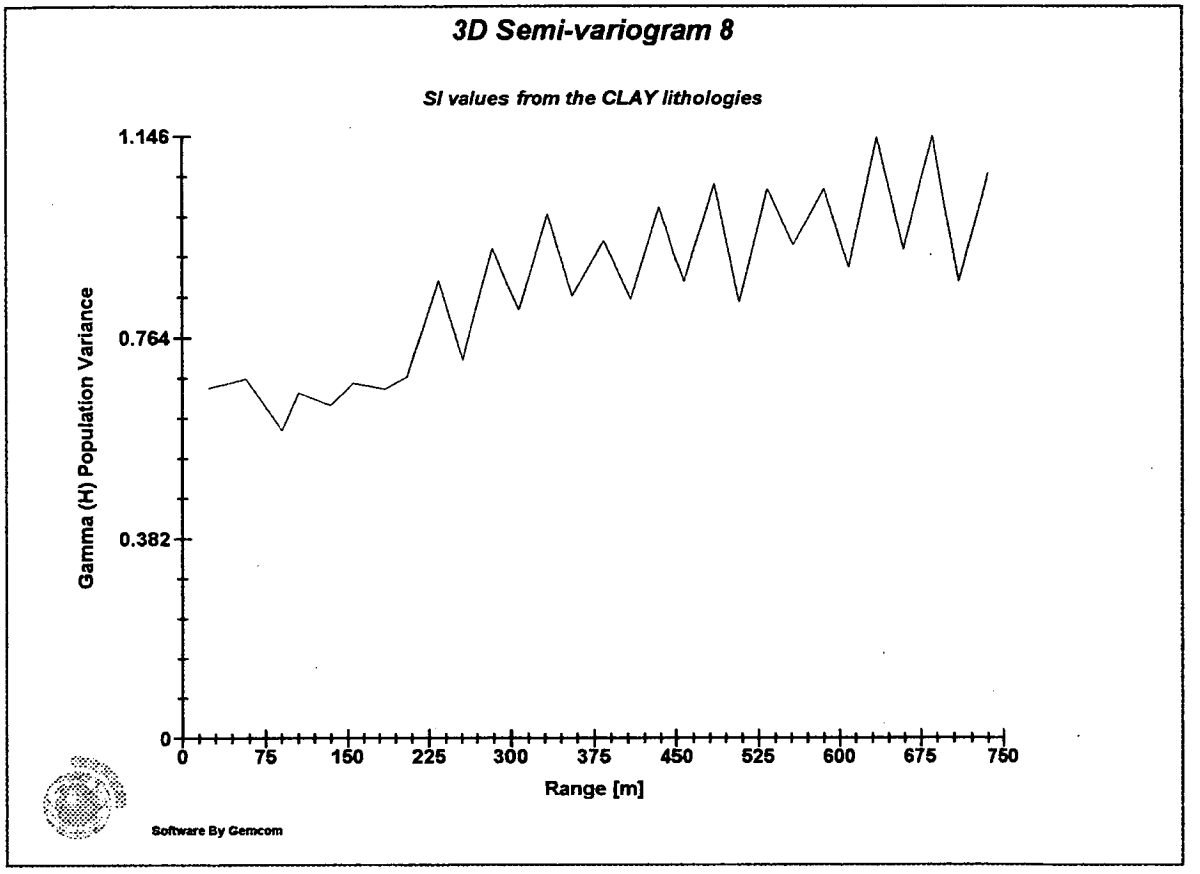
3D Semi-variogram 8
SI values from the CLAY lithologies
1.146
0.764
0.382
0
Gamma (H) Population Variance
0
75
150
225
300
375
450
525
600
675
750
Range [m]
Software By Gemcom

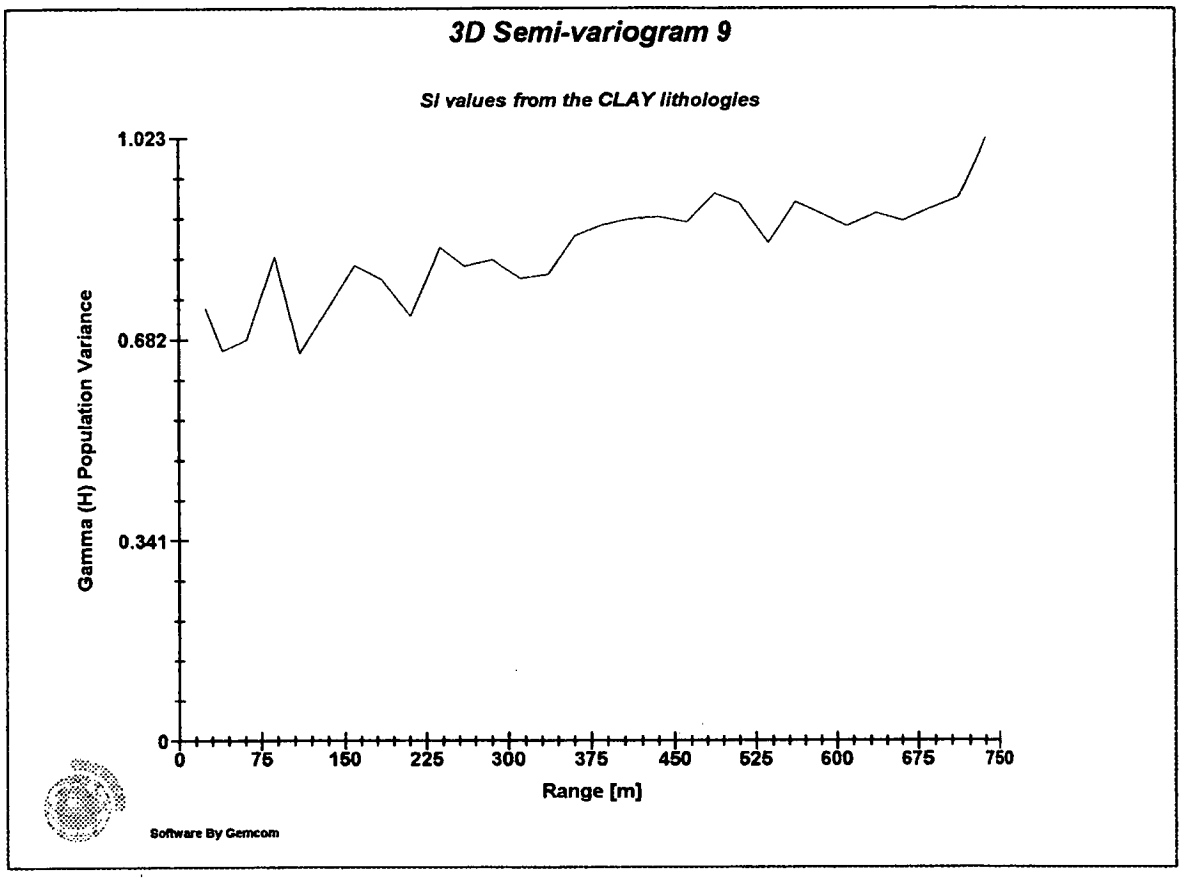
3D Semi-variogram 9
SI values from the CLAY lithologies
Gamma (H) Population Variance
1.023
0.682
0.341
0
0
75
150
225
300
375
450
525
600
675
750
Range [m]
Software By Gemcom

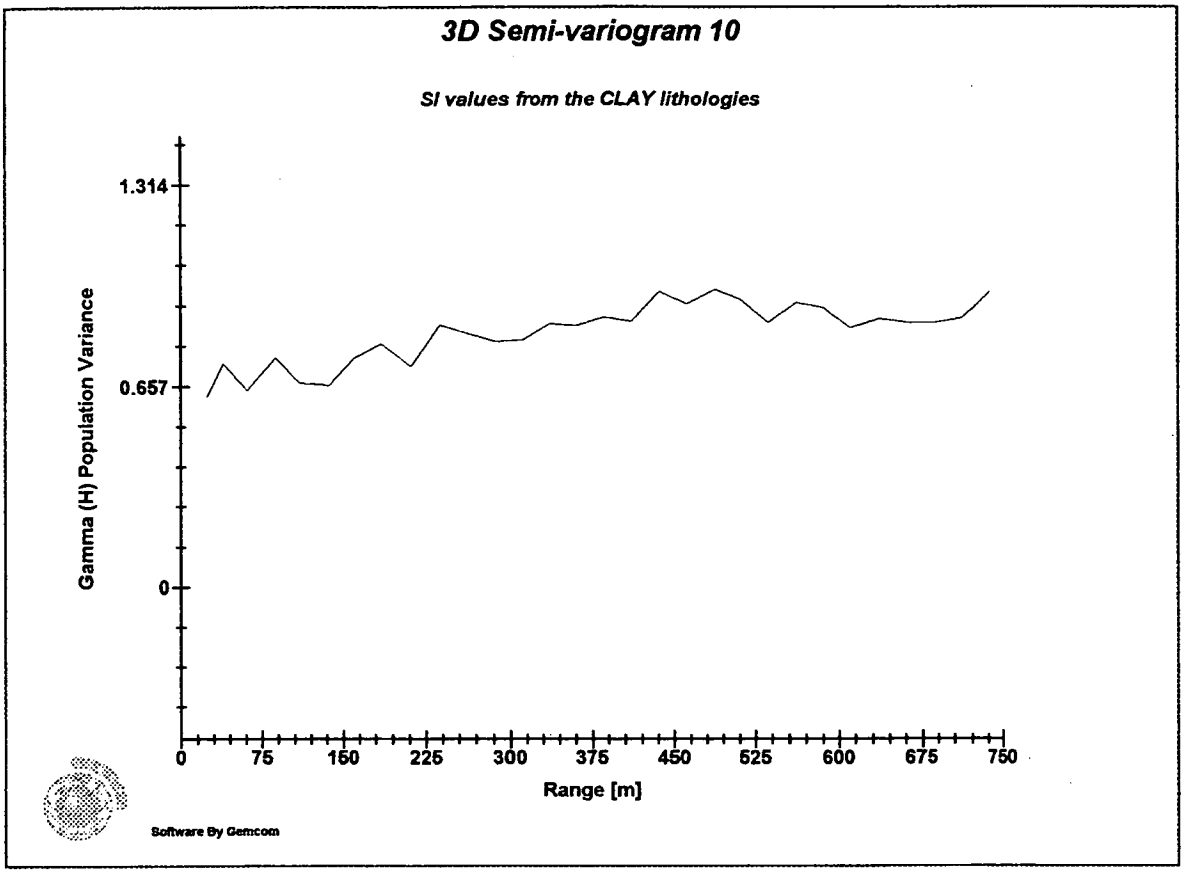
3D Semi-variogram 10
SI values from the CLAY lithologies
Gamma (H) Population Variance
1.314
0.657
0
0
75
150
225
300
375
450
525
600
675
750
Range [m]
Software By Gemcom

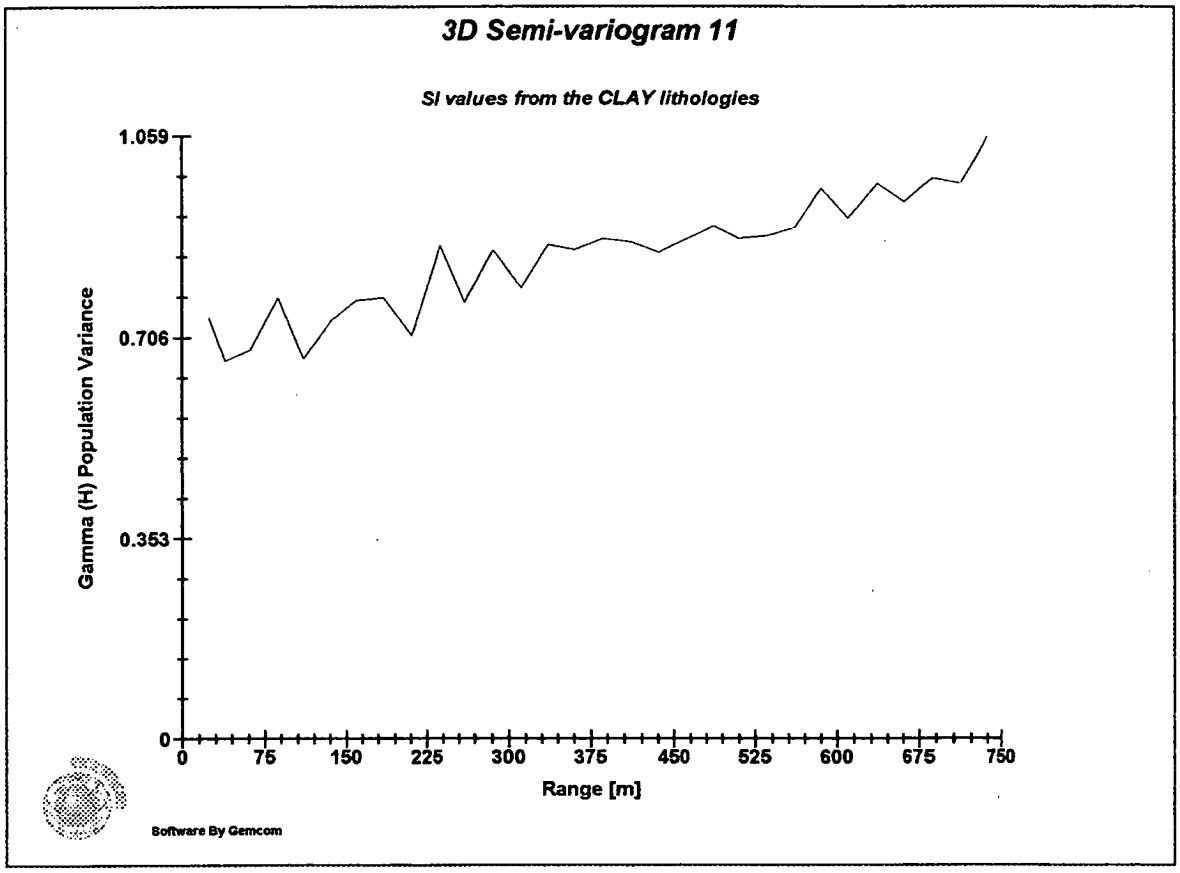
3D Semi-variogram 11
SI values from the CLAY lithologies
Gamma (H) Population Variance
1.059
0.706
0.353
0
0
75
150
225
300
375
450
525
600
675
750
Range [m]
Software By Gemcom

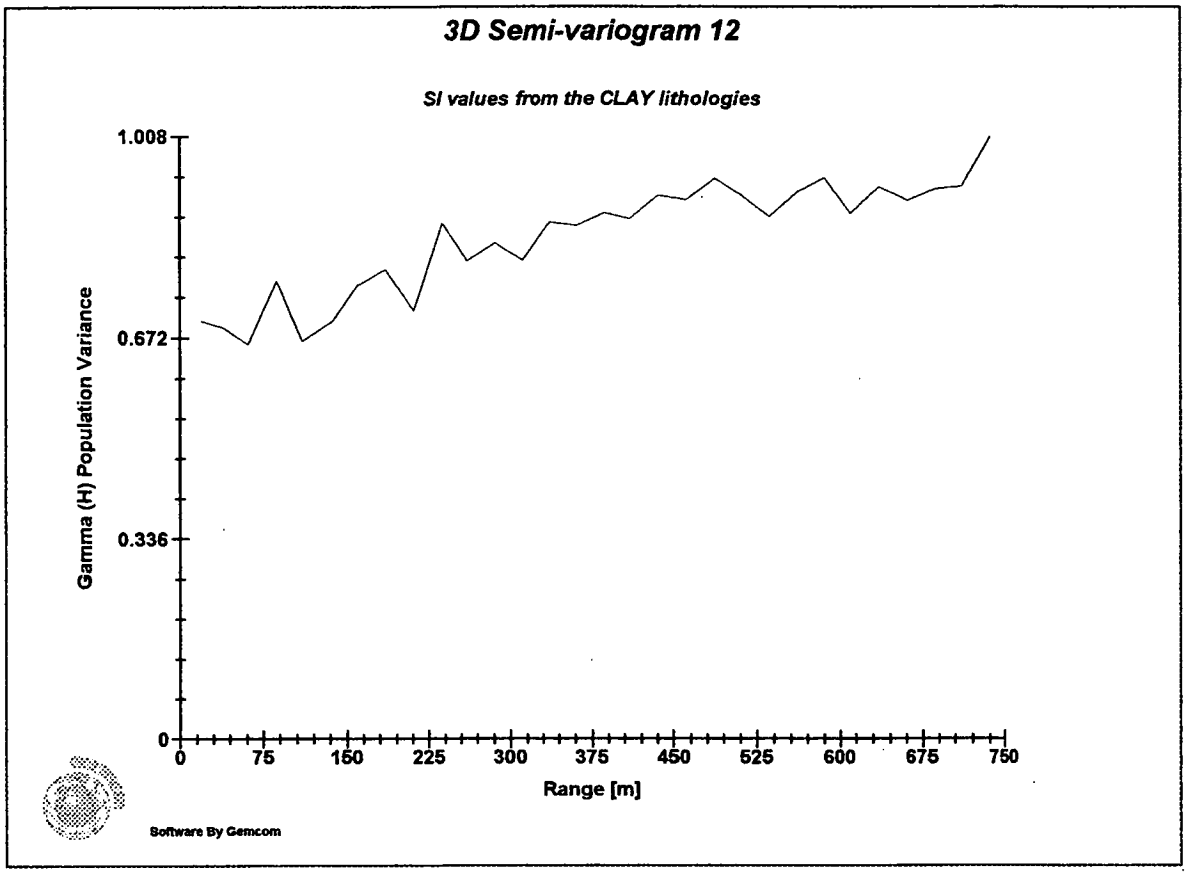
3D Semi-variogram 12
SI values from the CLAY lithologies
1.008
0.672
0.336
0
Gamma (H) Population Variance
0
75
150
225
300
375
450
525
600
675
750
Range [m]
Software By Gemcom

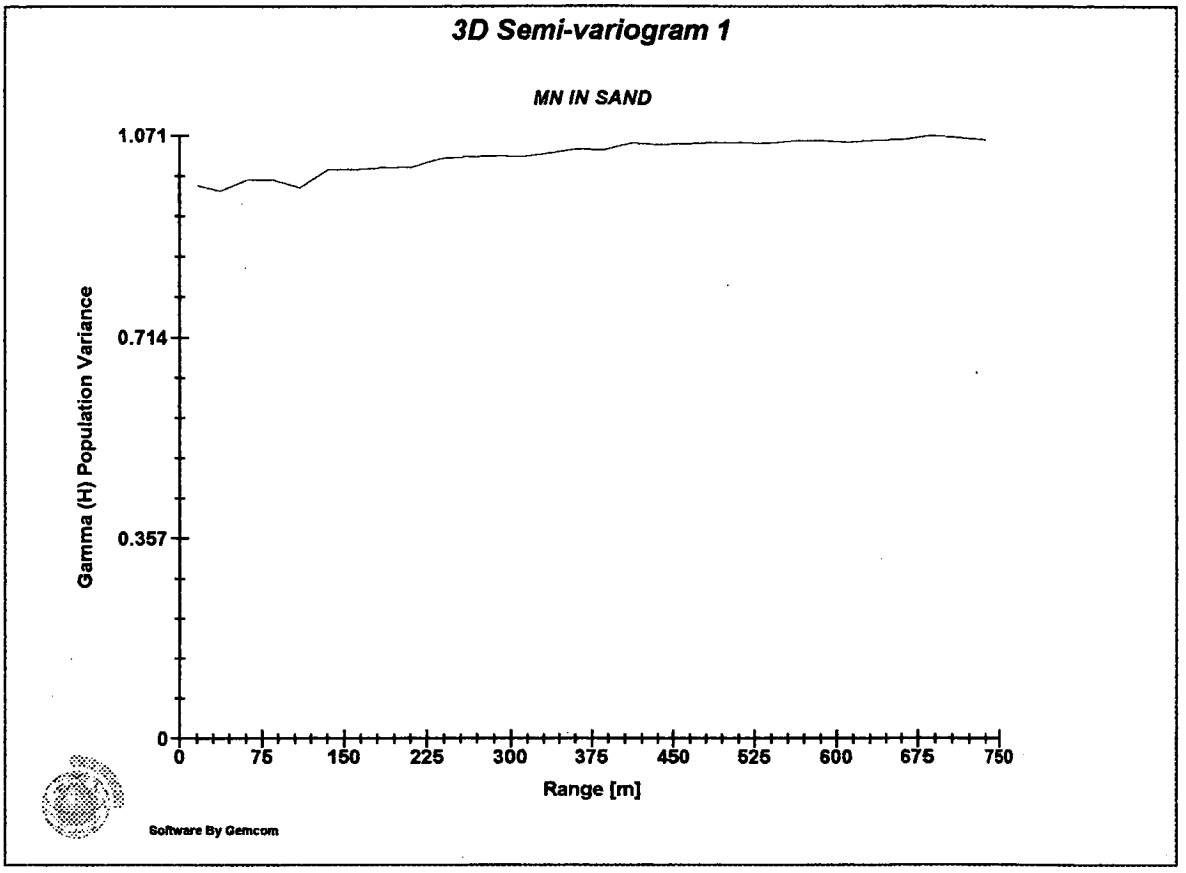
3D Semi-variogram 1
MN IN SAND
1.071
0.714
0.357
0
Gamma (H) Population Variance
0
75
150
225
300
375
450
525
600
675
750
Range [m]
Software By Gemcom

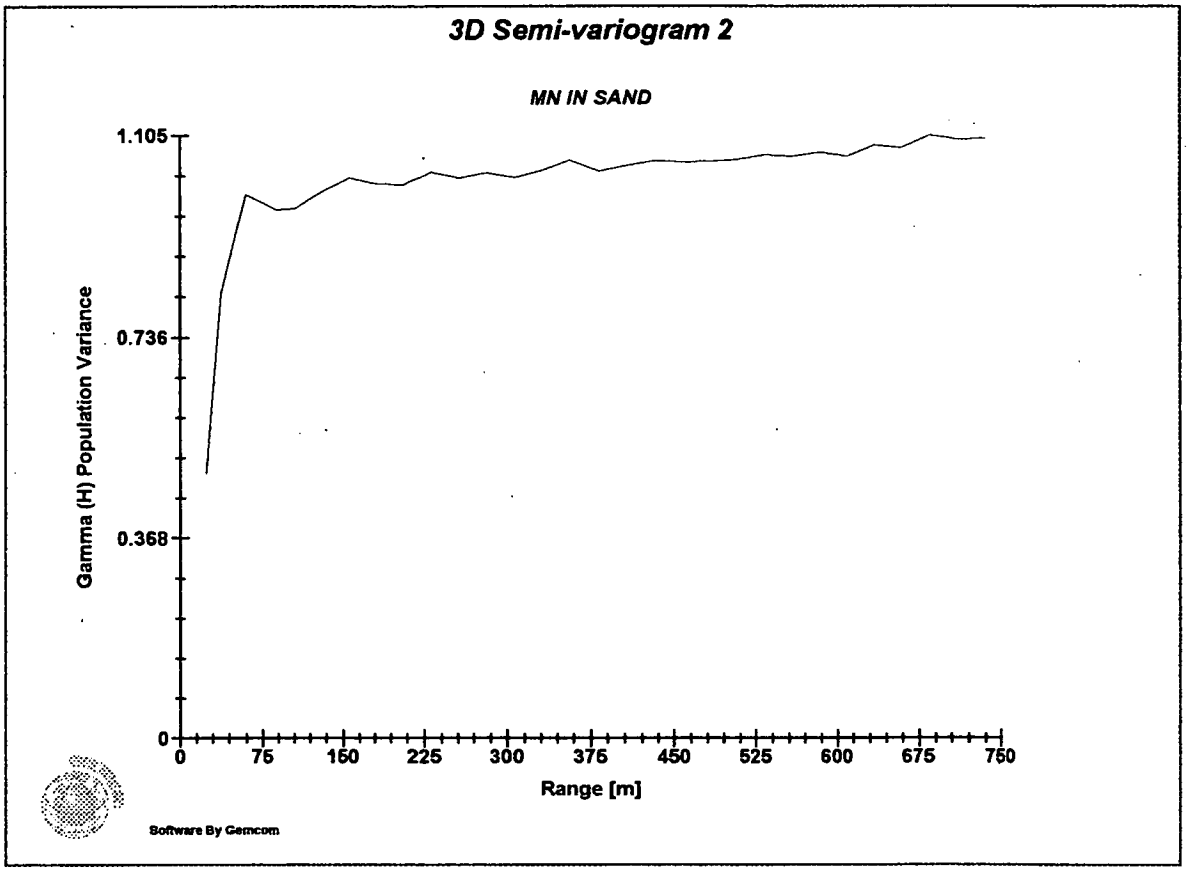
3D Semi-variogram 2
MN IN SAND
1.105
0.736
0.368
0
Gamma (H) Population Variance
0
75
150
225
300
375
450
525
600
675
750
Range [m]
Software By Gemcom

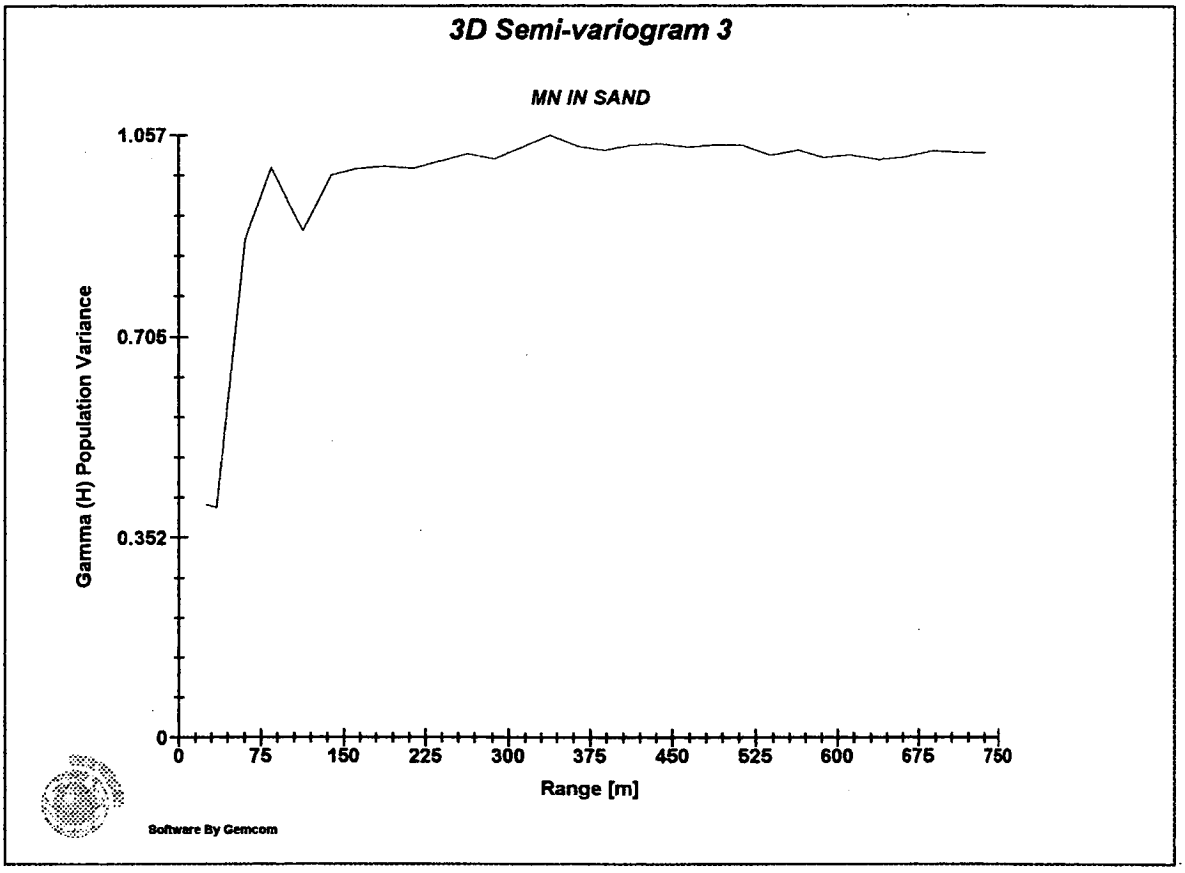
3D Semi-variogram 3
MN IN SAND
1.057
0.705
0.352
0
Gamma (H) Population Variance
0
75
150
225
300
375
450
525
600
675
750
Range [m]
Software By Gemcom

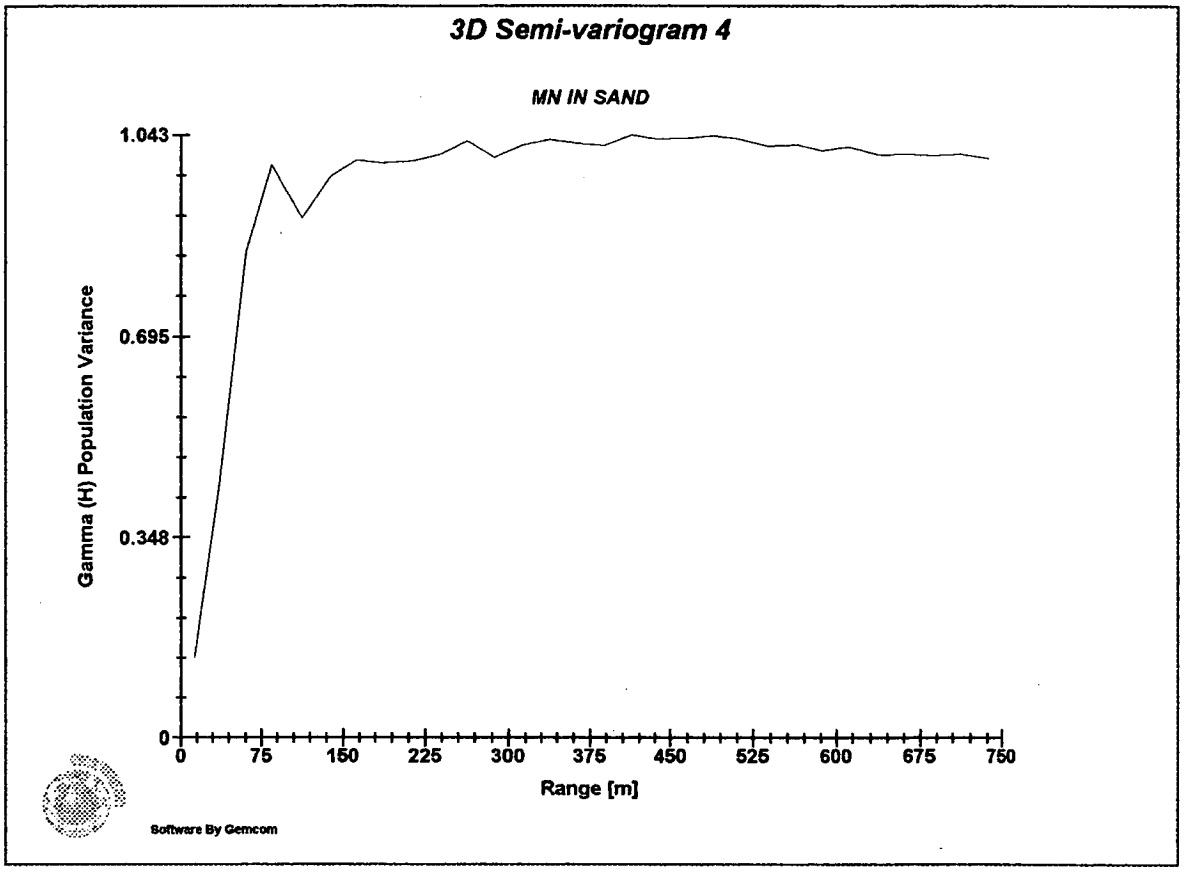
3D Semi-variogram 4
MN IN SAND
Gamma (H) Population Variance
1.043
0.695
0.348
0
0
75
150
225
300
375
450
525
600
675
750
Range [m]
Software By Gemcom

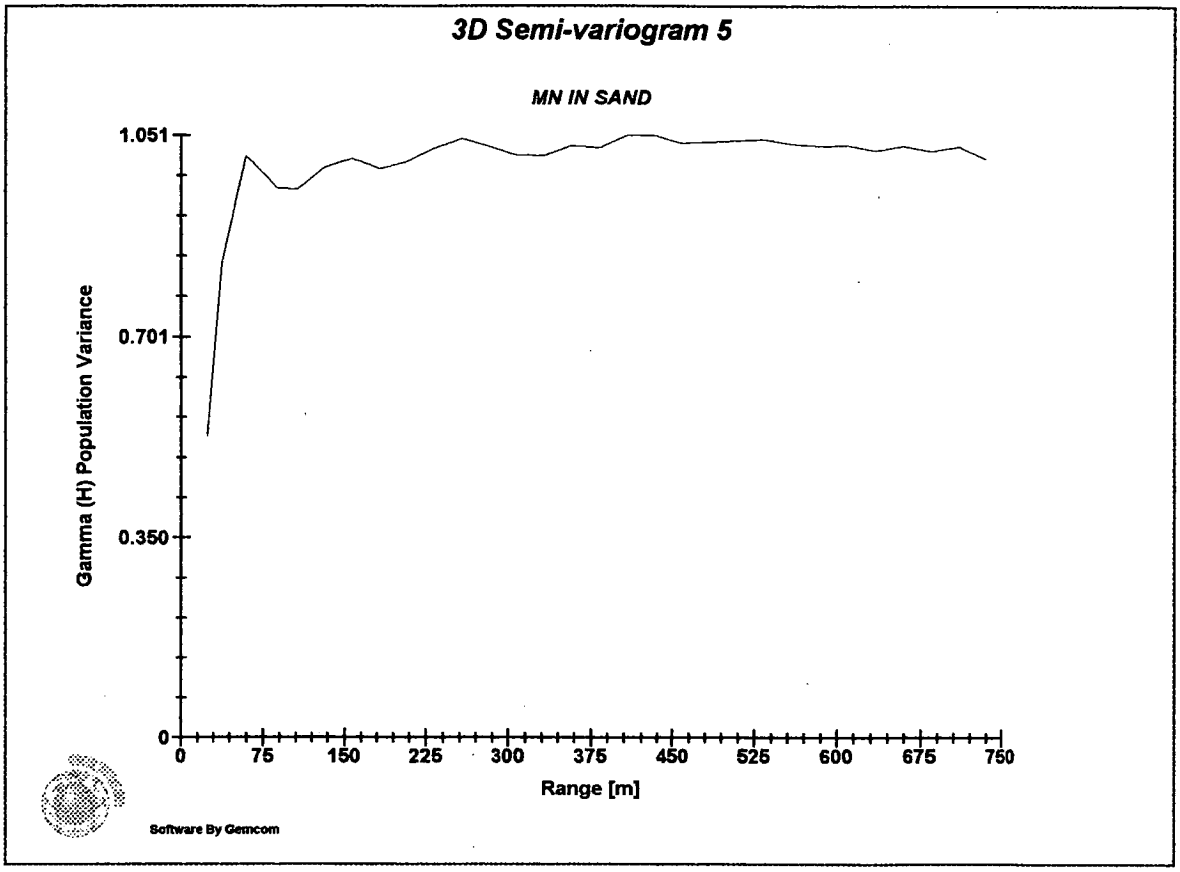
3D Semi-variogram 5
MN IN SAND
1.051
0.701
0.350
0
Gamma (H) Population Variance
0
75
150
225
300
375
450
525
600
675
750
Range [m]
Software By Gemcom

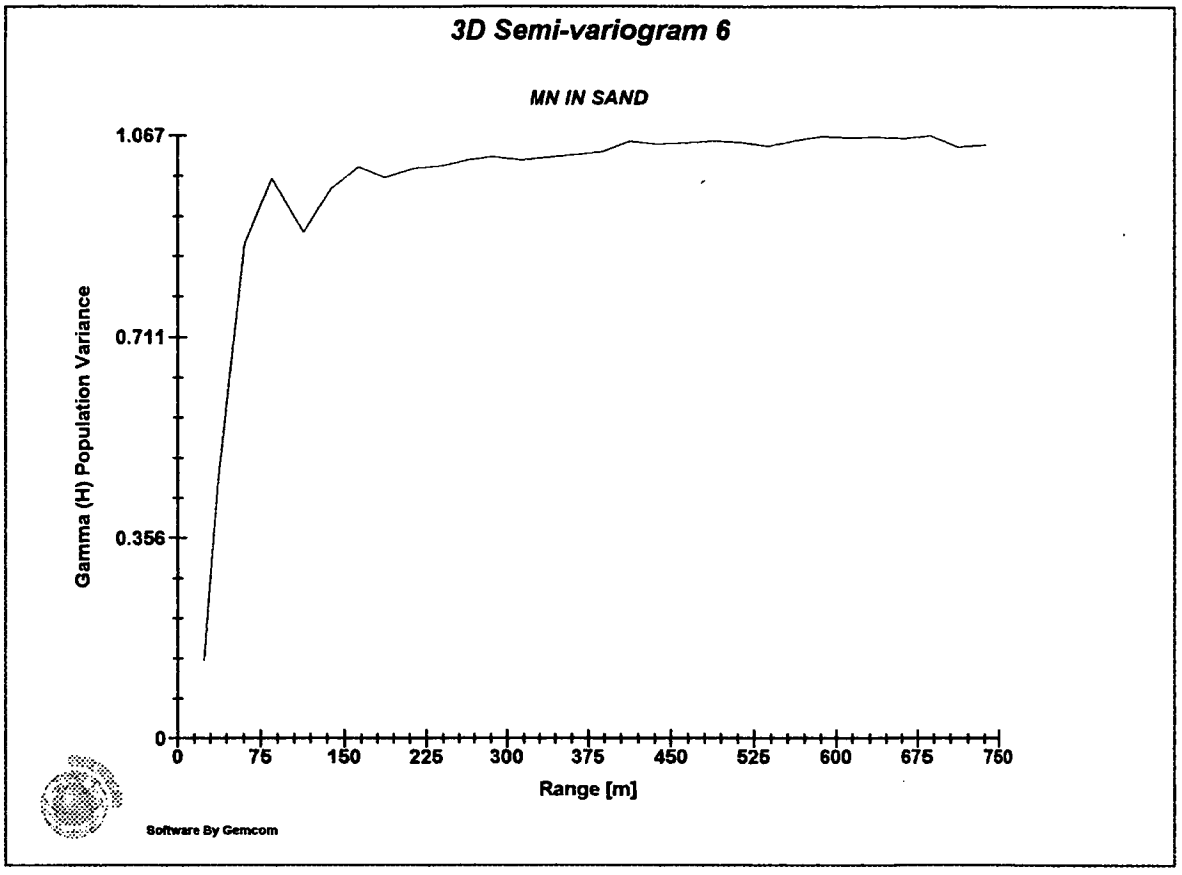
3D Semi-variogram 6
MN IN SAND
1.067
0.711
0.356
0
Gamma (H) Population Variance
0
75
150
225
300
375
450
525
600
675
750
Range [m]
Software By Gemcom

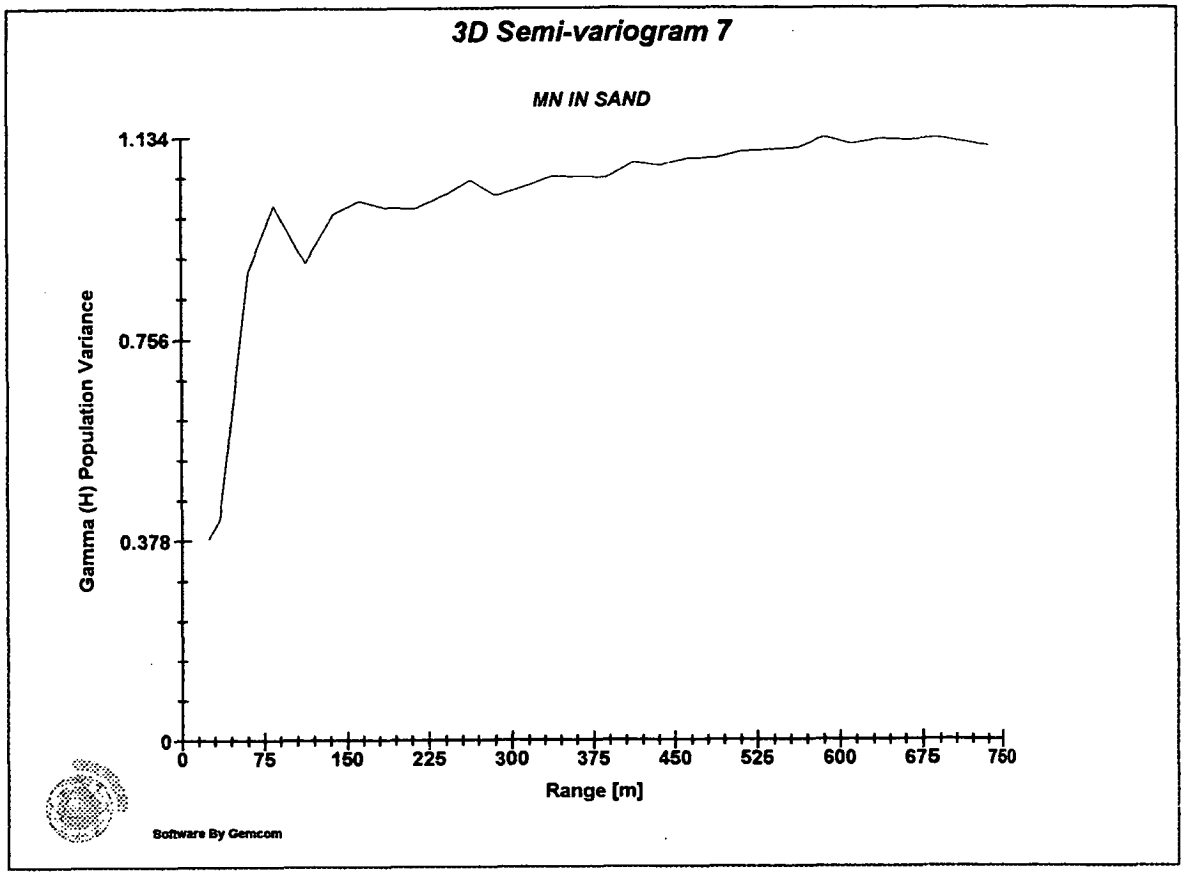
3D Semi-variogram 7
MN IN SAND
1.134
0.756
0.378
0
Gamma (H) Population Variance
0
75
150
225
300
375
450
525
600
675
750
Range [m]
Software By Gemcom

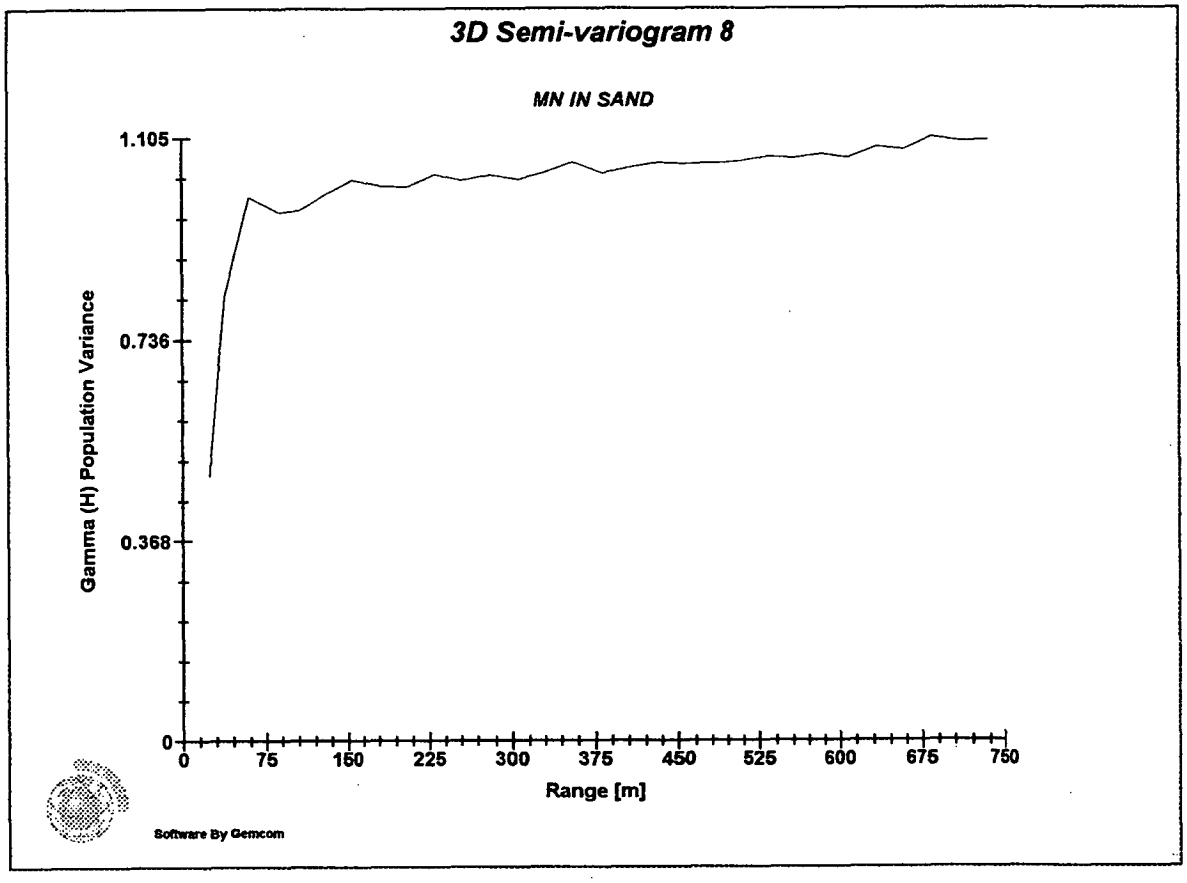
3D Semi-variogram 8
MN IN SAND
1.105
0.736
0.368
0
Gamma (H) Population Variance
0
75
150
225
300
375
450
525
600
675
750
Range [m]
Software By Gemcom

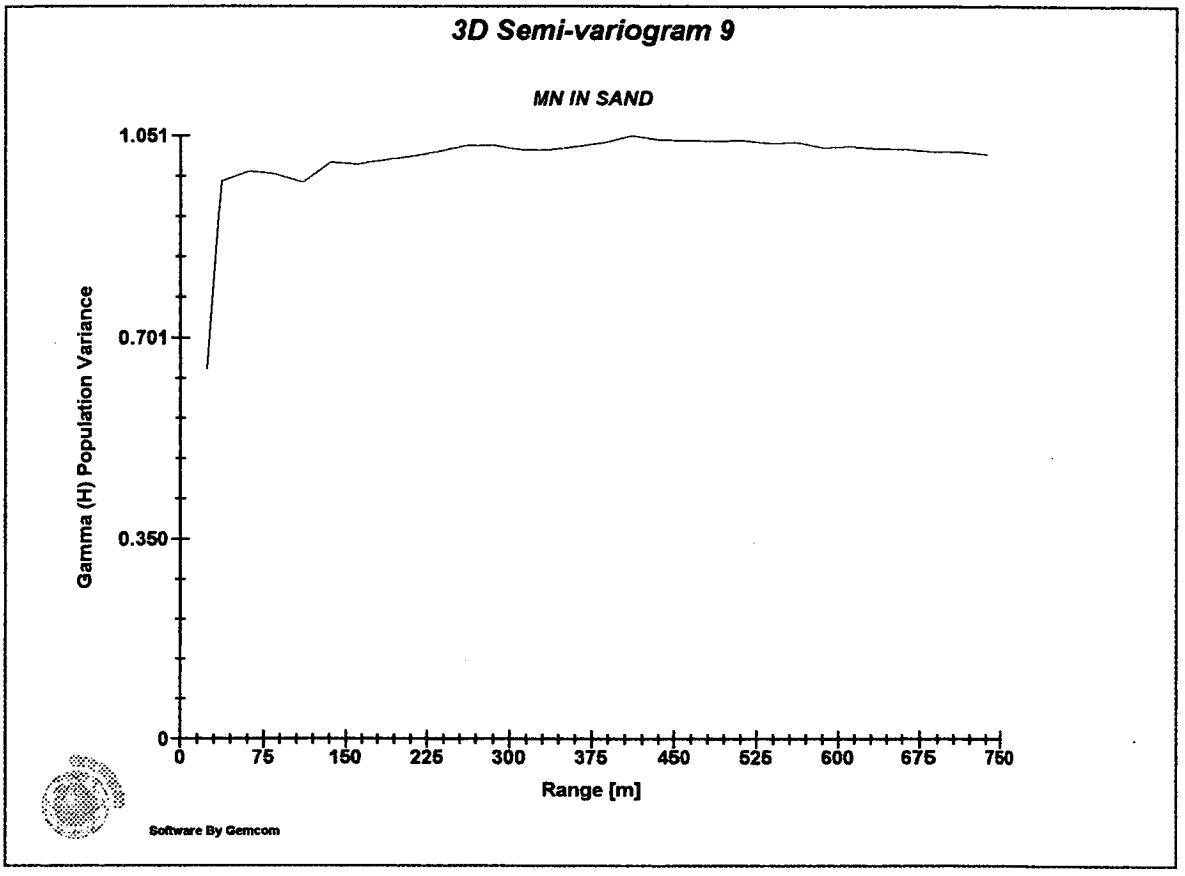
3D Semi-variogram 9
MN IN SAND
1.051
0.701
0.350
0
Gamma (H) Population Variance
0
75
150
225
300
375
450
525
600
675
750
Range [m]
Software By Gemcom

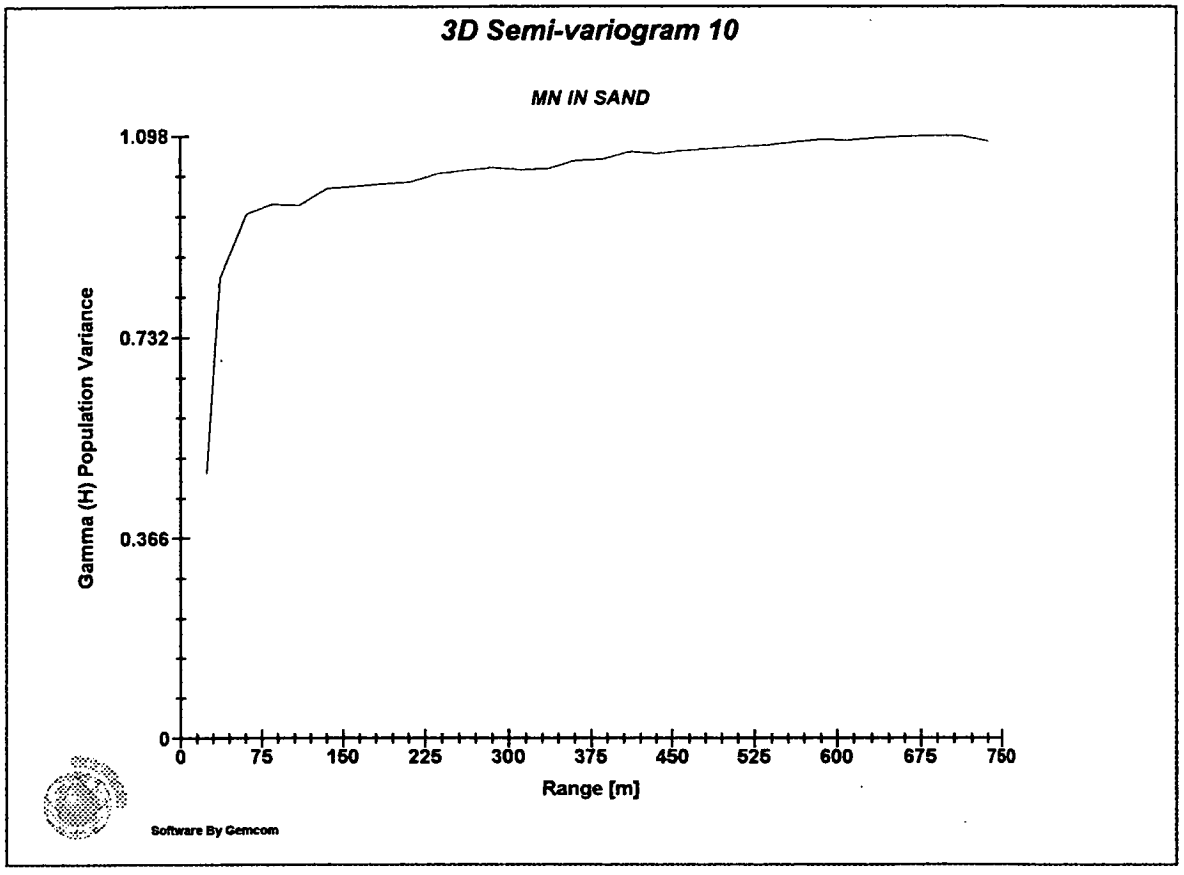
3D Semi-variogram 10
MN IN SAND
1.098
0.732
0.366
0
Gamma (H) Population Variance
0
75
150
225
300
375
450
525
600
675
750
Range [m]
Software By Gemcom

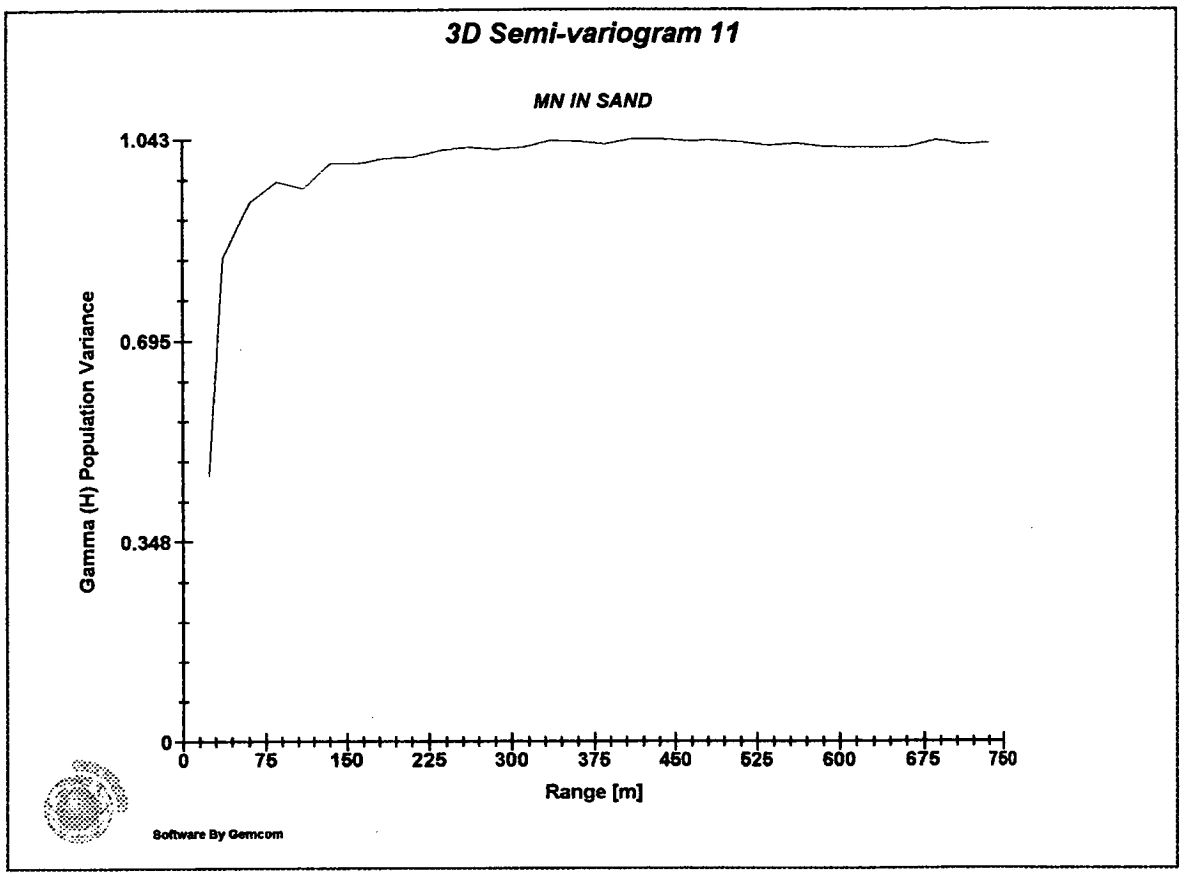
3D Semi-variogram 11
MN IN SAND
1.043
0.695
0.348
0
Gamma (H) Population Variance
0
75
150
225
300
375
450
525
600
675
750
Range [m]
Software By Gemcom

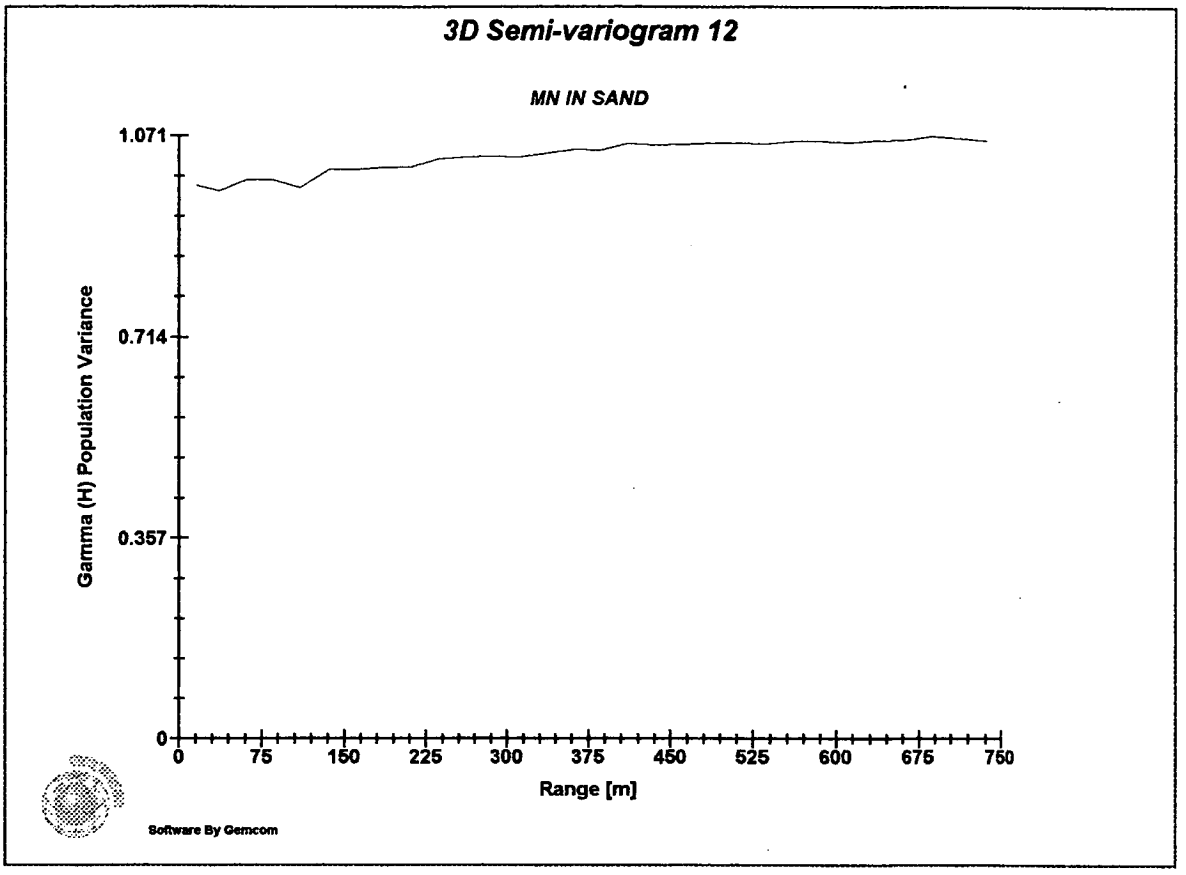
3D Semi-variogram 12
MN IN SAND
1.071
0.714
0.357
0
Gamma (H) Population Variance
0
75
150
225
300
375
450
525
600
675
750
Range [m]
Software By Gemcom

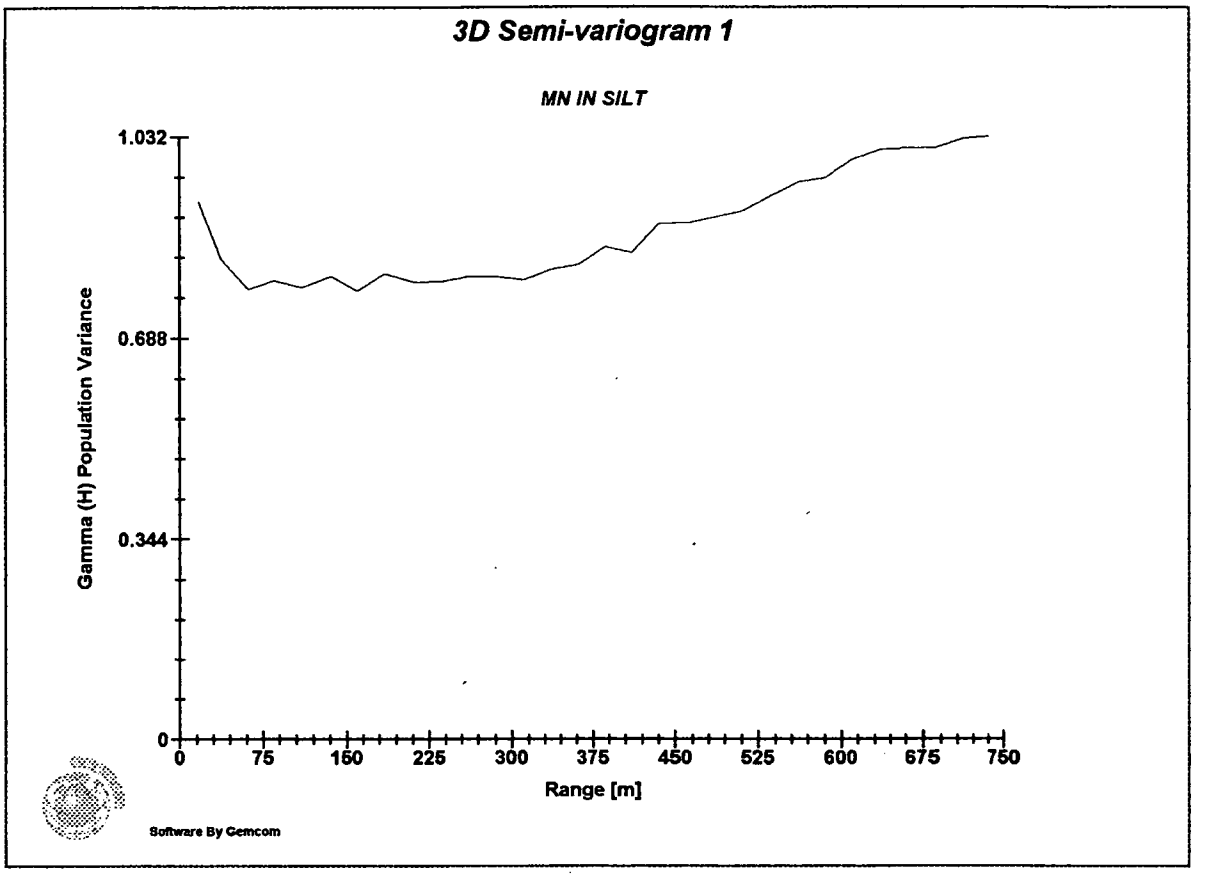
3D Semi-variogram 1
MN IN SILT
1.032
0.688
0.344
0
Gamma (H) Population Variance
0
75
150
225
300
375
450
525
600
675
750
Range [m]
Software By Gemcom

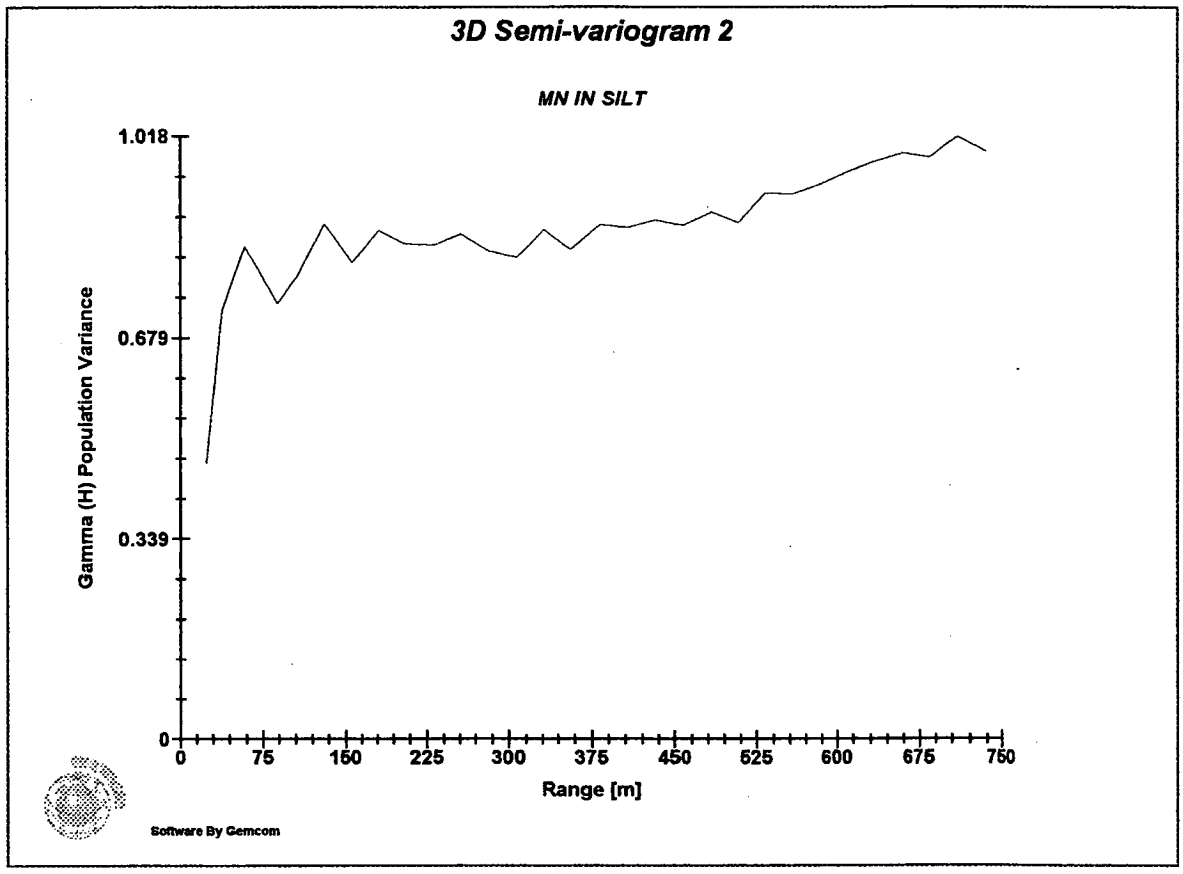
3D Semi-variogram 2
MN IN SILT
1.018
0.679
0.339
0
Gamma (H) Population Variance
0
75
150
225
300
375
450
525
600
675
750
Range [m]
Software By Gemcom

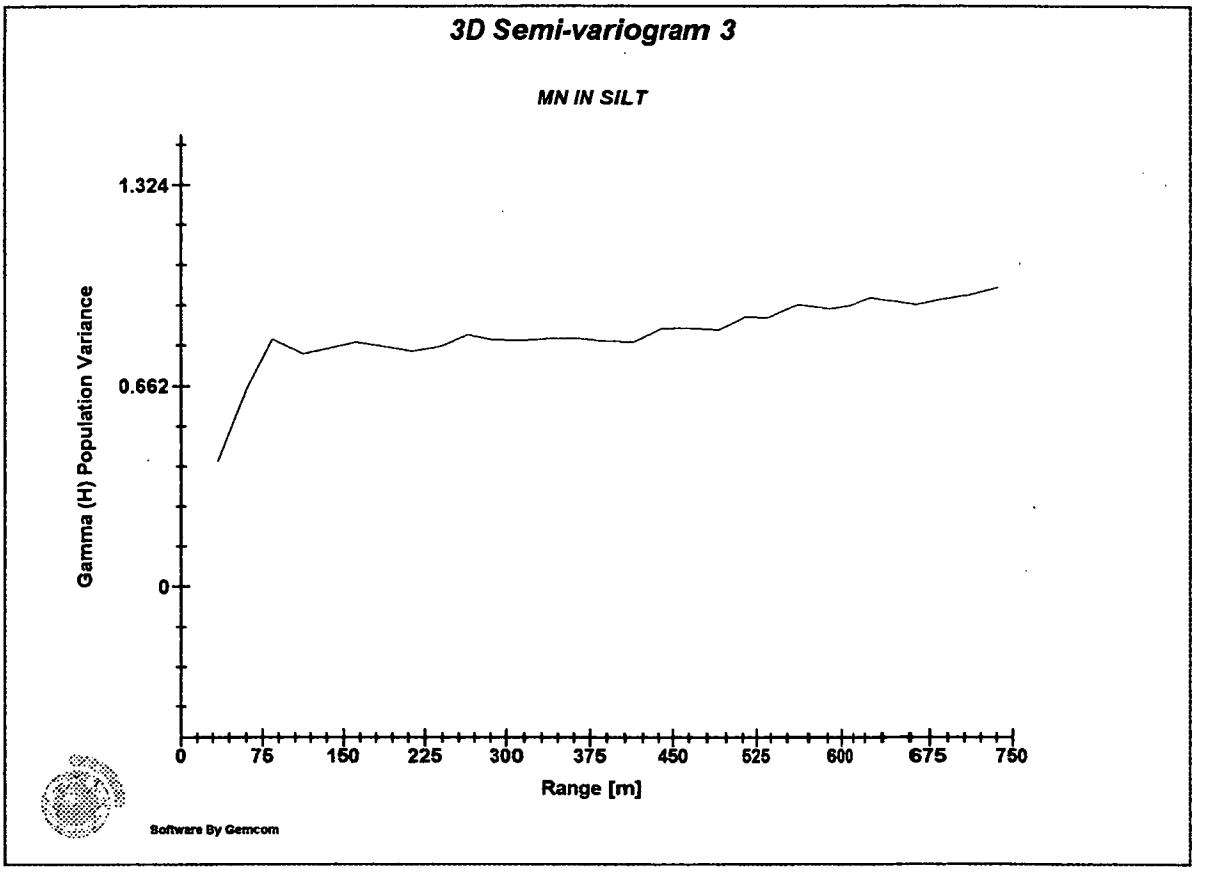
3D Semi-variogram 3
MN IN SILT
Gamma (H) Population Variance
1.324
0.662
0
0
75
150
225
300
375
450
525
600
675
750
Range [m]
Software By Gemcom

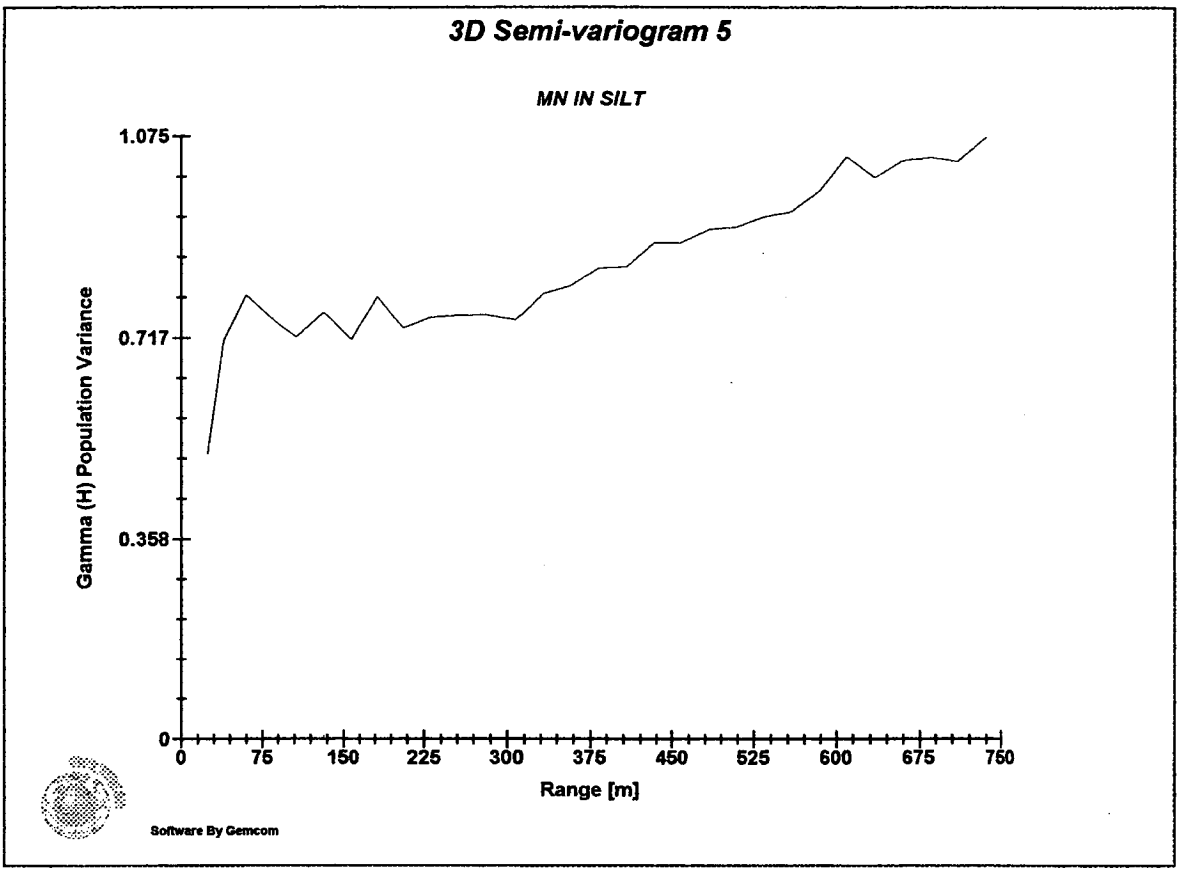
3D Semi-variogram 5
MN IN SILT
1.075
0.717
0.358
0
Gamma (H) Population Variance
0
75
150
225
300
375
450
525
600
675
750
Range [m]
Software By Gemcom

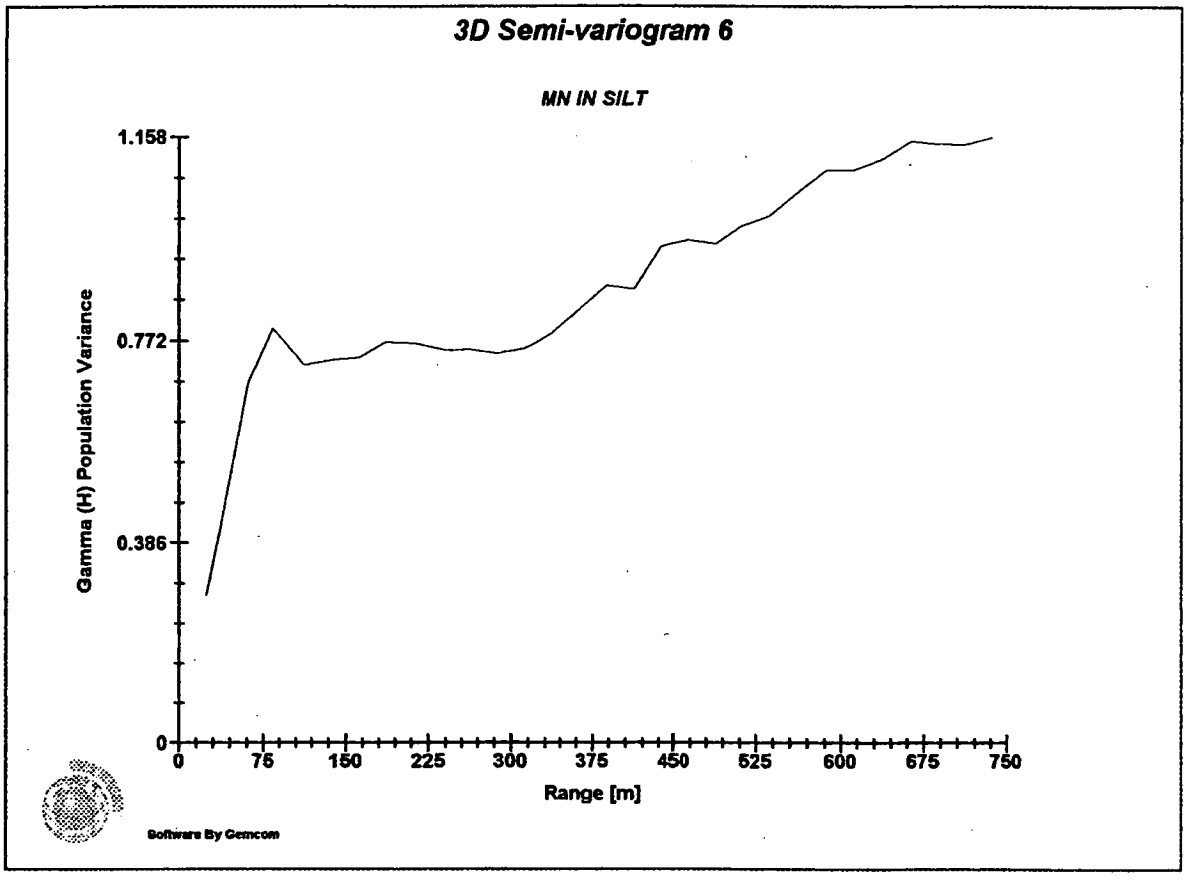
3D Semi-variogram 6
MN IN SILT
Gamma (H) Population Variance
1.158
0.772
0.386
0
0
75
150
225
300
375
450
525
600
675
750
Range [m]
Software By Gemcom

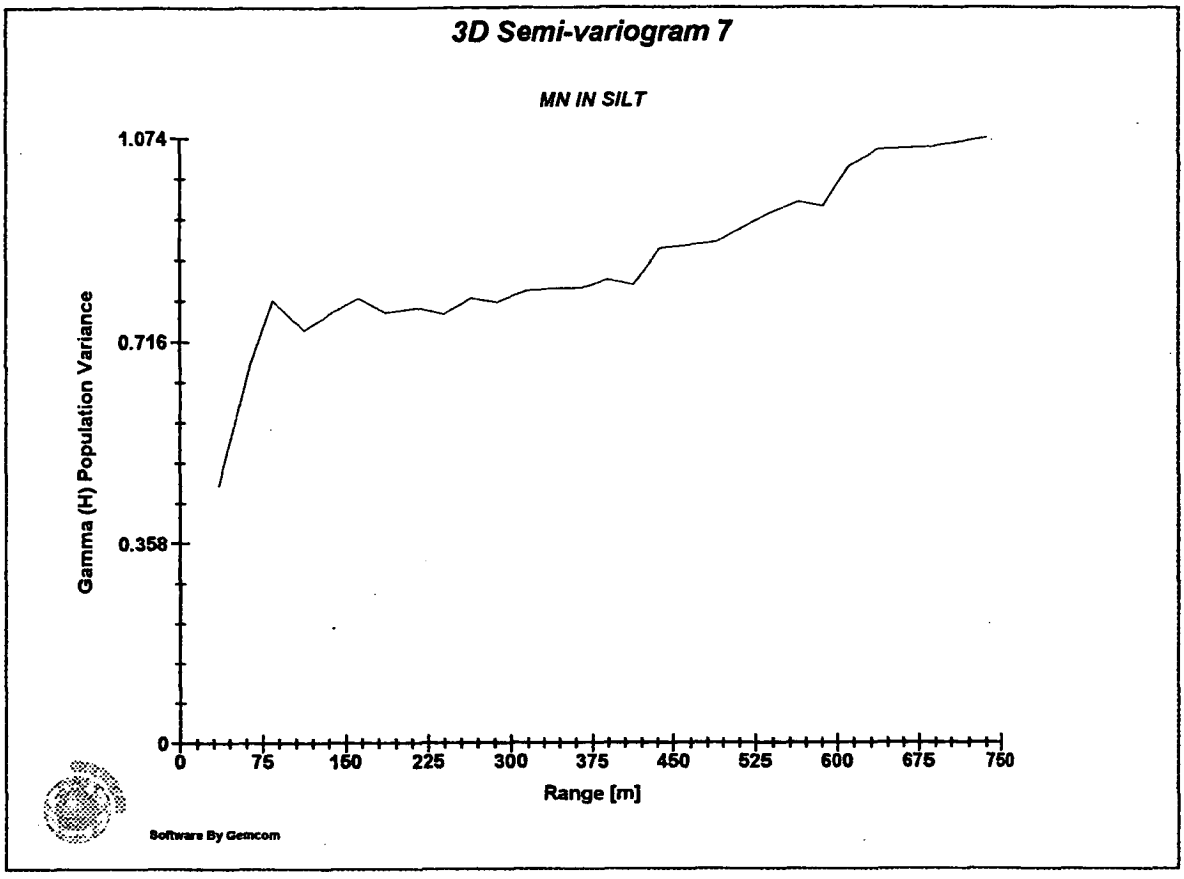
3D Semi-variogram 7
MN IN SILT
1.074
0.716
0.358
0
Gamma (H) Population Variance
0
75
150
225
300
375
450
525
600
675
750
Range [m]
Software By Gemcom

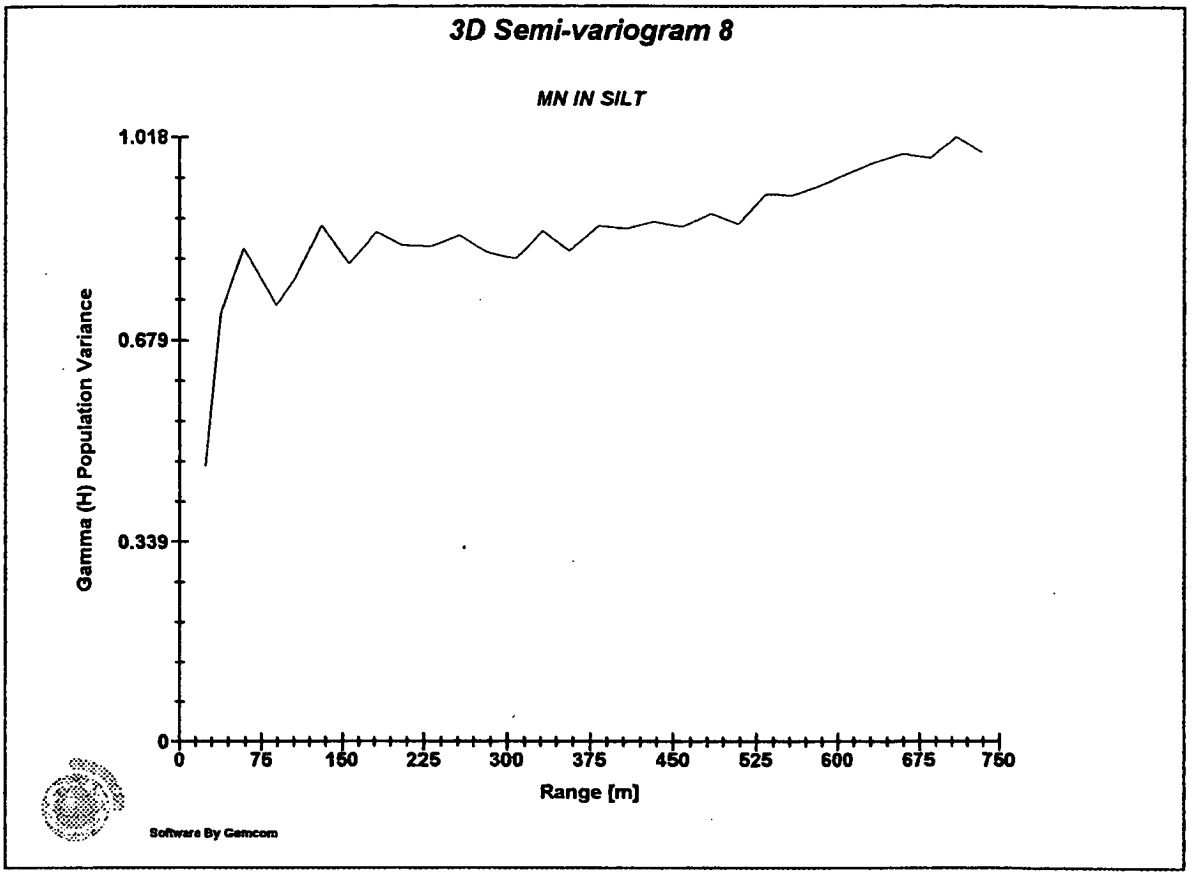
3D Semi-variogram 8
MN IN SILT
1.018
0.679
0.339
0
Gamma (H) Population Variance
0
75
150
225
300
375
450
525
600
675
750
Range [m]
Software By Gemcom

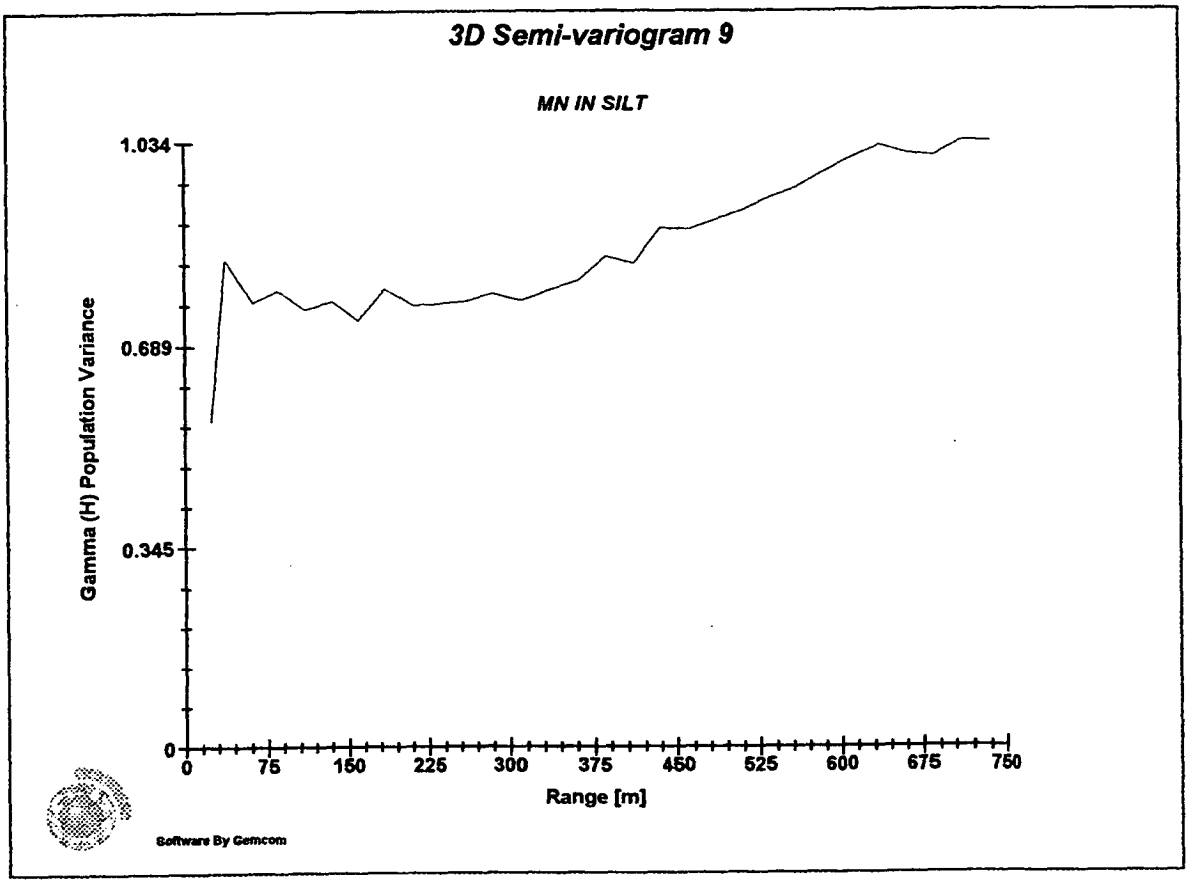
3D Semi-variogram 9
MN IN SILT
1.034
0.689
0.345
0
Gamma (H) Population Variance
0
75
150
225
300
375
450
525
600
675
750
Range [m]
Software By Gemcom

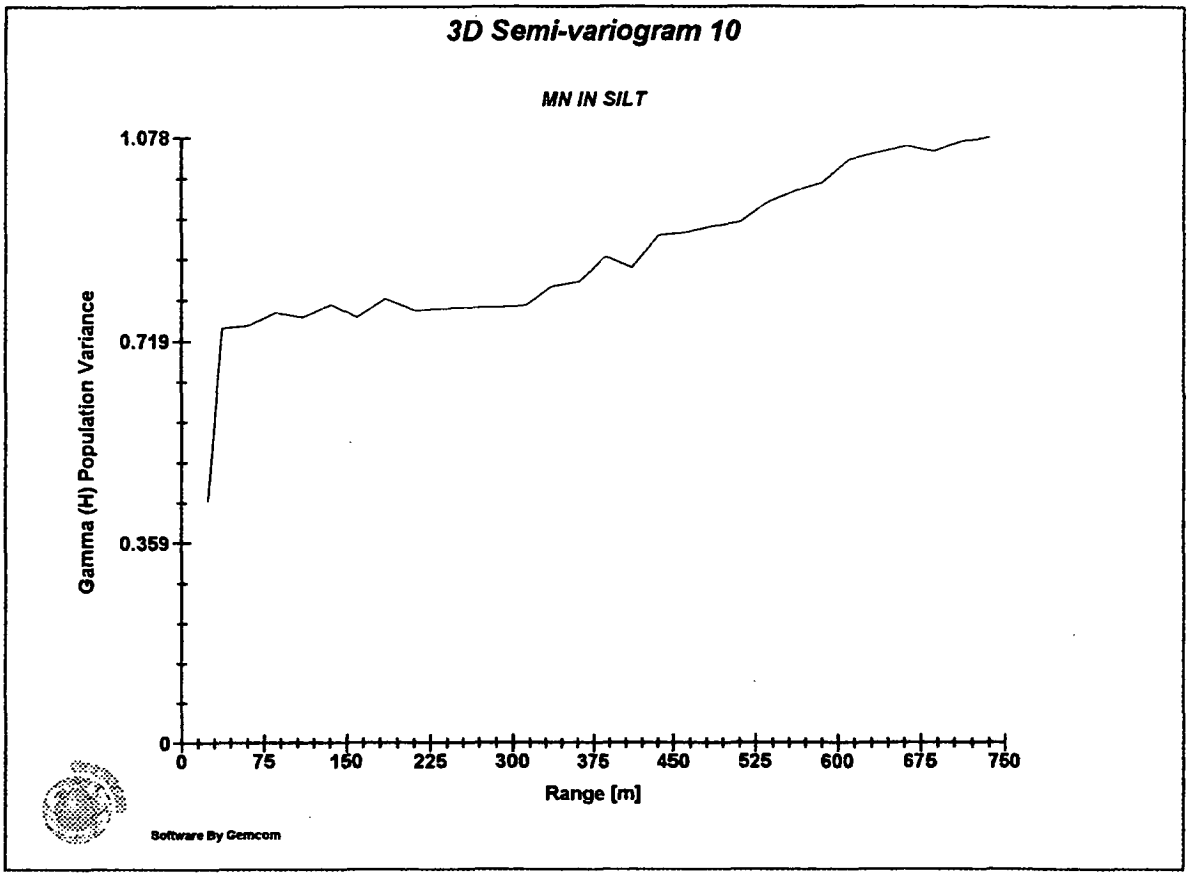
3D Semi-variogram 10
MN IN SILT
Gamma (H) Population Variance
1.078
0.719
0.359
0
0
75
150
225
300
375
450
525
600
675
750
Range [m]
Software By Gemcom

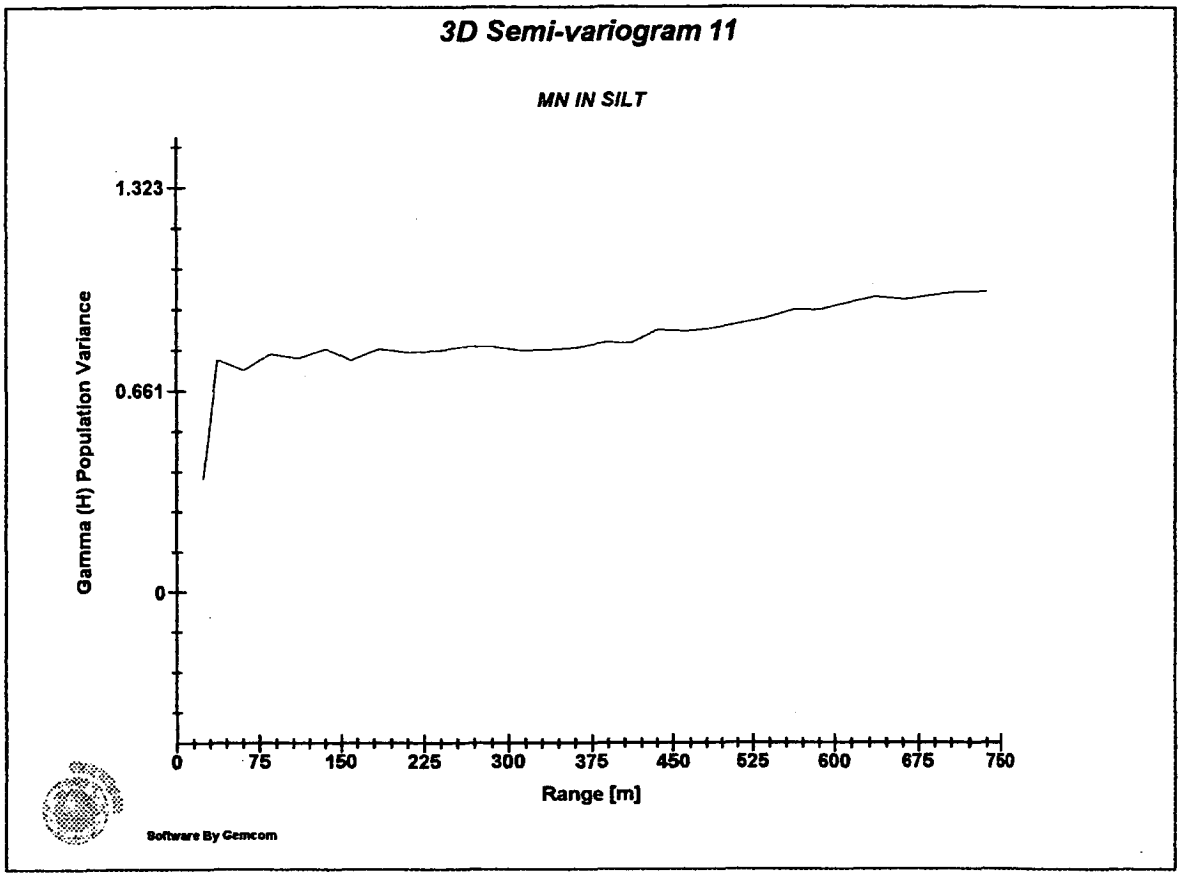
3D Semi-variogram 11
MN IN SILT
1.323
0.661
0
Gamma (H) Population Variance
0
75
150
225
300
375
450
525
600
675
750
Range [m]
Software By Gemcom

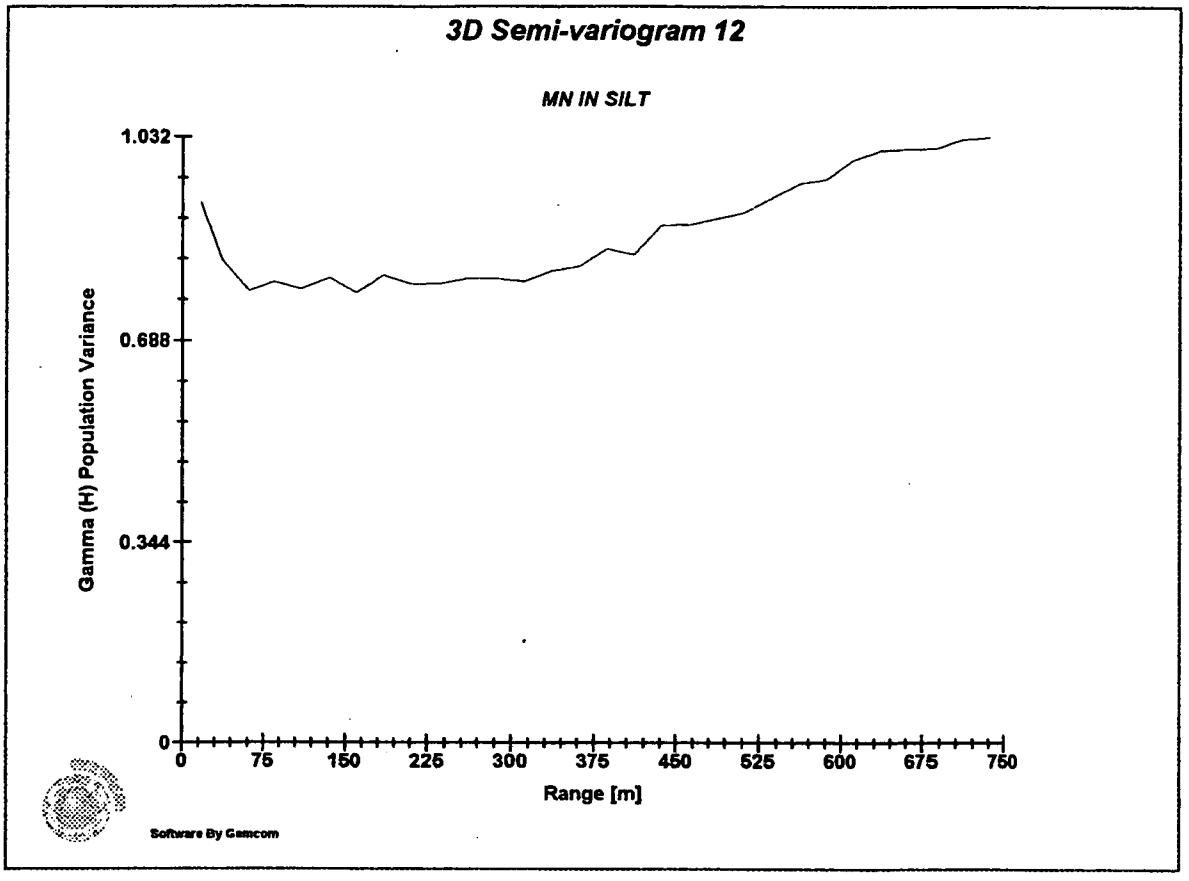
3D Semi-variogram 12
MN IN SILT
1.032
0.688
0.344
0
Gamma (H) Population Variance
0
75
150
225
300
375
450
525
600
675
750
Range [m]
Software By Gamcom

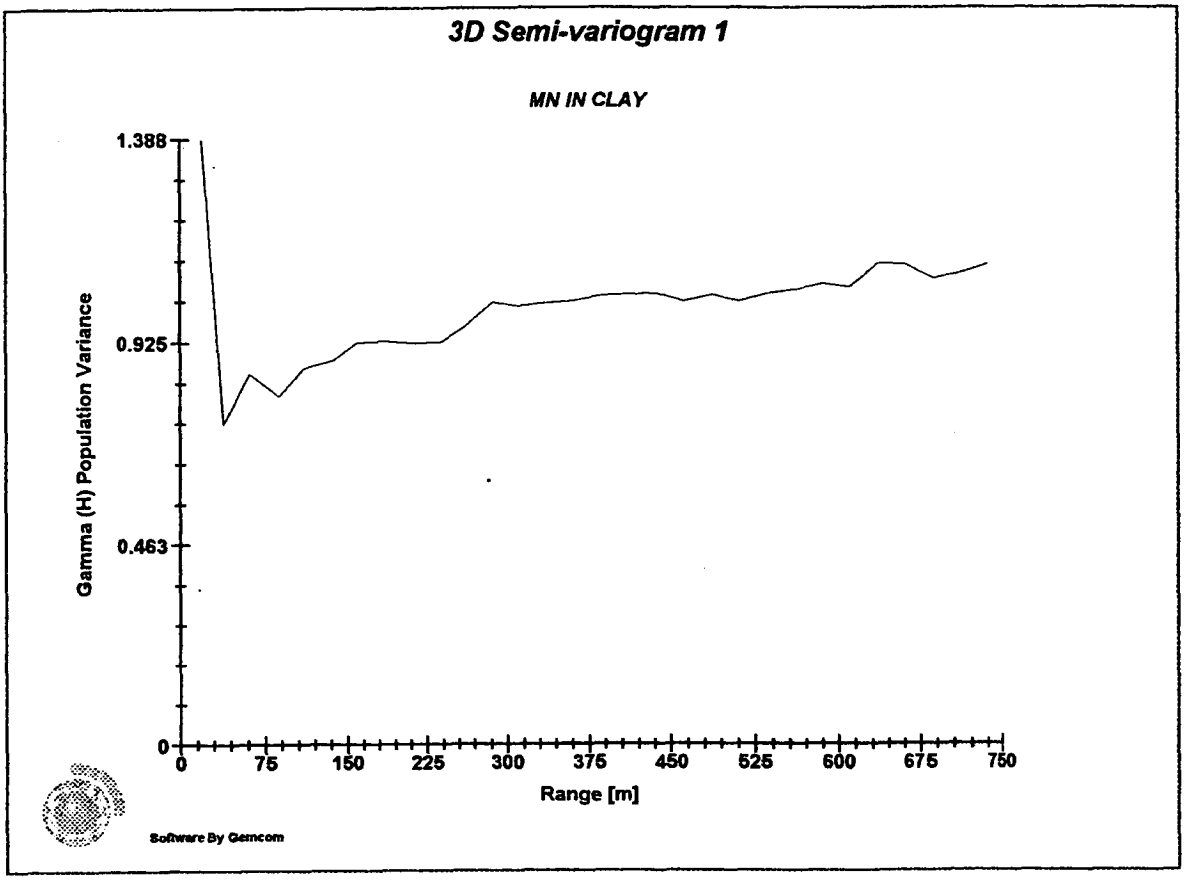
3D Semi-variogram 1
MN IN CLAY
1.388
0.925
0.463
0
Gamma (H) Population Variance
0
75
150
225
300
375
450
525
600
675
750
Range [m]
Software By Gemcom

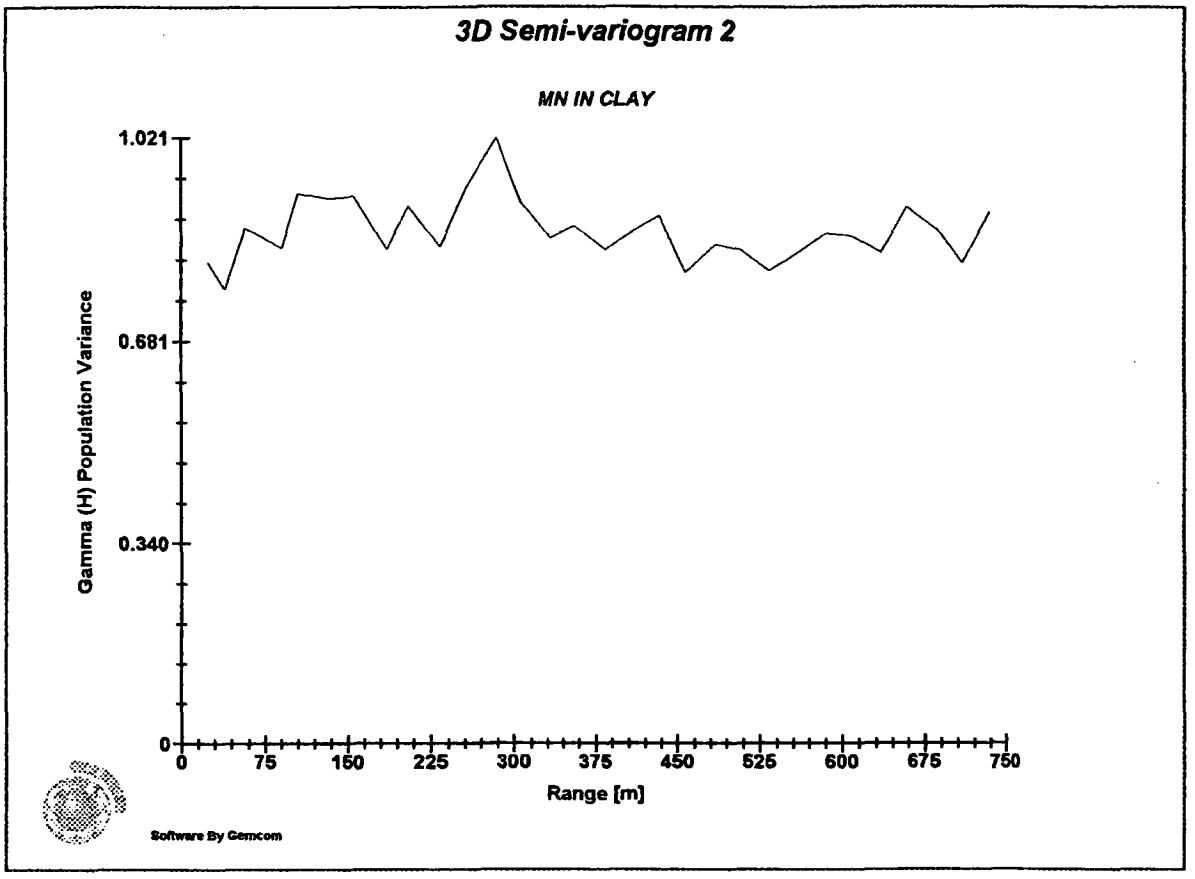
3D Semi-variogram 2
MN IN CLAY
1.021
0.681
0.340
0
Gamma (H) Population Variance
0
75
150
225
300
375
450
525
600
675
750
Range [m]
Software By Gemcom

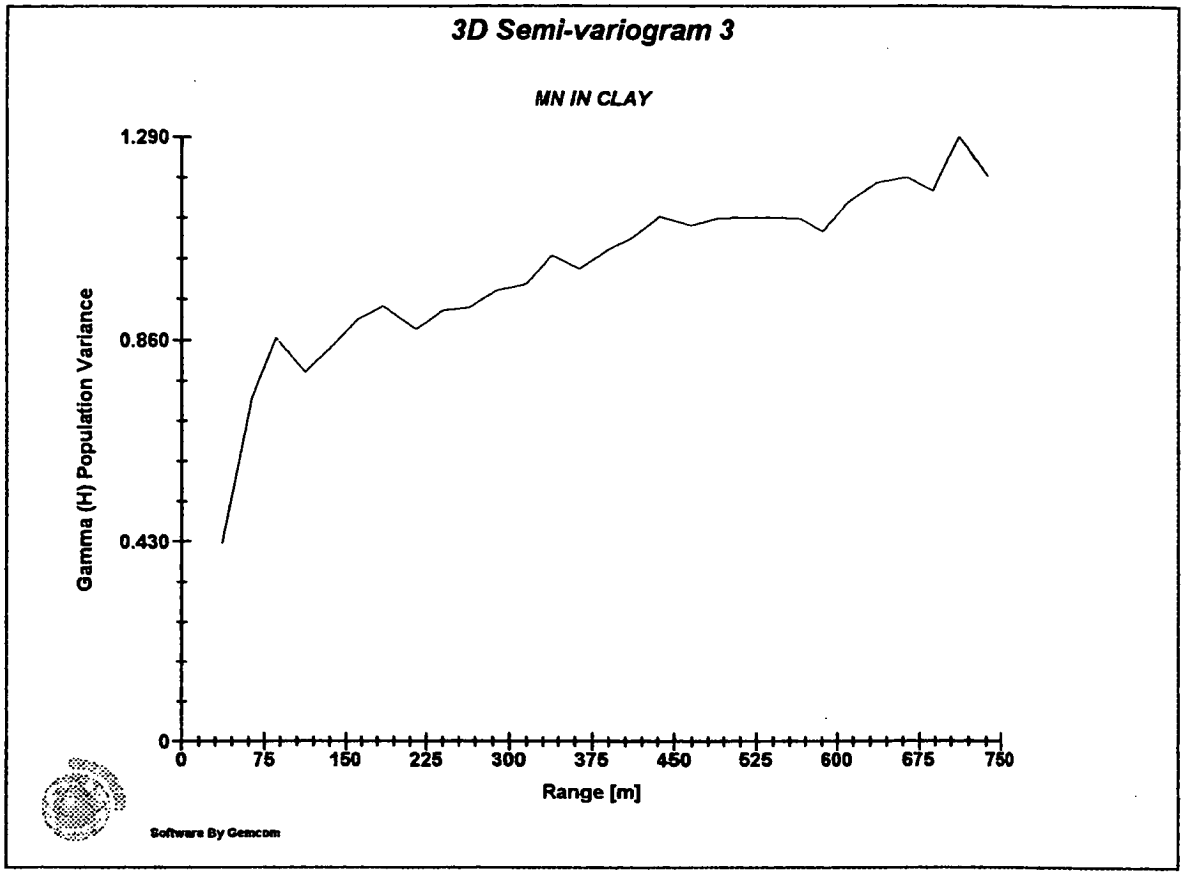
3D Semi-variogram 3
MN IN CLAY
Gamma (H) Population Variance
1.290
0.860
0.430
0
0
75
150
225
300
375
450
525
600
675
750
Range [m]
Software By Gemcom

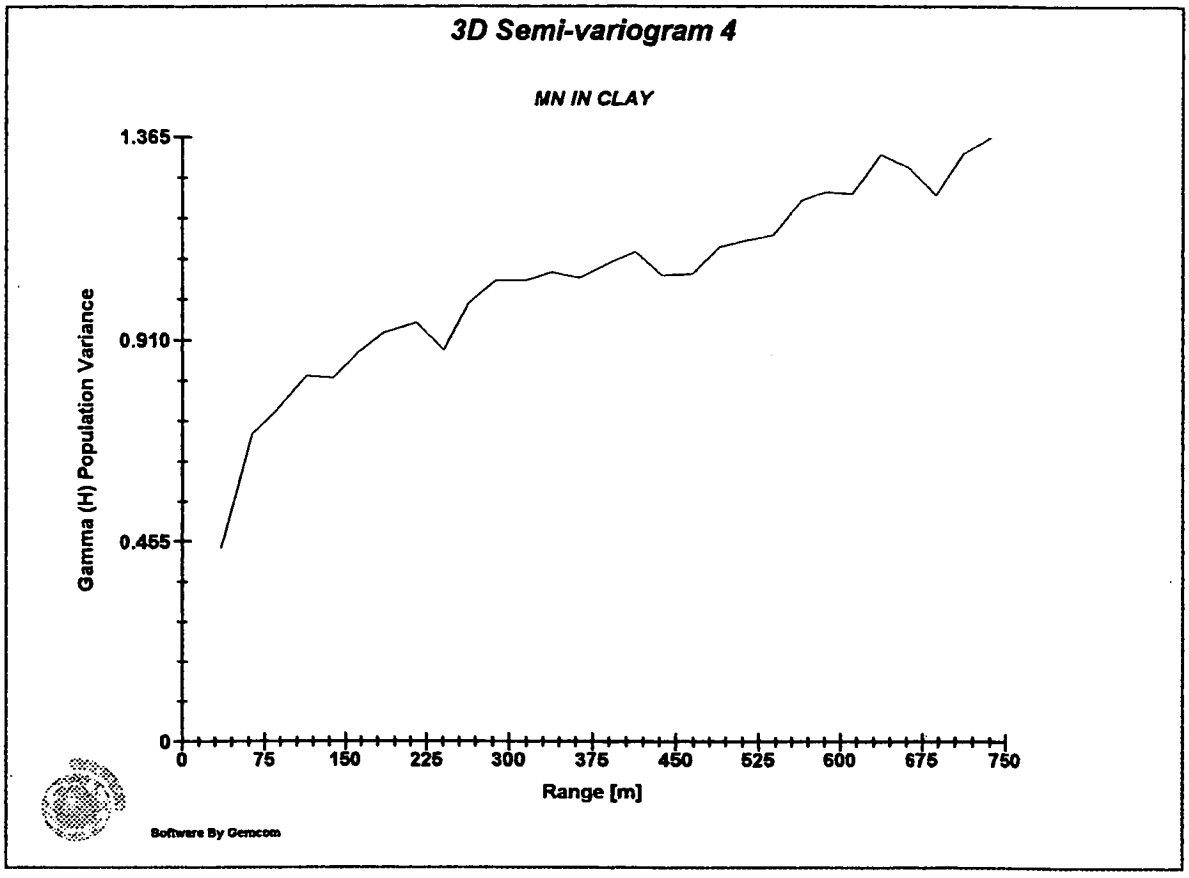
3D Semi-variogram 4
MN IN CLAY
1.365
0.910
0.455
0
Gamma (H) Population Variance
0
75
150
225
300
375
450
525
600
675
750
Range [m]
Software By Gemcom

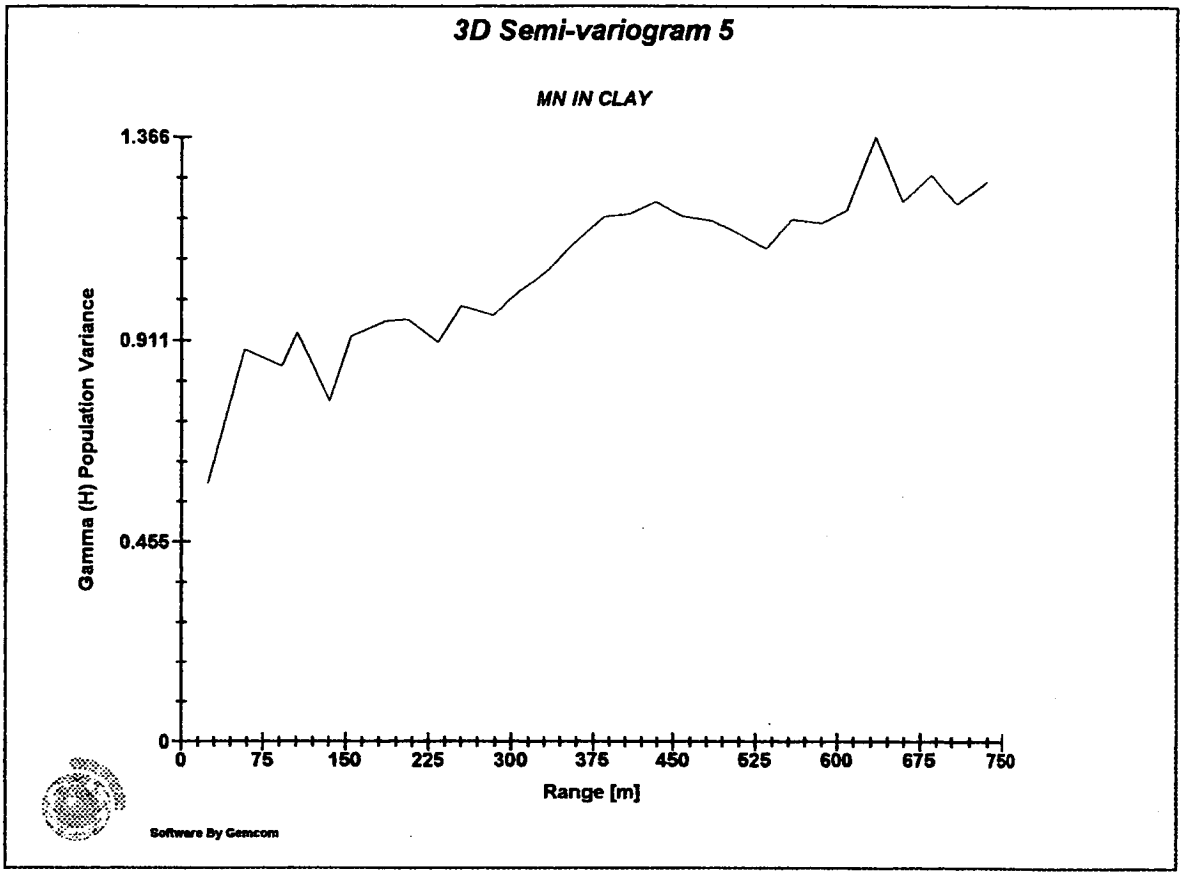
3D Semi-variogram 5
MN IN CLAY
Gamma (H) Population Variance
1.366
0.911
0.455
0
0
75
150
225
300
375
450
525
600
675
750
Range [m]
Software By Gemcom

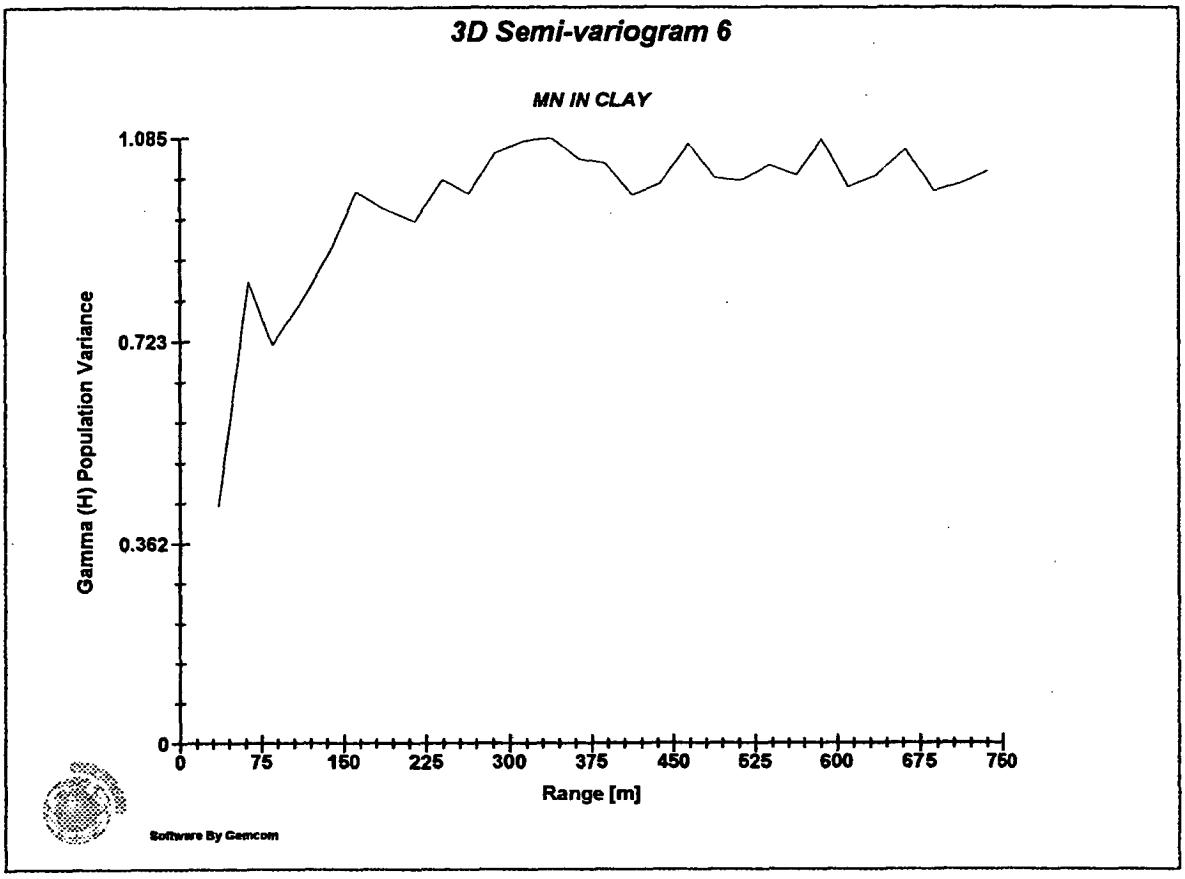
3D Semi-variogram 6
MN IN CLAY
1.085
0.723
0.362
0
Gamma (H) Population Variance
0
75
150
225
300
375
450
525
600
675
750
Range [m]
Software By Gemcom

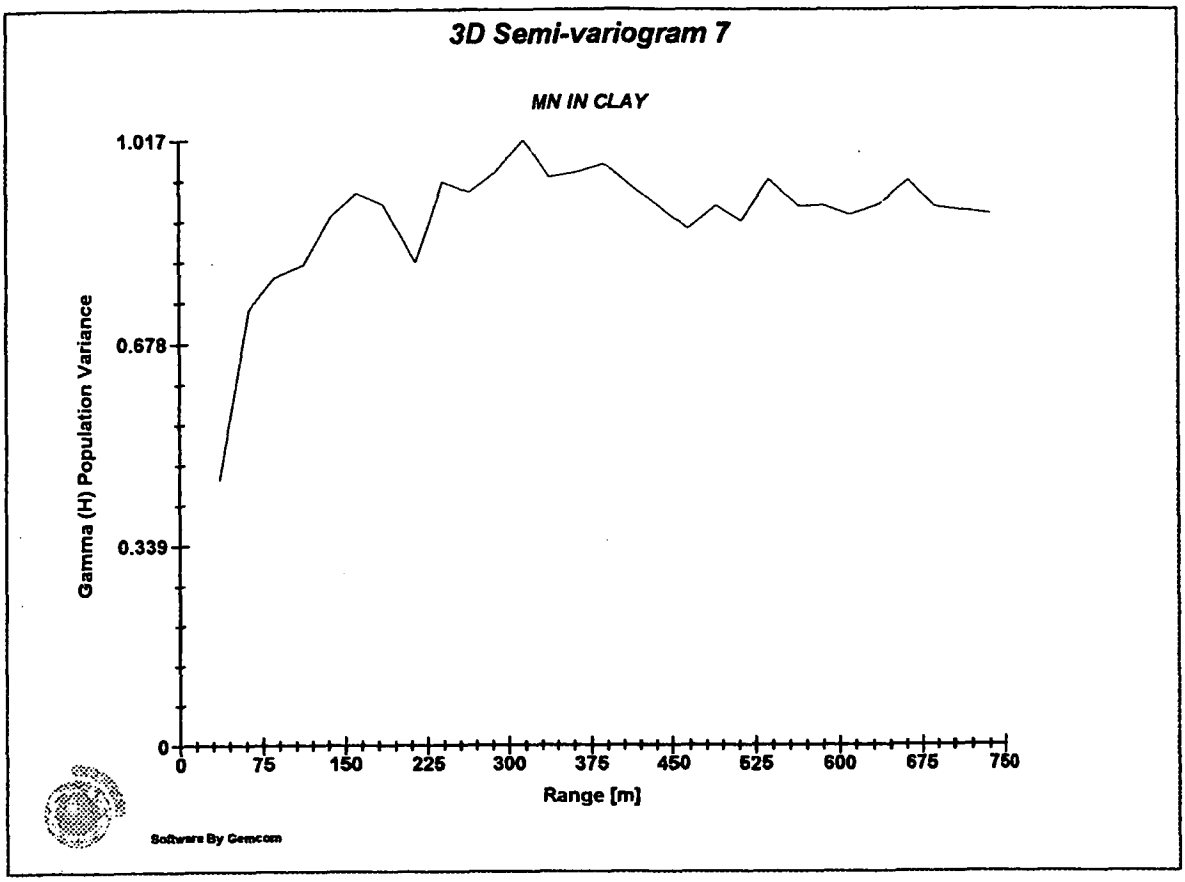
3D Semi-variogram 7
MN IN CLAY
1.017
0.678
0.339
0
Gamma (H) Population Variance
0
75
150
225
300
375
450
525
600
675
750
Range [m]
Software By Gemcom

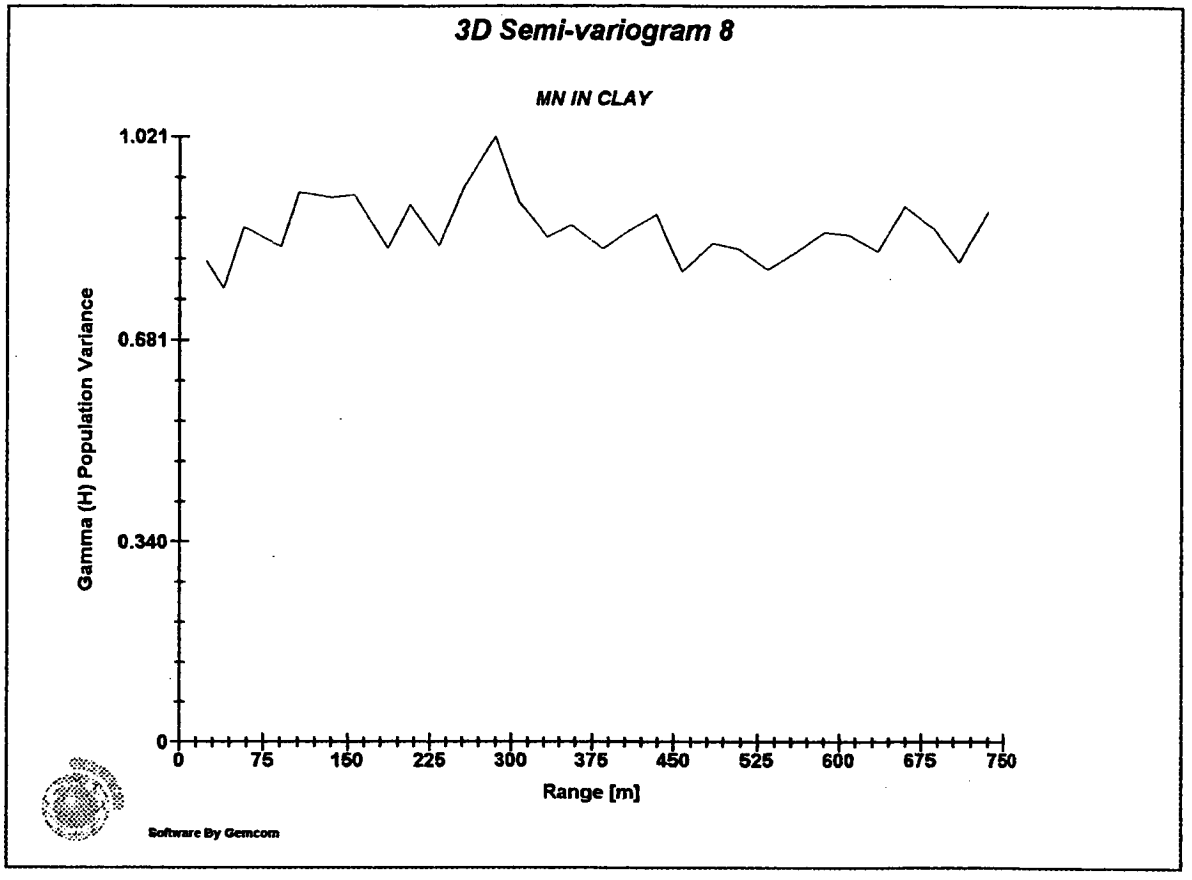
3D Semi-variogram 8
MN IN CLAY
1.021
0.681
0.340
0
Gamma (H) Population Variance
0
75
150
225
300
375
450
525
600
675
750
Range [m]
Software By Gemcom

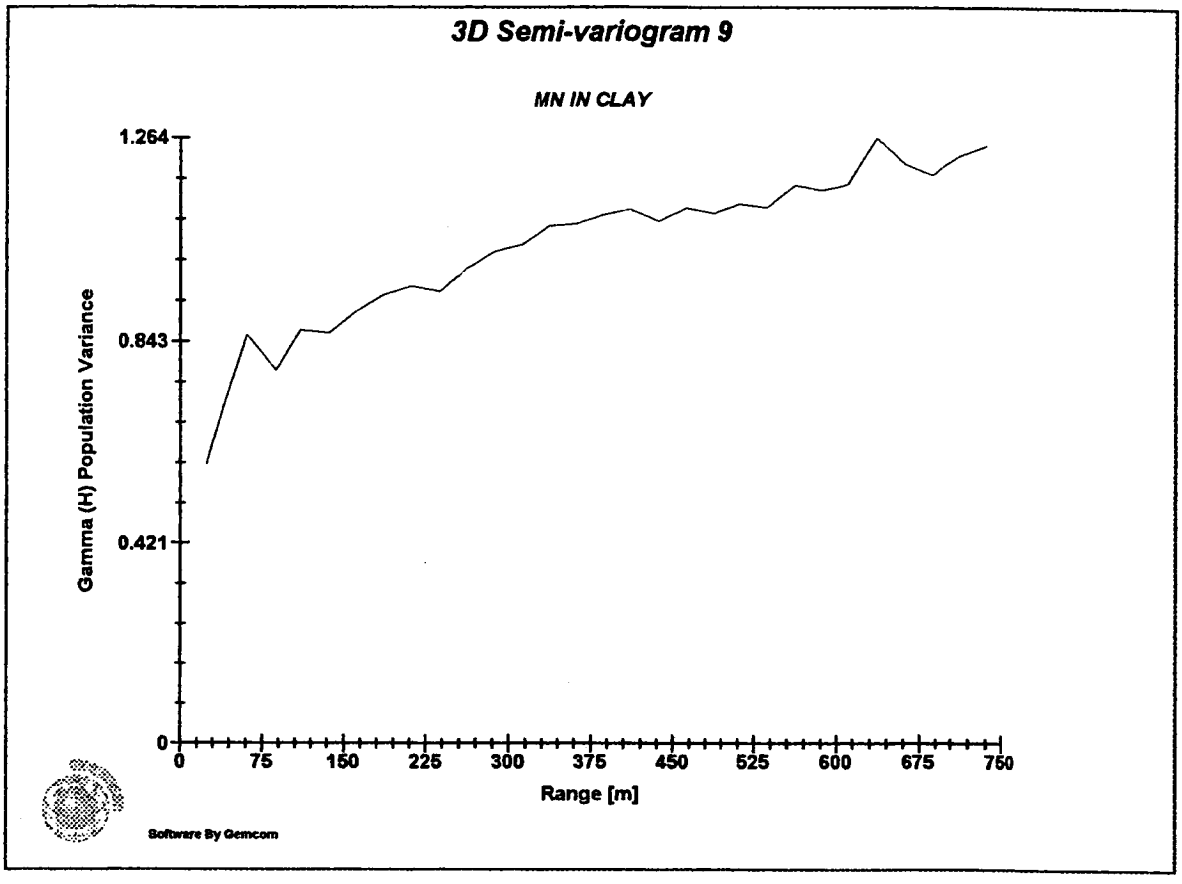
3D Semi-variogram 9
MN IN CLAY
Gamma (H) Population Variance
1.264
0.843
0.421
0
0
75
150
225
300
375
450
525
600
675
750
Range [m]
Software By Gemcom

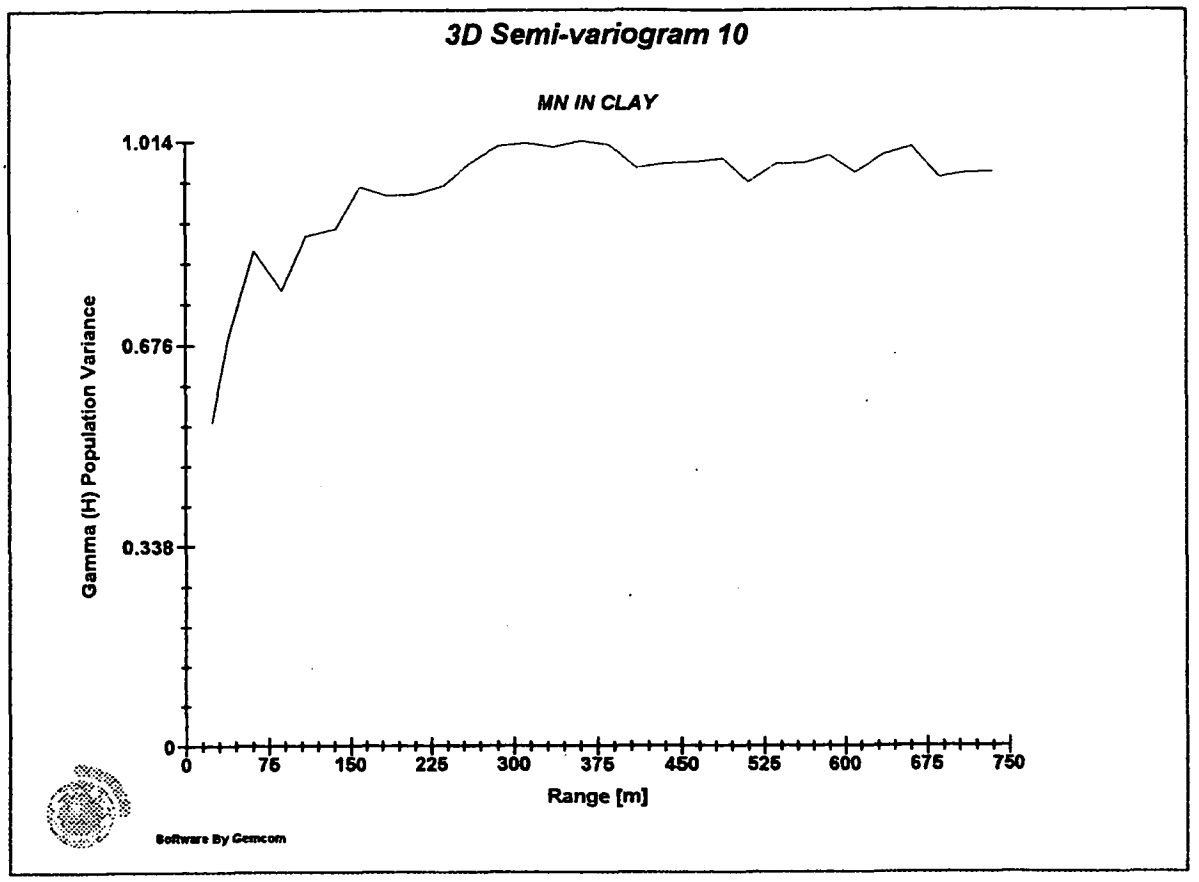
3D Semi-variogram 10
MN IN CLAY
1.014
0.676
0.338
0
Gamma (H) Population Variance
0
75
150
225
300
375
450
525
600
675
750
Range [m]
Software By Gemcom

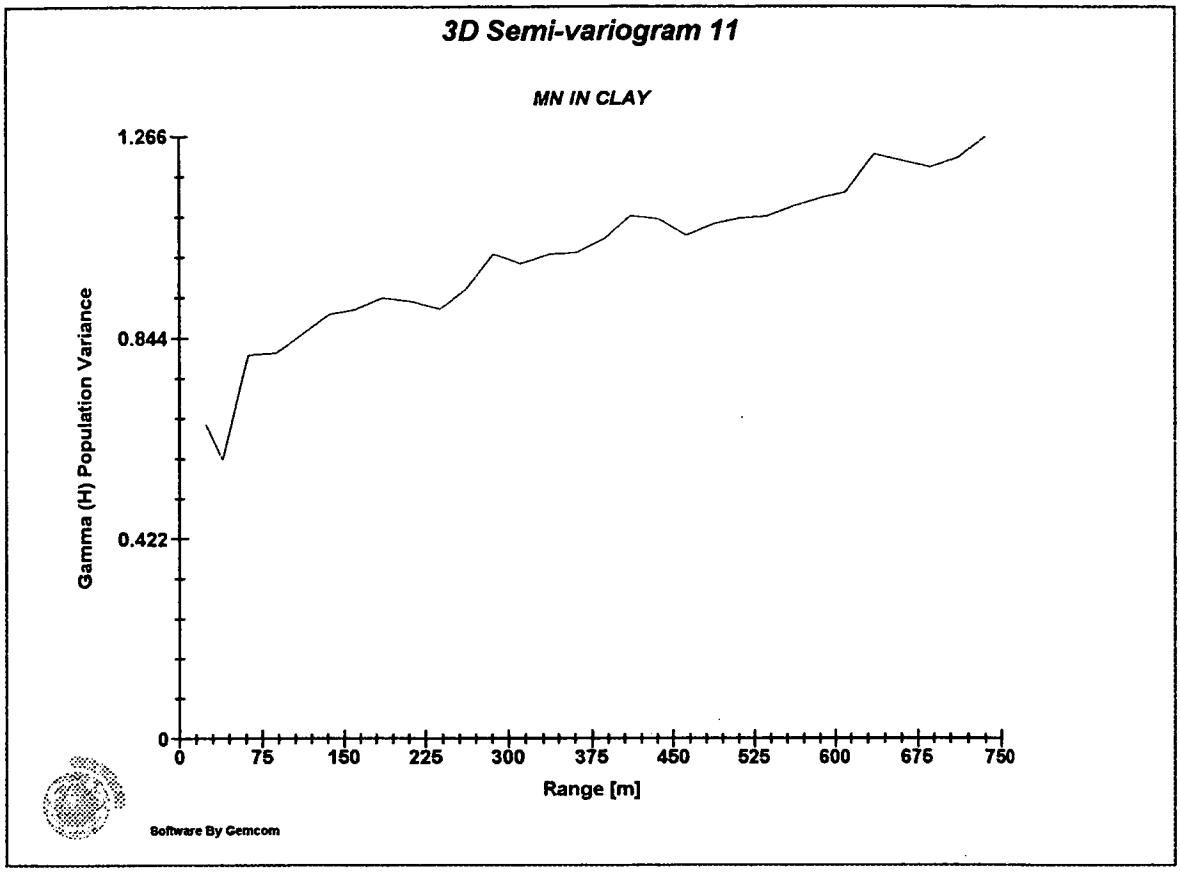
3D Semi-variogram 11
MN IN CLAY
1.266
0.844
0.422
0
Gamma (H) Population Variance
0
75
150
225
300
375
450
525
600
675
750
Range [m]
Software By Gemcom

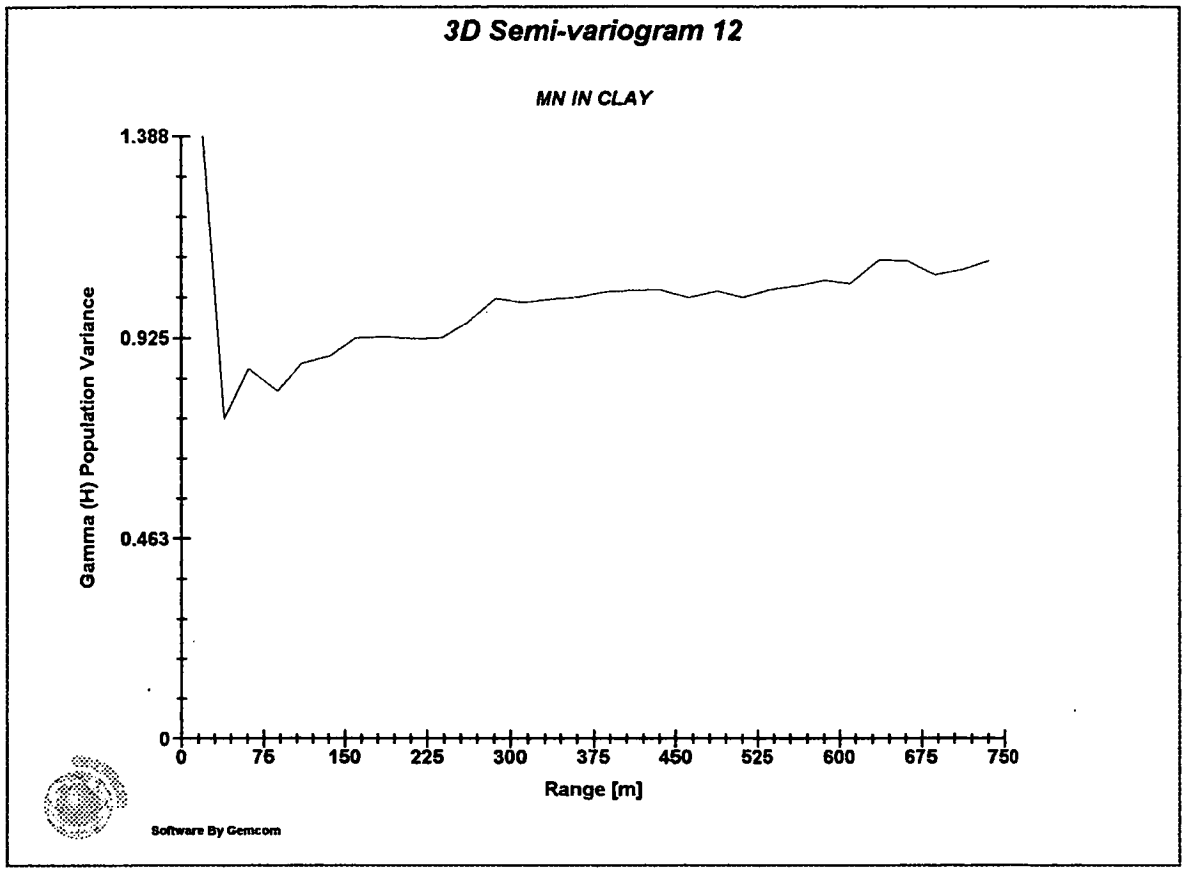
3D Semi-variogram 12
MN IN CLAY
1.388
0.925
0.463
0
Gamma (H) Population Variance
0
75
150
225
300
375
450
525
600
675
750
Range [m]
Software By Gemcom

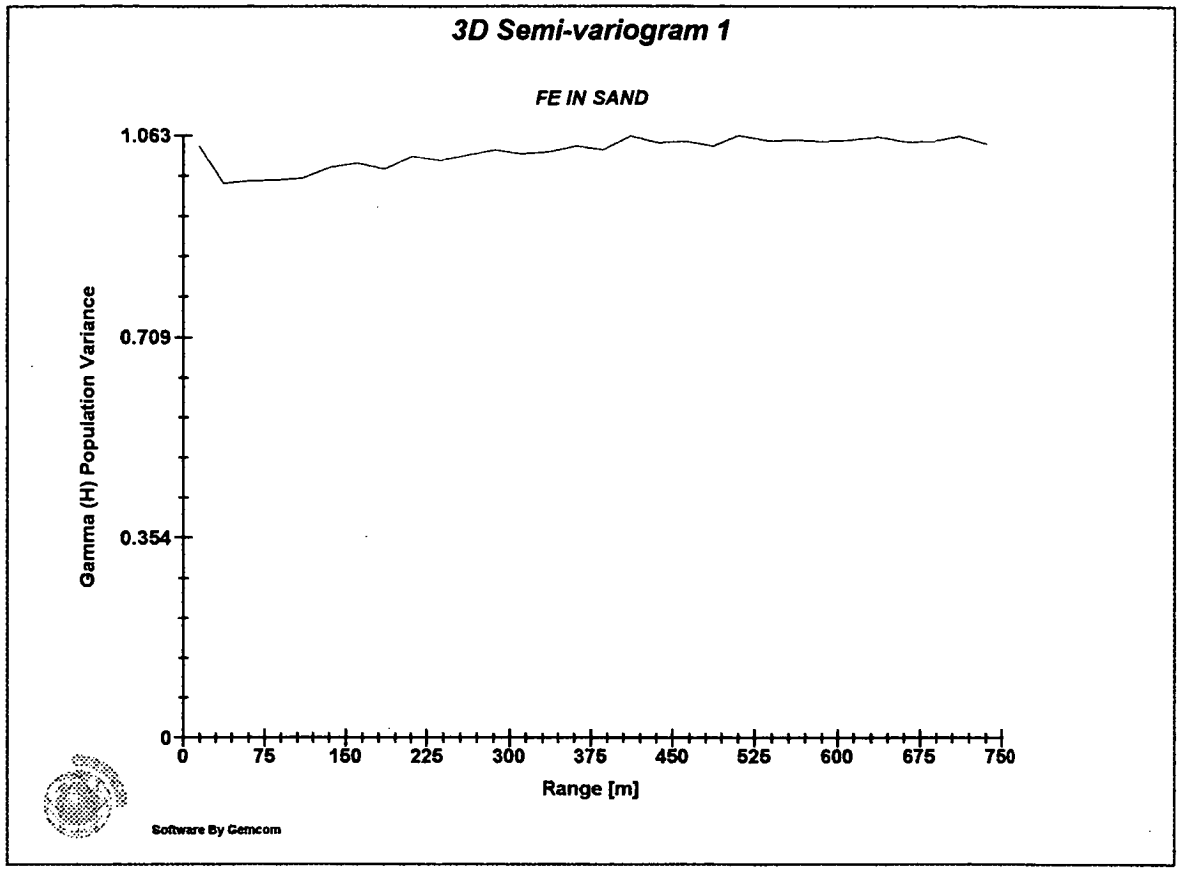
3D Semi-variogram 1
FE IN SAND
1.063
0.709
0.354
0
Gamma (H) Population Variance
0
75
150
225
300
375
450
525
600
675
750
Range [m]
Software By Gemcom

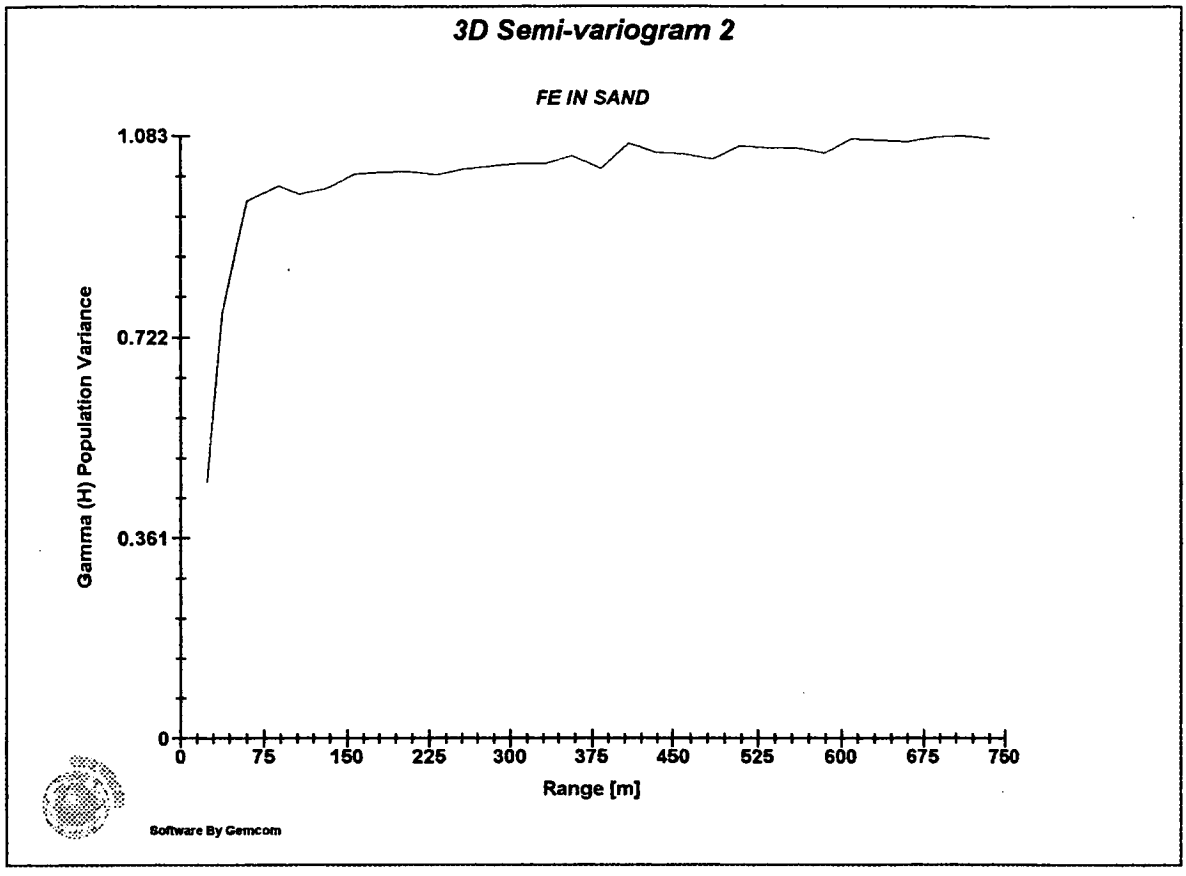
3D Semi-variogram 2
FE IN SAND
1.083
0.722
0.361
0
Gamma (H) Population Variance
0
75
150
225
300
375
450
525
600
675
750
Range [m]
Software By Gemcom

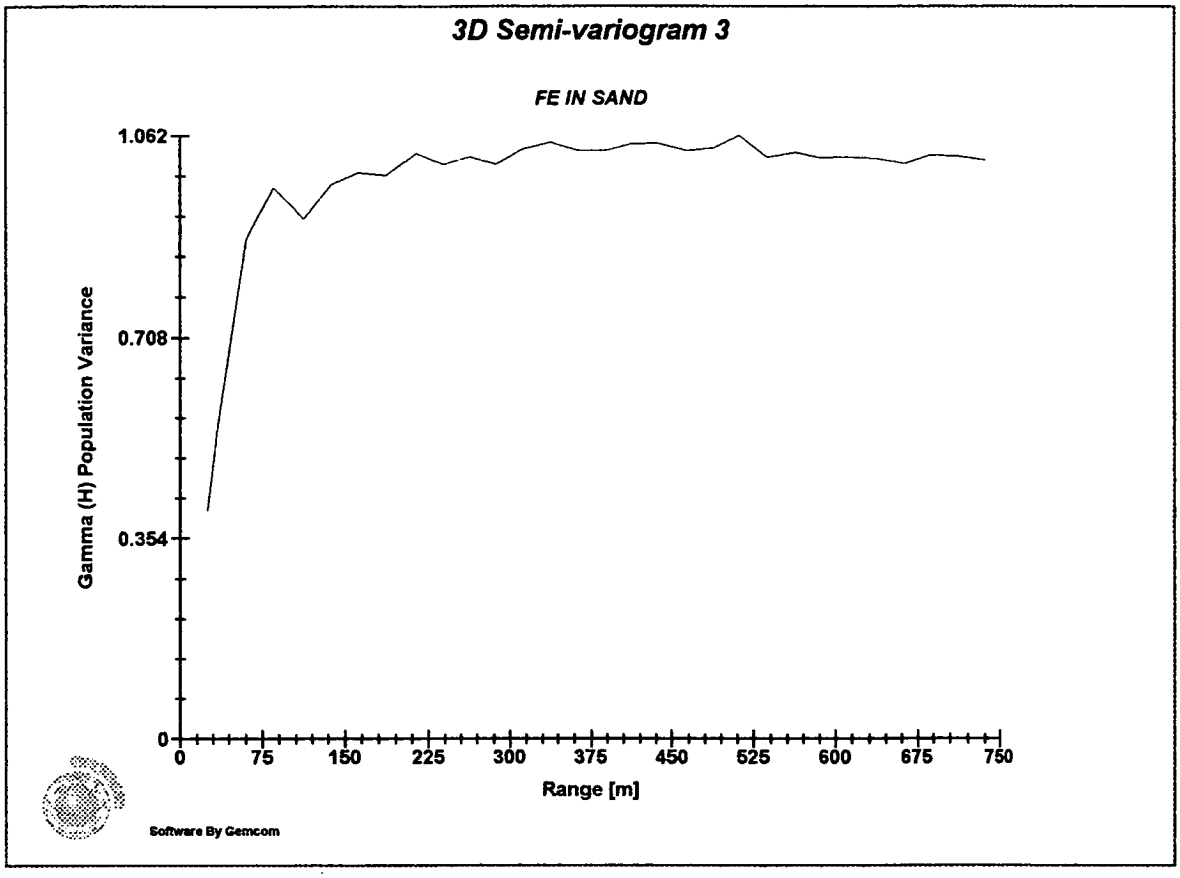
3D Semi-variogram 3
FE IN SAND
1.062
0.708
0.354
0
Gamma (H) Population Variance
0
75
150
225
300
375
450
525
600
675
750
Range [m]
Software By Gemcom

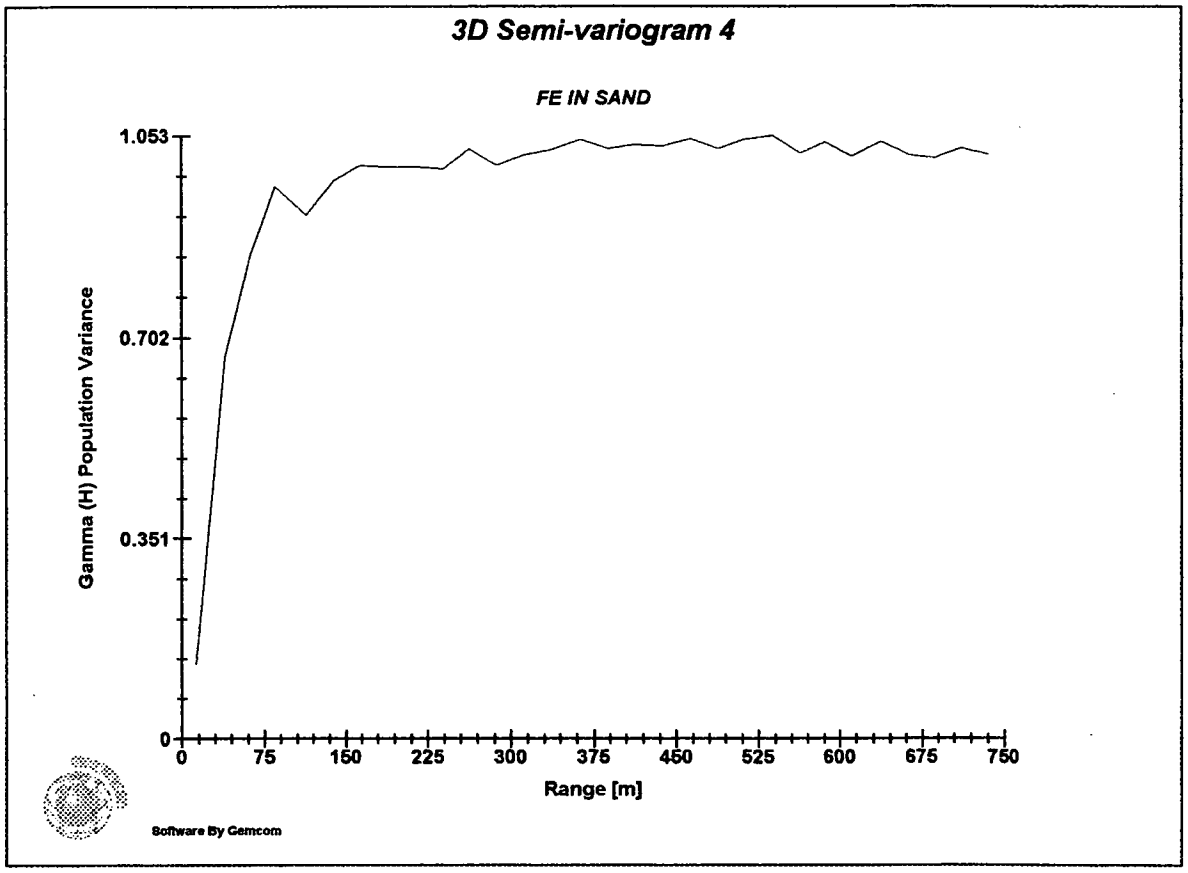
3D Semi-variogram 4
FE IN SAND
1.053
0.702
0.351
0
Gamma (H) Population Variance
0
75
150
225
300
375
450
525
600
675
750
Range [m]
Software By Gemcom

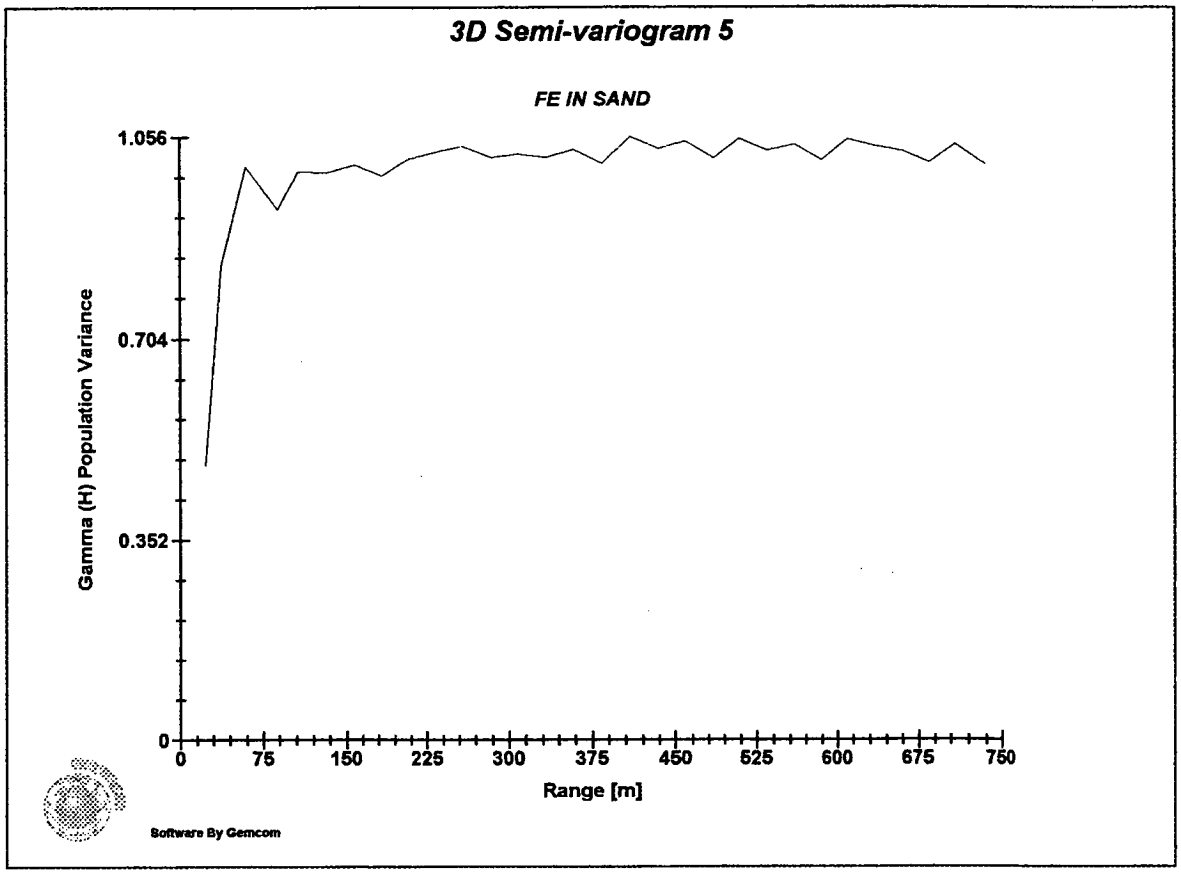
3D Semi-variogram 5
FE IN SAND
1.056
0.704
0.352
0
Gamma (H) Population Variance
0
75
150
225
300
375
450
525
600
675
750
Range [m]
Software By Gemcom

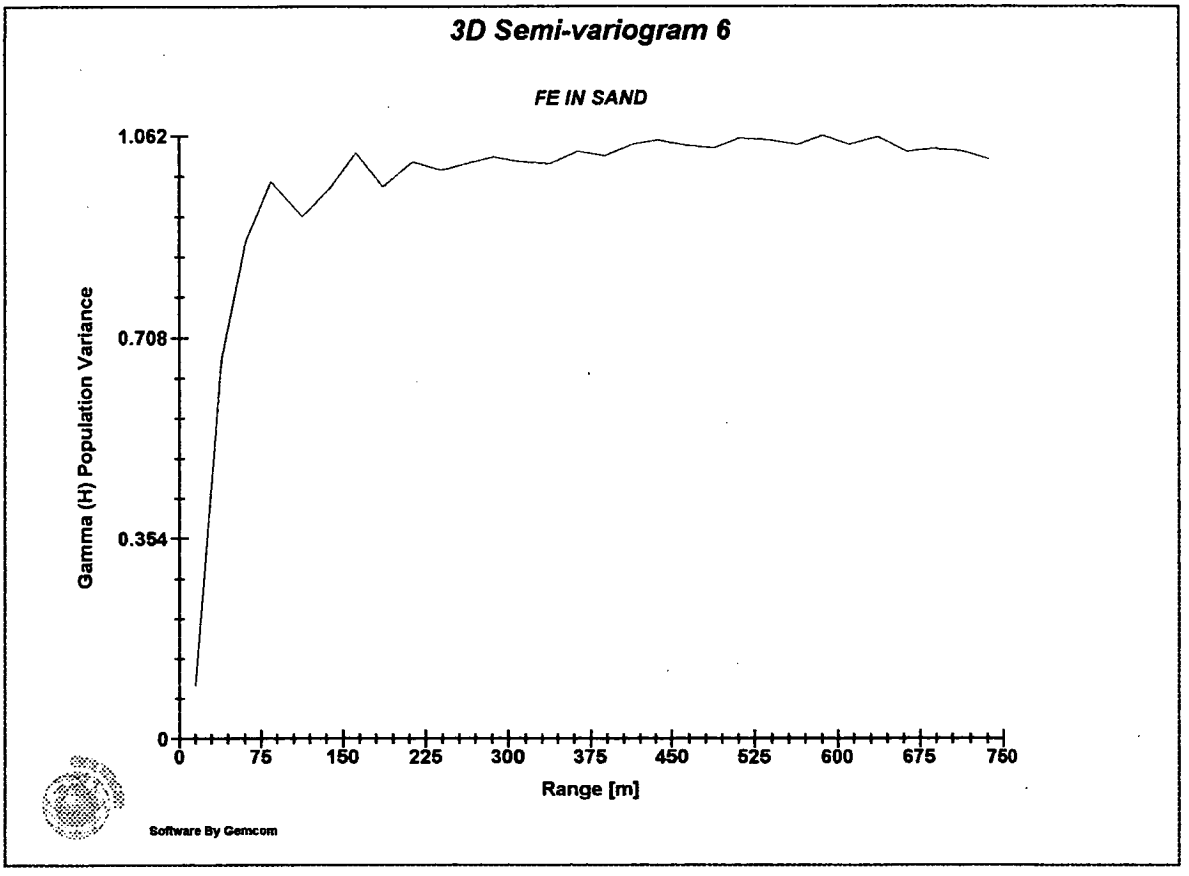
3D Semi-variogram 6
FE IN SAND
1.062
0.708
0.354
0
Gamma (H) Population Variance
0
75
150
225
300
375
450
525
600
675
750
Range [m]
Software By Gemcom

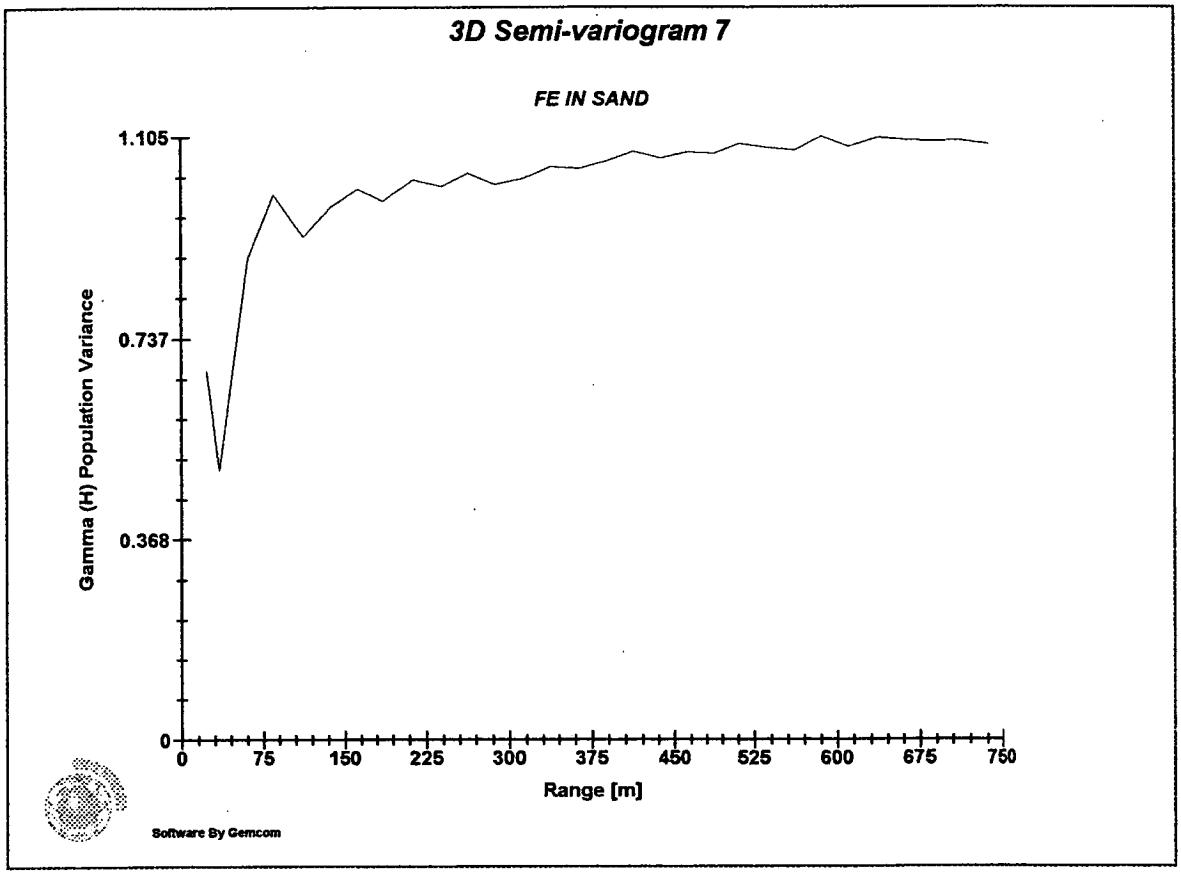
3D Semi-variogram 7
FE IN SAND
1.105
0.737
0.368
0
Gamma (H) Population Variance
0
75
150
225
300
375
450
525
600
675
750
Range [m]
Software By Gemcom

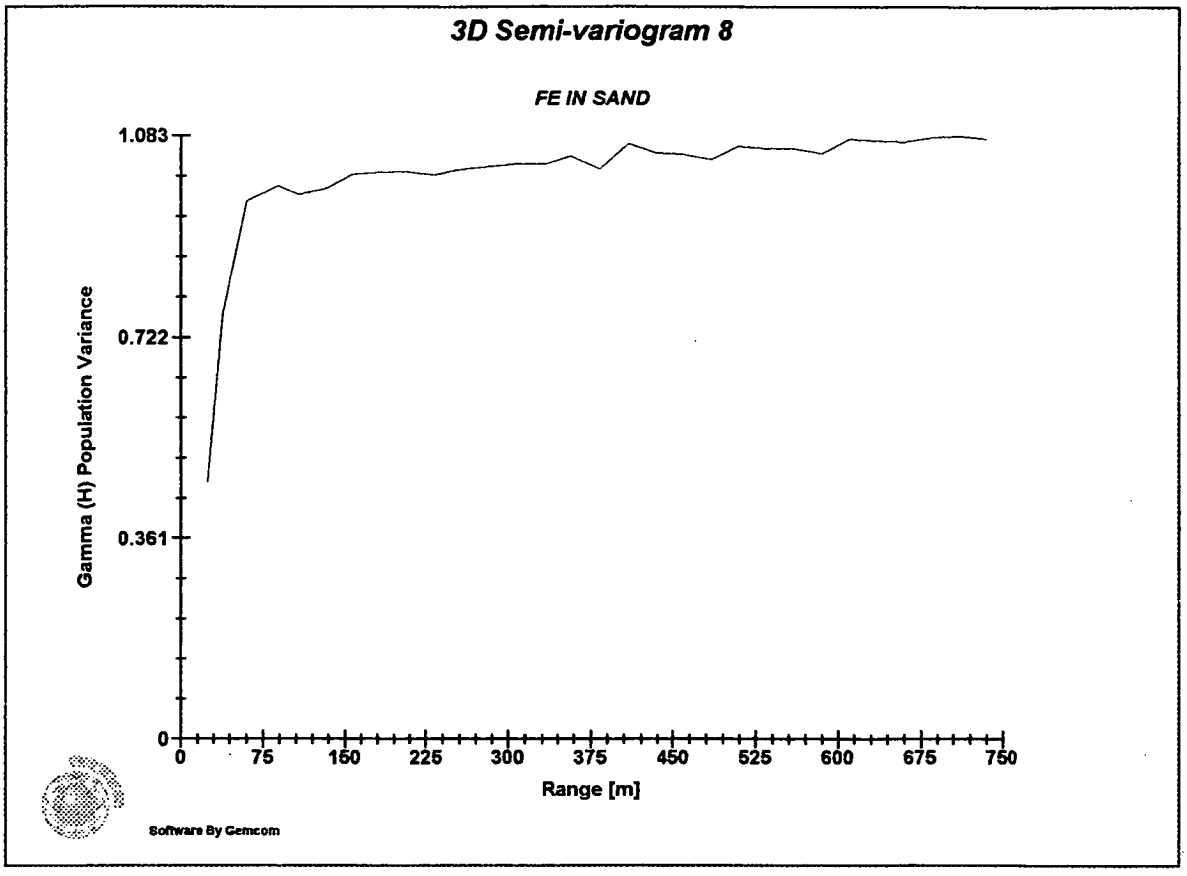
3D Semi-variogram 8
FE IN SAND
1.083
0.722
0.361
0
Gamma (H) Population Variance
0
75
150
225
300
375
450
525
600
675
750
Range [m]
Software By Gemcom

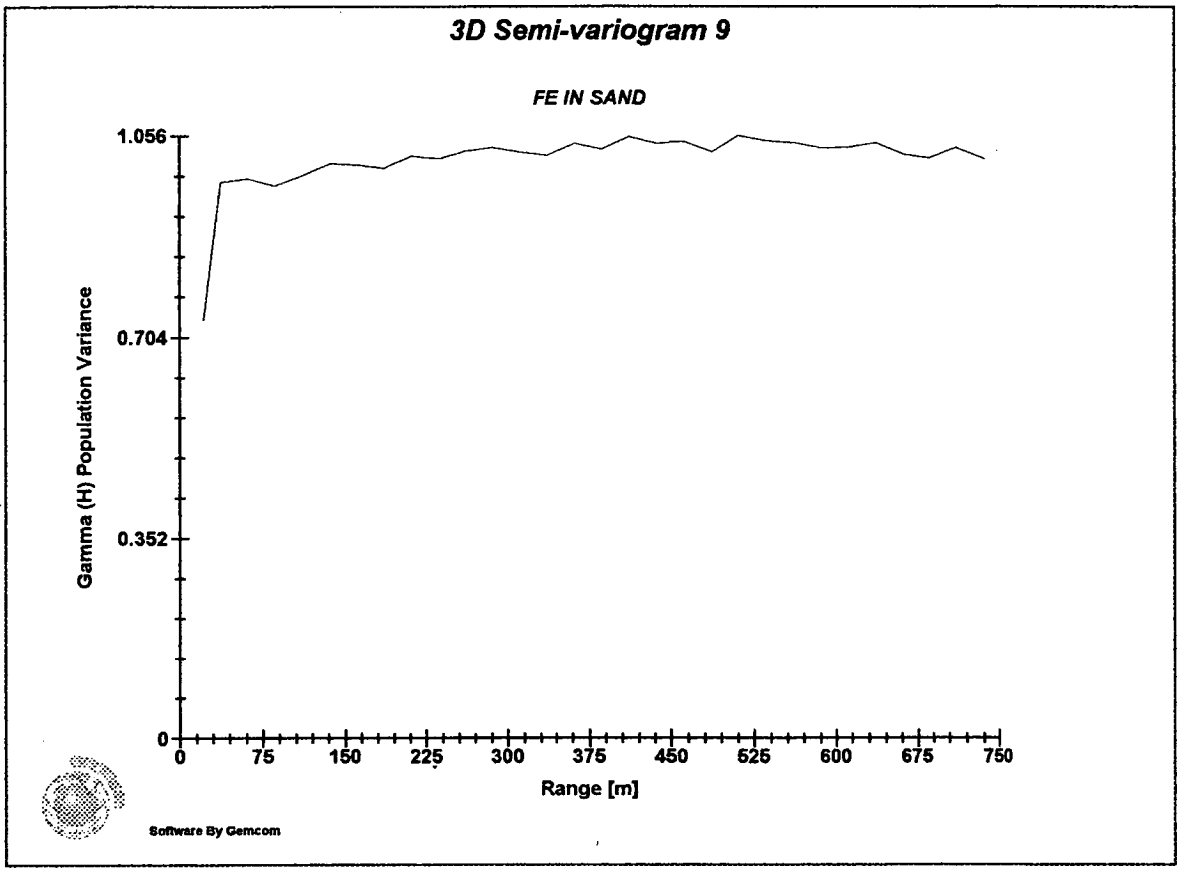
3D Semi-variogram 9
FE IN SAND
1.056
0.704
0.352
0
Gamma (H) Population Variance
0
75
150
225
300
375
450
525
600
675
750
Range [m]
Software By Gemcom

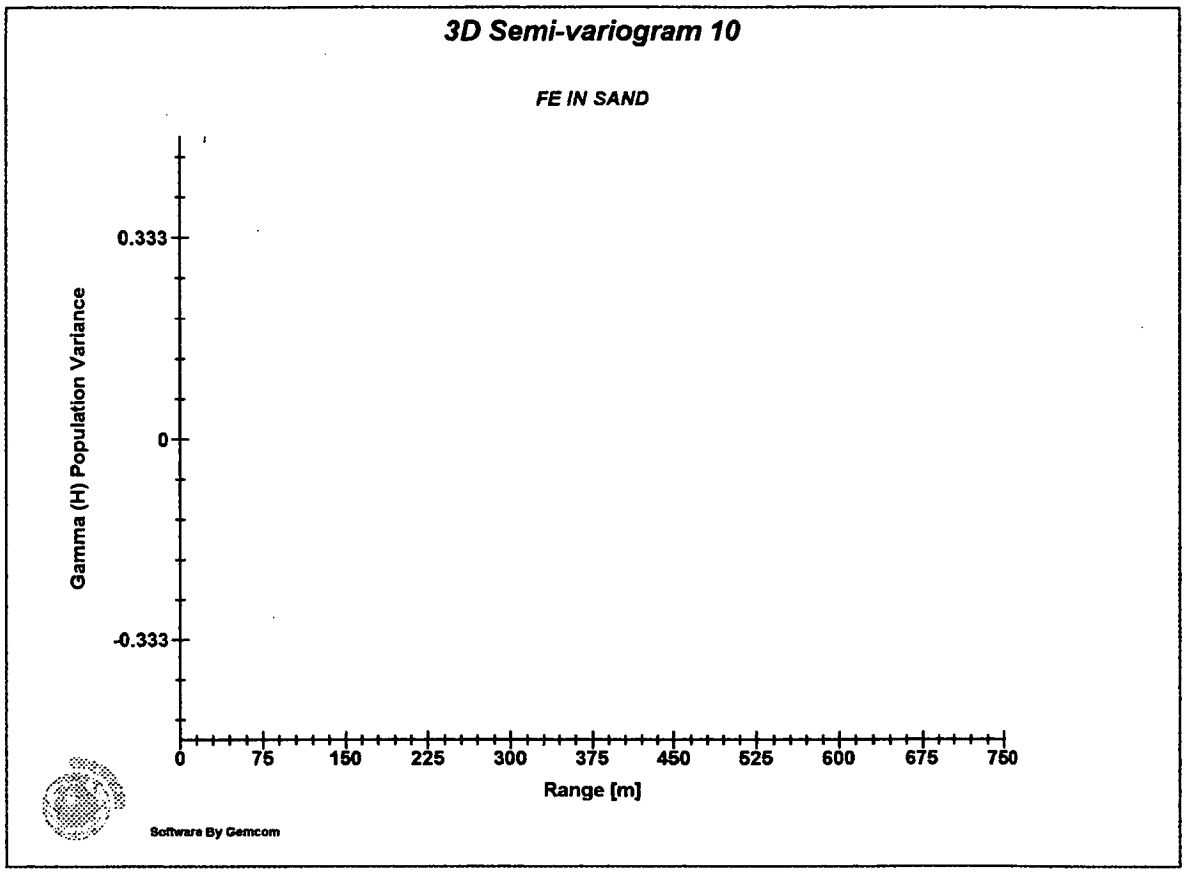
3D Semi-variogram 10
FE IN SAND
Gamma (H) Population Variance
0.333
0
-0.333
0
75
150
225
300
375
450
525
600
675
750
Range [m]
Software By Gemcom

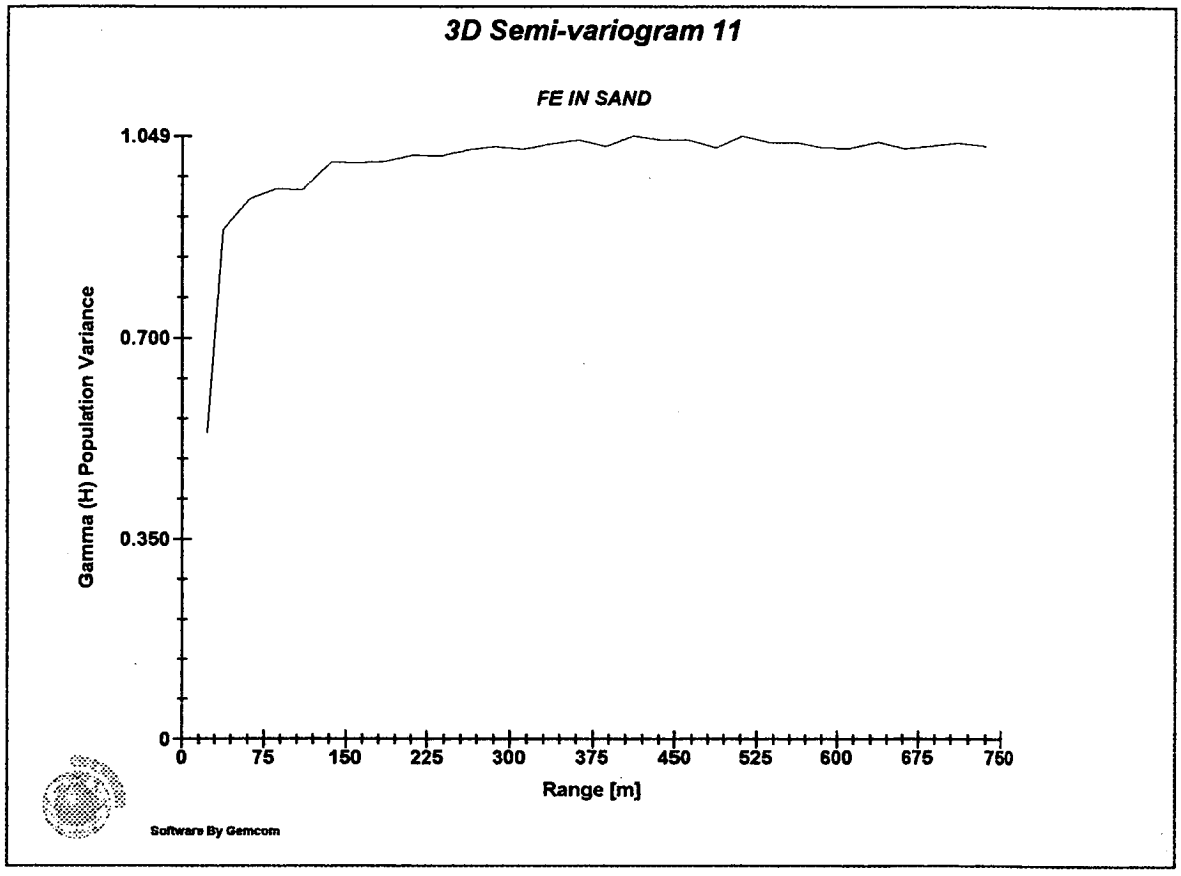
3D Semi-variogram 11
FE IN SAND
Gamma (H) Population Variance
1.049
0.700
0.350
0
0
75
150
225
300
375
450
525
600
675
750
Range [m]
Software By Gemcom

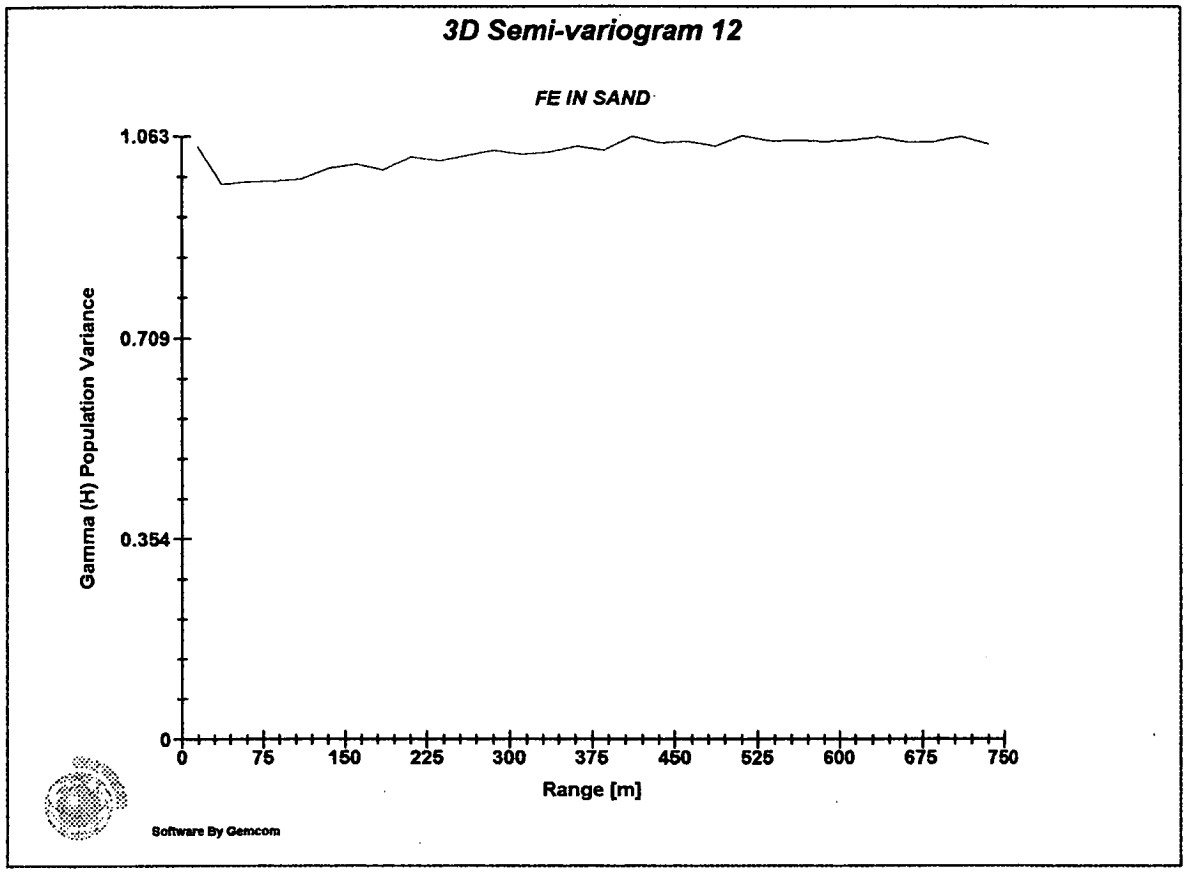
3D Semi-variogram 12
FE IN SAND
1.063
0.709
0.354
0
Gamma (H) Population Variance
0
75
150
225
300
375
450
525
600
675
750
Range [m]
Software By Gemcom

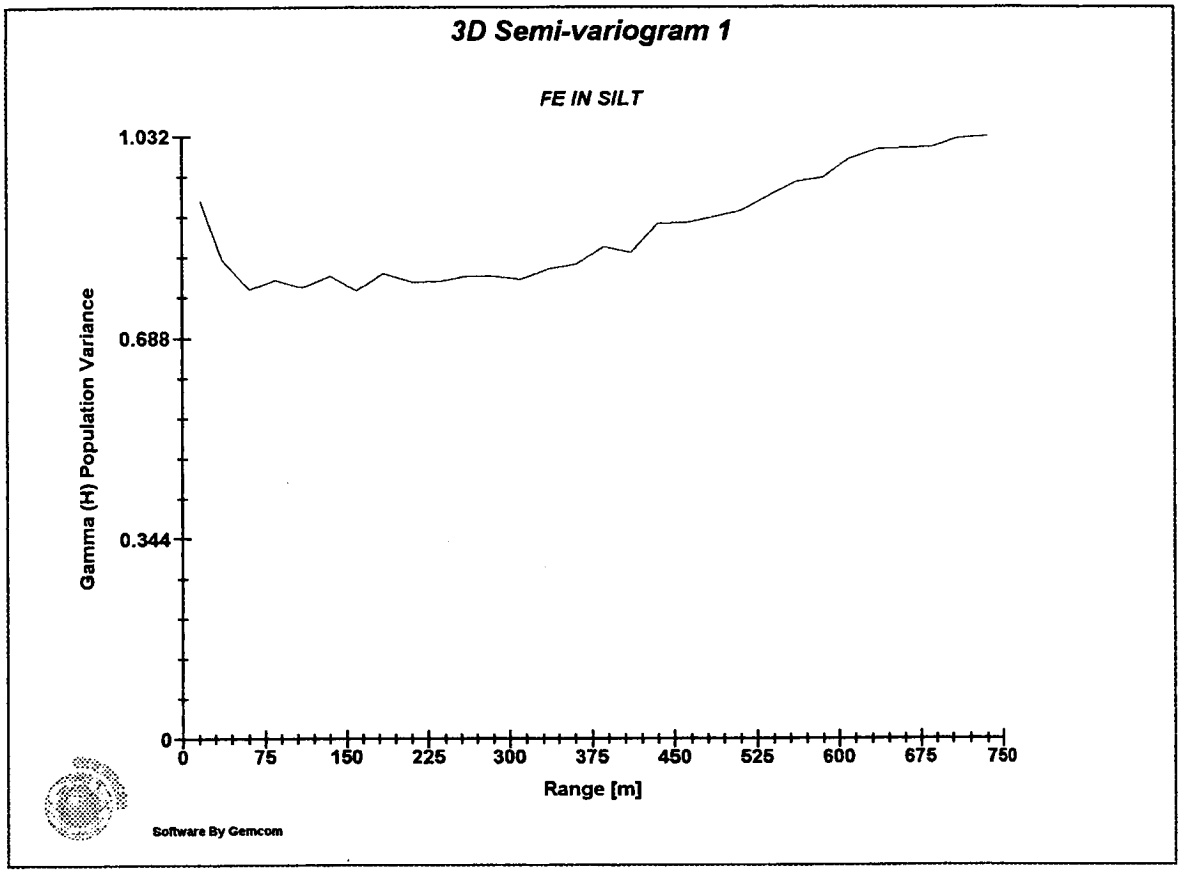
3D Semi-variogram 1
FE IN SILT
1.032
0.688
0.344
0
Gamma (H) Population Variance
0
75
150
225
300
375
450
525
600
675
750
Range [m]
Software By Gemcom

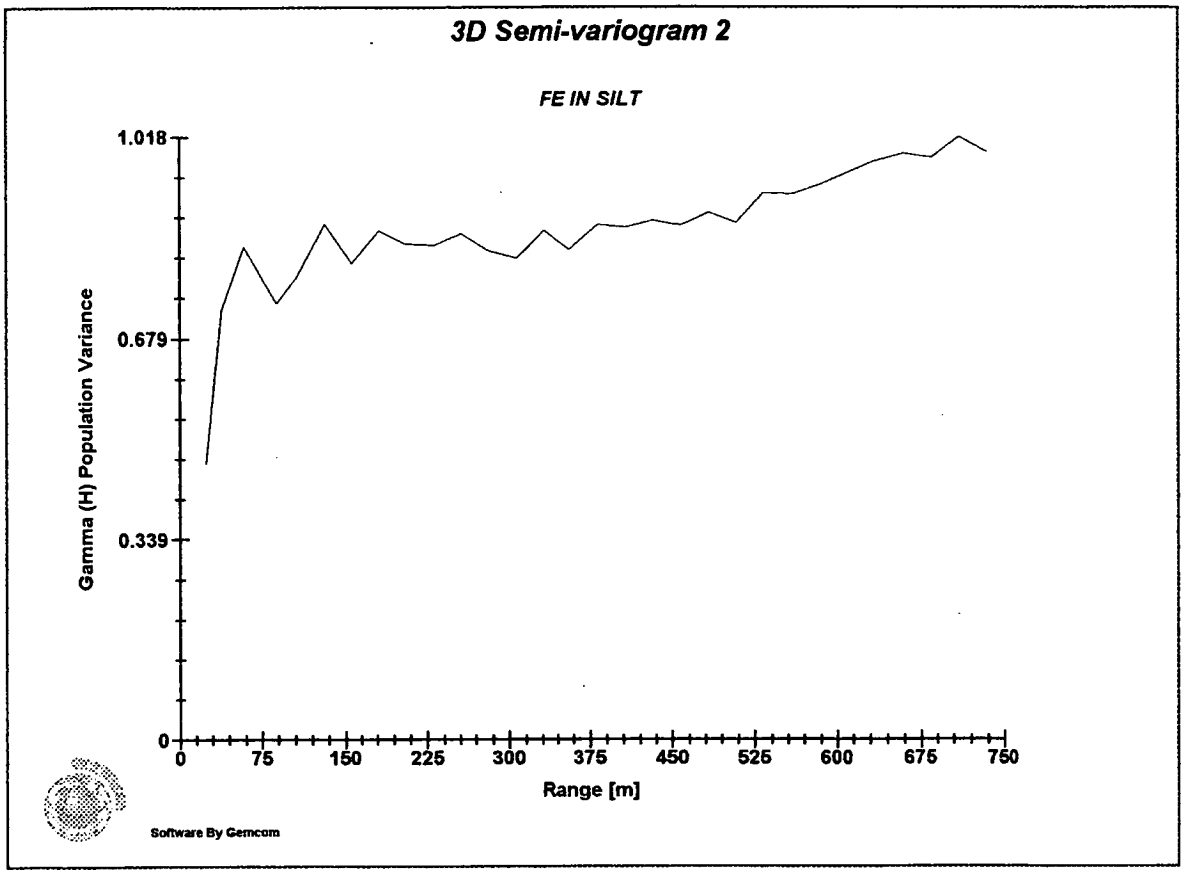
3D Semi-variogram 2
FE IN SILT
1.018
0.679
0.339
0
Gamma (H) Population Variance
0
75
150
225
300
375
450
525
600
675
750
Range [m]
Software By Gemcom

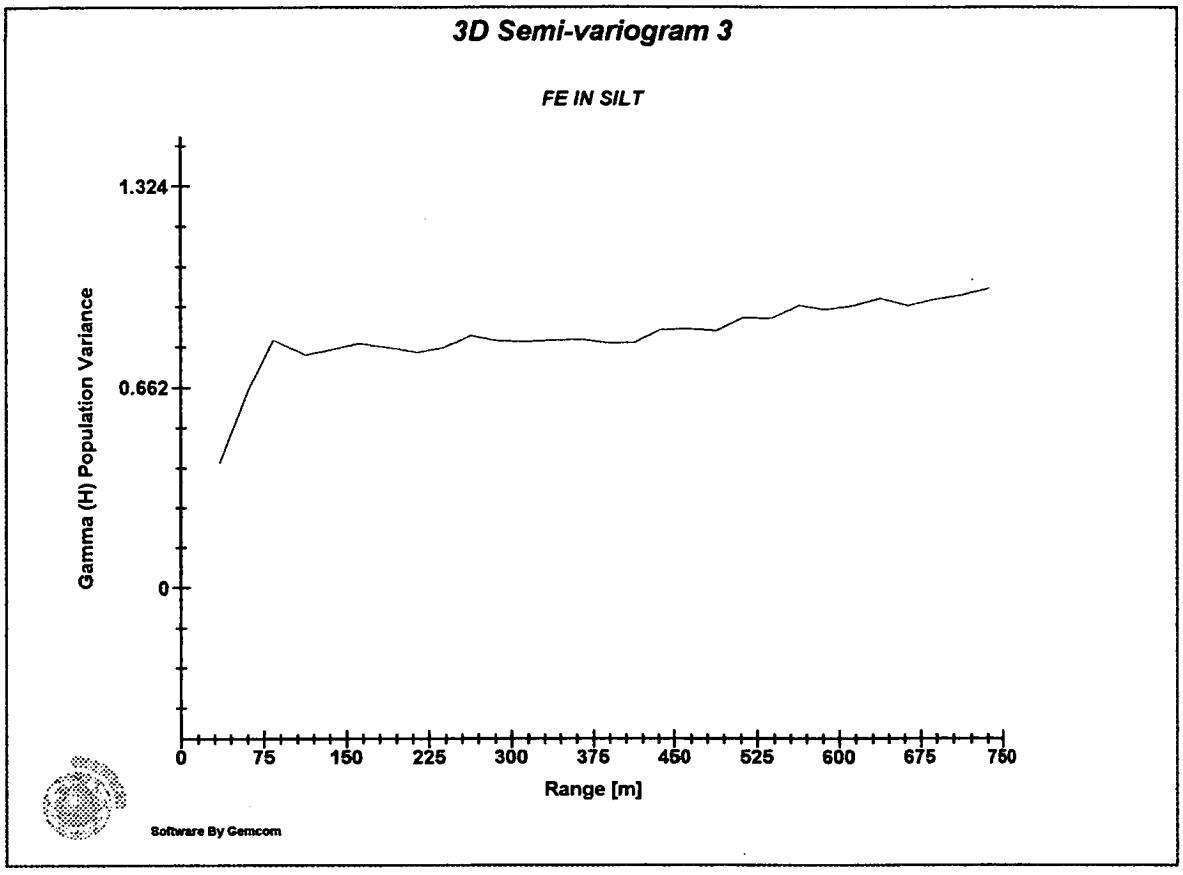
3D Semi-variogram 3
FE IN SILT
1.324
0.662
0
Gamma (H) Population Variance
0
75
150
225
300
375
450
525
600
675
750
Range [m]
Software By Gemcom

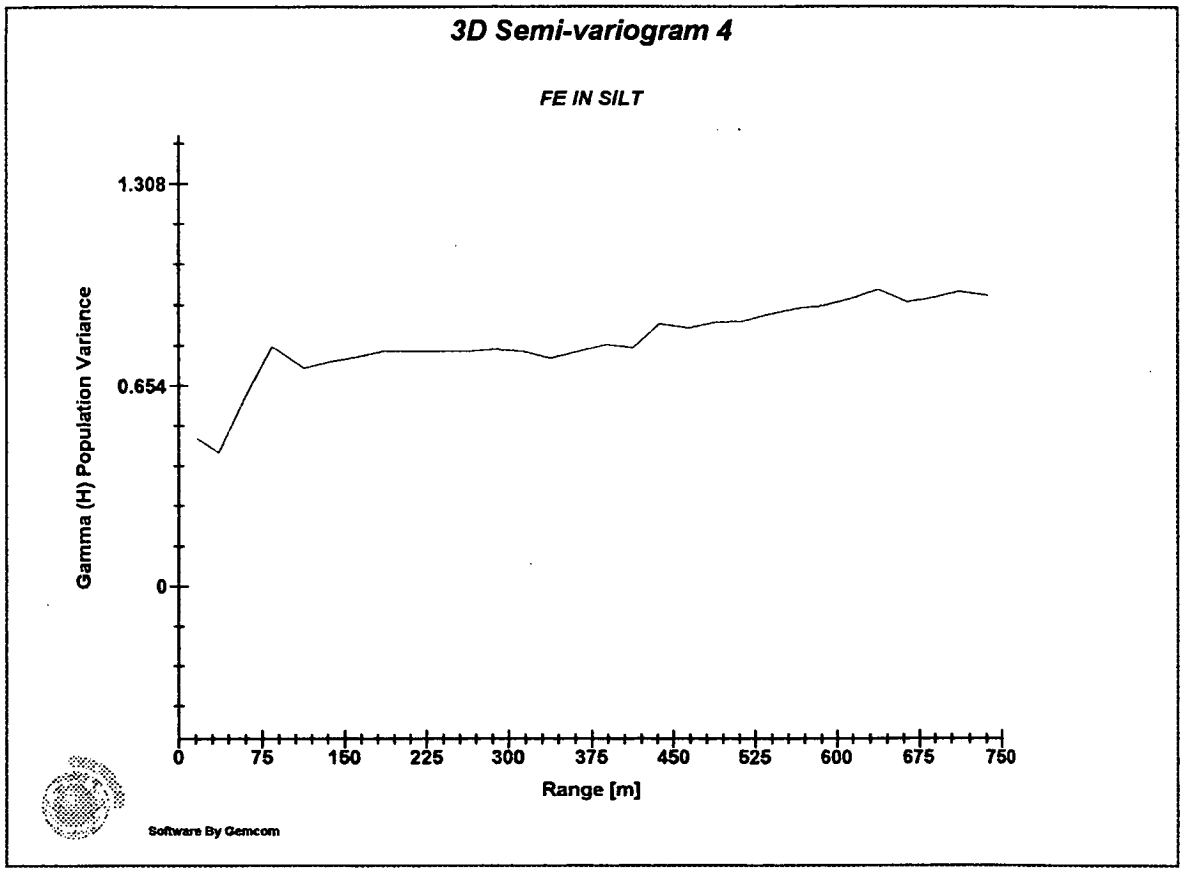
3D Semi-variogram 4
FE IN SILT
1.308
0.654
0
Gamma (H) Population Variance
0
75
150
225
300
375
450
525
600
675
750
Range [m]
Software By Gemcom

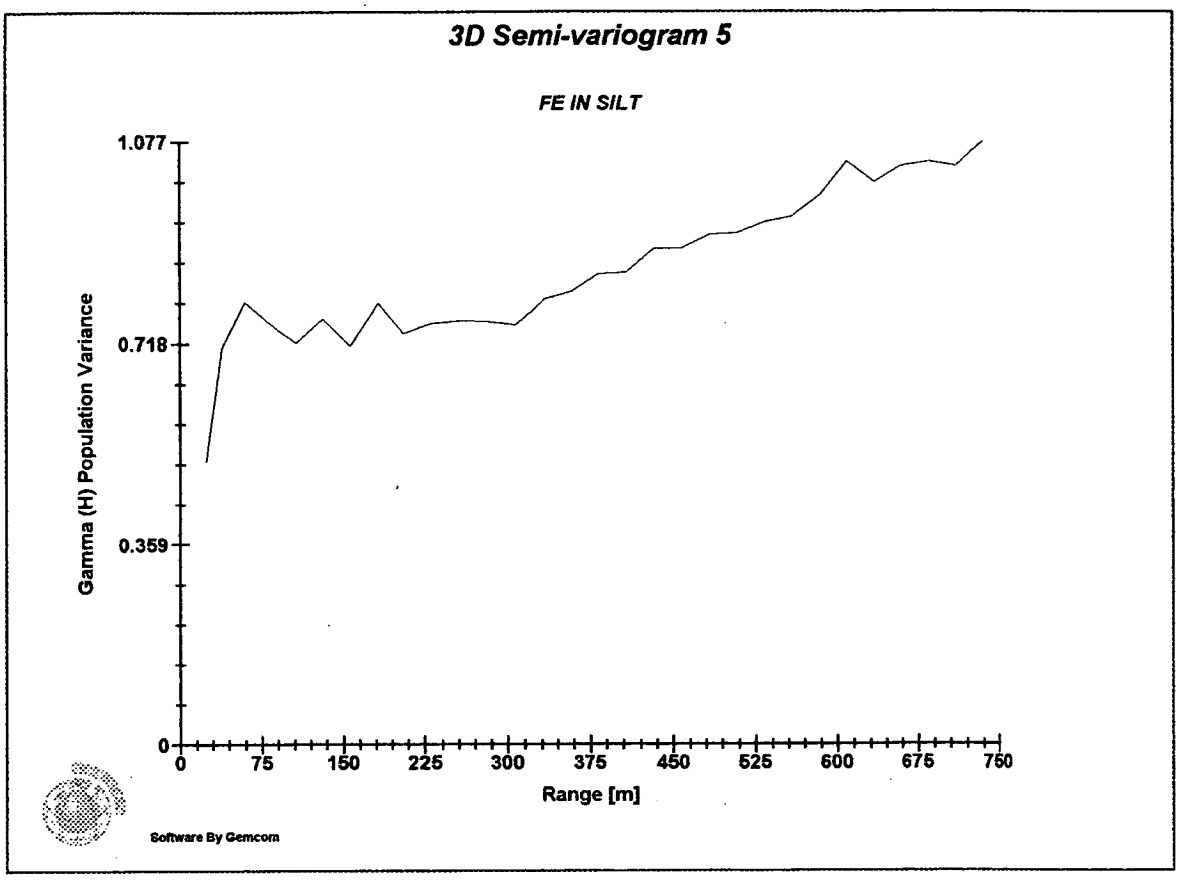
3D Semi-variogram 5
FE IN SILT
1.077
0.718
0.359
0
Gamma (H) Population Variance
0
75
150
225
300
375
450
525
600
675
750
Range [m]
Software By Gemcom

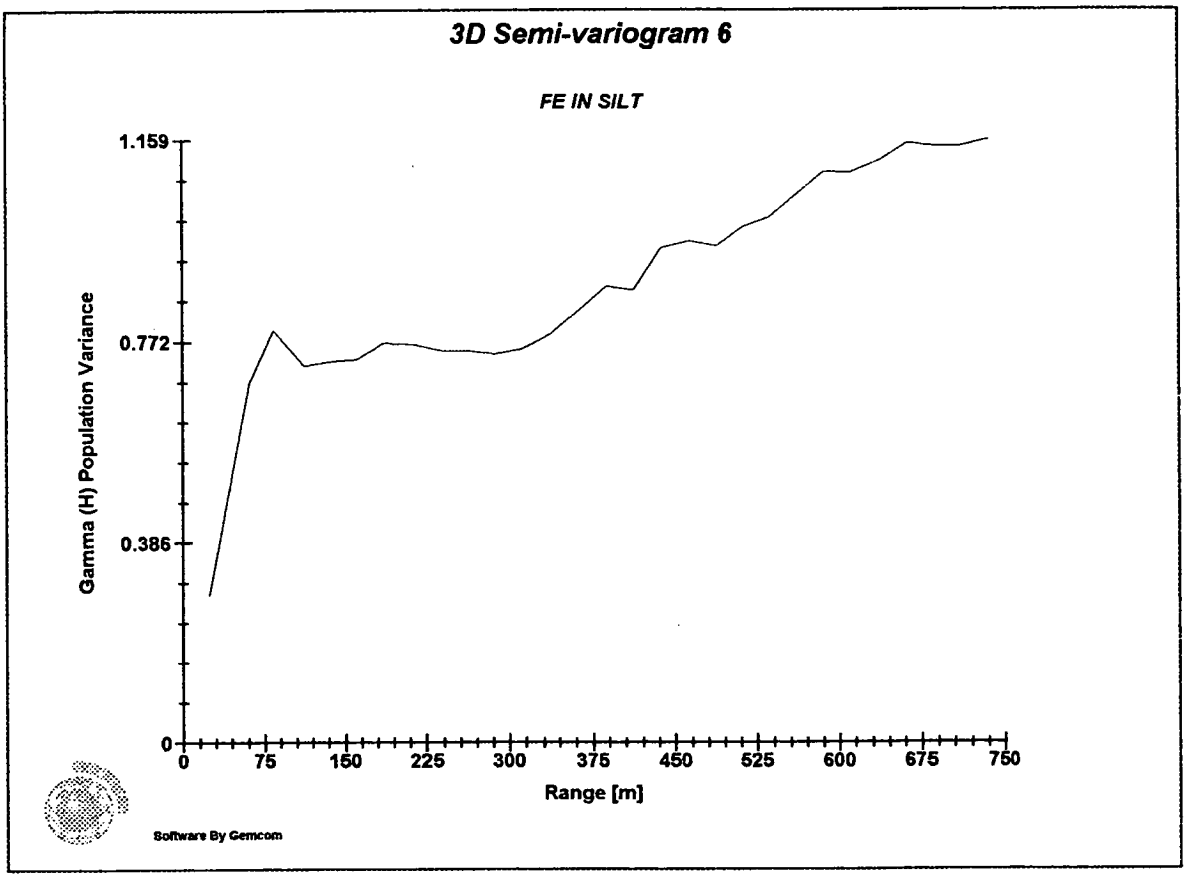
3D Semi-variogram 6
FE IN SILT
1.159
0.772
0.386
0
Gamma (H) Population Variance
0
75
150
225
300
375
450
525
600
675
750
Range [m]
Software By Gemcom

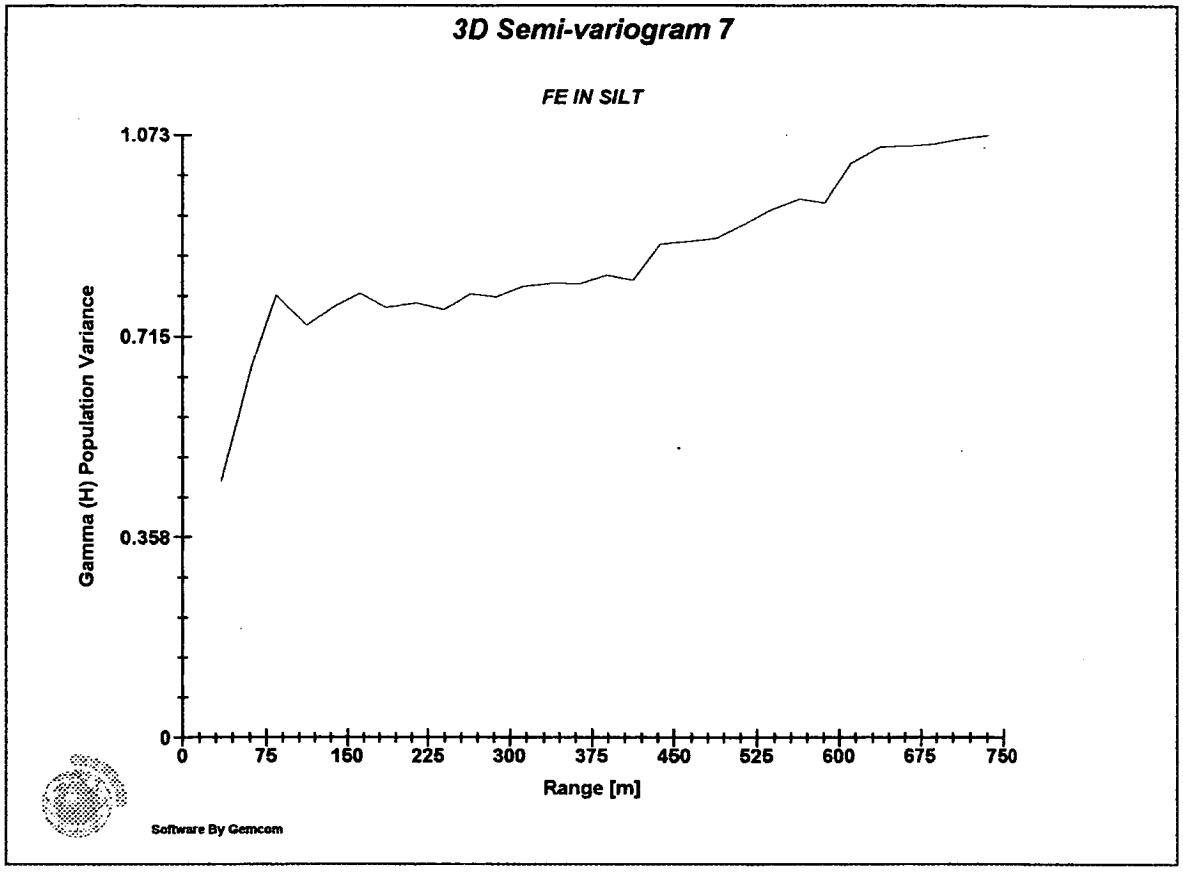
3D Semi-variogram 7
FE IN SILT
1.073
0.715
0.358
0
Gamma (H) Population Variance
0
75
150
225
300
375
450
525
600
675
750
Range [m]
Software By Gemcom

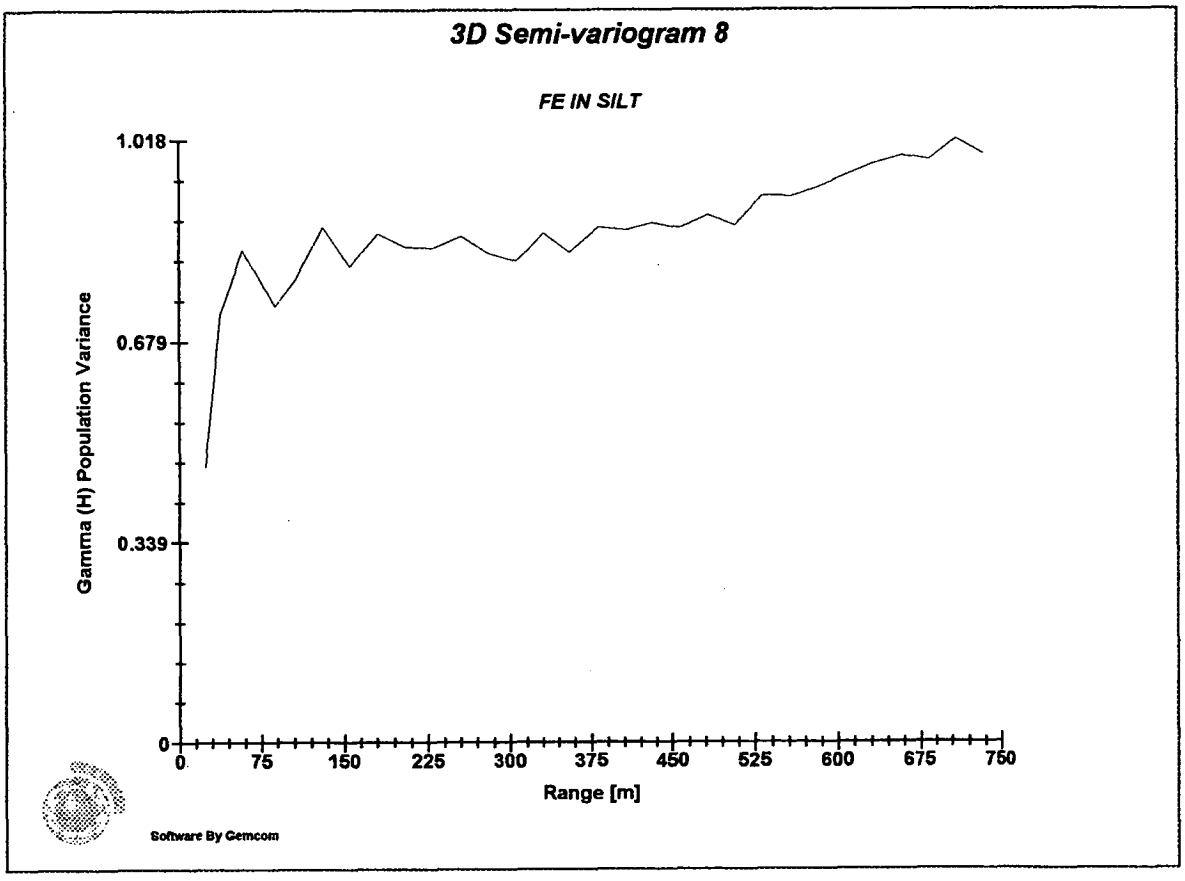
3D Semi-variogram 8
FE IN SILT
1.018
0.679
0.339
0
Gamma (H) Population Variance
0
75
150
225
300
375
450
525
600
675
750
Range [m]
Software By Gemcom

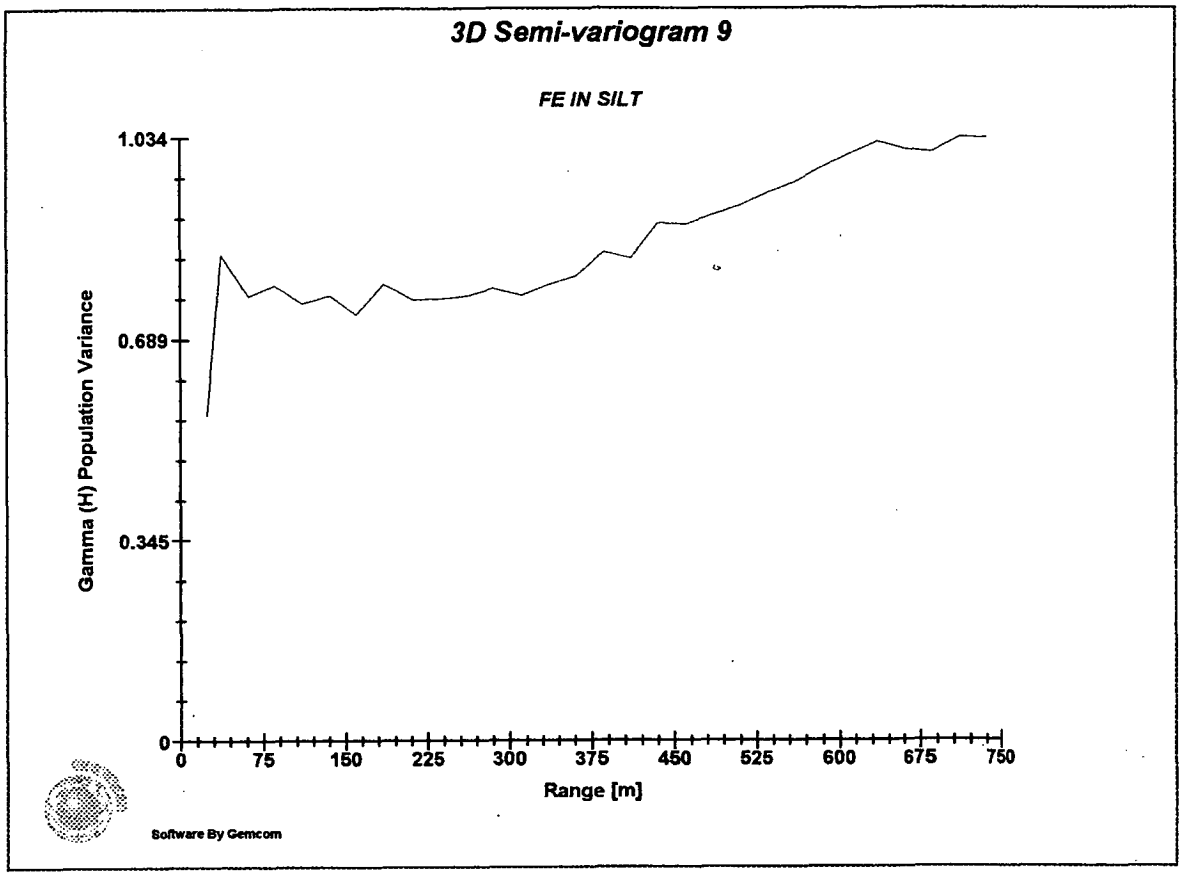
3D Semi-variogram 9
FE IN SILT
1.034
0.689
0.345
0
Gamma (H) Population Variance
0
75
150
225
300
375
450
525
600
675
750
Range [m]
Software By Gemcom

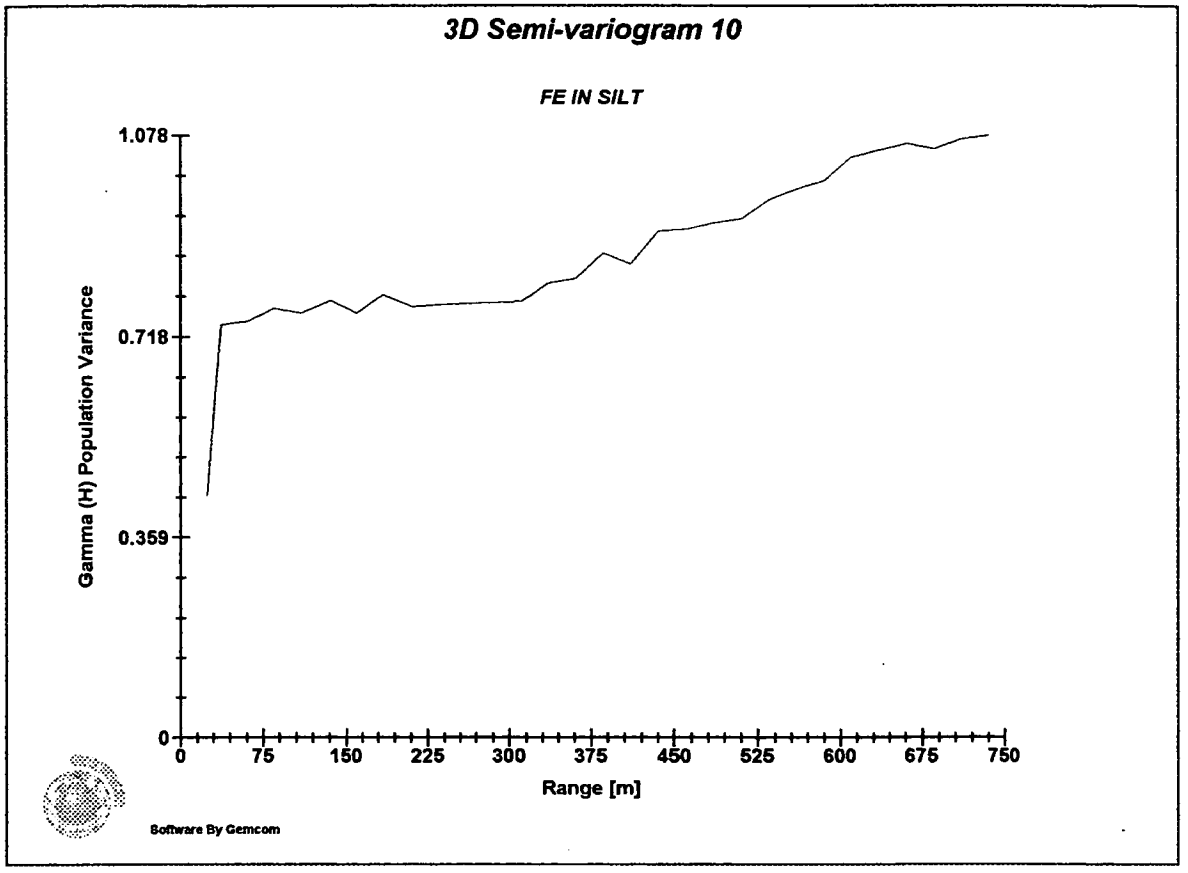
3D Semi-variogram 10
FE IN SILT
1.078
0.718
0.359
0
Gamma (H) Population Variance
0
75
150
225
300
375
450
525
600
675
750
Range [m]
Software By Gemcom

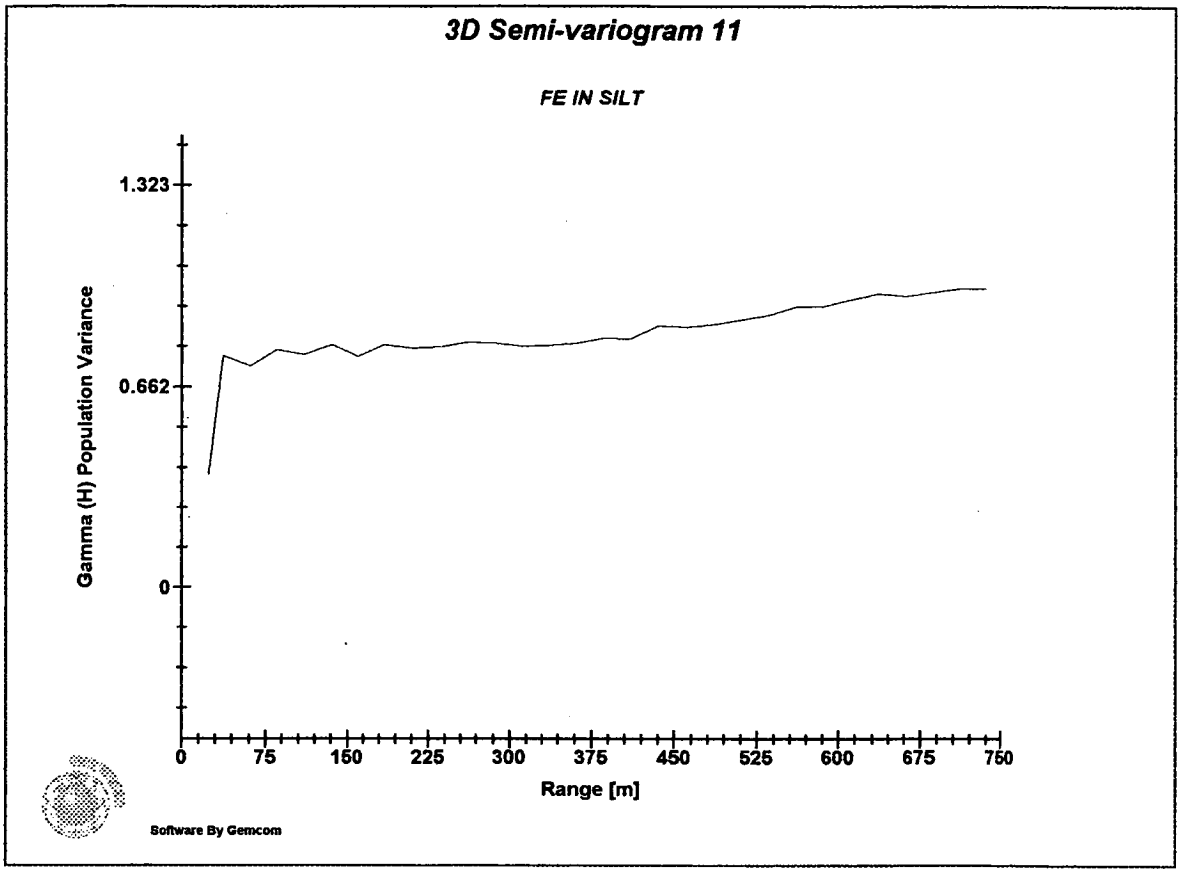
3D Semi-variogram 11
FE IN SILT
1.323
0.662
0
Gamma (H) Population Variance
0
75
150
225
300
375
450
525
600
675
750
Range [m]
Software By Gemcom

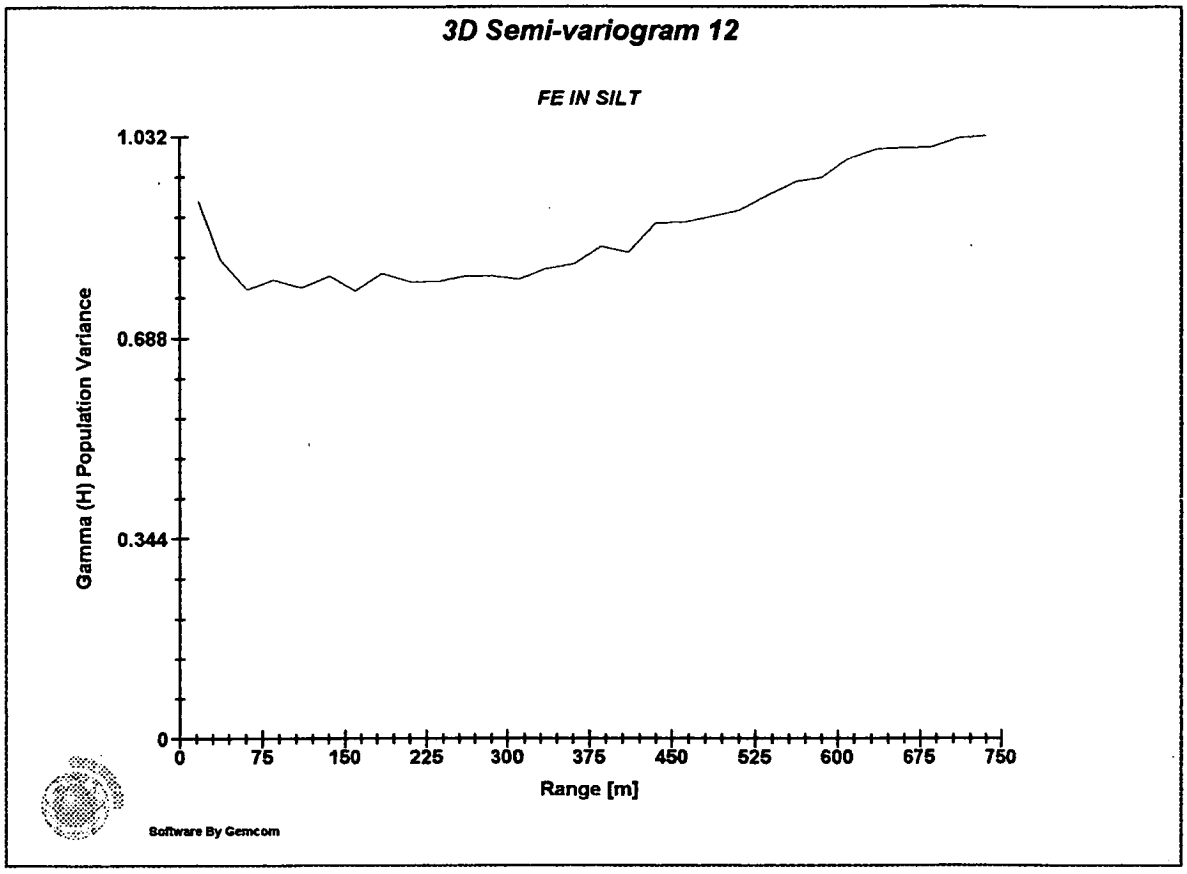
3D Semi-variogram 12
FE IN SILT
1.032
0.688
0.344
0
Gamma (H) Population Variance
0
75
150
225
300
375
450
525
600
675
750
Range [m]
Software By Gemcom

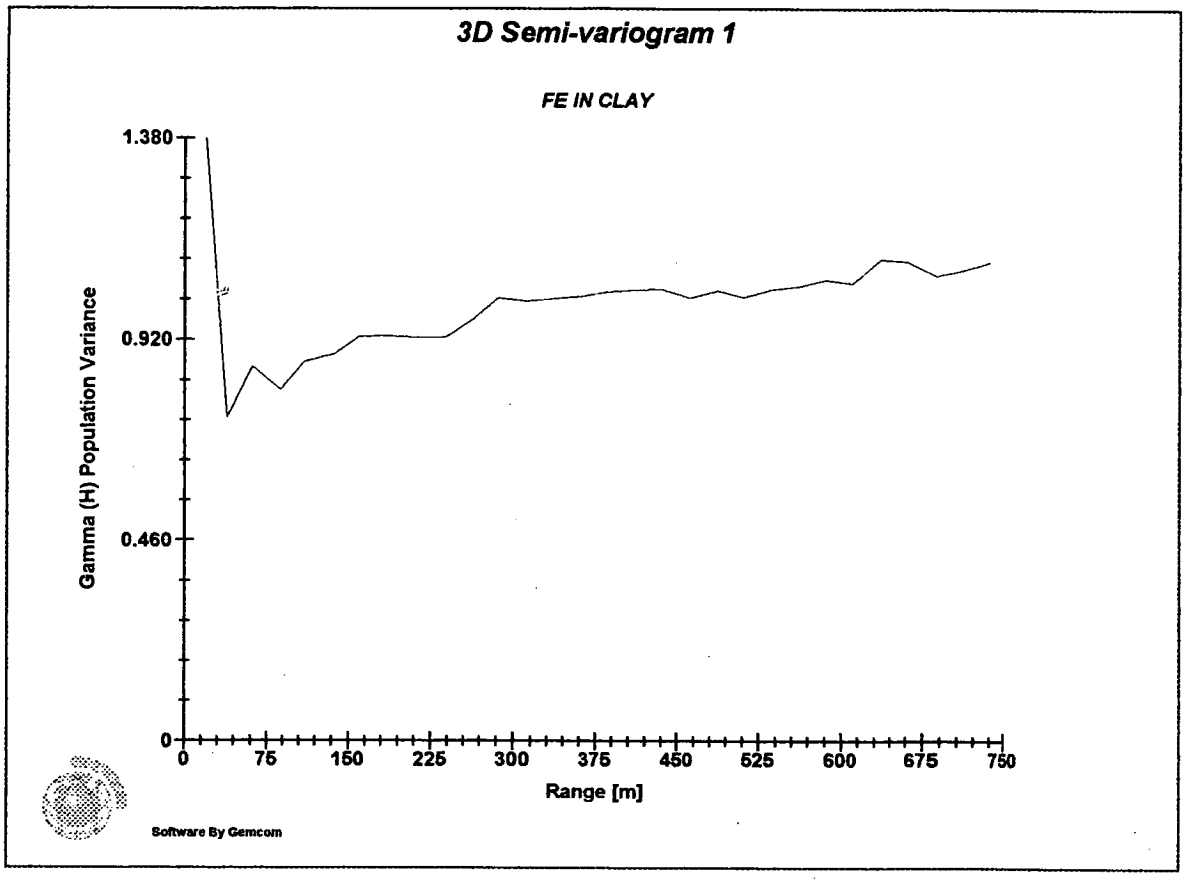
3D Semi-variogram 1
FE IN CLAY
1.380
0.920
0.460
0
Gamma (H) Population Variance
0
75
150
225
300
375
450
525
600
675
750
Range [m]
Software By Gemcom

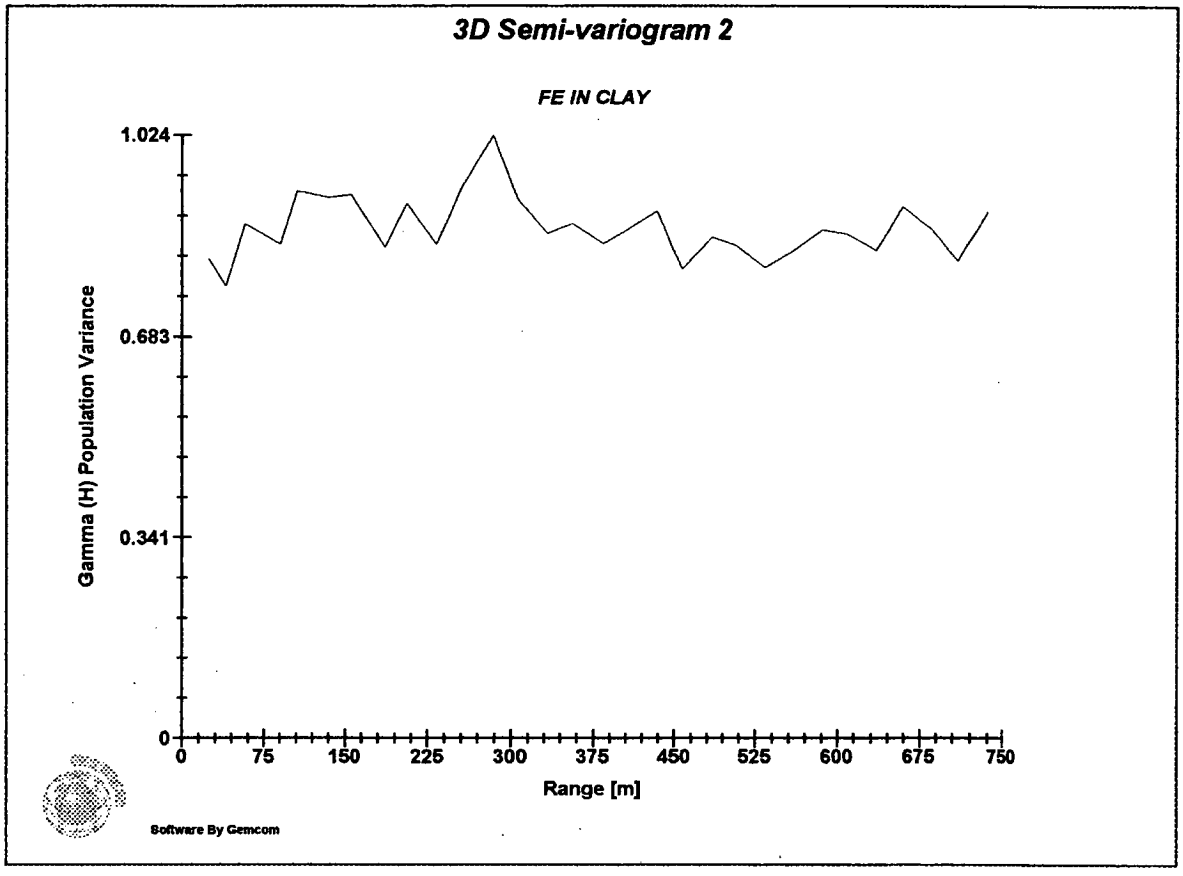
3D Semi-variogram 2
FE IN CLAY
1.024
0.683
0.341
0
Gamma (H) Population Variance
0
75
150
225
300
375
450
525
600
675
750
Range [m]
Software By Gemcom

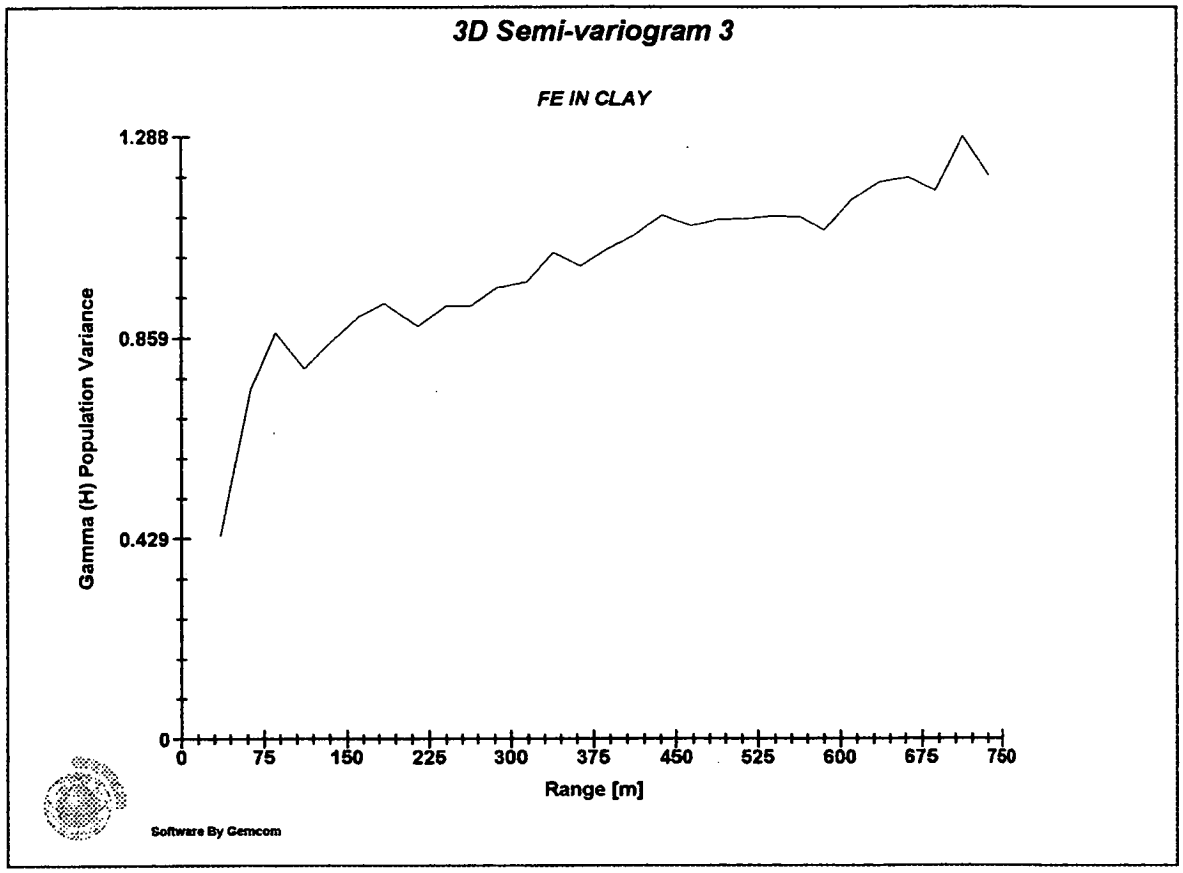
3D Semi-variogram 3
FE IN CLAY
1.288
0.859
0.429
0
Gamma (H) Population Variance
0
75
150
225
300
375
450
525
600
675
750
Range [m]
Software By Gemcom

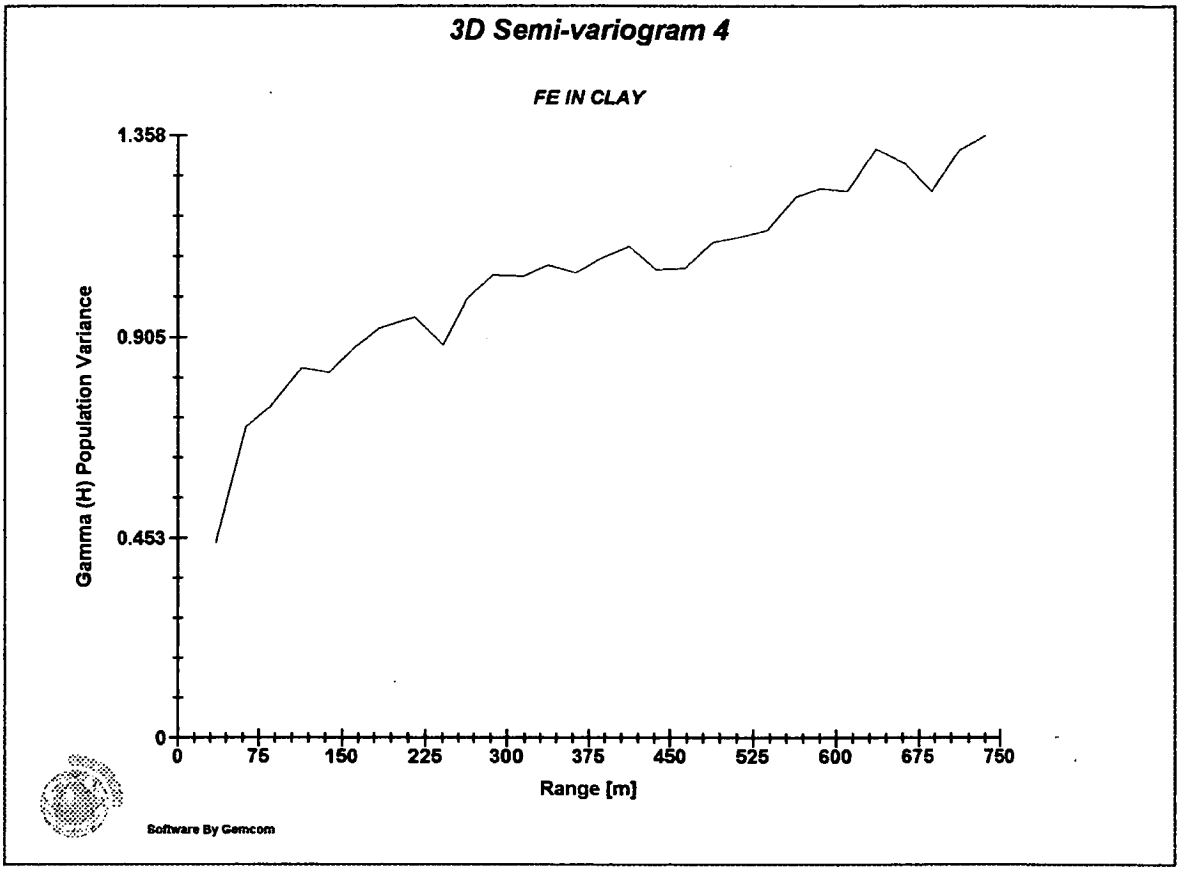
3D Semi-variogram 4
FE IN CLAY
1.358
0.905
0.453
0
Gamma (H) Population Variance
0
75
150
225
300
375
450
525
600
675
750
Range [m]
Software By Gemcom

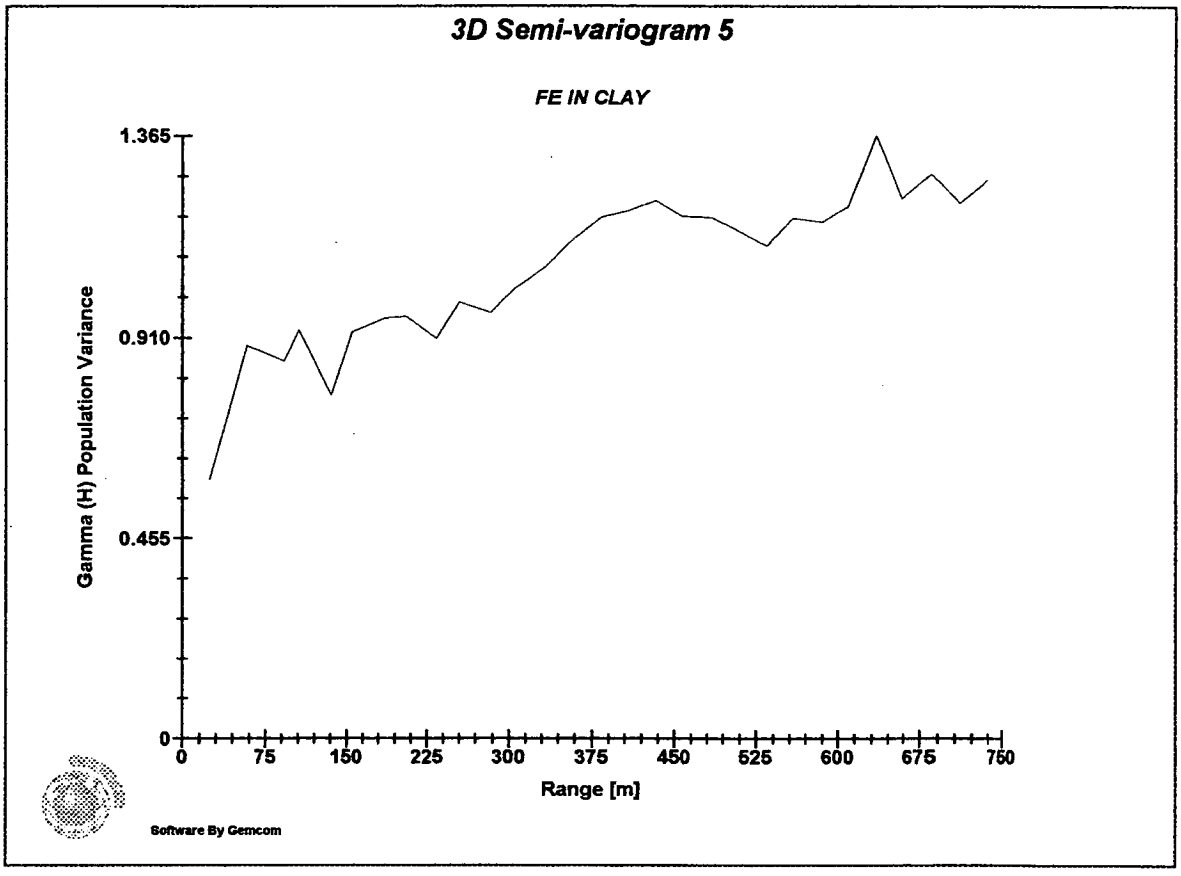
3D Semi-variogram 5
FE IN CLAY
1.365
0.910
0.455
0
Gamma (H) Population Variance
0
75
150
225
300
375
450
525
600
675
750
Range [m]
Software By Gemcom

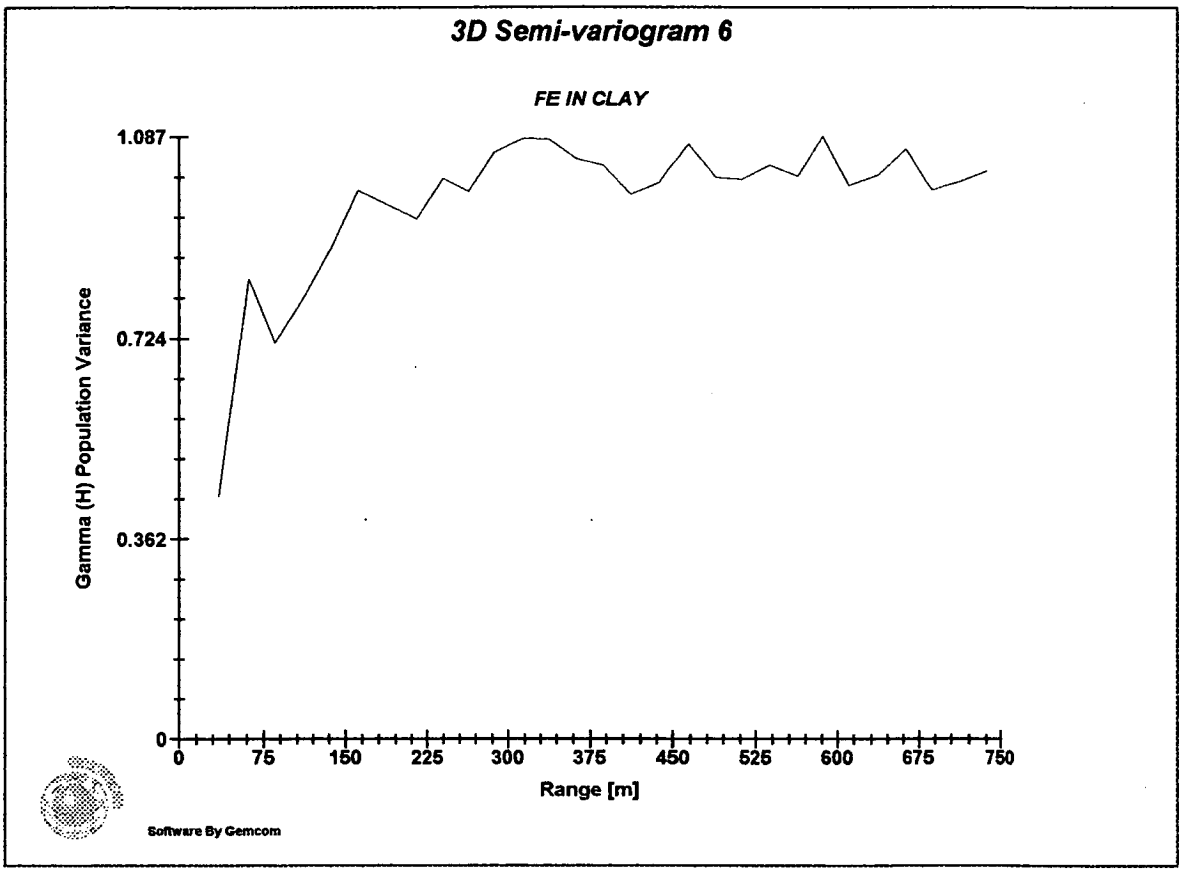
3D Semi-variogram 6
FE IN CLAY
1.087
0.724
0.362
0
Gamma (H) Population Variance
0
75
150
225
300
375
450
525
600
675
750
Range [m]
Software By Gemcom

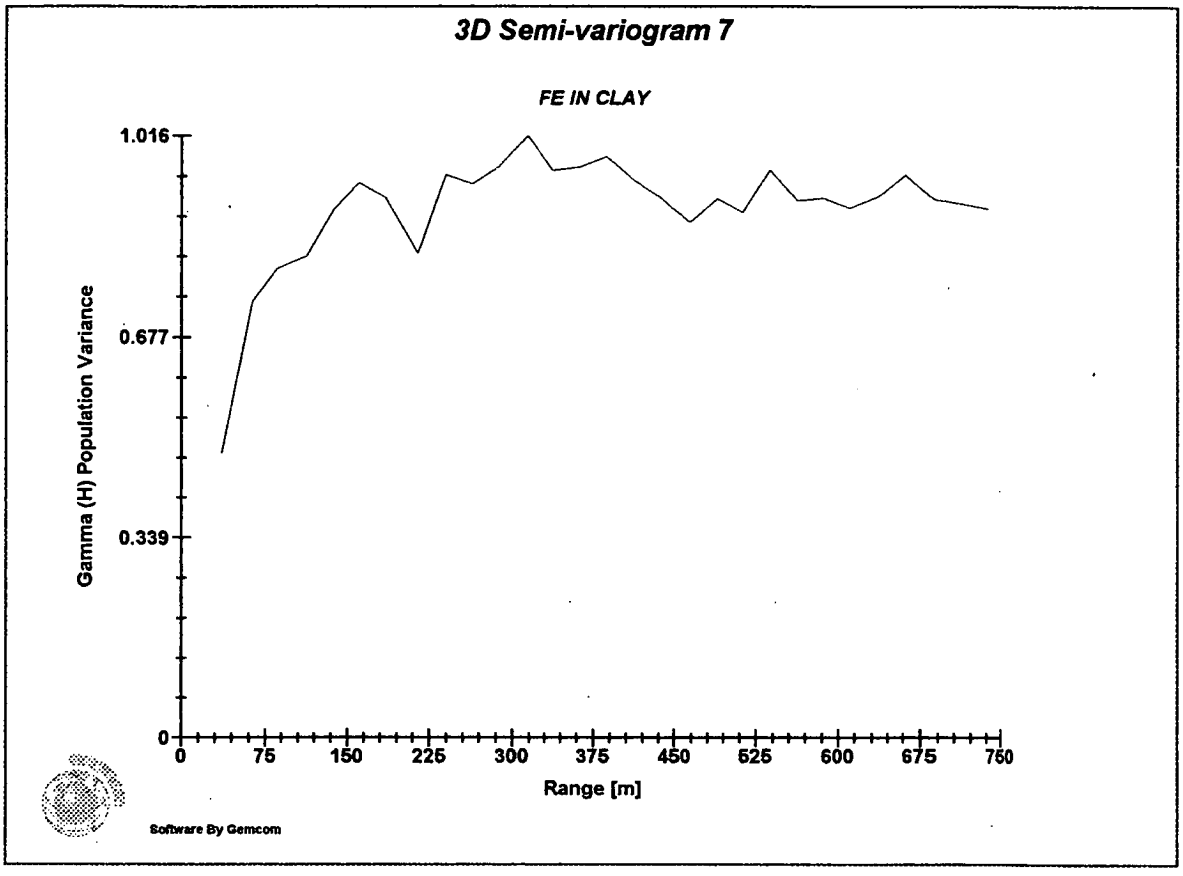
3D Semi-variogram 7
FE IN CLAY
1.016
0.677
0.339
0
Gamma (H) Population Variance
0
75
150
225
300
375
450
525
600
675
750
Range [m]
Software By Gemcom

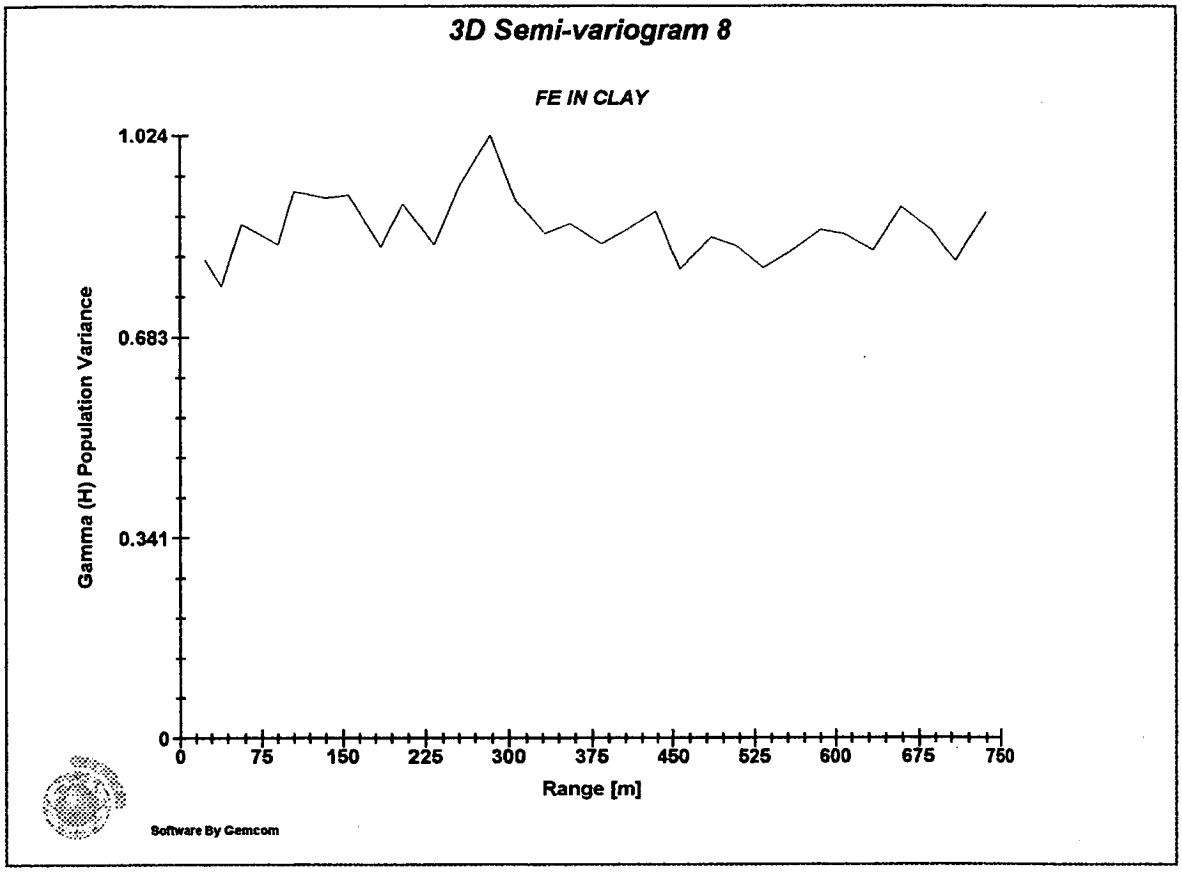
3D Semi-variogram 8
FE IN CLAY
1.024
0.683
0.341
0
Gamma (H) Population Variance
0
75
150
225
300
375
450
525
600
675
750
Range [m]
Software By Gemcom

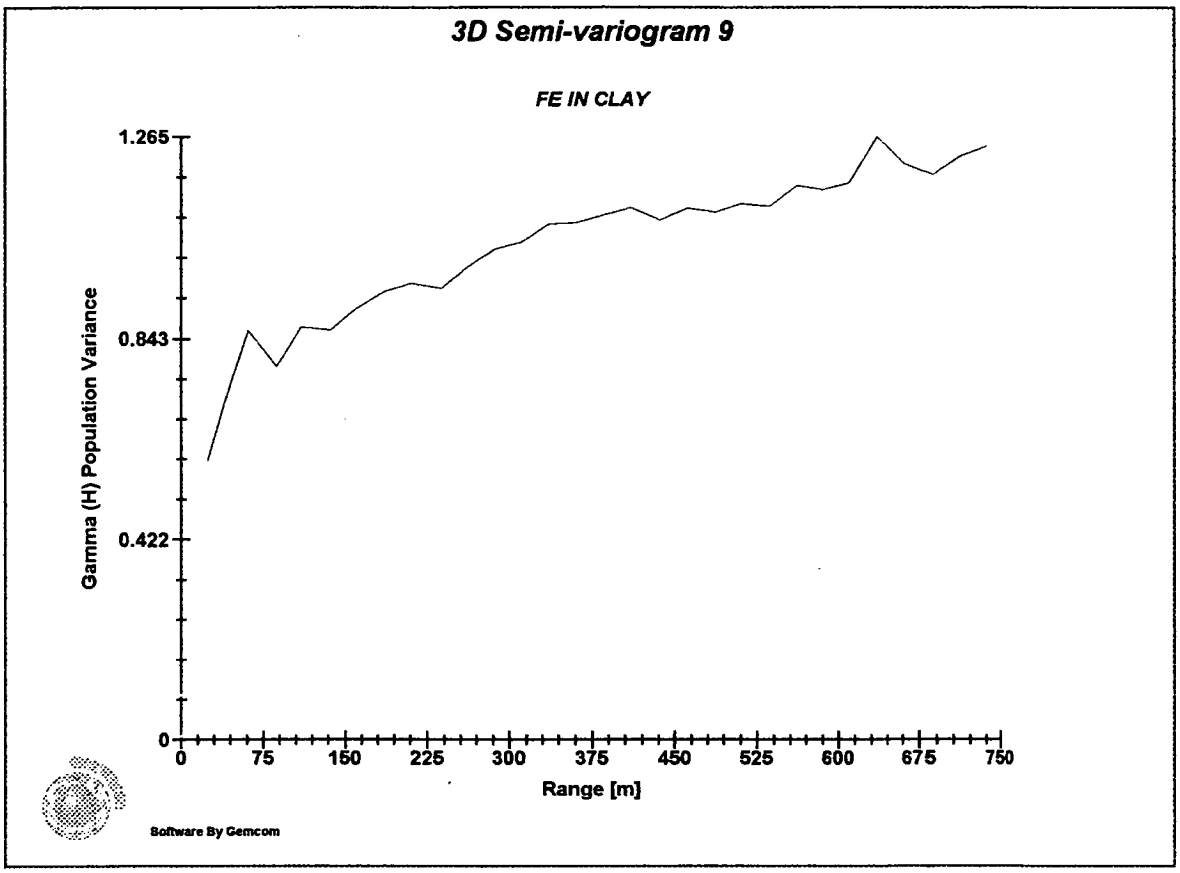
3D Semi-variogram 9
FE IN CLAY
1.265
0.843
0.422
0
Gamma (H) Population Variance
0
75
150
225
300
375
450
525
600
675
750
Range [m]
Software By Gemcom

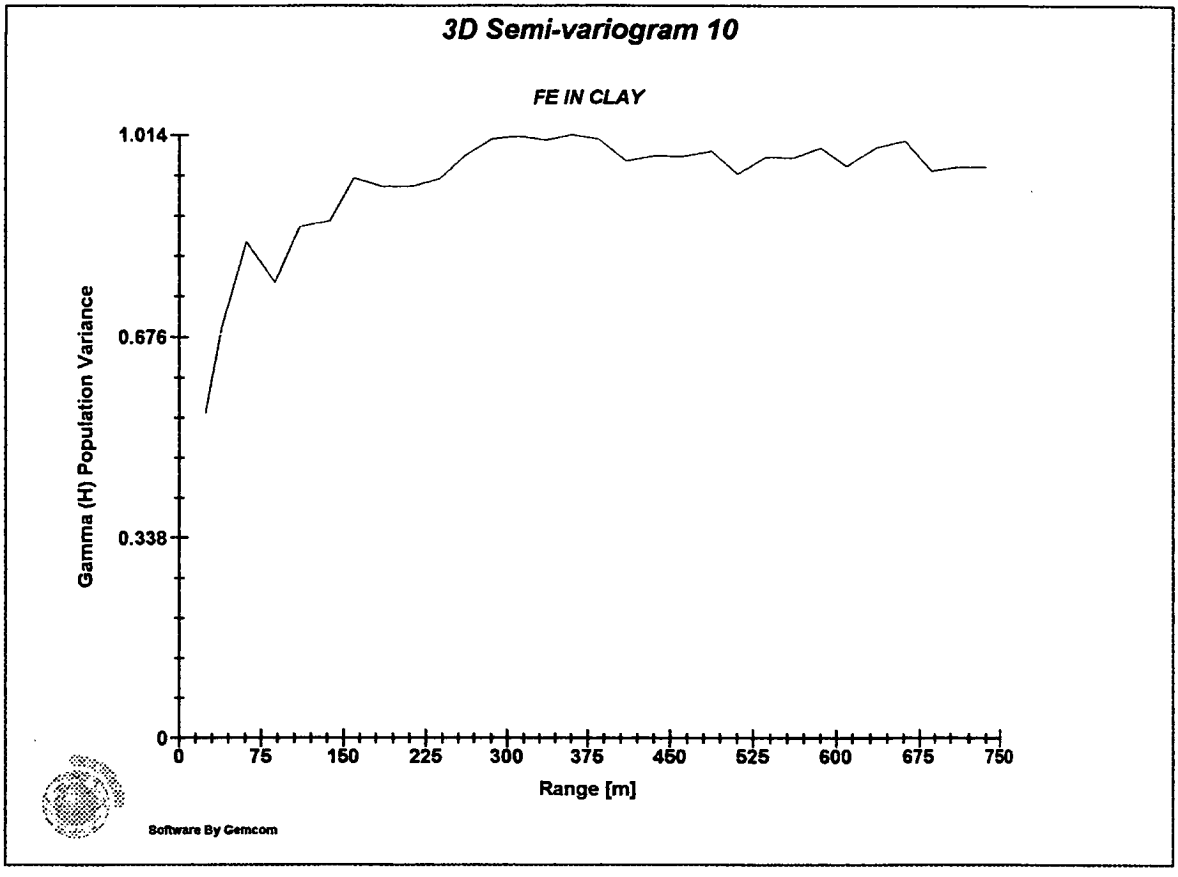
3D Semi-variogram 10
FE IN CLAY
1.014
0.676
0.338
0
Gamma (H) Population Variance
0
75
150
225
300
375
450
525
600
675
750
Range [m]
Software By Gemcom

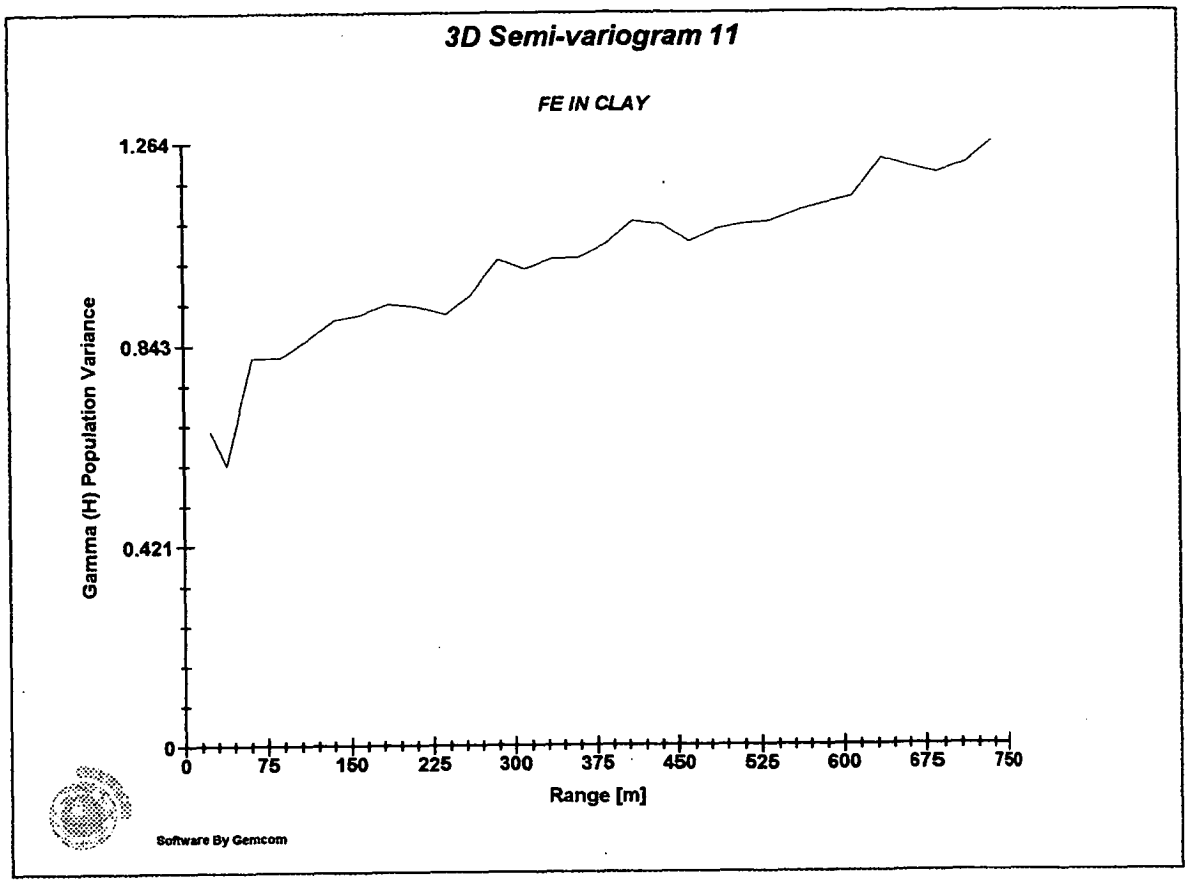
3D Semi-variogram 11
FE IN CLAY
1.264
0.843
0.421
0
Gamma (H) Population Variance
0
75
150
225
300
375
450
525
600
675
750
Range [m]
Software By Gemcom

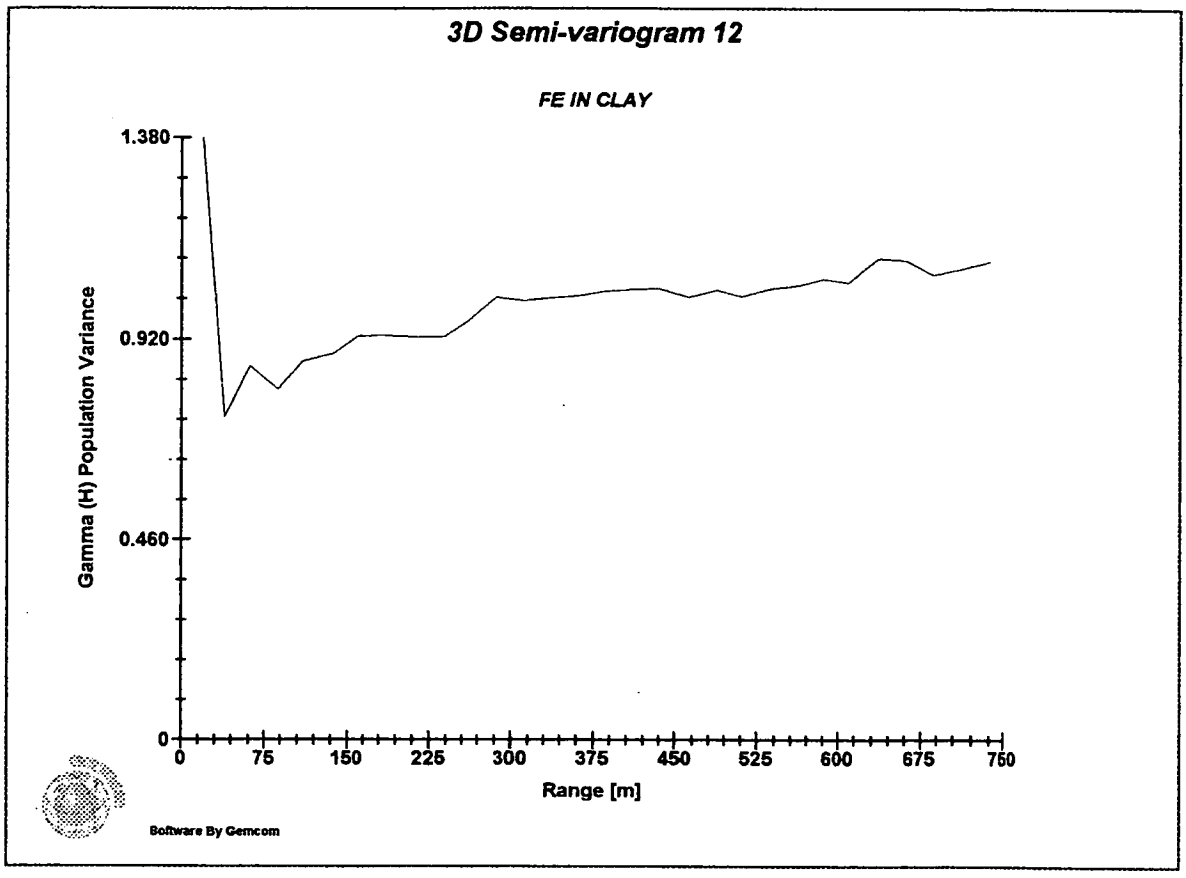
3D Semi-variogram 12
FE IN CLAY
1.380
0.920
0.460
0
Gamma (H) Population Variance
0
75
150
225
300
375
450
525
600
675
750
Range [m]
Software By Gemcom

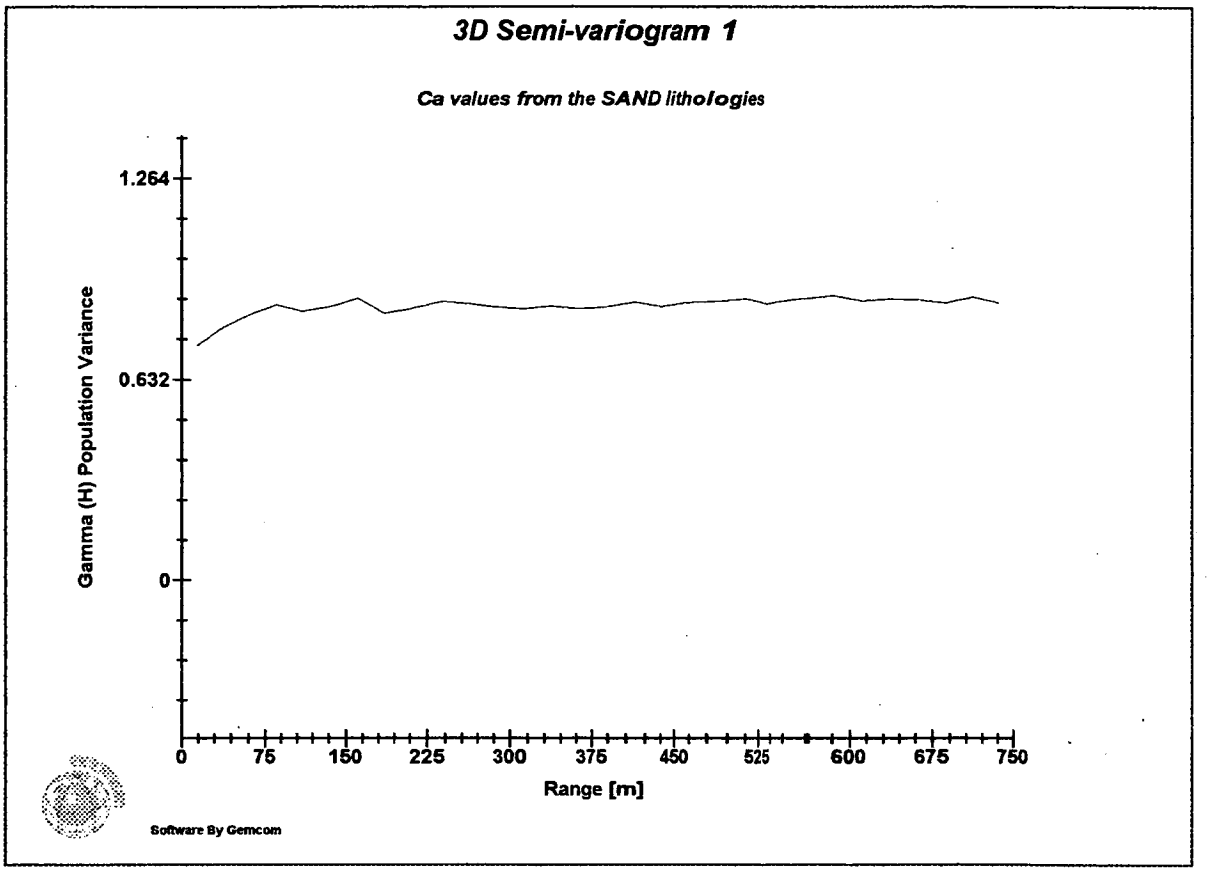
3D Semi-variogram 1
Ca values from the SAND lithologies
1.264
0.632
0
Gamma (H) Population Variance
0
75
150
225
300
375
450
525
600
675
750
Range [m]
Software By Gemcom

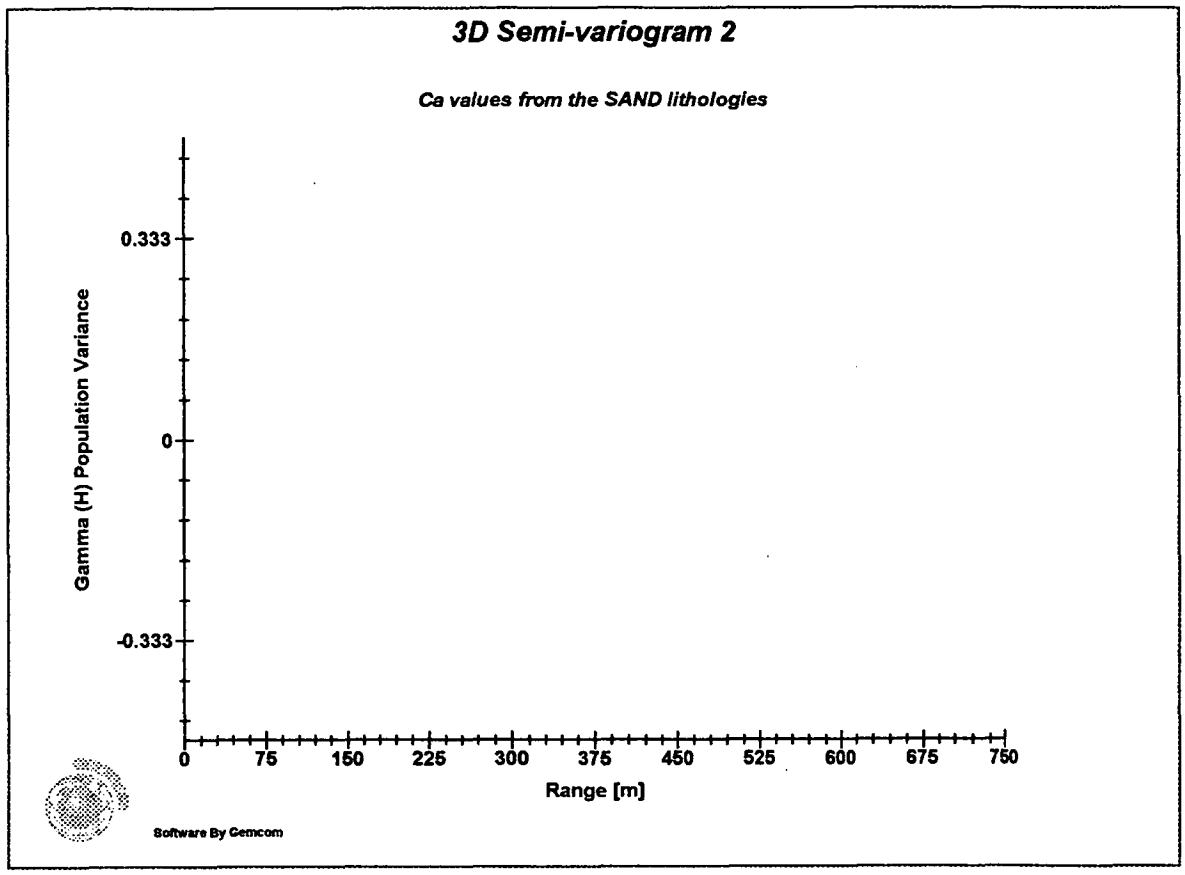
3D Semi-variogram 2
Ca values from the SAND lithologies
Gamma (H) Population Variance
0.333
0
-0.333
0
75
150
225
300
375
450
525
600
675
750
Range [m]
Software By Gemcom

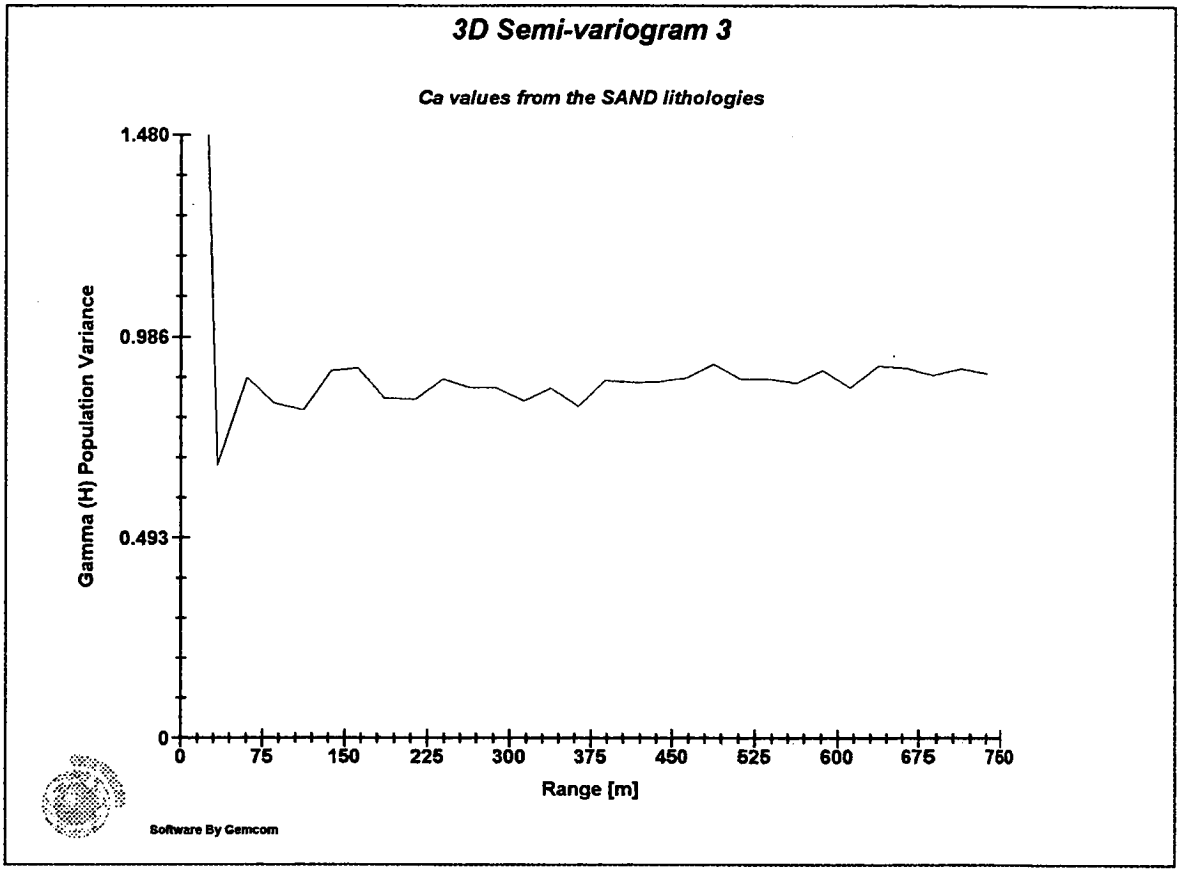
3D Semi-variogram 3
Ca values from the SAND lithologies
1.480
0.986
0.493
0
Gamma (H) Population Variance
0
75
150
225
300
375
450
525
600
675
750
Range [m]
Software By Gemcom

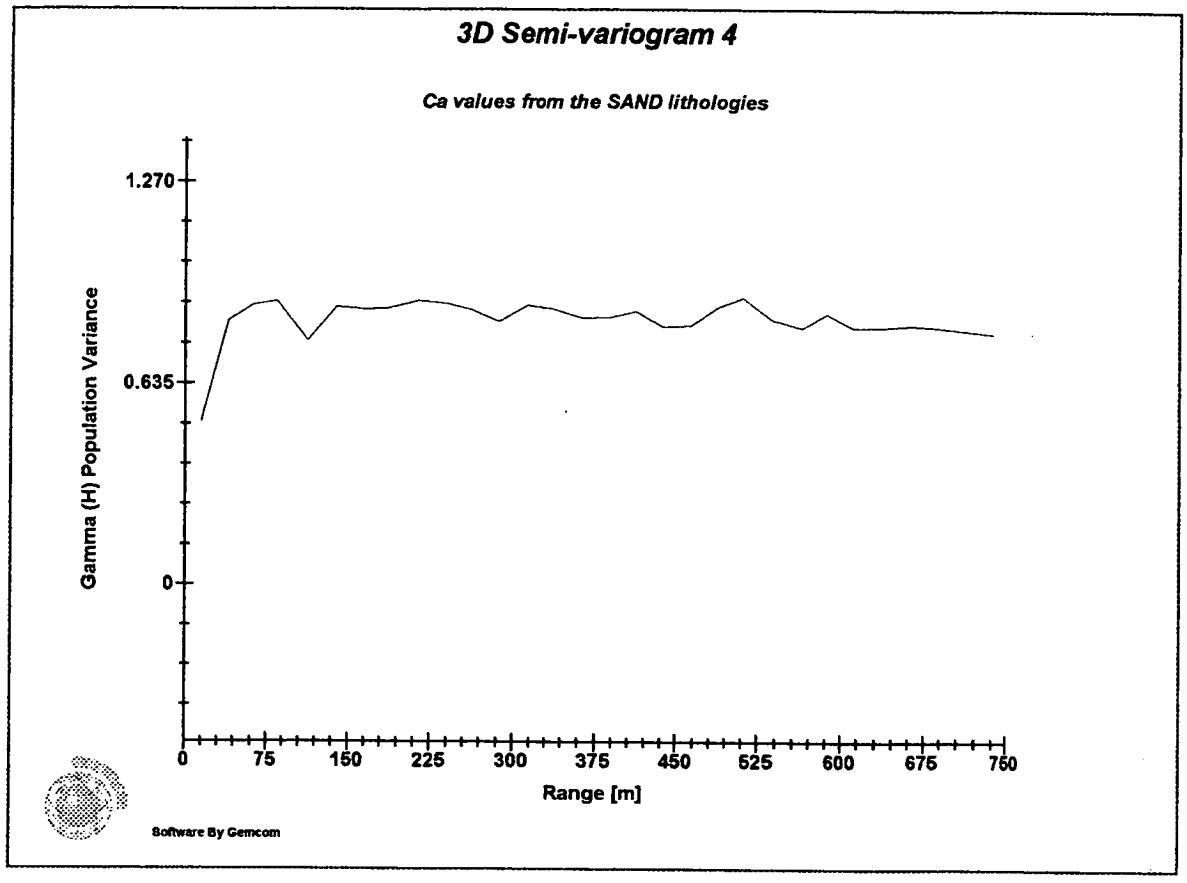
3D Semi-variogram 4
Ca values from the SAND lithologies
1.270
0.635
0
Gamma (H) Population Variance
0
75
150
225
300
375
450
525
600
675
750
Range [m]
Software By Gemcom

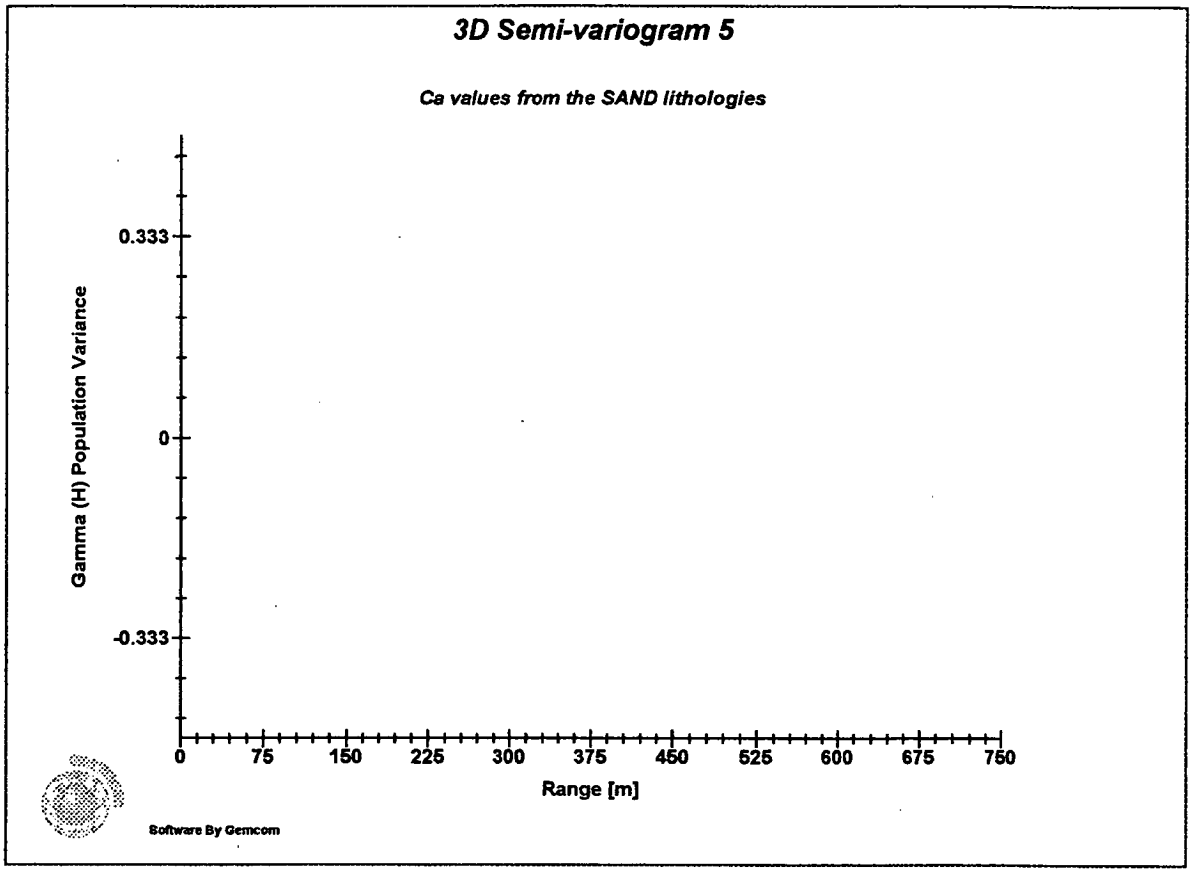
3D Semi-variogram 5
Ca values from the SAND lithologies
Gamma (H) Population Variance
0.333
0
-0.333
0
75
150
225
300
375
450
525
600
675
750
Range [m]
Software By Gemcom

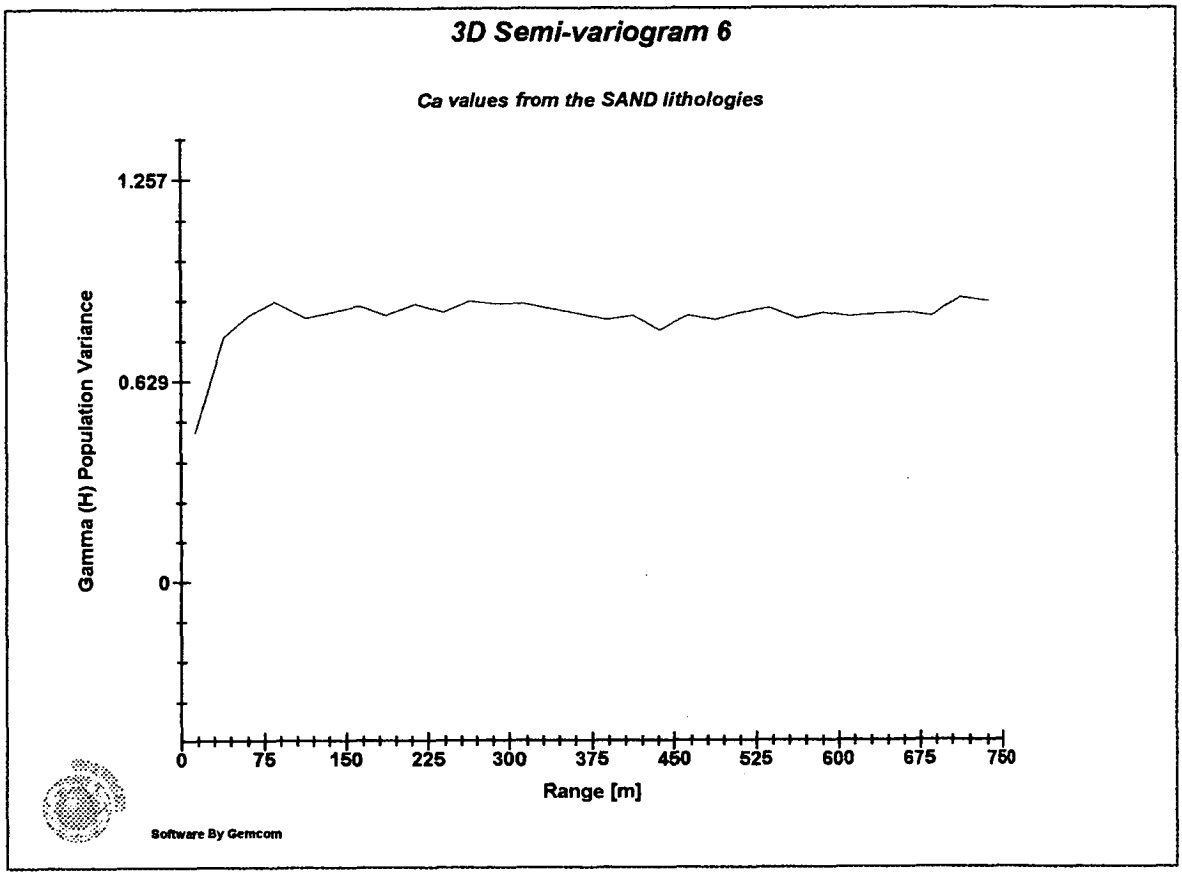
3D Semi-variogram 6
Ca values from the SAND lithologies
1.257
0.629
0
Gamma (H) Population Variance
0
75
150
225
300
375
450
525
600
675
750
Range [m]
Software By Gemcom

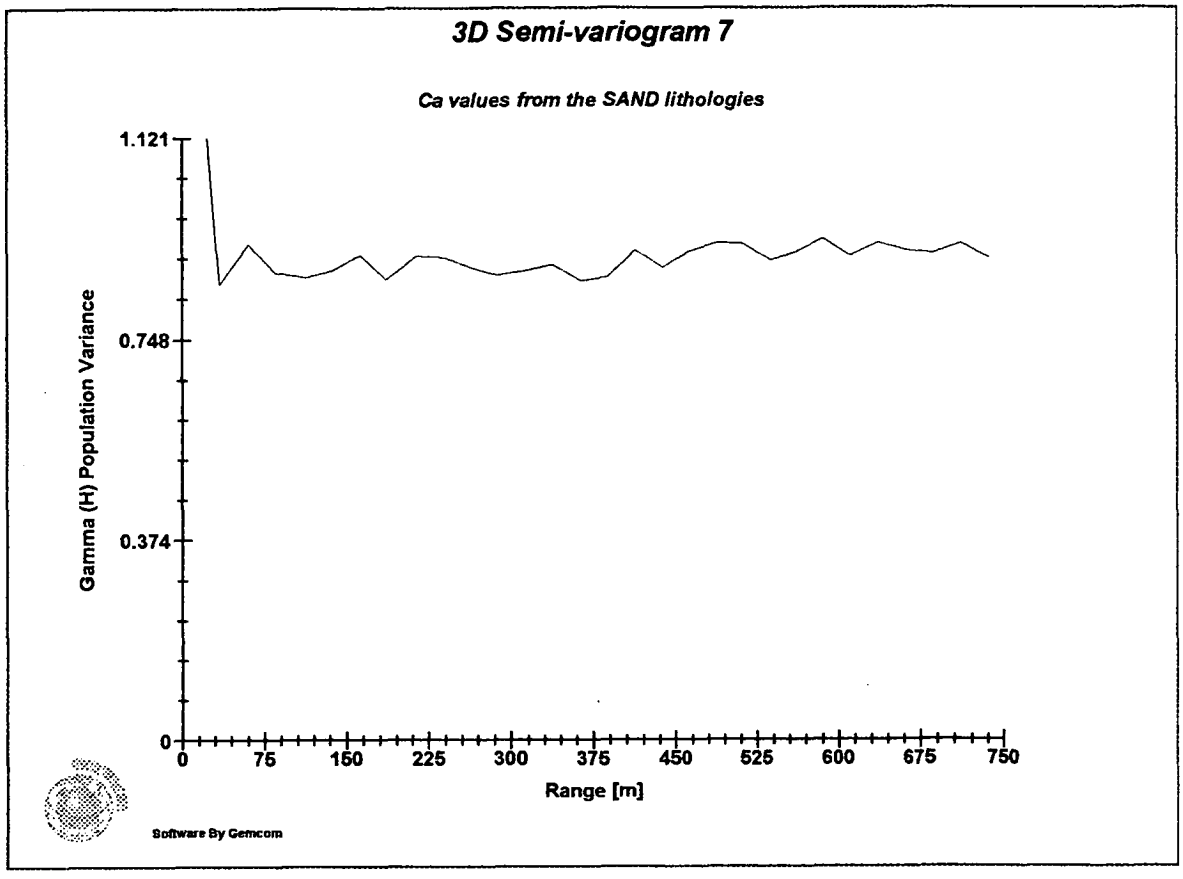
3D Semi-variogram 7
Ca values from the SAND lithologies
1.121
0.748
0.374
0
Gamma (H) Population Variance
0
75
150
225
300
375
450
525
600
675
750
Range [m]
Software By Gemcom

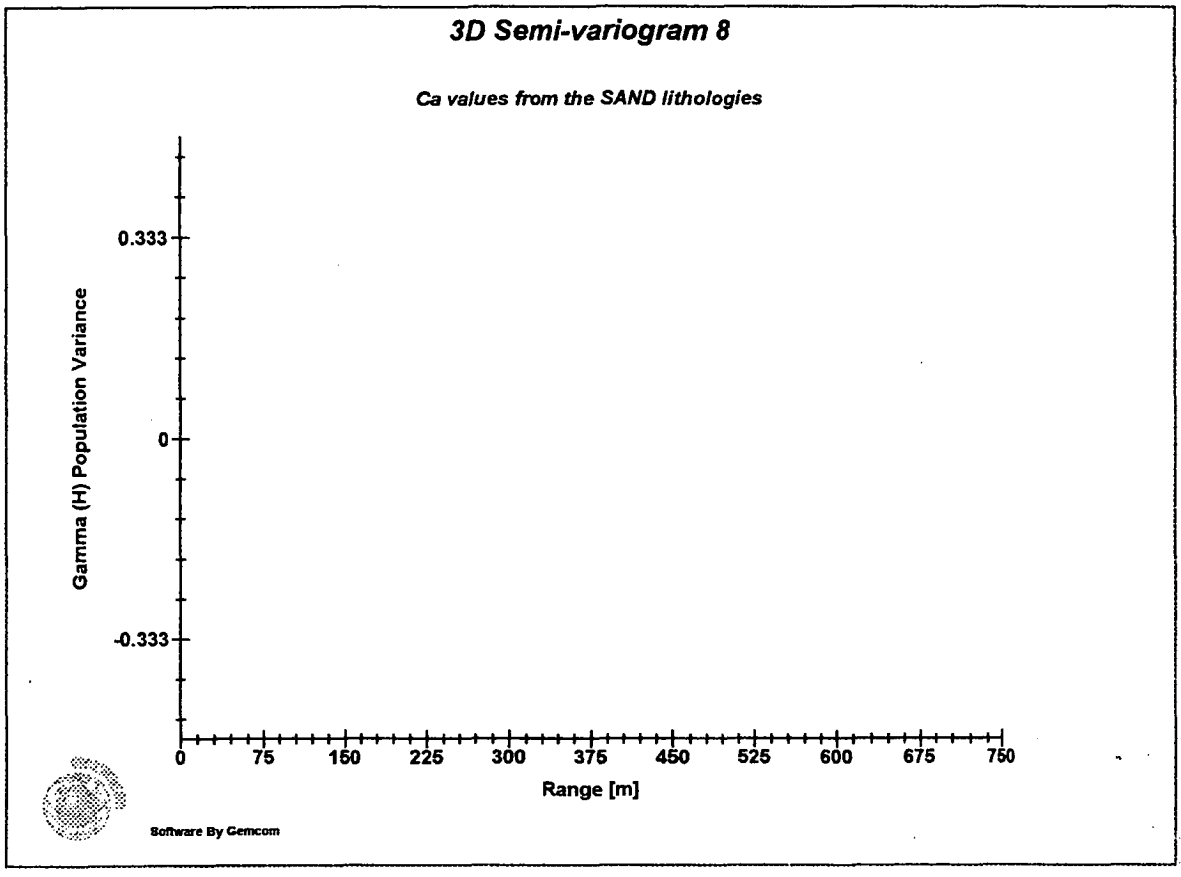
3D Semi-variogram 8
Ca values from the SAND lithologies
Gamma (H) Population Variance
0.333
0
-0.333
0
75
150
225
300
375
450
525
600
675
750
Range [m]
Software By Gemcom

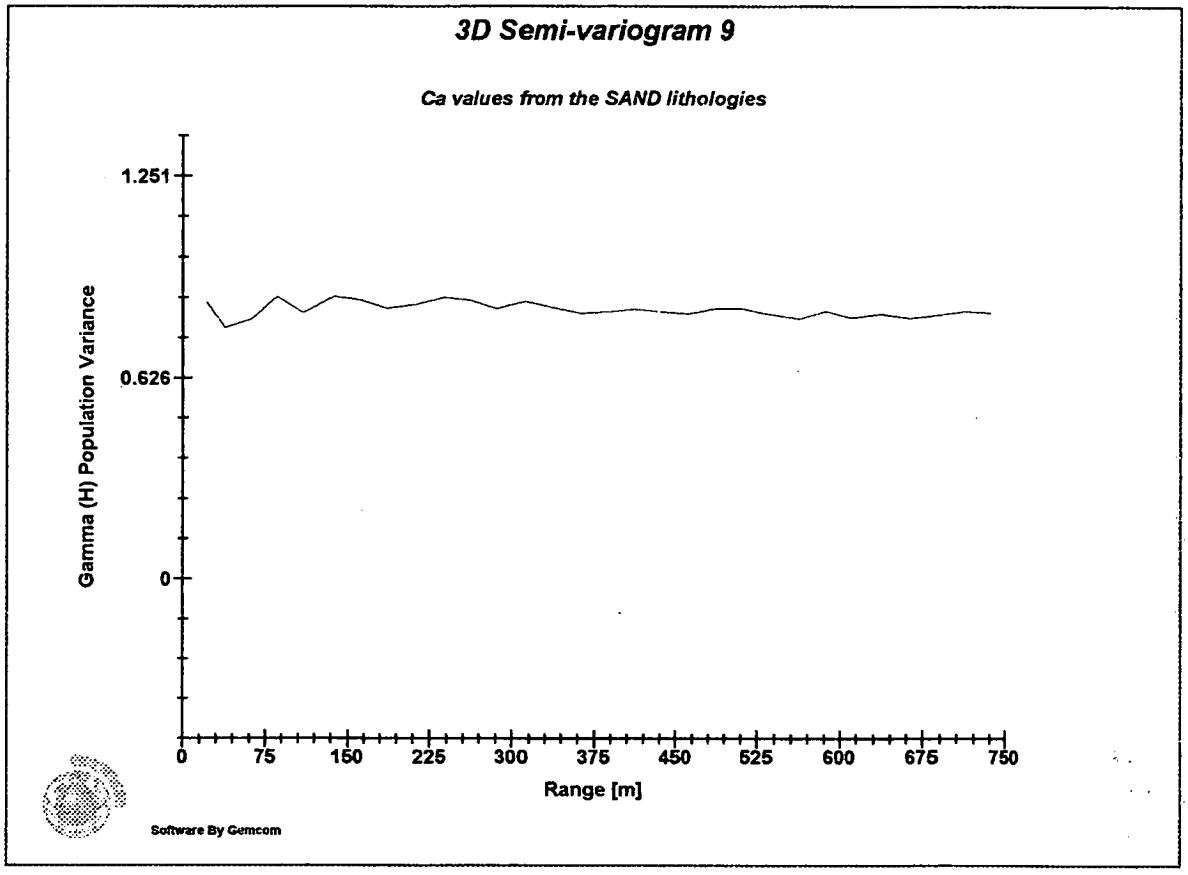
3D Semi-variogram 9
Ca values from the SAND lithologies
1.251
0.626
0
Gamma (H) Population Variance
0
75
150
225
300
375
450
525
600
675
750
Range [m]
Software By Gemcom

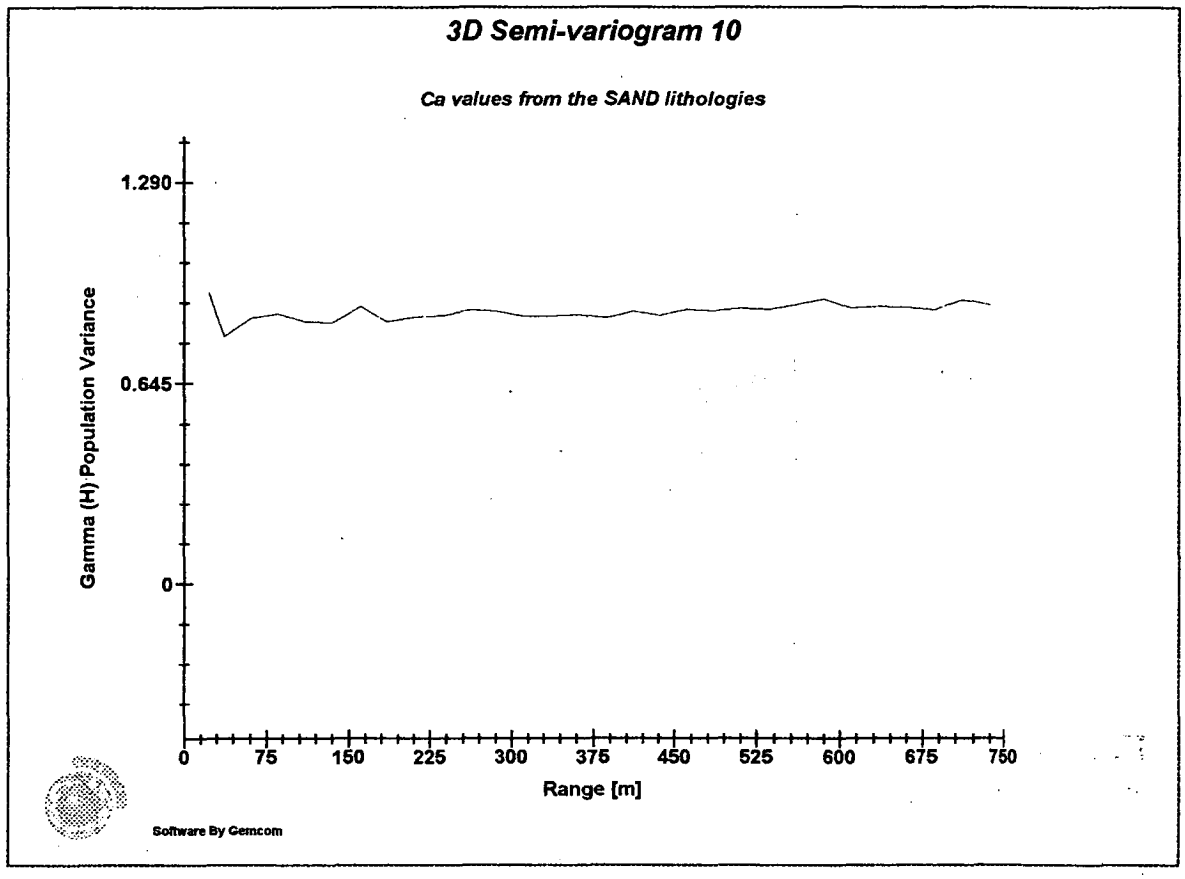
3D Semi-variogram 10
Ca values from the SAND lithologies
1.290
0.645
0
Gamma (H) Population Variance
0
75
150
225
300
375
450
525
600
675
750
Range [m]
Software By Gemcom

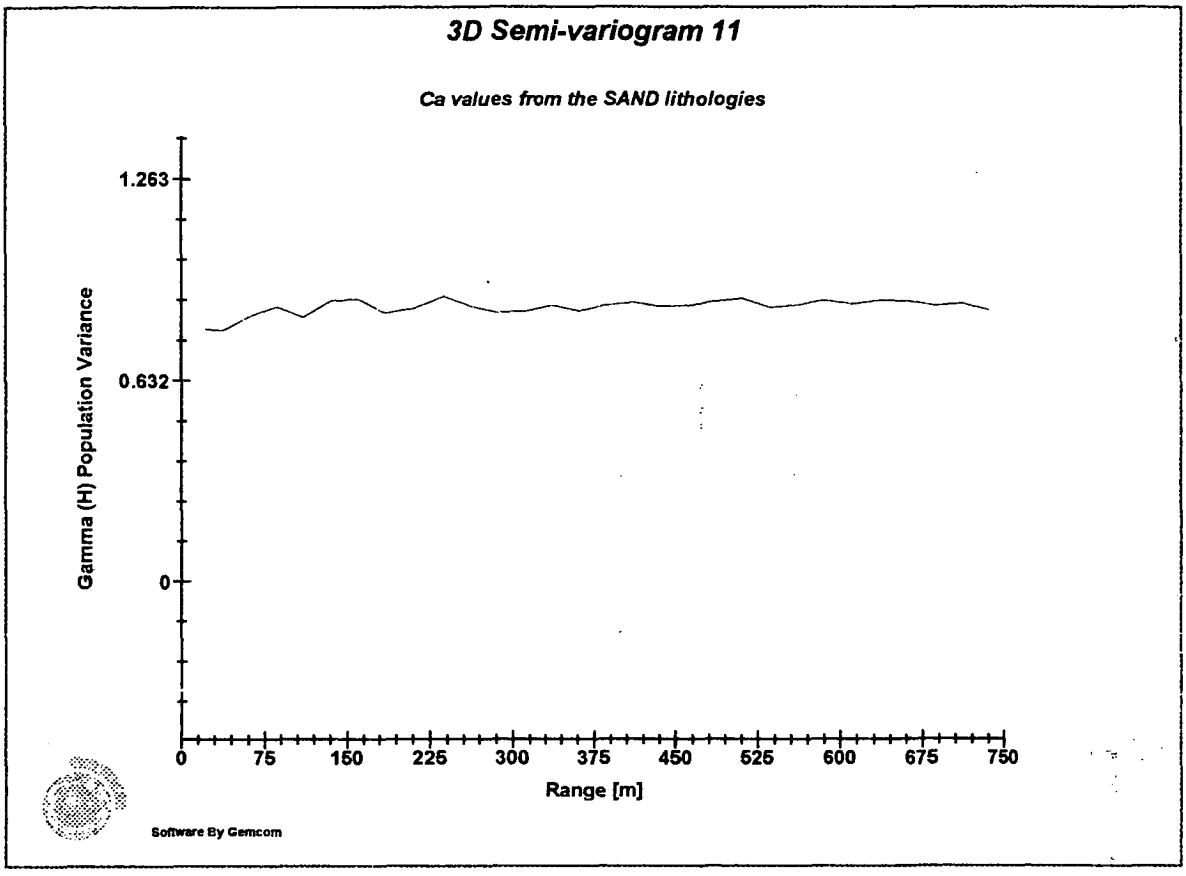
3D Semi-variogram 11
Ca values from the SAND lithologies
1.263
0.632
0
Gamma (H) Population Variance
0
75
150
225
300
375
450
525
600
675
750
Range [m]
Software By Gemcom

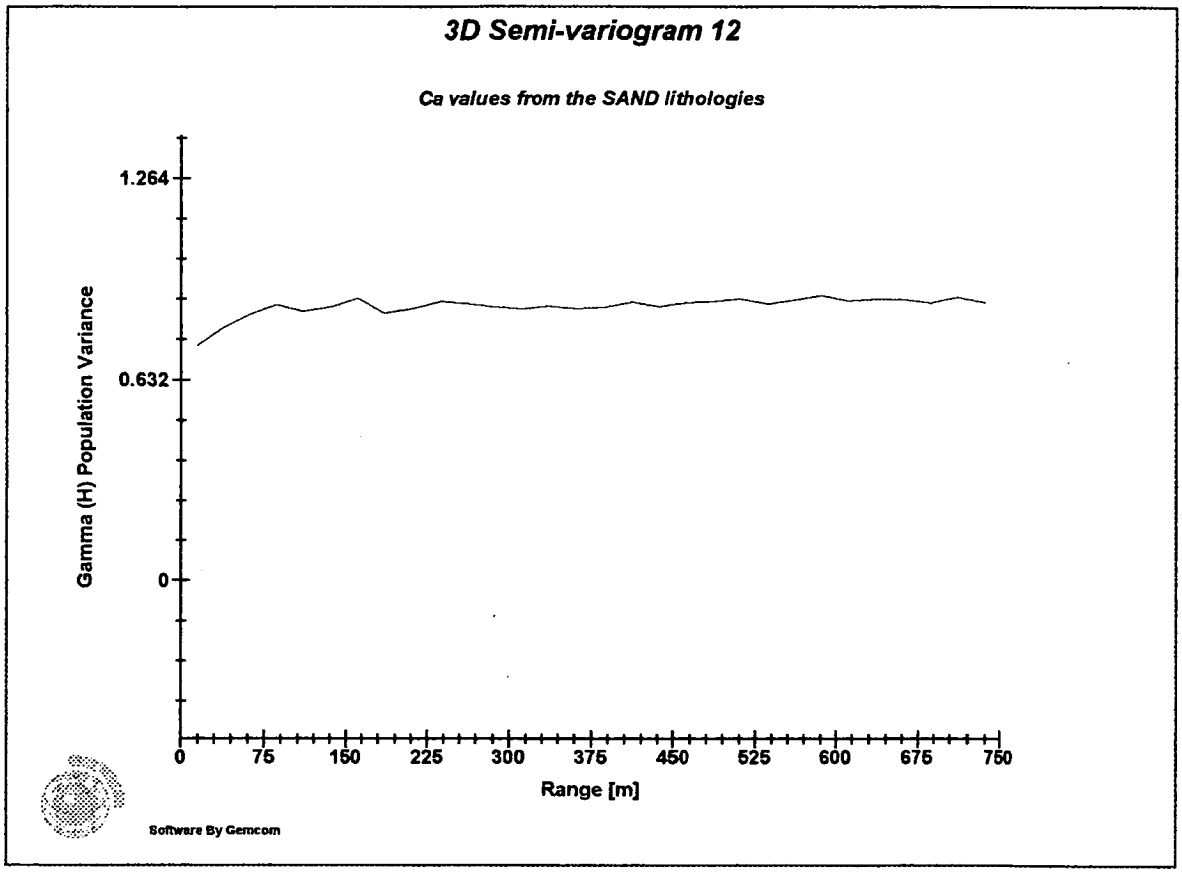
3D Semi-variogram 12
Ca values from the SAND lithologies
1.264
0.632
0
Gamma (H) Population Variance
0
75
150
225
300
375
450
525
600
675
750
Range [m]
Software By Gemcom

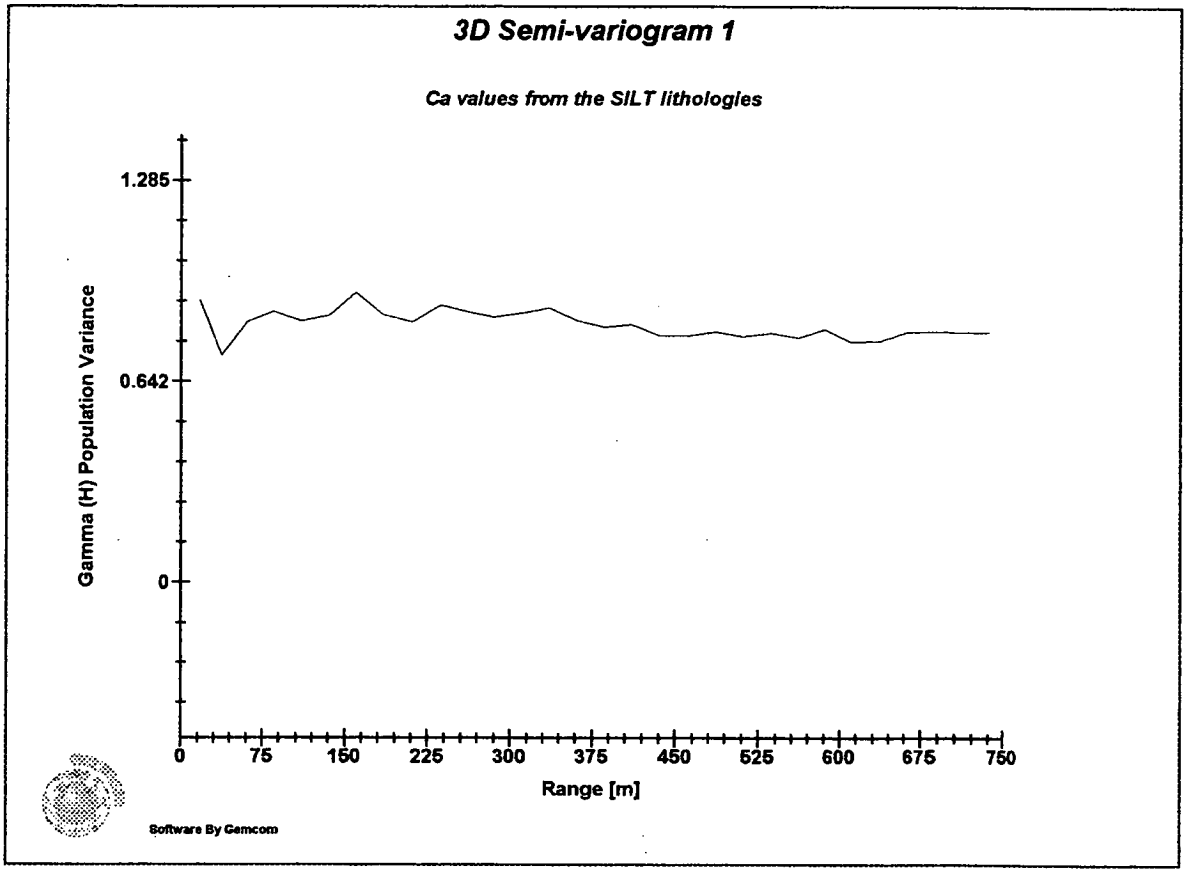
3D Semi-variogram 1
Ca values from the SILT lithologies
1.285
0.642
0
Gamma (H) Population Variance
0
75
150
225
300
375
450
525
600
675
750
Range [m]
Software By Gemcom

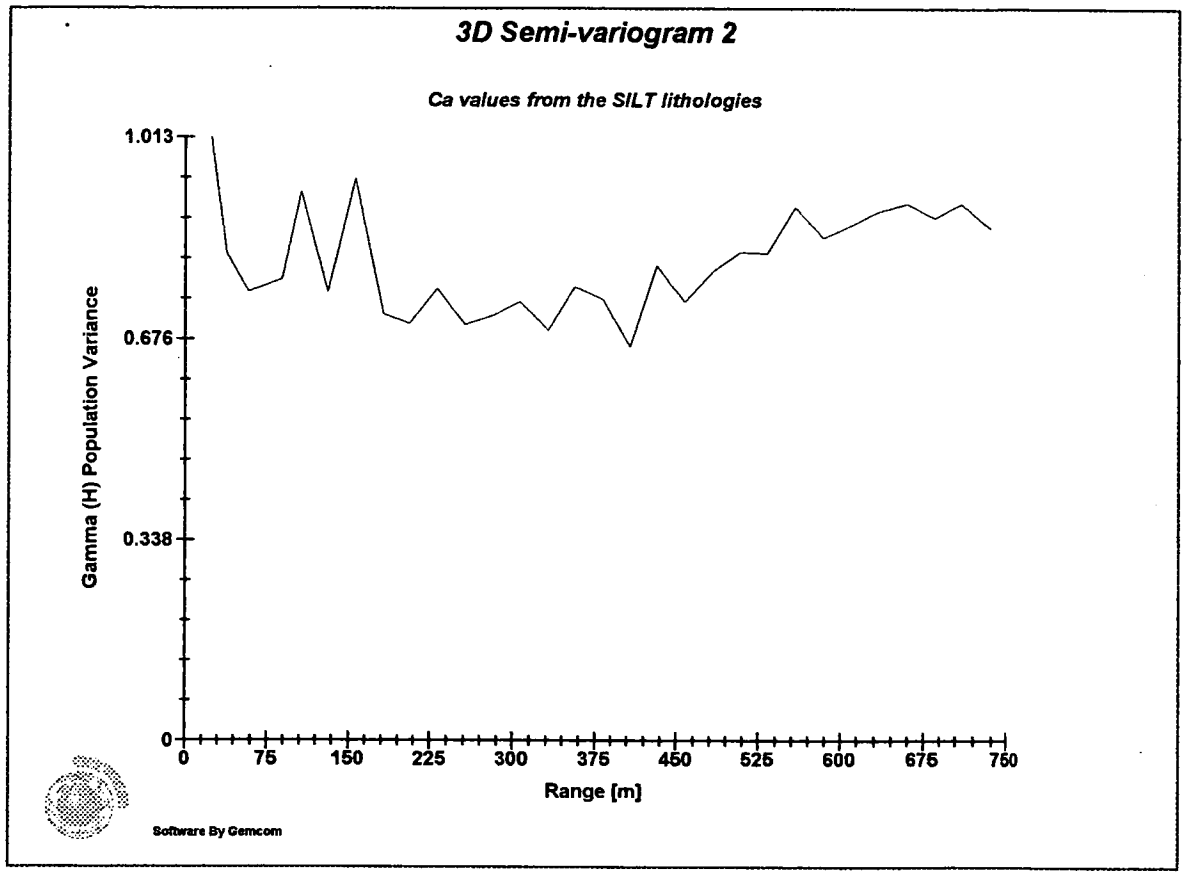
3D Semi-variogram 2
Ca values from the SILT lithologies
1.013
0.676
0.338
0
Gamma (H) Population Variance
0
75
150
225
300
375
450
525
600
675
750
Range [m]
Software By Gemcom

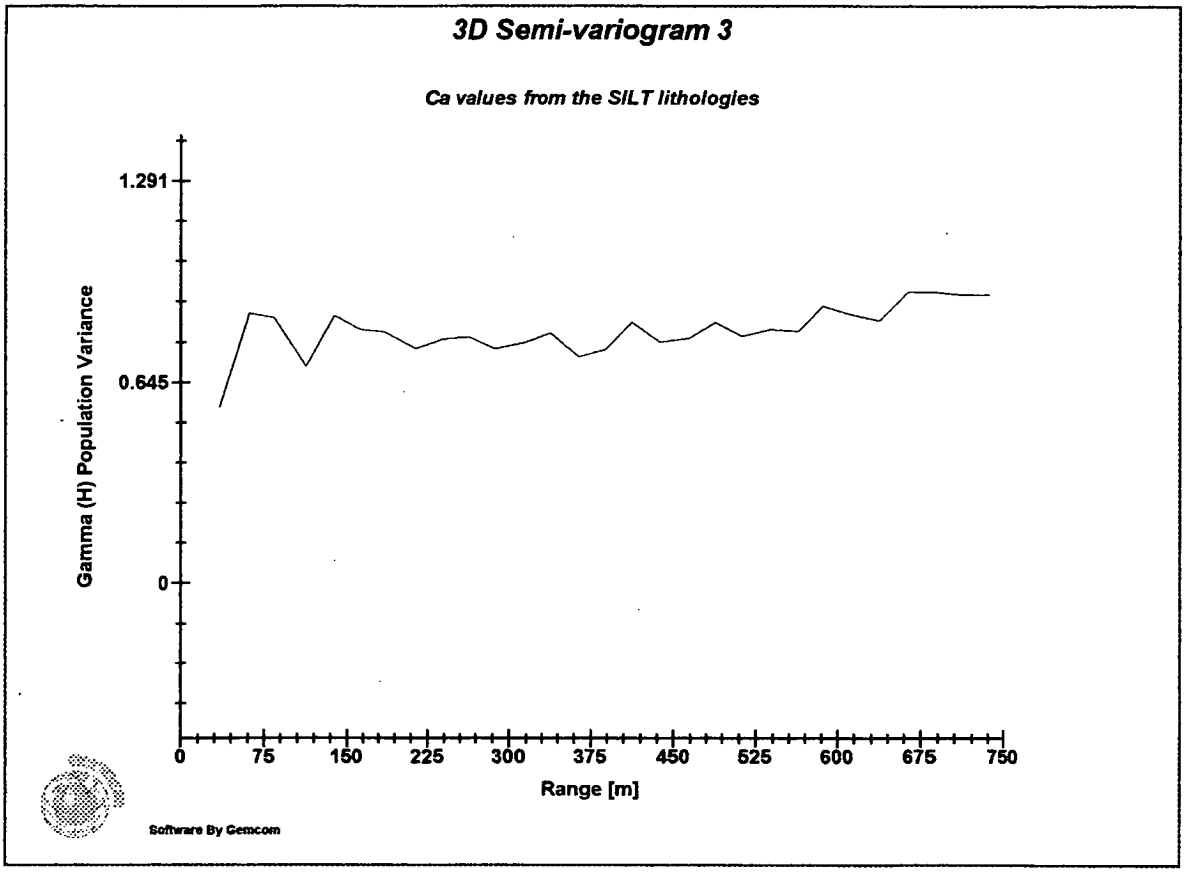
3D Semi-variogram 3
Ca values from the SILT lithologies
1.291
0.645
0
Gamma (H) Population Variance
0
75
150
225
300
375
450
525
600
675
750
Range [m]
Software By Gemcom

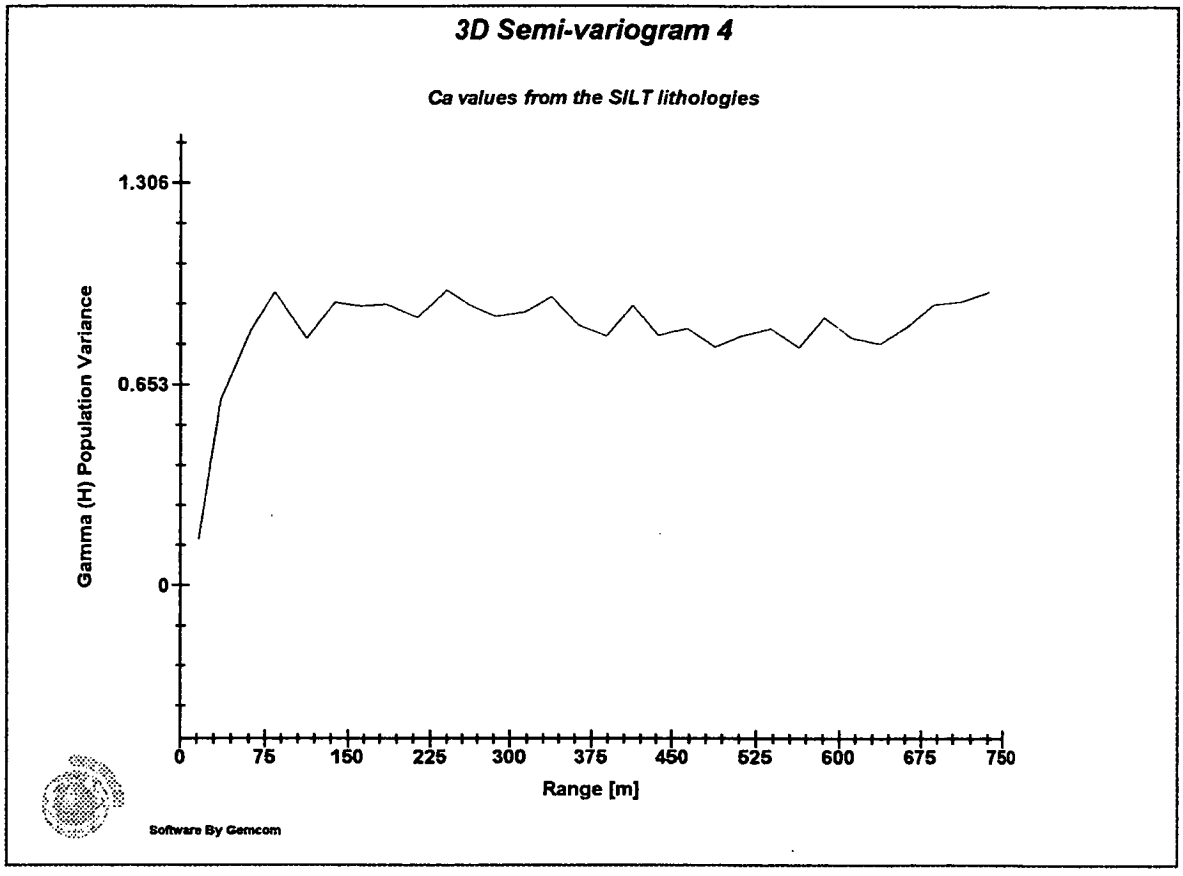
3D Semi-variogram 4
Ca values from the SILT lithologies
Gamma (H) Population Variance
1.306
0.653
0
0
75
150
225
300
375
450
525
600
675
750
Range [m]
Software By Gemcom

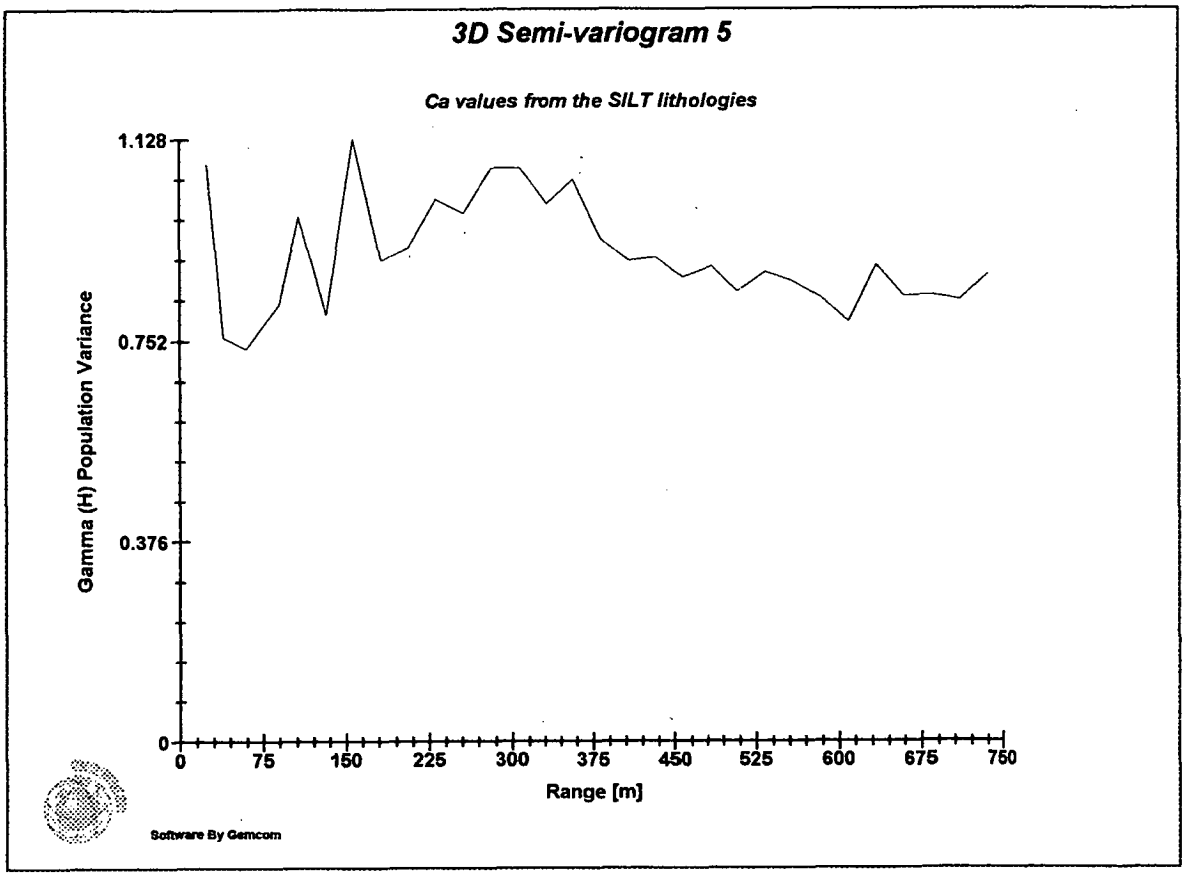
3D Semi-variogram 5
Ca values from the SILT lithologies
1.128
0.752
0.376
0
Gamma (H) Population Variance
0
75
150
225
300
375
450
525
600
675
750
Range [m]
Software By Gemcom

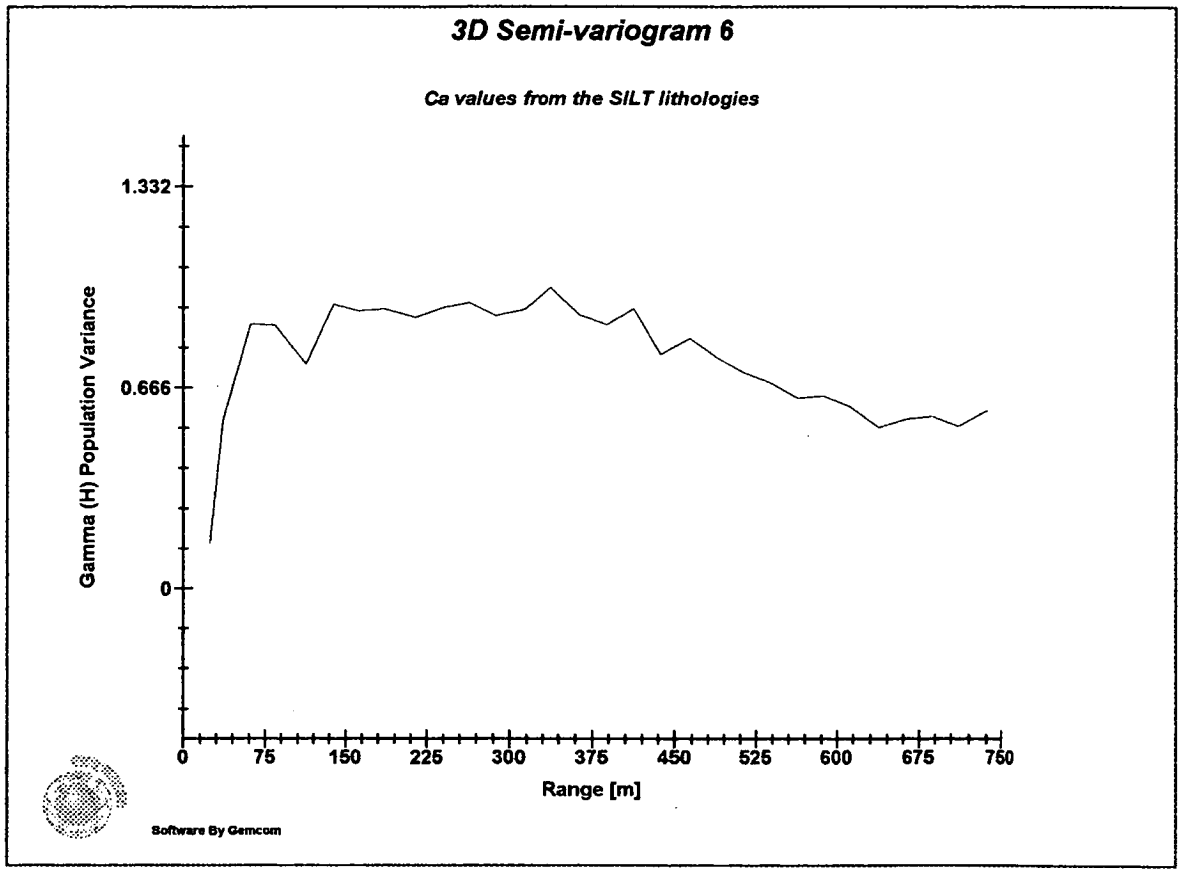
3D Semi-variogram 6
Ca values from the SILT lithologies
Gamma (H) Population Variance
1.332
0.666
0
0
75
150
225
300
375
450
525
600
675
750
Range [m]
Software By Gemcom

3D Semi-variogram 7

Ca values from the SILT lithologies

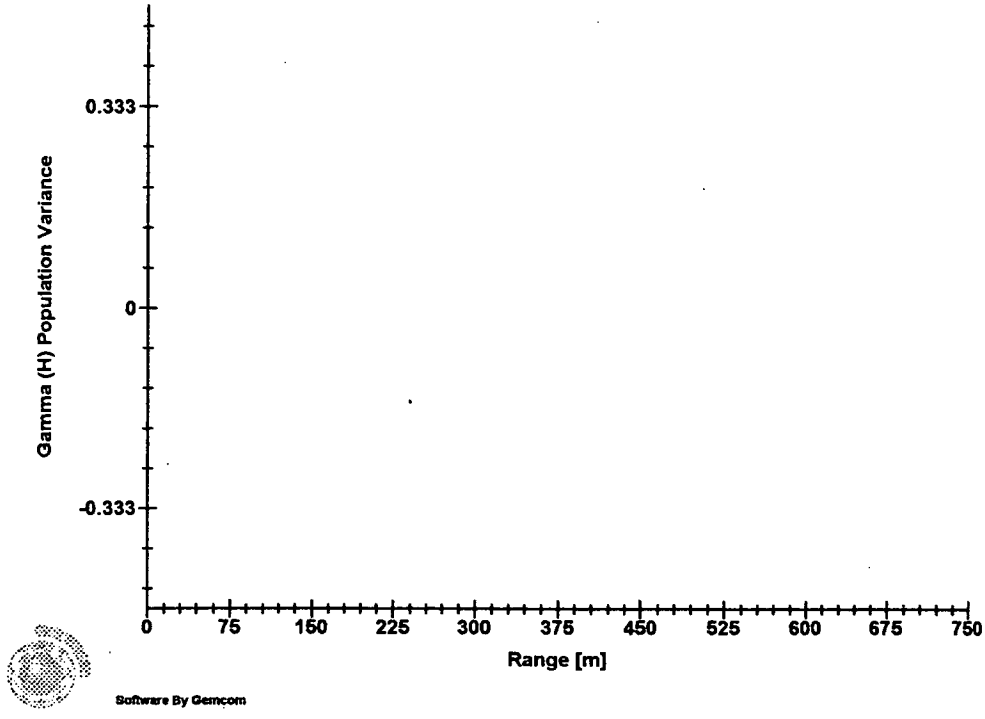

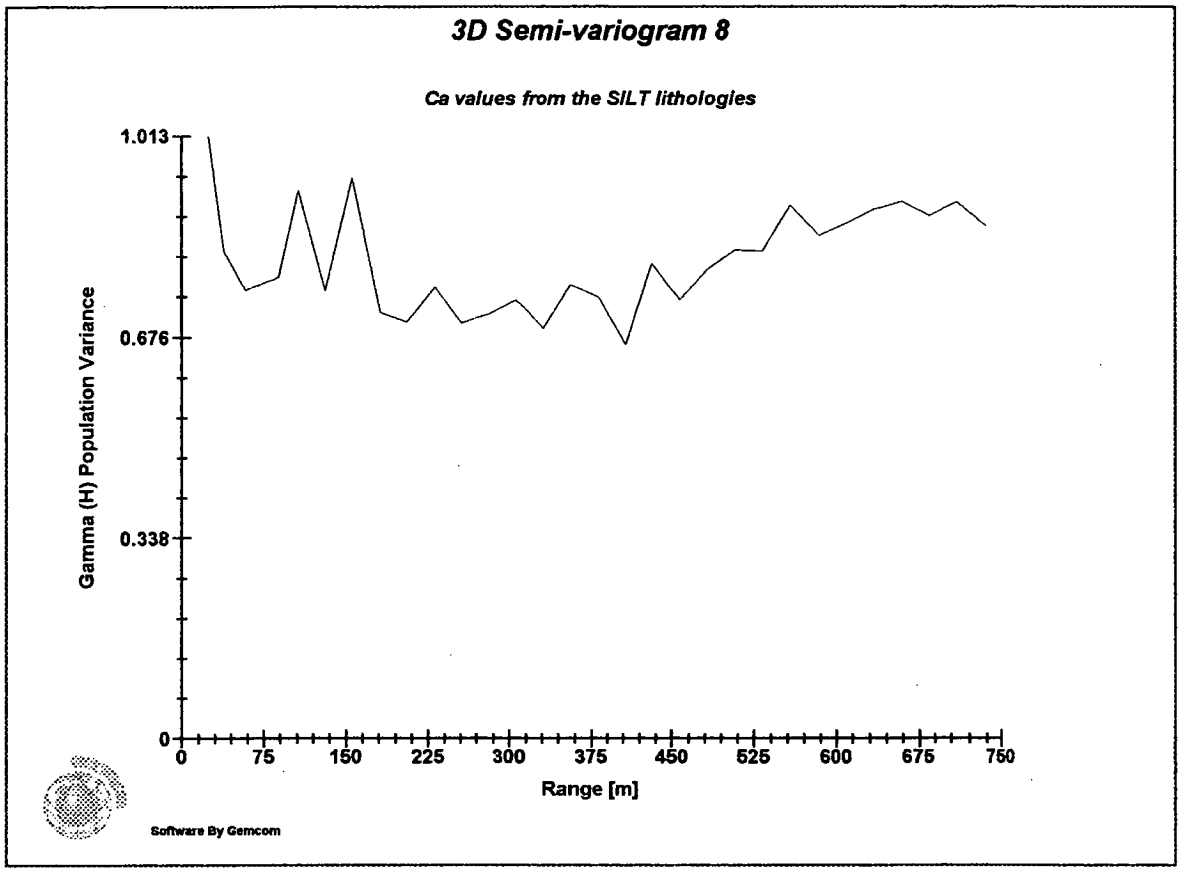
3D Semi-variogram 8
Ca values from the SILT lithologies
1.013
0.676
0.338
0
Gamma (H) Population Variance
0
75
150
225
300
375
450
525
600
675
750
Range [m]
Software By Gemcom

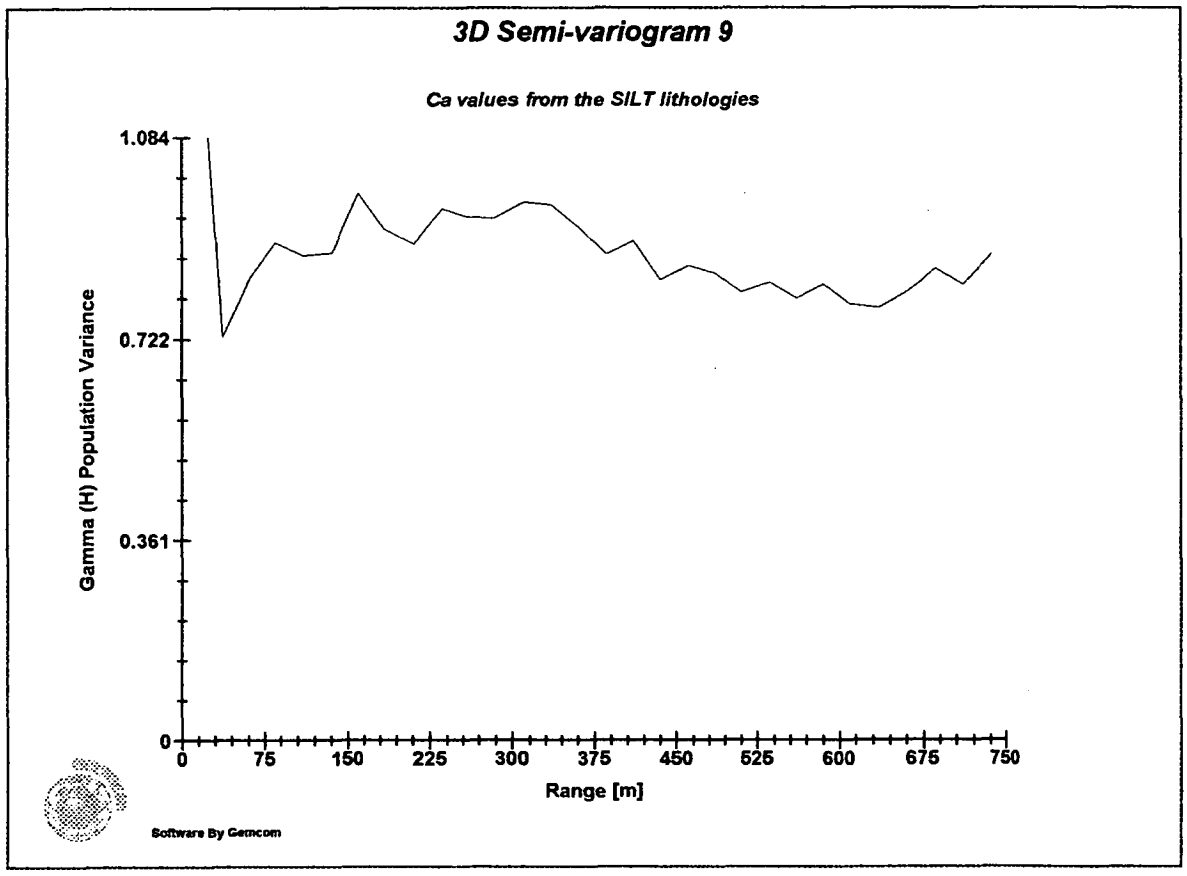
3D Semi-variogram 9
Ca values from the SILT lithologies
1.084
0.722
0.361
0
Gamma (H) Population Variance
0
75
150
225
300
375
450
525
600
675
750
Range [m]
Software By Gemcom

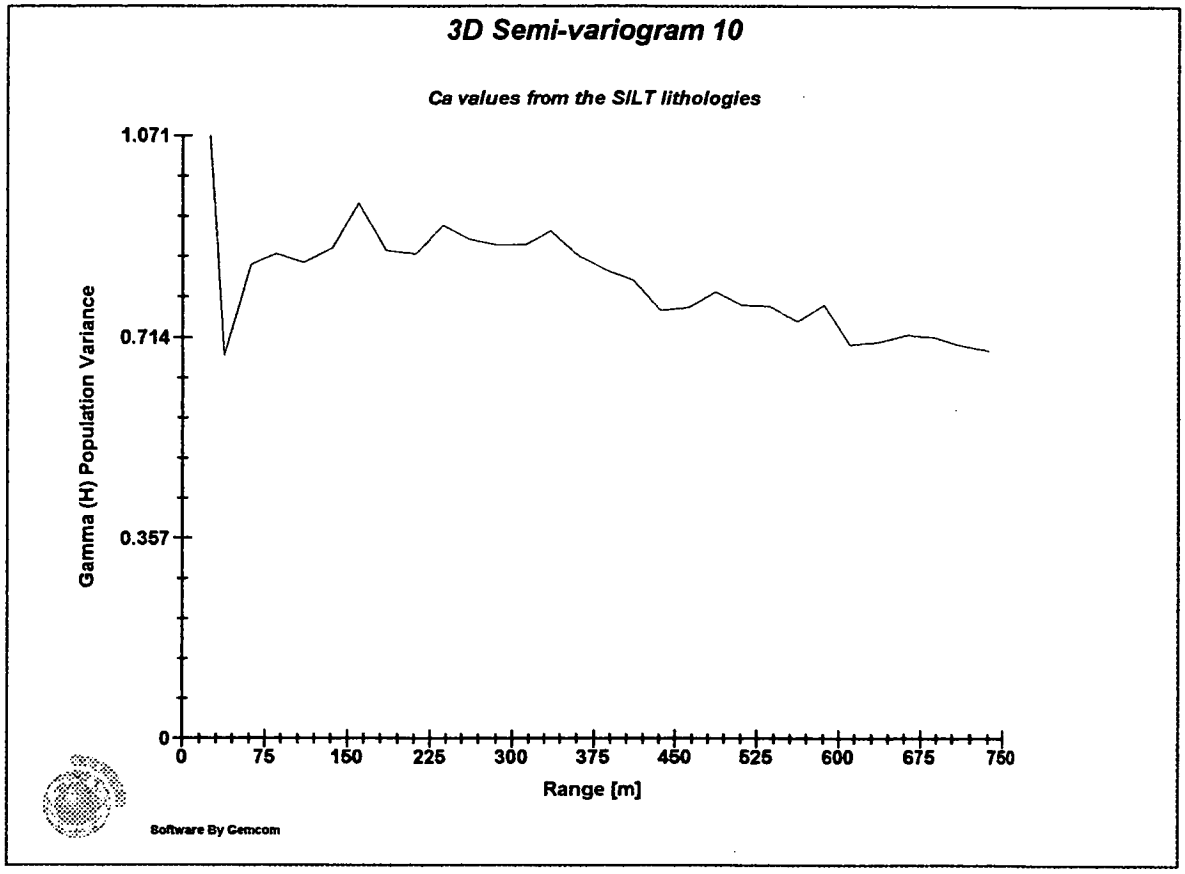
3D Semi-variogram 10
Ca values from the SILT lithologies
Gamma (H) Population Variance
1.071
0.714
0.357
0
0
75
150
225
300
375
450
525
600
675
750
Range [m]
Software By Gemcom

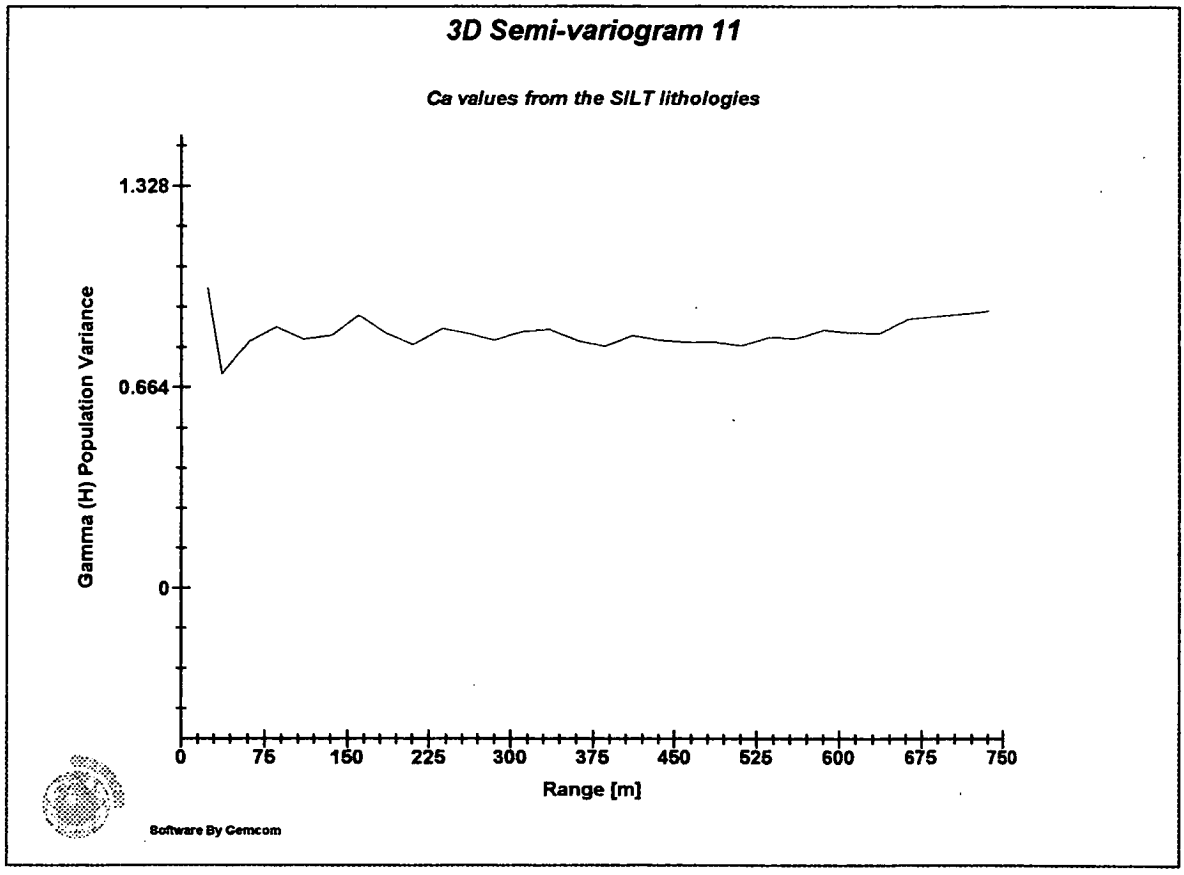
3D Semi-variogram 11
Ca values from the SILT lithologies
1.328
0.664
0
Gamma (H) Population Variance
0
75
150
225
300
375
450
525
600
675
750
Range [m]
Software By Gemcom

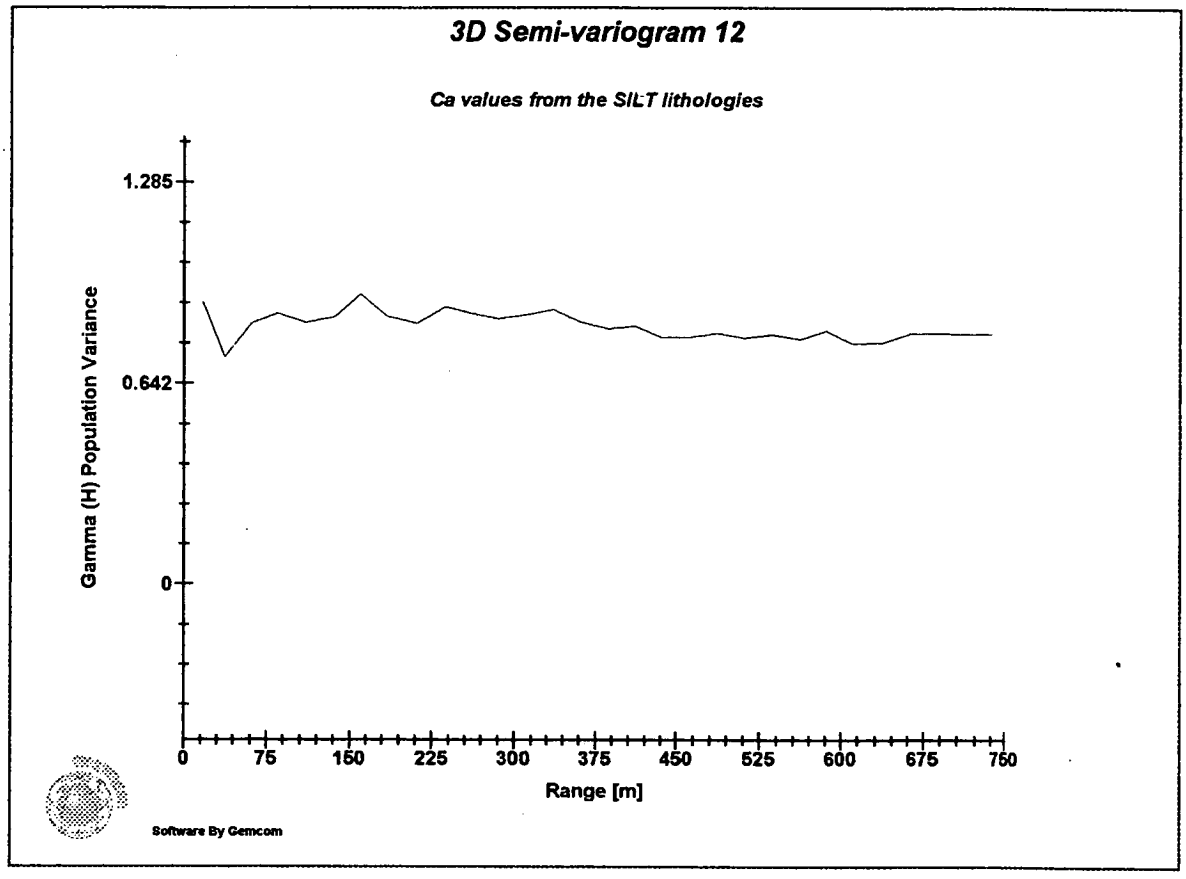
3D Semi-variogram 12
Ca values from the SILT lithologies
Gamma (H) Population Variance
1.285
0.642
0
0
75
150
225
300
375
450
525
600
675
750
Range [m]
Software By Gemcom

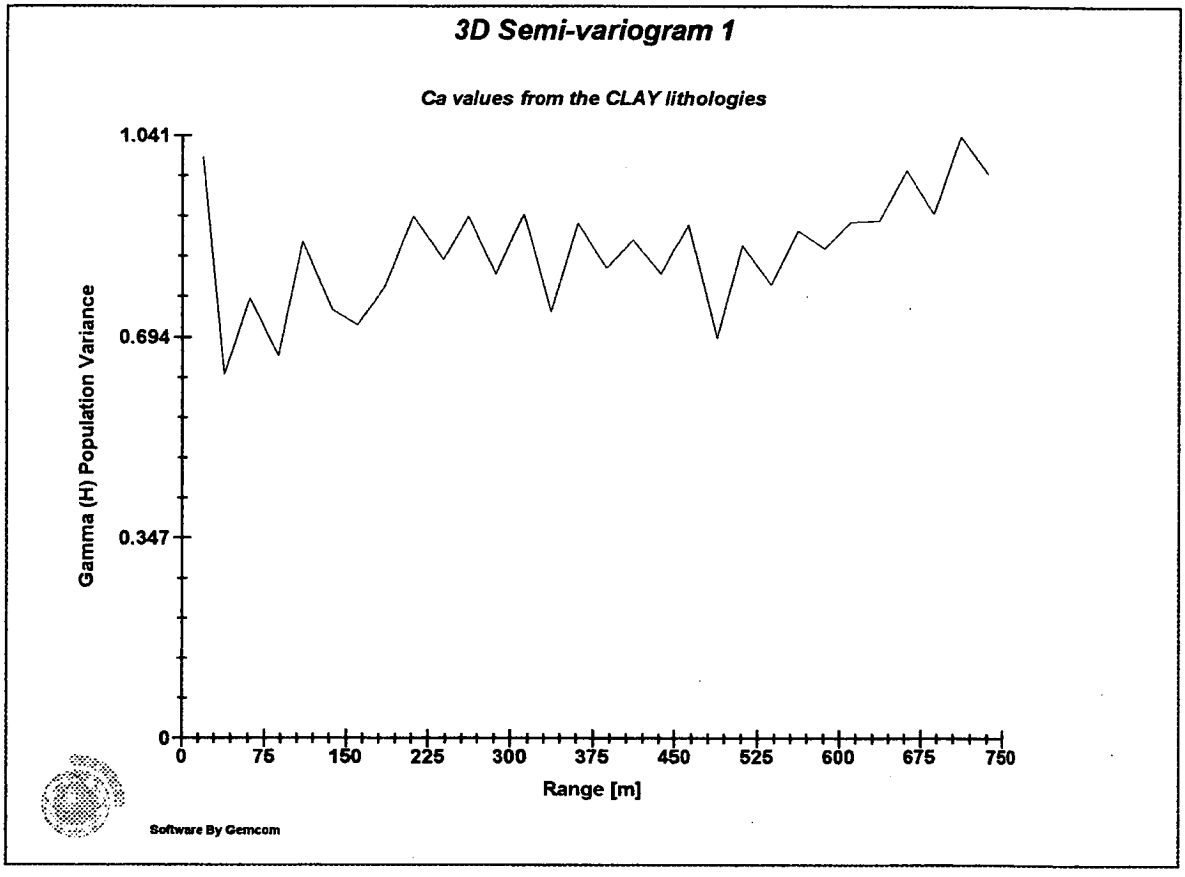
3D Semi-variogram 1
Ca values from the CLAY lithologies
Gamma (H) Population Variance
1.041
0.694
0.347
0
0
75
150
225
300
375
450
525
600
675
750
Range [m]
Software By Gemcom

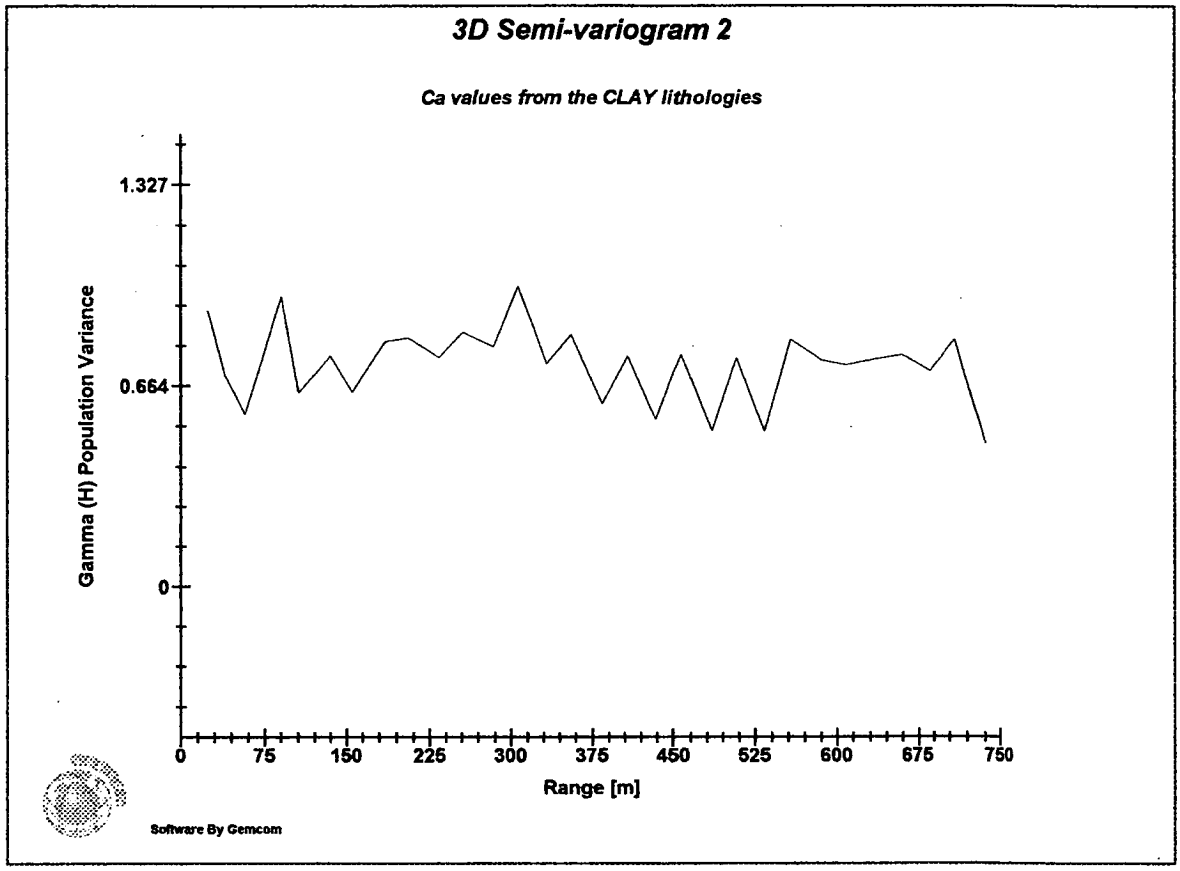
3D Semi-variogram 2
Ca values from the CLAY lithologies
Gamma (H) Population Variance
1.327
0.664
0
0
75
150
225
300
375
450
525
600
675
750
Range [m]
Software By Gemcom

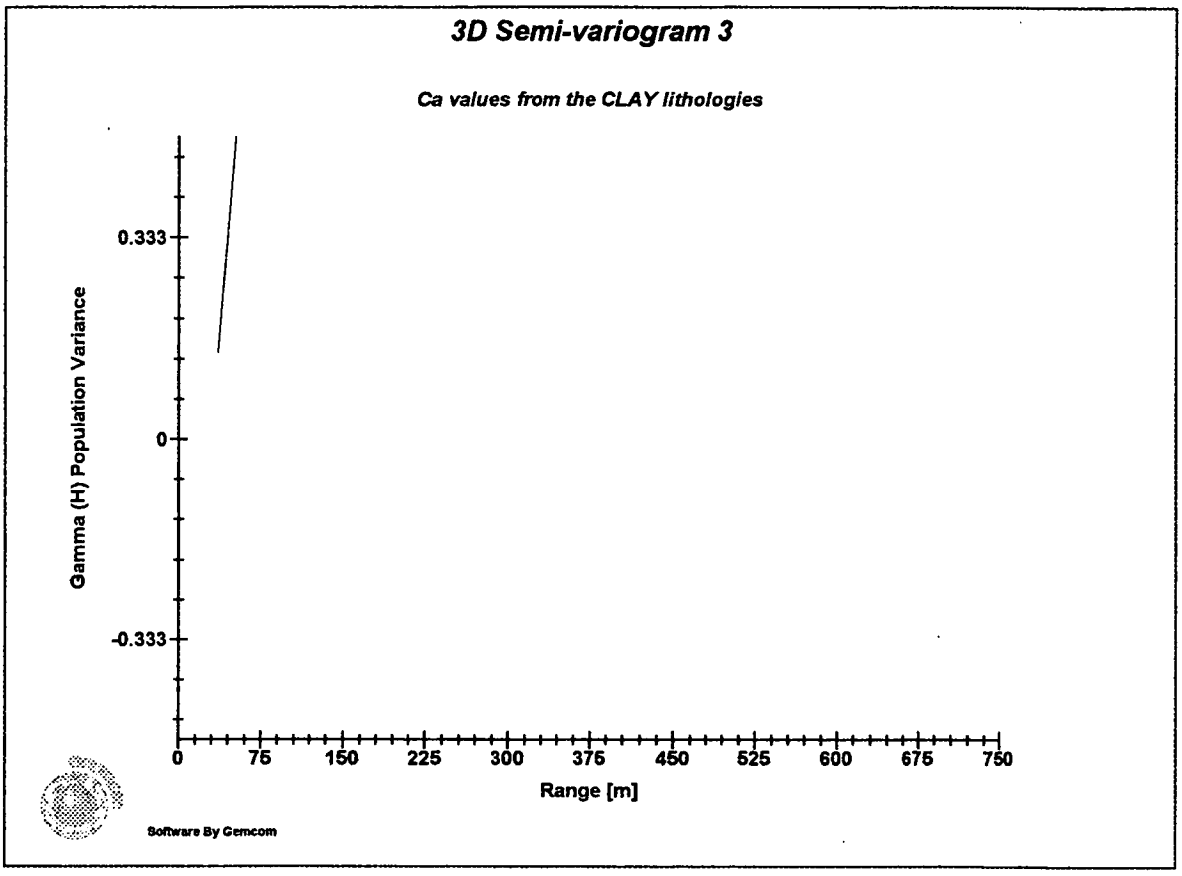
3D Semi-variogram 3
Ca values from the CLAY lithologies
Gamma (H) Population Variance
0.333
0
-0.333
0
75
150
225
300
375
450
525
600
675
750
Range [m]
Software By Gemcom

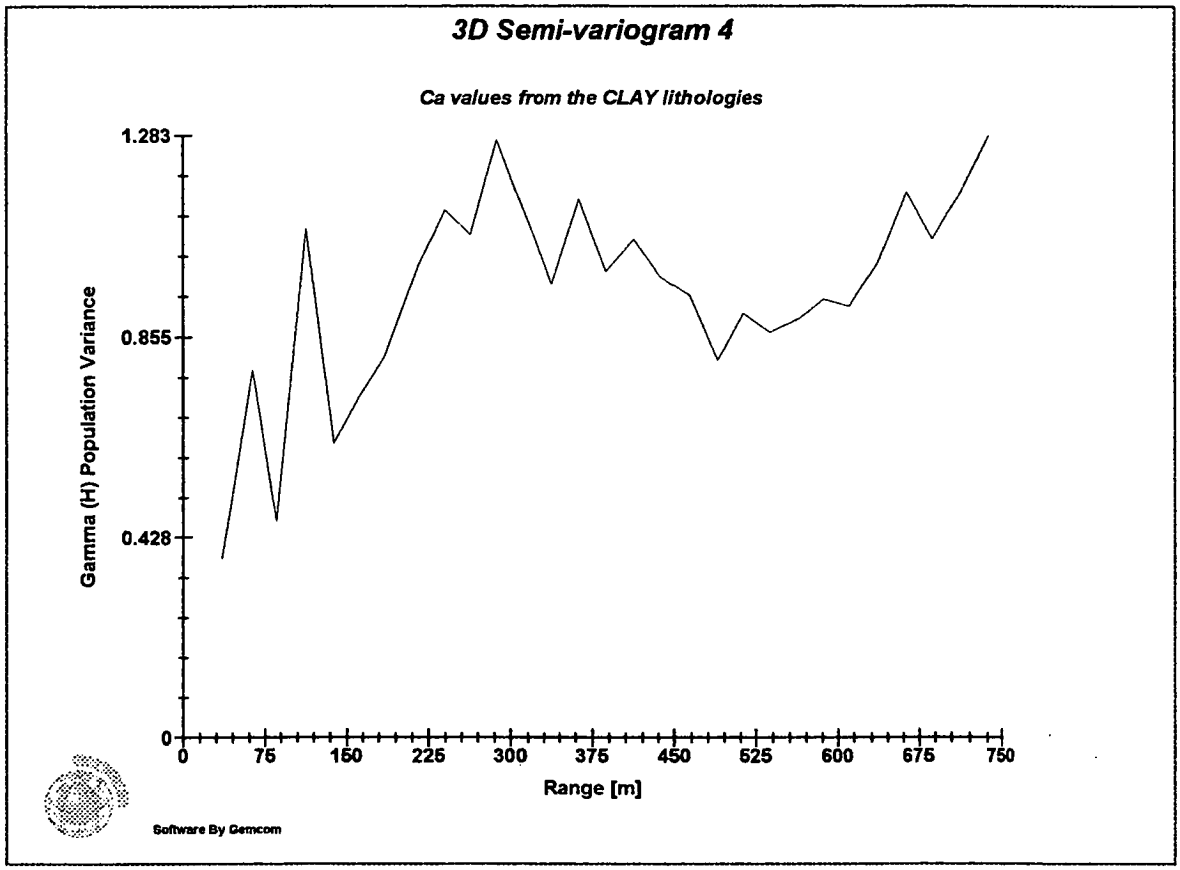
3D Semi-variogram 4
Ca values from the CLAY lithologies
Gamma (H) Population Variance
1.283
0.855
0.428
0
0
75
150
225
300
375
450
525
600
675
750
Range [m]
Software By Gemcom

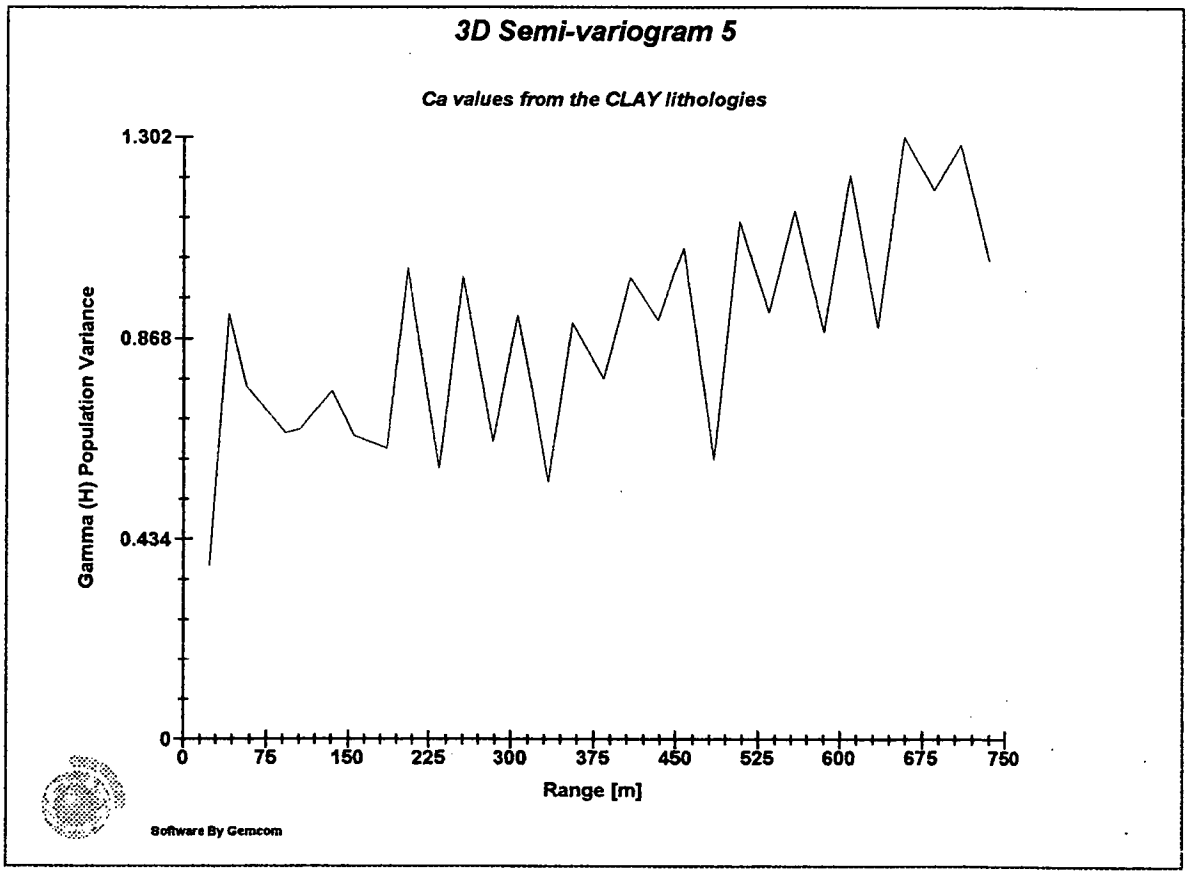
3D Semi-variogram 5
Ca values from the CLAY lithologies
1.302
0.868
0.434
0
Gamma (H) Population Variance
0
75
150
225
300
375
450
525
600
675
750
Range [m]
Software By Gemcom

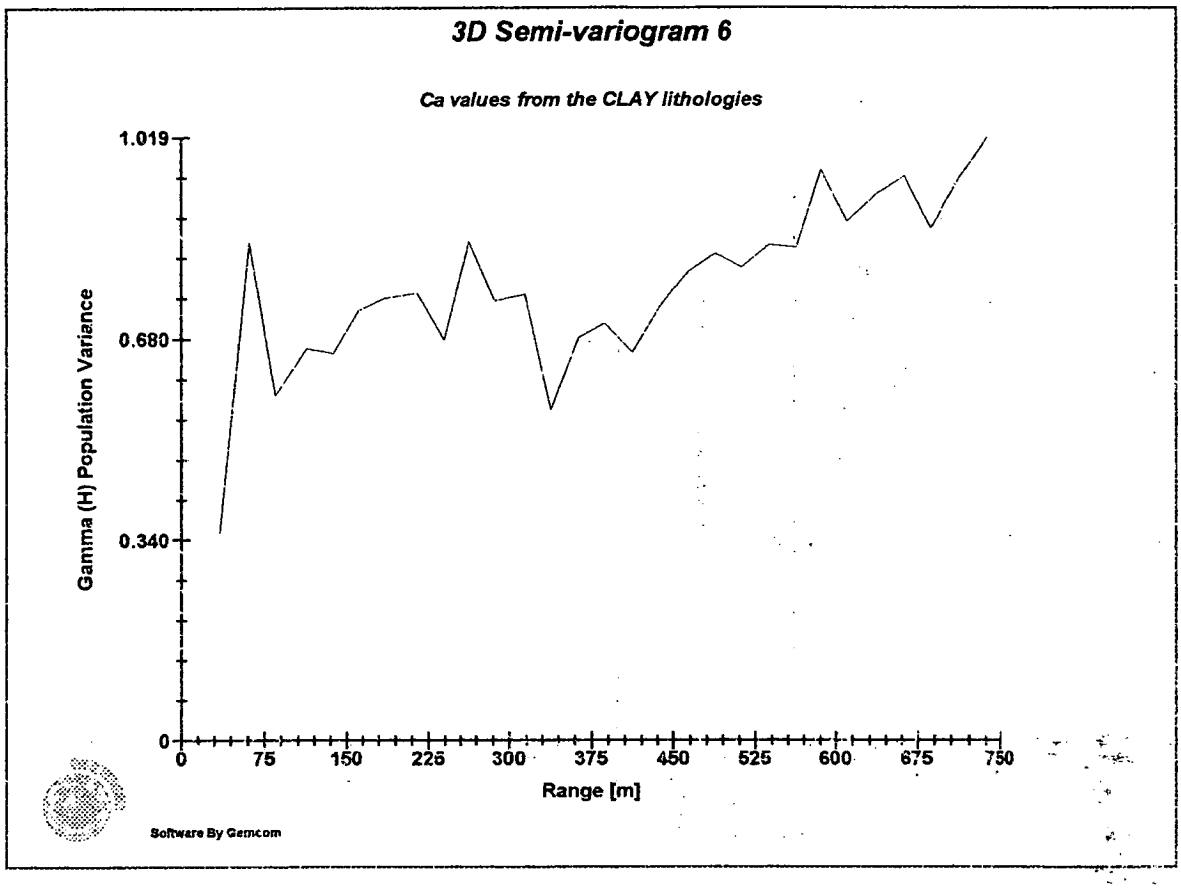
3D Semi-variogram 6
Ca values from the CLAY lithologies
1.019
0.680
0.340
0
Gamma (H) Population Variance
0
75
150
225
300
375
450
525
600
675
750
Range [m]
Software By Gemcom

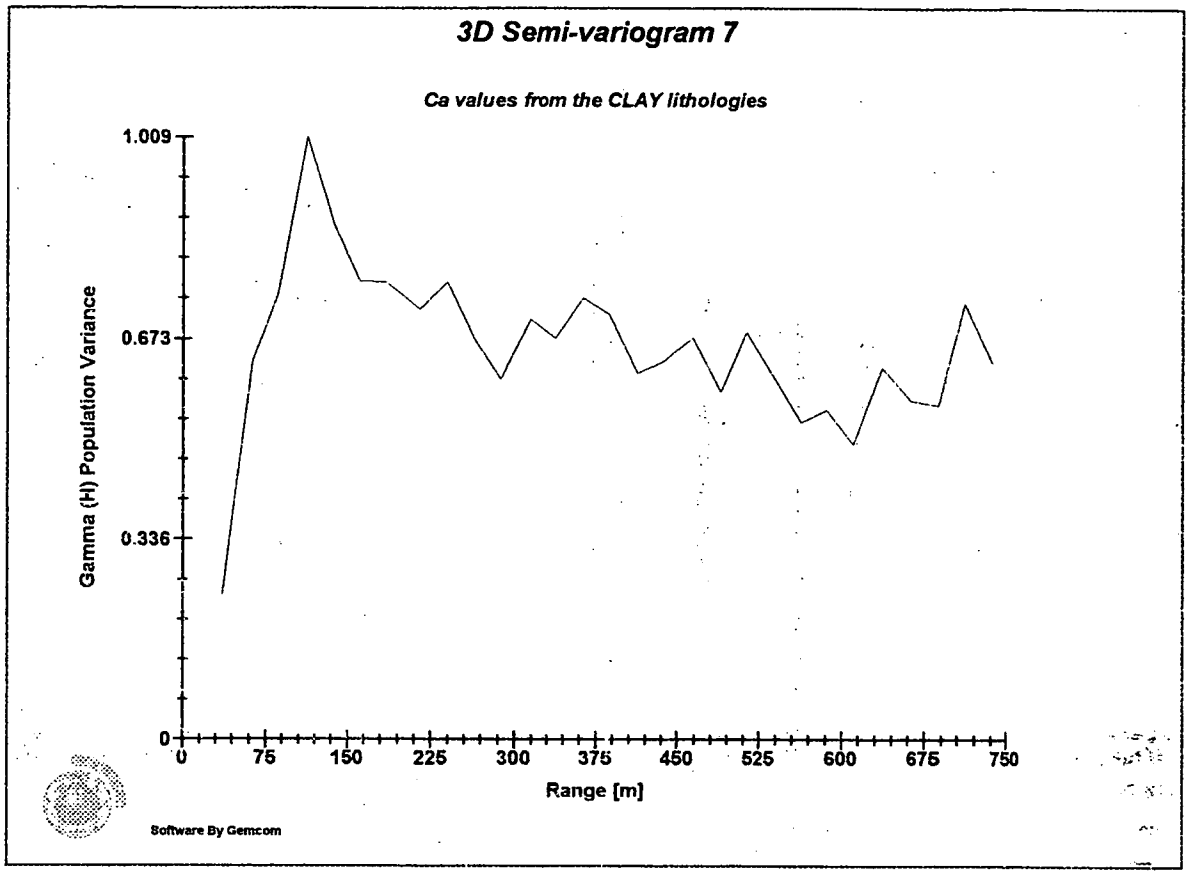
3D Semi-variogram 7
Ca values from the CLAY lithologies
1.009
0.673
0.336
0
Gamma (H) Population Variance
0
75
150
225
300
375
450
525
600
675
750
Range [m]
Software By Gemcom

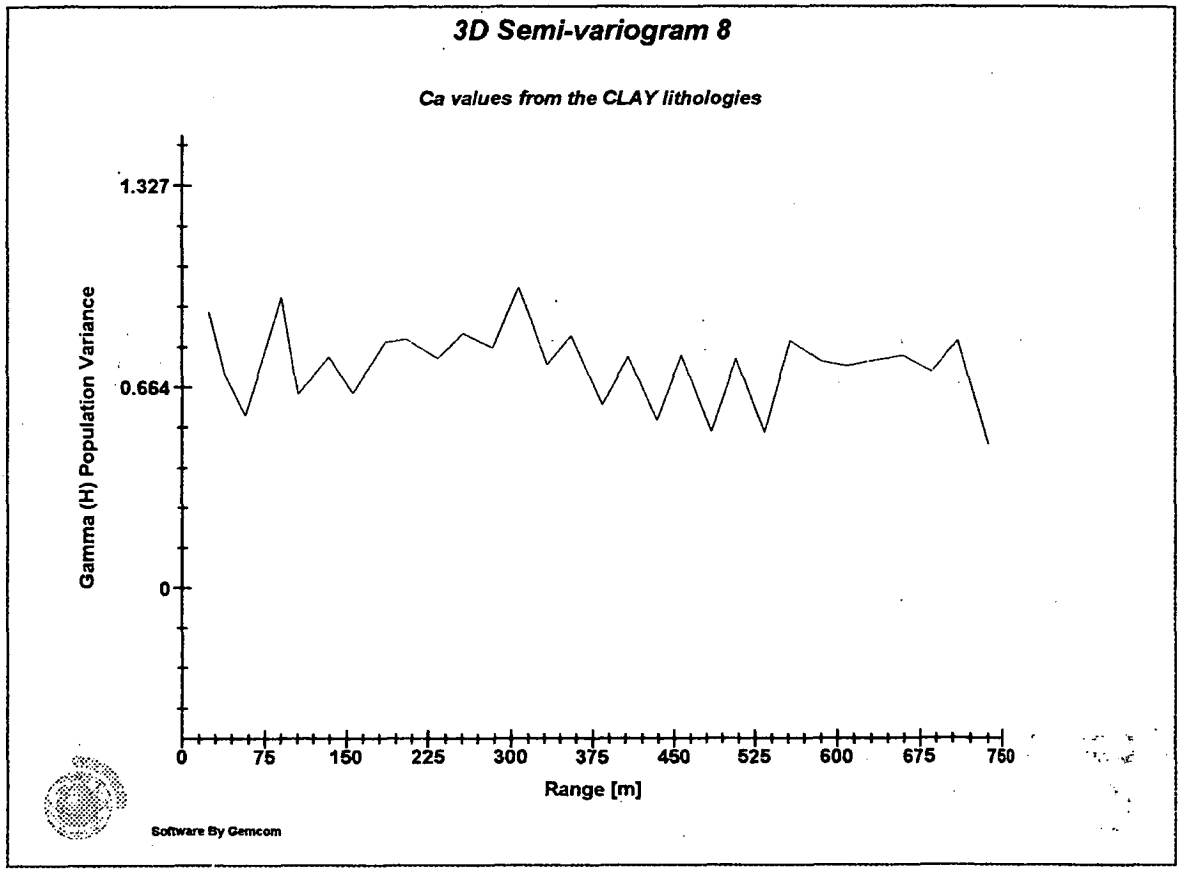
3D Semi-variogram 8
Ca values from the CLAY lithologies
1.327
0.664
0
Gamma (H) Population Variance
0
75
150
225
300
375
450
525
600
675
750
Range [m]
Software By Gemcom

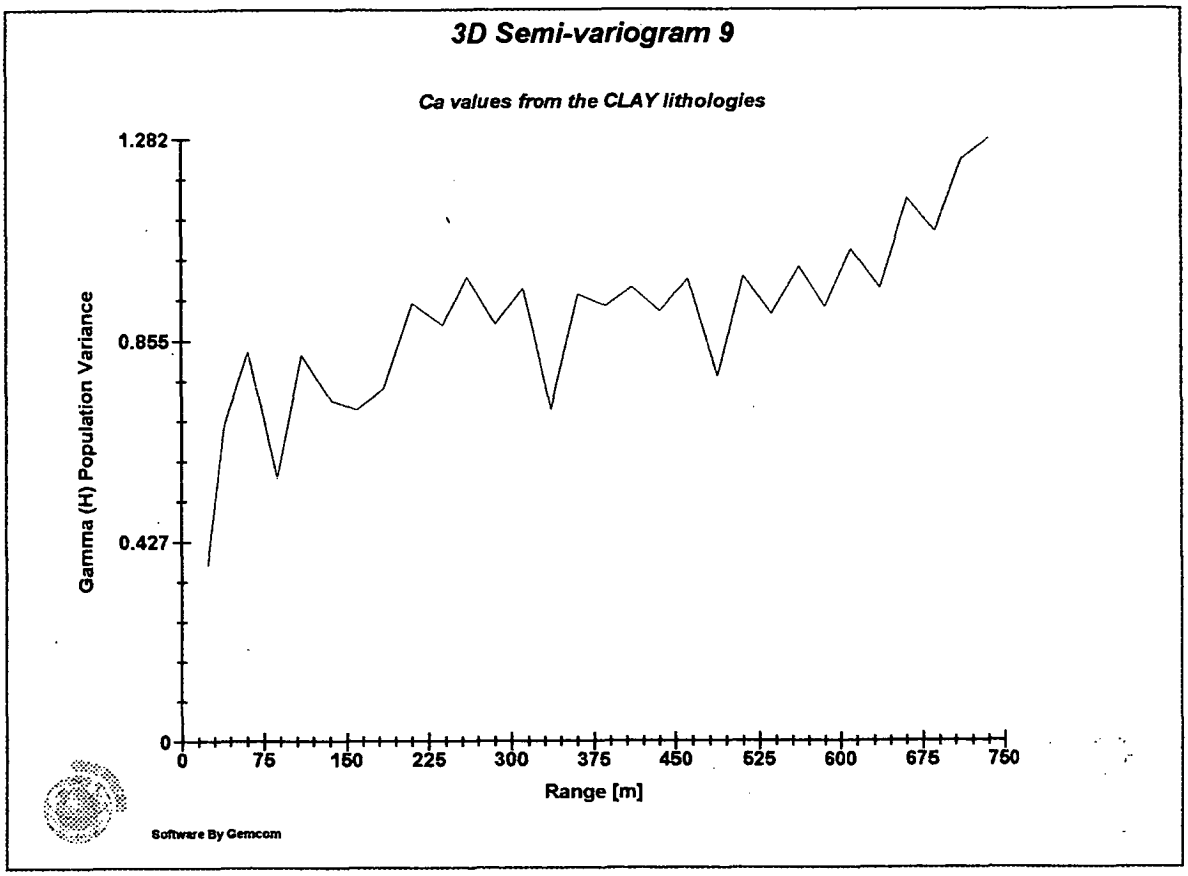
3D Semi-variogram 9
Ca values from the CLAY lithologies
Gamma (H) Population Variance
1.282
0.855
0.427
0
0
75
150
225
300
375
450
525
600
675
750
Range [m]
Software By Gemcom

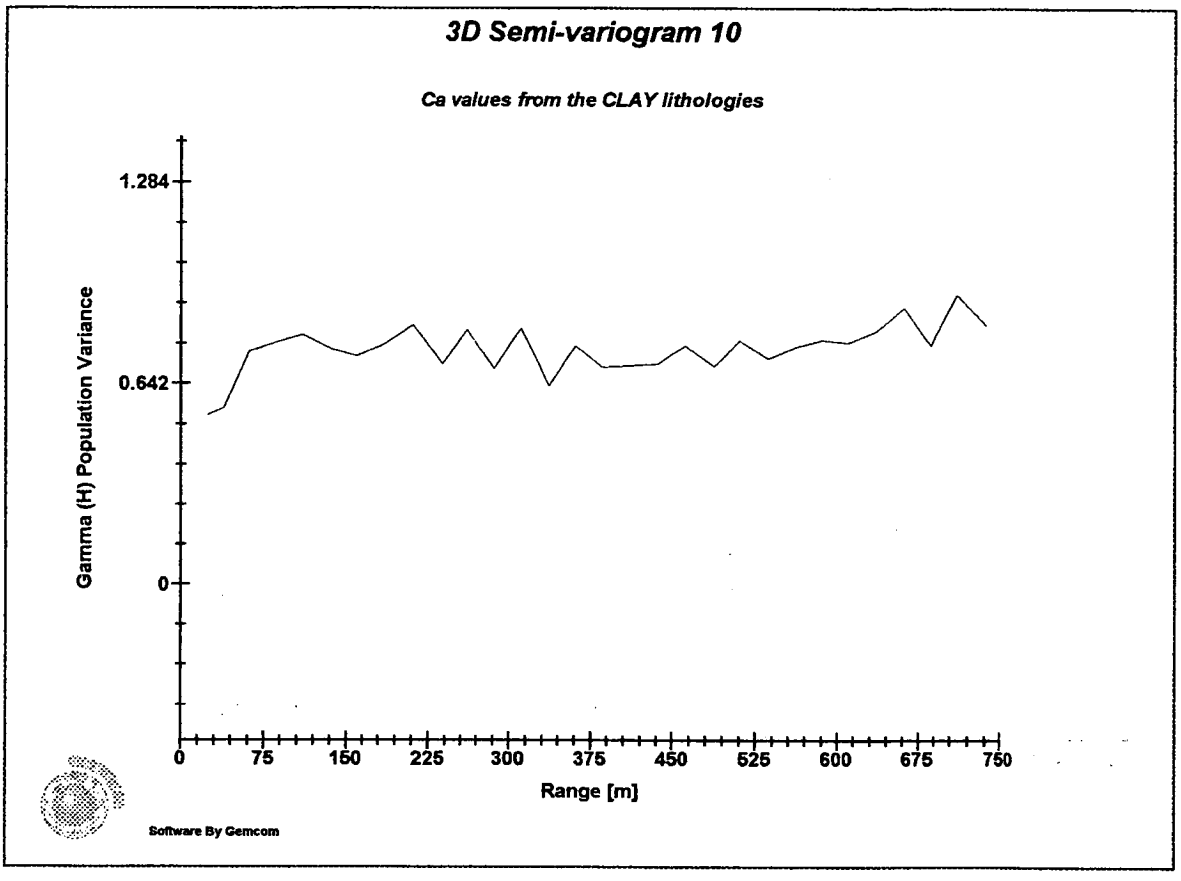
3D Semi-variogram 10
Ca values from the CLAY lithologies
1.284
0.642
0
Gamma (H) Population Variance
0
75
150
225
300
375
450
525
600
675
750
Range [m]
Software By Gemcom

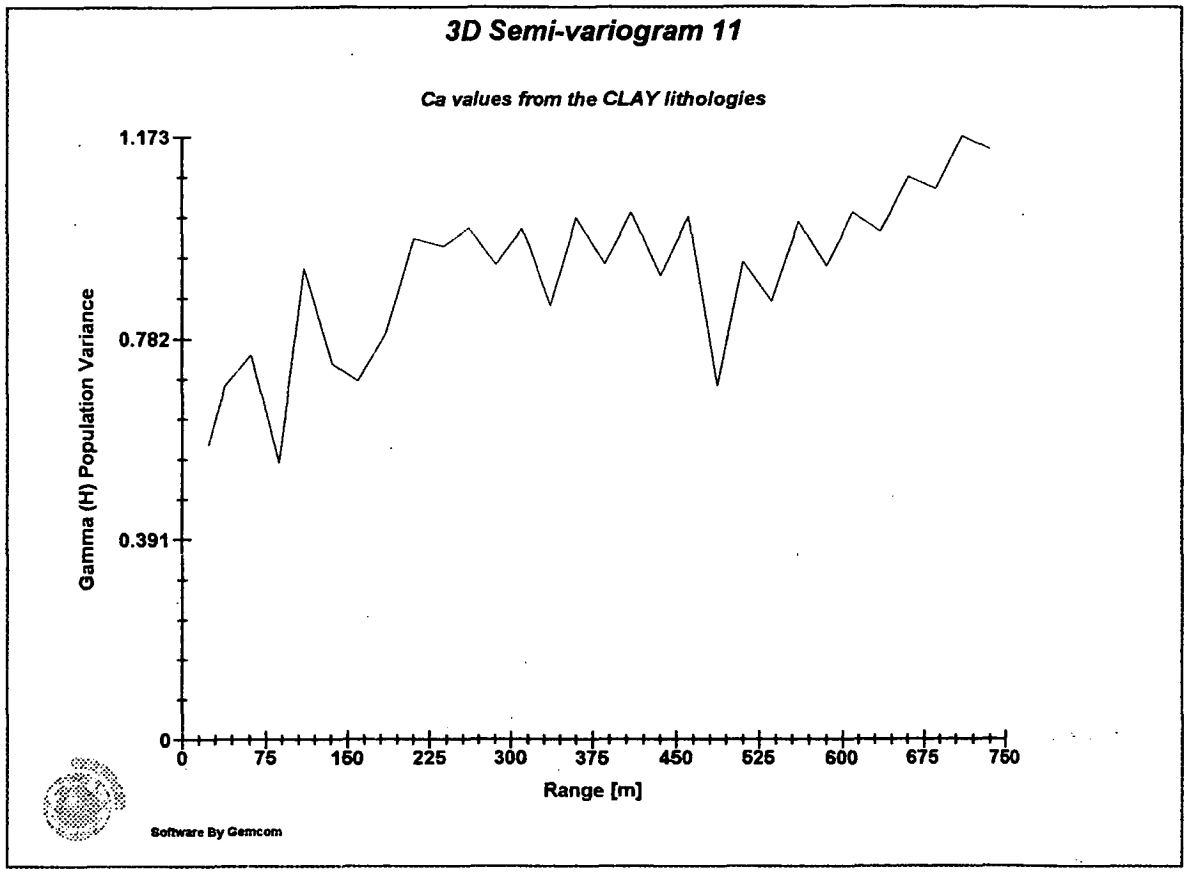
3D Semi-variogram 11
Ca values from the CLAY lithologies
Gamma (H) Population Variance
1.173
0.782
0.391
0
0
75
150
225
300
375
450
525
600
675
750
Range [m]
Software By Gemcom

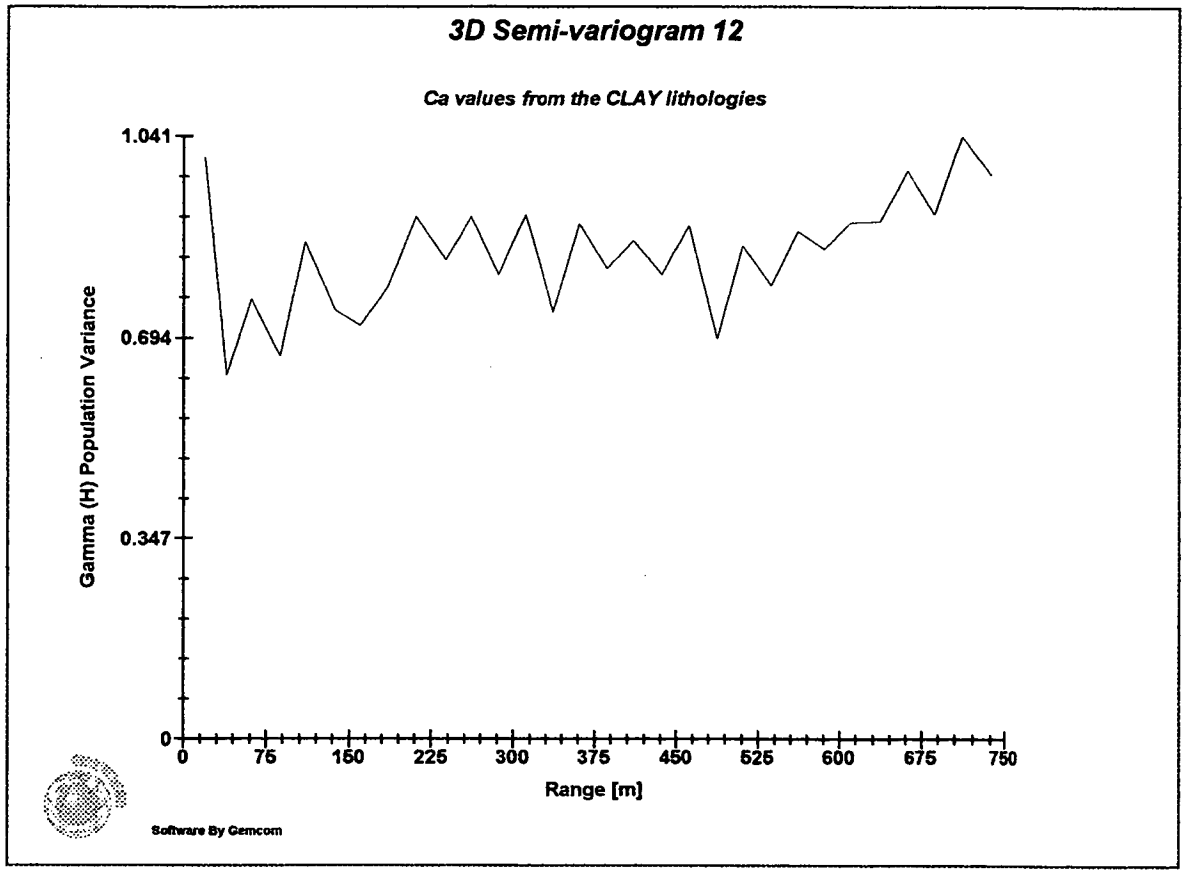
3D Semi-variogram 12
Ca values from the CLAY lithologies
1.041
0.694
0.347
0
Gamma (H) Population Variance
0
75
150
225
300
375
450
525
600
675
750
Range [m]
Software By Gemcom

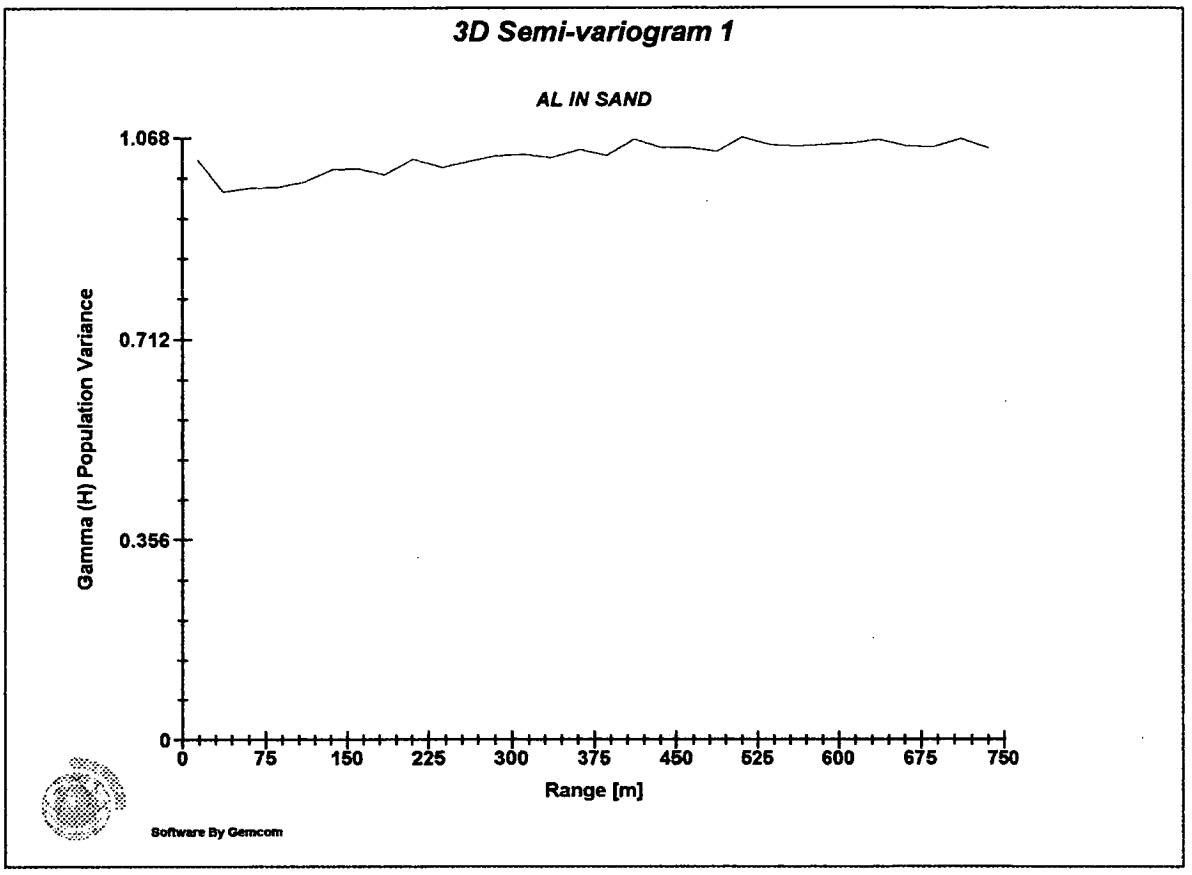
3D Semi-variogram 1
AL IN SAND
1.068
0.712
0.356
0
Gamma (H) Population Variance
0
75
150
225
300
375
450
525
600
675
750
Range [m]
Software By Gemcom

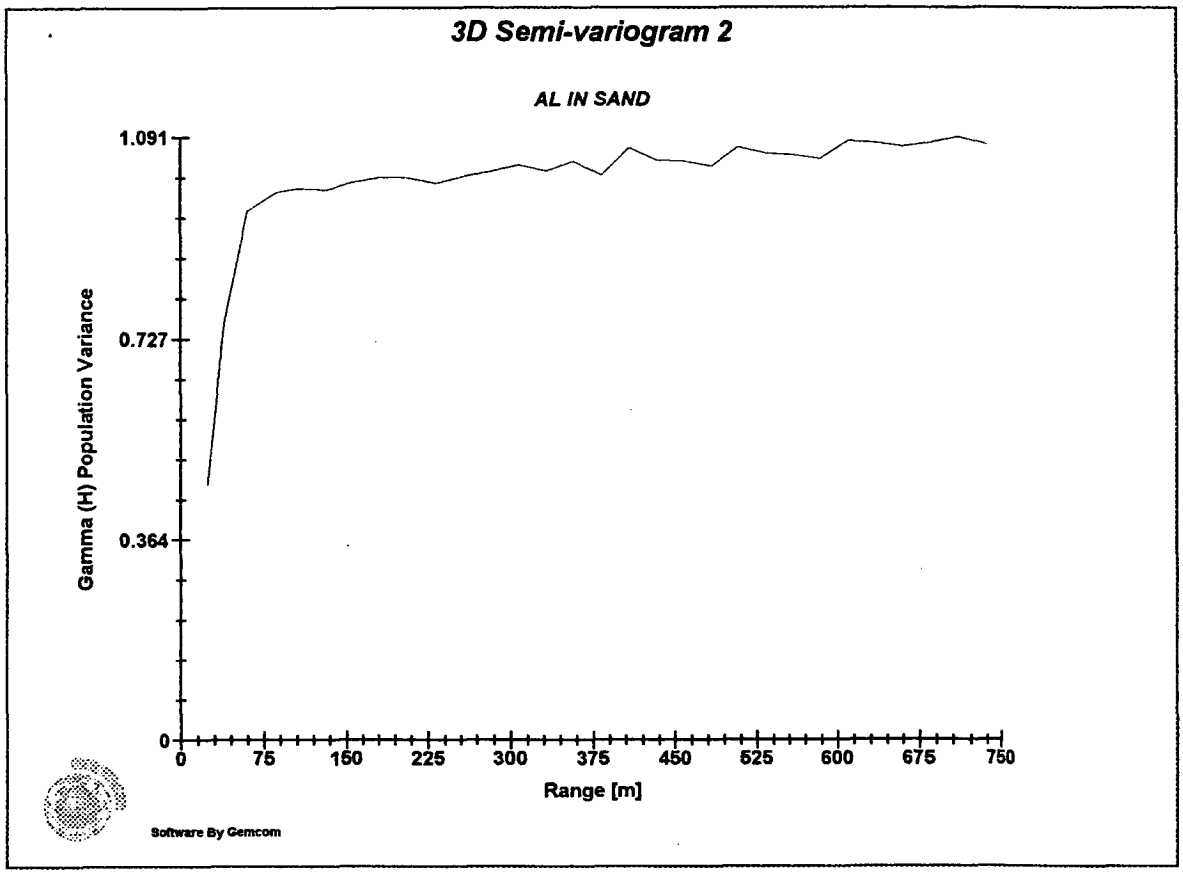
3D Semi-variogram 2
AL IN SAND
1.091
0.727
0.364
0
Gamma (H) Population Variance
0
75
150
225
300
375
450
525
600
675
750
Range [m]
Software By Gemcom

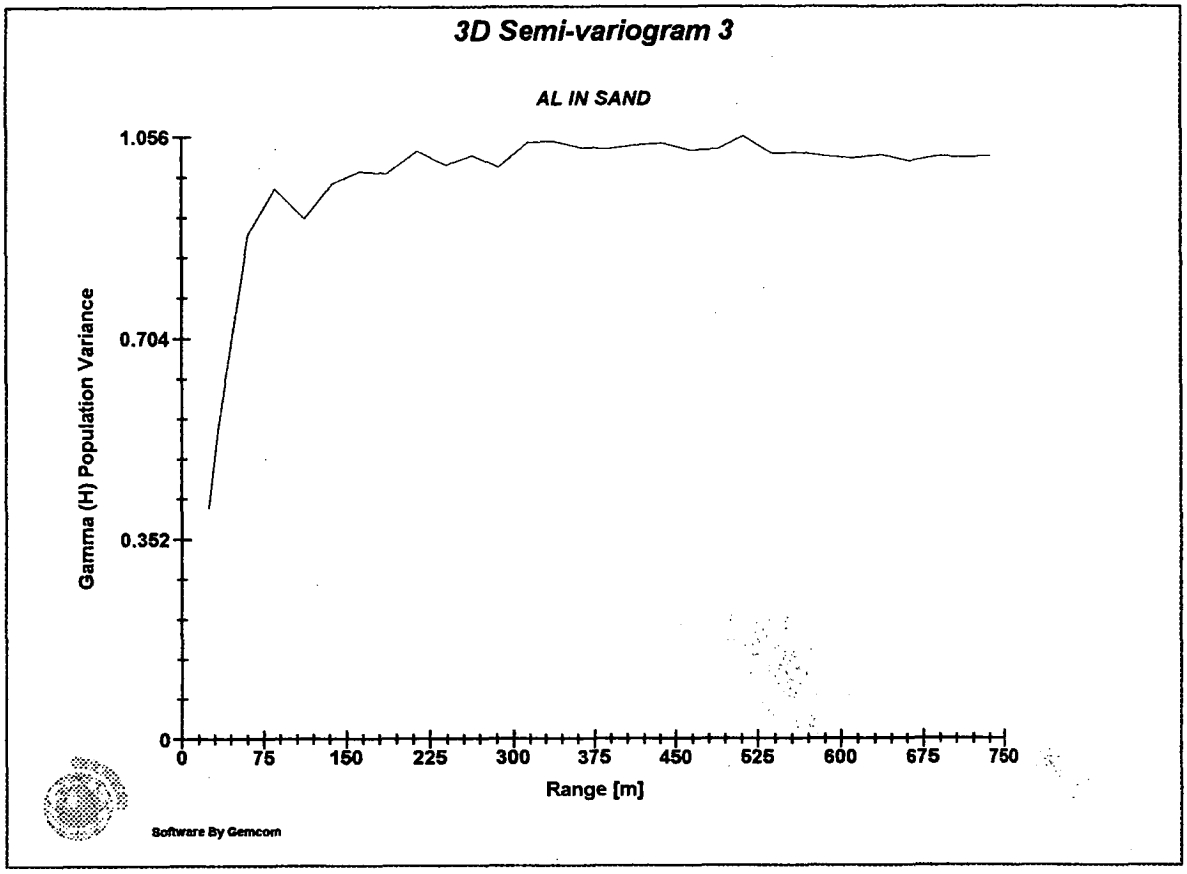
3D Semi-variogram 3
AL IN SAND
1.056
0.704
0.352
0
Gamma (H) Population Variance
0
75
150
225
300
375
450
525
600
675
750
Range [m]
Software By Gemcom

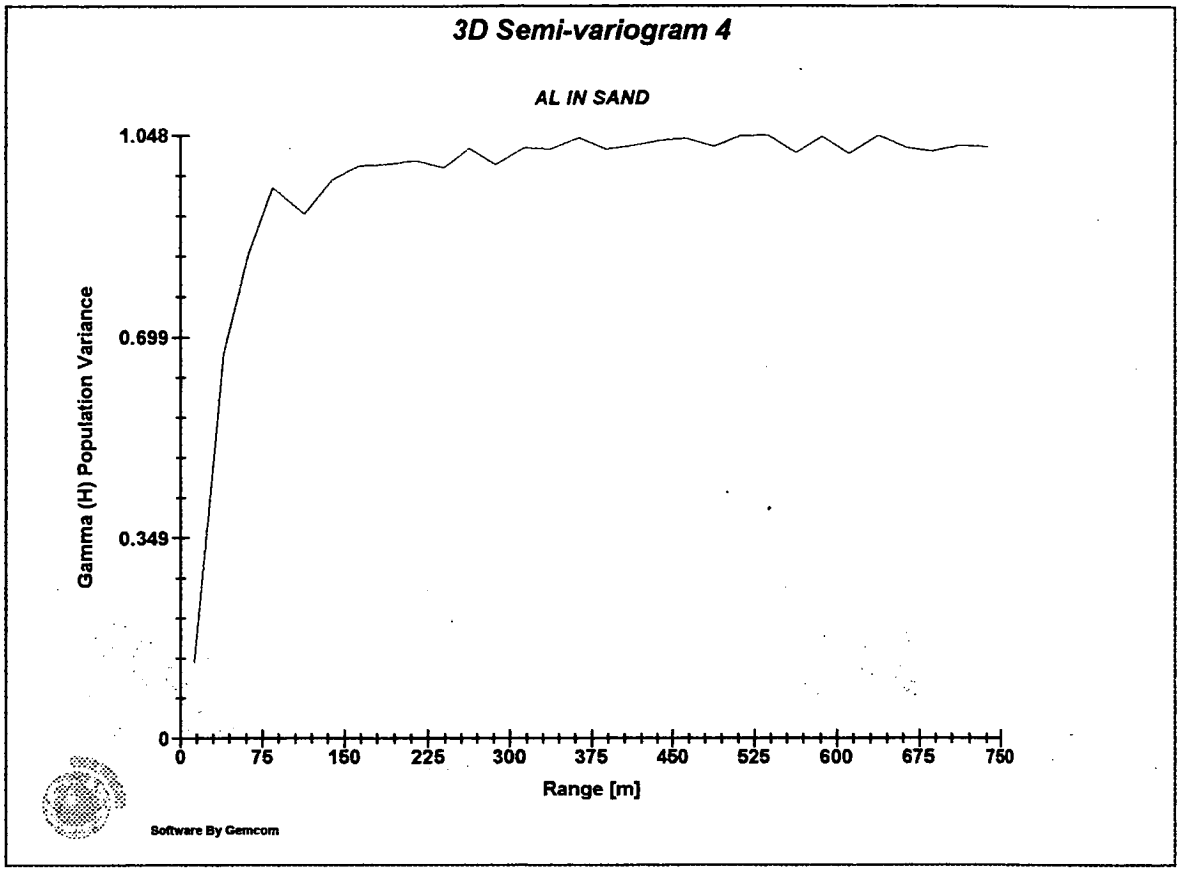
3D Semi-variogram 4
AL IN SAND
1.048
0.699
0.349
0
Gamma (H) Population Variance
0
75
150
225
300
375
450
525
600
675
750
Range [m]
Software By Gemcom

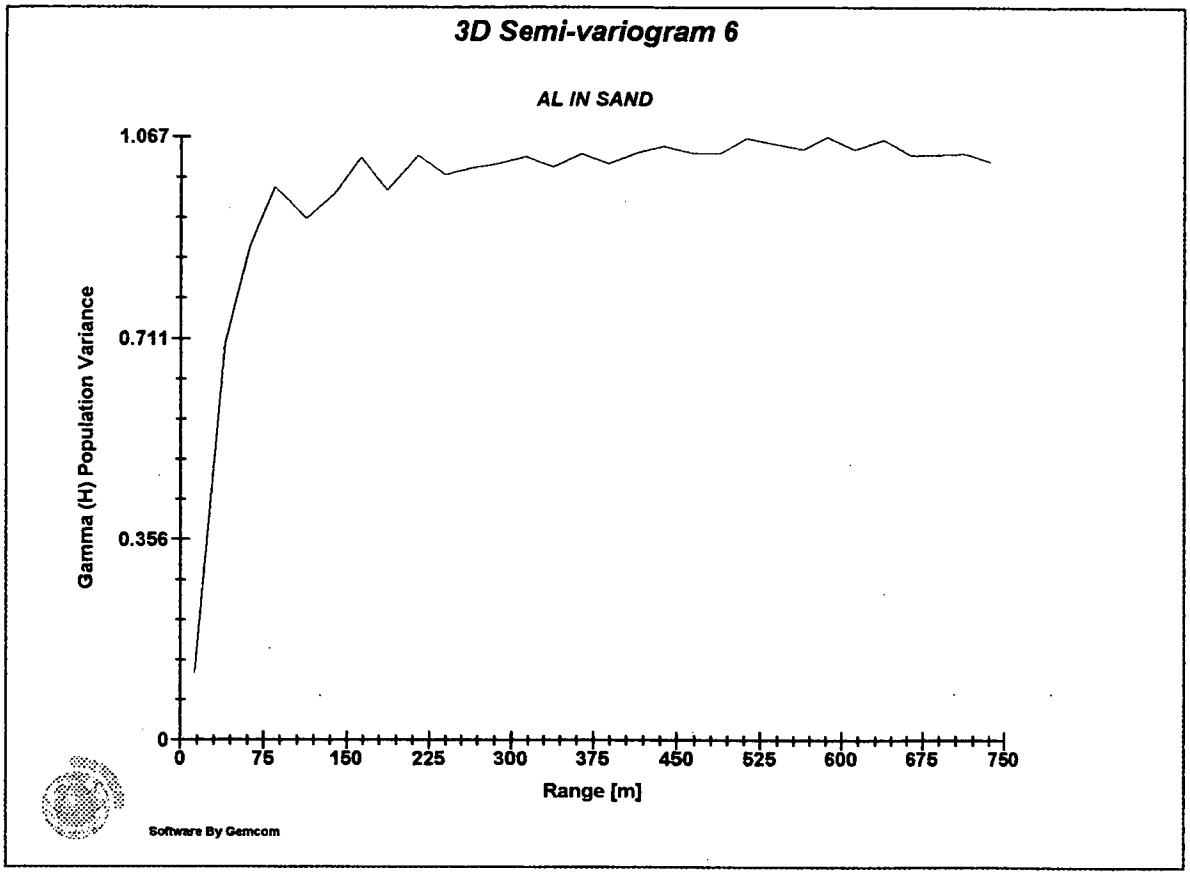
3D Semi-variogram 6
AL IN SAND
1.067
0.711
0.356
0
Gamma (H) Population Variance
0
75
150
225
300
375
450
525
600
675
750
Range [m]
Software By Gemcom

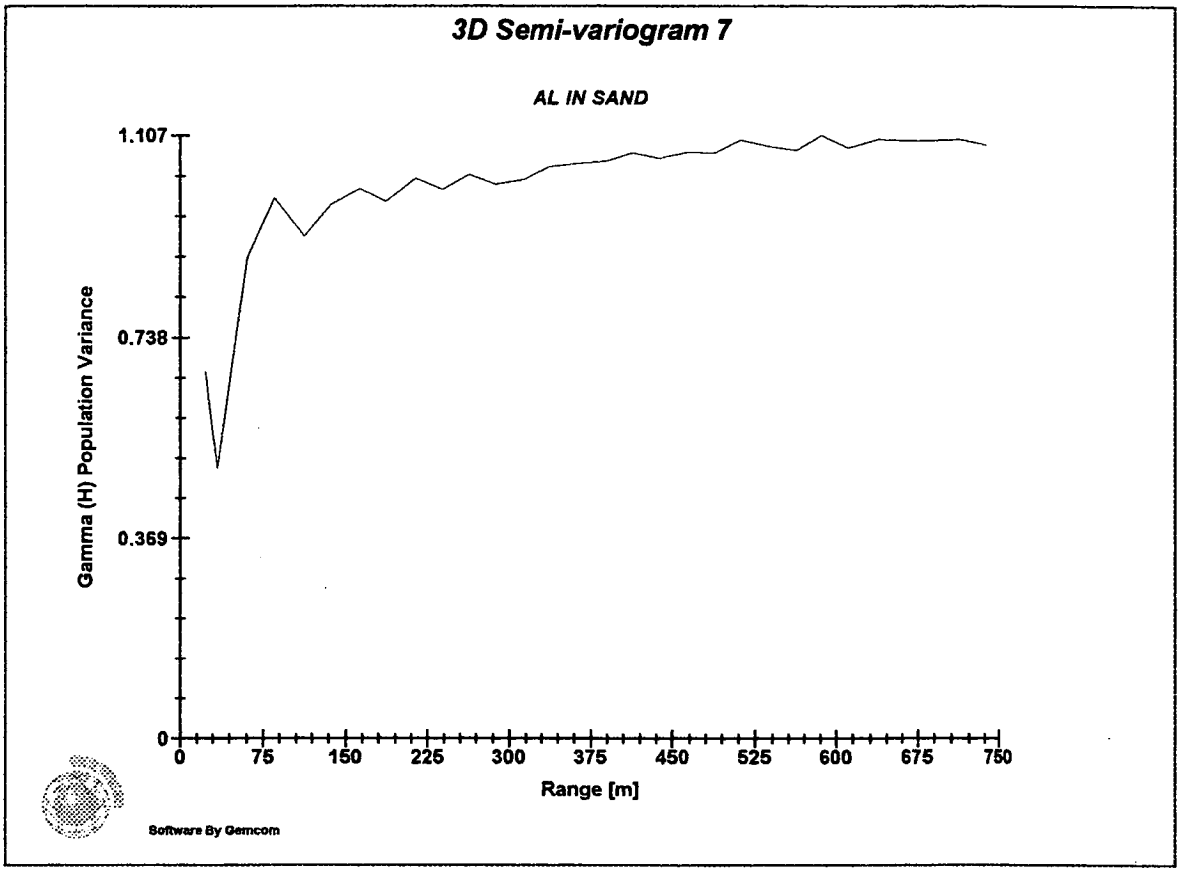
3D Semi-variogram 7
AL IN SAND
1.107
0.738
0.369
0
Gamma (H) Population Variance
0
75
150
225
300
375
450
525
600
675
750
Range [m]
Software By Gemcom

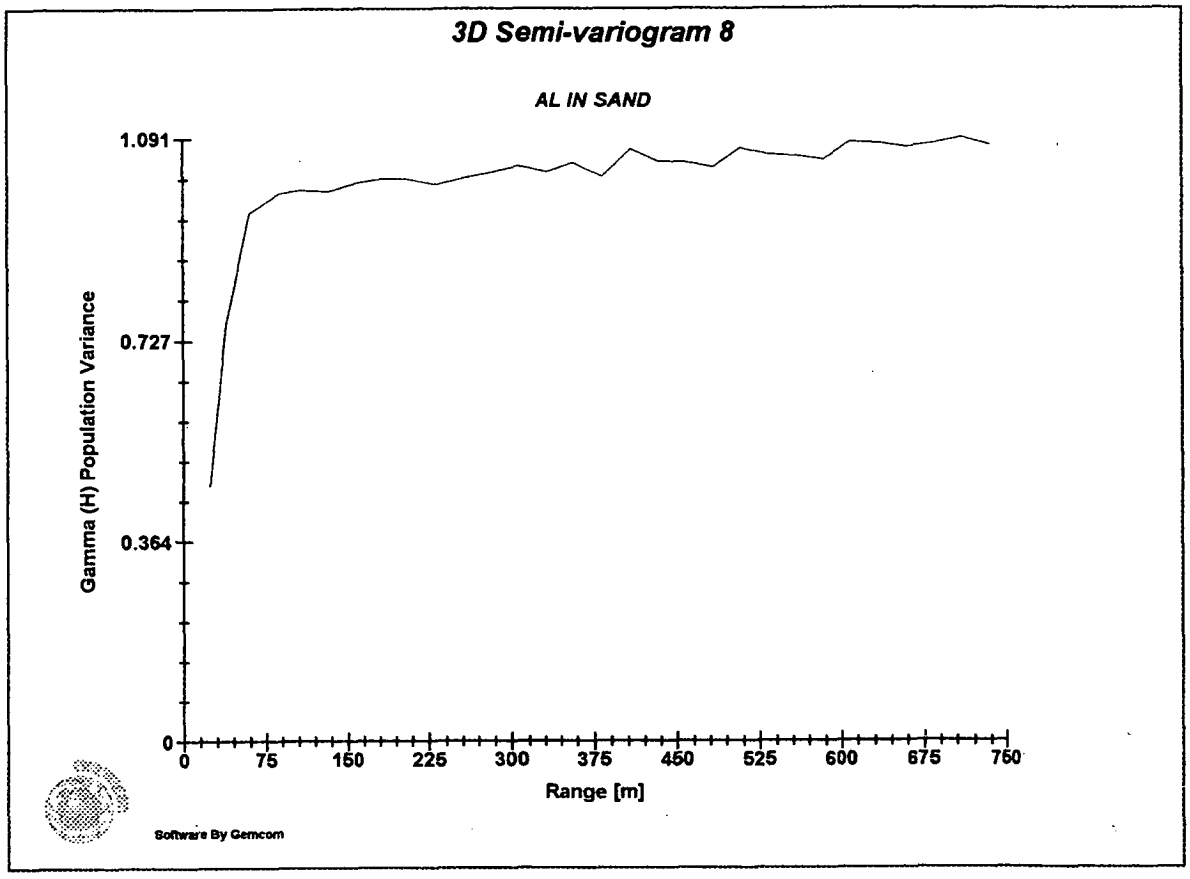
3D Semi-variogram 8
AL IN SAND
1.091
0.727
0.364
0
Gamma (H) Population Variance
0
75
150
225
300
375
450
525
600
675
750
Range [m]
Software By Gemcom

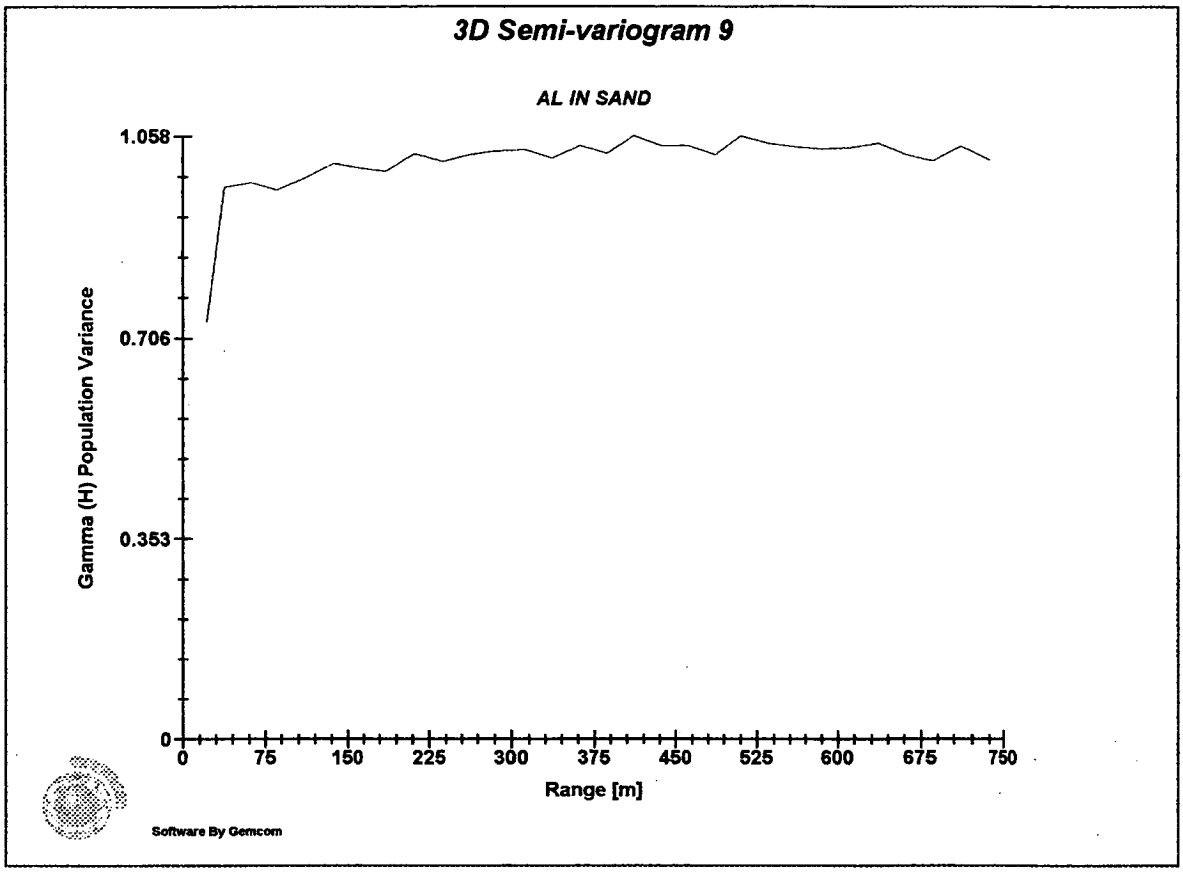
3D Semi-variogram 9
AL IN SAND
1.058
0.706
0.353
0
Gamma (H) Population Variance
0
75
150
225
300
375
450
525
600
675
750
Range [m]
Software By Gemcom

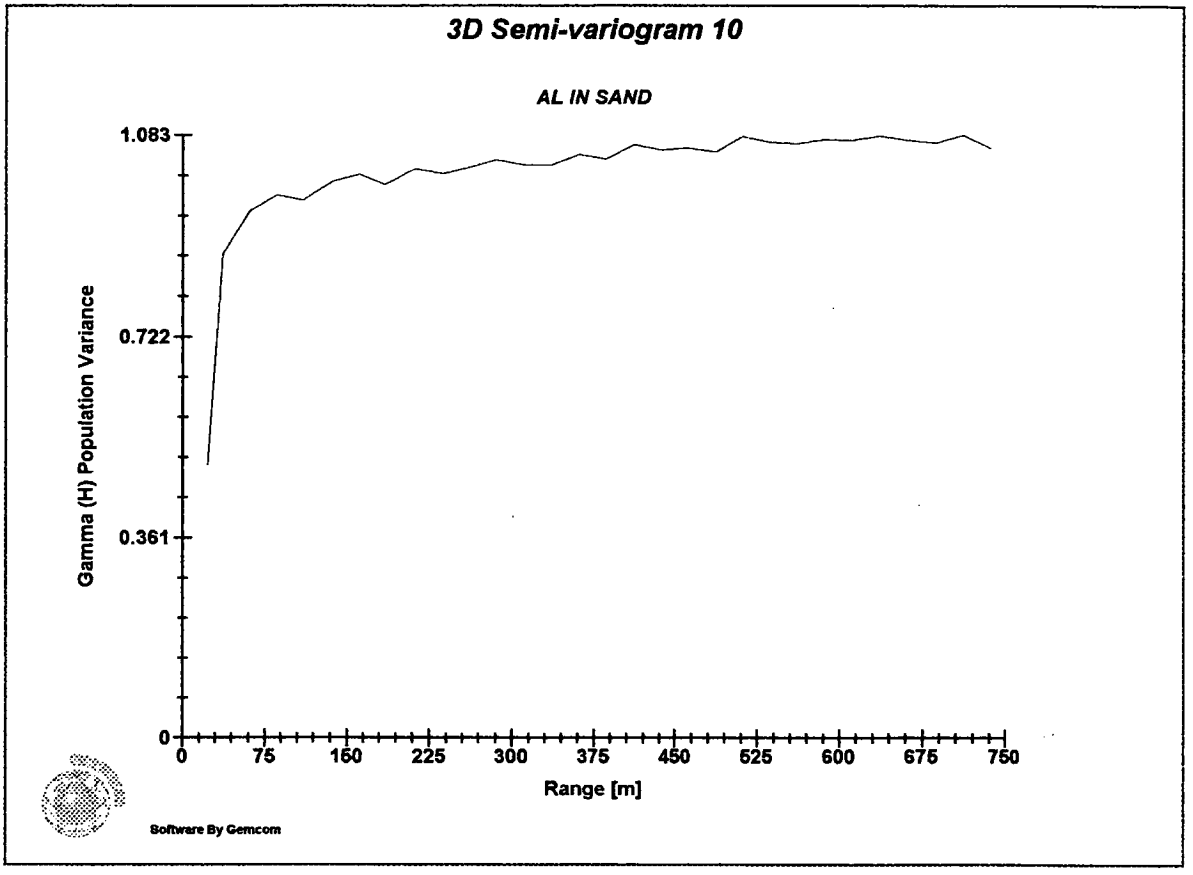
3D Semi-variogram 10
AL IN SAND
1.083
0.722
0.361
0
Gamma (H) Population Variance
0
75
150
225
300
375
450
525
600
675
750
Range [m]
Software By Gemcom

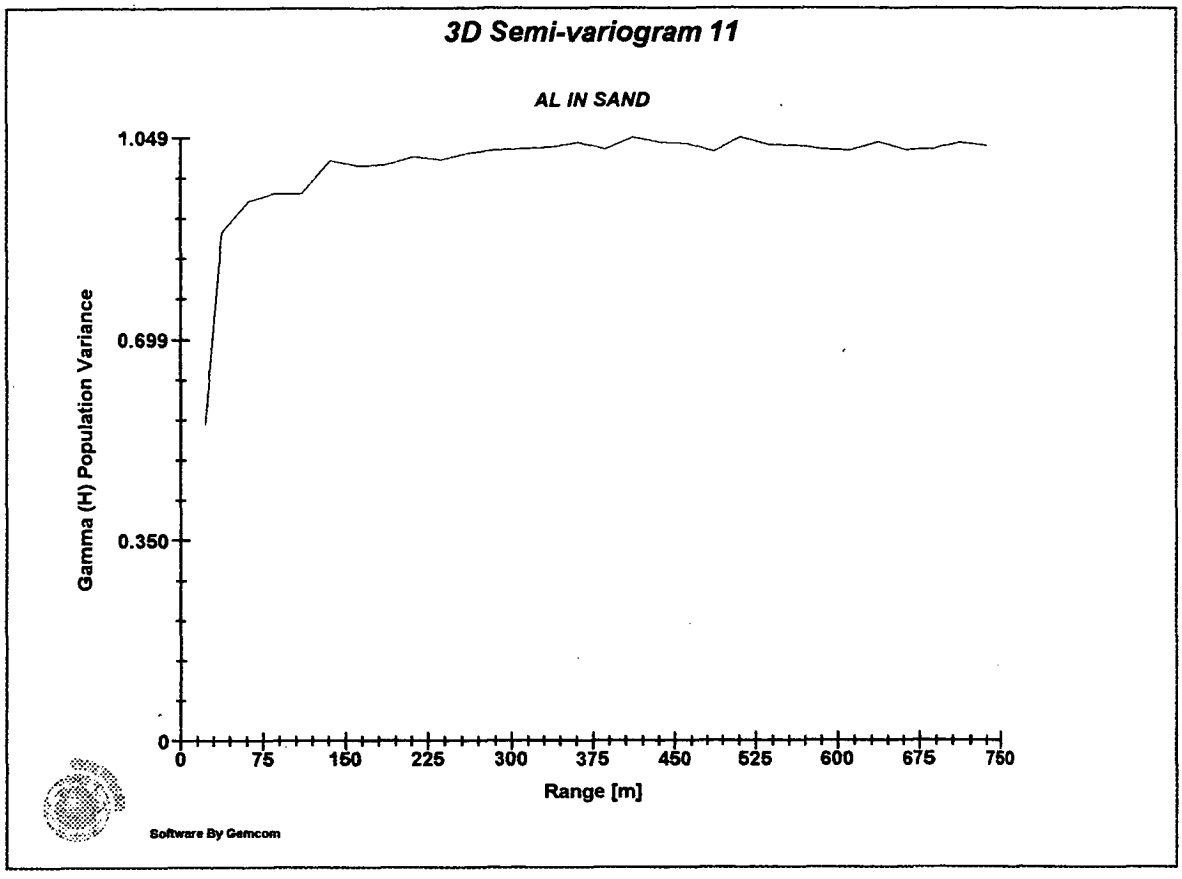
3D Semi-variogram 11
AL IN SAND
1.049
0.699
0.350
0
Gamma (H) Population Variance
0
75
150
225
300
375
450
525
600
675
750
Range [m]
Software By Gemcom

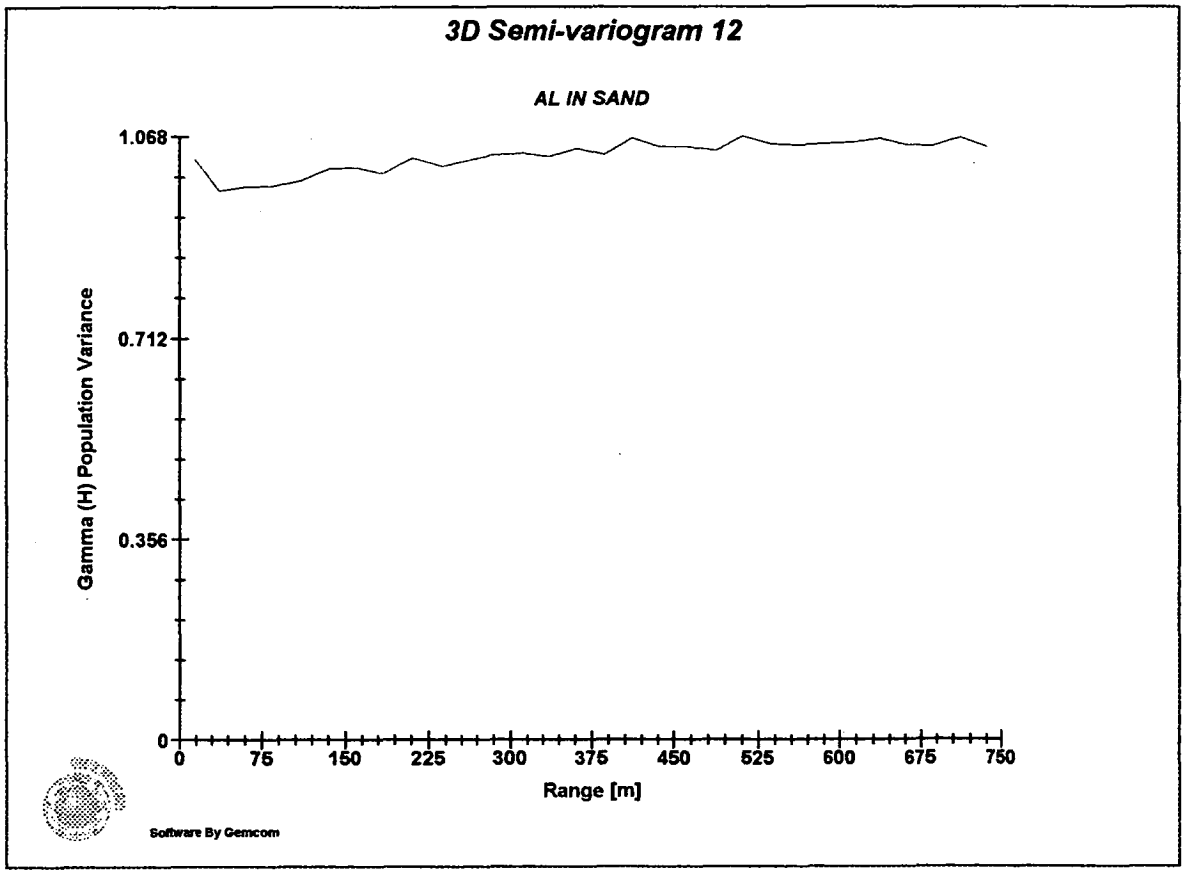
3D Semi-variogram 12
AL IN SAND
1.068
0.712
0.356
0
Gamma (H) Population Variance
0
75
150
225
300
375
450
525
600
675
750
Range [m]
Software By Gemcom

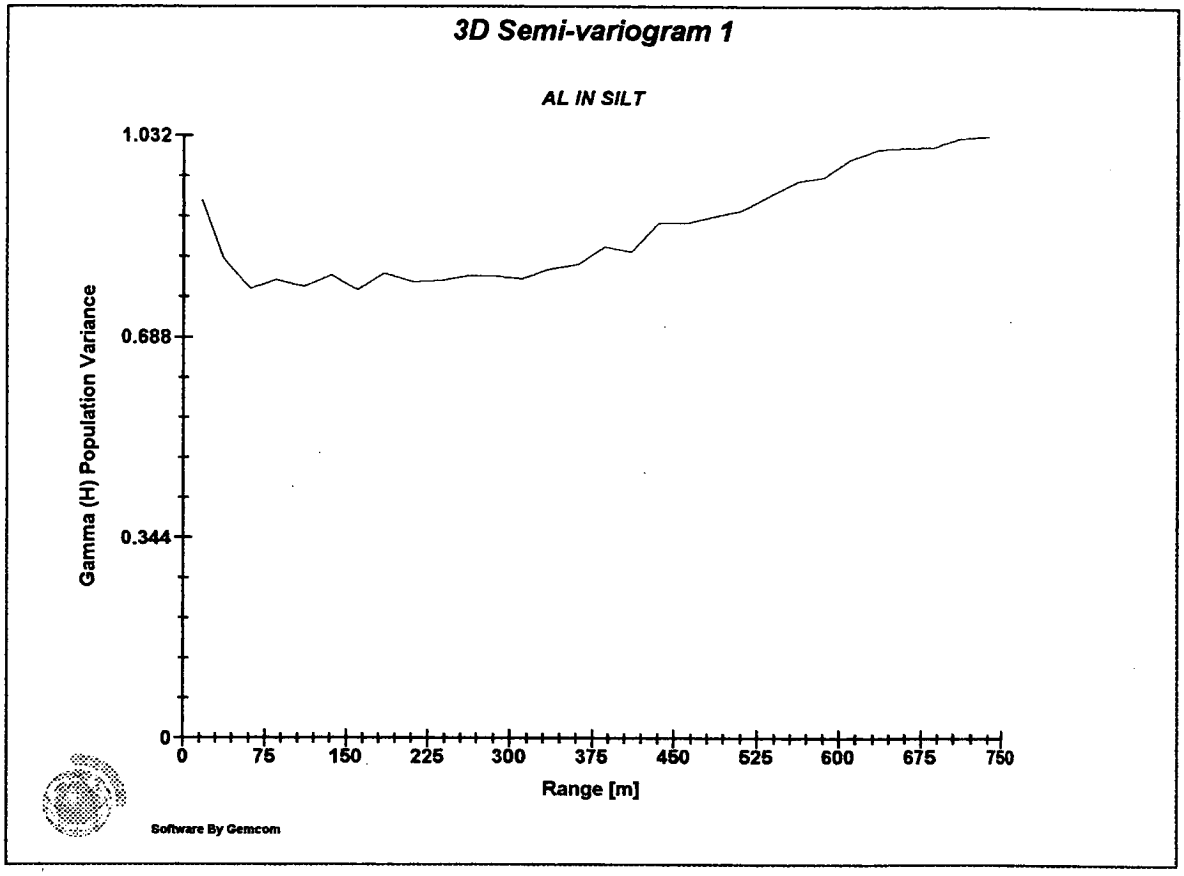
3D Semi-variogram 1
AL IN SILT
1.032
0.688
0.344
0
Gamma (H) Population Variance
0
75
150
225
300
375
450
525
600
675
750
Range [m]
Software By Gemcom

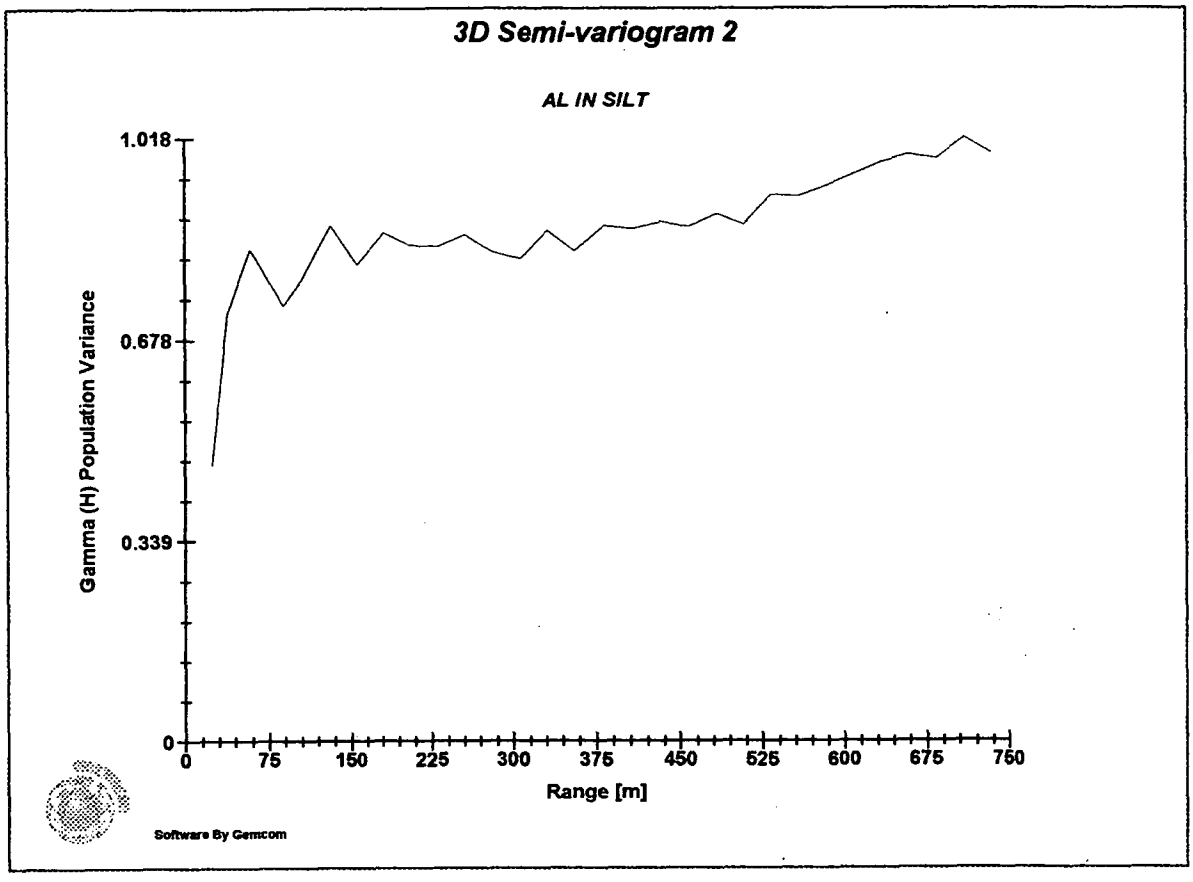
3D Semi-variogram 2
AL IN SILT
1.018
0.678
0.339
0
Gamma (H) Population Variance
0
75
150
225
300
375
450
525
600
675
750
Range [m]
Software By Gemcom

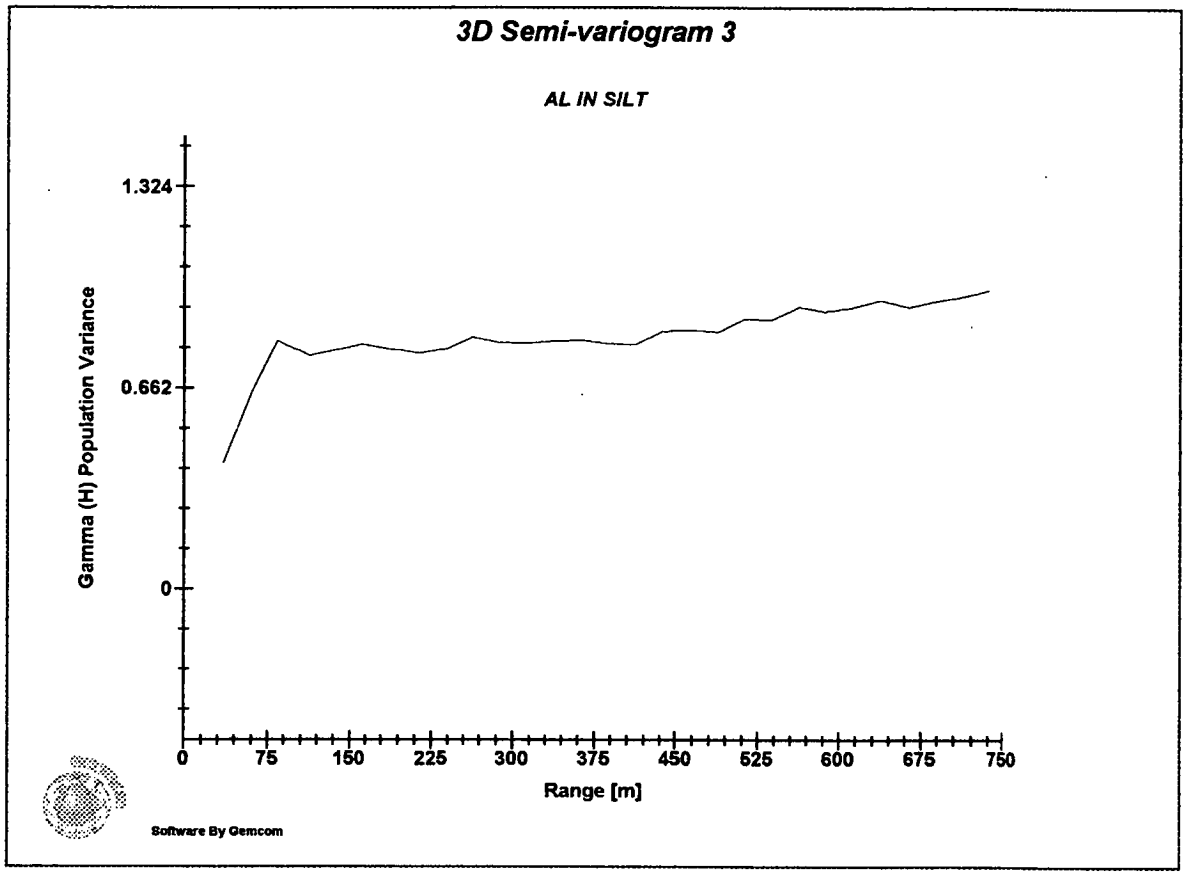
3D Semi-variogram 3
AL IN SILT
1.324
0.662
0
Gamma (H) Population Variance
0
75
150
225
300
375
450
525
600
675
750
Range [m]
Software By Gemcom

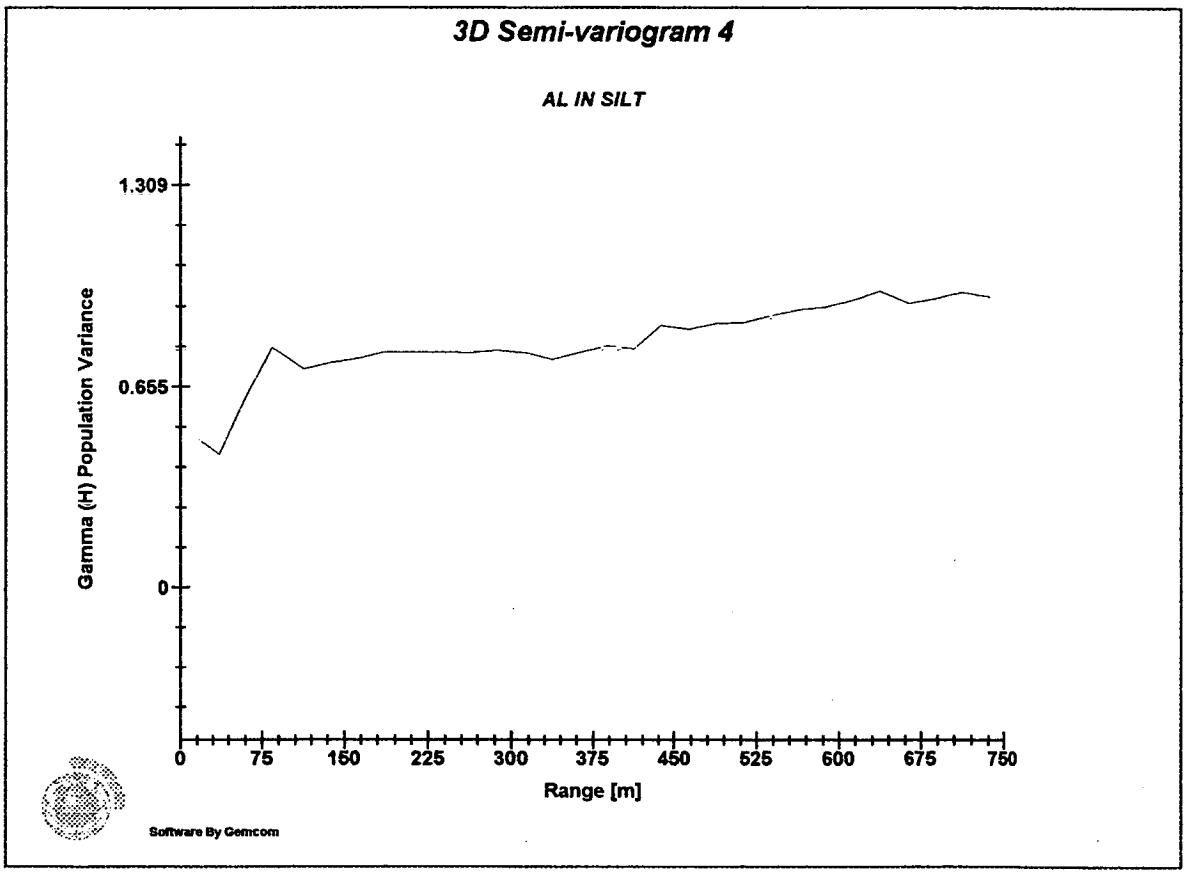
3D Semi-variogram 4
AL IN SILT
1.309
0.655
0
Gamma (H) Population Variance
0
75
150
225
300
375
450
525
600
675
750
Range [m]
Software By Gemcom

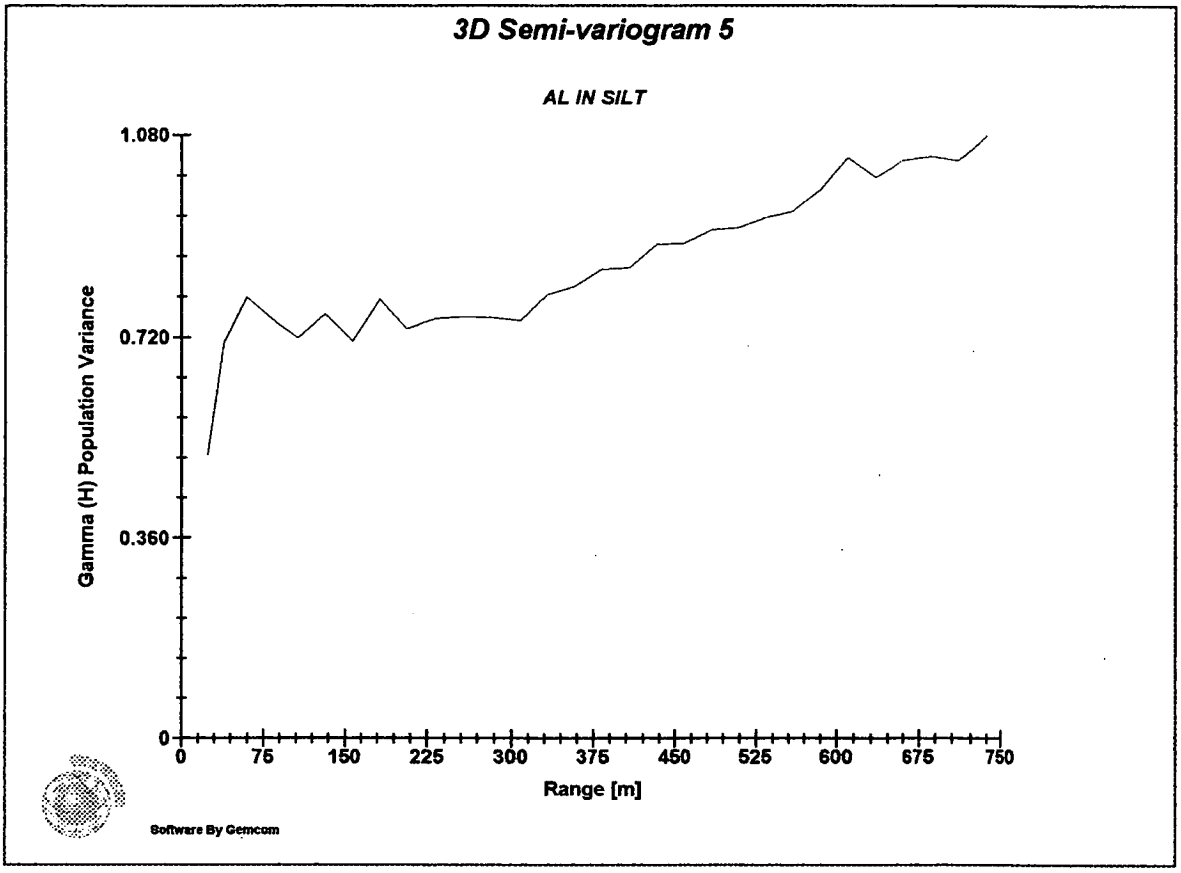
3D Semi-variogram 5
AL IN SILT
1.080
0.720
0.360
0
Gamma (H) Population Variance
0
75
150
225
300
375
450
525
600
675
750
Range [m]
Software By Gemcom

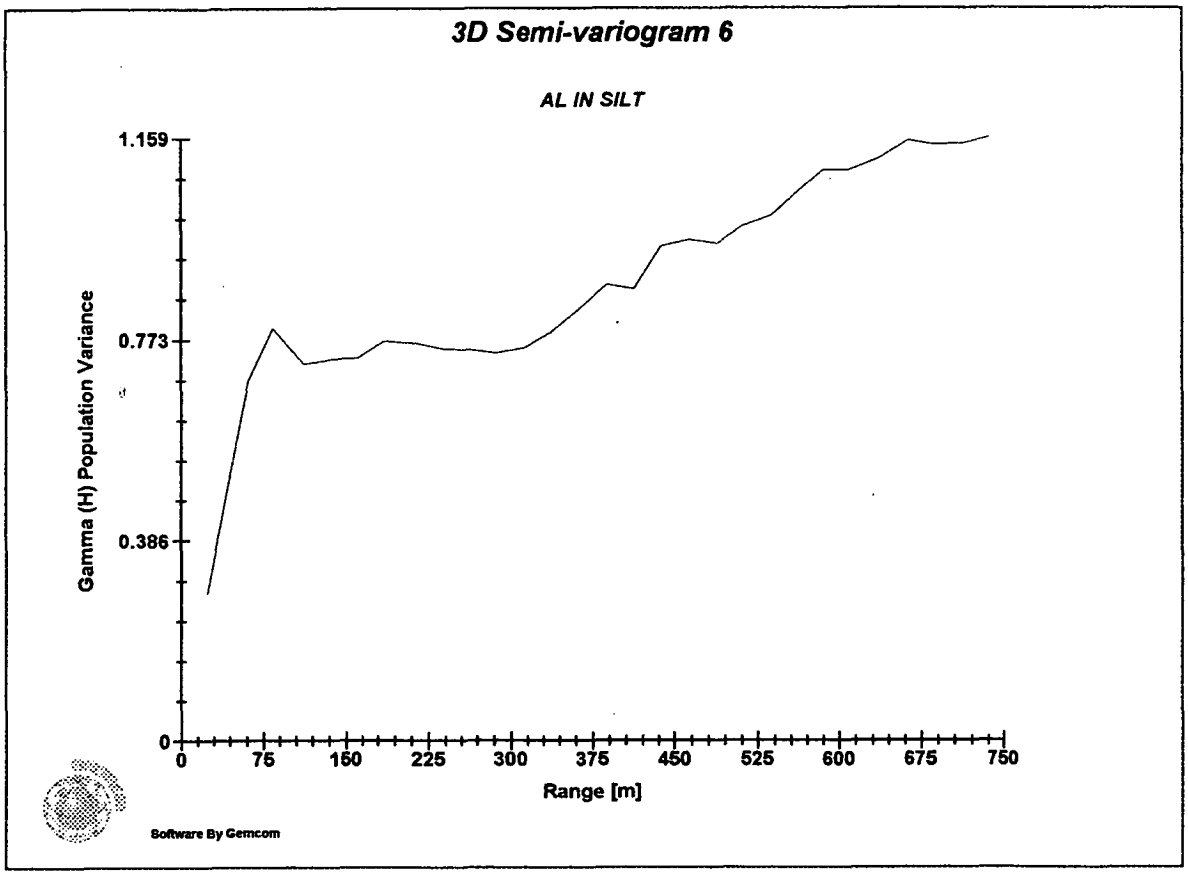
3D Semi-variogram 6
AL IN SILT
1.159
0.773
0.386
0
Gamma (H) Population Variance
0
75
150
225
300
375
450
525
600
675
750
Range [m]
Software By Gemcom

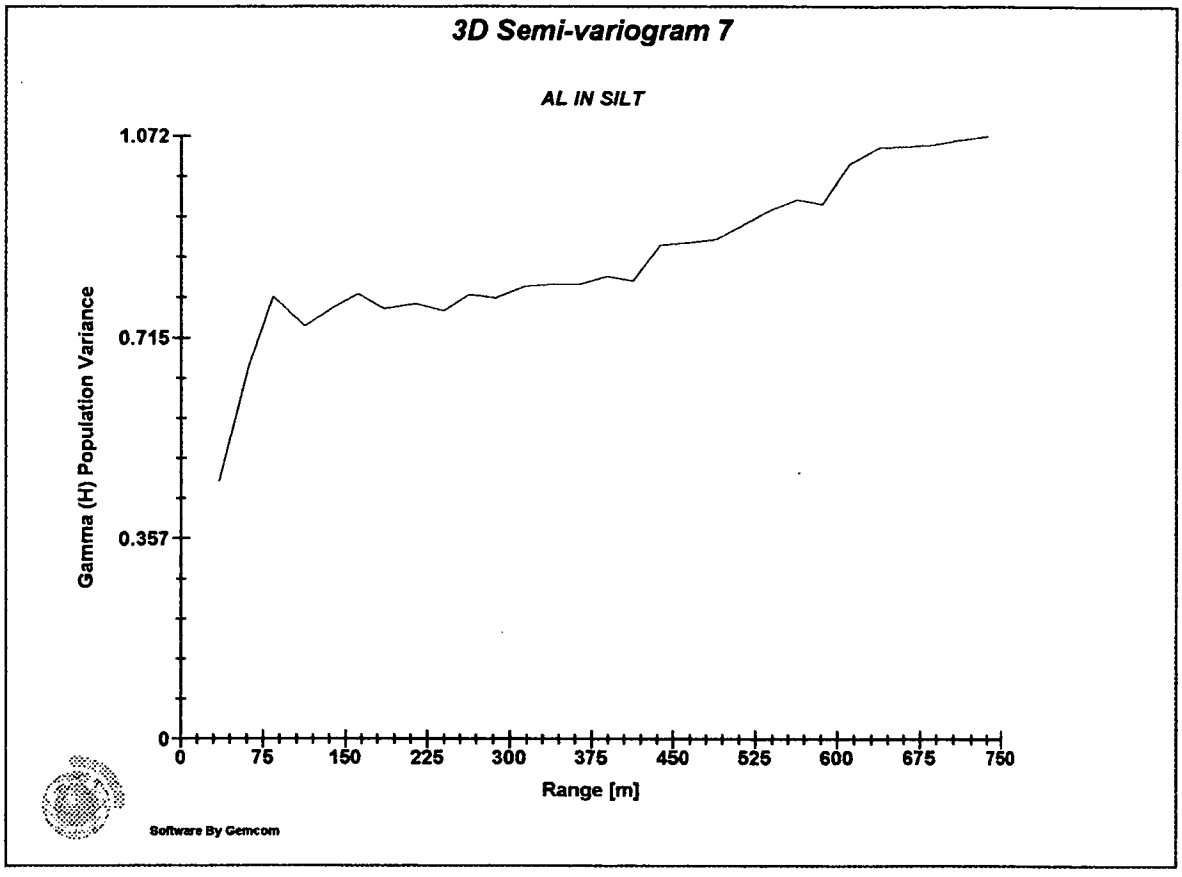
3D Semi-variogram 7
AL IN SILT
1.072
0.715
0.357
0
Gamma (H) Population Variance
0
75
150
225
300
375
450
525
600
675
750
Range [m]
Software By Gemcom

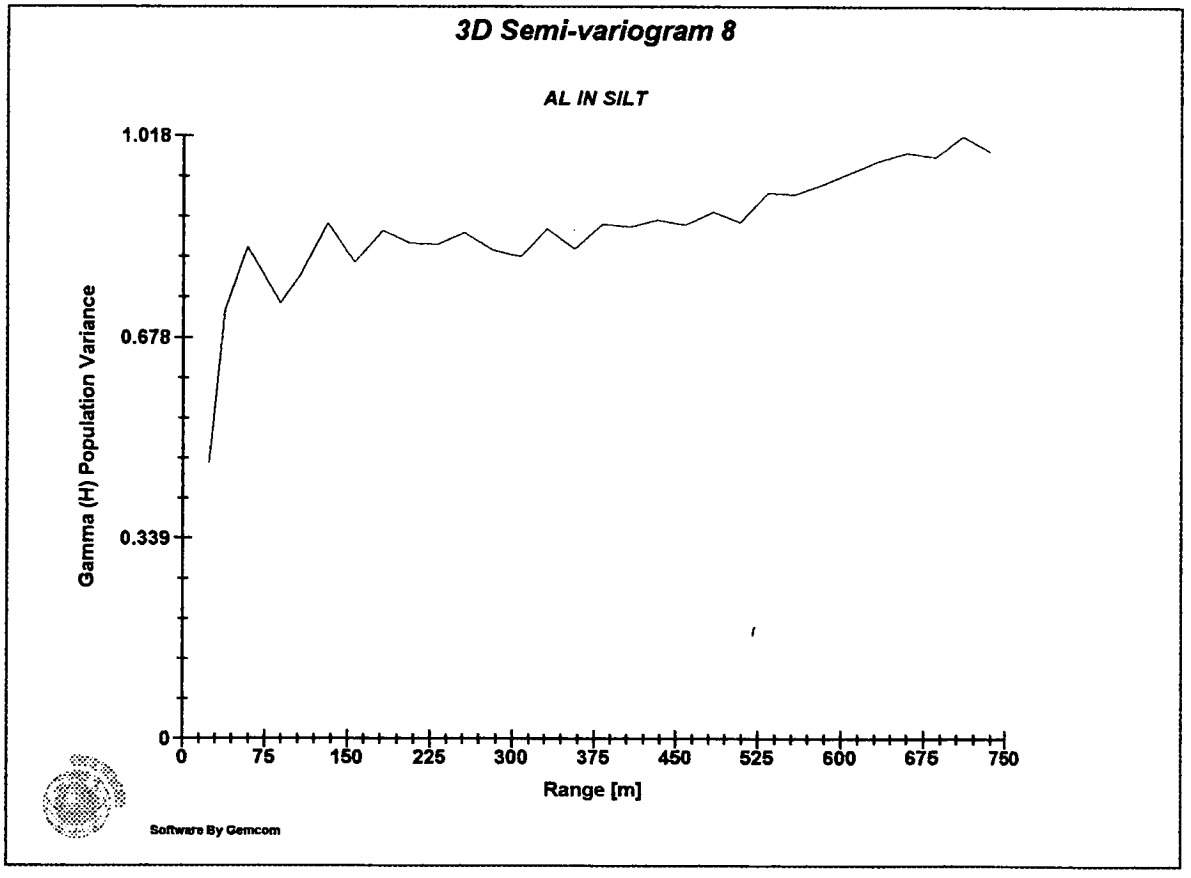
3D Semi-variogram 8
AL IN SILT
1.018
0.678
0.339
0
Gamma (H) Population Variance
0
75
150
225
300
375
450
525
600
675
750
Range [m]
Software By Gemcom

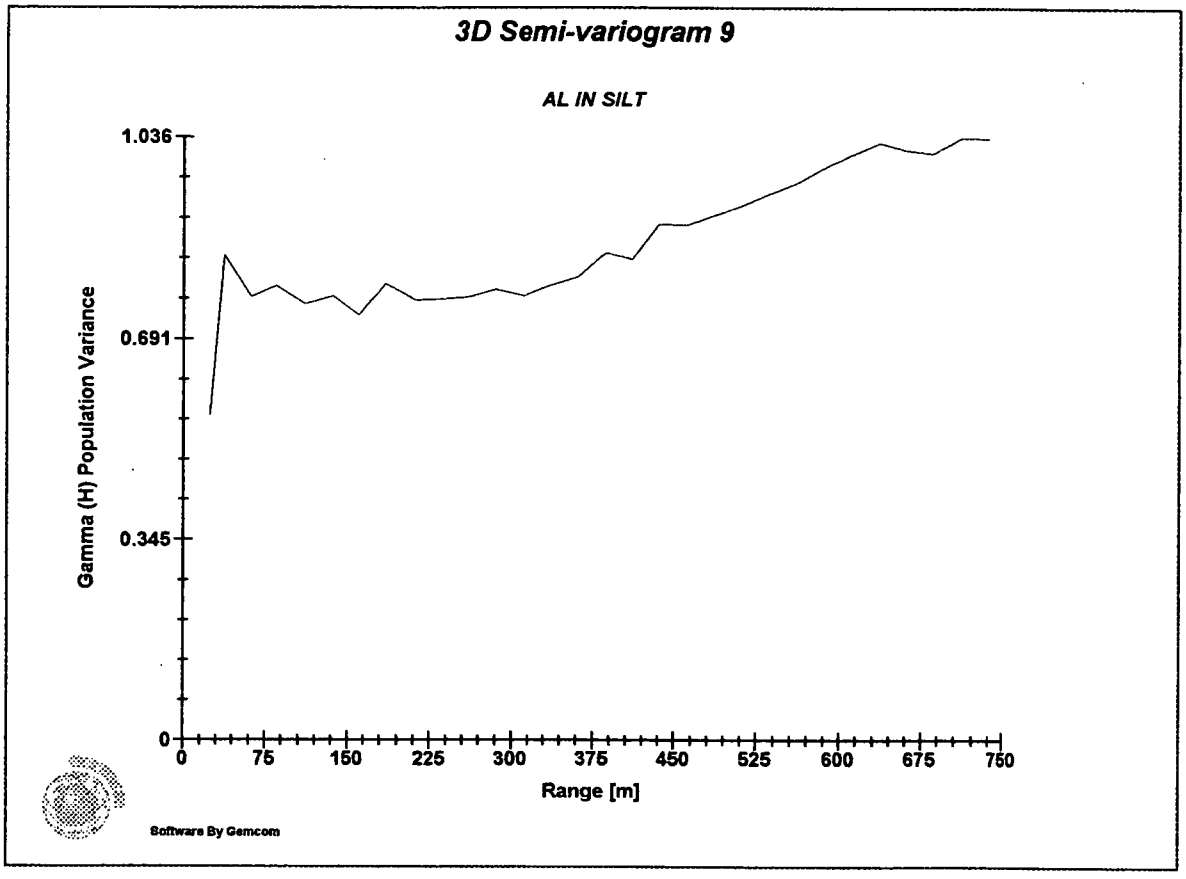
3D Semi-variogram 9
AL IN SILT
1.036
0.691
0.345
0
Gamma (H) Population Variance
0
75
150
225
300
375
450
525
600
675
750
Range [m]
Software By Gemcom

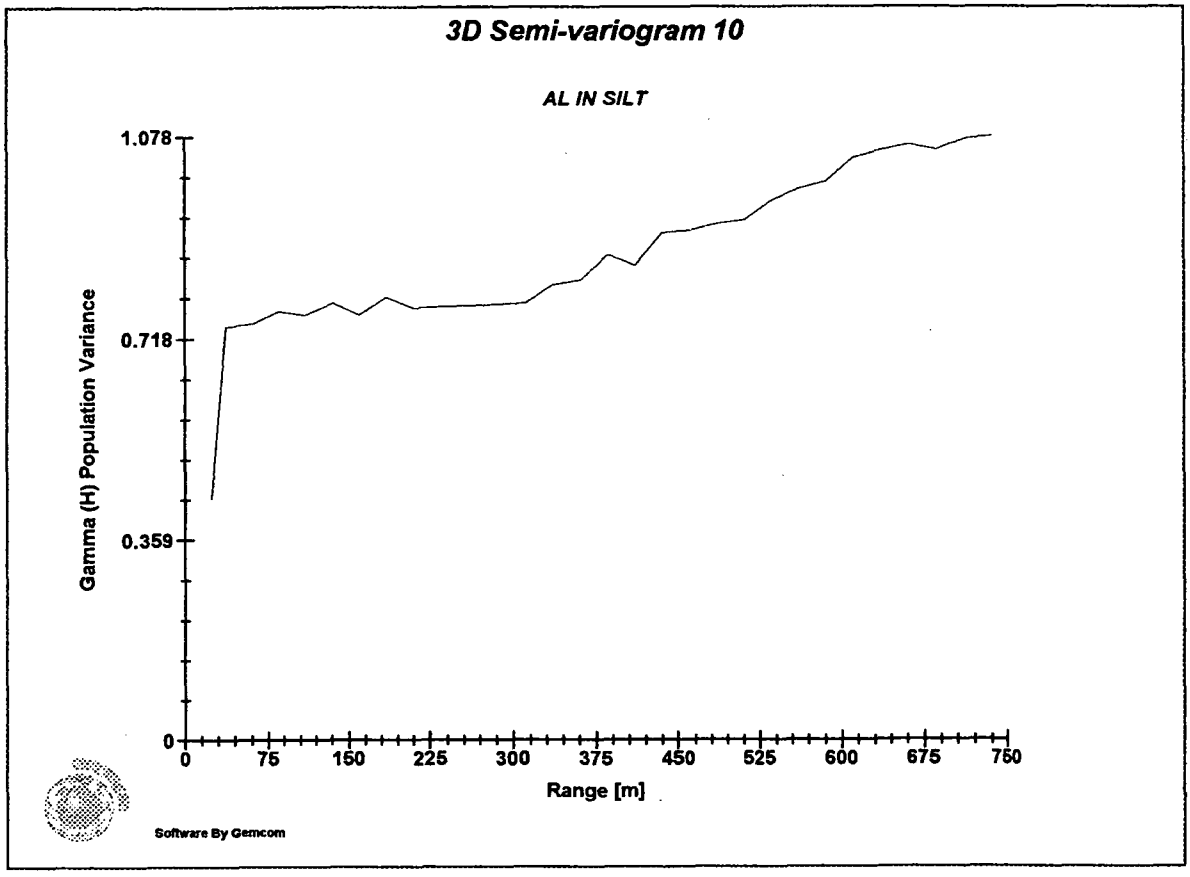
3D Semi-variogram 10
AL IN SILT
1.078
0.718
0.359
0
Gamma (H) Population Variance
0
75
150
225
300
375
450
525
600
675
750
Range [m]
Software By Gemcom

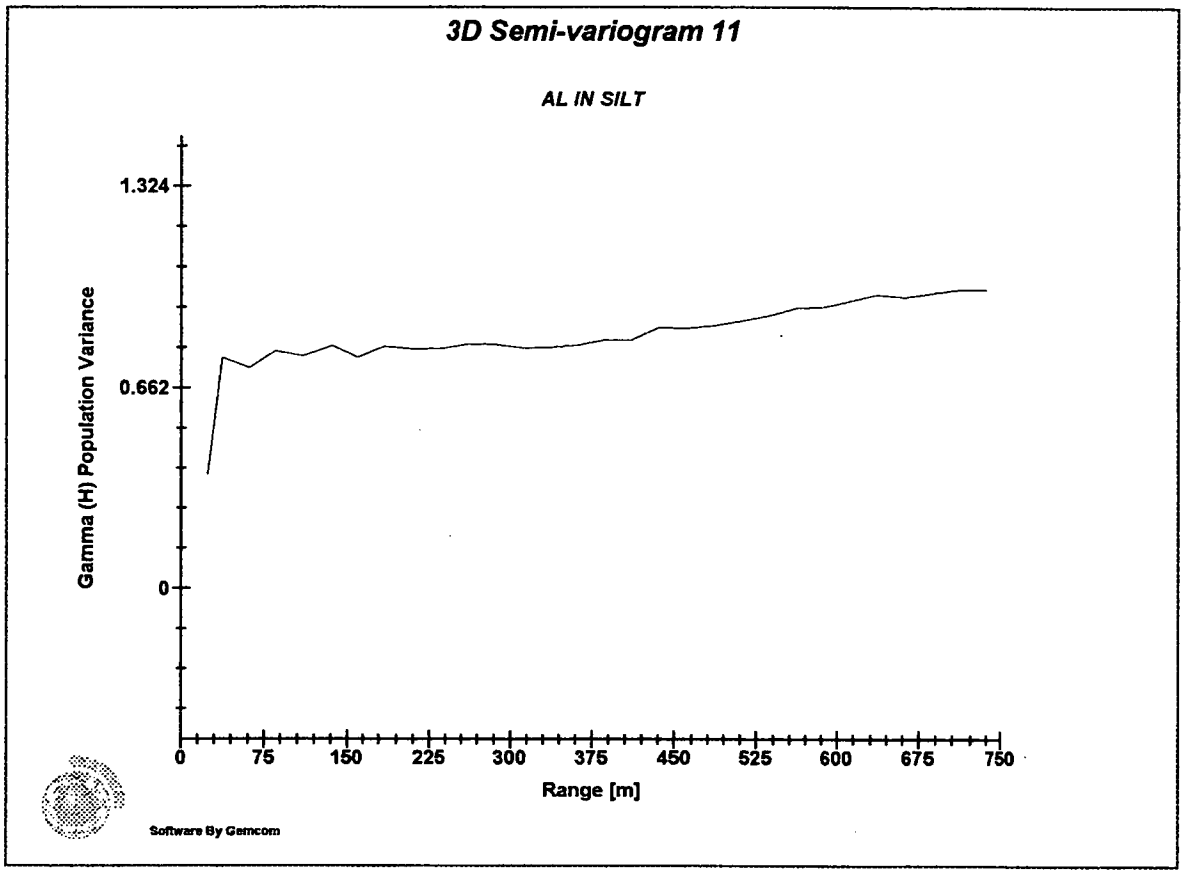
3D Semi-variogram 11
AL IN SILT
1.324
0.662
0
Gamma (H) Population Variance
0
75
150
225
300
375
450
525
600
675
750
Range [m]
Software By Gemcom

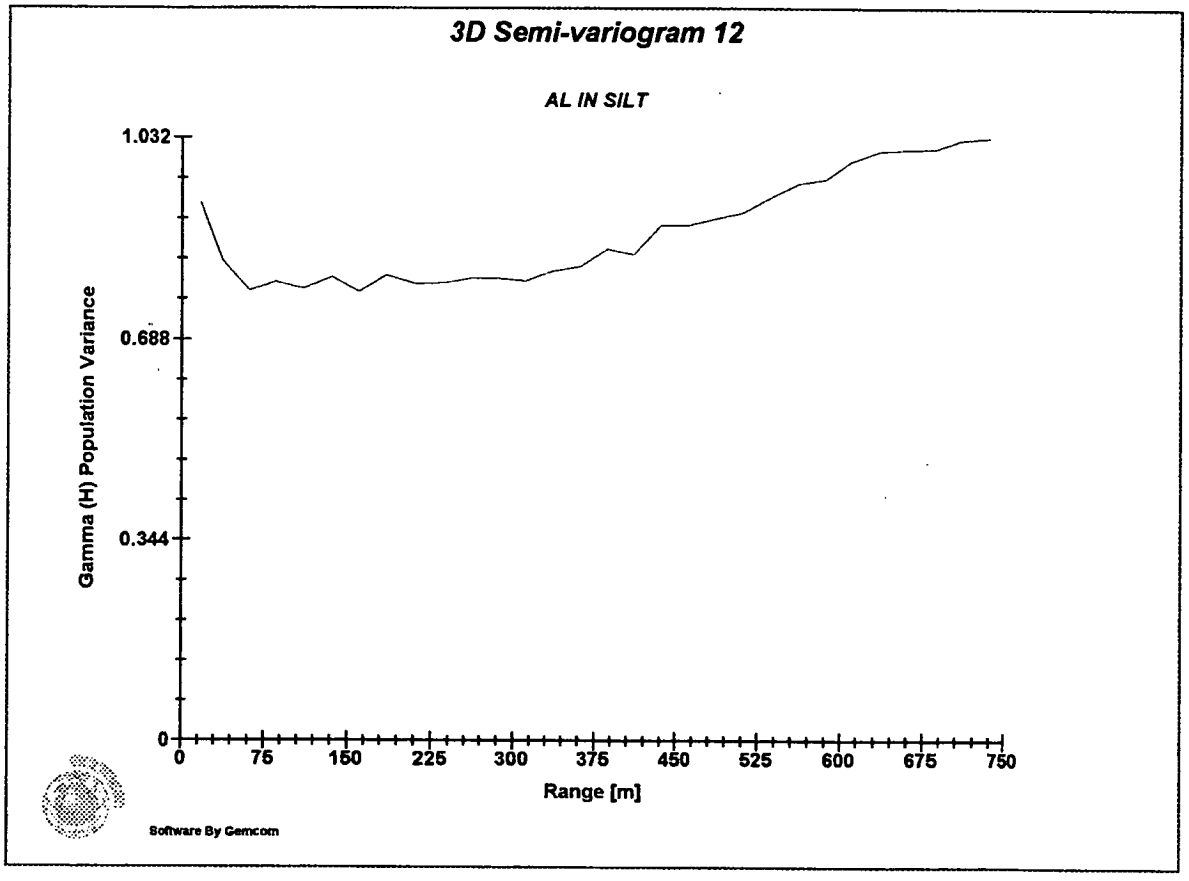
3D Semi-variogram 12
AL IN SILT
1.032
0.688
0.344
0
Gamma (H) Population Variance
0
75
150
225
300
375
450
525
600
675
750
Range [m]
Software By Gemcom

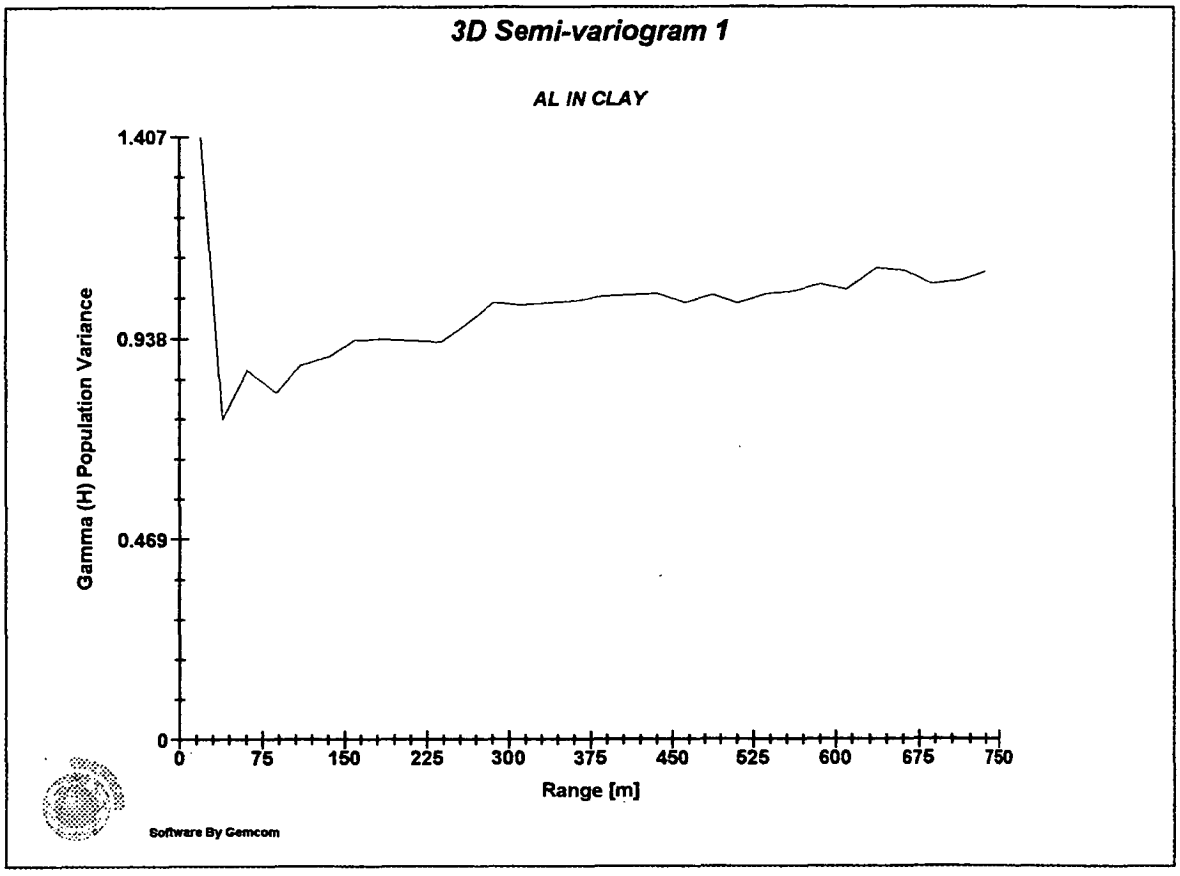
3D Semi-variogram 1
AL IN CLAY
1.407
0.938
0.469
0
Gamma (H) Population Variance
0
75
150
225
300
375
450
525
600
675
750
Range [m]
Software By Gemcom

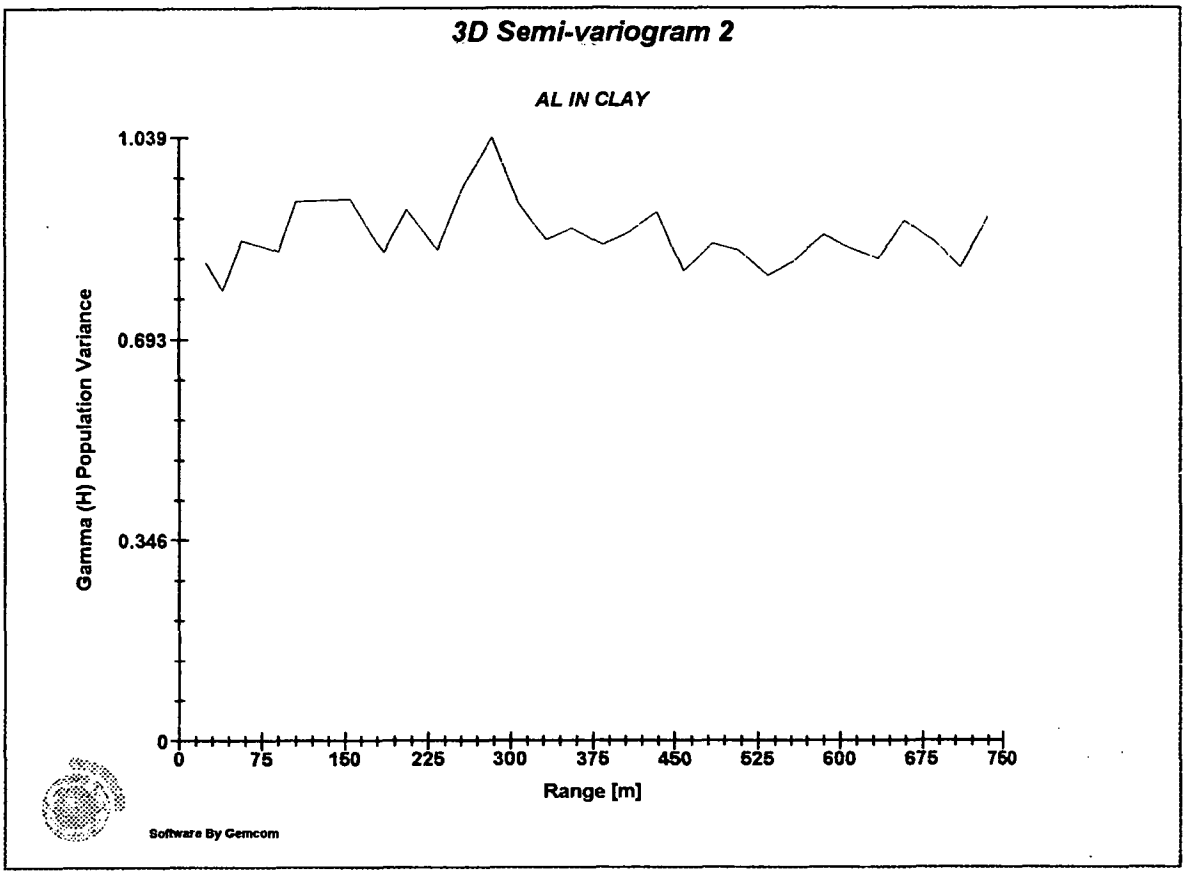
3D Semi-variogram 2
AL IN CLAY
1.039
0.693
0.346
0
Gamma (H) Population Variance
0
75
150
225
300
375
450
525
600
675
750
Range [m]
Software By Gemcom

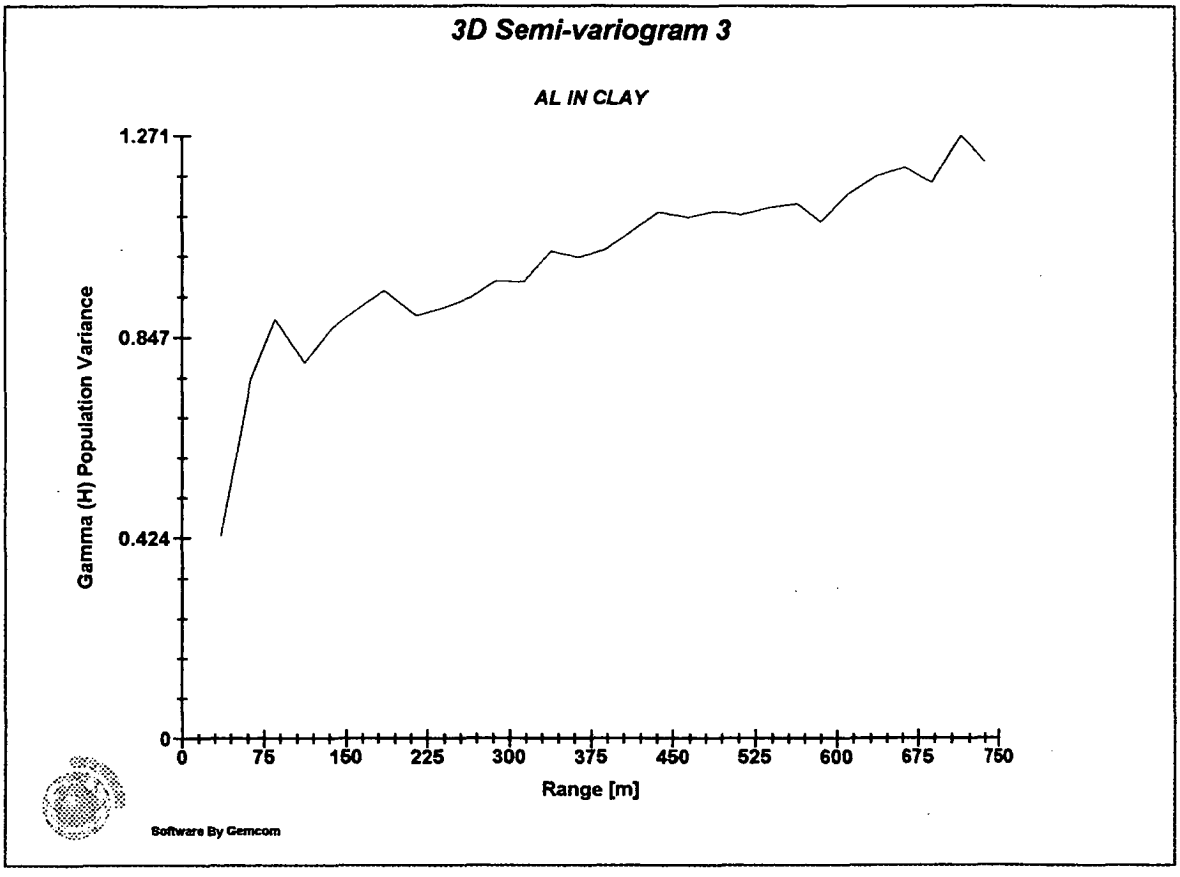
3D Semi-variogram 3
AL IN CLAY
1.271
0.847
0.424
0
Gamma (H) Population Variance
0
75
150
225
300
375
450
525
600
675
750
Range [m]
Software By Gemcom

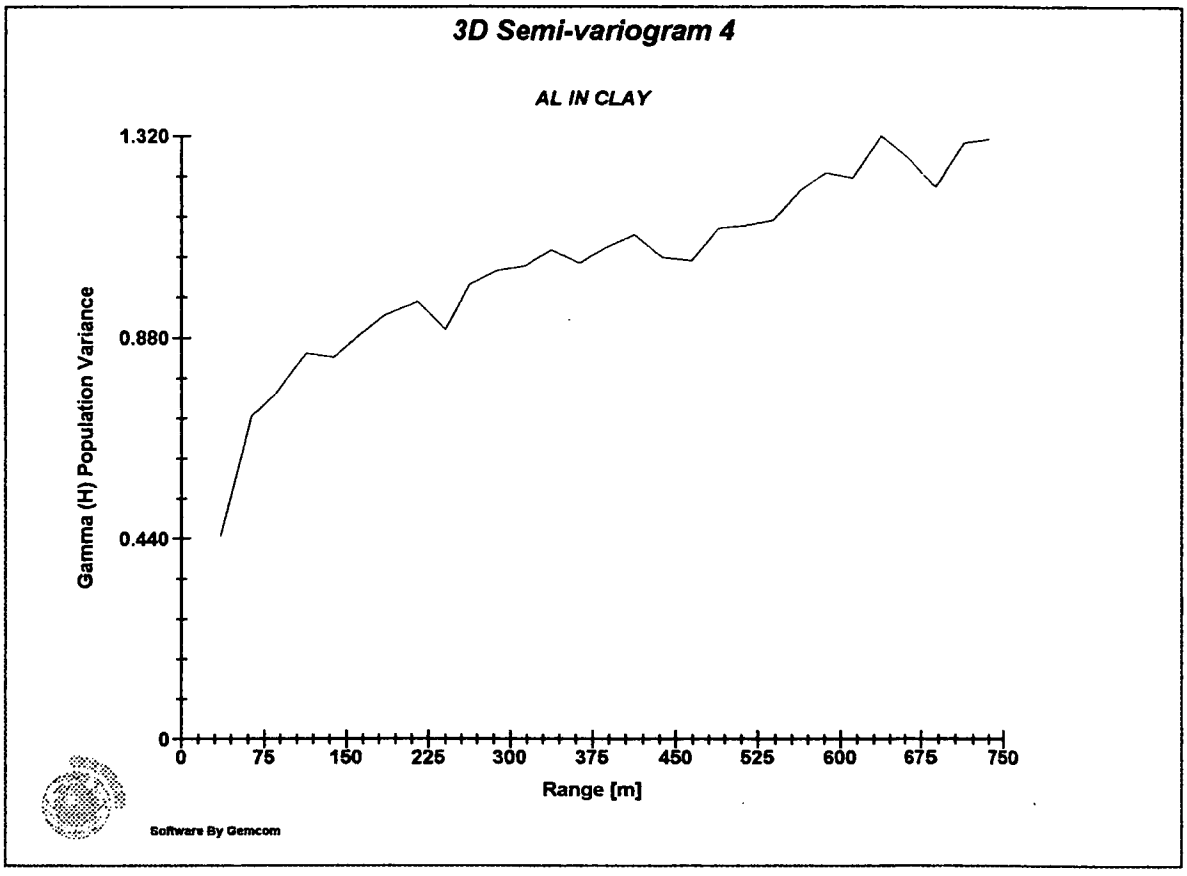
3D Semi-variogram 4
AL IN CLAY
1.320
0.880
0.440
0
Gamma (H) Population Variance
0
75
150
225
300
375
450
525
600
675
750
Range [m]
Software By Gemcom

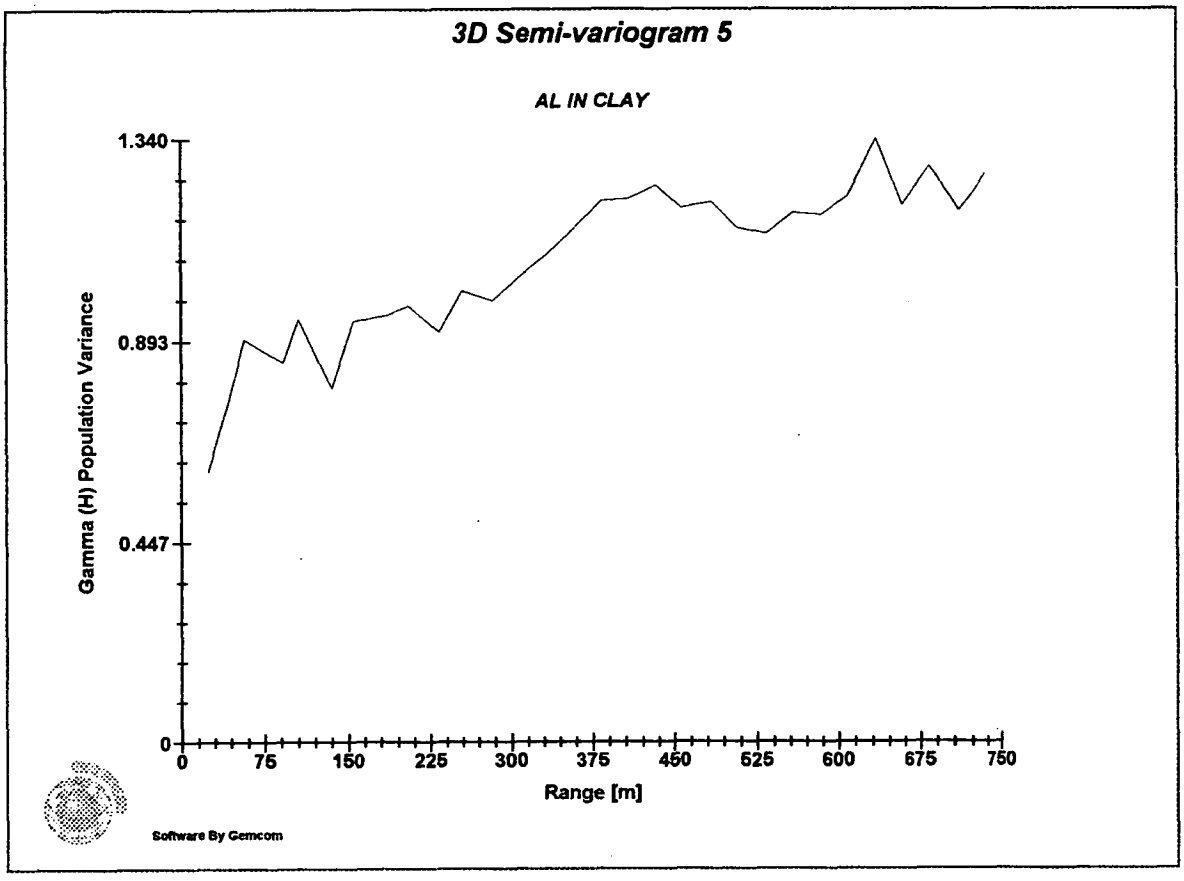
3D Semi-variogram 5
AL IN CLAY
1.340
0.893
0.447
0
Gamma (H) Population Variance
0
75
150
225
300
375
450
525
600
675
750
Range [m]
Software By Gemcom

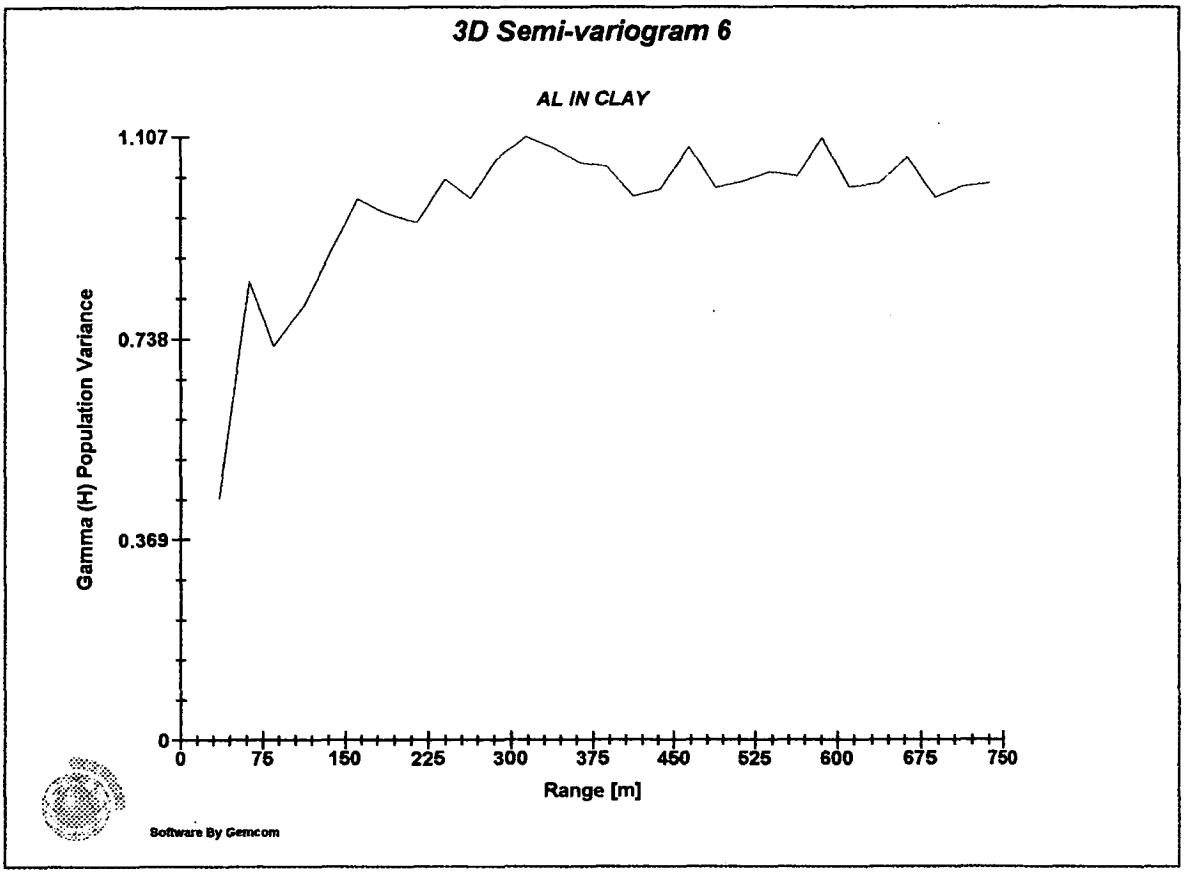
3D Semi-variogram 6
AL IN CLAY
1.107
0.738
0.369
0
Gamma (H) Population Variance
0
75
150
225
300
375
450
525
600
675
750
Range [m]
Software By Gemcom

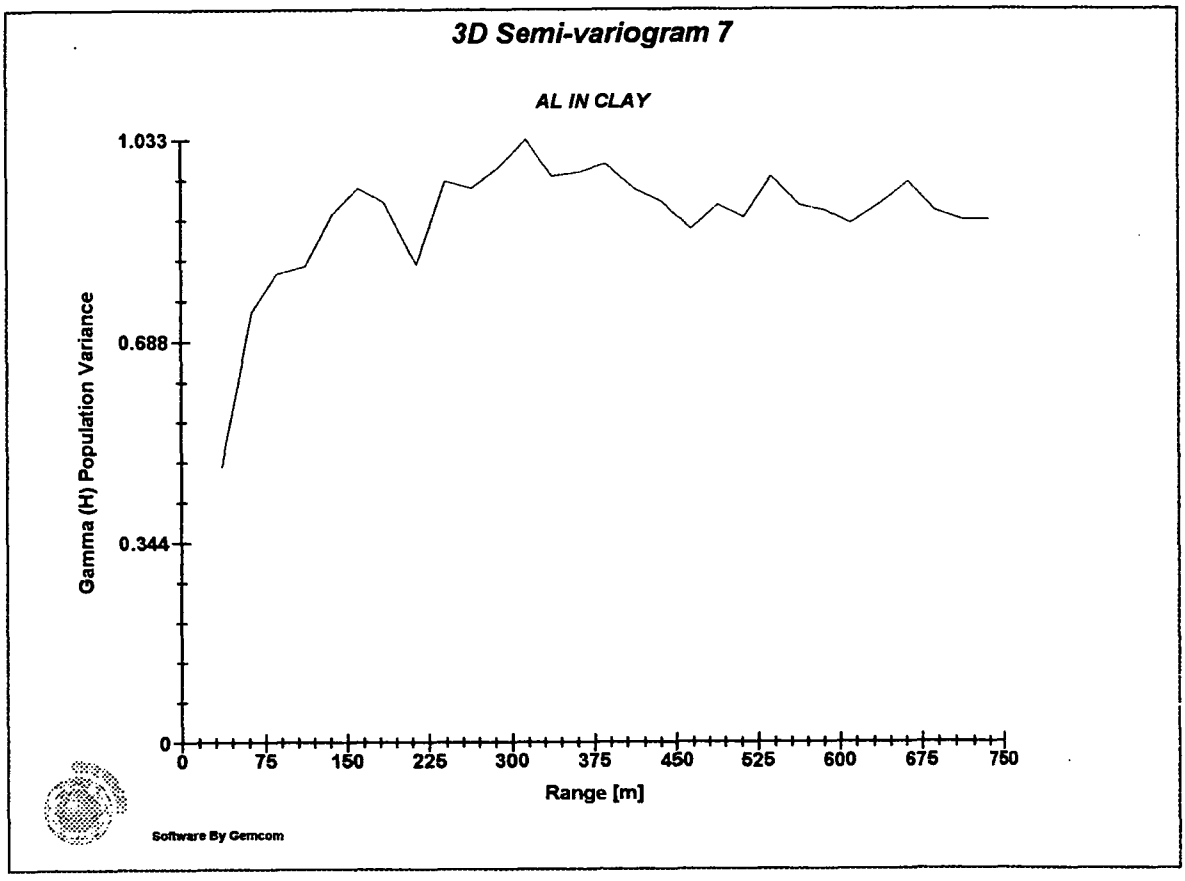
3D Semi-variogram 7
AL IN CLAY
1.033
0.688
0.344
0
Gamma (H) Population Variance
0
75
150
225
300
375
450
525
600
675
750
Range [m]
Software By Gemcom

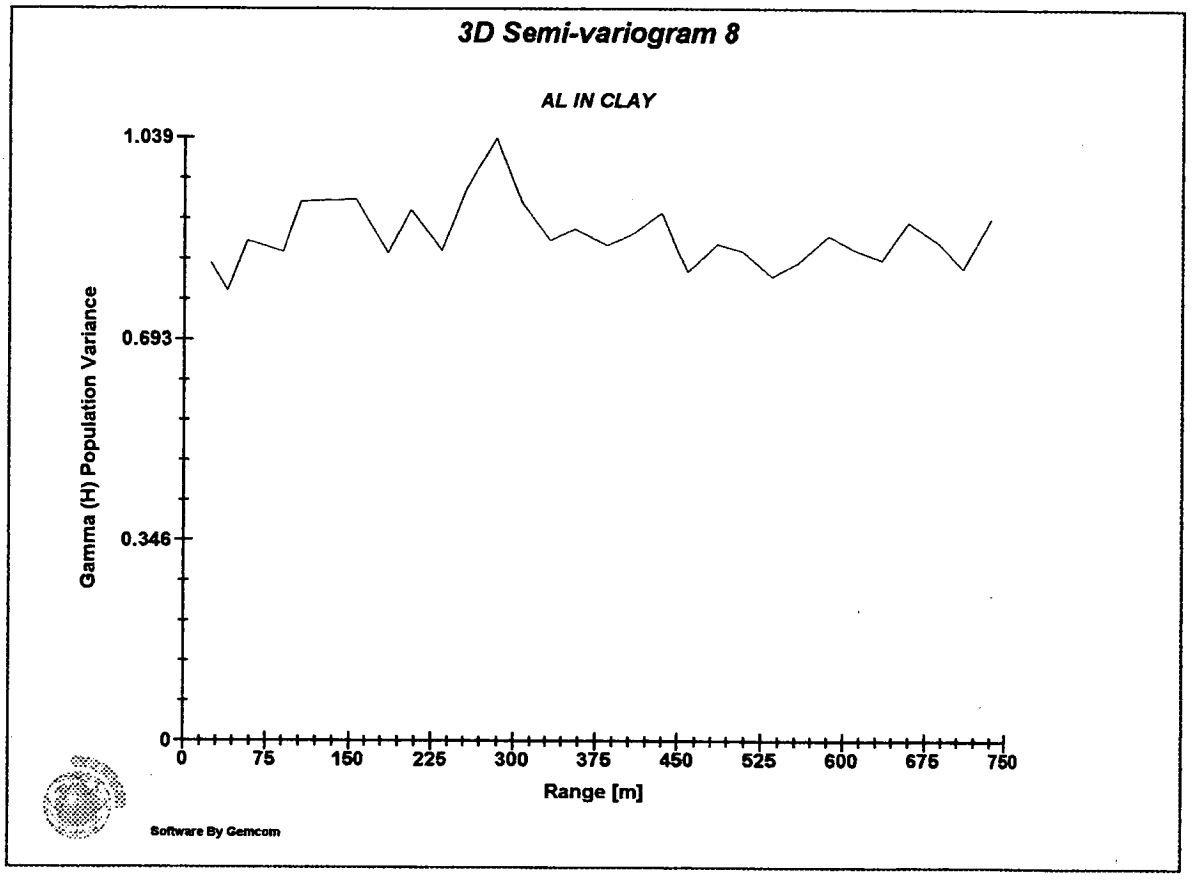
3D Semi-variogram 8
AL IN CLAY
1.039
0.693
0.346
0
Gamma (H) Population Variance
0
75
150
225
300
375
450
525
600
675
750
Range [m]
Software By Gemcom

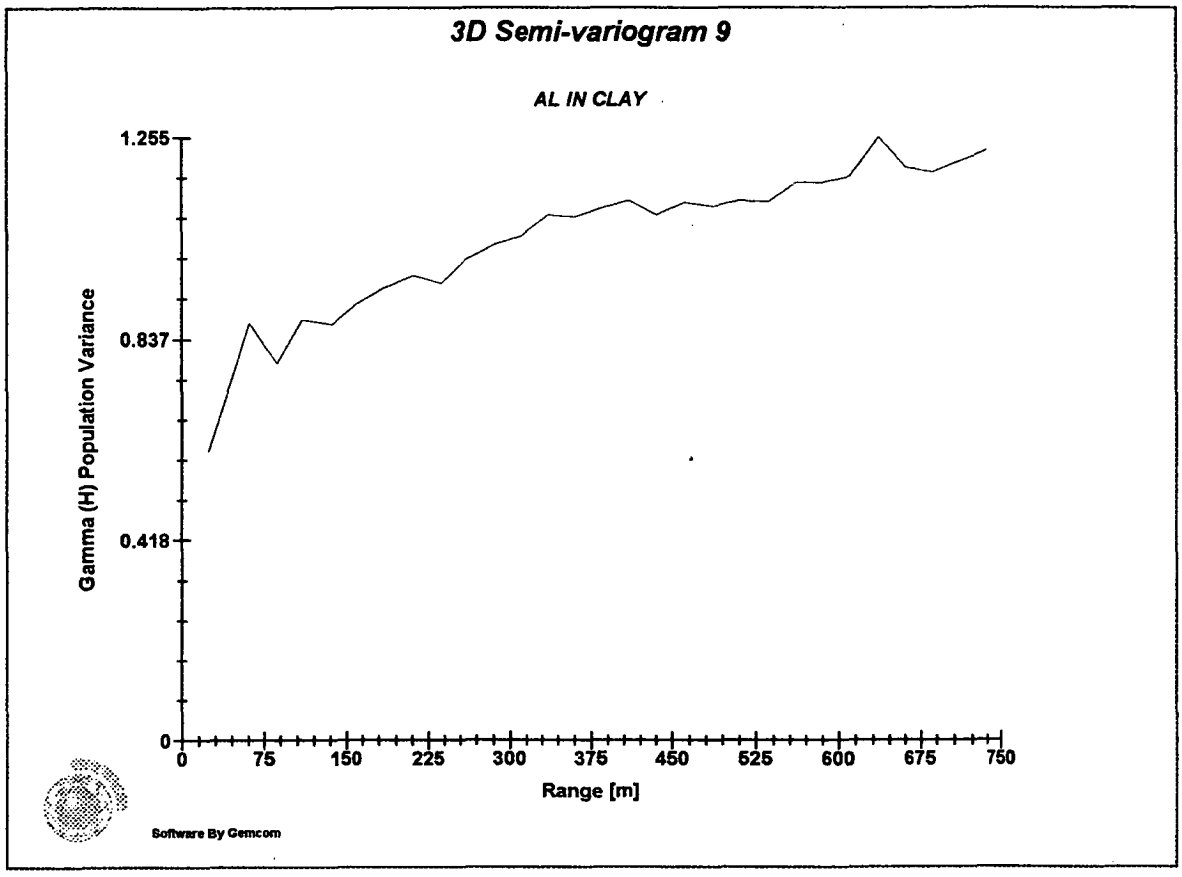
3D Semi-variogram 9
AL IN CLAY
1.255
0.837
0.418
0
Gamma (H) Population Variance
0
75
150
225
300
375
450
525
600
675
750
Range [m]
Software By Gemcom

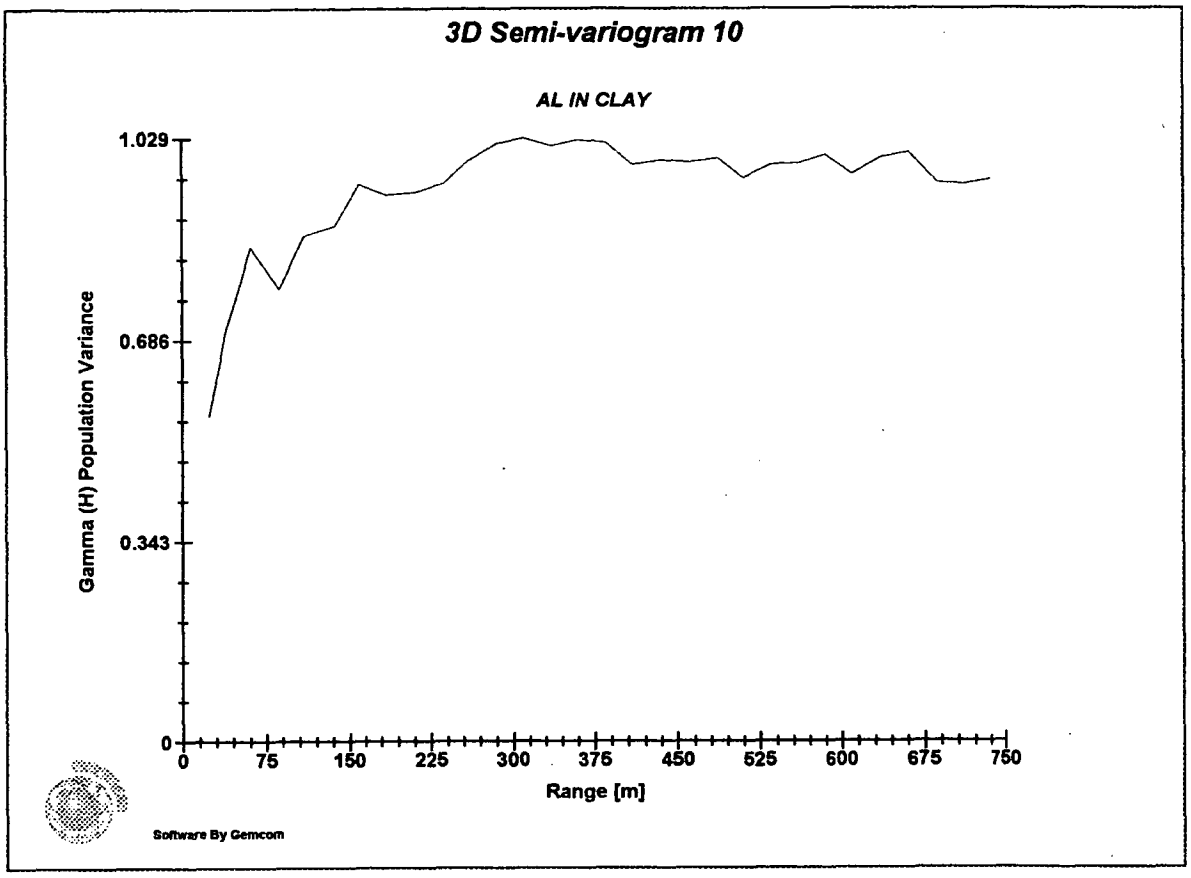
3D Semi-variogram 10
AL IN CLAY
1.029
0.686
0.343
0
Gamma (H) Population Variance
0
75
150
225
300
375
450
525
600
675
750
Range [m]
Software By Gemcom

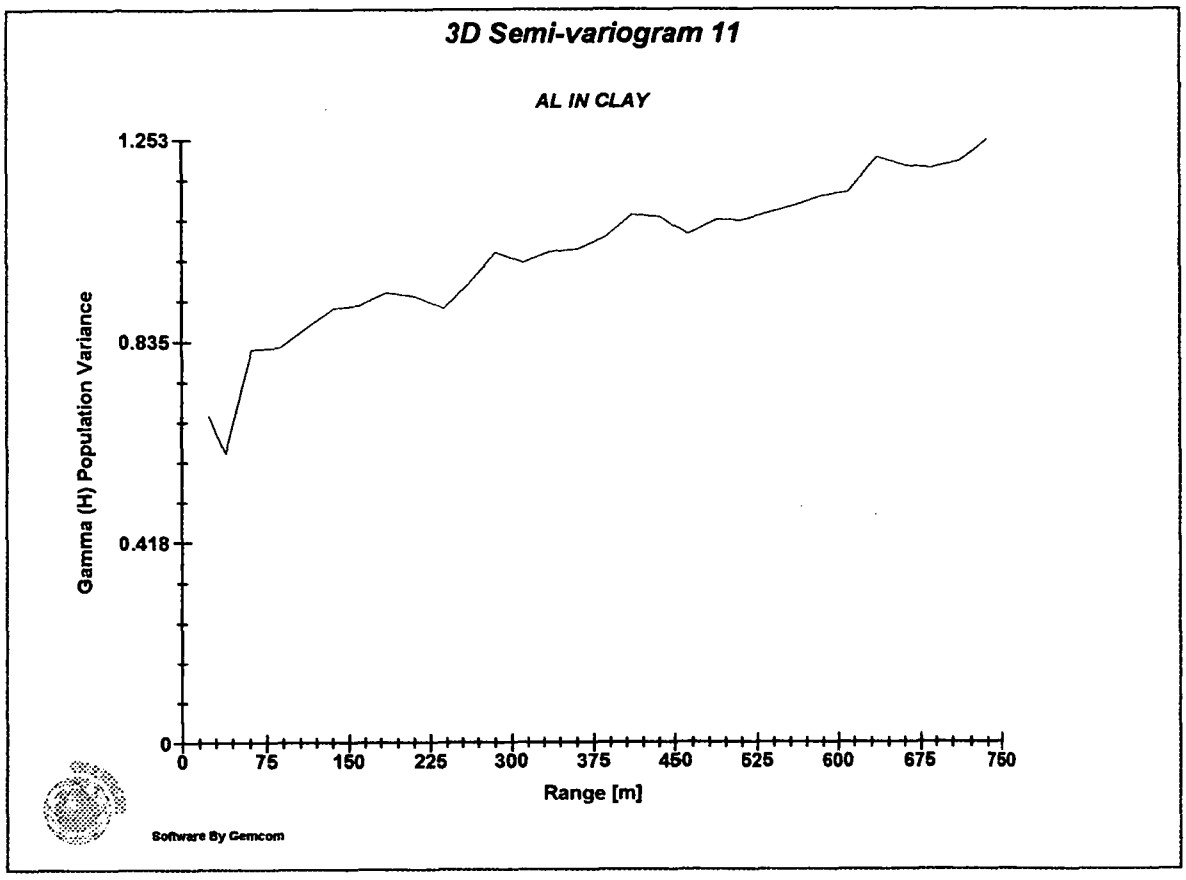
3D Semi-variogram 11
AL IN CLAY
1.253
0.835
0.418
0
Gamma (H) Population Variance
0
75
150
225
300
375
450
525
600
675
750
Range [m]
Software By Gemcom

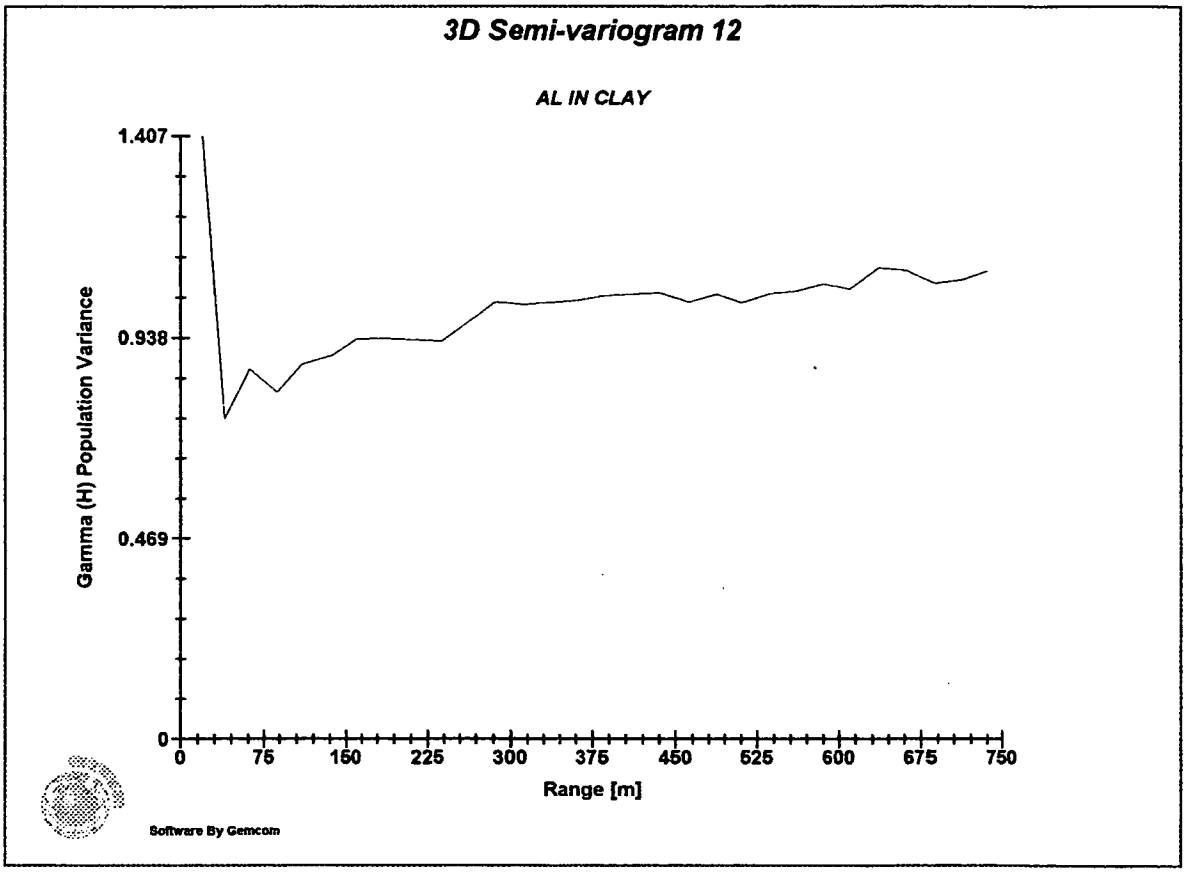
3D Semi-variogram 12
AL IN CLAY
Gamma (H) Population Variance
1.407
0.938
0.469
0
0
75
150
225
300
375
450
525
600
675
750
Range [m]
Software By Gemcom

APPENDIX TWO

Linear Variograms

MEAN =	92.92039	STD. DEV=	4.49480	NO. =	6804
LOG MEAN=	.00000	LOG STDV=	.00000	C.V.=	.05

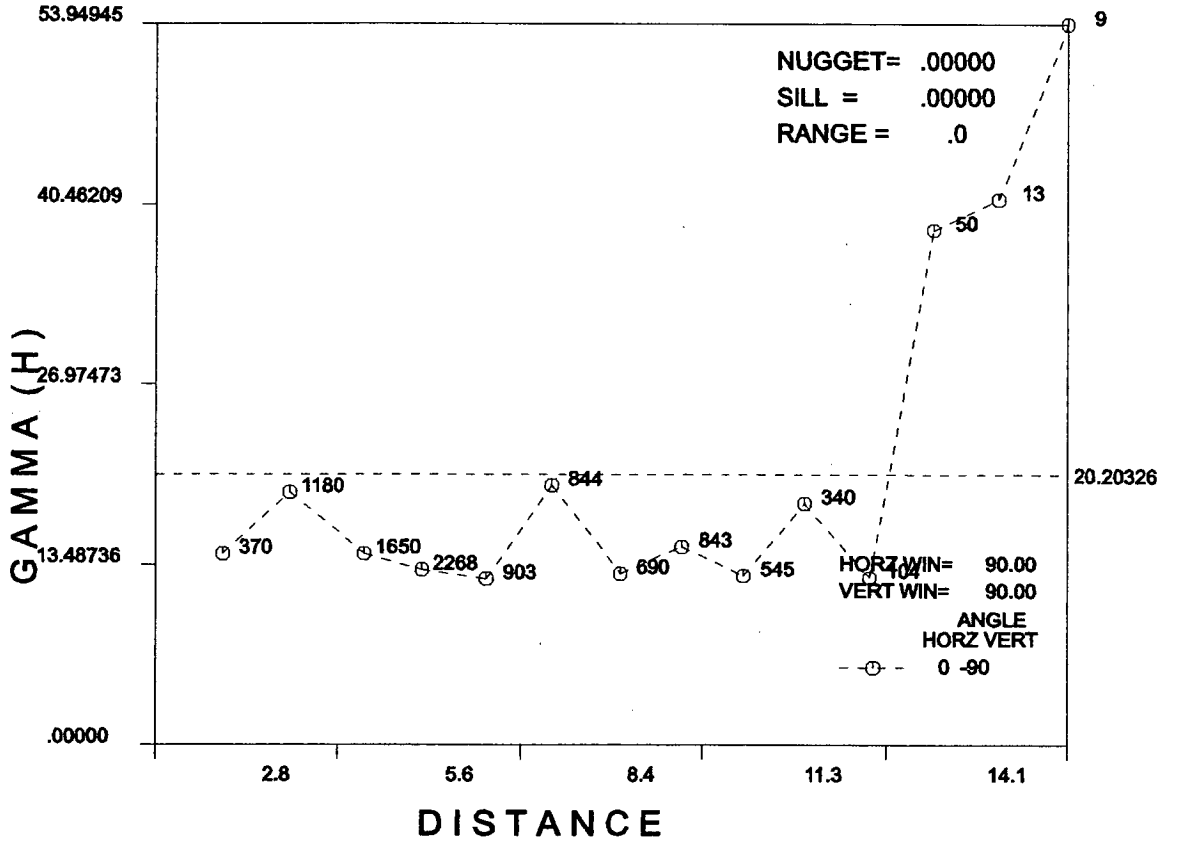

DwnH, Norm, MgO=10-100, Lag=1(+/-)0m, All Samples.

MEAN = 92.92039 STD. DEV= 4.49480 NO. = 6804
LOG MEAN= .00000 LOG STDV= .00000 C.V.= .05

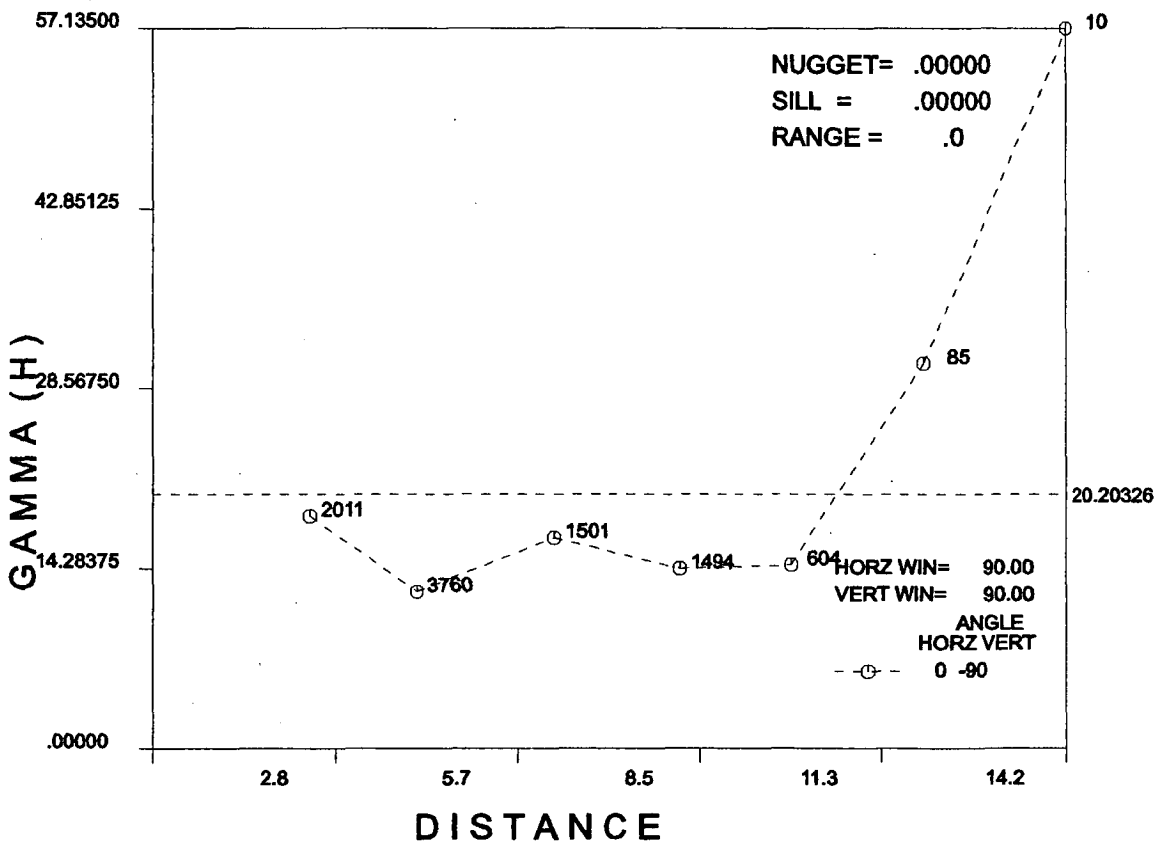

DwnH, Norm, MgO=10-100, Lag2m(+/-)0m, All Samples.

MEAN =	2.88953	STD. DEV=	1.89939	NO. =	4515
LOG MEAN=	.00000	LOG STDV=	.00000	C.V.=	.66

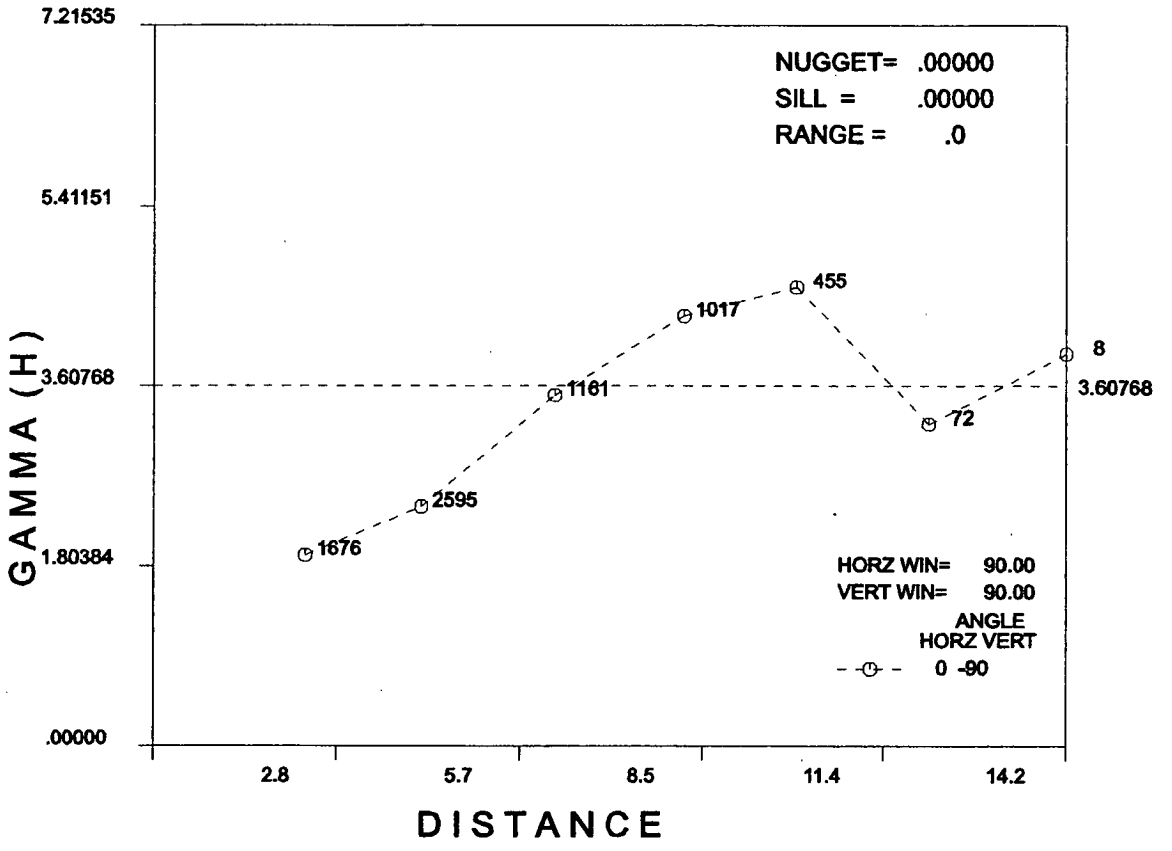

DwnH, Norm, Sio2=0.3-20, Lag=2(+/-)0m, All Samples.

MEAN =	2.88953	STD. DEV=	1.89939	NO. =	4515
LOG MEAN=	.00000	LOG STDV=	.00000	C.V.=	.66

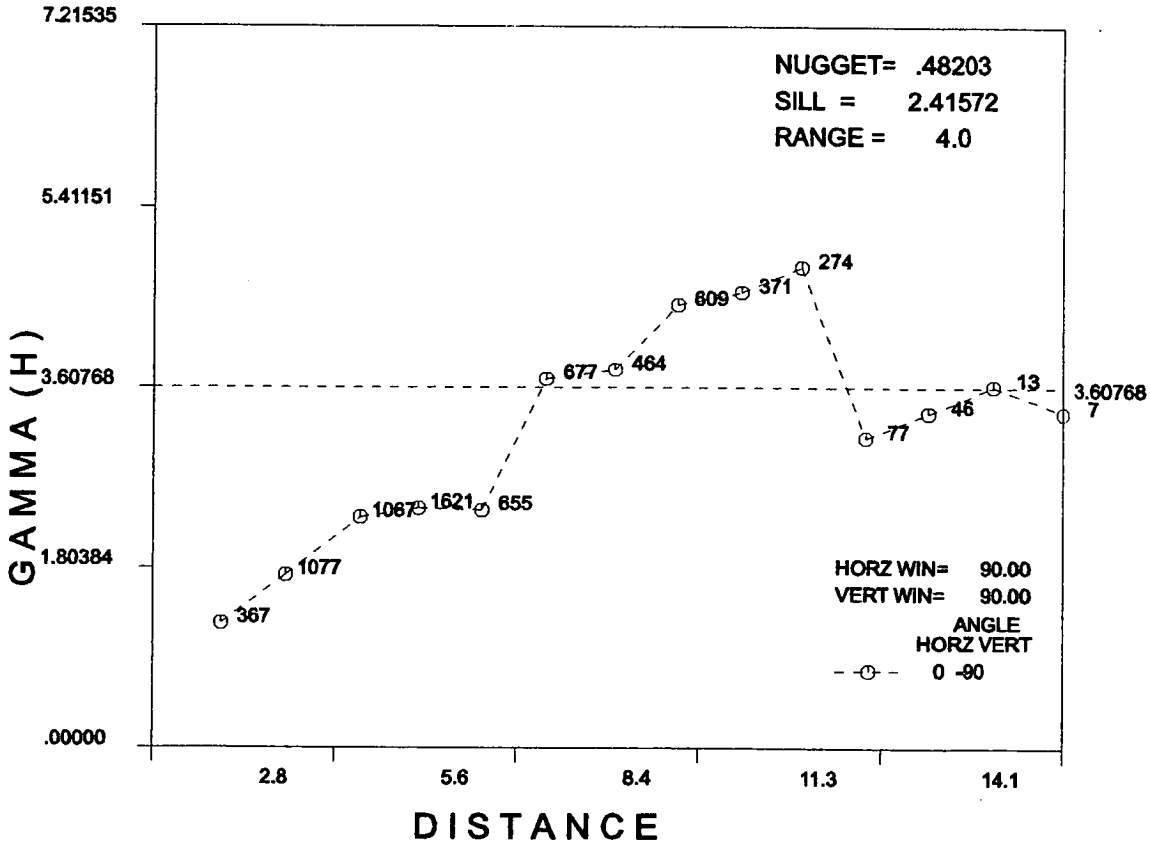

DwnH, Norm, SiO2=0.3-20, Lag=1(+/-)0m, All Samples.

MEAN =	.14373	STD. DEV=	.05387	NO. =	5673
LOG MEAN=	.00000	LOG STDV=	.00000	C.V.=	.37

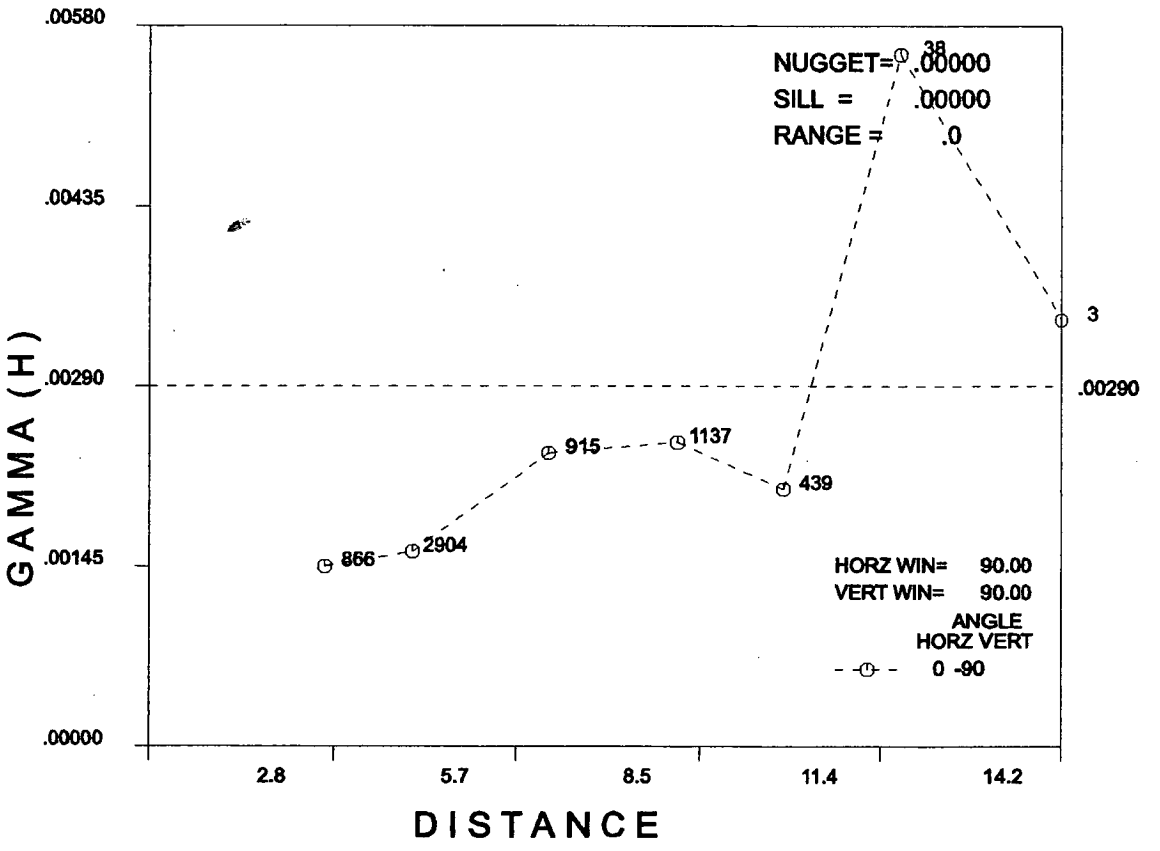

DwnH, Norm, Mn3O4=0.02-1, Lag=2(+/-)0m, All Samples.

MEAN =	.14373	STD. DEV=	.05387	NO. =	5673
LOG MEAN=	.00000	LOG STDV=	.00000	C.V.=	.37

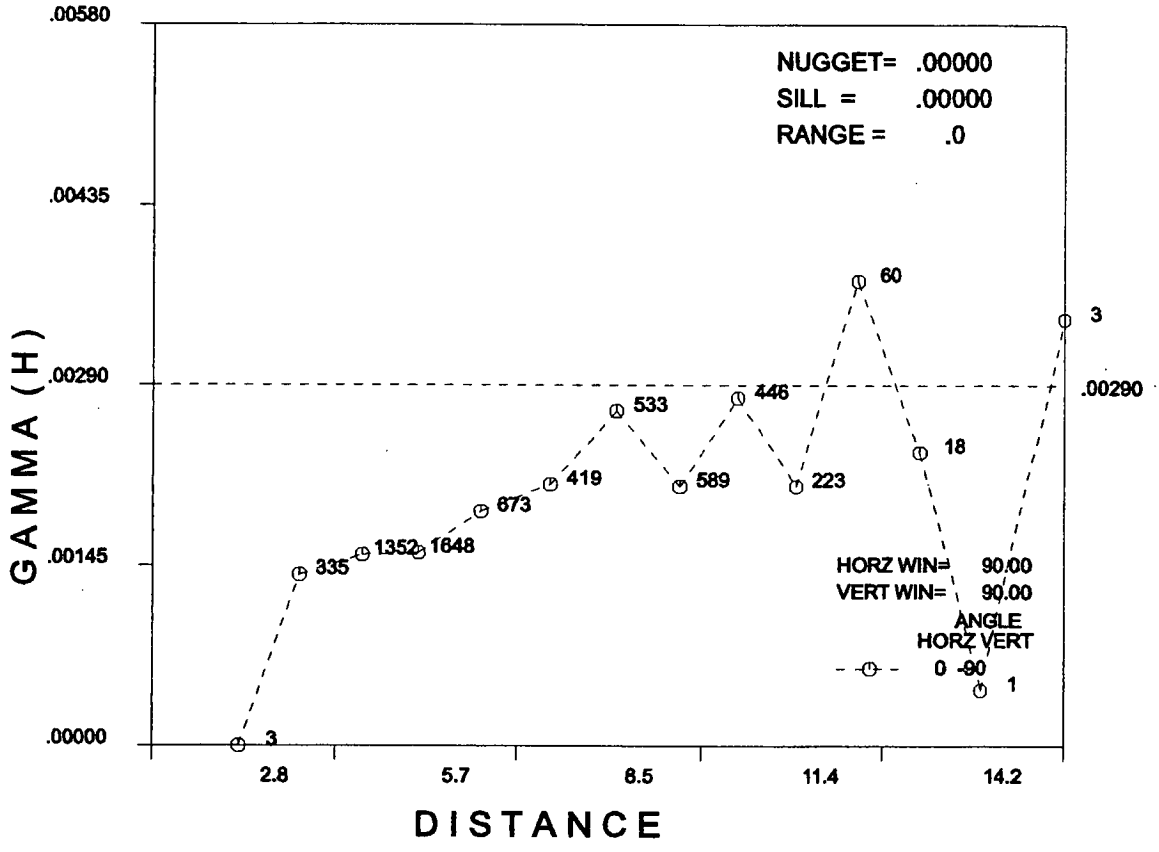

DwnH, Norm, Mn3O4=0.02-1, Lag=1(+/-)0m, All Samples.

MEAN =	.25302	STD. DEV=	.17324	NO. =	4197
LOG MEAN=	.00000	LOG STDV=	.00000	C.V.=	.68

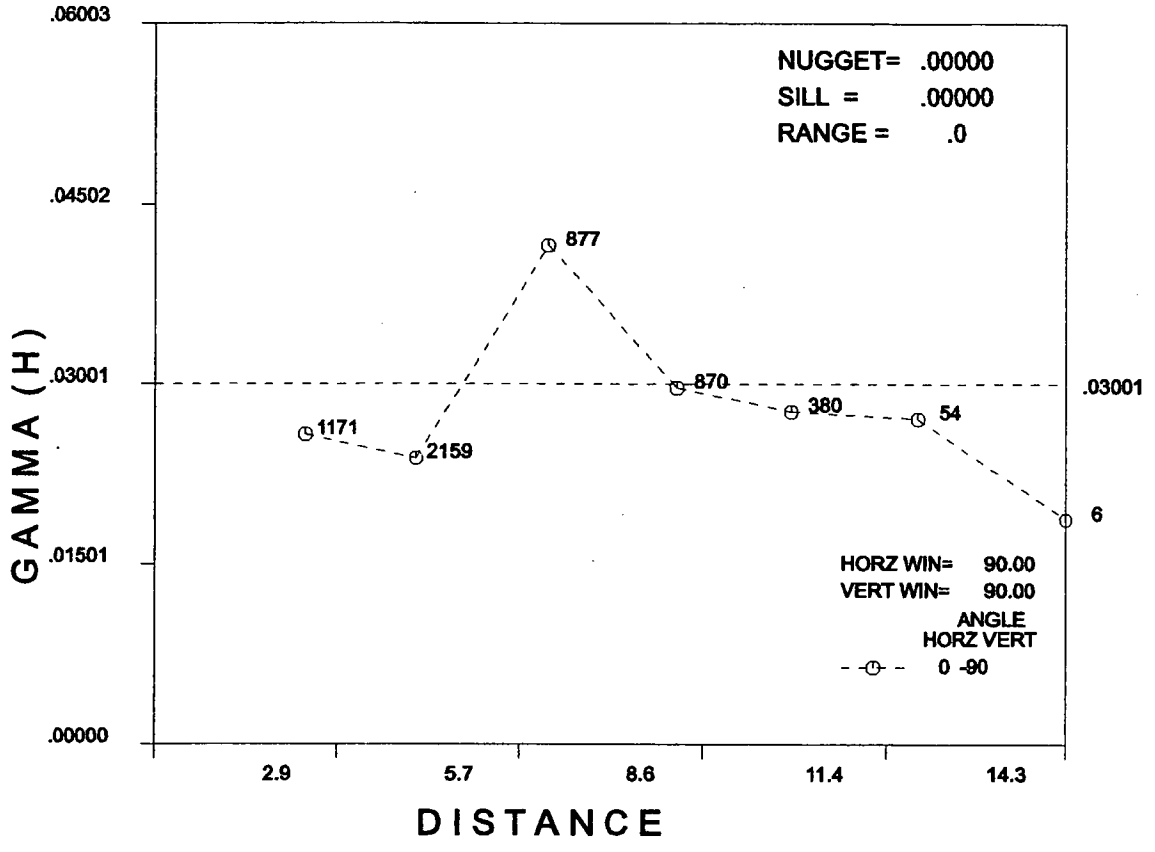

DwnH, Norm, Fe2O3=0.1-4, Lag=2(+/-)0m, All Samples.

MEAN =	.25302	STD. DEV=	.17324	NO. =	4197
LOG MEAN=	.00000	LOG STDV=	.00000	C.V.=	.68

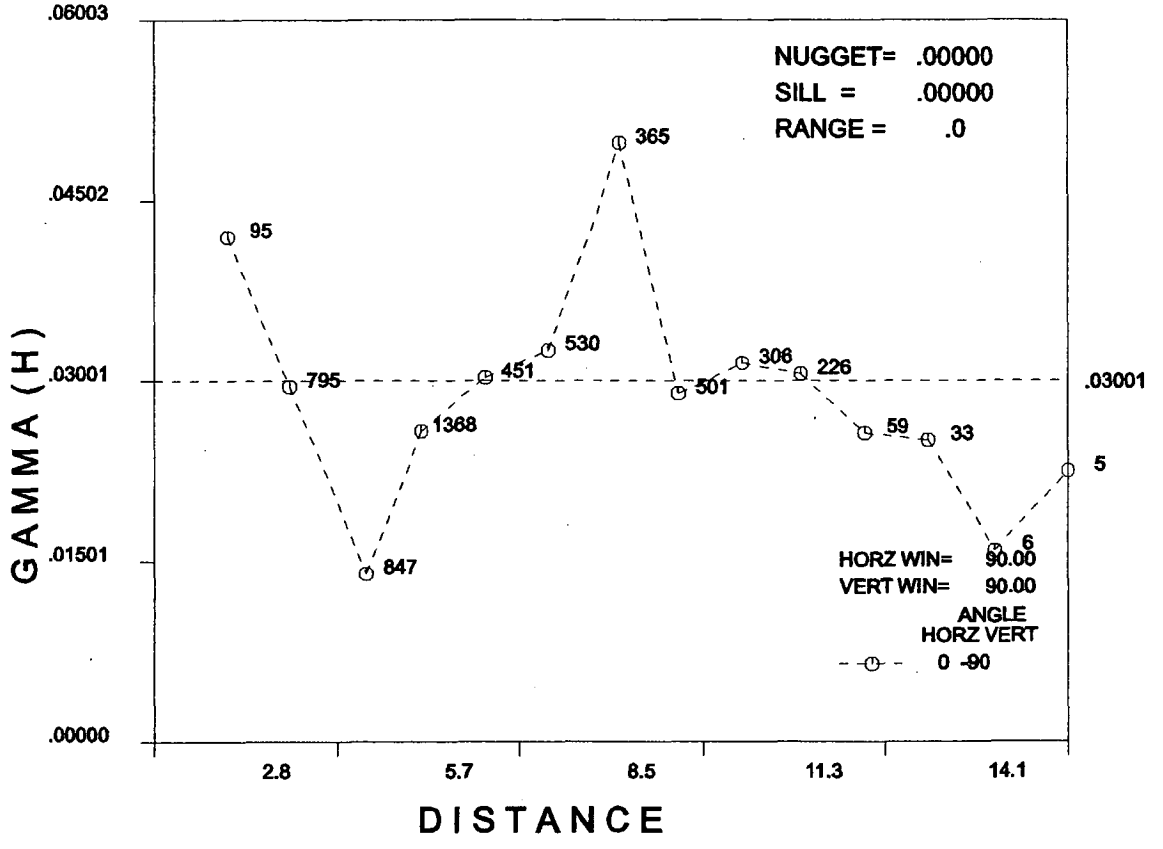

DwnH, Norm, Fe203=0.1-4, Lag=1(+/-)0m, All Samples.

MEAN = 4.86922 STD. DEV= 3.91411 NO. = 4509

LOG MEAN= .00000 LOG STDV= .00000 C.V.= .80

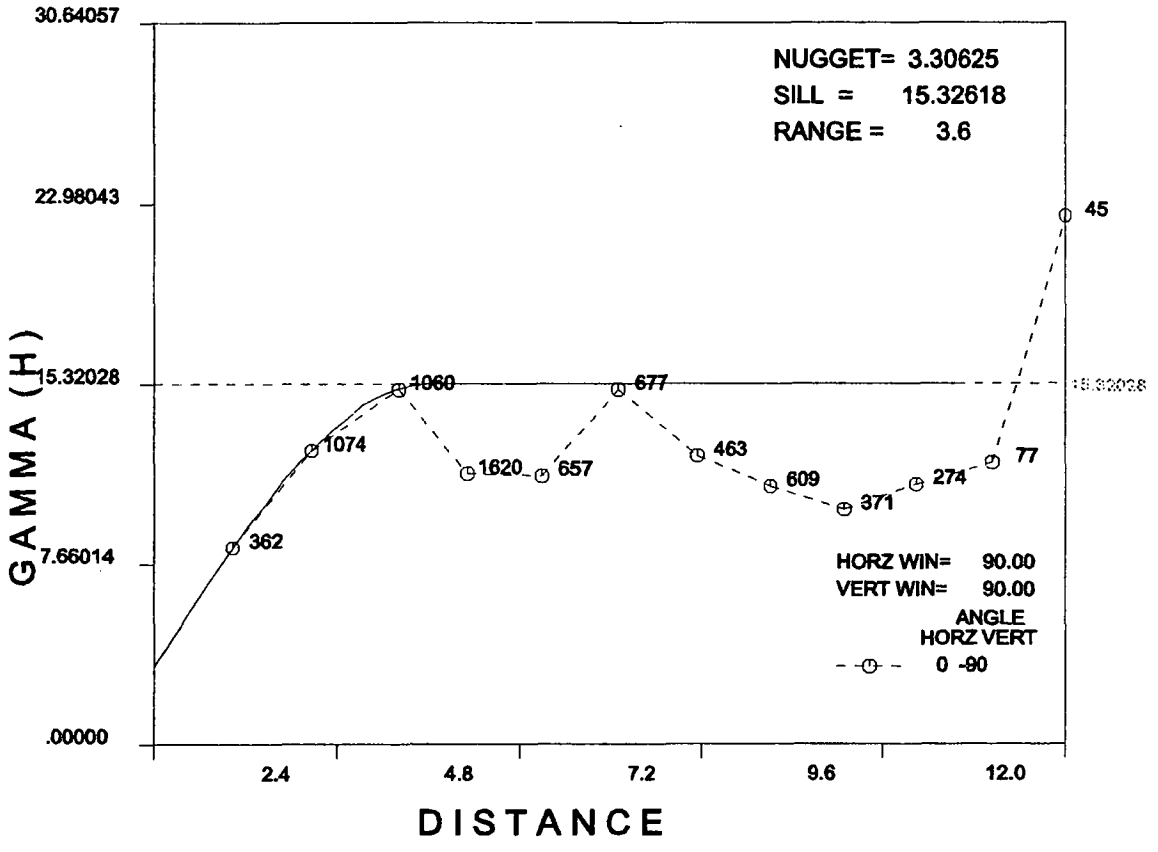

DwnH, Norm, Ca0=1-30, Lag=1(+/-)0m, All Samples.

MEAN =	4.86922	STD. DEV=	3.91411	NO. =	4509
LOG MEAN=	.00000	LOG STDV=	.00000	C.V.=	.80

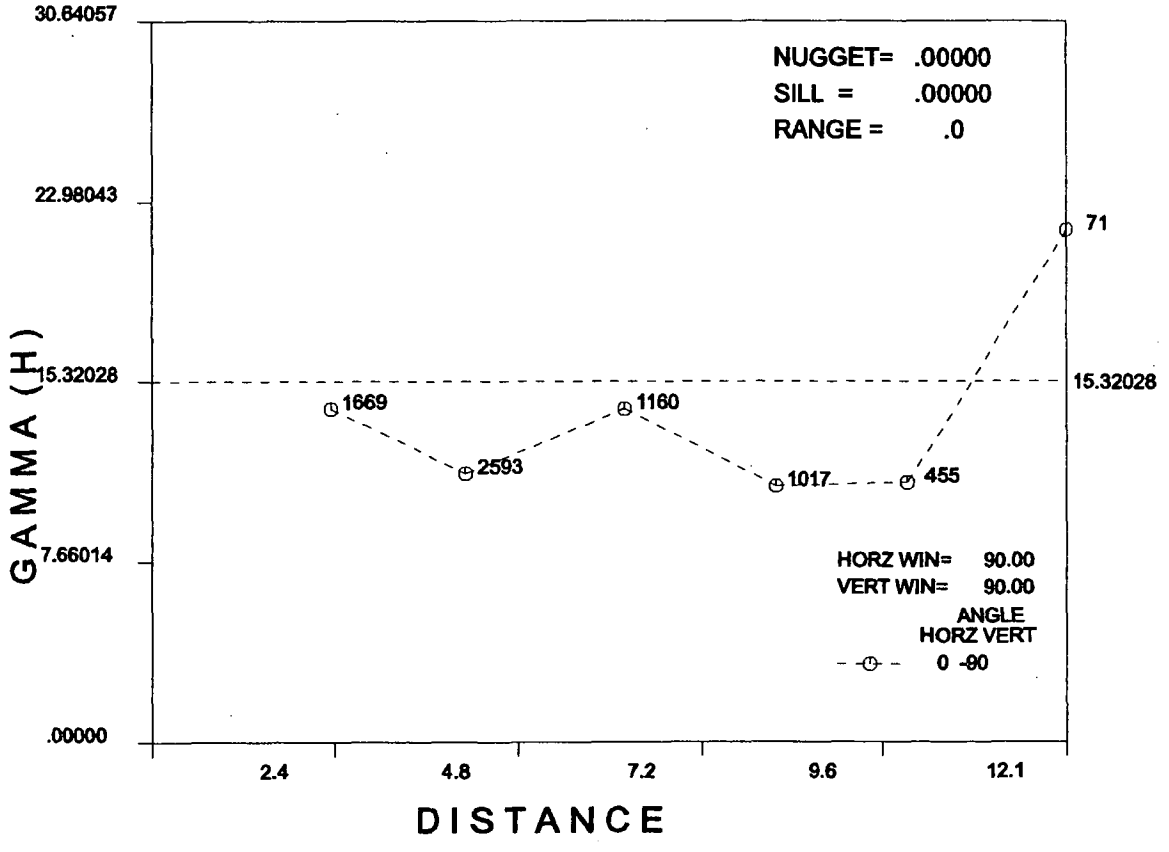

DwnH, Norm, CaO=1-30, Lag=2(+/-)0m, All samples.

MEAN =	.31286	STD. DEV=	.20864	NO. =	3997
LOG MEAN=	.00000	LOG STDV=	.00000	C.V.=	.67

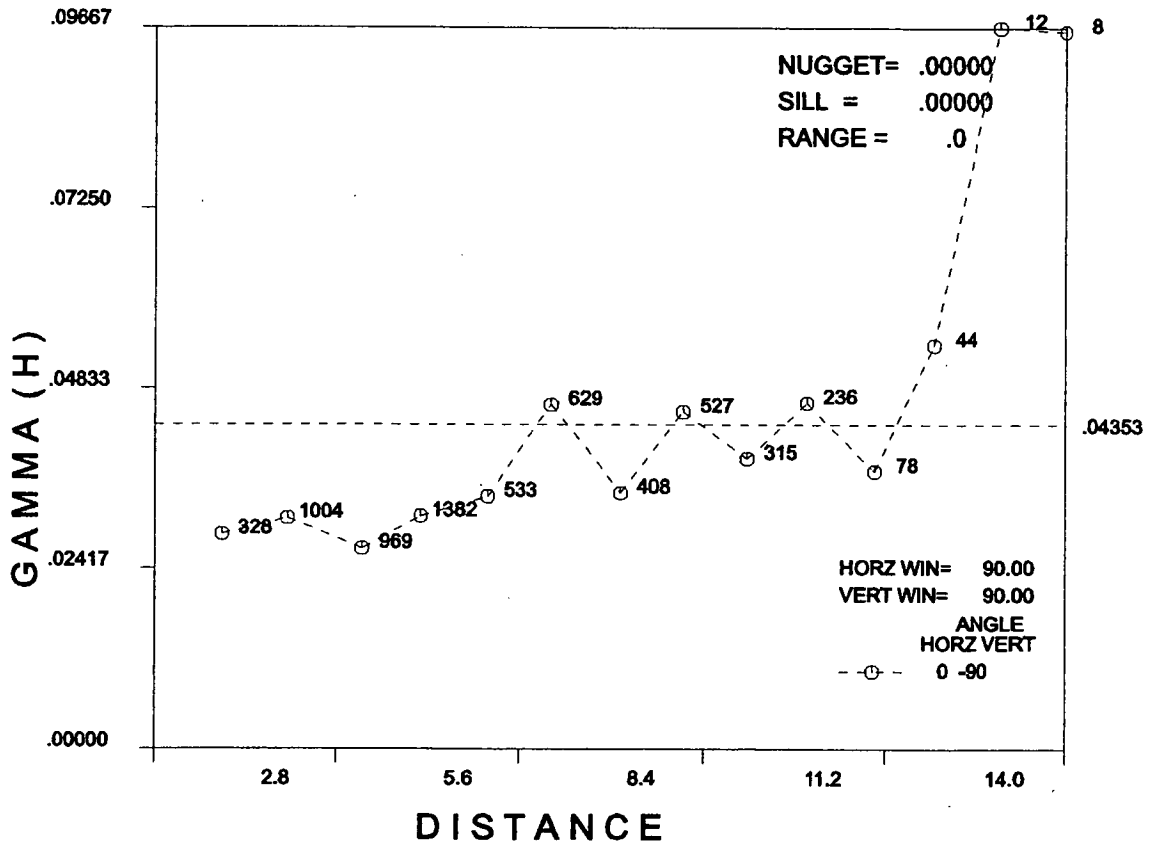

DwnH, Norm, Al2O3=0.1-3, Lag=1(+/-)0m, All Samples.

MEAN =	.31286	STD. DEV=	.20864	NO. =	3997
LOG MEAN=	.00000	LOG STDV=	.00000	C.V.=	.67

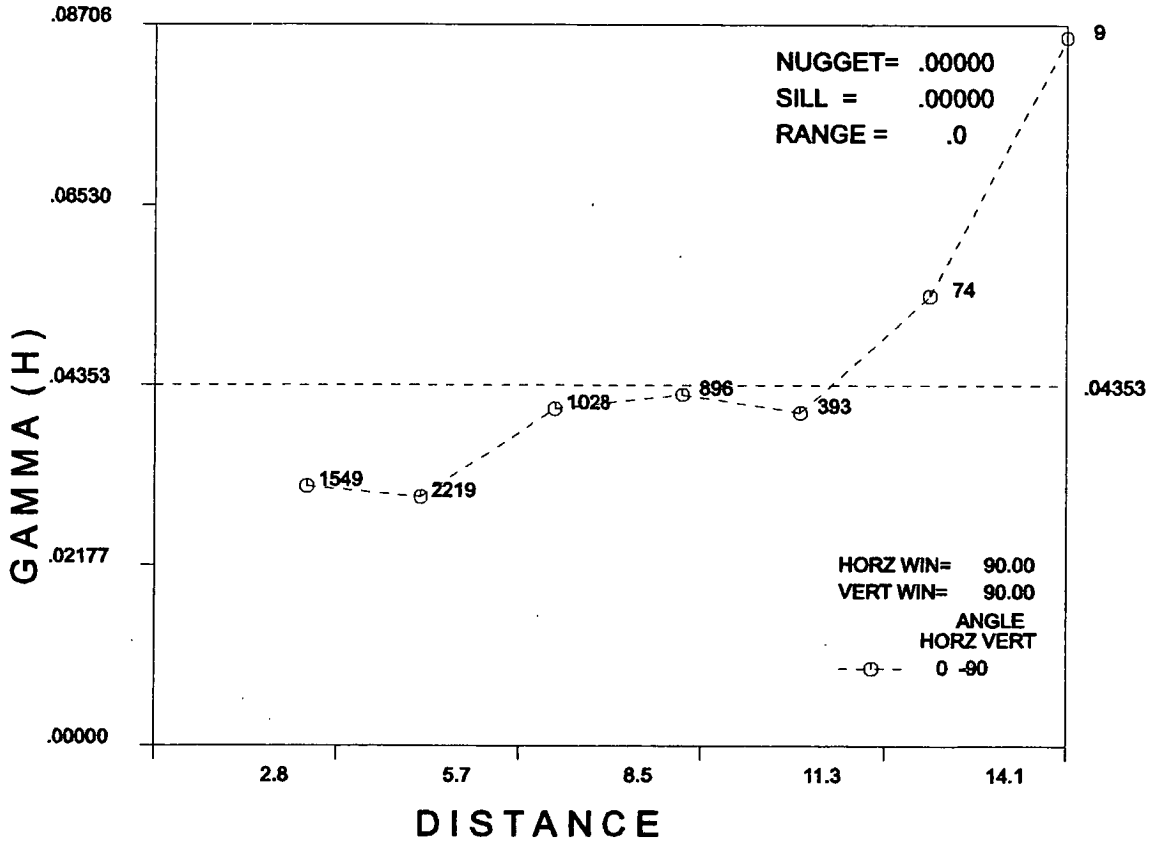

DwnH, Norm, Al2O3=0.1-3, lag=2(+/-)0m, All Samples.

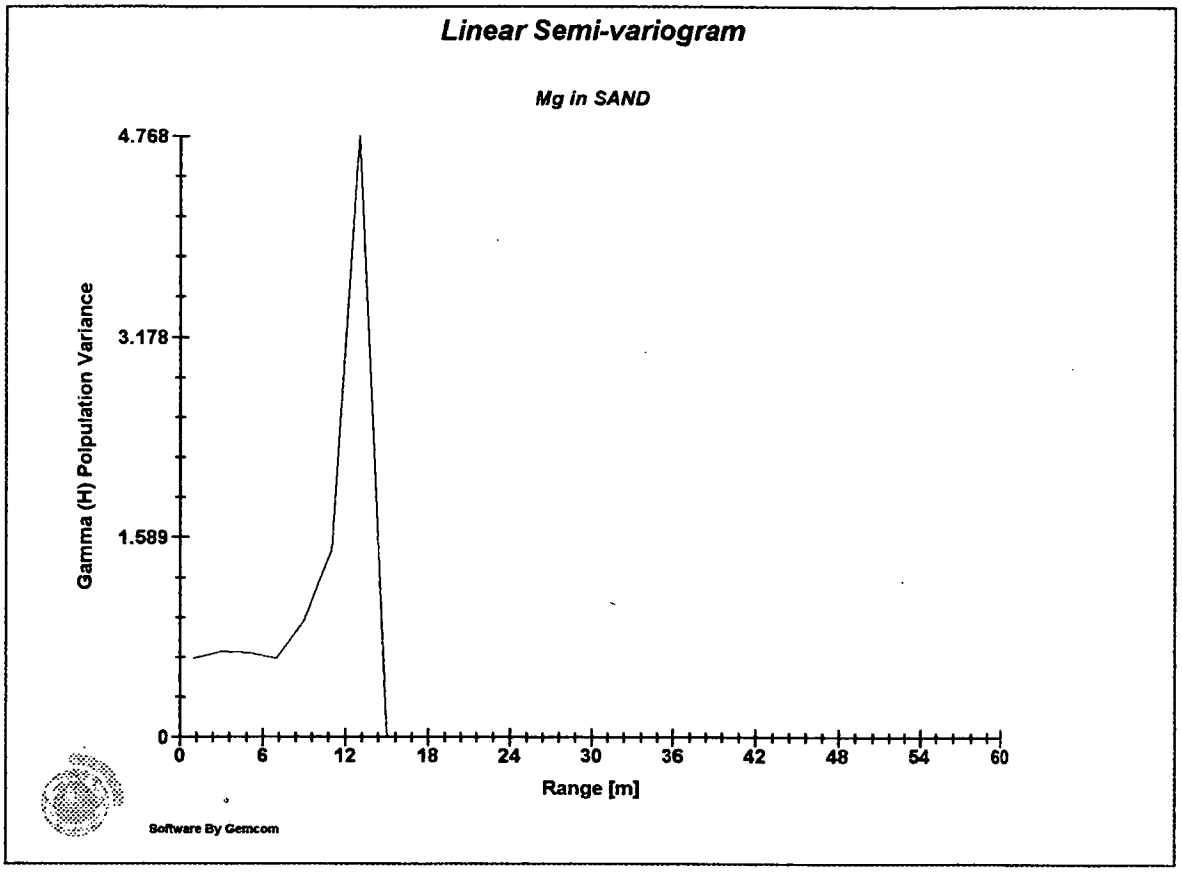
Linear Semi-variogram
Mg in SAND
4.768
3.178
1.589
0
Gamma (H) Polpulation Variance
0
6
12
18
24
30
36
42
48
54
60
Range [m]
Software By Gemcom

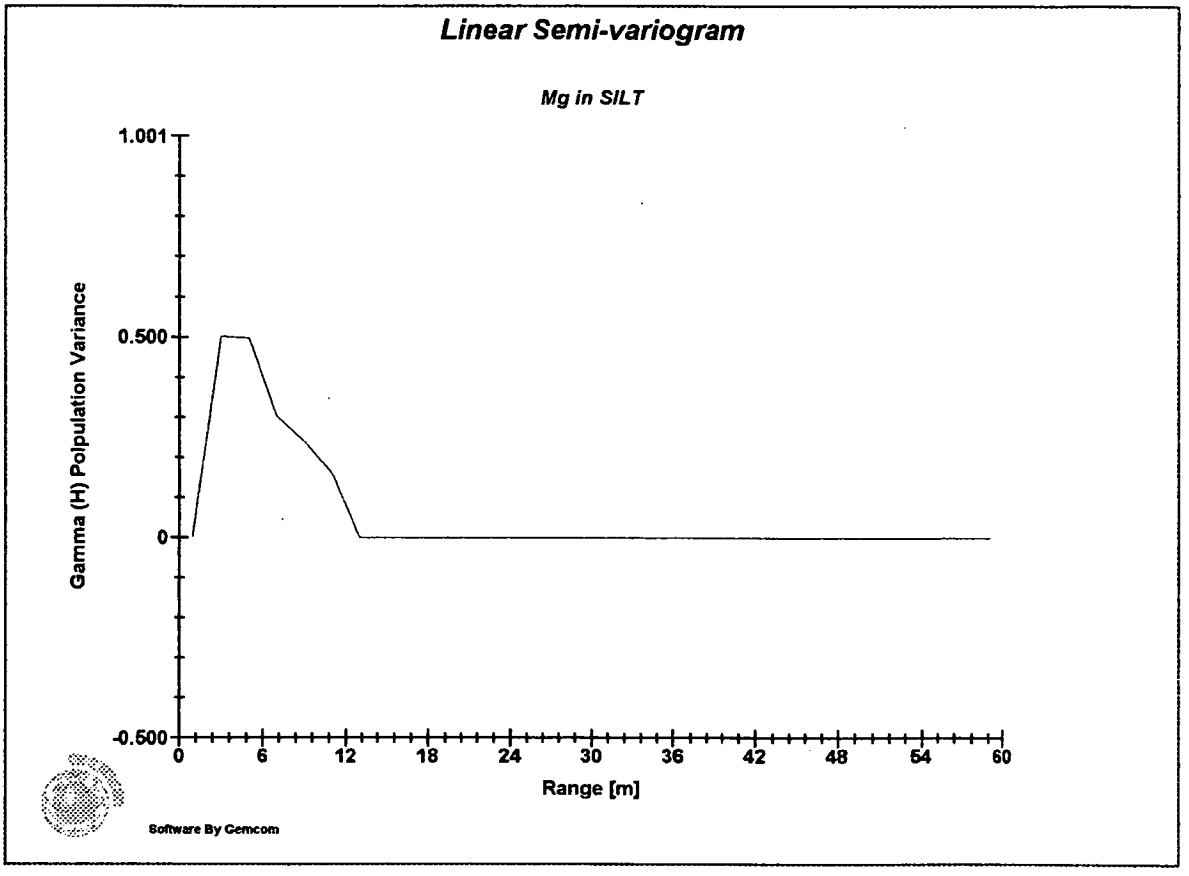
Linear Semi-variogram
Mg in SILT
1.001
0.500
0
-0.500
Gamma (H) Polpulation Variance
0
6
12
18
24
30
36
42
48
54
60
Range [m]
Software By Gemcom

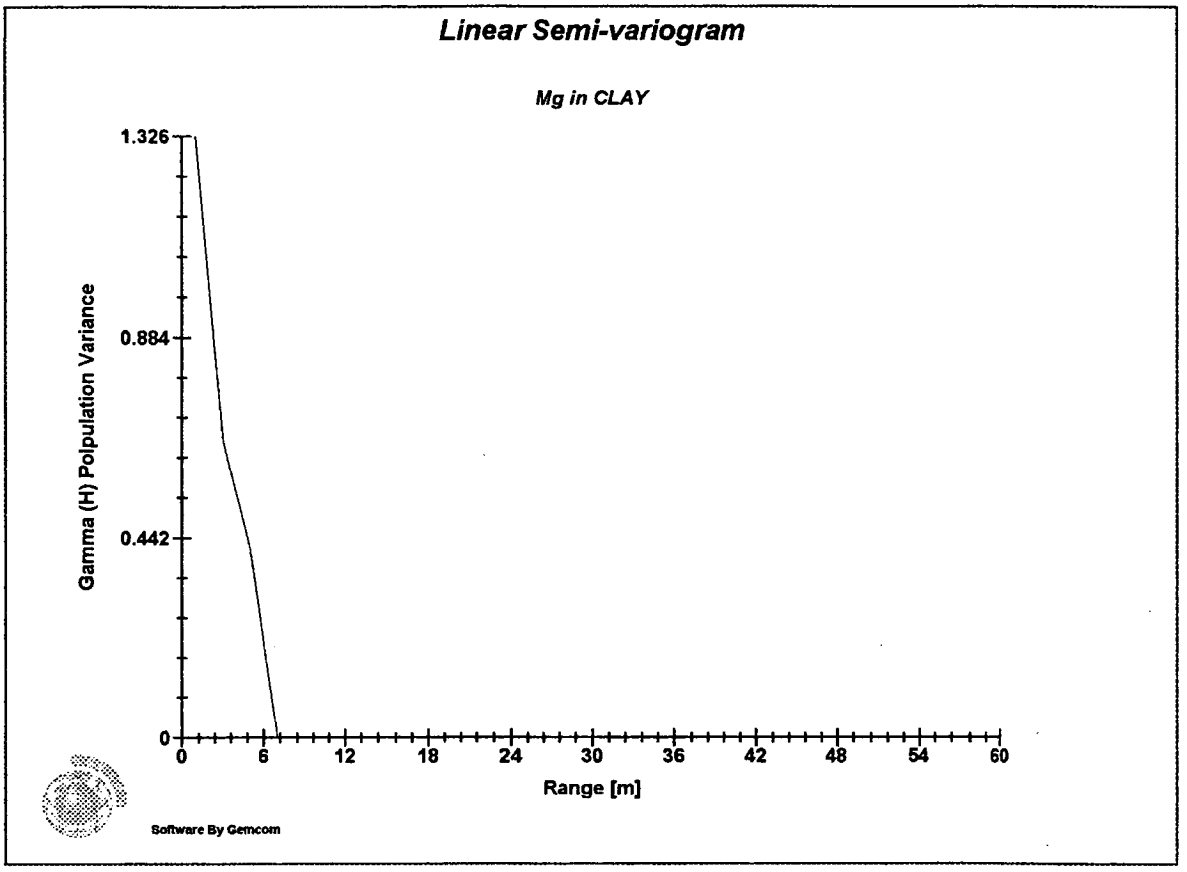
Linear Semi-variogram
Mg in CLAY
Gamma (H) Polpulation Variance
1.326
0.884
0.442
0
0
6
12
18
24
30
36
42
48
54
60
Range [m]
Software By Gemcom